Developing a Holocene Tephrostratigraphy for Ethiopia

Catherine Mariel Martin-Jones

BSc, MPhil (Aberystwyth)

Thesis submitted in fulfilment of the requirements for the degree of Doctor of Philosophy

Aberystwyth University

June 2016

Abstract

Explosive eruptions occurred throughout the Ethiopian Rift Valley during the Quaternary, depositing tephras that have provided crucial chronology for archaeological sites in eastern Africa. However, Holocene tephras are largely unstudied and the recent volcanic history of Ethiopia remains poorly constrained.

The first < 17 ka regional tephrostratigraphy is presented here, constructed using sediments from seven Ethiopian lakes: Ashenge and Hayk (Ethiopian Highlands), Dendi and Hora (Yerer-Tullu Wellel Volcano Tectonic Lineament, YTVL) and Awassa, Tilo and Chamo (central Main Ethiopian Rift, CMER). A database of ~ 2100 major and trace element single grain glass analyses will aid the future identification of these tephras at proximal and distal locations.

Peralkaline rhyolitic tephras are dominant throughout the Ethiopian Rift. Tephras are more differentiated in the central Main Ethiopian Rift than those deposited in northern Ethiopia. The uniquely phonolitic-trachytic Dendi tephras are derived from volcanoes on the rift shoulders, where magma evolved under high pressure.

Archives from the Ethiopian Highlands record < 17 ka distal volcanism from seven unknown volcanic centres in the Afar Rift. Eruptions occurred every <1000 years between $15.3 - 1.6$ cal. ka BP. Different tephras were deposited in lakes Ashenge and Hayk, and they were not dispersed towards lakes further south.

Tephras erupted from centres in the CMER are recorded in the Awassa, Tilo and Chamo archives. Glass compositions are indistinguishable from recent Corbetti eruptives. During < 10 ka, eruptions from Corbetti occurred every < 800 years and 6 eruptions were highly explosive. Two tephras are correlated between Tilo and Chamo (170 km SW of Tilo). However, eruptions from Corbetti are not recorded in archives from Ashenge, Hayk and Dendi.

These findings demonstrate the potential for further study to construct a comprehensive tephra framework, enabling assessment of regional volcanic hazards. Further geochemical characterisation of regional volcanoes will constrain the sources of these tephras and their petrogenesis.

WORD COUNT: 42,627

DECLARATION

This work has not previously been accepted in substance for any degree and is not being concurrently submitted in candidature for any degree.

Signed: .....(candidate)
Date: .....

STATEMENT 1

This thesis is the result of my own investigations, except where otherwise stated. Where **correction services* have been used, the extent and nature of the correction is clearly marked in a footnote(s).

Other sources are acknowledged by footnotes giving explicit references.
A bibliography is appended.

Signed: .....(candidate)
Date: .....

[*this refers to the extent to which the text has been corrected by others]

STATEMENT 2

I hereby give consent for my thesis, if accepted, to be available for photocopying and for inter-library loan, and for the title and summary to be made available to outside organisations.

Signed: .....(candidate)
Date: .....

Acknowledgements

This research was funded by a NERC algorithm studentship. This work would not have been possible without the assistance and insight provided by a multitude of people.

Most importantly, I thank my supervisors, Prof. Henry Lamb, Prof. Nick Pearce and Dr Christine Lane (University of Manchester), who have provided support, encouragement and constructive criticism throughout my research.

I thank Prof. Frank Schaebitz (University of Cologne) and the Hominin Sites and Palaeolakes Drilling Project for inviting me to participate in fieldwork in Ethiopia, providing me with an unforgettable experience.

Numerous people have assisted me during my never-ending quest for Ethiopian lake sediment cores and tephra deposits. Prof. Frank Schaebitz and Dr. Verena Foerster (University of Cologne) provided me with access to core sediments and helped me with shipping them. Dr Keith Haylock devoted days to helping me catalogue forgotten lake archives in the depths of the cold store. Dr. Giday WoldeGabriel (Los Alamos National Laboratory) and Prof. Clive Oppenheimer (University of Cambridge) supplied proximal tephra samples from Ethiopia.

Drs. Katie Loakes (Loughborough University), Helene Ducrotoy (Aberystwyth University) and Tsige Kassa and Bernd Wagner (University of Cologne) provided unpublished radiocarbon dates. Prof. Christopher Bronk Ramsey (University of Oxford) and the OxCal Google Group assisted me with Bayesian age modelling.

Analytical costs at LacCore were supported by the Visiting Graduate Student Travel Grant Program (University of Minnesota). Lorraine Morrison and Hollie Wynne helped me with cryptotephra sample processing. Tommy Ridway is thanked for helping mount tephra samples for analysis. Prof. John Westgate (University of Toronto) assisted me with polishing epoxy mounts and offered advice on geochemical analysis. Dr Victoria Smith (University of Oxford) assisted me greatly with EPMA glass analysis. Dr Bill Perkins and Andy Brown helped me with the LA-ICP-MS analysis at Aberystwyth University.

I thank Dr Asfawossen Asrat and Bahru Adugna (Addis Ababa University). Their wealth of knowledge on Ethiopian geology provided a wider perspective to my research findings. Dr Giacomo Corti (National Research Council of Italy) provided DEM data files for Ethiopia.

Thank you to Drs Ian Saunders, Jo Matthews, Marrie-Jeanne Royer and Keith Haylock and Vicky Mann, Alice Court and Alun James for supporting me and never failing to make me laugh. Drs Jo Matthews, Melissa Chapot and Sara Rassner have helped me so much with typesetting my thesis. I will greatly miss the excellent company and stories at tea time in the L floor common room.

A special thank you to Huw, who has been my rock. I thank Kayleigh and Amy, for always being there when I need them. Finally, I am hugely grateful for the support of my family, and to my Mum - who's rock collections inspired me as a child.

Contents

List of Figures

List of Tables

Chapter 1

Context and aims

1.1 Research context

The Ethiopian Rift is one of the few locations worldwide where active continental rifting can be observed (Macgregor, 2015). The rift extends from the intersection of the Red Sea and Gulf of Aden oceanic rifts through to southern Ethiopia in a south-west direction.

Whilst geologically intriguing, magmatic and tectonic processes of the Ethiopian Rift remain poorly understood (Macgregor, 2015). The early stage of regional geological studies is partly associated with the logistical difficulties of undertaking field work; e.g. the remote Afar region of northern Ethiopia is regarded as one of the hottest and most inhospitable areas of the world (Oppenheimer and Francis, 1997).

Explosive volcanic eruptions occurred throughout the Ethiopian Rift Valley during the Quaternary and into the Holocene (Pyle, 1999; Siebert *et al.*, 2011). Volcanic ash (*tephra*) produced by explosive eruptions is typically dispersed and deposited over hundreds to thousands of kilometres (e.g. Jensen *et al.*, 2014)

within a geologically instantaneous time frame (e.g. Rose and Durant, 2009). Due to this rapid dispersal and deposition, tephra layers record a 'moment in time' and can therefore be used as chronostratigraphic markers. Distal tephra records provide a dossier of past eruptions from multiple sources and an insight into eruption tempo and magnitude (e.g. Smith *et al.*, 2011*a*, 2013). Furthermore, the temporal and spatial precision of tephrochronology has been exploited by Quaternary researchers in order to corroborate other dating techniques and synchronize palaeoenvironmental proxy data, providing invaluable information on the leads and lags of palaeoclimate change (e.g. Lane *et al.*, 2013*a*,*b*).

Early Pliocene to late Pleistocene tephra deposits preserved in sedimentary archives throughout eastern Africa provide chronological control on hominin fossil sites in Ethiopia and Kenya (e.g. Clark *et al.*, 2003; WoldeGabriel and Hart, 2005; Brown *et al.*, 2006). The region is regarded as the crucible of human evolution and, since the discovery of the first hominid remains at Olduvai Gorge, Tanzania (Leakey *et al.*, 1961), has been a magnet for interdisciplinary research. Tephra studies have provided important temporal and spatial control on geological, archaeological and palaeoclimatic records from the region and have therefore been crucial in understanding the context of hominin evolution (Wolde-Gabriel and Hart, 2005). Stratigraphic controversies at numerous archaeological sites throughout eastern Africa have been resolved using tephrochronology (e.g. McDougall, 1985; Renne *et al.*, 1999; WoldeGabriel, 1994). The controversial age of the famous 'Lucy' (*Australopithecus afarensis*) fossil remains were corroborated through tephra correlations (Brown and Cerling, 1982).

However, younger Holocene tephras remain unstudied in Ethiopia. Ethiopia has 65 volcanoes of suspected Holocene age, only 14 of which have recorded historic eruptions (Siebert *et al.*, 2011). The historic record of volcanism is

sparse, and 85% of Africa's 155 recent eruptions recorded since 1870. The main historical record of volcanism followed the construction of the Suez Canal in 1869 and subsequent exploration of Africa. Those historic eruptions recorded are typically VEI$<$ 4 (Newhall and Self, 1982), due to the typically milder nature of rift volcanism. However, the rift volcanism is bimodal and large volume explosive eruptions are suspected to have occurred during the late Pleistocene to early Holocene (Siebert *et al.*, 2011).

Africa ranks within the top five volcanic regions in terms of people living close to volcanoes, and high population densities live in the vicinity of silicic volcanoes and calderas in the Ethiopian Rift Valley (Siebert *et al.*, 2011). Currently 12 volcanoes throughout eastern Africa are known to be actively deforming; 4 of which are within the Main Ethiopian Rift (Alutu, Corbetti, Bora and Haledebi) and many are undergoing fumarolic activity (Biggs *et al.*, 2009, 2011; Lenhardt and Oppenheimer, 2014). Despite this, the hazards remain underestimated (Lenhardt and Oppenheimer, 2014). The Main Ethiopian Rift volcanoes are listed by the World Bank report of volcanic hazards at a zero level of monitoring and the highest level of uncertainty in terms hazard and risk (Biggs *et al.*, 2011).

The potential for volcanoes in East Africa to erupt suddenly is demonstrated by the 2011 eruption of Nabro (Eritrea). Eritrea had no volcano monitoring network at this time and, until further inspection of higher spatial resolution satellite data, Dubbi (a volcano 25 km to the NE) was initially thought to be the source (Lenhardt and Oppenheimer, 2014). A lack of seismometers in Eritrea meant that seismic unrest during the weeks before was not interpreted as a precursor to an eruption. The eruption displaced thousands of people and the ash plume caused widespread disruption to international air-traffic (Lenhardt and

Oppenheimer, 2014). The Nabro eruption is believed to have caused the largest aerosol perturbation since the 1991 Pinatubo eruption (Sawamura *et al.*, 2012).

The Holocene record of volcanism in Ethiopia is therefore poorly documented. In order to prepare for hazards posed by future volcanic eruptions, it is important to understand how frequently they occur and their magnitude.

1.2 Research aims

The principal aim of this study is to construct a Holocene tephra framework for Ethiopia, the first tephrostratigraphy to cover this temporal and spatial range. To achieve this, tephras in < 17 ka lake sediment cores from seven lakes throughout the Ethiopian Rift are studied. A selection of samples from potential source volcanoes are also studied to test the provenance of these tephras. This study focusses on lake sediments because they often contain a more comprehensive and accessible record of distal tephras from multiple volcanic sources than proximal tephra deposits (Lowe, 2011). Linking tephras between different archives in Ethiopia will provide an insight into the dispersal of the tephras and their potential volcanic sources. Modelled radiocarbon ages for the tephras will give information on the tempo of past eruptions. Furthermore, this record of previous eruptions can also be used to mitigate against hazards of future events (Swindles *et al.*, 2011).

This study addresses the following specific research questions:

1. **Do the lake sediment cores available to the study contain tephra layers (including visible and microscopic tephras)?**

2. **If so, what are their approximate ages, and can any of these layers be correlated from lake to lake?**

3. **Can any tephras be attributed to known deposits on land, particular volcanoes, or particular eruptive events of known volcanoes? Where exact matches cannot be made, can affinities nevertheless be established through modelling of geochemical trends?**

4. **Based on the ages and characteristics of discrete ash layers, what if anything can be said about rates of volcanism in the Ethiopian Rift and adjacent Rift Shoulders?**

1.3 Thesis outline

This thesis is divided into eight chapters. This chapter has discussed the context and rationale behind the research and set out the aims of the study. Chapter 2 describes the principles of tephrochronology and the methods involved in this geochronological technique. Chapter 3 discusses Quaternary tephra deposits in eastern Africa and their importance in providing chronologies for fossil sites. Importantly, Chapter 3 outlines the lack of Holocene tephra studies in Ethiopia and the necessity for further investigation of these deposits. The methodological rationale is detailed in Chapter 4, which outlines the research design, gives site descriptions and provides information on the analytical methods employed to identify and characterise the tephras. Chapter 5 presents the tephrochronology of each archive and the major and trace element composition of the tephras. Chapter 5 goes on to investigate whether the composition of tephras varies spatially and if there is potential for tephra correlation between archives. The record of volcanism preserved in archives from the Ethiopian Highlands is presented in Chapter 6. Chapter 7 discusses the composition and timing of eruptions in the central Main Ethiopian Rift. Chapter 8 presents the conclusions of this study.

Chapter 2

Tephrochronology and its application

In this chapter, tephrochronology is discussed with specific reference to the fundamentals of this stratigraphic linking and dating technique, its applications and utility for providing records of past volcanism. The methodological approaches used in tephrochronology and analytical advances which have extended its geographical scope are later described.

2.1 Principles of tephrochronology

Tephra (originating from the Greek *'ashes'*) describes the loose fragmental material ejected by explosive volcanic eruptions and may range in grainsize from volcanic ash to volcanic blocks (Walker, 1971; Heiken, 1972; Fisher and Schminke, 1984). Explosive volcanic eruptions generate large volumes of tephra which is transported over thousands of kilometres (Jensen *et al.*, 2014) and deposited in sedimentary sequences over a geologically instantaneous time frame (Rose and Durant, 2009). Therefore a tephra layer represents a plane of equal

age in the host sediments which may be used to link archives over a wide geographic area (Lowe, 2011). A tephra layer from the same eruption has a unique geochemical fingerprint, allowing it to be identified and correlated across the fallout zone (Alloway *et al.*, 2007; Lowe, 2011). Tephrochronology can be used to test whether past events were synchronous or time-transgressive, the technique has been used in Quaternary science, with applications to hominin evolution (WoldeGabriel *et al.*, 2013), the hominin genetic bottleneck (Lane *et al.*, 2013*b*), the Neanderthal extinction (Lowe *et al.*, 2012) and the asynchronicity of climatic changes associated with the Younger Dryas in northern Europe (Lane *et al.*, 2013*a*).

2.2 Characteristics of tephra

2.2.1 Macroscopic tephra

Volcanic ash clouds are generally produced either by Plinian eruption columns or are elutriated from pyroclastic clouds formed by column collapse (Sparks and Walker, 1977; Woods and Wohletz, 1991; Sparks *et al.*, 1997) (see Fig. 2.1). The dispersal of tephra depends on a number of factors, including, column height, wind direction and speed and the grain size distribution of the ejecta (Sparks *et al.*, 1992). More powerful eruptions producing higher volumes of finer grained ejecta are likely to disperse tephra over greater spatial areas (Walker, 1973).

Tephra particles from within the ash plume are typically deposited rapidly, within minutes to days (Lowe, 2011). Tephra particles are deposited on the lake bed rapidly, although secondary transportation processes (e.g. turbidity currents) and depositional processes (e.g. settling of tephra particles through lake sediments) may compromise the stratigraphic position of the tephra layer

(Boygle, 1999; White and Riggs, 2001). Tephra particles sink rapidly in still lake waters and, assuming a particle size of fine sand, the fall velocity can exceed 40 m h^{-1} (Julien, 1995). Once saturated, even pumice will sink to the lake bed rapidly (Manville *et al.*, 2002).

Tephras typically become exponentially thinner with distance from the volcanic source, ranging in thickness from metres at proximal locations to sub-millimetres at distal locations (Pyle, 1989). Proximal deposits typically blanket the existing topography and contain a greater range of components, including heavier lithics and loose crystals, than their distal counterparts (Lowe, 2011). Proximal tephras can be traced locally between outcrops on the basis of stratigraphic relationships and physical characteristics, including, colour, bedding, pumice density or colour, the presence of accretionary lapilli or unique mineral assemblages (e.g. Brown, 1969; Brown *et al.*, 1970). Further stratigraphic information, such as palaeoenvironmental and archaeological associations, may also enable correlation of tephras (Feibel, 1999).

Tephras are generally better preserved in subaqueous settings as opposed to subaerial settings (Köninger and Stollhofen, 2001). Proximal deposits in subaerial settings are prone to erosion, local reworking and burial and therefore tracing these deposits over wide geographic areas becomes more challenging (Lowe, 2011). Distal tephra records, preserving tephras from multiple volcanic sources, therefore provide a more comprehensive record of past volcanism (Lowe, 2011).

2.2.2 Microscopic tephra

Cryptotephra (from the Greek, *'kryptein'* to hide) are 'non-visible' tephras and are typically far-travelled 'distal' deposits. They are commonly constituted of

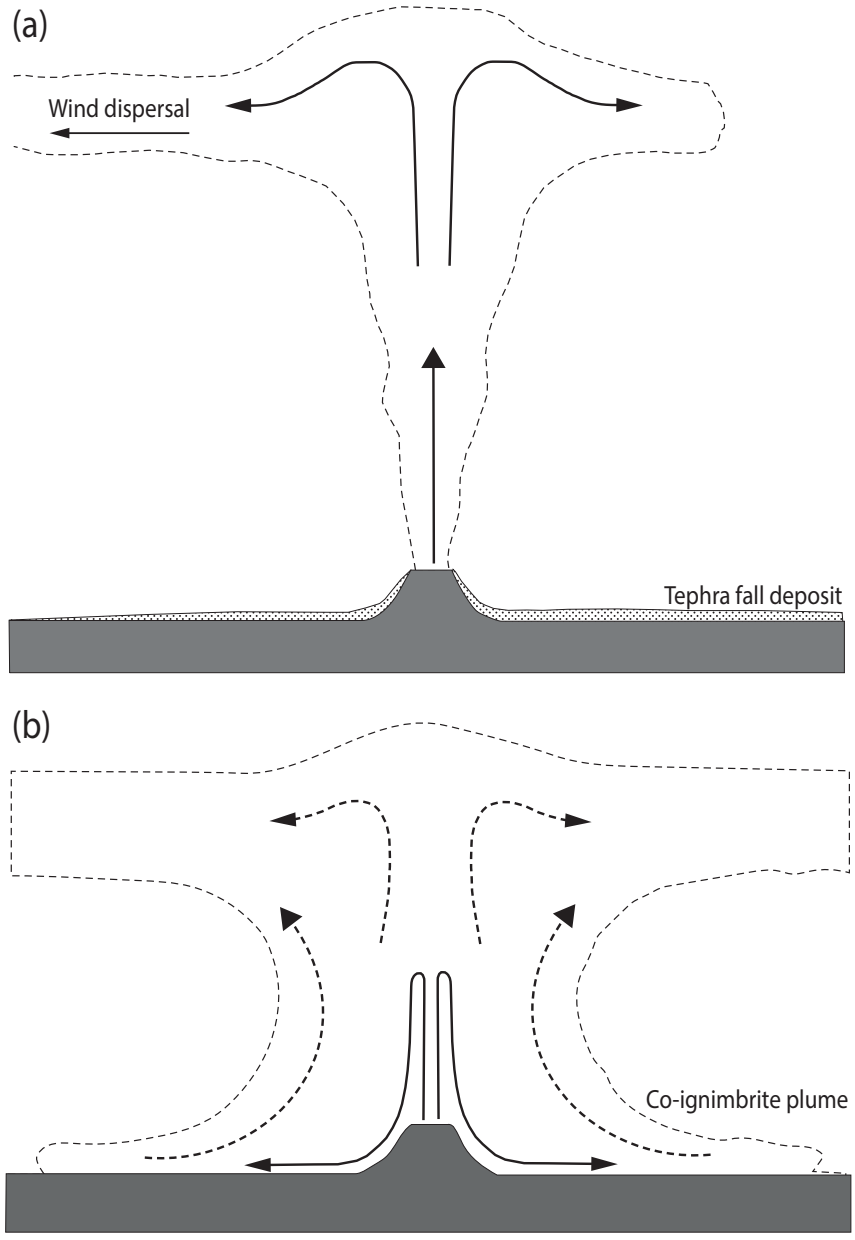

Figure 2.1: Tephra dispersal and deposition. Two mechanisms produce a widely dispersed tephra: (a) Tephra fall out from volcanic ash cloud generated by Plinian-style eruption (b) Tephra elutriated from extensive pyroclastic flows and forming co-ignimbrite plumes. Figure adapted from Dartevelle *et al.* (2002).

fine grained (typically $< 125\,\mu$m) glass shards present at dilute concentrations and are difficult to distinguish from host sediments which may have a similar grain size and colour (Lane *et al.*, 2014; Davies, 2015).

Cryptotephras were first studied by Christer Persson, who described microscopic Icelandic tephra layers occurring in peat bogs in Sweden (Persson, 1966; Wastegård, 2005). Dugmore (1989) documented the first occurrence of an Icelandic cryptotephra in the UK (in a Scottish peat bog) and kick-started the search for cryptotephra in Holocene deposits across Europe. Dugmore (1989) used an acid digestion technique to remove organic material and identify a cryptotephra which was correlated to the Hekla 4 eruption of ~ 4 ka on the basis of the unique geochemical fingerprint of its glass shards.

Less destructive methods of cryptotephra identification have since been developed, for example, the density separation procedures of Turney (1998) and Blockley *et al.* (2005) which were designed to isolate glass shards from host sediments.

Applications of cryptotephrochronology have now been undertaken in more than 24 countries, where sub-millimetre tephra have been traced over hundreds to thousands of kilometres (Lowe, 2011). Cryptotephras have greatly extended the scope of tephrochronology, allowing correlation over much greater areas and leading to the discovery of new tephras (Blockley *et al.*, 2005).

The fallout distribution of cryptotephra is exemplified by recent and historic eruptions. The AD $833-850$ Alasksan White River Ash, erupted from the Bona-Churchill massif, south-eastern Alaska, forms a prominent visible marker for 1000 km to the east. Recently the Alaskan White River Ash has been found to correlate to the'AD860B' cryptotephra (AD $846-848$) occurring in Greenland and northern Europe, 7000 km to the east (Jensen *et al.*, 2014). The eruption had

an explositivity of VEI=6 (an order of magnitude greater than Pinatubo 1991), which illustrates how even moderate size eruptions can disperse tephra over greater geographical distances than previously thought (Jensen *et al.*, 2014).

Recent applications of cryptotephrochronology include the discovery of tephra from the most explosive eruption of the Quaternary, the ~ 75 ka Younger Toba Tuff (YTT), in Lake Malawi sediments (East Africa), $> 7,000$ km to the west of the source volcano (Lane *et al.*, 2013*b*) (Fig. 2.2). Numerous studies have linked a supposed human genetic bottleneck with a dramatic climatic shift in eastern Africa resulting from the YTT supereruption (Gibbons, 1993; Ambrose, 1998; Hewlitt, 2000; Rampino and Ambrose, 2000). The identification of the YTT in the Lake Malawi sediments is significant because the sediments record no climatic changes at the position of the cryptotephra. This demonstrates that the eruption did not impact the East African climate significantly and may not have been responsible for a human genetic bottleneck (Lane *et al.*, 2013*b*). This is reiterated by Jackson *et al.* (2015) who observed no palaeoecological changes recorded in the Lake Malawi sediments before, during and after the deposition of the YTT.

2.3 Tephra records as dossiers of past eruptions

Tephras preserved in East African sedimentary archives have been used to elucidate the frequency, magnitude and style of past eruptions and also provide information on tectonic processes and petrogenesis (WoldeGabriel *et al.*, 1990, 1999, 2005; Ukstins Peate *et al.*, 2003; Feakins *et al.*, 2007). For instance, Feakins *et al.* (2007) identified 155 cryptotephras in the DSDP Site 231 Gulf of Aden marine core. The cryptotephras were geochemically linked to East African

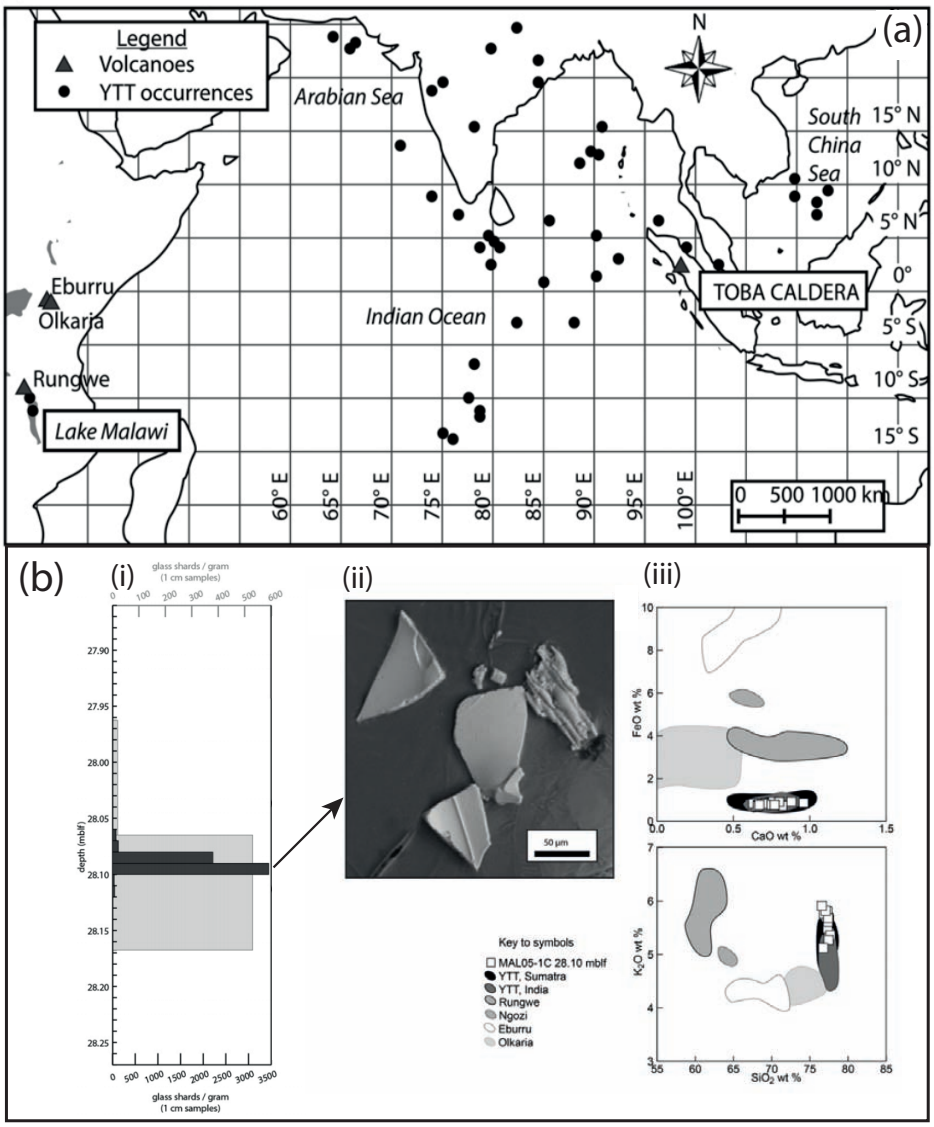

Figure 2.2: Cryptotephra from the Youngest Toba Tuff ($\sim$ 75 ka) found in Lake Malawi, eastern Africa; (a) Map showing the Toba caldera (Sumatra) and distribution of the YTT (b) the position of the YTT cryptotephra in sediments from Lake Malawi; (i) Glass shard counts in the Malawi lake sediments, the peak indicates the isochron position, (ii) SEM image of glass shards in the Malawi sediments, (iii) Glass shards from the Malawi cryptotephra have an identical composition to the YTT tephra. Figures from Lane *et al.* (2013*b*).

tephras and reveal three main volcanic episodes; at $\sim 4.0 - 3.2$ Ma, 2.4 Ma and $1.7 - 1.3$ Ma. Larger volume eruptions between $4.0 - 3.2$ Ma were inferred from the generally thicker tephras deposited in the Gulf of Aden during this time interval.

The tephra record has important implications for hazard assessments, giving insight into the tempo and magnitude of eruptions from multiple volcanic centres (Lowe, 2011). Tephra records have been used in numerous studies to provide information on past eruptive frequencies and therefore future hazards (Shane and Hoverd, 2002; Hurst and Smith, 2004; Jenkins *et al.*, 2007; Turner *et al.*, 2009). The Eyjafjallajökull 2010 eruption (Davies *et al.*, 2010) and Grímsvötn 2011 Icelandic eruptions and subsequent disruption to air-traffic demonstrated the importance of studying previous eruptive deposits and their dispersal. These eruptions prompted Swindles *et al.* (2011) to compile information on the tephra deposits sourced from Icelandic volcanoes over the past 7000 years. Swindles *et al.* (2011) demonstrated that within any decade over the past millennium there was a 16% probability of an eruption from Iceland producing a visible tephra deposit in northern Europe. Through understanding the past and therefore future eruptions from Iceland the impact on aviation, public health and economy can be lessened (Lawson *et al.*, 2012).

The lack of documented Holocene eruptions and their tephra deposits in eastern Africa, coupled with the absence of a volcano monitoring network, meant that the Nabro 2011 (Eritrea) eruption occurred unexpectedly. Although tephra studies have been used for hazard mitigation to great effect elsewhere, this approach is yet to be used in eastern Africa. In order to prevent future disruption to the aviation industry and the displacement of thousands of people,

it is crucial that previous eruptions from regional volcanoes and their deposits are investigated.

2.4 Lakes as tephrostratigraphic repositories

Subaerial tephras may be obscured by dense vegetation, buried and extensively eroded. For instance the subaerial Dubbi (Eritrea) 1861 tephra deposit has been eroded since its deposition (Lenhardt and Oppenheimer, 2014). The most complete records of volcanism therefore occur where tephras are deposited in aggrading sediment records, rather than eroding systems (White and Riggs, 2001).

Sediments from Ethiopian Rift lakes provide records of past volcanism, and an archive of core material is held at Aberystwyth University. The accessibility of these tephra records is crucial in a region where fieldwork is regarded as logistically challenging and where proximal tephra deposits at volcanoes may be poorly exposed, buried or eroded (Wiart and Oppenheimer, 2004). This study uses Holocene Ethiopian lake sediment cores as dossiers of past regional volcanic activity.

Lake sediments provide ideal records of past volcanic activity because:

1. Lakes are **low energy** depositional environments that may record near continuous sedimentation, allowing high resolution tephra records to be preserved (White and Riggs, 2001).

2. Tephra particles fall rapidly to the lake bed and their deposition is typically geologically **instantaneous** (Julien, 1995; Manville *et al.*, 2002).

3. Lacustrine sediments contain **age-diagnostic material** which is useful for chronostratigraphic correlation (White and Riggs, 2001).

4. Tephras from multiple volcanic sources are preserved, enabling **inter-relationships** between different centres to be investigated (Smith *et al.*, 2013).

2.4.1 Factors impacting tephra deposition and preservation in lake sediments

Prior to investigating tephra records preserved in Ethiopian lake sediments, it is important to consider factors that may determine the distribution of tephras and their subsequent preservation in disparate lake sediments. These factors may determine the potential for tephra correlations between lake archives and have implications for interpretations of past eruption frequency.

As discussed above, the physical characteristics of a volcanic eruption, including the volcanic explosivity, column height and grain size directly determine the spatial distribution of tephra deposits (Sparks *et al.*, 1997). Furthermore, differences in tephra occurrence in lake sediments are related to meteorological conditions, and their deposition in precipitation bearing systems may cause sporadic fall out patterns (Boygle, 1999). Importantly, tephra dispersal is dependant on wind direction and speed (Carey and Bursik, 2015). Figure 2.3 shows recent wind regimes during summer and winter, averaged over Ethiopia. Wind directions vary seasonally over Ethiopia, and this will determine the spatial distribution of tephras over time. During the wet season westerly winds predominate, potentially dispersing tephra away from Ethiopia towards the east. However, during the dry season months, the wind directions reverse causing

tephras to be dispersed towards the west. It is therefore apparent that the preservation of tephras in lake sediments may be governed in part by variations in wind direction. However, these are recent wind regimes, which may have varied throughout the Holocene.

Processes including sediment focussing, slumping, turbidity currents, bioturbation and tectonic movement may also compromise the stratigraphic position of a tephra (Boygle, 1999; White and Riggs, 2001; Payne *et al.*, 2005). Tephra particles may also migrate vertically through lake sediments; typically causing the tephra to appear older (Anderson *et al.*, 1985; Payne *et al.*, 2005). Furthermore, the fragmental nature of tephra deposit means that they can be redistributed throughout the lake catchment by aeolian and fluvial processes (Boygle, 1999).

The controls on the deposition and preservation of tephras therefore varies between sites and these factors need to be considered when constructing a tephra framework. Nevertheless, lake sediments frequently provide more complete tephra records than those proximal to volcanic centres.

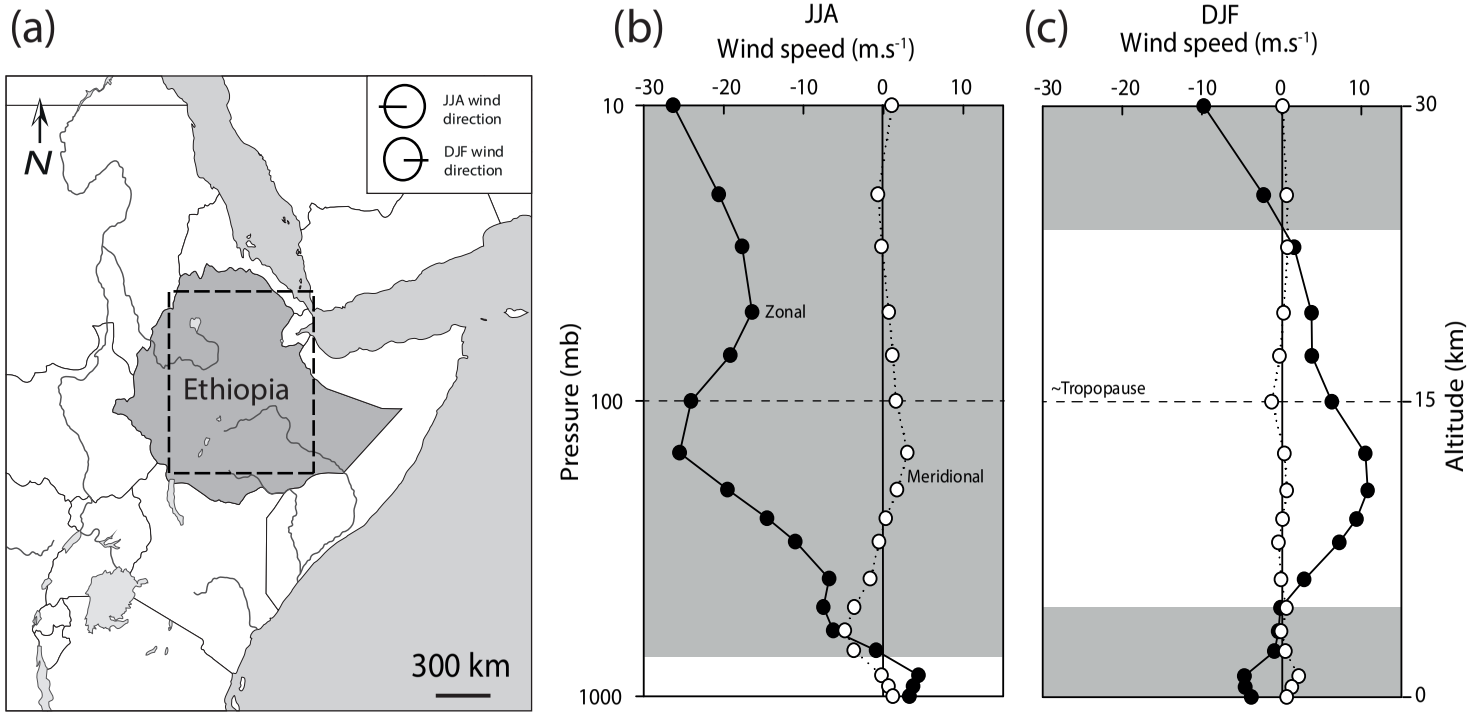

Figure 2.3: (a) Map of Ethiopia, dashed area indicates approximate region represented in (b) and (c). (b) Profile through atmosphere showing the speed of zonal and meridional winds during the summer and (c) winter monsoon months - after Feakins *et al.* (2007). Wind velocities obtained from the NOAA NCEP CDAS-1 monthly pressure level climatology dataset spanning January 1949 - January 2016 (Kalnay *et al.*, 1996), averaged over $40-45^{O}$E, $6-15^{O}$N. Negative wind speed values indicate easterly flow of zonal winds and southerly flow of meridional winds. Positive values indicate westerly zonal winds and northerly meridional winds. Grey shading indicates favourable wind trajectories from the Afar Rift towards the Ethiopian Highlands in the west. The approximate altitude of the tropopause is given for reference, based on vertical pressure.

2.4.2 Identifying cryptotephras in lake sediments

Whilst distal records often preserve a more complete record of past volcanism, they typically receive lower volumes of finer grained tephra than proximal locations, making tephra identification more difficult.

This study investigates both visible tephras and cryptotephras in Ethiopian lake sediments. Studying cryptotephras promises to build a higher resolution tephra framework for Ethiopia, facilitating correlation over wider spatial areas and providing insight into the dispersal of ultra-distal deposits.

Various methods have been used in the literature to identify 'non-visible' cryptotephras in lake sediments; these are briefly outlined below to provide a rationale for the methods used in this work.

Cryptotephras hosted in terrestrial and marine sediments are typically identified using the standard density separation technique reviewed by Blockley *et al.* (2005), Lane *et al.* (2014) and Davies (2015). The technique involves first sampling the sediments at contiguous ~ 10 cm depths and extracting tephra glass shards using the high density liquid, sodium polytungstate ($1.95 - 2.55$ g/cm^3). The glass shards from each sample can then be counted under an optical microscope and regions containing high concentrations of shards resampled at 1 cm intervals in order to define the position of the isochrons. Shard counts are typically expressed as shards per gram (s/g) of dried sediment and can be plotted against the site's stratigraphy in order to review the position of a cryptotephra (e.g. see Fig. 2.2b). The profile of the cryptotephra is influenced by the eruption duration and characteristics along with secondary processes such as bioturbation and soil erosion, which may distribute the cryptotephra throughout the stratigraphy. If glass shards show a sudden appearance in the host sediment

and tail off gradually, the basal rise is typically interpreted as the primary airfall event (Lane *et al.*, 2014).

Counting procedures are time consuming; numerous studies have utilised other methods to successfully identify cryptotephras in terrestrial and marine sediments. These techniques are reviewed by Gehrels *et al.* (2008) and include ground-penetrating radar (Lowe, 1985), remnant magnetisation and magnetic susceptibility (Hodgson *et al.*, 1998; Takemura *et al.*, 2000; de Fontaine *et al.*, 2007; Carter *et al.*, 2002; Rasmussen *et al.*, 2003; Gomez *et al.*, 2007; Venuti and Verosub, 2010; McCanta *et al.*, 2015), spectrophotometry (sediment reflectance and luminescence) (Caseldine *et al.*, 1999; Gehrels *et al.*, 2008; McCanta *et al.*, 2015) X-radiography (Turner *et al.*, 2008; Lowe, 2011), X-ray fluorescence (XRF) (Hogg and McCraw, 1983; Gehrels *et al.*, 2008) and XRF core scanning (Gehrels *et al.*, 2008; Marshall *et al.*, 2009; Langdon *et al.*, 2011; Vogel *et al.*, 2010; Kylander *et al.*, 2011; McCanta *et al.*, 2015). To date, none of these techniques have proved as effective in detecting the finest cryptotephras as density separation techniques.

This study uses XRF core scanning, in combination with density separation techniques, to identify cryptotephras in lake sediments. Comparatively few studies have combined these techniques to identify cryptotephras, particularly in lake sediments. The first systematic study to apply this technique to cryptotephra detection in lakes sediments was undertaken by Kylander *et al.* (2011) on archives from the Faroe Islands. Kylander *et al.* (2011) successfully identified basaltic visible and crypto-tephras (containing $>1,000$ shards/cm^3) on the basis of elevated K, Mn, Fe, Ca and Ti counts. Damaschke *et al.* (2013) identified alkaline visible tephras in sediments from Lake Prespa (Balkans) based on increased K and Rb and/or Sr counts. However, cryptotephras were not associated with

this geochemical signature. Wulf *et al.* (2013) identified the phonolitic Laacher See cryptotephra using XRF mapping of resin-impregnated sediments from Trzechowskie palaeolake (Poland) on the basis of increased K, Al and Fe counts (Fig. 2.4).

Silicic cryptotephras are generally more difficult to identify using XRF core scanning. For example, Wastegård *et al.* (2013) found that even visible rhyolitic tephras in the Laguna Potrok Aike (Argentina) core were associated with only slight variations in K and Ti counts. Furthermore, Kylander *et al.* (2011) found that rhyolitic cryptotephras of low shard concentrations (<850 shards/cm^3) in Faroe Island lake sediments were not detected by XRF core scanning. Balascio *et al.* (2015) created synthetic core sediments spiked with basaltic and rhyolitic cryptotephras. Basaltic cryptotephras were identifiable using XRF core scanning, but more silicic cryptotephras were not associated with a distinct elemental response.

Few studies have used XRF core scanning to identify cryptotephras in Ethiopian lake sediments. Marshall (2006) identified elevated K, Zr and Rb counts associated with visible silicic tephras in sediments from Lake Ashenge (northern Ethiopia). Marshall (2006) also suggested that increased K, Zr and Rb counts at other depths throughout the sediments may be associated with cryptotephras. This is verified in this study through higher resolution XRF scanning and glass shard counting.

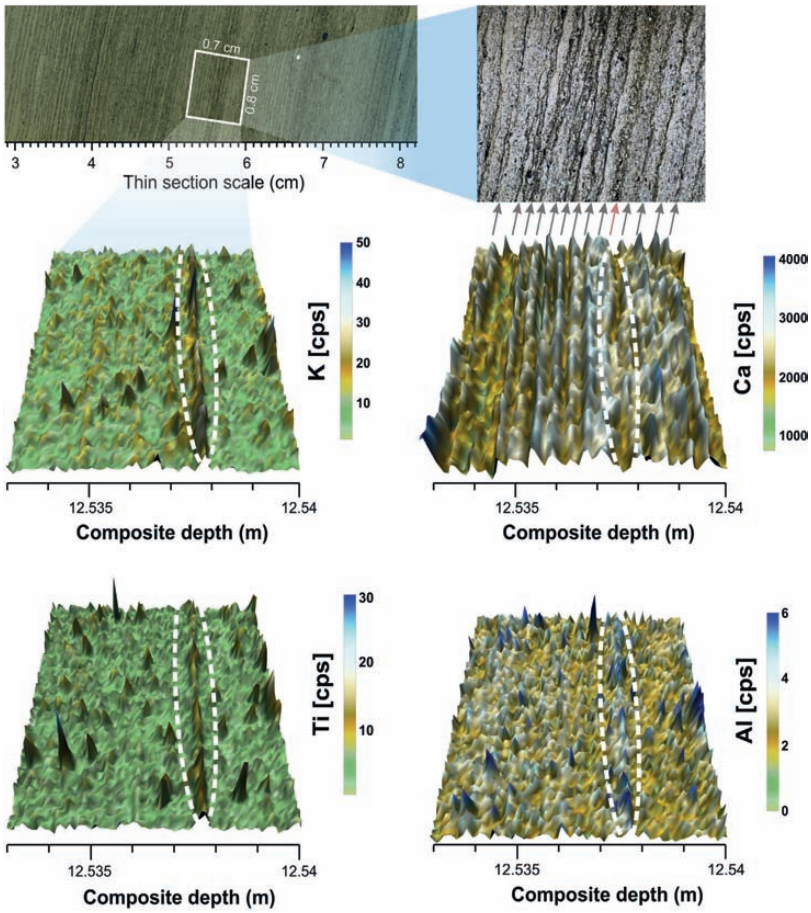

Figure 2.4: Thin section images and 3D images showing the K, Ti, Ca and Al distribution (obtained through XRF scanning) in sediments from the Trzechowskie palaeolake containing the Laacher See Tephra. The continuous line of increased K, Ti and Al counts represents the Laacher See cryptotephra. Figure from Wulf *et al.* (2013).

2.5 Tephra fingerprinting

The unique physical and geochemical properties of a tephra from the same eruption allow it to be identified across the fallout zone and distinguished from other tephras of similar ages (Alloway *et al.*, 2007).

Tephra fingerprinting may be undertaken using a variety of analytical instruments on various components of the tephra deposits, including, the individual glass shards, free crystals and phenocrysts or microcrysts (Table 2.1).

Where tephras of different ages have similar geochemical fingerprints; age data and good stratigraphic information are essential for narrowing down the potential correlatives (e.g. Lane *et al.*, 2012).

Commonly multiple criteria are necessary in order to distinguish between tephra deposits; Tryon *et al.* (2008) suggest that tephra correlations are best considered as testable hypotheses, subject to continual revision and expanded data sets.

2.5.1 Glass shard morphology

The morphology of tephra glass shards varies between deposits depending on the magma composition, eruption style and other factors (Heiken, 1972). Shard morphology may be studied under optical microscopy or scanning electron microscopy (SEM) and, in favourable circumstances, may provide a means for discriminating between tephra deposits.

Three main morphological types have been described (Fig. 2.5): bubble wall or cuspate shards, platy shards and pumiceous shards, although other morphologies are common (Heiken, 1972, 1974; Fisher and Schminke, 1984; Rose and Chesner, 1987; Heiken and Wohletz, 1991). Katoh *et al.* (2000) used

Table 2.1: Summary of analytical methods used for characterising tephras, adapted from Lowe (2011). INAA: instrumental neutron activation analysis, XRF: X-ray fluorescence, LA- or SN-ICP-MS: laser ablation or solution nebulisation inductively coupled plasma mass spectrometry, SEM: scanning electron microscopy, EDS or WDS: energy or wavelength dispersive spectrometry, SSMS: spark source mass spectrometry, SIMS: secondary ionization mass spectrometry.

Tephra component	**Method of analysis**
Bulk tephra samples	
Bulk samples	INAA, XRF, SN-ICP-MS
Glass shards	
Shard morphology	Optical microscope/SEM
Major and minor elements	EDS or WDS Electron probe micro-analyser
Rare earth and trace elements	LA- or SN-ICP-MS, INAA, SSMS, SIMS
Pb isotopes	LA-ICP-MS
Fe-Ti oxides	
Major and minor elements	EDS or WDS Electron probe micro-analyser
Eruption temperatures & oxygen fugacities	Mössbauer spectroscopy and EDS or WDS Electron probe micro-analyser
Ferromagnesian mineals	
Assemblages	Petrographic microscope
Pyroxene, amphibole, olivine, biotite crystals	Electron microscope
Feldspars	
Anorthite content of plagioclase crystals	EDS or WDS Electron probe micro-analyser

the morphological properties of glass shards combined with tephra chemistry to create a tephra framework for the Konso Formation, southern Ethiopia.

However, tephras produced by eruptions with similar characteristics and similar melt compositions may have indistinguishable shard morphologies. Therefore correlation based on shard morphology may be inconclusive and this technique is more effective when used alongside other techniques.

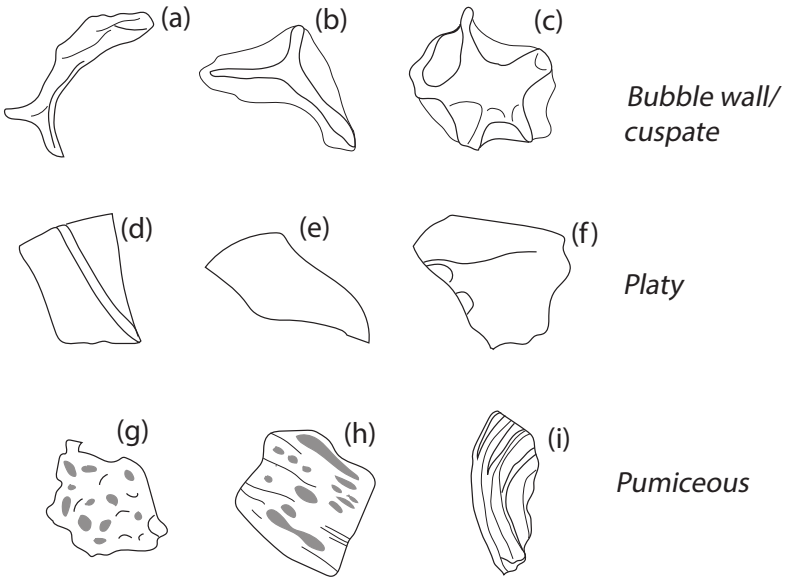

Figure 2.5: The three main glass shard morphologies (author's image). (a-c) Bubble wall / cuspate glass shard morphologies, (d-f) platy shards possessing a blocky shape and (g-i) pumiceous shards containing vesicles. Note the differing types of pumiceous shards - the vesicles have been stretched to produce (h) and (i), the latter has a more fluted shape.

2.5.2 Mineral assemblages

Tephra deposits proximal to the volcanic source ($\sim<$ 100 km) may contain unique assemblages of minerals which may be used to discriminate between tephra deposits. Orthopyroxenes, clinopyroxenes, amphiboles and biotite are common minerals associated with tephras derived from calc-alkaline volcanic centres, whilst peralkaline tephras may contain sodic phases such as aegirine, riebeckite, ferrohedenbergite and aenigmatite (Alloway *et al.*, 2007). Mineral assemblages were used by Brown (1969) and Walter *et al.* (1987) to identify and trace tephras locally in the Omo Basin (southern Ethiopia) and to identify the Cindery Tuff in the Awash Basin (northern Ethiopia).

The relative abundance of ferromagnesian and accessory minerals in tephras may also provide a valuable correlative tool (e.g. Lowe *et al.*, 2008). However,

these denser minerals may be preferentially deposited close to the source (Sparks *et al.*, 1997) causing variations in their abundance in deposits. Biotite and Fe-Ti oxides may also be dissolved in acidic peat bogs and olivine may be altered by weathering (Hodder *et al.*, 1991). Furthermore, tephras derived from the same source, or with similar compositions, may have comparable mineral assemblages.

Therefore mineral assemblages may not be a diagnostic tool for correlation beyond proximal areas and this technique is better used in combination with other characterisation methods.

2.5.3 Glass chemistry

Glass shards in a tephra have a unique geochemical fingerprint which approximates the composition of the magma at the time of eruption (Lowe, 2011).

Grain specific geochemical analysis of glass shards in tephra deposits is now considered the most diagnostic tool for correlation where stratigraphic, mineralogical and physical properties are inconclusive. Shard-specific analyses are preferable to whole rock analyses because bulk tephra samples may contain variable quantities of accessory and accidental material with distance and direction from the source including phenocrysts, xenocrysts, xenoliths and detrital grains (Shane and Smith, 2000).

Although glass chemistry is extensively used for correlation in Quaternary science, different tephras may have identical compositions (e.g. Lane *et al.*, 2012) and therefore a combination of characterisation methods and stratigraphic and age data provide the most robust correlations.

Two analytical techniques are used in this study to characterise Holocene tephras from Ethiopia in terms of their major (electron probe micro-analyser) and trace element (laser ablation inductively coupled plasma-mass spectrometry)

concentrations and therefore these methods are discussed below. Advances in these analytical techniques, extending the spatial area of tephra correlation, are also described.

2.5.3.1 Electron probe micro-analysis of glass

Since its development in the late 1960*s* (Smith and Westgate, 1968), single shard electron probe micro analysis (EPMA) now forms the foundation of tephra studies. Notably, the technique has been extensively used to correlate Pliocene to late Pleistocene tephra in eastern Africa and the Gulf of Aden (e.g. Brown, 1982; Sarna-Wojcicki *et al.*, 1985; WoldeGabriel *et al.*, 1990; Pickford *et al.*, 1991; Brown *et al.*, 1992; Hart *et al.*, 1992; Katoh *et al.*, 2000; WoldeGabriel *et al.*, 2005; Brown *et al.*, 2006; Feakins *et al.*, 2007; Campisano and Feibel, 2008; DiMaggio *et al.*, 2008; Deino *et al.*, 2010; Lane *et al.*, 2013*b*).

Typically, $10-13$ major elements (Si, Al, Ti, Fe, Mn, Mg, Ca, Na, K and P), dependant on glass composition, can be routinely determined using EPMA (Lowe, 2011). Over the past years several analytical limitations have been overcome, allowing accurate and precise analysis of fine glass shards at a high resolution (Hayward, 2011).

Subtle geochemical differences between some tephras require high levels of analytical precision and accuracy (Hayward, 2011). Different laboratories employ variable analytical methods which create inter-laboratory variations when analysing the same materials (Pearce *et al.*, 2014). Therefore, numerous inter-laboratory comparisons have been undertaken to ensure robust correlations can be made using different instruments (e.g. Kuehn *et al.*, 2011).

EPMA analysis is associated with 'alkali element migration', the chemical modification of glass during analysis, causing an underestimation of Na and

overestimation of Si and Al (Morgan and London, 1996, 2005; Humphreys *et al.*, 2006). This element migration is overcome by the use of a defocussed, ~ 10 μm diameter beam, at a low (< 10 nA) current and the determination of Na at the start of the analysis (Hunt and Hill, 2001). Hayward (2011) successfully conducted glass analysis with no detected alkali element loss, using a narrower 3 μm diameter focused beam, operating at a low beam current of < 0.1 nA/μm^2. X-rays signals can be measured using two different analysis types: energy dispersive spectrometry (EDS) and wavelength dispersive spectrometry (WDS). EDS analysis measures X-ray energies simultaneously and is therefore favoured for its speed. WDS analysis is capable of measuring individual wavelengths at a higher beam current and monitoring sodium loss (Coulter *et al.*, 2009).

These analytical improvements enable fully quantitative analysis at a high resolution, extending the scope for finer grained and more distal tephras to be correlated.

2.5.3.2 Laser ablation ICP-MS analysis of glass

Many tephras can be distinguished between on the basis of their major element composition. However, different melts may share similar crystallisation trends and mixing patterns prior to their eruption, so tephras of different ages may have similar major element compositions (e.g. Westgate *et al.*, 2013).

In these instances, trace element analysis of tephra glass shards may allow compositional discrimination. This technique was used by Westgate *et al.* (2013) to discriminate between the Older, Middle and Younger Toba Tuff, which possess a similar major element composition (Fig. 2.6) (Chesner, 1998; Lee *et al.*, 2004). Westgate *et al.* (2013) identified four primary glass populations with differing Sr, Ba and Y concentration within the Younger Toba Tuff (YTT) which easily

distinguish it from the homogeneous glass populations of the Older and Middle Toba Tuffs.

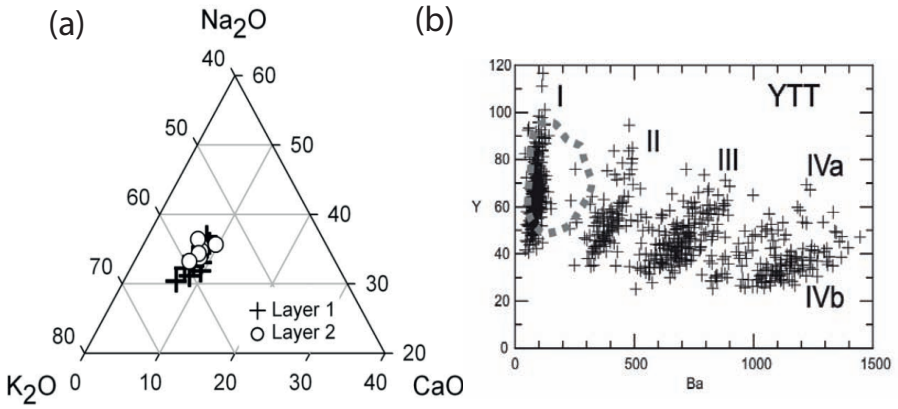

Figure 2.6: Trace element composition of the Youngest Toba Tuff distinguishes it from the Oldest and Middle Toba Tuff. (a) CaO-Na_2O-K_2O ternary diagram showing the compositional similarity between the Oldest Toba Tuff (open circles) and Youngest Toba Tuff (crosses), figure from Lee *et al.* (2004). (b) Bi-plots of Ba-Y (ppm) concentrations divide the YTT tephra into four major glass compositions and a smaller, fifth compositional group (IVa). In contrast the OTT and MTT have homogeneous trace element compositions (dotted grey outline shows the homogeneous composition of OTT glass shards). Figure from Pearce *et al.* (2014).

The potential of laser ablation inductively coupled plasma-mass spectrometry (LA-ICP-MS) for analysing trace elements in tephra glass shards was first realised by Westgate *et al.* (1994). Since then, LA-ICP-MS has been used frequently in Quaternary science to characterise tephras (Bryant *et al.*, 1999; Pearce *et al.*, 2008; Harangi *et al.*, 2005; Narcisi *et al.*, 2006; Jordan *et al.*, 2007; Brendryen *et al.*, 2010; Tomlinson *et al.*, 2010; Abbott *et al.*, 2011, 2012; Smith *et al.*, 2011*b*,*a*; Bramham-Law *et al.*, 2013). Contrastingly, LA-ICP-MS is rarely used to discriminate east African tephras; this is due, in part, to the comparatively later development of LA-ICP-MS over the past $10-15$ years (Pearce *et al.*, 2011). However, Ukstins Peate *et al.* (2003, 2008) used LA-ICP-MS to correlate

Indian Ocean deep sea tephras to Oligocene silicic pyroclastic units in the Afro-Arabian Flood Volcanic Province of Ethiopia. Numerous studies have used instrumental neutron activation analysis (INAA) to characterise trace elements in early-Pliocene to late Pleistocene tephras from eastern Africa (Walter *et al.*, 1987; Hart *et al.*, 1992; Walter and Aronson, 1993; WoldeGabriel *et al.*, 1999; Clark *et al.*, 2003).

The desire to analyse finer, more distal, glass shards has driven analytical improvements to LA-ICP-MS (Bryant *et al.*, 1999; Pearce *et al.*, 1999, 2014). However, analytical precision and accuracy is affected by element fractionation. This process is caused by calibration of glass analyses against National Institute of Technology (NIST) reference materials, which possess a different matrix to any geological sample. The calibration standard and sample therefore respond differently to ablation, causing an analytical bias known as element fractionation (Günther and Hattendorf, 2005). During sample ablation a surface condensate forms on inner walls of the ablation crater (Fig. 2.7) and this is widely cited as the cause of element fractionation (Eggins *et al.*, 1998; Hergenröder, 2006; Sylvester, 2008; Pearce *et al.*, 2011). This melt film occupies a greater proportion of narrower < 20 μm diameter ablation craters and therefore the analytical bias increases with decreasing crater diameter. Element fractionation compromises the accurate and precise analysis of fine grained shards, but can be corrected for by applying a 'fractionation correction factor' (Pearce *et al.*, 2011). This enables 25 petrogenically significant trace elements to be determined when analysing using 10 μm crater diameters.

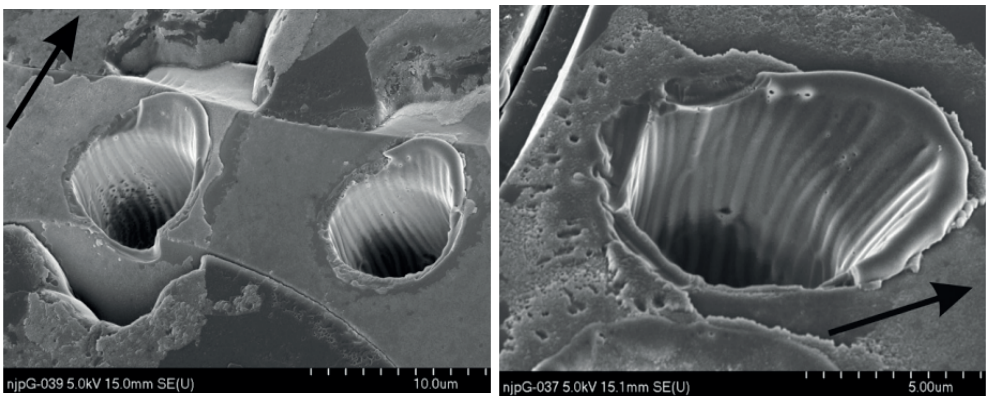

Figure 2.7: SEM images of 6 μm and 4 μm ablation craters in Minoan glass from Santorini. Note the melt film lining the interior of the craters, the gas flow through the sample chamber is indicated with an arrow. Element fractionation is widely attributed to this melt film, figure from Pearce *et al.* (2011).

2.5.4 Fe-Ti oxide and silicate mineral chemistry

The composition of minerals within a tephra, including feldspars, pyroxene, amphibole, biotite and olivine can be used to discriminate between tephras (Lowe, 2011).

Analyses of the Fe-Ti oxides, titanomagnetite and illmenite by EPMA have been extensively used to distinguish between tephra deposits (Hogg and McCraw, 1983; Cronin *et al.*, 1997; Smith *et al.*, 2002; McHenry, 2005; Turner *et al.*, 2009). For instance, Smith *et al.* (2011*b*) noted lower FeO/MgO in biotite from the proximal and distal deposits (in India) of the Younger Toba Tuff as opposed to biotite in the Middle Toba Tuff and Oldest Toba Tuff, and used this to identify and correlate the YTT (Fig. 2.8).

At the Hadar hominin fossil site (northern Ethiopia), Campisano and Feibel (2008) used magnetite, feldspar and glass major element chemistry to characterise Pliocene-Pleistocene tephras from the Hadar and Busidima formations.

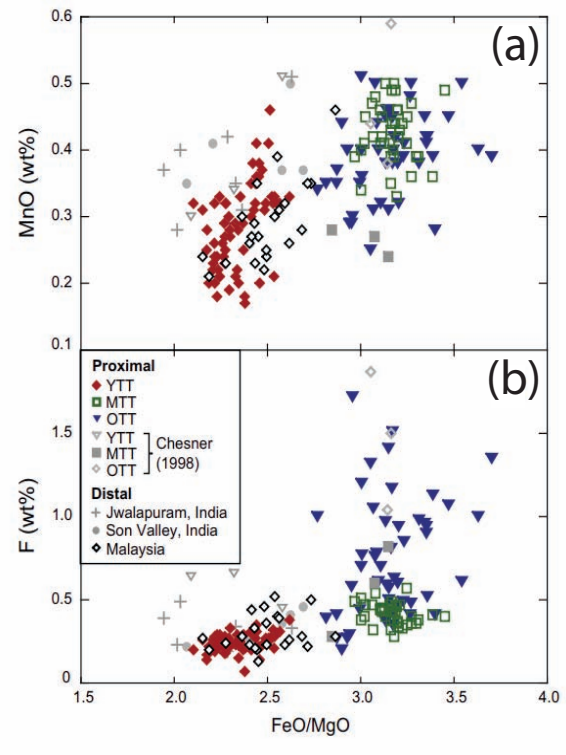

Figure 2.8: Biotite chemistry of proximal and distal Toba deposits; FeO/MgO versus (a) MnO (wt.%) and (b) F (wt.%). Biotite within the YTT is of a different composition to those within the MTT and OTT. Figures from Smith *et al.* (2011*b*)

.

However, due to the high specific gravity of Fe-Ti oxide minerals, they are generally not found at distal locations and are therefore less frequently used in distal tephra studies (Lowe, 2011).

2.6 Using geochemical data for tephra studies

This study uses major and trace element glass data to investigate tephra correlations, volcanic sources and magmatic processes. This section provides a brief overview of the presentation and interpretation of geochemical data for tephra studies.

2.6.1 Rock classification

Igneous rocks are commonly classified using bi-variate oxide-oxide major element plots. The total alkalis-silica (TAS) diagram (Le Bas *et al.*, 1986) is the most commonly used classification scheme for volcanic rocks and an example is shown in Figure 2.9 . Concentrations of SiO_2 and ($Na_2O + K_2O$) in a volcanic rock are plotted onto the TAS classification diagram, which divides igneous rocks into ultrabasic, basic, intermediate and acidic types according to their silica content (Fig. 2.9).

Thereafter, igneous rocks can be classified into subalkali and alkali groups. Figure 2.9 shows subalkali and alkali rocks divided according to the dashed line, defined by Irvine and Barager (1971). Alkaline rocks are those that possess an excess of ($Na_2O + K_2O$) over silica, whilst rocks undersaturated with alkali metals with respect to silica are subalkaline. Alkali rocks constitute < 1 % of all igneous rocks exposed on the Earth surface. They attain their largest volume in continental rift settings (Gill, 2010), notably the East African Rift System (EARS), and are therefore the focus of this study.

Alkali and subalkaline basalts are the parent liquid for many intermediate and acidic magmas. They evolve through extraction of phenocryst phases, typically starting with olivine, followed by plagioclase, clinopyroxene and an oxide,

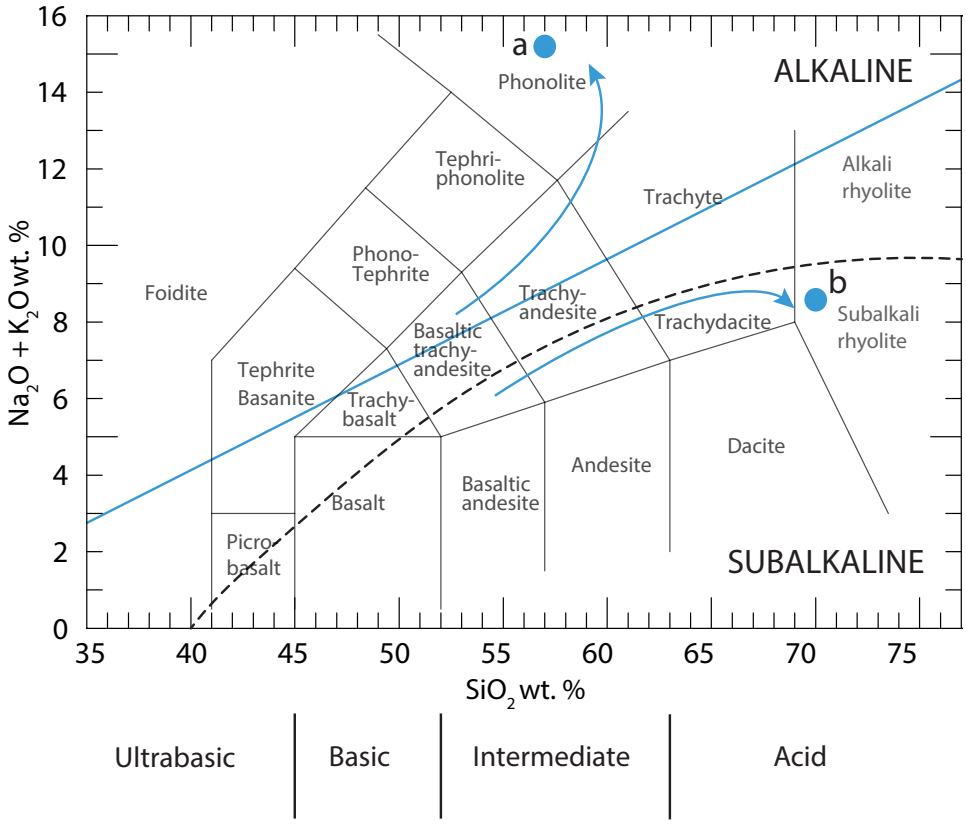

Figure 2.9: Chemical classification of volcanic rocks using the total alkalis versus silica diagram (TAS) of Le Bas *et al.* (1986). The dashed line subdivides alkalic from subalkalic rocks, co-ordinates from Irvine and Barager (1971). The blue solid line represents the albite-orthoclase thermal barrier, temperature contours decrease away from this plane (Sørensen, 1974). Blue arrows indicate the evolution of silica undersaturated compositions to (a) the feldspar-nepheline minimum and silica oversaturated compositions to (b) the feldspar-quartz minimum.

according to their stability at different temperatures. However, the sequence of crystallising minerals varies between these two magma types, producing differently evolved magmas. Therefore, alkali basalt magmas cannot evolve into subalkaline basalts, and vice versa (Rogers, 2015). This is related to reactions between the crystallising minerals and melt that consume silica (Rogers, 2015). In alkali melts, the SiO_2 deficiency may result in the crystallisation of feldspathoid minerals (silica deficient variants of feldspar) e.g. nepheline, leucite and rare kalsilite.

The reaction between nepheline and quartz, produces albite:

$$NaAlSi_2O_6 + SiO_2 = NaAlSi_3O_8 \tag{2.1}$$

In magmas containing an excess of quartz, olivine and quartz further react to produce orthopyroxene:

$$Mg_2SiO_4 + SiO_2 = 2MgSiO_3 \tag{2.2}$$

Therefore, nepheline and orthopyroxene can never co-exist in a magma and be in equilibrium (Rogers, 2015). This is explained further using the quartz-nepheline-kalsilite or Petrogeny's residua system (Fig.2.10). This system demonstrates the effect of the crystallisation of these end members on the evolution of a melt. Temperature contours decrease away from the albite-orthoclase feldspar thermal barrier, dividing silica oversaturated compositions (containing quartz) from silica undersaturated compositions (containing nepheline) and preventing magma evolution across the barrier (Gill, 2010; Rogers, 2015). Melts that have compositions either side of this thermal divide will follow different fractionation paths towards low temperature compositions that are either silica oversaturated

(feldspar-quartz minima) or silica undersaturated (feldspar-nepheline minima). For reference, the albite-orthoclase join and feldspar-nepheline and feldspar-quartz cotectics are illustrated on a TAS diagram in Fig. 2.9. This thermal barrier causes subalkali basalts to evolve towards the feldspar-quartz cotectic into low alkali dacitic and rhyolitic magmas. In contrast alkali basalts evolve towards the felsdpar-nepheline cotectic to more alkali rich melts, such as trachytes or phonolites (Gill, 2010; Rogers, 2015). Whilst phonolites are highly differentiated, they are classified as intermediate according to their silica content (Fig.2.9), therefore they can be more accurately described as felsic.

Alkali rocks can be further subdivided by comparing the total alkali content of a volcanic rock with its Al_2O_3 content, in molar proportions (Eqs. 2.3- 2.5) following Le Bas *et al.* (1986). Silicic volcanism in Ethiopia has a predominantly peralkaline composition (Peccerillo *et al.*, 2007). Peralkaline rhyolites can be further classified as either pantellerites or comendites (Eqs. 2.6 and 2.7), after Le Maitre (2002).

Peralkaline

$$[Na_2O + K_2O]_{mol} > [Al_2O_3]_{mol} \tag{2.3}$$

Peraluminous

$$[Al_2O_3]_{mol} > [Na_2O + K_2O + CaO]_{mol} \tag{2.4}$$

Metaluminous

$$[Na_2O + K_2O]_{mol} < [Al_2O_3]_{mol} < [Na_2O + K_2O + CaO]_{mol} \tag{2.5}$$

Pantellerites

$$Al_2O_3 < [FeO^T + 4] \tag{2.6}$$

Comendites

$$Al_2O_3 > [FeO^T + 4] \tag{2.7}$$

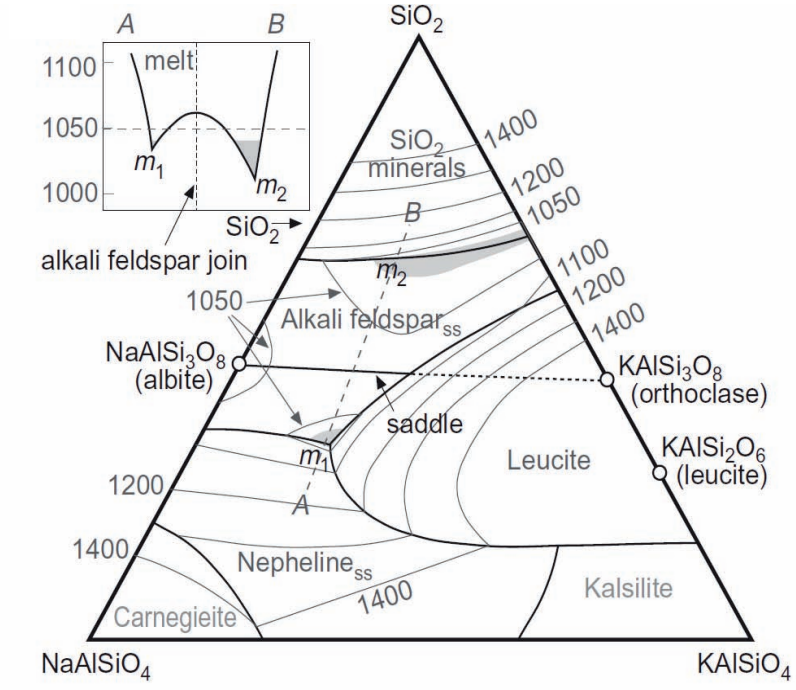

Figure 2.10: Phase relations in the residua system, quartz, nepheline and kalsilite (mass proportions), from Gill (2010). Open circles indicate the composition of the end-member albite, orthoclase and leucite and $m1$ and $m2$ show the feldspar-nepheline and feldspar-quartz cotectic, respectively. Temperature contours decrease away from the albite-orthoclase thermal barrier, dividing silica oversaturated compositions from silica undersaturated compostions (shown in inset, along line AB). This prohibits the evolution of melts across this thermal barrier.

The silica saturation of a rock can be calculated using the CIPW norm, developed by the petrologists Cross, Iddings, Pirsson and the geochemist Washington,

during the early 1900s. The major element analysis of a rock is translated into weight proportions of hypothetical minerals. Calculation of the CIPW norm determines the ideal mineralogy of an igneous rock. Rocks that have the potential to crystallise out nepheline are silica undersaturated, whilst those containing orthopyroxene are silica oversaturated.

Furthermore, once the CIPW norm has been calculated, the composition of natural silicate glasses can be projected onto the 'haplogranite' quartz-albite-orthoclase system (Fig. 2.11 - the silica oversaturated portion of Fig. 2.10), following Blundy and Cashman (2001). Prior to translation onto the haplogranite system, the CIPW norms must be recalculated, to account for the effect of anorthite on the feldspar compositions in the projection.

This enables variations in glass compositions to be related to changes in temperature and pressure in the magma chamber. Additionally, this gives an insight into whether crystallisation of the magma was driven by cooling or ascent (decompression). The haplogranite system is used in this study to investigate how variations in tephra composition recorded at different lakes may be related to differing magmatic conditions.

2.6.2 Magmatic differentiation

The array of rock compositions seen in see Fig. 2.9 is related to four principal factors. Firstly, the chemistry of magmatic rocks is ultimately determined by and mineralogy of the source region, i.e. crust or mantle. Secondly, magma composition is influenced by the depth and extent of melting. Thirdly, numerous magma chamber processes influence the primary melt composition en route to the surface. These include; fractional crystallisation, magma mixing and contamination or a combination of these processes. Following eruption, the composition

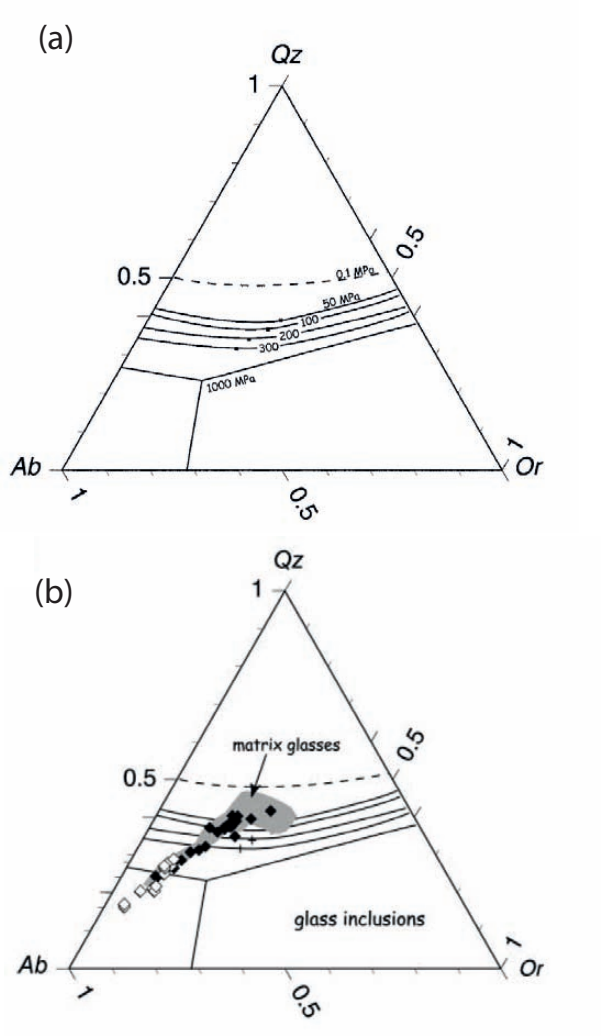

Figure 2.11: The haplogranite, Q-Ab-Or system, figures from Blundy and Cashman (2001). (a) Cotectic lines and compositions of H_2O saturated minima and eutectics as a function of pressure, units are in weight fraction. (b) Projection of the composition of glass from the 1980 Mount St Helens eruption onto the Q-Ab-Or ternary.

of igneous rocks may be further modified by outgassing or interaction with a fluid. Therefore, fresh and unaltered samples for geochemical analysis are thus required in order to determine geological processes effectively (Rollinson, 1993; Gill, 2010).

Major elements dominate the bulk composition of igneous rocks, and their abundance and variation give an insight into the depths at which melting took place and the magmatic evolution that followed. Trace elements are more sensitive to melting and crystallisation and give further insight into these processes (Rollinson, 1993). The natural variation in trace element concentrations relates to the differing geochemical behaviour of trace elements in magmatic systems. When the Earth's mantle is melted, trace elements display a preference for either the solid (mineral) phase or the melt phase (Rollinson, 1993). Trace elements which have a preference for the melt are termed incompatible elements. Those which have a preference for mineral phases are termed compatible (Rollinson, 1993). This compatibility and incompatibility will varying in different melt compositions (Rollinson, 1993). The behaviour and distribution of trace elements can be defined using the partition coefficient:

$$Kd = c_1/c_2 \tag{2.8}$$

where c_1 and c_2 are the concentrations of a trace element in the mineral and the melt, respectively.

If a trace element is equally distributed throughout the melt and mineral phase, it will have a distribution coefficient of 1.0. If a trace element is incompatible and has a preference for the melt, it will have a distribution (or partition) coefficient < 1.0. Whereas, a compatible trace element, with a preference for the mineral

phase will have a distribution coefficient > 1.0 (Rollinson, 1993). Peralkaline rocks typically contain high concentrations of incompatible elements, leading to the formation of unusual accessory minerals. This is associated with higher concentrations of alkalis in the melt, which increase the solubility of these elements. For instance, Watson (1979) demonstrated that Zr forms a NaZr complex in peralkaline melt, preventing the mineral zircon from forming. This enables Zr concentrations to reach higher concentrations than peraluminous melts and melts lying in the quartz-orthoclase-albite composition plane.

2.6.2.1 Fractional crystallisation

The behaviour of trace elements is also determined by various geological processes, including fractional crystallisation, crustal assimilation and magma mixing.

A key process causing variation in natural silicate melts is fractional crystallisation. It has been shown that fractional crystallisation of alkaline basalts is the most likely process responsible for generating peralkaline rhyolites in the Ethiopian Rift (Walter *et al.*, 1987; Peccerillo *et al.*, 2007; Ukstins Peate *et al.*, 2008; Rooney *et al.*, 2012). Magma chambers consist of molten areas (above the liquidus temperature) and areas of crystal mush, which behave rheologically as solids. The temperature difference between the liquidus and solidus is $\sim 200^{o}$C in subalkaline basalts. Minerals with the highest melting temperatures will form first, leaving an increasingly acidic magma, following Bowen's Reaction Series (Fig. 2.13). Fractional crystallisation is the removal and segregation of the residual melt from the minerals it precipitates, changing the composition of the magma (Marsh, 2015).

The equation for Rayleigh fractionation is:

$$C_L/C_0 = F^{(D-1)} \tag{2.9}$$

where C_L and C_0 are concentrations of a trace element in the melt and the initial system, respectively. F is the weight fraction of the remaining melt and D is the bulk partition coefficient of the fractionating assemblage.

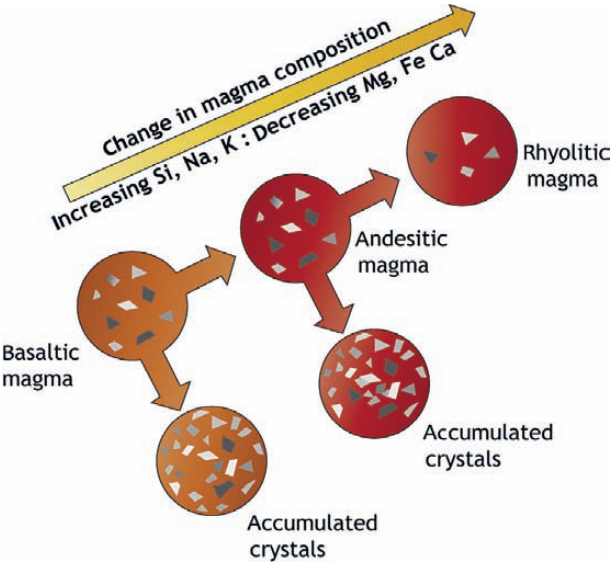

Figure 2.12: Illustration of the evolution of a subalkaline magma by fractional crystallisation as a result of cooling and removal of crystals from the melt, from Rogers (2015).

With increasing fractional crystallisation the residual magma will become increasingly fractionated or 'evolved'. Fractional crystallisation of plagioclase and olivine from basalts simultaneously increases concentrations of Si, Na and K and decreases Mg, Fe and Ca concentrations in the residual melt (see Fig. 2.12). With increasing fractional crystallisation, incompatible elements will also become enriched in the melt. In contrast, concentrations of compatible elements will typically decrease with increasing fractional crystallisation (Rollinson, 1993).

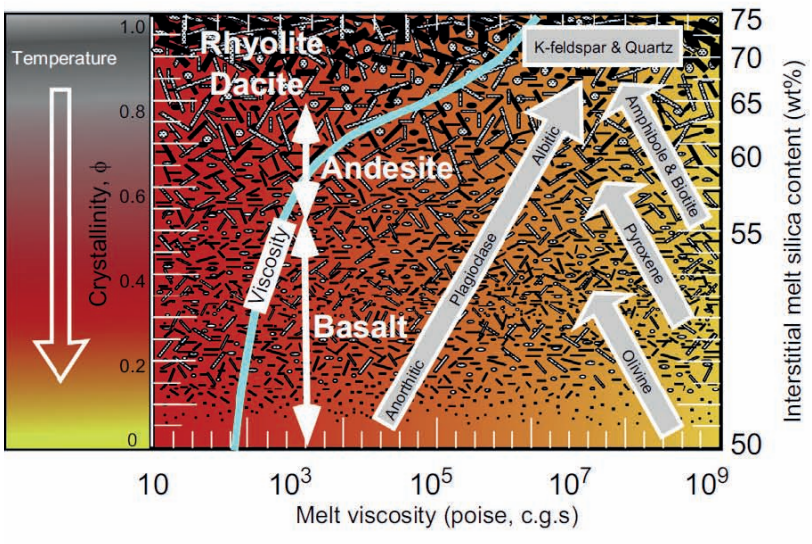

Figure 2.13: Bowen's Reaction Series operating within a zoned magma chamber from Marsh (2015). With the progression of crystallisation, the residual melt becomes increasingly enriched in silica.

The rare earth elements (REE) are amongst the most useful of trace elements for investigating petrogenic processes. The REE comprise La to Lu (atomic numbers 57 to 71) and display slight differences in size and behaviour. Therefore, petrogenic processes cause them to be differently fractionated (Rollinson, 1993). In order to study petrogenic processes, REE concentrations can be normalised to chrondritic meteorite compositions. Figure 2.14 shows chondrite normalised compositions of $\sim$ 3.1 Ma rhyolitic and trachytic tephras from Ethiopia (Rooney *et al.*, 2012). The tephras show distinct negative Eu anomalies. Europium, unlike other REE, can have a $+2$ valency and substitute for Ca in feldspars, thus this anomaly indicates that these compositions have evolved through extraction of a feldspar dominated assemblage (Rollinson, 1993). Furthermore, higher concentrations of incompatible elements in the rhyolitic tephras than the trachytic tephras reflect their more evolved composition (Rooney *et al.*, 2012).

Pyroclastic deposits frequently show compositional zoning, from highly evolved compositions at the base to less evolved compositions at the top. The earlier, more evolved subunits are typically more widespread due to their generally greater crystallinity and viscosity. This compositional change is a result of the eruption tapping a zoned magma chamber, containing more evolved compositions and the top and denser, less evolved compositions at the base. For example, proximal tephra from the Laacher See $\sim$ 12.9 ka eruption (Reide *et al.*, 2011) exhibits dramatic colour changes upwards, associated with the tapping of a compositionally zoned magma chamber.

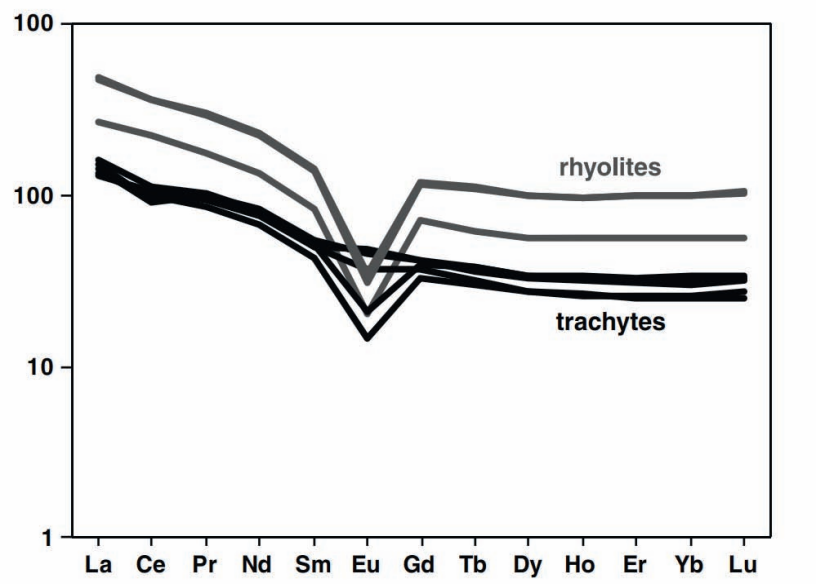

Figure 2.14: Spiderdiagram showing chondrite normalised compositions of tephras from Chefe Donsa, Ethiopia, from Rooney *et al.* (2012).

2.6.2.2 Assimilation fractional crystallisation

Crustal assimilation is believed to contribute significantly to the diversity of natural magma compositons in continental regions (Gill, 2010). During fractional

crystallisation, latent heat is realised and passes through and promotes the melting of the wall-rocks (Marsh, 2015). Peccerillo *et al.* (2007) studied the role of assimilation of Precambrian crust in generating peralkaline rhyolitic magmatism from the Gedemsa Volcano, Ethiopia. Ratios of incompatible elements, particularly large ion lithophile and high field strength elements (LILE/HFSE, e.g. Rb/Nb, Th/Ta, La/Ta, Rb/Zr) are higher in the Precambrian rocks than the Gedemsa volcanic products. Large ion lithophile elements are more incompatible than HFSE during crustal assimilation and therefore melting preserves or increases LILE/HFSE ratios (Watt and Harley, 1993; Beard *et al.*, 1994; Ayres and Harris, 1997). Concentrations of Rb are higher in the crust than the mantle, and therefore Rb and Sr radiogenic isotopes are frequently used to identify assimilation (Rollinson, 1993).

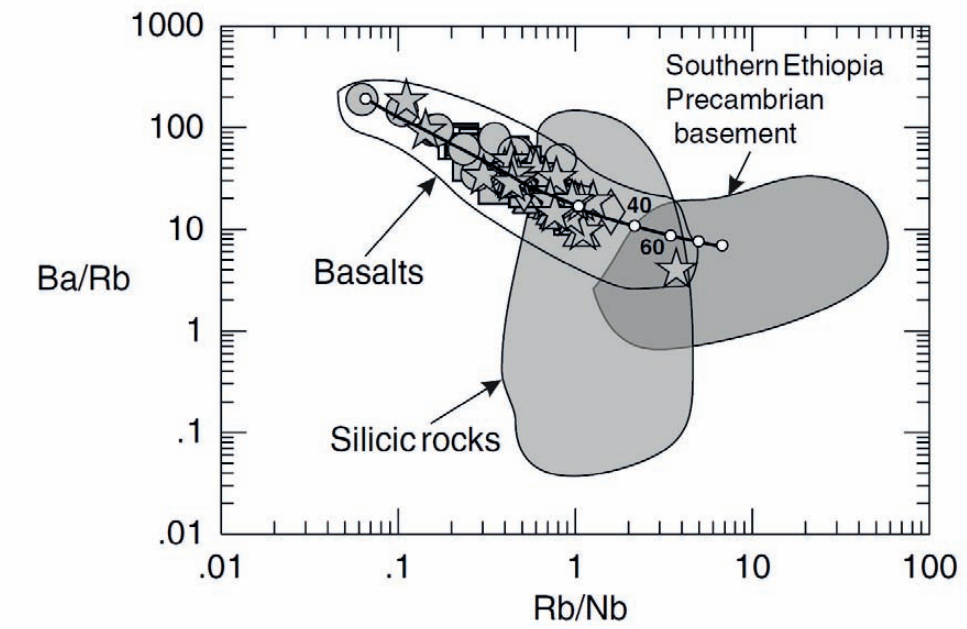

Figure 2.15: Ba/Rb vs. Rb/Nb diagram for basaltic rocks from the Ethiopian Rift, from Peccerillo *et al.* (2007), compared to compositional fields occupied by Precambrian basement and silicic rocks. The thick black line represents an assimilation trend of Precambrian basement by basaltic magma, dots indicate the proportion of melting.

2.6.2.3 Magma mixing

If two magmas with differing compositions come into contact prior to their eruption, they may co-mingle, producing a new intermediate composition between the end members. Mixing of two melts will therefore produce element concentrations along a simple mixing line (Rollinson, 1993). However, melts of very different compositions may not mix effectively, due to differences in their viscosity and density. For example, Walter *et al.* (1987) investigated the petrogenesis of the Cindery Tuff (3.9 Ma) derived from the Afar region of northern Ethiopia. This is a valuable tephrostratigraphic marker, and preserves evidence of magma mixing; containing rhyolitic, basaltic are rare intermediate glass compositions. Walter *et al.* (1987) suggested that, due to the non-linear array of selected major element ratios, the range of compositions was not related to simple mixing alone.

2.6.3 The use of bi-variate plots

Major and trace element bi-plots are of immense value for tephra studies, and can be used to:

1. Investigate the **range of compositions** within a tephra deposit and ascertain whether there are any **magmatic trends**.

2. Compare the range of glass compositions in one tephra deposit with another, specifically to **identify differences and similarities**.

3. Identify glass shards which are compositional **outliers**, e.g. accidental mineral analyses.

4. Recognise contaminant glass shards of older tephras as a result of **reworking**.

Electron microprobe analyses of glass typically determine 10 major element oxides (Si, Ti, Al, Mg, Fe, Mn, Ca, Na, K and P) and using these elements it is possible to generate 45 different bi-variate plots (Pearce *et al.*, 2008). However, some major elements are of more use for distinguishing between tephras. The choice of elements included in a major element plot is a function of the composition and petrogenesis of the glass. A selection of major element bi-plots showing the composition of Oligocene tephras derived from Yemen and Ethiopia (Ukstins Peate *et al.*, 2008) are shown in Fig. 2.16. These bi-plots distinguish between some of the glass compositions and show linear compositional arrays (Fig. 2.16 b, c, d). These trends indicate that the tephras evolved through fractionational crystallisation of feldspar, clinopyroxene and Fe-Ti oxides, causing the glass to become enriched in SiO_2 and depleted in TiO_2, MgO and FeO^T.

The previous discussion demonstrated that trace elements are more sensitive to magmatic differentiation. Trace elements are therefore indicative of the processes involved in their petrogeneis, and this determines which trace elements are included in bi-plots. Amongst the $25-28$ trace elements typically determined by LA-ICP-MS glass analyses, the most useful are those which exhibit extreme behaviour, including the highly incompatible or highly compatible elements. Selected trace element concentrations in Oligocene tephras derived from Yemen and Ethiopia are plotted as bi-plots in Fig. 2.17 (from (Ukstins Peate *et al.*, 2008)). Bi-plots of two incompatible elements, e.g. Nb vs. U (Fig. 5.10a), show that the tephra glass shards exhibit positive linear trends which are related to enrichment of these elements in the melt during fractional crystallisation. Ukstins Peate *et al.* (2008) noted that one tephra (4W) exhibited two different incompatible element arrays, suggesting that this tephra may have been reworked

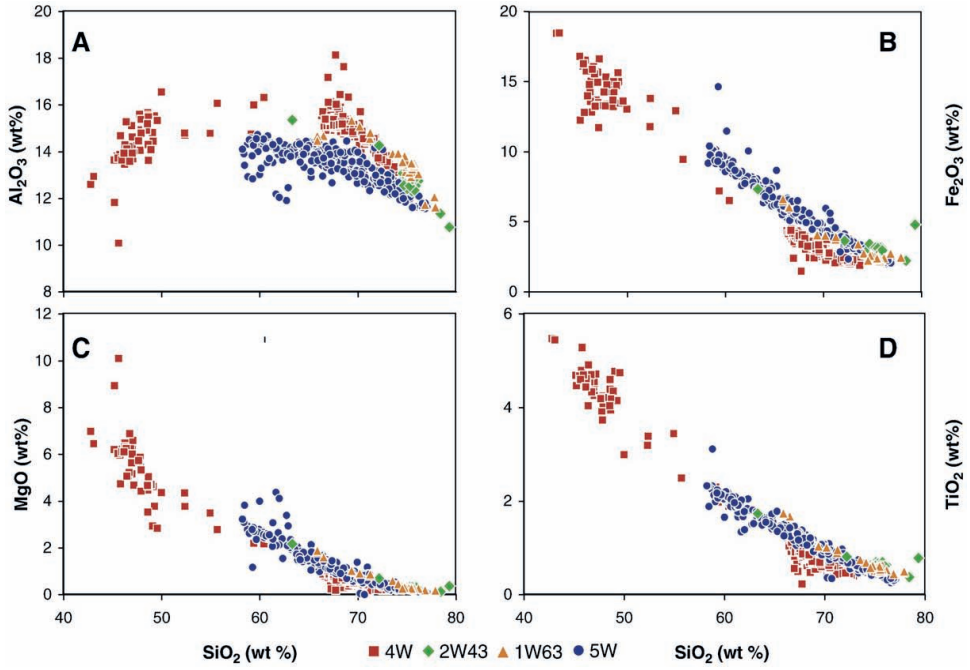

Figure 2.16: Using major element data to distinguish between tephras, an example from Ukstins Peate *et al.* (2008). Anydrous concentrations of selected major elements are used to distinguish between Indian Ocean tephra layers, correlated to Oligocene pyroclastic units from Yemen and Ethiopia. Data points indicate a major element analysis of a tephra glass shard, showing the full range of compositional variations in a tephra layer.

and includes older glass compositions. Differences in these incompatible element trends may indicate that these tephras are derived from different sources, which exhibit different geochemical signatures.

Incompatible elements with similar bulk partition coefficients behave similarly during fractional crystallisation, and their relative concentrations will vary little during partial melting. Thus, the slope of the correlation line between two incompatible elements gives the ratio of the concentration of trace elements at the source volcano. This is exemplified in Fig. 2.18, which shows different incompatible element ratios for Red Sea basalts, indicating they have three different mantle sources.

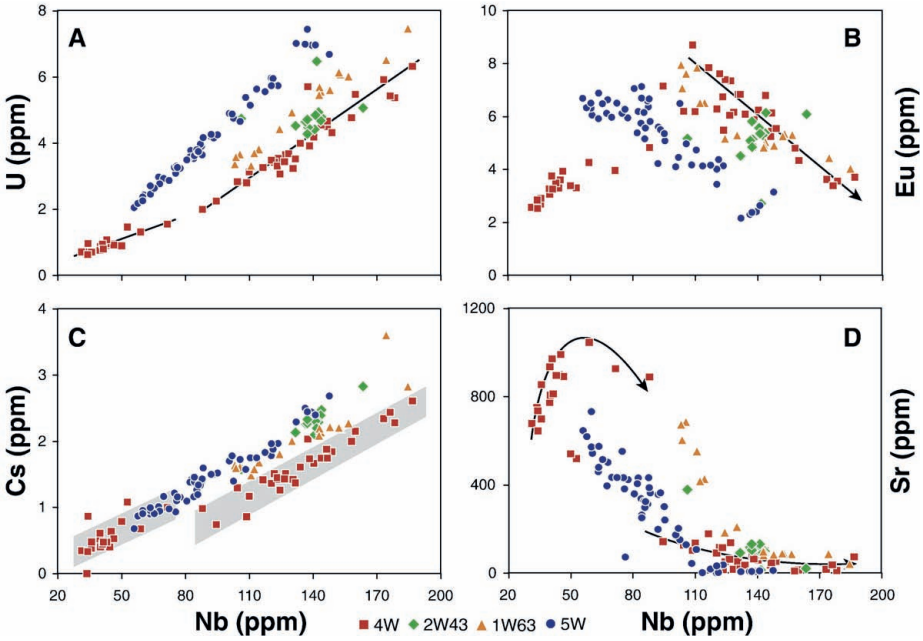

Figure 2.17: Distinguishing between tephras using trace element concentrations. Fig. from Ukstins Peate *et al.* (2008). Selected trace element concentrations in glass shards from NW Indian Ocean tephras, derived from Ethiopia and Yemen. Individual points indicate an analysis of a single tephra glass shard using LA-ICP-MS. Incompatible elements (e.g. Nb, Y) plotted against one another form strong positive linear trends. Arrows indicate changes in slope with increasing Nb concentrations. Tephra 4W contains two compositional groups, based on Nb vs. Cs concentrations in the glass shards.

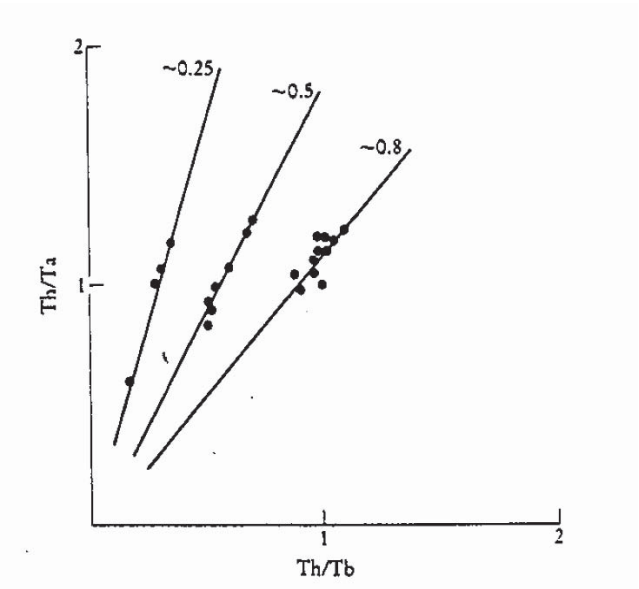

Figure 2.18: Bi-variate plot of Th/Ta vs. Th/Tb for Red Sea basalts from Eissen *et al.* (1989). The trends of 0.25, 0.5 and 0.8 may represent three different mantle sources.

2.6.4 Principal component analysis

Principal component analysis is a statistical approach which converts a large number of variables (e.g. major and trace element concentrations) into a smaller set of variables (principal components) which feature the variance of the original data set (Rollinson, 1993). The first principal component (PC 1) includes most of the variance from the original dataset and following principal components include decreasing amounts of residual variation (Rollinson, 1993; Pearce *et al.*, 2008).

The principal components generated can then be used to produce variation diagrams, which include a large number of variables, as opposed to the typical two or three. A large data set, including multiple samples and variables is produced as part of this study, therefore PCA provides an effective means of

testing compositional similarities between tephras noted using major and trace element bi-plots. The choice of variables (element concentrations) included in the PCA determines how effective this analysis may be for discrimination. If element concentrations which show a large amount of variance are included in the dataset, smaller scale variance may be masked. Therefore, PCA is most useful when only those tephras which cannot be clearly distinguished using major and trace element bi-plots are included in the analysis.

Pearce *et al.* (2008) advocate the importance of using major and trace element bi-plots in combination with PCA. The previous section has highlighted that bi-plots provide a valuable means of identifying geochemical trends, outliers and tephra reworking in a dataset. As an example, two potential correlative tephra deposits may share similar compositions and incompatible element ratios, suggesting they may derived from a shared source. However, one tephra may be slightly more evolved and PCA of their compositions may indicate they are not correlatives. However, these tephras may have been produced from a zoned magma chamber, which tapped successively less evolved compositions during the eruption. If the wind direction changed mid-eruption, more evolved compositions would be deposited in some locations and not others. Therefore, these deposits may be correlatives and this exemplifies why PCA should only be used in combination with major and trace element bi-plots.

2.7 Dating tephras

In addition to providing isochrons, tephra layers may also be dated using both direct or indirect methods. Primary minerals (including zircon, hornblende, orthoclase, biotite and quartz) and glass contained within the tephra may be

directly dated, whilst materials enclosed or encapsulating a tephra may be used to indirectly date a horizon (Lowe, 2011).

Tephra may be dated using radiometric, incremental and age-equivalent methods and age-modelling of sediment sequences. These dating techniques and their application to dating tephras in East Africa are summarized in Table 2.2.

In eastern Africa, early Pliocene to late Pleistocene tephras have been directly dated to provide chronologies for hominin fossil sites (e.g. Aronson *et al.*, 1977; Walter, 1989; Deino and Potts, 1990; Walter, 1994; Wiart and Oppenheimer, 2000; Deino and McBrearty, 2002; Deino *et al.*, 2002, 2010). Walter (1994) dated two tephras within the Hadar Formation, Ethiopia, using $^{40}Ar/^{39}Ar$ and provided the first reliable dates for the *Australopithecus afarensis* fossils 'Lucy' and the 'First Family' (3.18 Ma and 3.20 Ma, respectively).

Few historical eruptions have been directly observed and documented in eastern Africa. In Ethiopia the only recorded historical eruptions are believed to have occurred from Fantale and Kone (northern Main Ethiopian Rift) during the 1800*s* (Harris, 1844; Gibson, 1969). In Eritrea, the Dubbi 1861 eruption, Africa's largest documented historical eruption, was observed by Captain R. L. Playfair who reported the eruption in the *Times* newspaper (Wiart and Oppenheimer, 2000).

Tephras throughout East Africa have also been indirectly dated using a range of techniques, from magnetostratigraphy (Shuey *et al.*, 1974; Aronson *et al.*, 1977; Harris, 1977; Brown *et al.*, 1978; WoldeGabriel *et al.*, 2001), nanofossil stratigraphy (Sarna-Wojcicki *et al.*, 1985) to $<$ 17 ka Ethiopian tephras dated by radiocarbon age-modelling (Telford, 1998; Marshall, 2006).

Tephras erupted over the past 50 ka years are typically dated using the radiocarbon technique (Lowe, 2011). In this study, the Holocene lake sediments

investigated have been previously used for palaeoclimatic reconstruction as part of numerous studies. Therefore, the core sediments have pre-existing radiocarbon age models, which will be used to calculate modelled ages for each of the tephras.

Table 2.2: Direct and indirect (shown in italics) methods of dating tephra, adapted from Lowe (2011) to include examples of dating volcanic deposits in East Africa. AMS, accelerator mass spectrometry; ITPFT, isothermal-plateau fission track; SCLP/F, single-crystal laser probe or fusion; LIH, laser incremental heating; TL, thermoluminescence; OSL, optically stimulated luminescence; IRSL, infra-red stimulated luminescence; SIMS, secondary ionization mass spectrometry; TIMS, thermal ionization spectrometry.

Method	**Technique**	**Applications in East Africa**
Radiometric	Radiocarbon dating (radiometric/beta counting, AMS), fission-track dating (zircon, glass-ITPFT dating), argon isotopes (K/Ar, Ar/Ar including SCLP/F) LIH, luminescence dating (TL, OSL, IRSL), U-series including (U-Th)/He dating and $^{238}U/^{230}Th$ zircon dating (via SIMS/TIMS), electron spin resonance (ESR), ^{210}Pb, ^{137}Cs, ^{3}He and ^{21}Ne surface exposure dating	$^{40}Ar/^{39}Ar$ dating: Deino and Potts (1990); Walter (1994); Deino and McBrearty (2002); Deino *et al.* (2002, 2010), K/Ar dating: Aronson *et al.* (1977), Zr fission track dating: Aronson *et al.* (1977); Walter (1989)
Incremental	Dendrochronology, varve chronology, layering in ice cores	
Age-equivalence	Magnetostratigraphy, palaeomagnetic secular variation (PSV), orbital tuning, correlation with marine oxygen istope stages, palynostratigraphy, biostratigraphy, palaeopedology	Nanofossil stratigraphy: Sarna-Wojcicki *et al.* (1985), magnetostratigraphy: Shuey *et al.* (1974); Aronson *et al.* (1977); Harris (1977); Brown *et al.* (1978); WoldeGabriel *et al.* (2001)
Relative	Obsidian hydration dating, amino acid racemisation (AAR)	Obsidian dating: Michels *et al.* (1983)
Historical	Eye-witness accounts and observations	Eye-witness accounts: Wiart and Oppenheimer (2000) Harris (1844); Gibson (1969), observations: Smeds (1964)
Age modelling	Statistical methods, including Bayesian depositional modelling, wiggle matching, free shape modelling and periodic time-series	Age modelling: Telford (1998); Marshall (2006)

2.8 Summary

This section has provided a background to the tephrochronological method used in this study. Tephrochronology is a uniquely high resolution correlation tool where widespread sedimentary archives are linked and dated through tracing tephra layers. The technique has immense practical value and has been applied to an extensive range of subjects; including palaeoenvironmental reconstruction, geochronology, volcanology, archaeology, human evolution and palaeoanthropology. This section has also discussed the advances in tephrochronology, allowing identification of far-travelled cryptotephras and their accurate and precise analysis at high resolutions, enabling correlation of tephras over greater geographical areas.

This chapter has emphasized that tephra deposits in sedimentary records can also provide powerful dossiers of past volcanic eruptions, which has important implications for predicting the occurence and magnitude of future eruptions and therefore hazard mitigation. Furthermore, the potential of lake sediments for providing comprehensive tephra repositories where proximal tephra deposits may be inaccessible has been highlighted.

A brief overview of the use of geochemical data for tephra studies has been provided. Importantly, this overview demonstrated how geochemical data, coupled with principal component analysis, can be used to discriminate and correlate between tephra deposits. Additionally, this outlined how major and trace element data can be used to provide an insight into magma petrogenesis and volcanic sources.

In the forthcoming section, the significant value of tephrochronology for dating early Pliocene to late Pleistocene hominin fossil sites throughout Ethiopia and Kenya is discussed. The contrasting lack of studies on Holocene tephras in

Ethiopia and absence of a regional volcanic history will be underlined. Through studying Holocene tephras in Ethiopian lake sediment cores, this study aims to construct a < 17 ka tephrostratigraphy that can be used to give insight into past volcanism and to enable correlation of regional palaeoclimate archives.

Chapter 3

East African tephra studies

This chapter discuses volcanic activity in Ethiopia and potential Quaternary-recent tephra sources. The second section of this chapter demonstrates how Quaternary tephras have been crucial in providing age control on archaeological sites in Ethiopia and Kenya. Finally, the lack of studies on Holocene tephra deposits in Ethiopia is reviewed.

3.1 Geological setting

Volcanic deposits in the East African Rift System (EARS) provide a valuable record of magmatic and related tectonics processes operating in one of the best exposed continental rift systems on Earth. The EARS extends through Ethiopia and Kenya, diverging around the Tanzanian Craton to form western and eastern branches before reuniting and terminating in Mozambique (Macgregor, 2015). Offshore, a third south-eastern branch occurs along the Mozambique channel. Generally, the eastern branch of the EARS is characterized by greater volcanic activity, whereas the western branch is associated with much deeper basins infilled with larger accumulations of sediment.

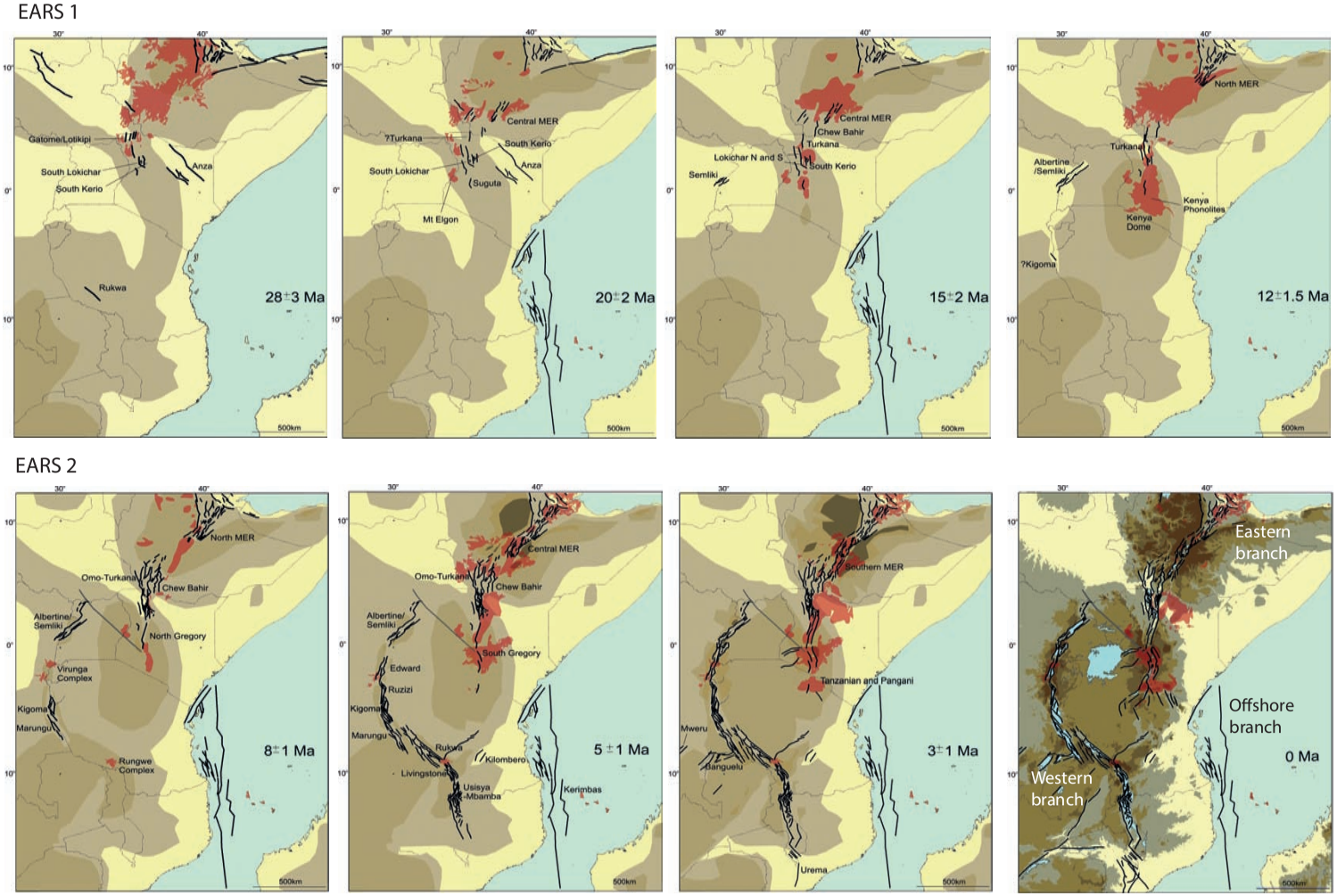

Figure 3.1: Maps of East Africa illustrating the development of rift branches through time. Darker colours indicate areas of higher elevation, red indicates volcanism. During the past 13 Ma distinct western and eastern branches formed. figure from Macgregor (2015)

.

The development of the EARS and associated volcanism is summarised below. The EARS rift propagation can be divided into two phases: EARS 1; rifting confined to the Afar, S. Ethiopia and N. Kenya and EARS 2; widespread rifting forming the western and eastern branches. Rifting processes in the Kenyan and Tanzanian portion of the eastern branch are better understood than those in Ethiopia, where there are conflicting interpretations over dated volcanic outcrops.

3.1.1 EARS 1: Oligocene - mid Miocene

Afar Dome and trap volcanism. Rifting confined to Afar, S. Ethiopia and N. Kenya. Development of Kenya Dome.

At 35 Ma a series of N-S trending Rifts were initiated in the South Lokichar Basin of northern Kenya (Fig. 3.1) , contrasting the orientation of pre-existing faults and signifying a significant change in stress direction (Macgregor, 2015). Plume related basalt trap volcanism began in Ethiopia at ~ 31 Ma with rhyolitic volcanism following at ~ 30 Ma, peak activity occurred between $\sim 31-28$ Ma (Bosworth *et al.*, 2005).

Marine sediments were first deposited on the continental crust of the Gulf of Aden between $\sim 30-29$ Ma. The development of a small basin followed at $\sim$28-24 Ma, forming the Eritrean Red Sea. At ~ 25 Ma rifting in the Afar was initiated and the main phase of rifting and shoulder uplift followed at 20 Ma (Bosworth *et al.*, 2005). During the late Oligocene early Miocene rifting commenced in the offshore branch of the EARS (Macgregor, 2015).

Rifting then shifted to the Broadly Rifted Zone of southern Ethiopia at $25-21$ Ma (Bonini *et al.*, 2005) and moved northwards to the central Main Ethiopian Rift (MER), where it was well established by $\sim 17-15$ Ma (WoldeGabriel *et al.*, 1990). To the south; volcanism occurred in northern Kenya at 15 Ma, infilling

the existing rift topography. Between $13.5 - 11$ Ma the 1400 m high Kenya Dome developed (Macgregor, 2015).

3.1.2 EARS 2: Mid Miocene - Recent

Widespread rifting and development of distinct western and eastern EARS branches.

During the last 13 Ma, rifting developed two distinct eastern and western branches. The onset of this second rifting phase is marked by the migration of rifting northwards in Kenya to Turkana and the initiation of rifts in the northern part of the western EARS branch. Rifting spread south from the Afar to the central MER at ~ 8 Ma and activated in the Turkana, Omo and Chew Bahir basins. Major topographic development and uplift occurred in Ethiopia at ~ 5 Ma. Over the past ~ 3 Ma rifting has propagated into the southern MER and also spread southwards to Lake Malawi and Tanganyika (Macgregor, 2015).

3.2 Volcanism and tephra deposits in Ethiopia

Ethiopia remains one of the most active regions in the EARS and a present phase of rifting in the Manda-Hararo segment (Afar) began in September 2005; accompanied by the formation of a 60 km long dyke and rhyolitic eruption (Field *et al.*, 2013).

The Ethiopian Rift System can be divided into sections; the Afar, the Main Ethiopian Rift, the Broadly Rifted Zone and the off-axis Yerer-Tullu Wellel Volcano Tectonic Lineament (WoldeGabriel *et al.*, 2013), each characterized with unique tectonic, volcanic and geomorphic features. Volcanism within each

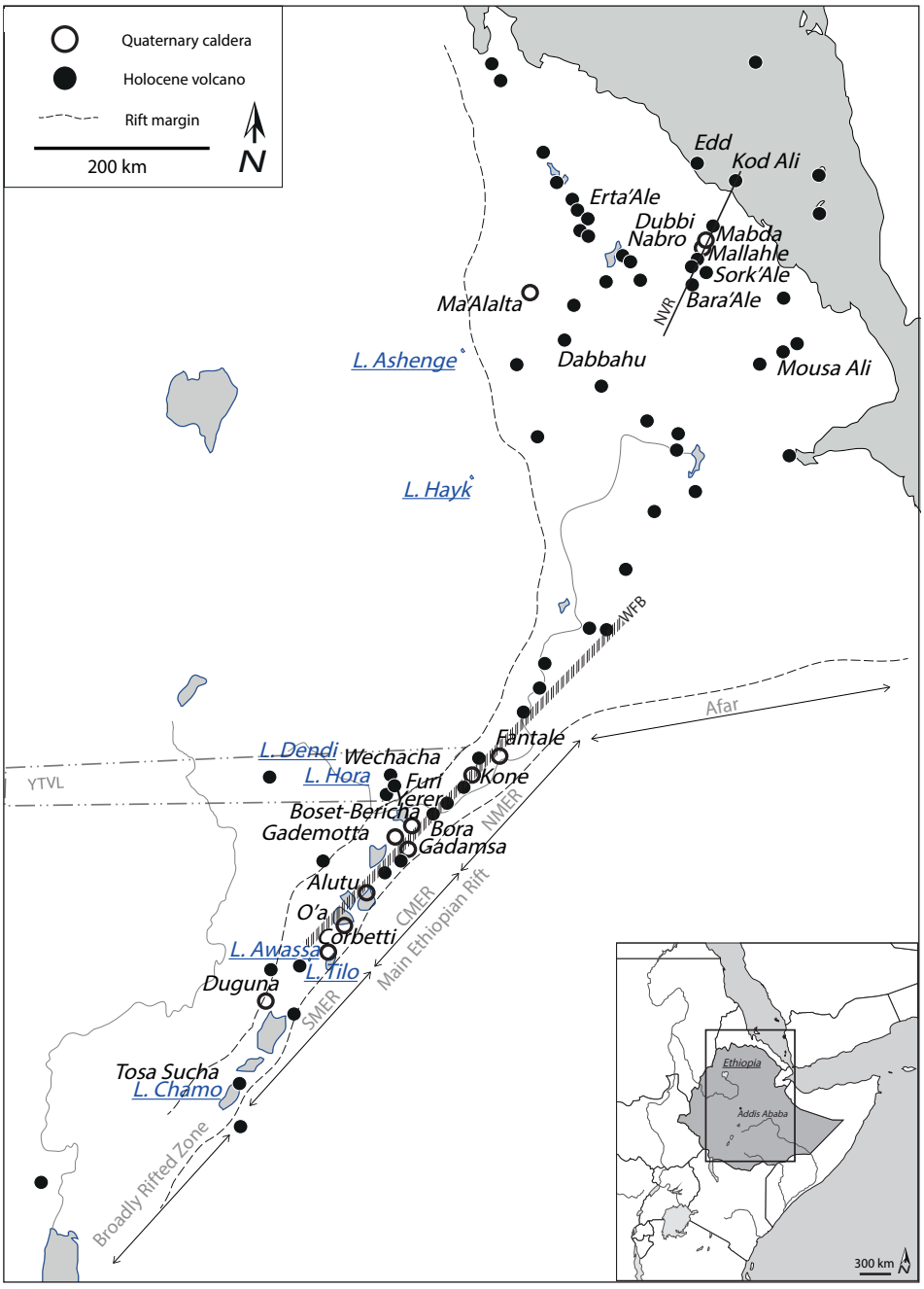

Figure 3.2: Map of Ethiopia showing Quaternary calderas and other volcanoes known or suspected to have been active during the Holocene (Siebert *et al.*, 2011). Lake core sites used in this study are also labelled in blue. It is likely that volcanoes which have not yet been recognised, or those with unknown ages, are not plotted. The Afar Rift, Main Ethiopian Rift and Broadly Rifted Zone are shown (NMER, CMER and SMER = northern, central and southern Main Ethiopian Rifts). NVR = Nabro Volcanic Range (N. Afar), WFB = Wonji Fault Belt (Main Ethiopian Rift), YTVL = Yerer-Tullu Wellel Volcano Tectonic Lineament (E-W trending lineament on the Ethiopian Plateau).

of these sections of the Ethiopian Rift System is discussed below; with particular reference to Quaternary-recent tephra producing eruptions.

3.2.1 The Afar Rift

The Afar Rift possesses a funnel shape spanning ~ 300 km in width and ~ 600 km from north to south. The rift is bounded by the Ethiopian and Somalian Plateaus and the Red Sea, marking the junction between the Arabian, Somalian and African plates (Mohr, 1978). Geological expeditions between $1968 - 1973$ (CNR-CNRS Afar Team 1973) lead to a four-fold classification of volcanic features in the Afar (Barberi and Varet, 1977); namely the centres associated with the Afar Stratoid Series and transverse, axial and marginal centres.

Flood basalts and ignimbrites were emplaced in the Afar at ~ 31 Ma, reaching thicknesses of ~ 2 km (Ebinger *et al.*, 1993; Hofmann *et al.*, 1997; Wolfenden *et al.*, 2004). Miocene igneous rocks were then emplaced; including peralkaline granites ($26 - 22$ Ma), trap basalts ($25 - 12$ Ma), the Mabla rhyolite series ($14 - 10$ Ma) and the Dahla series of basalt flows ($8 - 6$ Ma) (Barberi and Varet, 1977).

During the Pliocene-Pleistocene the Afar Stratoid Series was extruded; consisting of basalt flows attaining 1500 m in thickness and silicic centres. At ~ 4 Ma E-NE trending volcanic centres were produced; comprising basaltic transverse centres towards the Red Sea (e.g. Dubbi) and silicic marginal centres and calderas on the borders of the Afar (e.g. Nabro, Ma'Alalta) (Barberi and Varet, 1977). Quaternary axial centres occur along NW-SE trending rift zones, associated fissure eruptions and shield volcanoes produced basalt flows and alkaline silicic rocks. These axial zones are typically interpreted as the equivalent of oceanic spreading centres (Barberi *et al.*, 1974).

The 100 km long Erta'Ale range, in the northern apex of the Afar triangle is a renowned and well-studied axial volcano in the region (Wiart and Oppenheimer, 2004; Mohr, 1978). The Quaternary axial volcano, Dabbahu, differs from typical axial volcanoes, showing a full fractional crystallisation suite from alkaline basalts to peralkaline rhyolites and has an estimated eruption volume of ~ 115 km^3. Dabbahu is one of the closest (< 70 km) volcanoes to the Ashenge lake core site, studied here. Field *et al.* (2013) describe extensive deposits of pumice of ~ 10 m thickness on the flanks of Dabbahu. This variation is due to its location at a higher elevation, at a shallower axial orientation and its closer proximity to the crystalline scarp border (Wiart and Oppenheimer, 2004). Fission track dates on obsidians from the upper flanks give ages of ~ 44 ka and ~ 1.5 ka. An eruption (VEI=3) in 2005 deposited tephra over 100 km^2, resulting in the formation of a small pumice cone (Ayele *et al.*, 2007*a*; Ferguson *et al.*, 2010). In September 2005 the eruption of rhyolitic ash from a small pumice cone on the northern flanks of Dabbahu and the largest dike-opening event ever witnessed reawakened interest in the volcano (Field *et al.*, 2013).

Whilst the basaltic axial ranges of the Afar rift are well studied (Barberi *et al.*, 1970; Barberi and Varet, 1977; Oppenheimer and Francis, 1997; Amelung *et al.*, 2000), few marginal and transverse centres have been studied and only smaller silicic centres, including Ma'Alalta (Barberi *et al.*, 1970) and Mousa Alli (de Fino *et al.*, 1973) have been described in any detail. Wiart and Oppenheimer (2004) demonstrate that large magnitude caldera forming eruptions are associated with marginal and transverse centres. The poorly studied Nabro Volcanic Range (NVR) runs for ~ 100 km from the margin of the Danakil Depression to the Red Sea and has a subaerial volume of 550 km^3. Wiart and Oppenheimer (2004) suggest that this volcanic range was the source of many large magnitude

silicic eruptions during the Quaternary. Several volcanoes comprise the NVR, including Sork'Ale, Bara'Ale, Mallahle, Nabro, Mabda, Dubbi, the Edd lava field and Kod Ali island located in the Red Sea (Wiart and Oppenheimer, 2004). There is a general trend of younging volcanism westwards along with NVR, associated with the change from mafic to ultramafic products of Kod Ali in the Red Sea, to trachytic tephra and basaltic lava erupted from Dubbi in the east to the youngest rhyolitic products of Nabro and Mallahle in the west (Wiart and Oppenheimer, 2000). Nabro volcano itself, standing at $2,248$ m high, marks the highest point of the NVR, and is formed of a double crater concomitant with the eruption of $20-100$ km^3 of ignimbrite, which may have formed a regional tephra stratigraphic marker (Wiart and Oppenheimer, 2004). In 2011, the first recorded eruption from Nabro occurred, satellite images show the eruption plume drifting over Sudan, $\sim$ 1000 km to the NW, and the ash clouds disrupted international flights over Eritrea and Ethiopia (Siebert *et al.*, 2011; Goitom *et al.*, 2015). Dubbi volcano, on the Red Sea coast, is responsible for the largest known historical eruption in Africa (Mohr, 1978; Wiart and Oppenheimer, 2004). The 1861 eruption was recorded by maritime traffic in the Red Sea; it is reported to have deposited volcanic ash 400 km to the west on the Ethiopian Plateau and a subsequent effusive phase produced lava flows with a volume of 3.5 km^3 (Wiart and Oppenheimer, 2004).

Archives from Lakes Ashenge and Hayk (Ethiopian Highlands) are used in this study; these are located $<$ 70 km from the volcanoes in the Afar, it is therefore possible that tephras from these volcanoes may be found in these records.

3.2.2 The Main Ethiopian Rift

The MER is a symmetrical graben, bounded by normal step faults and antithetic faults, lying between 5^o-9^o N and $37^o30 - 40^o$ E. Volcanism in the Main Ethiopian Rift (MER) can be broadly split into two phases, reflecting rifting stages. During the Mio-Pliocene volcanism occurred throughout the whole MER, associated with the activity of large boundary fault systems. Deformation and magmatism within the MER is controlled along the Wonji Fault Belt; a $5 - 12$ km wide, NNE-SSW orientated system of en echelon faults associated with Quaternary calderas (Gibson, 1967; WoldeGabriel *et al.*, 1990; Boccaletti *et al.*, 1999). Pyle (1999) states that the MER was most likely the source of explosive volcanic eruptions during the Quaternary. The MER, can be further subdivided into northern, central and southern sections; volcanism within these sections is described below.

3.2.2.1 Northern MER

In the northern MER, the first volcanic deposits were flood basalts related to the Afar plume, erupted at 30 Ma and shield volcanoes subsequently developed on the rift shoulders (Corti, 2009). During the Mio-Pliocene, syn-rift widespread ignimbrites were deposited across the northern MER with intercalated minor silicic and mafic lavas (Chernet *et al.*, 1998). Upper Pliocene basalts ($3.5 - 1.6$ Ma) and contemporaneous rhyolitic pyroclastic deposits ($2.5 - 1.7$ Ma) outcrop above (Corti, 2009). Subsequent, syn-rift bimodal volcanic activity is spatially associated with the oblique faults of the Wonji Fault Belt (WoldeGabriel *et al.*, 1990).

The large caldera forming eruptions are typically characterised by trachytic to peralkaline rhyolitic compositions, with a lack of intermediate compositions

(Corti, 2009). This volcanism is typically $<$ 1.8 Ma (WoldeGabriel *et al.*, 1990; Chernet *et al.*, 1998; Wolfenden *et al.*, 2004), forming large scale calderas at Gademotta, Gadamsa, Kone , Fantale, Bora and Corbetti. Volcanism continued until Holocene-historic times (Corti, 2009). Di Paola (1972) states that Holocene volcanic deposits occur inside the caldera of Gadamsa and Boset-Boricha, which are presently at fumarolic stage. Fantale (Fentale) and Kone (Garibaldi), erupted during the 1800's. Fantale is one of the most active volcanoes in the Ethiopian Rift, it reaches $\sim$ 600 m a.s.l. and is topped by a central elliptical caldera of $\sim$ 3.5 km diameter and $\sim$ 300 m depth (Acocella *et al.*, 2002). The volcano is constructed predominantly from trachytic and alkali rhyolitic tuffs and lava flows erupted from a zoned magma chamber (Webster *et al.*, 1993; Giordano *et al.*, 2014). An eruption from the volcano during the 13th century destroyed a town to the south (Siebert *et al.*, 2011) and two recent episodes of basaltic volcanism produced a lava flow covering $\sim$ 3 km^2. The latest of these was produced by an eruption dated by historical reports and oral tradition to AD 1820 (Gibson, 1967). The Kone volcanic complex is located $\sim$ 30 km SW of Fantale (Fig. 3.2) . It is composed of two calderas, measuring $\sim$ 8 km and $\sim$ 11 km each, which may be associated with the formation of a regional tephra marker (Rampey *et al.*, 2010).

3.2.2.2 Cental MER

Early flood basalt extrusion (30 Ma) also occurs throughout the central MER. Preceding the main rifting, late Miocene ($11-8$ Ma) basalts and trachybasalts were erupted (Corti, 2009). The onset of major rifting was marked by bimodal volcanism; characterised by voluminous silicic pyroclastics and associated minor basalts which occur extensively across the rift floor and attain thicknesses of $<$ 700 m. These ignimbrites are associated with large calderas; including the

3.5 Ma 'Munesa Crystal Tuff caldera, presently buried beneath the Ziway-Shala lakes. This caldera produced the 3.446 Ma Sidi Hakoma Tuff ; one of the only regional tephras in Ethiopia to be traced to its source (WoldeGabriel *et al.*, 2013). Subsequent volcanism during the Quaternary ($<$ 1.6 Ma) was related to the oblique faults of the Wonji Fault Belt. The bimodal volcanism is associated with major ignimbritic eruptions from large scale calderas; including Duguna, Corbetti and Aluto, O'a (Shalla) (Pyle, 1999; Corti, 2009). The collapse volume of these calderas ranges from ~ 3 to ~ 45 km^3, however, O'a, active between $280 - 180$ ka BP, is estimated to have had a collapse volume of 120 km^3 (WoldeGabriel *et al.*, 1990).

Holocene pyroclastic deposits and obsidians occur at Alutu and Corbetti (Di Paola, 1971, 1972). The 15 km wide Quaternary Corbetti caldera, located in the central MER, is superimposed on the Pliocene, 30 km wide, Awassa caldera. Corbetti is the closest volcano to two sites studied here, $<$ 40 km from Lake Tilo and Lake Awassa is situated in the Awassa caldera.

The recent volcanic history of the Corbetti caldera is poorly documented (Hutchison *et al.*, 2015). The Corbetti caldera is formed exclusively of pyroclastic deposits, including ignimbrite deposits intercalated with pumice and ash layers (Di Paola, 1971). Following the collapse of Corbetti; a large pyroclastic volcano, Wendo Koshe and a composite volcano, Chabbi, emerged in the centre of the caldera during the late Pleistocene (Rapprich *et al.*, 2016). The Chabbi volcano occurs on the eastern margin of the Corbetti caldera, and is constructed from obsidian lava flows, interbedded with pumice fall deposits (Di Paola, 1971; Rapprich *et al.*, 2013, 2016). The Wendo Koshe volcano is located to the west of Chabbi, it is formed of interbedded pumice deposits with a 'monotonous' appearance, thus the eruptive history of this centre is difficult to constrain

(Rapprich *et al.*, 2016). The most recent eruption from Wendo Koshe at 400 BC formed a widespread pumice deposit, described by Žáček *et al.* (2014) and Rapprich *et al.* (2016). This retains a thickness of 10 cm over 1000 km^2 and has been reworked in the Corbetti caldera, and redeposited on the shores of Lake Awassa.

Sediment cores from Lakes Awassa and Chamo are used in this study to construct a tephra framework. These lakes are located proximal to volcanoes in the CMER which may have been active during the Holocene; notably Lake Awassa is formed within the Corbetti caldera. The approach taken in this study, where the distribution of Holocene tephras is mapped, is key to further understanding the scale and hazards posed by these volcanoes, including those which are showing recent signs of unrest.

3.2.2.3 Southern MER

In the southern MER a basaltic phase of volcanism occurred at 11 Ma, resulting in the eruption of stratoid basalts. During the upper Miocene-lower Pliocene, volcanism was markedly reduced, to be resumed in the late Pliocene-early Pleistocene with bimodal volcanism and the eruption of widespread ignimbrites ($1.6 - 0.5$ Ma) (Bonini *et al.*, 2005; Corti, 2009). At 0.66 Ma, trachybasalts, pumice deposits and obsidian flows were emplaced in the Tosa Sucha (northern shores of Lake Chamo). Fissure eruptions and scoria cones have also been emplaced in the Tosa Sucha area during historic times (Corti, 2009).

This study investigates the tephra record preserved in sediments from lake Chamo. There is a lack of recent explosive volcanic activity in the southern MER. Therefore, the Chamo archive may provide a valuable record of distal volcanism from the central and northern MER, and potentially the Afar.

3.2.2.4 The Broadly Rifted Zone, SW Ethiopia

The 300 km wide, broadly rifted zone of SW Ethiopia represents the most southerly set of N-S trending basins comprising the EARV. The zone forms the northern extension of the Kenya rift and is made up of three half grabens and a fully developed rift basin. The oldest 45 Ma flood basalts outcrop in the broadly rifted zone (Davidson and Rex, 1980; Ebinger *et al.*, 1993; George *et al.*, 1998). In contrast with the MER, no post-rift volcanic eruptions have been noted in the broadly rifted zone, except for early Pliocene basaltic flows to the north of the failed Chew Bahir rift (WoldeGabriel *et al.*, 2013). The broadly rifted zone represents the waning stages of tectonic and volcanic activity to the north of the Kenyan Rift and displays the characteristics of rift basin terminations (WoldeGabriel *et al.*, 2013).

3.2.2.5 Off-axis volcanism: The YTVL

The Yerer-Tullu Wellel Volcano Tectonic Lineament (YTVL) is an E-W trending fault system or failed rift which extends for $>$ 500 km from Addis Ababa (Mount Yerer) to the border with Sudan (Tullu Wellel). Two volcanic successions outcrop along the YTVL. The Oligocene - lower Miocene lower succession consists of strongly weathered and faulted flood basalts and associated phonolitic domes (Abebe *et al.*, 1998). The upper volcanic succession is of late Miocene - recent age and is comprised of central volcanoes and small domes aligned in an E-W direction (Abebe *et al.*, 1998). The central volcanoes young from $12-7$ Ma in the west (Tullu Wellel) to $<$ 1 Ma in the east (Wenchi, Dendi and Bishoftu) (Adhana, 2014). Volcanism along this volcanic lineament generally becomes more alkaline and less silica saturated towards the west (Adhana, 2014). Lake sediment cores from Lakes Dendi and Lake Hora (Bishoftu) are used in this

study; both of the lakes are located on the YTVL and therefore may record tephras erupted from this region. A volcanic eruption at $\sim$ 1400 BP may have occurred from Mount Wenchi, 13 km to the southwest of Lake Dendi (Smeds, 1964).

3.2.3 Quaternary tephras from further afield

This study focuses on tephras in Ethiopian lake sediments; there is potential for some of these tephras to be derived from further afield. Potential sources of recent tephras throughout Africa, the Mediterranean, Middle East and Atlantic are outlined briefly below.

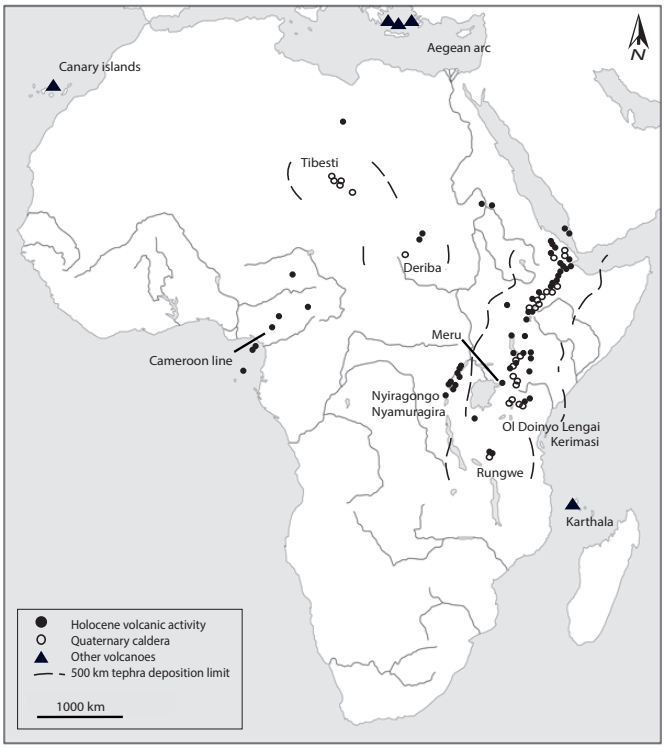

Figure 3.3: Tephra sources from further afield: in Africa, the Mediterranean, Middle East and Atlantic

3.2.3.1 Potential tephra sources in other areas of the EARS

In the eastern branch of the EARS; trachytic volcanoes in central and southern Kenya have undergone cycles of Krakatoan style collapse, producing voluminous ignimbrite and fall deposits, however few have been correlated. In the Tanzanian sector of the rift, Kerimasi and Ol Doinyo Lengai volcanoes have produced carbonatitic tephra which are regarded as the sources of surface limestones ~ 100 km to the west on the Crater Highlands and Serengeti Plains (Pyle, 1999). One of the largest volcanoes in Africa, Meru, located to the south of Kilimanjaro, exhibited major volcanic activity over the past 300 ka years and experienced large-scale collapse at 7.8 ka years BP producing widespread tephra which is likely to form a prominent distal tephra marker (Wilkinson *et al.*, 1986; Pyle, 1999). Tephra layers from Meru, recorded in sediments from Lake Challa (S. Kenya), indicate that Meru erupted explosively at least five times throughout the Holocene (C. Lane 2015, pers. comm. 15th Jan 2015). The western sector of EARS produced large volumes of basalt from the Nyamuragira and Nyiragongo centres, however, the only explosive volcanism during the Quaternary occurred in the Rungwe mountains to the north of Lake Malawi (Pyle, 1999).

3.2.3.2 Potential tephra sources in central and northern Africa

Quaternary volcanism in central and northern Africa is, in contrast to that in eastern Africa, typically of a smaller scale. Numerous volcanic calderas are visible in the Tibesti mountains and are believed to be of Quaternary age. The Deriba caldera to the east, in Sudan, is regarded as Holocene in age (Pyle, 1999).

3.2.3.3 Potential tephra sources in western Africa

The volcanoes comprising the Cameroon line in western Africa are thought to have been active during the Quaternary. However, they tend to produce more localised alkaline and basaltic lavas as opposed to widespread pyroclastic deposits. In western Senegal and the Tefidet rift Quaternary volcanism is also recorded, however, no significant tephra production has been attributed to these centres (Pyle, 1999). The distance of these volcanoes from Ethiopia and their localised eruptions means that is unlikely that tephras will be recorded in lake sediments studied here.

3.2.3.4 Potential tephra sources in the Mediterranean, Middle East and Atlantic

Pyle (1999) suggests that major explosive eruptions from caldera volcanoes in the Mediterranean, Middle East and the Atlantic have the potential to disperse distal tephra layers across Africa. Glass shards from the $\sim$3.5 ka Minoan eruption of Santorini have been recorded the sediments of Lake Manzala, in the north-eastern section of the Nile Delta (Eastwood *et al.*, 1999). Distal tephras from the Canary Islands have been recorded in DSDP cores from the west African continental margin and Pyle (1999) suggests these tephras may also have been deposited on the western coast of Africa. Holocene volcanism occurred on the Indian ocean islands of Comoros, Madagascar and Reunion, however, the deposits are primarily basaltic and therefore the likelihood of voluminous tephra production is low (Pyle, 1999). Microscopic cryptotephra from the $\sim$75 ka Younger Toba Tuff, the largest eruption of the Quaternary, has recently been discovered in lake sediments from Malawi, extending the known dispersal limits of this eruption

(Lane *et al.*, 2014). This was however, an exceptional event and as of yet, no other eruptions of this nature have been located in the tropics.

3.3 Tephra studies in East Africa

Geological and palaeoanthropological exploration of Ethiopian Rift basins over the past 50 years has led to the discovery of the most comprehensive record of human biological and technological change extending over the last 6 million years (WoldeGabriel *et al.*, 2013). Since the discovery of the first fossil remains from Olduvai Gorge (Tanzania) (Leakey *et al.*, 1961), hominid fossils have been recovered from the Afar Rift, Main Ethiopian Rift and the Omo Basin of the broadly rifted zone of SW Ethiopia (see Fig. 3.4). Determining accurate temporal and contextual constraints for these records is crucial.

Early Pliocene to late Pleistocene distal and proximal tephras identified across Ethiopia, Kenya and in marine sediments from the Gulf of Aden and NW Indian Ocean provide key chronological control on these hominin fossils. The tephras have proved essential in unravelling our understanding of hominid evolution and furthermore have resolved controversial ages of the hominin fossils, including age of the renowned 'Lucy' *Australopithecus afarensis* fossils from Hadar (Afar) (Brown and Cerling, 1982).

The successful application of tephrochronology in eastern Africa is exemplified by the Turkana Basin (northern Kenya). The site is one of the most well preserved and chronologically controlled Plio-Pleistocene fossil records in eastern Africa, containing a total of 135 tephra layers (Feibel, 1999, 2011). Many of the regional tephras were first described in the Turkana Basin by Howell (1968); Bowen and Vondra (1973); Brown and Feibel (1986) during the late

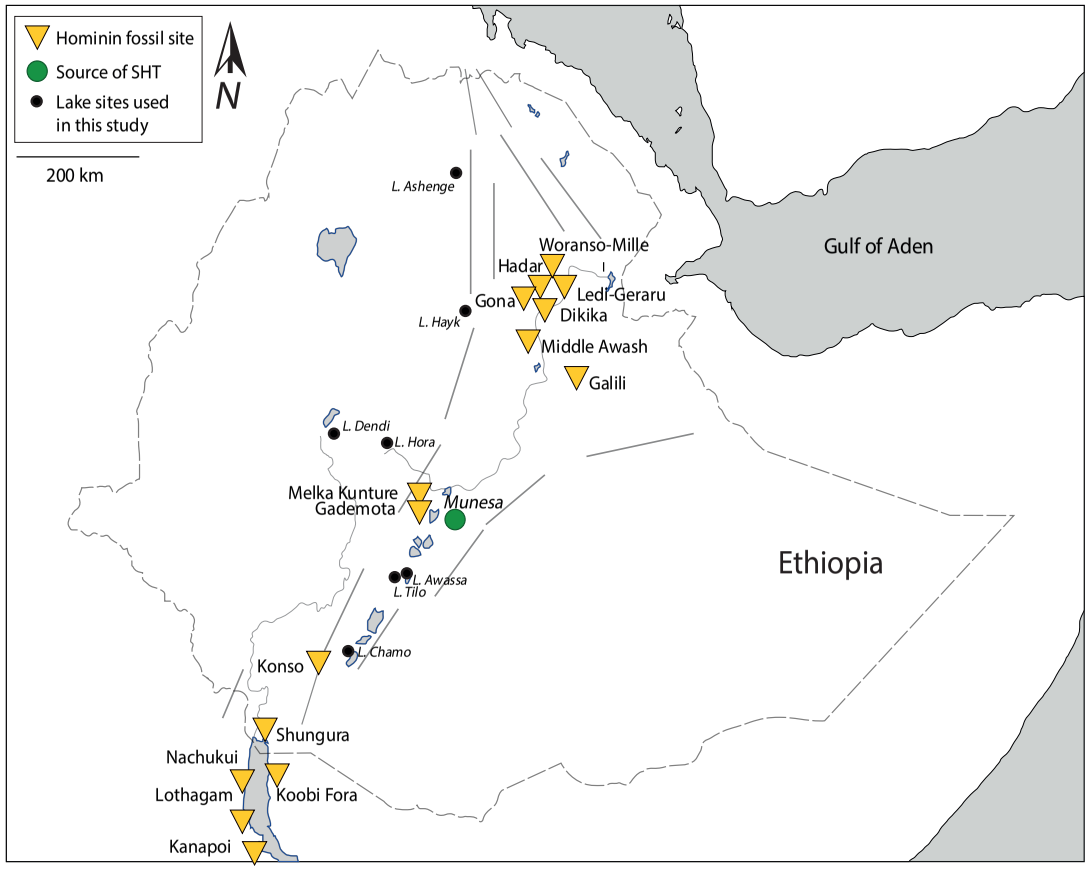

Figure 3.4: Map of Ethiopia showing regional hominin fossil sites (yellow triangles), many of these have been dated using tephrochronology. Green circle indicates the Munesa vitrophyre, which is geochemically and chronologically identical to the Sidi Hakoma Tuff (SHT) and is located close to the buried source caldera. Lake core sites used in this study are labelled. Adpated from WoldeGabriel *et al.* (2013).

1960*s*. The first local tephra correlations within the Turkana Basin were based on outcrop tracing and lithological features (Brown, 1969; Brown *et al.*, 1970). This approach proved successful in the Lower Omo Valley section of the Turkana basin, however, correlations were unsuccessful in Koobi Fora Region due to it's complex stratigraphy (Feibel, 1999).

The potential for tephra correlation on a basinal scale in Turkana was realised in the 1970*s* when three tephras were geochemically correlated between the Koobi Fora and Shungura Formations in the Turkana Basin (Cerling *et al.*, 1979; Cerling and Brown, 1982).

Correlation over regional scales quickly became feasible when the composition of the Tulu Bor Tuff at Turkana was found to geochemically correlate with the Sidi Hakoma Tuff at Hadar in the Afar (northern Ethiopia) (Brown, 1982). Correlative units were then identified at other sites in the MER (Haileab and Brown, 1992; WoldeGabriel *et al.*, 1992; Haileab and Brown, 1994; WoldeGabriel *et al.*, 1999, 2005), Afar Rift (Hart *et al.*, 1992), Uganda (Pickford *et al.*, 1991), the Baringo Basin of N Kenya (Namwamba, 1993) and in marine sediments in the Gulf of Aden (Sarna-Wojcicki *et al.*, 1985) and the Indian Ocean (Brown *et al.*, 1992); linking terrestrial and marine archives.

Tephra from the East African Rift have since been correlated 2700 km away from their source volcanoes to the Gulf of Aden and the NW Indian Ocean (deMenocal and Brown, 1999; Ukstins Peate *et al.*, 2003; Feakins *et al.*, 2007). Feakins *et al.* (2007) correlated a cryptotephra in the DSDP site 231 Gulf of Aden core to the Lokochot Tuff (first described at Koobi Fora, Turkana) and identified a further 67 cryptotephras in the marine core; all originating from the East African Rift System and revealing three pulses in volcanism at $\sim 4.0 - 3.2$ Ma, 2.4 Ma and $1.7 - 1.3$ Ma.

Table 3.1: Regional tephra stratigraphic markers, their age and distribution in the eastern African rift and the NW Indian Ocean, from WoldeGabriel *et al.* (2013)

Tephra	**Age (Ma)**	**Occurences**
Waidedo Vitric	0.16	Konso, Middle Awash, Gona
Silbo, Upper White	0.75	Omo-Turkana Basin, Konso, Gulf of Aden, NW Indian Ocean
Chari, Bright White	1.38	Omo-Turkana Basin, Konso, Gulf of Aden, NW Indian Ocean
KBS Turoha	1.87	Omo-Turkana Basin, Konso, Gulf of Aden, NW Indian Ocean
Sidi Hakoma, Tulu Bor, Tuff B. U-10/11	3.45	Kipcherere Section (Baringo Basin), Omo-Turkana Basin, central MER, Middle Awash, Hadar, Dikika, Ledi-Geraru, Gulf of Aden, NW Indian Ocean
Lokochot	3.57	Western Rift (Uganda), Kipcherere Section (Baringo Basin), Omo-Turkana Basin, central MER, Middle Awash, Woranso-Mille, Gulf of Aden, NW Indian Ocean
Lomogol	3.62	Western Rift (Uganda), Omo-Turkana Basin, Gulf of Aden, NW Indian Ocean
Wargolo/VT-3	3.80	Omo-Turkana Basin, Middle Awash, Dikika, Gulf of Aden, NW Indian Ocean
Moiti/ VT-1	3.97	Omo-Turkana Basin, central MER, Middle Awash, Gulf of Aden, NW Indian Ocean

Several regional tephras are now recognised (Table 3.1) and range in age from early Pliocene (3.97 Ma) to late Pleistocene (0.16 Ma) and, of these, the 3.446 ± 0.041 Ma Sidi Hakoma Tuff (SHT) is the most widely recognised and well-characterised. These tephras are believed to have originated from the central sector of the MER, however, the SHT is the only regional tephra which has been reliably correlated to its volcanic source, between the Baringo Basin of central Kenya and the NW Indian Ocean (Hart *et al.*, 1992; Walter and Aronson, 1993).

Of the regional tephra markers, the SHT has gained prominence as a regional stratigraphic marker in Ethiopia due to its distinct properties, versatility and chronostratigraphic and palaeoanthropological importance (WoldeGabriel *et al.*, 2013). The SHT acts as a marker within fossiliferous sediments containing important *A. afarensis* remains, namely two partial skeletons of 'Lucy' and 'Lucy's Baby-Selam' at Hadar, Dikika and Maka in the SW Afar Rift (Fig. 3.5)

(WoldeGabriel *et al.*, 2013). The first tuff chemically correlated to the SHT was described in the Omo-Turkana Basin (Howell, 1968; Bowen and Vondra, 1973) but the first regional correlation was not reported until the early 1980*s* by (Brown, 1982). The importance of the SHT and other regional and local tephra at the Middle Awash site is discussed in detail below.

3.3.1 The Middle Awash

The Middle Awash site (southern Afar) has yielded eight hominid species, $\sim 21,000$ vertebrate fossils and thousands of archaeological artefacts (WoldeGabriel *et al.*, 2013).

Tephra deposits from the Ayelu volcano and surrounding Yardi Floodplain (part of Middle Awash) are investigated in this study to see if they are geochemically related to Holocene tephra deposits in Ethiopian lake sediment cores. Therefore tephra studies in the Middle Awash are briefly discussed below.

Unlike other archaeological sites in Ethiopia, Middle Awash palaeoanthropological sites are scattered across a large area and separated by Quaternary lava fields and tephra deposits, modern flood plains, outwash plains, riverine forests and Lake Yardi (Fig. 3.5) (WoldeGabriel *et al.*, 2013). Due to poor exposure, isolated outcrops and dense faulting, the tephrostratigraphy has developed more slowly than in the Turkana Basin (Feibel, 1999; WoldeGabriel *et al.*, 2013).

The palaeoanthropological potential of the Middle Awash site was first realised by Taieb (1974) who collected palaeontological specimens and measured geological sections in the area. The Rift Valley Research Mission in Ethiopia (RVRME) later established several stratigraphic sections using biochronological records, identified hundreds of fossil and archaeological localities and collected many fossils and stone tools (Kalb, 1976). However, data published from

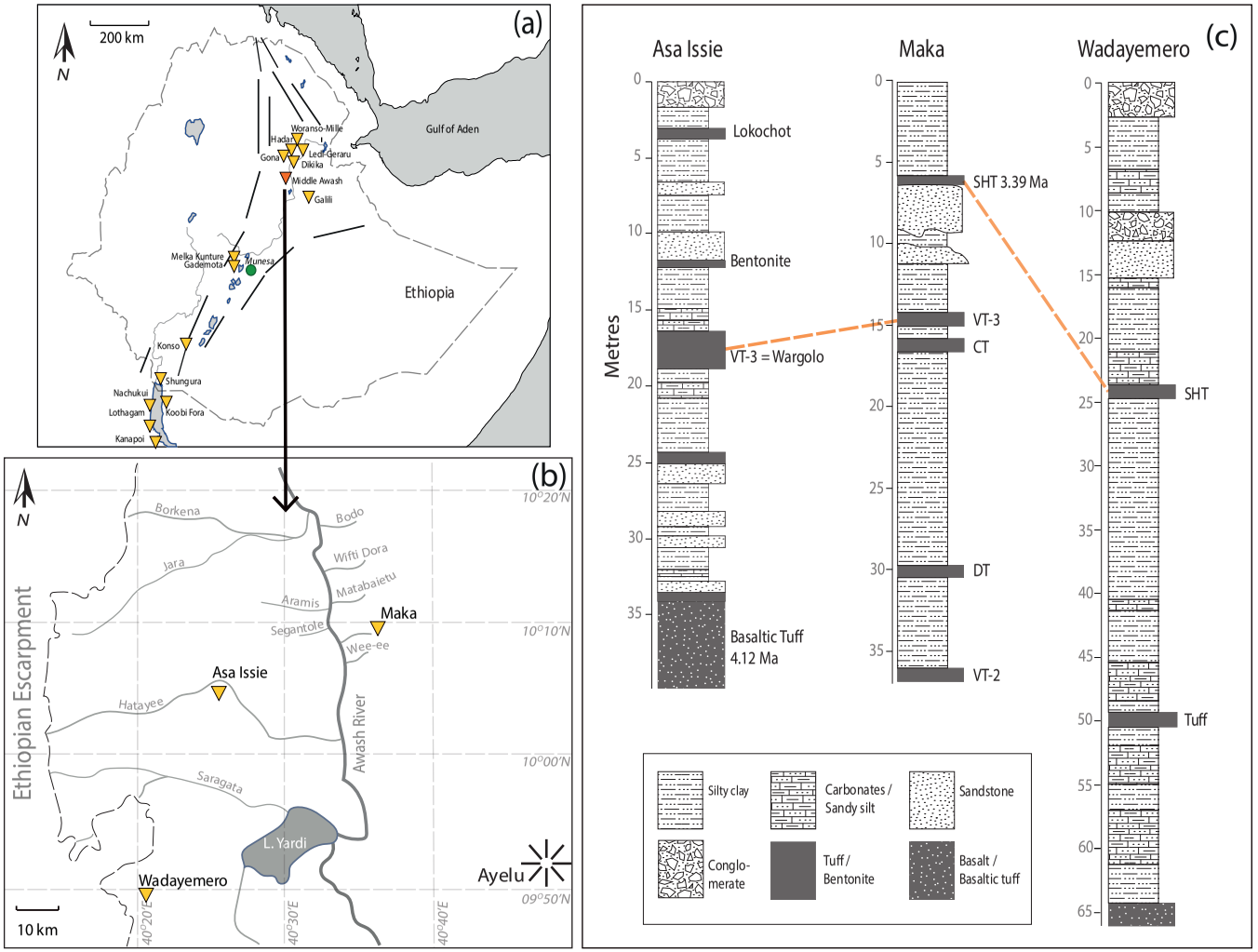

Figure 3.5: (a) Location of the Middle Awash in northern Ethiopia, (b) location of the Asa Issie, Maka and Wadayemero study areas comprising the Middle Awash Site (c) Stratigraphies of the Middle Awash study areas, correlated using tephras WoldeGabriel *et al.* (2013).

these investigations relied on lithostratigraphic similarities, coarse biochronology and broad structural interferences in order to form a stratigraphic framework, therefore estimated ages proved inaccurate (Kalb, 1993, 1995).

Tephrochonology has successfully synchronized the disparate study areas of the Middle Awash (Fig. 3.5) (de Heinzelin *et al.*, 1999; Asfaw *et al.*, 2002; Clark *et al.*, 2003). This framework allows the accurate and precise dating of fauna and artefacts from archaeological sites and subsequently provides insight into hominin evolution (Clark *et al.*, 2003).

3.4 A lack of Holocene Ethiopian tephra studies

The previous section has illustrated that tephrochronology has been successfully applied to early Pliocene - late Pleistocene archaeological sites throughout Ethiopia. However; younger Holocene tephras in Ethiopia remain unstudied and the record of volcanism in this volcanically active region remains brief (Siebert *et al.*, 2011).

In the $15th$ Century two eruptions from Ethiopia were recorded by Vasco de Gama en route to India via the Cape of Good Hope (Siebert *et al.*, 2011). In the early $1800s$, eruptions from Fantale and Kone (northern Main Ethiopian Rift) were recorded (Harris, 1844; Gibson, 1969). However, it was not until the opening of the Suez Canal in 1869 and the subsequent exploration of Africa that regional historic eruptions were recorded in detail; 85% of the 155 historic eruptions from the African continent were reported after 1870. Volcanoes of suspected Holocene age in Ethiopia, Eritrea and the Ethiopian borders are detailed in Table 3.2. Although 65 volcanoes of this age occur in the region, only 14 of them have recorded historic eruptions (Siebert *et al.*, 2011).

The largest known eruption from Africa occurred in 1861 from Dubbi in Eritrea (Wiart and Oppenheimer, 2000) (Fig. 3.6 and 3.7). The volcano lies along the Nabro Volcanic Range, which runs from the Eritrean coast in a south-western direction into Ethiopia (Wiart and Oppenheimer, 2000).

Earthquakes during the opening phases of the Dubbi eruption were felt 180 km away in Yemen and explosions were heard 330 km away. Pyroclastic density currents destroyed two villages and killed 100 local inhabitants and herds of cattle. Tephra was reported to have fallen across the Ethiopian Plateau, 300 km to the west and pyroclastic and lava flows travelled ~ 20 km from the vent. Volcanism then switched to fire-fountain activity along a 4 km long fissure; a lava flow associated with this phase travelled ~ 20 km from the vent.

Due to aeolian erosion, the tephra deposit from the initial eruption has since been deflated, and no reliable tephra volumes have therefore been calculated (Lenhardt and Oppenheimer, 2014). The 3.5km^3 lava flow volume alone (equivalent to VEI =6), makes this the largest historic eruption recorded in Africa. An anomalously cold Northern Hemisphere 1862 summer recorded in the tree ring record has been tentatively attributed to sulphate aerosols produced by the Dubbi eruption (Wiart and Oppenheimer, 2000).

Lake Ashenge is located $<$ 300 km to the west of Dubbi; there may be potential for preservation of the Dubbi 1861 tephra in the sediments from this lake, which may give insight into the dispersal of volcanic ash from the eruption.

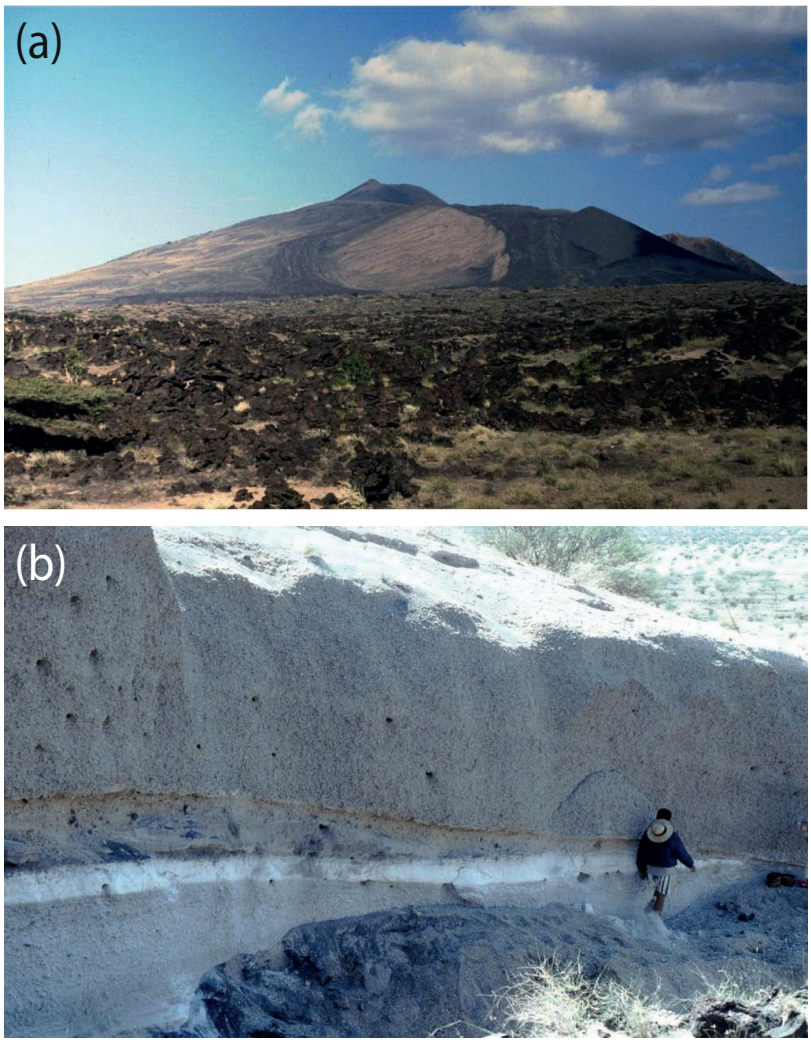

Figure 3.6: (a) The Dubbi volcano (1625 m a.s.l), (b) proximal pumice and ash deposits from the Dubbi 1861, figures from Oppenheimer (2011).

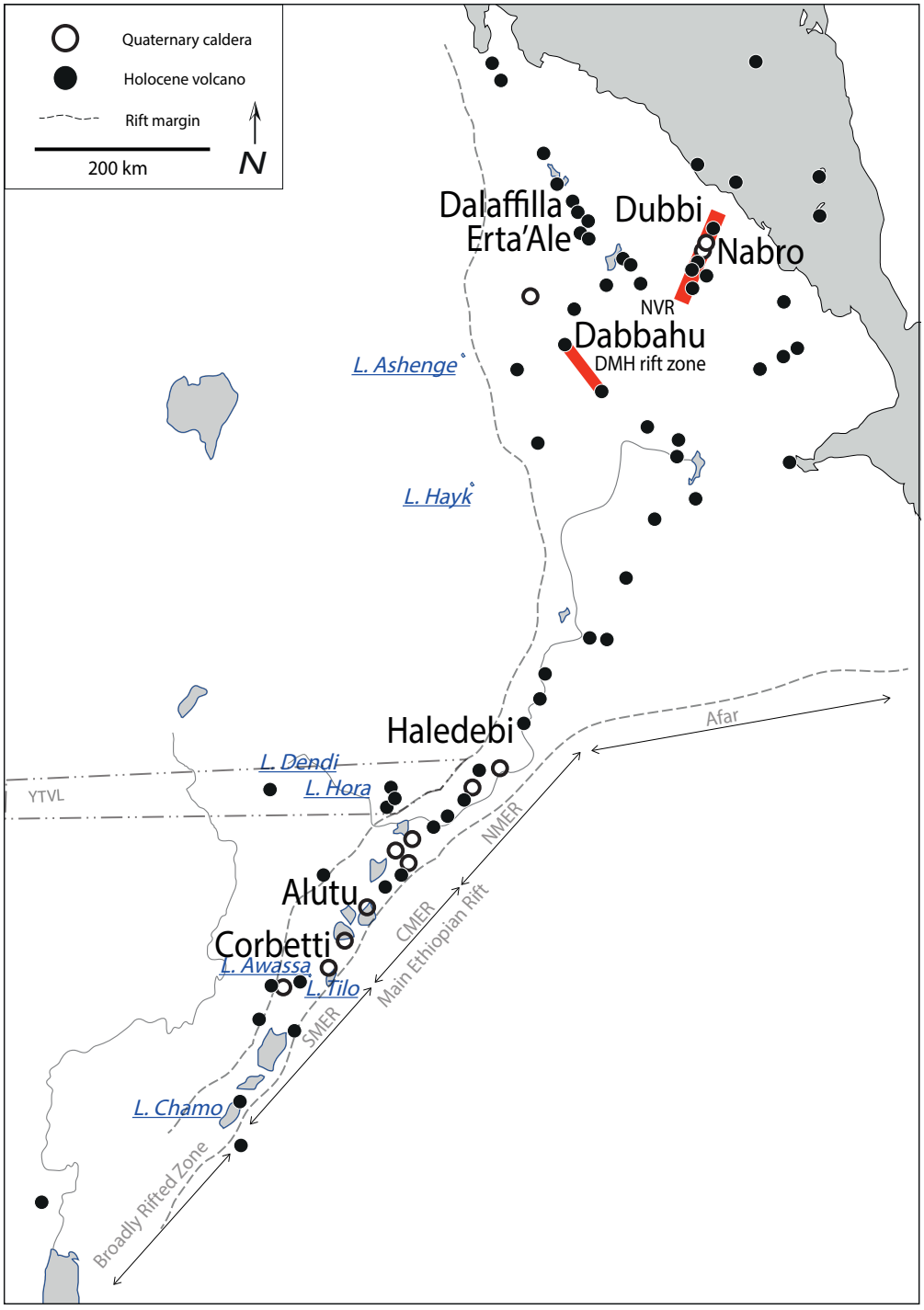

Figure 3.7: Location of volcanoes which have erupted historically or recently in the Afar and those in the Main Ethiopian Rift which are actively deforming. DMH = Dabbahu-Manda Hararo Rift Segment, NVR=Nabro Volcanic Range.

3.4.1 Volcanic hazards in Ethiopia

Numerous eruptions have occurred in the Afar during the last decade, notably at Dabbahu (2005), Dalaffilla (2008), Erta'Ale (2011) and Nabro (2011) (see Fig. 3.7) (Ferguson *et al.*, 2010; Wiart and Oppenheimer, 2000). In the Main Ethiopian Rift, significant pulses of deformation beneath Alutu, Corbetti, Bora, Haledebi (Fig. 3.7) have been observed over the past 20 years (Biggs *et al.*, 2011). This is indicative of magmatic unrest beneath these volcanoes and is often interpreted as a precursor to an eruption. Furthermore, numerous volcanoes throughout Ethiopia are currently at a fumarolic stage (Lenhardt and Oppenheimer, 2014).

Lenhardt and Oppenheimer (2014) cite the potential for a range of volcanic hazards to occur in Ethiopia; including lava flows, pyroclastic density currents, ash falls and volcanic gases.

The hazards posed by volcanoes in this region are exemplified by two recent explosive eruptions. Since September 2005, the Dabbahu-Manda Hararo rift (Fig. 3.7) has been undergoing active rifting, initiated by the opening of a dyke along a $\sim$60 km rift segment over a time span of $<$ 8 m (Ferguson *et al.*, 2010) (Fig. 3.8a). The rifting was associated with a small silicic eruption (VEI=3) from Dabbahu, which deposited tephra over 100 km^2 and resulted in the evacuation of $>$ 6000 people from nearby villages (Ayele *et al.*, 2007*a*; Ferguson *et al.*, 2010).

On June 12th 2011, Nabro volcano (20 km to the SW of Dubbi and on the same volcanic lineament, Fig. 3.7 3.8b,c) erupted explosively (VEI=4) displacing thousands of people. In Eritrea, 7 people were killed, although it is believed there were more fatalities in Ethiopia. Volcanic ash was dispersed over northern Africa and Eurasia 3 days after the eruption, causing disruption to air traffic (Fig. 3.8) (Lenhardt and Oppenheimer, 2014). Prior to the eruption

14 earthquakes (M> 4.5) occurred in the region, but the eruption remained unexpected due to a lack of monitoring and volcanic history for the volcano (Lenhardt and Oppenheimer, 2014). The Nabro eruption was ranked the largest source of sulphate aerosols to the atmosphere since the 1991 Pinatubo eruption (Sawamura *et al.*, 2012).

Whilst the Afar is sparsely populated, recent and historic eruptions from Dubbi, Dabbahu and Nabro highlight the potential for volcanic events to cause fatalities, displace inhabitants and disrupt international air and maritime traffic (Lenhardt and Oppenheimer, 2014). In the less extreme temperatures of the Main Ethiopian Rift, high population densities inhabit volcanic areas; with 570,000 people living within 5 km of the actively deforming Corbetti caldera (Siebert *et al.*, 2011) (see Table 3.2).

The lack of volcanic history for this region, coupled with limited volcano monitoring, means that the risks posed by these volcanoes remain uncertain. The World Bank report on volcanic hazards lists the Main Ethiopian Rift volcanoes at a zero level of monitoring and the highest uncertainty level for hazards posed (Biggs *et al.*, 2011). Numerous volcanoes have erupted after centuries of repose, e.g. El Chichón (1982), Mount Pinatubo (1991) and Nabro (2011), and it is therefore possible that Ethiopian volcanoes may erupt suddenly (Lenhardt and Oppenheimer, 2014).

Following the Dabbahu 2005 volcano-seismic crisis, the Afar Rift Consortium (http://www.see.leeds.ac.uk/afar/) was concieved. The project installed a volcano and seismic monitoring network in the Afar and set out to investigate magmatic and tectonic processes and the timing of past eruptions. The later discovery of the active deformation of volcanoes in the Main Ethiopian Rift lead to the formation of the RiftVolc project (http://www.geos.ed.ac.uk/riftvolc) in 2014.

RiftVolc aims to investigate the controls on active magmatic systems and the potential threats from future volcanic activity. These projects have been crucial in developing our understanding of magmatic processes in Ethiopia and the risk posed by future eruptions, however, their primary focus is on proximal volcanic deposits.

Distal tephras deposited in Holocene lake sediments throughout Ethiopia provide an ideal method to assess how frequently these volcanoes have erupted in the recent past and when future eruptions may occur. Furthermore, data on distal tephras in lake sediments will compliment research by the Afar Rift Consortium and RiftVolc; providing insight into the dispersal of tephras and the interrelationships between volcanic centres.

Table 3.2: List of volcanoes of known or suspected Holocene age in Ethiopia and bordering areas, modified from and Siebert *et al.* (2011) and Lenhardt and Oppenheimer (2014). It is likely that there are further volcanoes of Holocene age that have yet to be recognised or dated.

Name	*Country*	*Type*	*Latitude*	*Longitude*	*Elevation asl (m)*	*Last known eruption*	*Population < 5 km*
Alid	Eritrea	Stratovolcano	14.88°N	13.92°E	904	?	517
Assab Volc. Field	Eritrea	Volcanic field	12.95°N	42.43°E	987	?	9
Dubbi	Eritrea	Stratovolcano	13.58°N	41.80°E	1625	1861	0
Jalua	Eritrea	Stratovolcano	15.04°N	39.82°E	713	?	2072
Nabro	Eritrea	Stratovolcano	13.37°N	41.70°E	2218	2011	24
Adwa	Ethiopia	Stratovolcano	10.07°N	40.84°E	1733	?	101
Adferá	Ethiopia	Stratovolcano	13.08°N	40.85°E	1295	?	51
Alayta	Ethiopia	Shield volcano	12.88°N	40.57°E	1501	1915	156
Ale Bagu	Ethiopia	Stratovolcano	13.52°N	40.63°E	1031	?	2
Alu	Ethiopia	Fissure vents	13.83°N	40.51°E	429	?	0
Alutu	Ethiopia	Stratovolcano	7.77°N	38.78°E	2335	50 BC (?)	6011
Asavyo	Ethiopia	Shield volcano	13.07°N	41.60°E	1200	?	84
Ayelu	Ethiopia	Stratovolcano	10.08°N	40.70°E	2145	?	193
Beru	Ethiopia	Volcanic field	8.95°N	39.75°E	1100	?	3850
Bilate River Field	Ethiopia	Maars	7.07°N	38.10°E	1700	?	359001
Bishoftu Volcanic Field	Ethiopia	Fissure vents	8.78°N	38.98°E	$>$ 1850	?	310101
Bora-Bericcio	Ethiopia	Pumice cones	8.27°N	39.03°E	2285	?	5822
Borale Ale	Ethiopia	Stratovolcano	13.73°N	40.60°E	668	?	0
Borawli	Ethiopia	Stratovolcano	13.30°N	40.98°E	812	?	920
Borawli	Ethiopia	Lava domes	11.63°N	41.45°E	875	?	38
Boset-Bericha	Ethiopia	Stratovolcanoes	8.56°N	39.48°E	2447	?	3267
Butajiri-Silti Field	Ethiopia	Fissure vents	8.05°N	38.35°E	2281	?	431631
Chiracha	Ethiopia	Stratovolcano	6.65°N	38.12°E	1650	?	14959
Corbetti caldera	Ethiopia	Caldera	7.18°N	38.43°E	2320	?	565206
Dabbahu	Ethiopia	Stratovolcano	12.60°N	40.48°E	1442	2005	204
Dabbayra	Ethiopia	Shield volcano	12.38°N	40.07°E	1302	?	804
Dalaffilla	Ethiopia	Stratovolcano	13.79°N	40.55°E	613	2008	0
Dallol	Ethiopia	Explosion craters	14.24°N	40.30°E	-48	1926	461
Dama Ali	Ethiopia	Shield volcano	11.28°N	41.63°E	1068	1631	24
Dofen	Ethiopia	Stratovolcano	9.35°N	40.13°E	1151	?	1900
East Ziway	Ethiopia	Fissure vents	7.95°N	38.93°E	1889	?	85845
Erta Ale	Ethiopia	Shield volcano	13.60°N	40.67°E	613	2011	2685
Fantale	Ethiopia	Stratovolcano	8.98°N	39.93°E	2007	1820 (?)	1919
Gabillema	Ethiopia	Stratovolcano	11.08°N	41.27°E	1459	?	248
Gada Ale	Ethiopia	Stratovolcano	13.98°N	40.41°E	287	?	101
Gedamsa	Ethiopia	Caldera	8.35°N	39.18°E	1984	?	216008
Groppo	Ethiopia	Stratovolcano	11.73°N	40.25°E	930	?	2411
Hayli Gubbi	Ethiopia	Shield volcano	13.50°N	40.72°E	521	?	0
Hertali	Ethiopia	Fissure vent	9.78°N	40.33°E	900 ?	?	474
Hobicha caldera	Ethiopia	Caldera	6.78°N	37.83°E	1800 ?	?	466462
Kone	Ethiopia	Calderas	8.80°N	39.69°E	1619	1820 $\pm$ 10	7289
Korath Range	Ethiopia	Tuff cones	5.10°N	35.88°E	912	?	24549
Kurub	Ethiopia	Shield volcano	11.88°N	41.21°E	625	?	8
Liado Hayk	Ethiopia	Maars	9.57°N	40.28°E	878	?	22847
Ma Alalta	Ethiopia	Stratovolcano	13.02°N	40.20°E	1815	?	3925
Manda Gargori	Ethiopia	Fissure vents	11.75°N	41.48°E	Unknown	?	284
Manda Hararo	Ethiopia	Shield volcanoes	12.17°N	40.82°E	$>$ 600	2009	191
Mat Ala	Ethiopia	Shield volcano	13.10°N	41.15°E	523	?	45
O'a caldera	Ethiopia	Caldera	7.47°N	38.58°E	2075	?	148588
Sodore	Ethiopia	Pyroclastic cones	8.43°N	39.35°E	1765	?	432998
Tat Ali	Ethiopia	Shield volcano	13.28°N	41.07°E	$>$ 700	?	32
Tepi	Ethiopia	Shield volcano	7.42°N	35.43°E	2728	?	63395
Tosa Sucha	Ethiopia	Cinder cones	5.93°N	37.57°E	1650	?	175047
Tullu Moje	Ethiopia	Pumice cones	8.16°N	39.13°E	2349	1900 (?)	11514
Unnamed	Ethiopia	Pyroclastic cones	8.70°N	39.63°E	1300	?	134853
Unnamed	Ethiopia	Fissure vents	8.62°N	38.95°E	1800 ?	?	290221
Unnamed	Ethiopia	Fissure vents	8.07°N	39.07°E	1800 ?	?	283786
Unnamed	Ethiopia	Cinder cones	5.65°N	37.67°E	1200	?	78416
Yangudi	Ethiopia	Complex volcano	10.58°N	41.04°E	1383	?	33
Gufa	Ethiopia/Djibouti	Volcanic field	12.55°N	42.53°E	$>$ 600	?	1651
Manda-Inakir	Ethiopia/Djibouti	Fissure vents	12.38°N	42.20°E	$>$ 600	1928	116
Mousa Alli	Ethiopia/Djibouti	Stratovolcano	12.47°N	42.40°E	2028	?	132
Mallahle	Ethiopia/Eritrea	Stratovolcano	13.27°N	41.65°E	1875	?	912
Sork Ale	Ethiopia/Eritrea	Stratovolcano	13.18°N	41.73°E	1611	?	174
Mega Basalt Field	Ethiopia/Kenya	Pyroclastic cones	4.08°N	37.42°E	1067	?	2815

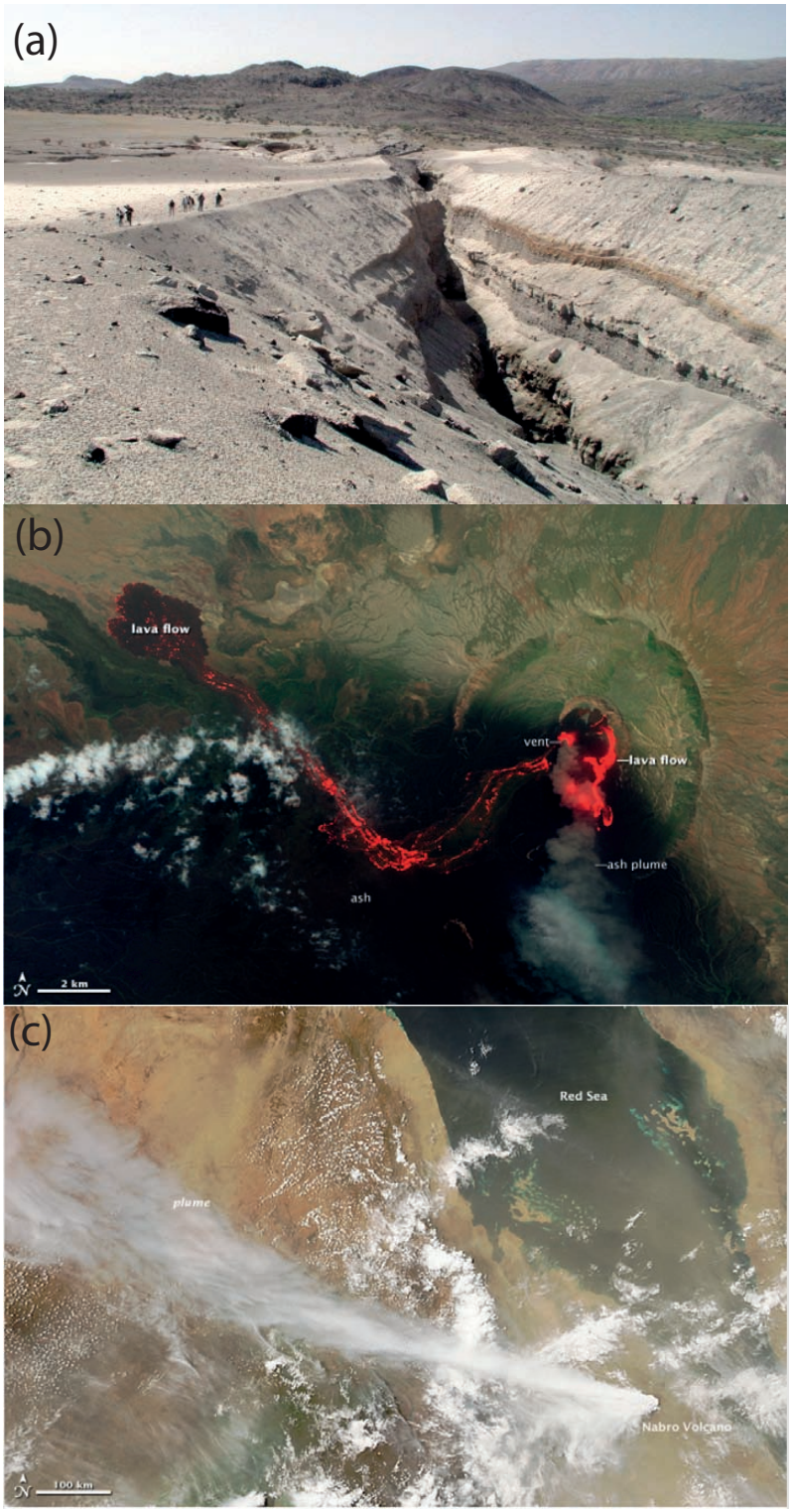

Figure 3.8: (a) Dabbahu 2005 volcano-seismic crisis; view of Dabbahu's newly formed pumice cone and fissure vent, from Siebert *et al.* (2011) (b) and (c) Satellite images showing lava flows and the ash plume associated with the Nabro 2011 eruption, from NASA (2011).

3.5 Summary

This chapter has demonstrated that numerous volcanic centres in the East African Rift Valley erupted explosively during the Quaternary - Holocene, producing widespread tephra layers. Early Pliocene (3.97 Ma) to late Pleistocene (0.16 Ma) tephra layers provide chronological control on important palaeoanthropological sites throughout eastern Africa and have also been correlated to the palaeoclimate archives within sediment cores from the Gulf of Aden and the NW Indian Ocean.

Numerous volcanoes believed to have been active during the Holocene occur throughout the Ethiopian Rift. Despite many of these being situated close to highly populous areas, their volcanic history and tephra deposits remain poorly understood and unstudied. This is related to the early stage of geological research in this region and the logistical difficulties of undertaking field work in regions such as the Afar. Tephra deposits in Ethiopia can give insight into the tempo and characteristics of past volcanism and therefore have useful implications for hazard monitoring. Furthermore, these tephra deposits can be used to date and correlate archives across this climatically sensitive region.

This study uses Holocene (< 17 cal. ka) sediment cores collected from Lakes Ashenge, Hayk and Dendi in the Ethiopian Highlands and Lakes Hora Awassa, Tilo and Chamo in the Ethiopian Rift. Correlations between different lake sites and to source volcanoes will enable a Holocene tephra framework to be constructed and will provide a dossier of past volcanism.

Chapter 4

Research design and methods

In the following chapter, field sampling methods are first discussed, including lake sediment coring and proximal tephra sampling. Laboratory methods are then described, including cryptotephra identification methods and the geochemical fingerprinting of tephras.

4.1 Research design

This study uses Holocene lacustrine sediment cores collected from Ethiopian lakes as part of a long term collaborative project between Aberystwyth University, Addis Ababa University and latterly the University of Cologne which aims to investigate regional palaeoclimate.

This study uses $<$ 17 cal. ka sediment cores collected from Lakes Ashenge, Hayk and Dendi in the Ethiopian Highlands and Lakes Hora Awassa, Tilo and Chamo in the Ethiopian Rift. Core site locations and core details are given in Fig. 4.1 and Table 4.1.

Lakes Ashenge, Hayk and Chamo are formed in tectonic basins, whilst Lakes Dendi, Hora, Awassa and Tilo are crater lakes.The core sites can be

divided geographically and tectonically into three groups (see Fig. 4.1). Lakes Ashenge and Hayk are the most northerly lakes studied here and are located on the Ethiopian Plateau. Lakes Awassa, Tilo and Chamo are located to the south in the Main Ethiopian Rift. Lakes Dendi and Hora are also located in the Ethiopian Plateau but are situated on the E-W orientated Yerer-Tullu Wellel Volcano Tectonic Lineament.

Primarily, these sites were chosen on the basis of their good preservation of tephra deposits. Sites distributed throughout the Ethiopian Rift and surrounding plateau were selected in order to provide a spatially comprehensive record of volcanism and ensure more opportunities for correlation. Core sites were also selected in order that both proximal and distal tephra layers could be studied, therefore providing insight into potential tephra sources and recording interfingering tephra deposits from multiple sources, respectively. Cores from Lakes Ashenge, Hayk and Chamo were used because these lakes are located $>$ 50 km away from volcanoes active during the Holocene and are therefore likely to receive only distal tephras from multiple volcanic sources. In contrast, Lakes Dendi, Hora, Awassa and Tilo are located close to Holocene volcanoes and contain proximal tephra deposits. Lake Dendi was chosen due to its proximity to volcanoes aligned along the E-W aligned Yerer-Tullu Wellel Volcano Tectonic Lineament. This volcanic lineament is offset from the NE-SW trending Ethiopian Rift and therefore the proximal tephra deposits may vary geochemically.

Lake sediment cores utilised in this study were cored by H. Lamb (Aberystwyth University) and F. Schäbitz (University of Cologne). Sediments were cored using a Livingstone piston corer (Lakes Ashenge, Hora, Awassa and Tilo) or a UWITEC corer (Lakes Hayk, Dendi and Chamo). Details of coring methods, the

length and temporal coverage of each core and previous studies on each record are given in Table 4.1.

In order to locate potential volcanic sources for tephras in lake sediment cores, proximal tephra samples from the Afar Rift and central Main Ethiopian Rift were geochemically fingerprinted. Ayelu and Dubbi (Afar) were selected due to their proximity to Lakes Ashenge and Hayk. The Dubbi 1861 eruption produced a widespread tephra layer and proximal tephras from Dubbi were analysed to check if they correlated with a historic tephra in the Ashenge core. Holocene activity has been recorded at the Chabbi volcano (in the Corbetti caldera, CMER) (Siebert *et al.*, 2011) and may be responsible for thick tephras in nearby Lakes Awassa and Tilo. Therefore samples from Chabbi were fingerprinted to check whether it is the source for the Awassa and Tilo tephras. Tephras from Mochena Borago (SW Ethiopia), were analysed to check whether they correlated with tephras occurring in lake sediments, therefore potentially tying down the chronology for this archaeological site and resolving dating problems.

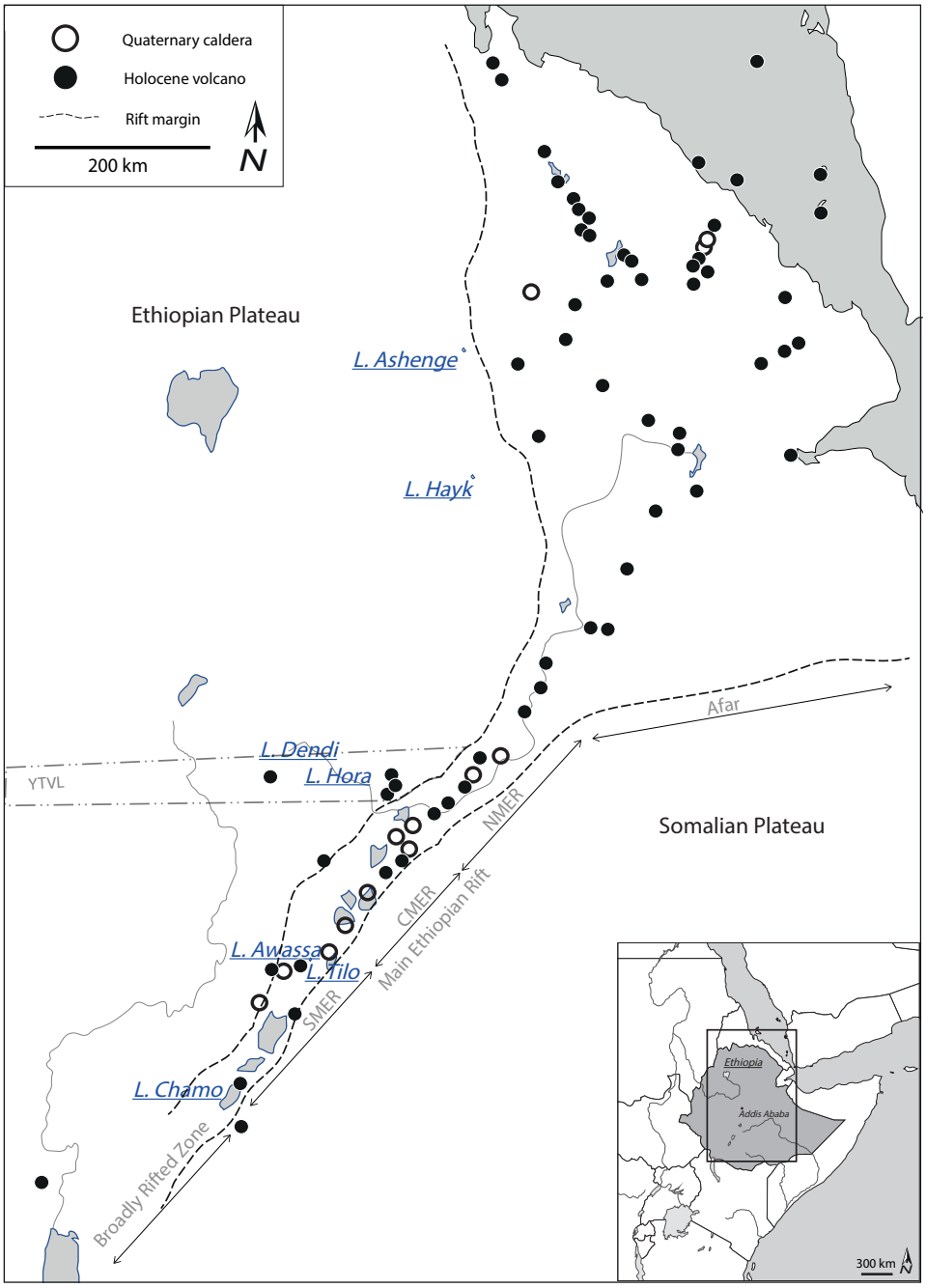

Figure 4.1: Locations of Holocene lake sediment cores collected from throughout Ethiopia, volcanoes suspected to have been active during the Holocene (Siebert *et al.*, 2011) are shown for reference. The lakes studied here can be grouped geographically; Lakes Ashenge and Hayk are located on the Ethiopian Plateau whilst Lakes Awassa, Tilo and Chamo are located to the south in the southern Main Ethiopian Rift. Lakes Dendi and Hora are located off the main rift axis on the E-W orientated Yerer-Tullu Wellel Volcano Tectonic Lineament (YTVL). NMER, CMER and SMER = northern, central and southern Main Ethiopian Rifts.

Table 4.1: Ethiopian lake sediment core details

Site name	Region	Latitute	Longitude	Collection date	Lake water depth (m)	Core length (m)	Age (cal. ka)	Studies
Ashenge	Tigray	12°34'39.28"N	39°30'6.67"E	2003	9	8	17.4	Marshall (2006); Marshall *et al.* (2009)
Hayk	Debub Wollo	11°20'44.49"N	39°42'40.23"E	2010	78	7.5	17.0	on-going study by K. Loakes (Loughborough University)
Dendi	Dendi	8°50'10.33"N	38°1'12.53"E	2012	54	12		on-going study by S. Meyer (University of Cologne)
Hora	Oromia	8°45'43.67"N	38°59'31.80"E	2001	30	12		Kebede *et al.* (2002); Lamb *et al.* (2002*b*)
Awassa	SNNPR†	7°3'11.31"N	38°26'25.29"E	1995	12	12	7.4	Telford (1998); Telford *et al.* (1999); Lamb (2000); Lamb *et al.* (2002*a*)
Tilo	SNNPR	7°3'48.12"N	38°5'41.94"E	1995/1997	10	18/21	10.0	Telford (1998); Leng *et al.* (1999); Telford and Lamb (1999); Lamb (2000); Lamb *et al.* (2000, 2004); Leng and Marshall (2004)
Chamo	SNNPR	5°52'38.54"N	37°34'25.66"E	2010	14	14.3	7.5	Kassa (2013)

† Southern Nations, Nationalities and Peoples' Region

4.2 Lake core sites

4.2.1 Lake core sites in the Ethiopian Highlands: Ashenge and Hayk

Lake Ashenge

Ashenge, a closed-basin lake, is the most northerly of the lakes studied here (Fig. 4.2). The lake lies at an altitude of 2400 m a.s.l. and has an area of $\sim$ 20 km^2 with a maximum depth of $\sim$ 20 m. The Lake Ashenge catchment covers $\sim$ 82 km^2; ephemeral streams (Chegwar, Haynet, Shanfa Adewt, Ada Ala) drain into the north of the lake and there is currently no surface outflow (Marshall, 2006). Lake Ashenge is formed within a graben consisting of mid-Tertiary flood basalt. Quaternary alluvial, colluvial and lacustrine deposits outcrop on the basin floor (Marshall, 2006).

Lake Hayk

Lake Hayk is located $\sim$ 140 km to the south of Lake Ashenge, lying at an elevation of 2000 m a.s.l. (Fig. 4.3). Lake Hayk has a maximum depth of 88 m and an area of $\sim$ 23 km^2. The principal inflow for this closed lake basin is via the Anchercah River which flows into the southeastern corner of Lake Hayk; there is currently no surface outflow (Lamb *et al.*, 2007; Ghinassi *et al.*, 2012). Lake Hayk is located within an extensional basin which developed in $\sim$ 1000 m of Miocene-Early Pliocene basalts, tuffs and rhyolitic lava flows. These are overlain by Quaternary colluvial, alluvial and lacustrine deposits (Ghinassi *et al.*, 2012).

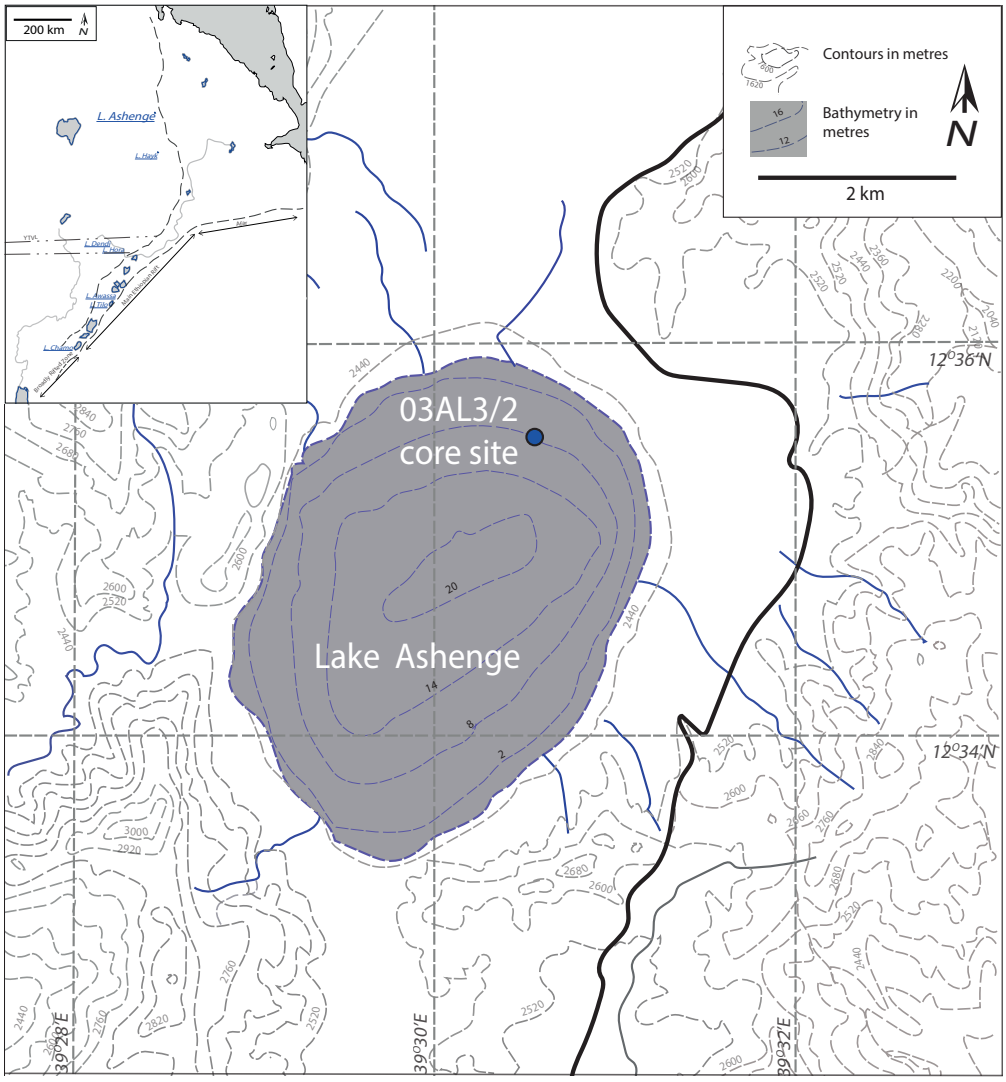

Figure 4.2: Lake Ashenge core 03AL3/2 location, indicated with blue circle. See inset for location of Lake Ashenge on the Ethiopian Plateau, northern Ethiopia.

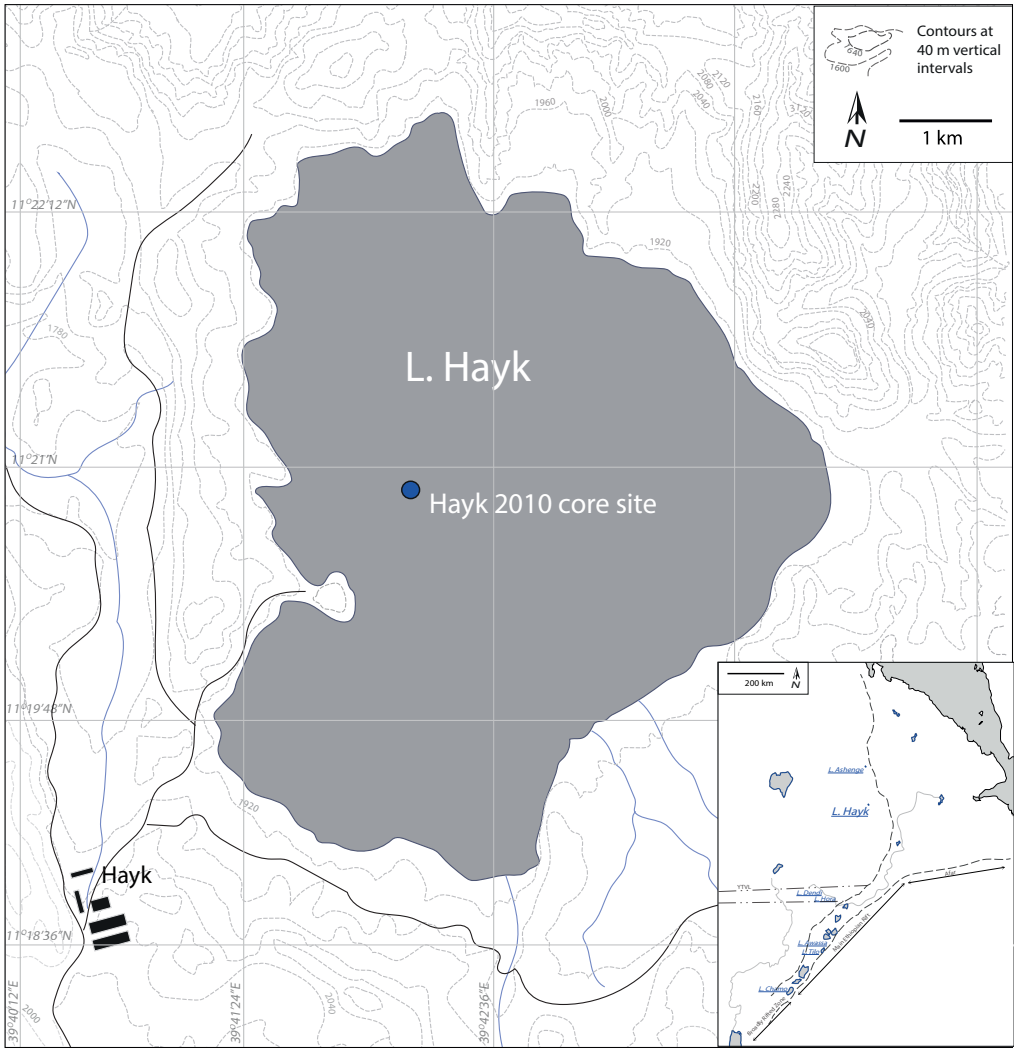

Figure 4.3: Lake Hayk 2010 core site (indicated with blue circle), see inset for location of Lake Hayk in the Ethiopian Plateau, northern Ethiopia.

Figure 4.4: (a) Lake Ashenge and (b) Lake Hayk, figure (b) from Ghinassi *et al.* (2012).

4.2.2 Lake core sites on the Yerer-Tullu Wellel Volcano Tectonic Lineament: Dendi and Hora

Lake Dendi

Lake Dendi is a double crater lake located 130 km west of Addis Ababa and at 2800 m a.s.l. (Fig. 4.5). The lake covers an area of 7.2 km^2 and has a maximum depth of 60 m. The lake has no permanent inlets and outlets, but is fed by seasonal springs and rivers during the rainy season.

The lake represents one of the central volcanoes aligned along the E-W trending Yerer-Tullu Wellel Volcano Tectonic Lineament (YTVL).

Lake Hora

Lake Hora is located at the town of Debre Zeit (Bishoftu) and $\sim$45 km to the south east of Addis Ababa at an elevation of 2000 m a.s.l. (Fig. 4.6). Lake Hora and the surrounding lakes Babogaya, Bishoftu, Kilole and Arenguade are maar lakes and collectively known as the Bishoftu Lakes. Lake Hora has a maximum depth of $\sim$ 38 m and an area of $\sim$ 1 km^2. The lake has no surface inlets or outlets and is fed by direct precipitation, run-off from the crater walls and by groundwater (Kebede *et al.*, 2002).

Lake Hora is located at the eastern limit of the Yerer-Tullu Wellel Volcano Tectonic Lineament, $\sim$100 km to the east of Lake Dendi. The bedrock in the Bishoftu area is comprised of 9 Ma-old basalts, overlain by $1-4$ Ma basaltic lavas and pyroclastics. Early Holocene volcanic activity in this area produced scoria cones, rhyolitic lava domes and the Bishoftu maars (Gasparon *et al.*, 1993).

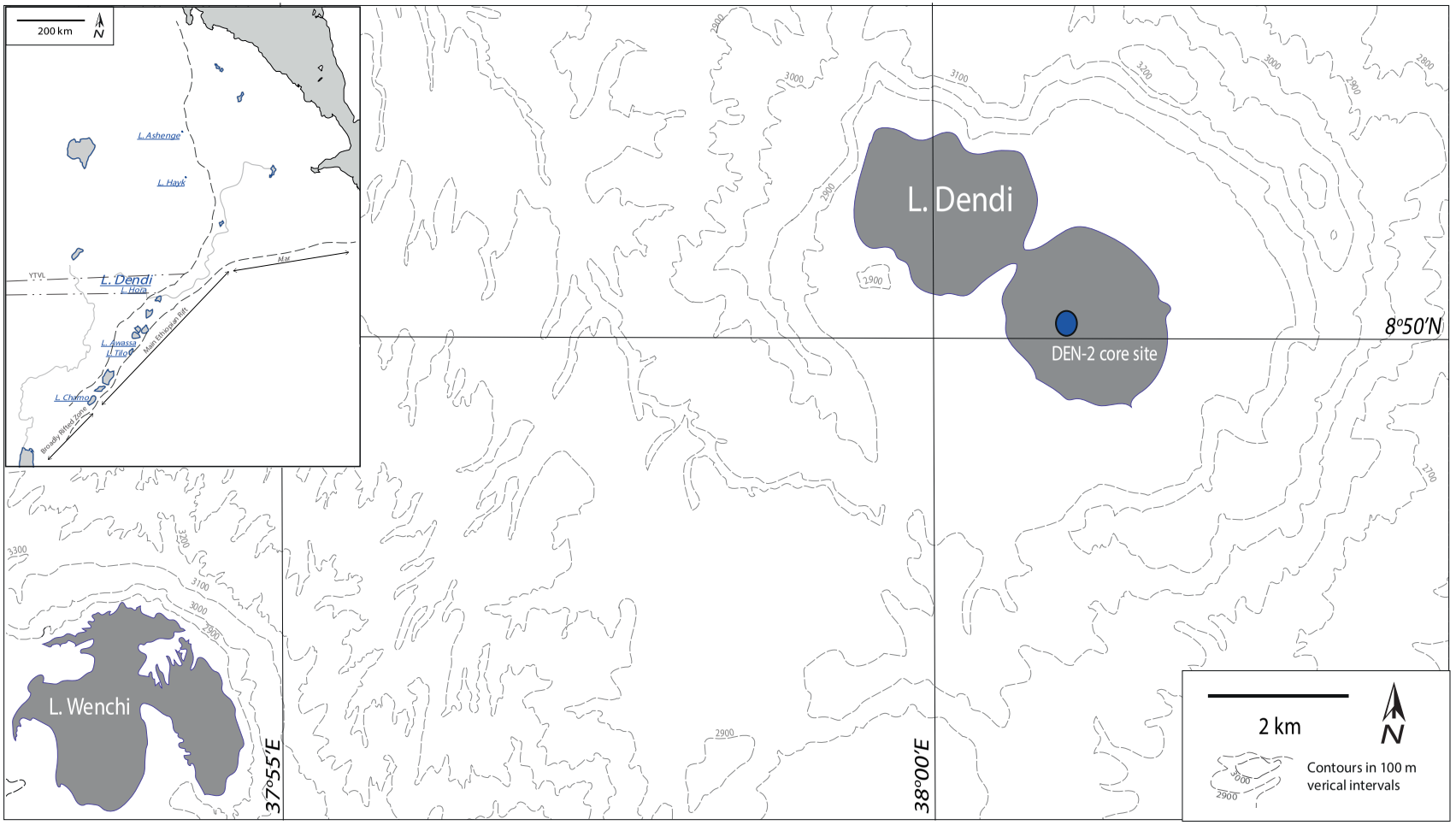

Figure 4.5: Location of DEN-2 in Lake Dendi, see inset for location of Dendi.

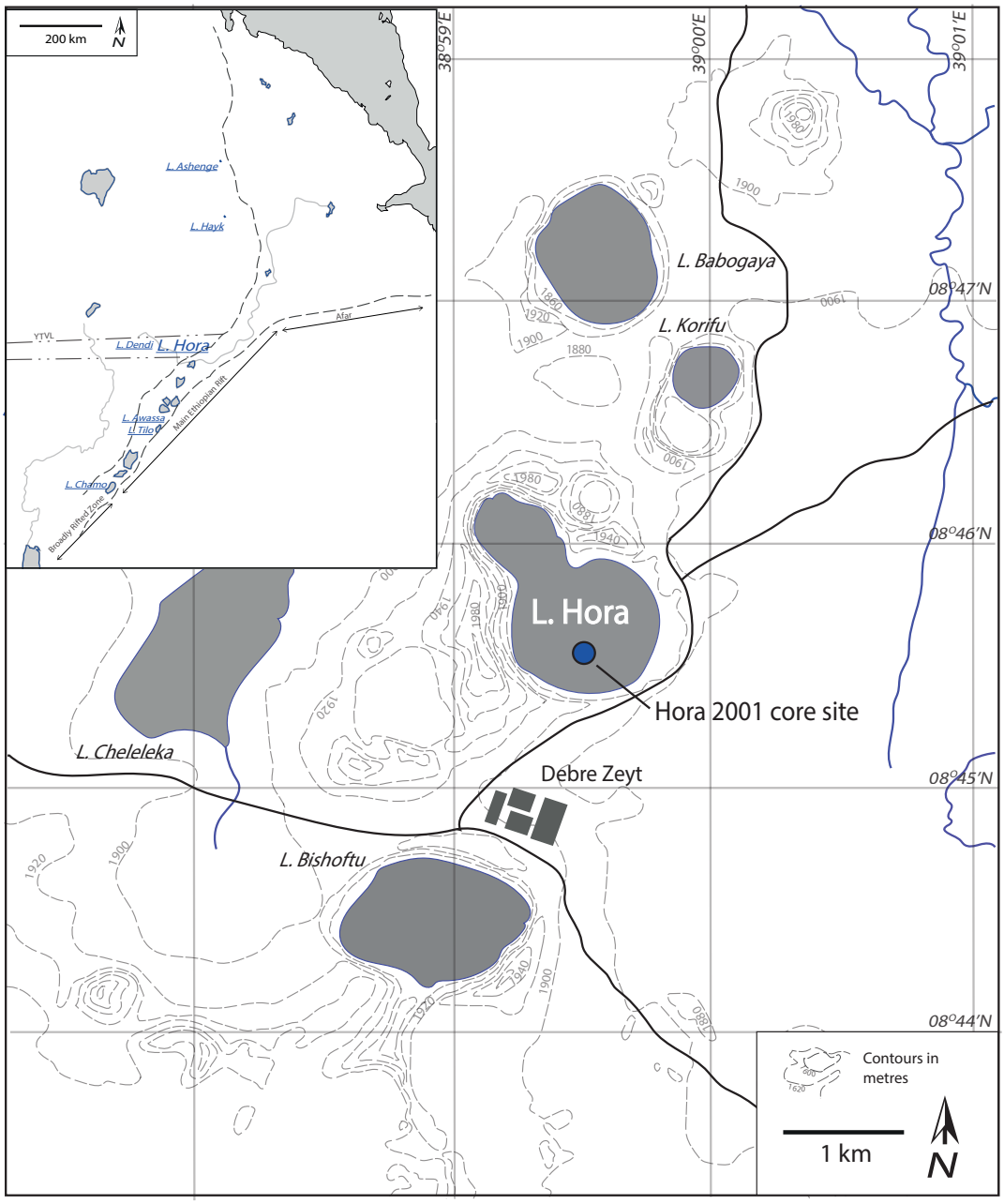

Figure 4.6: Lake Hora 2001 core site location, see inset for location of Lake Hora in Ethiopia.

Figure 4.7: (a) the infilled crater of Wenchi, 13 km to the west of Lake Dendi, (b) Lake Bishoftu, a maar lake located $\sim$ 1.5 km to the south of Lake Hora, images from Corti (2015).

4.2.3 Lake core sites in the Main Ethiopian Rift: Awassa, Tilo & Chamo

Lake Awassa

Lake Awassa is located in the central Main Ethiopian Rift and lies at an elevation of 1680 m a.s.l. (Fig. 4.8). The lake currently has a surface area of $\sim$ 92 km^2 with a maximum depth of 23 m. The lake is located within the nested Corbetti caldera complex which forms a $\sim$ 1300 km^2 closed drainage basin. Lake Awassa is fed by streams on the northern and western slopes of the catchment and the Tikur Wuha River which enters via the Dabashi swamp to the north-east (Lamb, 2000).

The oldest deposits within the Corbetti caldera were erupted from the Chilalo Volcano ($\sim$ 120 km to the NE) consisting of 4.5 – 1.5 Ma trachytic lavas and unwelded ignimbrites (WoldeGabriel *et al.*, 1990). Elsewhere in the catchment, highly faulted ignimbrites associated with the Wonji fault belt occur; on the eastern shores of Lake Awassa these are overlain by hyaloclastites (Di Paola, 1971, 1972). Wendo Koshe and Chabbi volcanoes within the Corbetti caldera and on the northern shore of Lake Awassa have erupted obsidian flows and peralkaline pumice falls recently (Fig. 4.8b) (Di Paola, 1971, 1972; Rapprich *et al.*, 2016). The most recent eruption from Wendo Koshe, at 400 BC (Rapprich *et al.*, 2016), produced a widespread pumice deposit that has been reworked and redeposited around the shores of Lake Awassa.

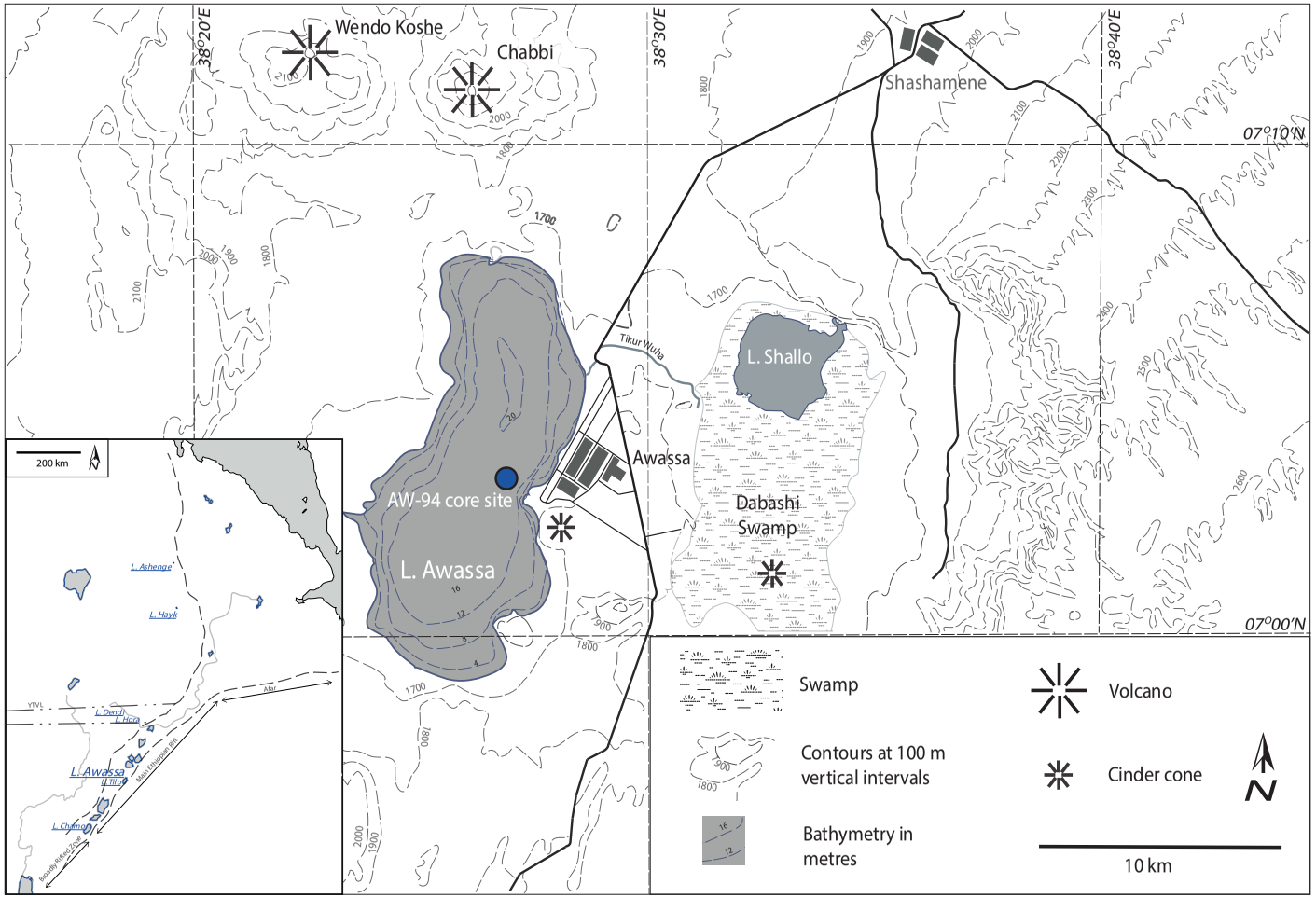

Figure 4.8: Core AW-94 core location in Lake Awassa (indicated with blue circle), see inset for the location of Lake Awassa in the CMER.

Lake Tilo

Lake Tilo is one of three crater lakes located 40 km to the west of Lake Awassa, at an elevation of 1550 m a.s.l. (Fig. 4.9). The crater lakes Budemeda, Tilo and Mechefera are orientated roughly north-south. Budemeda is the deepest of these lakes (~ 30 m) contained within a ~ 70 m crater. Mechefera is the shallowest (~ 5 m) within a ~ 30 m deep crater with a basaltic cinder cone in the centre. Tilo is intermediate in depth ($\sim 7-11$ m), with steep crater rims of $40-80$ m in height (Fig. 4.10b).

Ignimbrite deposits generally form the bedrock in the area surrounding Lake Tilo (Di Paola, 1972) and these are exposed at the base of the Tilo crater walls. Overlying this, $40-80$ m of pyroclastic deposits are exposed in the Tilo crater walls and a porphyritic basalt lava flow outcrops in the southern edge of the crater rim (Lamb *et al.*, 2002*a*). Lakes Budemeda, Tilo and Mechefera are probably maars occurring above an igneous dyke (Telford, 1998; Lamb, 2000).

Lake Chamo

Lake Chamo, the most southerly lake investigated in this study, is located ~ 140 km to the south-west of Lake Awassa and 6 km south of the town of Arba Minch. The lake lies at an elevation of 1100 m a.s.l. and has a surface area of ~ 551 km^2 with a maximum depth of 13 m (Kebede *et al.*, 1994; Kassa, 2013). The Kulfo River drains water from Lake Abaya into Lake Chamo and overflow from Lake Chamo ultimately drains into the Chew Bahir Basin. Lakes Chamo and Abaya were formerly part of a much larger drainage basin which includes Lakes Chew Bahir and Turkana, on the Ethiopia-Kenya border (Awulachew, 2006).

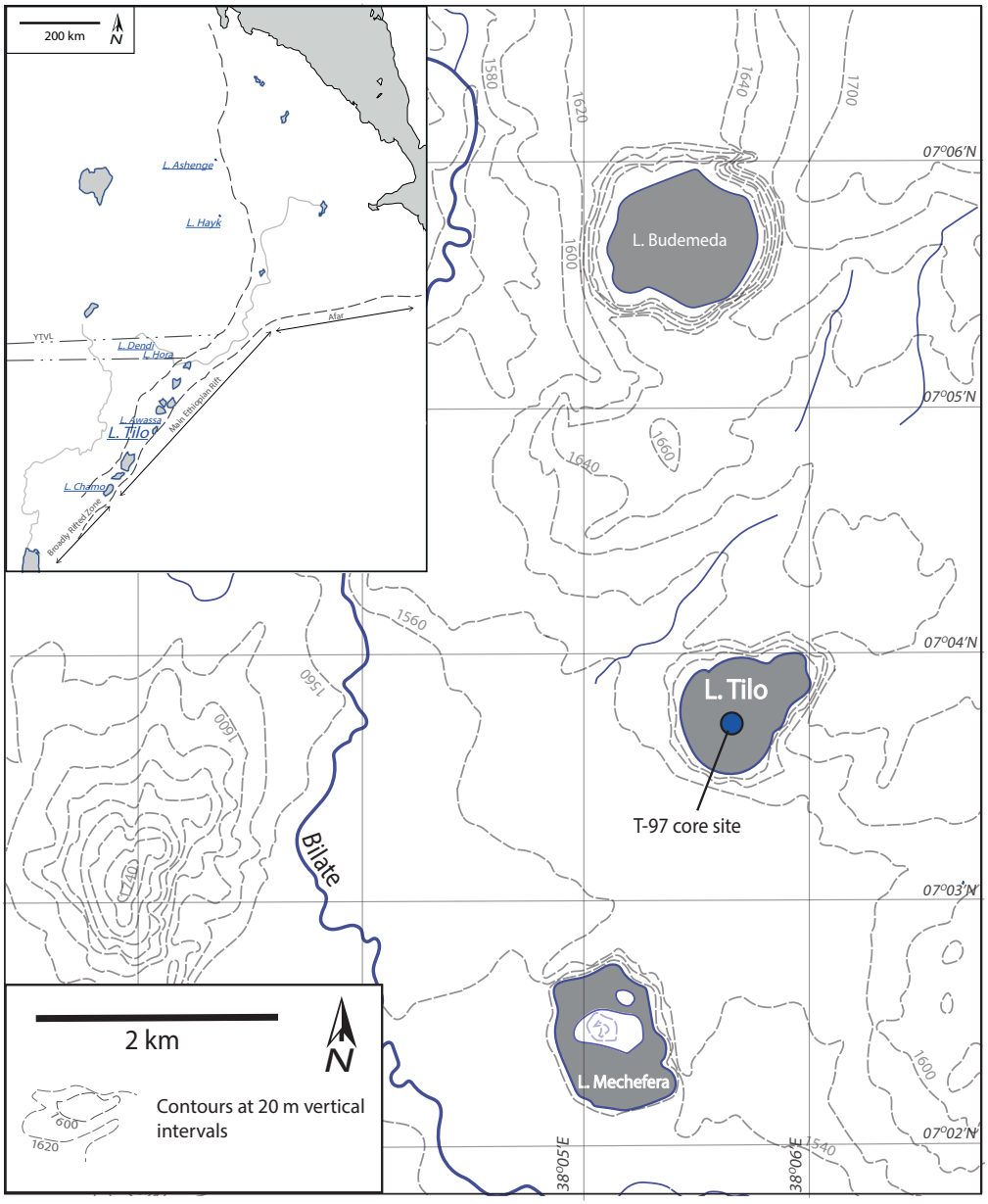

Figure 4.9: Lake Tilo T-97 core site, see inset for location of Lake Tilo in the CMER.

Figure 4.10: (a) the Corbetti caldera in which lake Awassa is situated (b) Lake Tilo, images from Corti (2015).

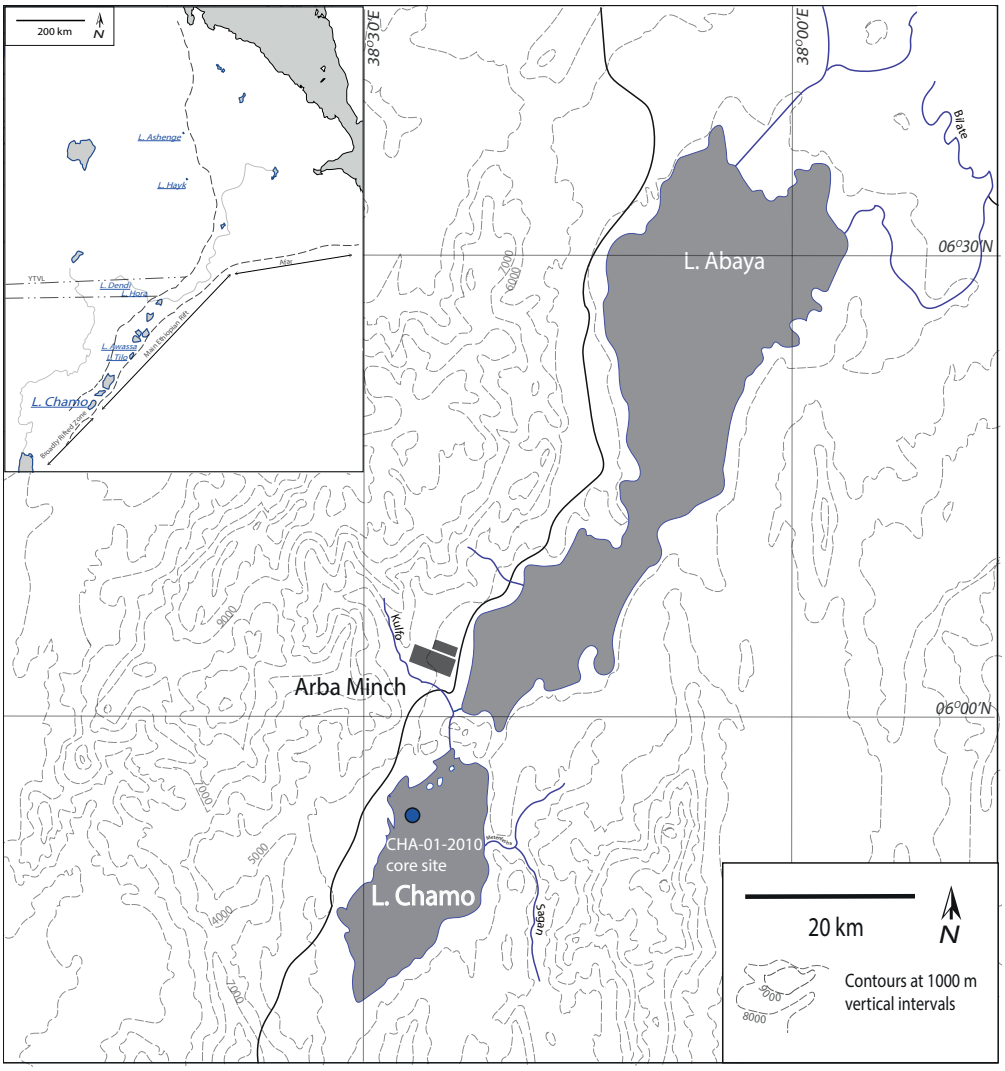

Figure 4.11: Location of core CHA-01-2010 collection in Lake Chamo, see inset for location of Lake Chamo in the CMER.

Lake Chamo occurs within the Ganjuli Graben, which extends from Lake Abaya to Konso, $\sim$ 80 km to the south. Lake Chamo is underlain by Precambrian crystalline basement and Eocene-Miocene mafic lava flows with Quaternary alluvial deposits outcropping above (Ebinger *et al.*, 1993; Nagaoka *et al.*, 2005). Lake Chamo is seperated from Lake Abaya by the Tosa Sucha (Bridge of God) chain of scoria cones; these may have been active historically and have produced olivine basalt flows (Ebinger *et al.*, 1993).

4.2.4 Proximal tephra samples

4.2.4.1 Proximal tephras from the Afar Rift

Details of a selection of samples collected from the Afar Rift are given below and are summarised in Table 4.2.

Dubbi

Two tephra samples were collected by C. Oppenheimer (University of Cambridge) from Dubbi volcano (Eritrea) in January 1998 (Fig. 4.13). Proximal deposits from the Dubbi 1861 eruption were studied by Wiart and Oppenheimer (2000) and are illustrated in the stratigraphic sections in Fig. 4.13. Glass samples from a pyroclastic density current deposit associated with the 1861 eruption have been analysed as part of this study.

Ayelu

Tephra samples were collected by G. WoldeGabriel (Los Alamos National Laboratory) from the Quaternary rhyolitic volcanic centre, Mount Ayelu, ($\sim$ 240 km to the north-east of Addis Ababa) and the surrounding areas during field work in 2000 (Fig. 4.14). Four late Pleistocene tephra samples were collected from

Figure 4.12: The Tosa Sucha chain of scoria cones, which separates Lake Abaya (to the left of image) from Lake Chamo (to the right of images), images from Corti (2015).

Table 4.2: Tephra and samples collected from Dubbi and Ayelu volcanoes in the Afar Rift, collected by C. Oppenheimer (C.O.) and G. WoldeGabriel (G.W.).

Sample ID	**Sample area**	**Latitude**	**Longitude**	**Sample type**	**Collected by**
Dubbi 1	Dubbi	13°30'53"N	41°42'48"E	PDC deposit	C. O.
Dubbi 2	Dubbi	13°30'53"N	41°42'48"E	PDC deposit	C. O.
MA00-2	Ayelu - E. Yardi Flood Plain	10°15'37"N	40°31'38"E	Ash-flow tuff	G.W.
MA00-4	Ayelu - E. Yardi Flood Plain	10°15'37"N	40°31'38"E	Reworked pumice	G.W.
MA00-7	Ayelu - E. Yardi Flood Plain	10°15'37"N	40°31'38"E	Ash-flow tuff	G.W.
MA00-8	Ayelu - E. Yardi Flood Plain	10°15'37"N	40°31'38"E	Ash-flow tuff	G.W.
MA00-9	Base of Mt. Ayelu	10°10'51"N	40°37'35"E	Ash-flow tuff	G.W.
MA00-10	Base of Mt. Ayelu	10°10'51"N	40°37'35"E	Ash-flow tuff	G.W.
MA00-11	Base of Mt. Ayelu	10°10'51"N	40°37'35"E	Ash-flow tuff	G.W.
MA00-12	Base of Mt. Ayelu	10°10'51"N	40°37'35"E	Pumice fallout	G.W.
MA00-13	Base of Mt. Ayelu	10°10'51"N	40°37'35"E	Ash-flow tuff	G.W.
MA00-14	Base of Mt. Ayelu	10°10'51"N	40°37'35"E	Pumice fallout	G.W.

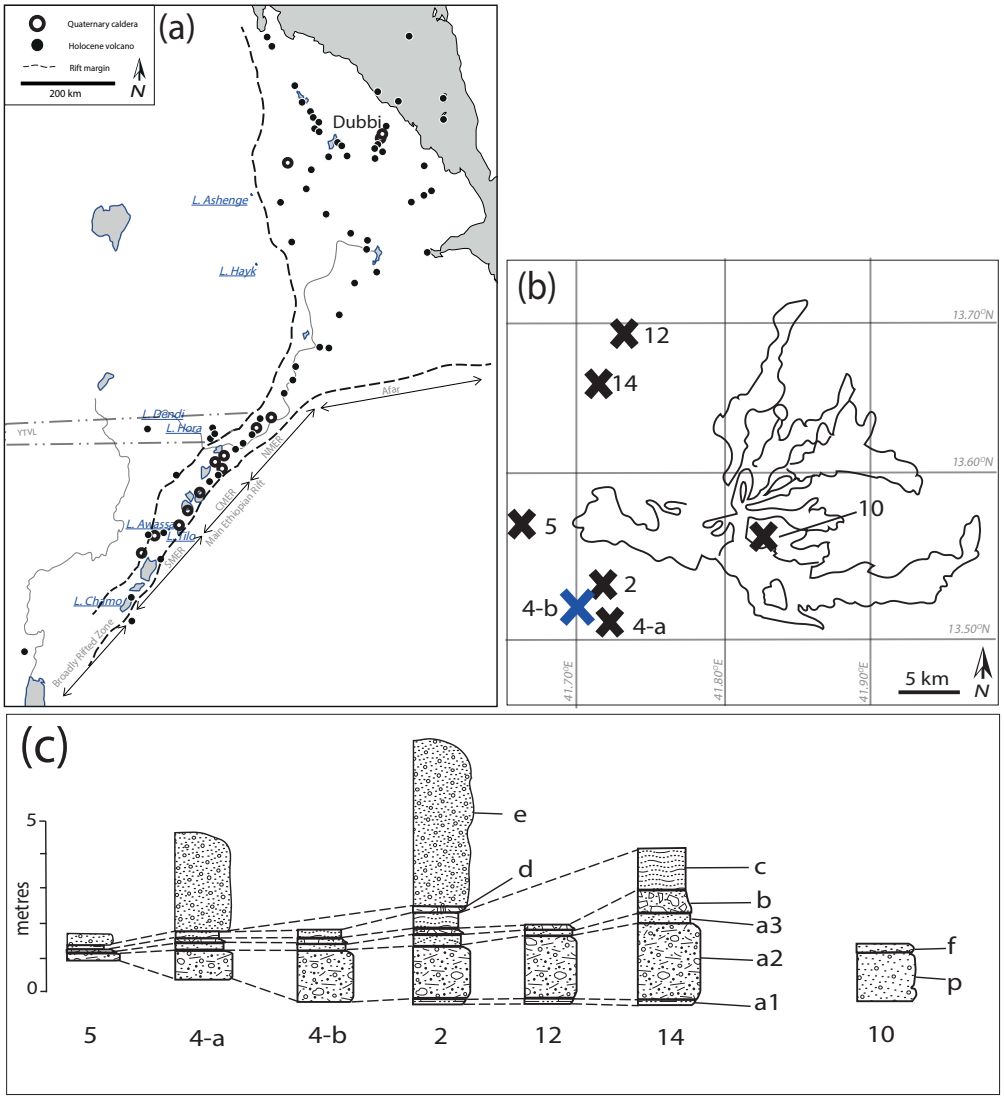

Figure 4.13: (a) Location of Dubbi in the Afar Rift, (b) Schematic of Dubbi volcano with stratigraphic sections logged by Wiart and Oppenheimer (2000) indicated with crosses, tephra from site 4-b (blue cross) has been analysed in this study, (c) Stratigraphic sections logged by Wiart and Oppenheimer (2000) from the areas around Dubbi volcano. a: Pyroclastic flow deposit (a1 = basal unit, a2 = pumice flow deposit, a3 = coignimbrite ash), b: scoria fall deposit, c: pyroclastic flow deposit, d: reworked deposit, e and p: pumice fall deposits, f: scoria fall deposits. Figures (b) and (c) are adapted from Wiart and Oppenheimer (2000).

the Bouri Formation on the East Yardi Flood Plain (Fig. 4.14). In order to check whether the Bouri Formation tephras were locally derived, six tephra samples were also collected from the north western slopes of the Ayelu volcano ($\sim$ 30 km to the SE of the East Yardi Flood Plain).

Figure 4.14b shows the location of samples collected from the eastern side of the Awash River Flood Plain and the base of Mount Ayelu; Fig. 4.14c shows stratigraphic sections at the two sampling localities.

4.2.4.2 Proximal tephras from the central Main Ethiopian Rift

Details of a selection of samples collected from the central Main Ethiopian Rift are given below and are summarised in Table 4.3 - a broad overview map of samples from this area is shown in Fig. 4.15.

Awassa and Tilo

During field campaigns in 1995 and 1997, N. Pearce (Aberystwyth University) collected a selection of tephra and obsidian samples from the shores of Lakes Tora, Awassa and Tilo and these have been analysed in this study.

Sample localities around Lake Awassa and inside the Corbetti caldera are seen in Fig. 4.16. Obsidian samples were collected from the northern shores of Lake Awassa (E95010, E95011 and E95019) and a small quarry on the Wondo-Genet - Shashamene road to the east of the Lake (E95003). Tephras were also sampled to the east of Lake Awassa, from a gully section on the Awassa - Shashamene road (E95006 and E95007) and from the Shallo swamp (ST1-NW).

Two samples were also collected from the northern shores of Lake Tilo (Fig. 4.17b) ; an obsidian clast (E95025) within an ignimbrite and, $\sim$ 600 m to the west, a pumice sample (E97003).

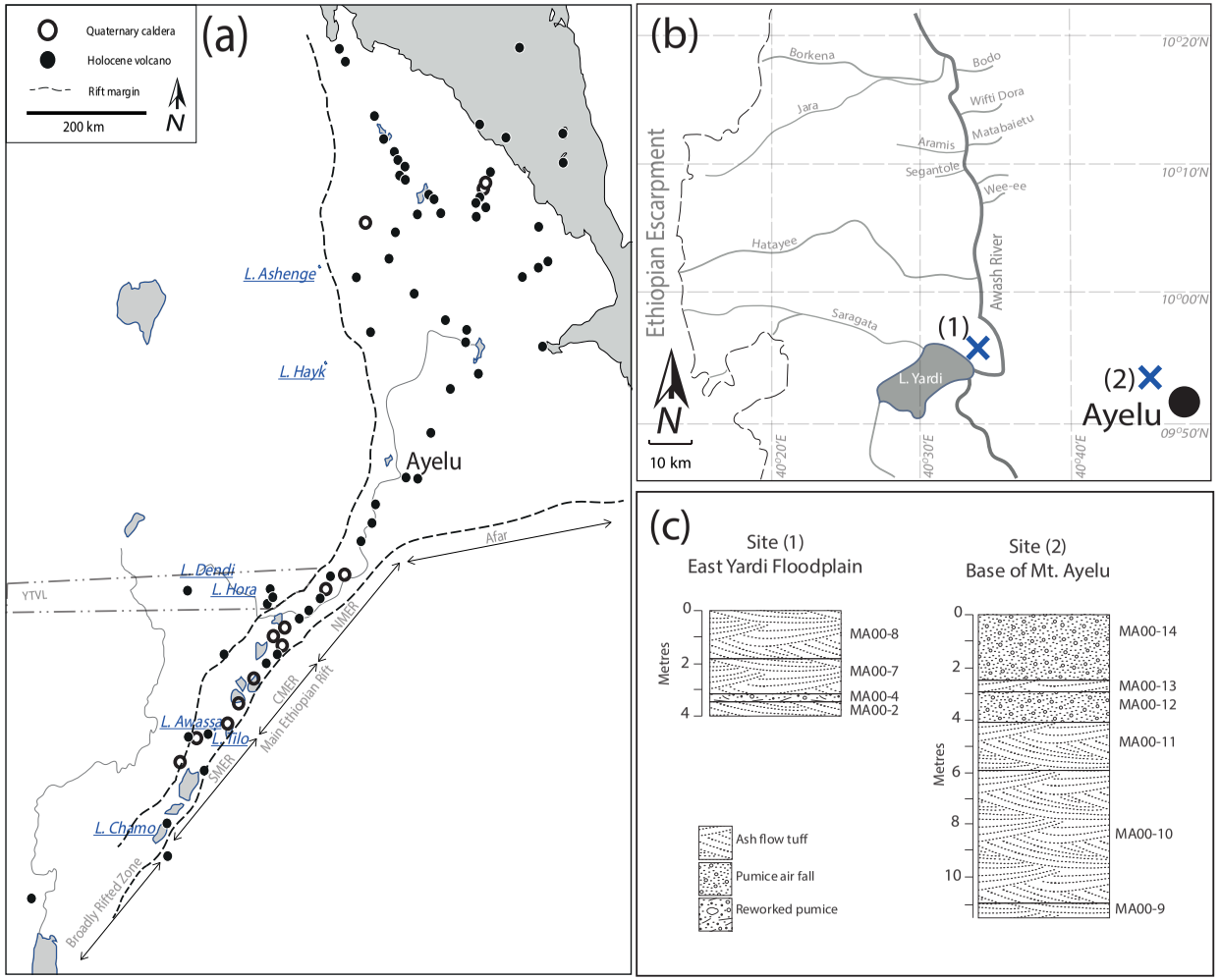

Figure 4.14: (a) Location of Ayelu in the Afar Rift; (b) Tephra sampling points surrounding Lake Yardi and the Ayelu volcano, samples points are indicated with blue crosses: (1) East Yardi Floodplain and (2) Base of Mt. Ayelu and (c) Stratigraphies at the East Yardi Floodplain and Base of Mt. Ayelu, tephra samples collected are labelled.

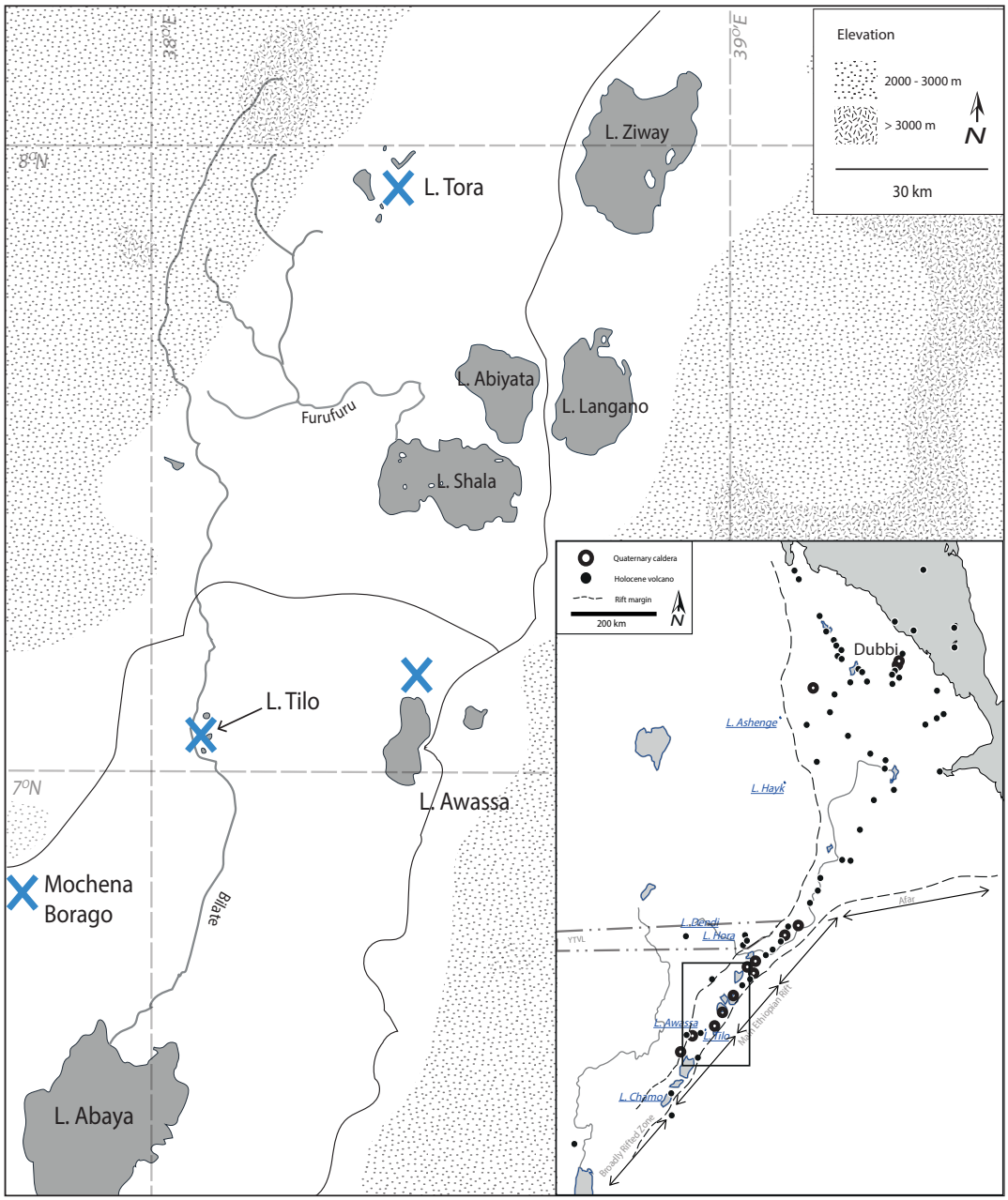

Figure 4.15: Locations of samples collected in Central Main Ethiopian Rift; for location in Ethiopia see inset. Tephra sample locations shown with blue crosses; samples from areas surrounding Lake Tora, Awassa and Tilo were collected by N. Pearce. Tephra samples collected from the Mochena Borago Rockshelter were collected by S. Meyer.

Table 4.3: Tephra and obsidian samples collected from locations throughout the central Main Ethiopian Rift, collected by N. Pearce (N.P.), H. Lamb (H.L.) and S. Meyer (S.M.)

Sample ID	Sample area	Latitude	Longitude	Sample type	Collected by
E95003	Lake Awassa: Quarry to east	7°7'34.03"N	38°55'55.94"E	Obsidian	N.P.
E95006	Lake Awassa: Shashamene-Awassa road cut	7°9'18.57"N	38°31'13.35"E	Tephra	N.P.
E95007	Lake Awassa: Shashamene-Awassa road cut	7°9'18.57"N	38°31'13.35"E	Tephra	N.P.
E95010	Lake Awassa: Promontory on northern shore	7°7'40.73"N	38°26'49.56"E	Obsidian	N.P.
E95011	Lake Awassa: Promontory on northern shore	7°7'40.73"N	38°26'49.56"E	Weathered obsidian	N.P.
E95019	Lake Awassa: Hill on northern shore	7°8'15.06"N	38°26'36.17"E	Obsidian xenoliths	N.P.
E95025	Lake Tilo: northern shore	7°3'56.36"N	38°6'4.34"E	Obsidian xenolith	N.P.
E97003	Lake Tilo: northern shore	7°3'56.36"N	38°6'4.34"E	Pumice in ignimbrite	N.P.
ST1-NW	Lake Awassa: Shallo Swamp	7°4'8.85"N	38°32'34.99"E	Pumice	H.L.
M14 0.27 m NW	Mochena Borago Rockshelter: Trench M14	6°52'58.40"N	37°46'5.35"E	Tephra	S.M
M14 0.47 m SW	Mochena Borago Rockshelter: Trench M14	6°52'58.40"N	37°46'5.35"E	Tephra	S.M
M14 0.75 m NE	Mochena Borago Rockshelter: Trench M14	6°52'58.40"N	37°46'5.35"E	Tephra	S.M
TU2	Mochena Borago Rockshelter: Trench TU2N	6°52'58.40"N	37°46'5.35"E	Tephra	S.M

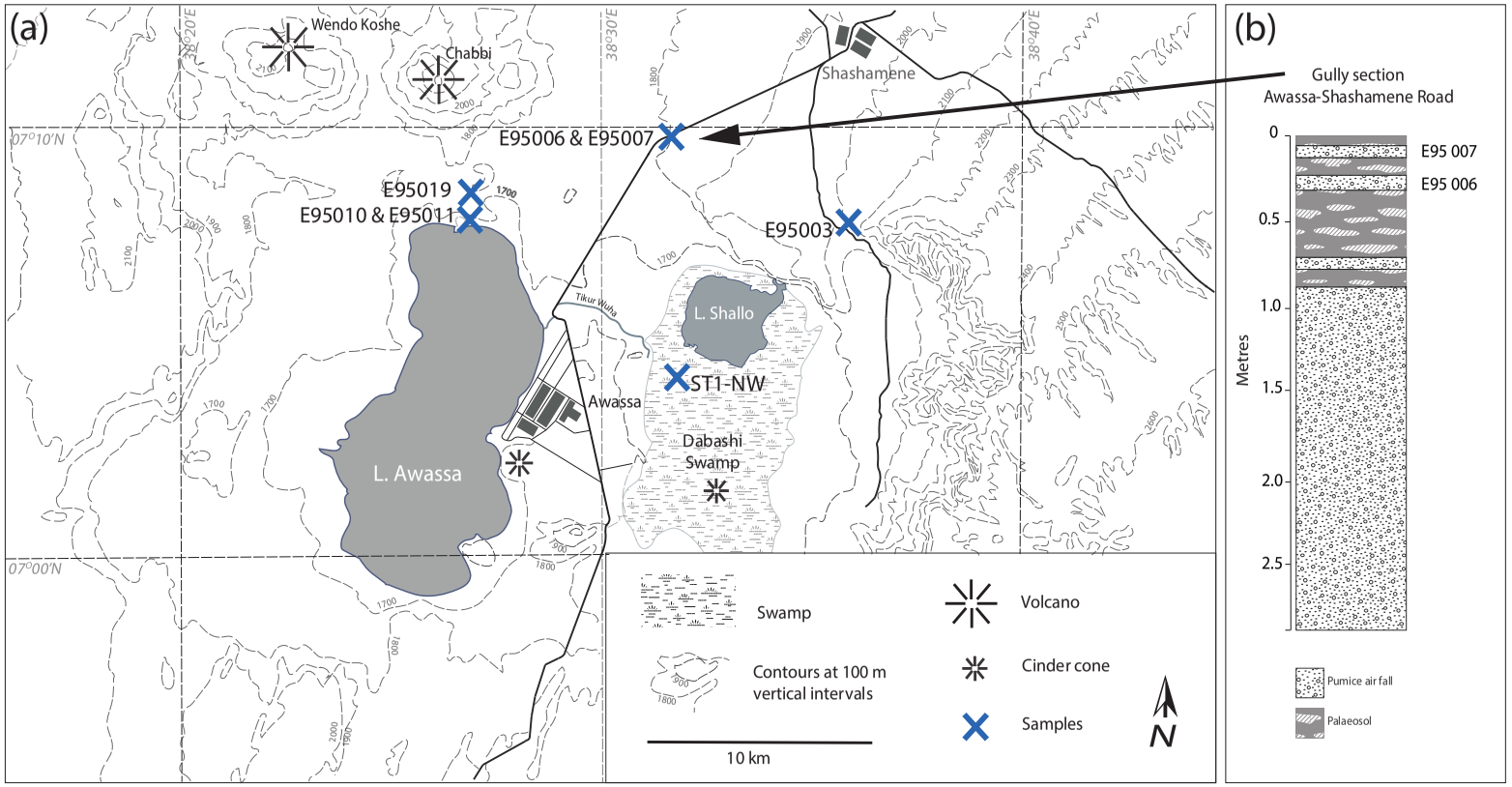

Figure 4.16: (a)Location of tephra samples collected from the Awassa area. E95003: obsidian collected from Quarry in the Awassa caldera wall; E95006 and E95007: tephras sampled from Awassa-Shashamene road-cut; E95010 and E95011: obsidians sampled from the northern shores of Lake Awassa; E95019: grab sample from pumice cone on northern shores of Lake Awassa; ST1-NW: sample from pumice layer. (b) Stratigraphic log noted by N. Pearce (Aberystwyth University) at the Awassa-Shashamene road cut.

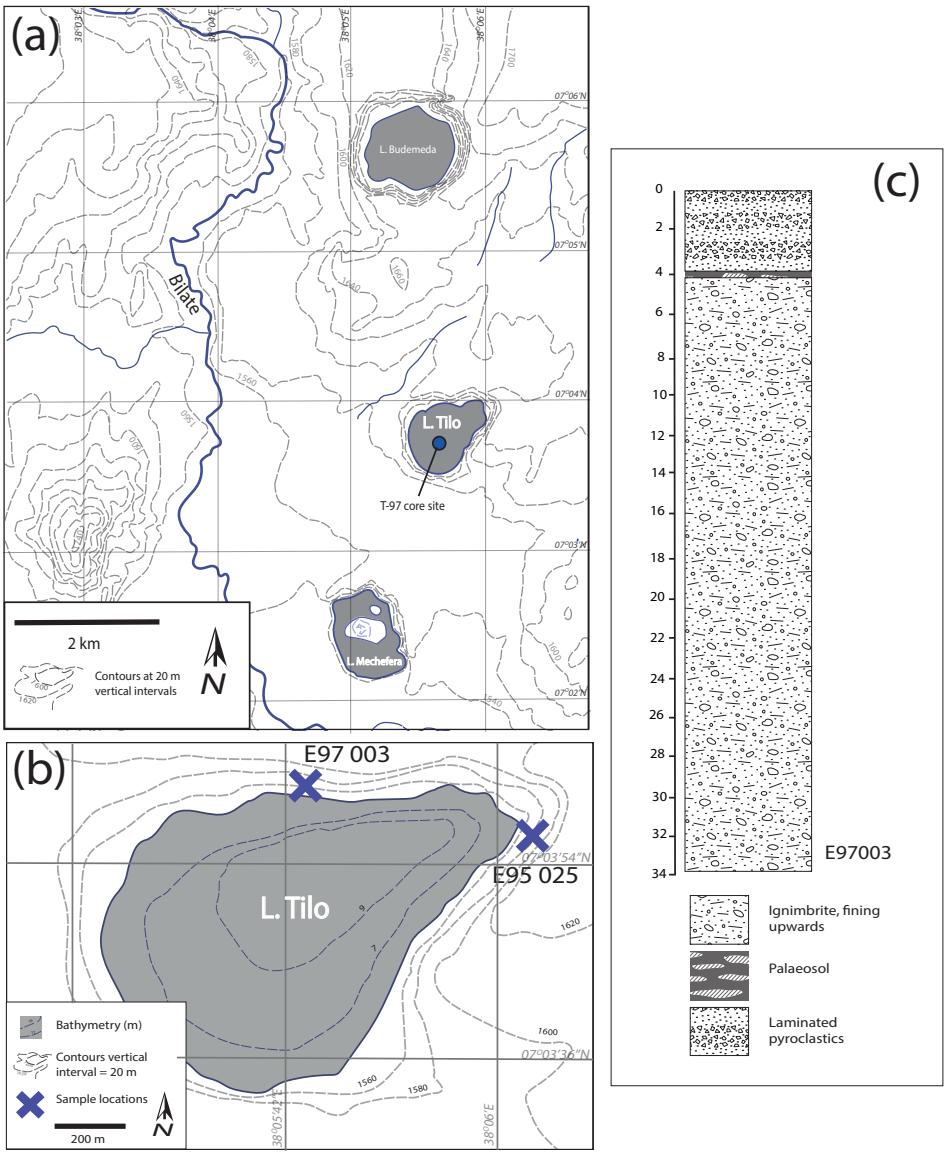

Figure 4.17: (a) and (b) Location of tephra samples collected from the shores of Lake Tilo, crosses indicate the locations from which and E95025 and E97003 were collected (c) Section showing lithology of the northern shore of Lake Tilo, noted by N. Pearce (Aberystwyth University). Sample E97003 was collected from the 'Valley Floor Ignimbrites' comprising the base of the sequence.

Mochena Borago Rockshelter

The Mochena Borago Rockshelter is located on the south-western flanks of Mount Damota (Fig. 4.18), a trachytic volcano $\sim$ 40 km to the southwest of Lake Tilo. The Mochena Borago Rockshelter deposits and archaeological finds are described in detail by Brandt *et al.* (2012). The rockshelter is formed within a non-welded ignimbrite which is under and overlain by mafic lava flows. Deposits on the cave-floor range in age from $\sim$53 ka to Holocene.

Three tephra deposits occur in sediments on the cave-floor. The oldest 'YBT' tephra is 20 cm thick, yellow-brown coloured and radiocarbon dates on charcoal give an age of 45.4 cal. ka BP. Deposits of clay rich silt separate the YBT tephra from a younger, $\sim$12 cm thick'YBS' ash and gravel rich volcaniclastic mud flow containing charcoal fragments with a radiocarbon age of 43.1 cal ka BP. This deposit is overlain by silty clay deposits. The youngest 'BWT' tephra caps a major unconformity in the Late Pleistocene sediments. The deposit is white in colour, $\sim$20 cm thick and radiocarbon dates on charcoal fragments in the BWT tephra give an age of 7.6 cal. ka BP. However, feldspars in the BWT tephra have an $^{40}Ar/^{39}Ar$ age of 3.16 $\pm$0.07 Ma. Brandt *et al.* (2012) suggest that the older feldspars within this Holocene tephra may be derived from the older ignimbrite in which the Mochena Borago Rockshelter has formed.

Samples from the youngest Holocene BWT tephra were collected by S. Meyer (University of Cologne) from the Mochena Borago Rockshelter and analysed as part of this study. The proximity of the Mochena Borago rockshelter to Lake Tilo may mean that there is potential for correlations between these sites, improving the Mochena Borago chronology.

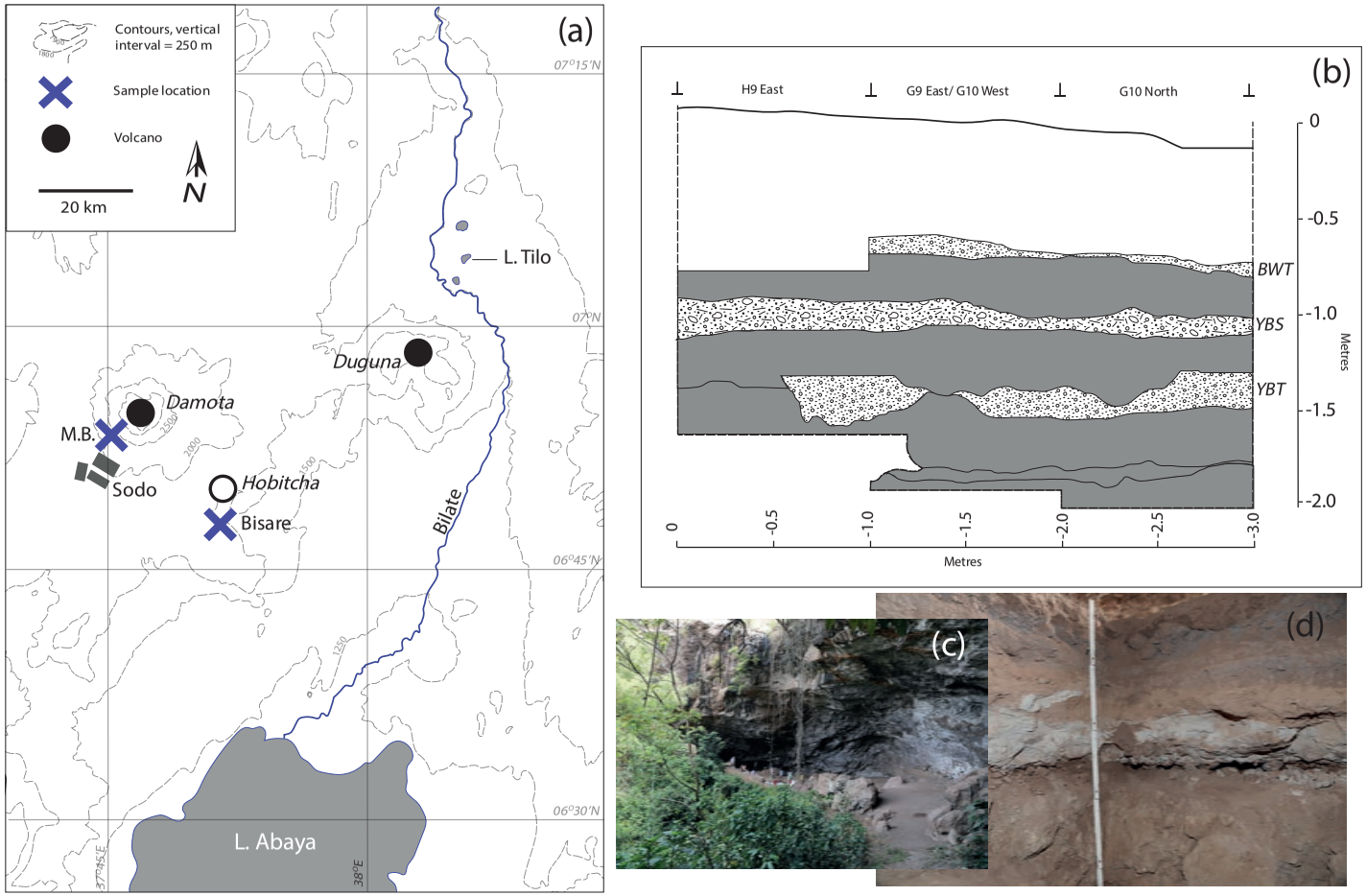

Figure 4.18: (a) Location of samples collected from the Mochena Borago Rockshelter and Bisare (marked with blue crosses) (b) Stratigraphy of the Mochena Borago Rockshelter sediments, containing three tephras: YBT, YBS and BWT (from Brandt *et al.* (2012), the BWT was analysed in this study, Photos provided by S. Meyer of (c) the Mochena Borago Rockshelter and (d) The BWT tephra.

4.3 Chronology

4.3.1 Lake cores

In this study, tephras in lake cores are dated indirectly on the basis of their modelled radiocarbon age. Most of the sediment cores used here have been previously studied (see Table 4.1), and their radiocarbon dates calibrated against the varying models available at that time.

A combination of new and previously published radiocarbon dates provide the chronologies for the seven lake archives studied here. Tilo sediments were dated using airfall sedimentary charcoal and the Chamo archive was dated using a combination of shell and plant material analyses. All other core sediments were dated using bulk sediment samples. The AMS ^{14}C measurements for the lake sediments are shown in Tables 4.4 and 4.5.

Samples for radiocarbon dating were digested in 2 M HCl for 8 h at 80°C, washed with distilled water and homogenised. Pre-treated samples were heated with CuO in sealed plastic tubes to recover the CO_2, which was then converted to graphite by Fe/Zn reduction. The radiocarbon was then measured using accelerator mass spectrometry at: Scottish Universities Environmental Research Centre (Ashenge), Oxford Radiocarbon Accelerator Unit, University of Oxford (Hayk) 14 CHRONO Centre, Queen's University Belfast (Hayk), Beta-Analytic (Hora, Awassa and Tilo) and the Cologne AMS Center (Dendi and Chamo).

Radiocarbon ages were recalibrated using IntCal13 (Reimer *et al.*, 2013), ensuring the ages of tephras in different archives could be compared. Unfortunately, due to uncertainities over coring depths for the Hora sediments, coupled with age reversal throughout the core, a new age model was not generated for this archive. Bayesian P_Sequence depositional models were run for Ashenge, Hayk, Awassa,

Tilo and Chamo sequences, using OxCal version 4.2 (Bronk Ramsey, 2009*a*) with outlier analysis (Bronk Ramsey, 2009*b*). Bernd Wagner (University of Cologne) supplied the Bayesian age model for the Dendi sediments, generated using Bacon software (Blaauw and Christen, 2011). Bayesian models do not assume uniform sedimentation rate or attempt to wiggle match to a calibration curve, whilst P_Sequence models allow for less rigid modelling of the data. Outlier analysis includes ages identified as statistical outliers in the model, but they are given a lower weight. Prior to analysis, sediment depths were converted to event free depths that do not include tephras of > 0.5 cm thickness, which are presumed to have been deposited instantaneously. Due to the presence of a significant hiatus at around 650 cm depth in the Lake Ashenge 03AL3/2 stratigraphy, separate P_Sequence age models were run to model deposition above and below this point. Interpolated tephra ages were retrieved using the *Date* function and are quoted herein as 95.4 % confidence intervals. These new age models are seen in Chapter 5 and were used to calculate tephra ages which include uncertainties in the modelled interpolation.

4.3.2 Proximal tephras

Samples collected from a recent tephra deposit at Dubbi volcano are associated with an eruption of the volcano dated at 1861 by historical accounts. Tephras sampled from the Lake Yardi area at the base of Ayelu have not been directly dated. However, they occur within the Bouri Formation, which has been divided into three chronostratigraphic sequences: Hatayae ($2.5 - 1.0$ Ma), Dakanihylo ($1.0 - 0.26$ Ma) and Herto ($0.25 - 0.16$ Ma) based on ^{40}Ar/^{39}Ar dating of tephras and biostratigraphy (de Heinzelin *et al.*, 1999; Asfaw *et al.*, 2002; Clark *et al.*, 2003). Whilst these tephras are older than Holocene tephras investigated in

Table 4.4: AMS ^{14}C measurements for the Ashenge and Hayk lake sediment cores. All analyses were undertaken on bulk sediment samples. Dates on Ashenge sediments from Marshall *et al.* (2009) are indicated in bold. Ages were calibrated using IntCal13 (Reimer *et al.*, 2013) run in OxCal version 4.2 (Bronk Ramsey, 2009*a*). * Sample SUERC-7178 from 645.5 cm depth was reanalysed (SUERC-7439) using archived CO_2 from original sample, both dates have been combined using the *R_Combine* function.

Laboratory number	**^{14}C ages yr BP ($\pm$ 1 σ)**	**Depth (cm)**	**δ^{13}C (‰PDB)**	**Calibrated ages yr BP**
Ashenge				
SUERC-29473	378 $\pm$ 37	3.5	-22.6	507 – 316
SUERC-6263	618 $\pm$ 31	51.5	-20.9	658 – 550
SUERC-29476	923 $\pm$ 35	104.5	-21.7	927 – 776
SUERC-6264	1609 $\pm$ 22	175.5	-24.0	1553 – 1415
SUERC-29477	2082 $\pm$ 37	246.5	-24.4	2150 – 1951
SUERC-6265	2865 $\pm$ 28	300.5	-23.0	3069 – 2883
SUERC-29478	3298 $\pm$ 35	341.5	-22.0	3611 – 3450
SUERC-29479	4143 $\pm$ 38	386.5	-22.2	4808 – 4527
SUERC-6266	4714 $\pm$ 30	440.5		5581 – 5324
SUERC-29480	4361 $\pm$ 38	485.5	-23.6	5039 – 4852
SUERC-6268	5063 $\pm$ 34	551.5	-22.1	5907 – 5741
SUERC-29481	5671 $\pm$ 39	600.5	-22.5	6564 – 6324
SUERC-7178	6696 $\pm$ 40	645.5	-20.8	7581 – 7476
SUERC-7439 *	6622 $\pm$ 40	645.5		*7581 - 7476*
SUERC-6269	10127 $\pm$ 66	657	-23.4	12015 – 11398
Beta-187297	11920 $\pm$ 40	739.5	-25.1	13961 – 13574
SUERC-6270	12810 $\pm$ 99	771.5	-21.3	15675 – 15005
Hayk				
UBA-27072	1583 $\pm$ 32	12.5		1546 - 1395
OxA-30960	2485 $\pm$ 32	100	-23.4	2729 - 2434
OxA-30883	2795 $\pm$ 31	140	-23	2974 - 2796
UBA-25092	3563 $\pm$ 36	172		3973 - 3724
OxA-30885	4068 $\pm$ 33	183	-23.1	4802 - 4436
OxA-30886	4914 $\pm$ 35	196	-23.6	5717 - 5591
OxA-30887	7650 $\pm$ 45	240	-24.2	8541 - 8383
UBA-27073	9643 $\pm$ 79	314.5		11193 - 10722
UBA-27074	10102 $\pm$ 44	396.5		11987 - 11415
UBA-25093	10393 $\pm$ 45	429		12237 - 11838
UBA-25094	10287 $\pm$ 46	442		12368 - 12020
UBA-27075	10254 $\pm$ 62	447.5		12383 - 12029
UBA-27076	12846 $\pm$ 67	657.5		15465 - 15069
UBA-25095	12873 $\pm$ 60	717.5		15726 - 15261

Table 4.5: Conventional AMS ^{14}C measurements for the Awassa, Tilo and Chamo lake sediment cores. Dates for Awassa are from Telford (1998), Tilo dates are from Telford and Lamb (1999) and Chamo dates are from (Kassa, 2013).

Laboratory number	**^{14}C ages yr BP ($\pm$ 1 σ)**	**depth (cm)**	**δ^{13}C (‰PDB)**	**Calibrated ages yr BP**	**Dated material**
Awassa					
Beta-100436	1450±80	259	-20.9	403 – 761	Bulk sediment
Beta-100437	3180±90	522	-19.9	1264 – 1684	Bulk sediment
Beta-81512	4500±110	687.5	-19.5	2532 – 3486	Bulk sediment
Beta-81513	6270±130	1132.5	-24.4	4935 – 5557	Bulk sediment
Tilo					
Beta-106145	1390±50	180	-15.9	556 – 764	Charcoal
Beta-106146	2400±50	347	-15.9	391 – 753	Charcoal
Beta-106147	4140±60	594.5	-19.1	2504 – 2888	Charcoal
Beta-90886	5520±80	804	-18.1	4070 – 4532	Charcoal
Beta-106148	6880±50	1289.5	-17.3	5664 – 5878	Charcoal
Beta-90887	7930±90	1764	-21.1	6613 – 7062	Charcoal
Beta-106149	8840±50	2316.5	-15.6	7763 – 8226	Charcoal
Chamo					
COL1244.1.1	1240±30	639	-12.7	670 – 861	Plant material
COL1246.1.1	1490±80	664	-56	410 – 711	Plant material
COL2455	3304±40	865.5	-18.7	234 – 19	Plant material
COL1240.1	4080±20	986	-2.4	2161 – 2839	Shell
COL1241.1	3980±50	987	4.4	2353 – 2943	Shell
COL1247.1.1	6580±30	1289	-34.8	3719 – 5618	Plant material

this study their geochemistry can still be used for broad comparison to identify potential volcanic sources.

Radiocarbon dates on charcoal within the BWT from Mochena Borago give an age of $7,589 \pm 689$ cal yr. BP. However, $^{40}Ar/^{39}Ar$ dates on (possibly older contaminant) feldspar within the tephra gives an age of 3.16 ± 0.07 Ma (Brandt *et al.*, 2012). Tephra and obsidian samples from Awassa, Tilo and Tora (in the CMER) do not have age control, but it is possible that they are contemporaneous with the Holocene tephras recorded in the lake sediments.

4.4 Tephra identification and analysis

4.4.1 Tephra sampling and laboratory processing

4.4.1.1 Visible tephra sampling

Tephras within lake sediment cores were described, recorded and imaged by the present author at LacCore (University of Minnesota). Tephras were sampled from the cores into sterile, labelled centrifuge tubes, taking care to avoid cross contamination. Tephra samples were wet sieved to $90 - 250$ μm and dried at 60°C. Where tephra in cores exceeded 5 cm thickness, subsamples were collected from the horizon, either at intervals of 5 cm or where a lithological change was noted. Coarser sand and gravel grade tephra were first disaggregated using an agate pestle and mortar and all samples were sieved to >25 μm.

4.4.1.2 Cryptotephra identification

Glass shard counting

Non-visible tephra horizons were primarily identified in lake cores through

extracting and counting the tephra glass shards within the host sediments. The procedure involves two stages: firstly the collection of continuous and contiguous sediment samples at a low resolution ($\sim$ 10 cm depth samples); followed by high resolution $\sim$1 cm sampling across a 10 cm region to pinpoint the tephra isochron (Lane *et al.*, 2014; Davies, 2015) (Fig. 4.19).

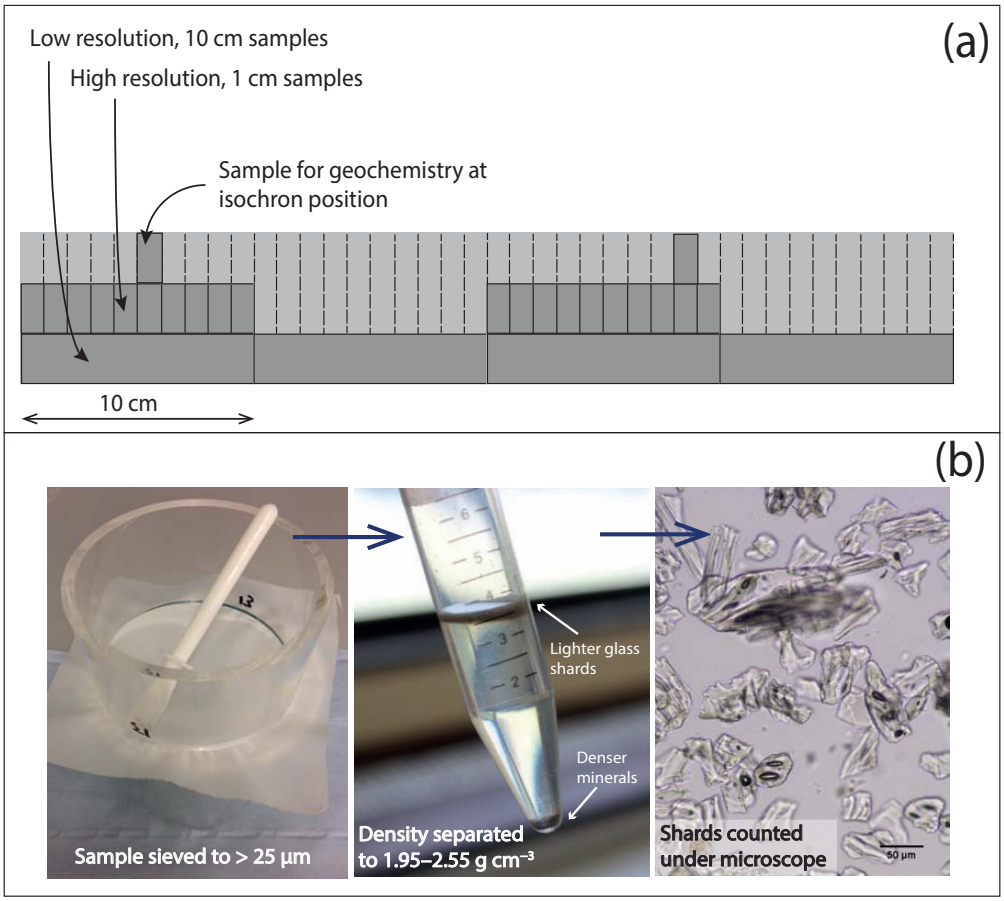

Figure 4.19: Cryptotephra sampling and processing. (a) Sampling core sediments first at a low (10 cm) resolution and resampling of sediments at a high (1 cm) resolution to identify the stratigraphic depth of the cryptotephra. (b) Sieving and density separation of sediment samples to isolate glass shards which can then be counted under a microscope.

Low resolution samples were dried and weighed and then treated with 1 M HCL to remove carbonates. Samples were then sieved to $>$25 μm, using dilute detergent to disaggregate samples with a clay content. Glass shards were then

extracted from the samples using sodium polytungstate at a density of $1.95-2.55$ g/cm^3, following the standard separation procedures described by Blockley *et al.* (2005).

The extracted residue from each 10 cm sample was then mounted on thin sections using glycerin jelly and counted under reflected light microscopy. Shard counts were recalculated to give shard concentrations per gram dry weight (gdw) of host sediment and these were plotted against the core stratigraphy. Regions containing tephra were then resampled at a 1 cm resolution and the samples reprocessed (see Fig. 4.19). The position of the cryptotephra isochron was evaluated through plotting the 1 cm resolution counts against core depth; where tephra glass shards show a sudden appearance in the stratigraphy and a gradual decrease upwards, the basal rise was typically identified at the isochron (Lane *et al.*, 2014). The core sediments were then resampled at the cryptotephra isochron position in order to obtain glass shards for geochemical analysis. In some instances insufficient core material necessitated the use of glass shards from the 1 cm interval thin sections for geochemical analysis. The entirety of the Ashenge core was sampled for cryptotephra. However, the Hayk and Chamo lake sediments were sampled at specific stratigraphic depths with the aim of finding dated tephra layers in the Ashenge, Dendi, Tilo and Awassa lake cores. To locate regions for sampling, minimum and maximum sediment depths (to 2 σ) corresponding to tephra age ranges were calculated using recalibrated age depth models for Hayk and Chamo.

XRF Core Scanning

Lake cores were also scanned to determine their geochemistry, magnetic susceptibility and reflectance in order to aid cryptotephra identification. Magnetic

susceptibility and reflectance measurements were undertaken at 2 mm intervals at LacCore (University of Minnesota) using a Geotek Multi-Sensor Core Logger. Core geochemistry was measured using an using the Itrax® X-ray fluorescence core scanner (Aberystwyth University) fitted with a 3 kW molybdenum tube.

The standard methods described by Croudace *et al.* (2006) were employed when analysing the geochemistry of lake cores. Core sections were loaded onto the horizontal sample cradle of the scanner, with the top of the core facing towards the right. Parameters for the analysis were set using the Core Scanner Navigator Programme on a representative area of the core. The excitation voltage and current of the X-ray tube were then set to 30 kV and 30 mA, respectively. The core dimension limits were set, the surface topography of the core was determined and the core imaged. The radiographic parameters, including the scan increment (120 μm) and dwell time (10 secs) were then set for the radiographic scan. Using the Q-spec programme, the elements for analysis and the spectral fitting parameters were refined. The Core Scanner Navigator was then used to move the core from under the X-ray beam and the X-ray line camera diode array was calibrated (Croudace *et al.*, 2006; Marshall, 2006).

The geochemical, magnetic susceptibility and reflectance data were then plotted against the stratigraphy and compared with the glass shard counts in order to test whether these sediment properties can be used to identify cryptotephra.

4.4.2 Preparation of samples for geochemical analysis

After core scanning, visible and crypto-tephras were prepared for geochemical analysis. Glass shards were separated from tephra samples for geochemical analysis using the standard separation procedures of Blockley *et al.* (2005). Tephra samples were mounted in 25 mm diameter resin blocks with predrilled

holes for geochemical analysis using procedures employed by J. Westgate (University of Toronto) and V. Smith (University of Oxford). The holes within the resin blocks were labelled and Sellotape® was affixed to the polishing face of the block (see Fig. 4.20). Stuers® Specifix-40 epoxy resin was added to the first sample hole and mixed with a tephra sample using a paper clip to remove air bubbles. The sample hole was then filled with tephra sample and more resin and mixed with a paper clip. This was then repeated until all the holes in each sample mount were filled with different samples, taking care not to cross contaminate samples.The mounts were then placed under weights for a minimum of 48 hours to allow the resin to cure.

In order to expose the interior of the shards for analysis, the mounts were lightly ground by hand on wet 600, 1000, 2000 and 3000 grit emery paper for a total of $\sim$15 minutes. After checking that the shards had been exposed for analysis, the mounts were polished. Firstly, the stubs were then polished using a 0.3 μm grade alumina powder solution for $\sim$ 15 minutes, followed by a 0.2 μm grade colloidal silica solution for $\sim$ 5 minutes, taking care not to develop topography on the samples. The polished surface of the mounts was then marked with a razor blade to allow location of the samples during geochemical analysis (see Fig. 4.20).

4.4.3 Electron microprobe analysis of glass shards

Tephra samples were analysed for major elements using a JEOL 8600 electron probe micro-analyzer (EPMA), equipped with four wavelength dispersive spectrometers and one energy dispersive spectrometer, at the Research Laboratory for Archaeology and the History of Art (RLAHA), Oxford University. Prior to major element analysis each sample mount was carbon coated. WDS-EPMA

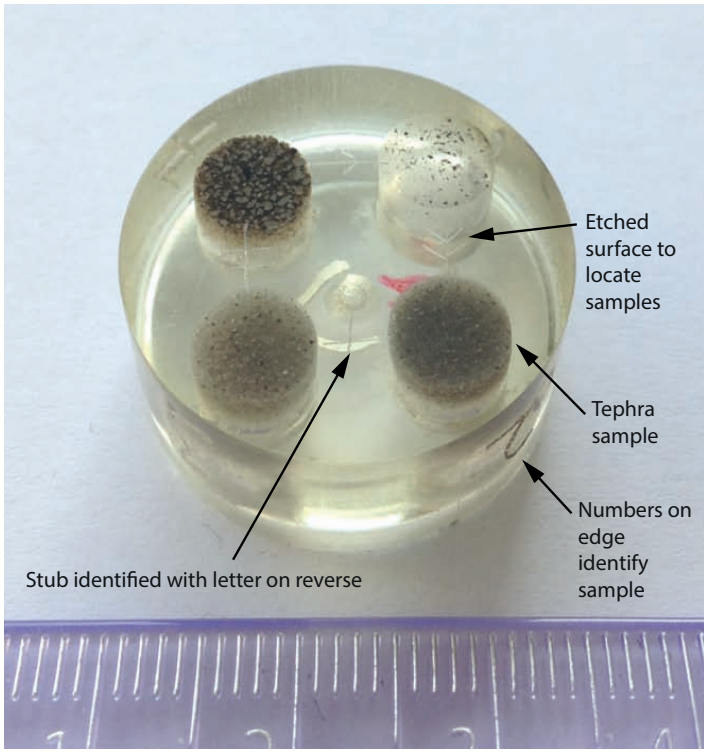

Figure 4.20: Epoxy resin stub containing tephra samples for geochemical analysis. Numbers on the edge of the resin mount identify the tephra sample, marks etched onto the surface aid location of samples during analysis. Scale at base in centimetres.

analytical conditions are given in Table 4.6. A minimum of 20 glass shards in each sample were analysed in order to determine compositional heterogeneity. To reduce alkali element migration glass analyses were undertaken using a 10 μm defocussed electron beam with a 6 nA current and 15 keV accelerating voltage. Sodium was collected for the first 10 secs of analysis, the majority of other elements were collected over 30 secs, however Cl and P were collected over 50 - 60 secs. Background counts for each analyte were collected for the same amount of time either side of the peak. Glass analyses were calibrated against a suite of mineral standards and analyte concentrations were calculated using the PAP absorption correction method. The calibration was verified by analysis of the MPI-DING geological reference materials; ATHO-G (rhyolite), StHs6/80-G

(dacite) and GOR128-G (basalt) (Jochum *et al.*, 2006) between every ten analyses of the tephra samples (Table 4.7). Typically, major element concentrations of the reference materials were determined to within 2 σ of the reported concentrations from GeoReM (Jochum *et al.*, 2005). The lower limit of detection (LLD) is defined as the concentration at which an element can be detected above the instrument background noise (Perkins and Pearce, 1995). Limits of detection for EPMA analysis, based on repeat analyses of ATHO-G, are given in Table 4.7. In Ethiopian tephras, most analytes were present at concentrations above these LLD. However, MnO, MgO and P_2O_5, are frequently present at concentrations below the detection limits in the tephras studied here. Analytical errors for the EPMA are typically $\sim$<5% for the majority of elements; $\sim$<0.9% for SiO_2, $\sim$<3.5% for FeO and $\sim$<1.2% for Al_2O_3. Less abundant elements typically were determined to a higher error; $\sim$<90% for P_2O_5, $\sim$<13% for TiO_2, and $\sim$<50% for MnO. Three reference points were marked onto each sample mount using the beam and the $x-y$ coordinates recorded to allow later relocation of the glass shards when analysing for trace elements.

4.4.3.1 Major element data reduction

Primary magmatic water can account for <10% in rhyolites, therefore tephra analyses with low analytical totals of <90% were rejected (Pearce *et al.*, 2008; WoldeGabriel and Hart, 2005). All analyses were normalised to an anhydrous basis (to 100%) to account for secondary hydration of glasses and magmatic water content (Pearce *et al.*, 2011, 2014). Analyses containing mineral contamination were filtered on the basis of anomalous major element concentrations, e.g. high SiO_2 indicates accidental quartz analysis, high MgO, CaO and FeO indicates clinopyroxene and high Na_2O, CaO and Al_2O_3 indicates feldspars.

Table 4.6: EPMA analytical operating conditions. Including beam conditions, analyte primary standards and analyte peak and background counting times. Counting times (secs.) are reported as: peak / background +/ background -

Jeol 8600 WDS EPMA		
Beam diameter	10 μm defocussed	
Accelerating voltage	15 keV	
Current	6 nA	
Analyte	**Mineral standard**	**Counting times (secs)**
Si	Wollastonite	30/15/15
Ti	Rutile	30/15/15
Al	Jadeite	30/15/15
Fe	Haematite	30/15/15
Mn	Fowlerite	40/20/20
Mg	Periclase	30/15/15
Ca	Wollastonite	30/15/15
Na	Jadeite	10/5/5
K	Orthoclase	30/15/15
P	$NdPO_4$	60/30/30
Cl	$BaFClPO_4$	50/25/25

4.4.4 Laser ablation inductively coupled plasma-mass spectrometry geochemical analysis

After major element analysis, the sample mounts were re-polished using alumina powder to remove the carbon coating. Tephra samples were then analysed for trace element concentrations using the Coherent GeoLas ArF 193 nm Excimer laser ablation system coupled to a Thermo Finnigan Element 2 magnetic sector ICP-MS based at Aberystwyth University. The laser and ICP-MS operating conditions are detailed in Table 4.8. The ICP-MS was tuned prior to each analytical session to optimise signal.

Glass shards previously analysed by EPMA were relocated for LA-ICP-MS analysis by inputting the $x-y$ coordinates of the three reference points on each sample mount into the coordinate transformation spreadsheet provided in the supplementary material from Kuehn and Froese (2010). Each shard was analysed at a laser fluence of 10 Jcm^{-2} and a repetition rate of 5 Hz. Where possible,

Table 4.7: Anydrous average major element concentrations in the MPI-DING reference materials, ATHO-G (rhyolite), St-Hs6/80-G (andesite), GOR128-G (komatiite) and ML3B-G (basalt), analysed over 8 EPMA analytical sessions. Concentrations are in wt. %, published concentrations, from the GeoReM reference material database (Jochum *et al.*, 2006), are given for comparison. Median lower limits of detection (wt.%), based on repeat analyses of ATHO-G during each EPMA session, are given in the the table heading.

ATHO-G	**SiO_2**	**TiO_2**	**Al_2O_3**	**MgO**	**FeO^T**	**MnO**	**CaO**	**Na_2O**	**K_2O**	**P_2O_5**	**Cl**
LLD	**0.08**	**0.05**	**0.05**	**0.04**	**0.08**	**0.07**	**0.04**	**0.08**	**0.03**	**0.10**	**0.02**
Average	**75.09**	**0.25**	**12.29**	**0.10**	**3.25**	**0.11**	**1.69**	**4.07**	**2.73**	**0.02**	**0.05**
2 σ	1.01	0.06	0.25	0.04	0.21	0.08	0.11	0.86	0.10	0.04	0.03
GeoReM	75.60	0.26	12.20	0.10	3.27	0.11	1.70	3.75	2.64	0.04	0.03
StHs6/80-G											
Average	**63.57**	**0.70**	**17.67**	**1.94**	**4.39**	**0.07**	**5.25**	**4.54**	**1.31**	**0.14**	**0.01**
2 σ	0.61	0.07	0.39	0.10	0.22	0.08	0.13	0.46	0.07	0.08	0.02
GeoReM	63.70	0.70	17.80	1.97	4.37	0.08	5.28	4.44	1.29	0.16	0.01
GOR128-G											
Average	**45.81**	**0.29**	**10.40**	**24.16**	**9.99**	**0.17**	**7.18**	**0.66**	**0.03**	**0.03**	**0.01**
2 σ	1.00	0.07	0.85	3.36	0.70	0.10	2.25	0.26	0.03	0.04	0.03
GeoReM	45.39	0.30	10.87	22.27	10.30	0.15	8.45	0.79	0.03	0.04	0.01
ML3B-G											
Average	**51.87**	**2.11**	**13.74**	**6.53**	**11.08**	**0.20**	**10.48**	**2.33**	**0.39**	**0.24**	
2 σ	0.44	0.09	0.27	0.17	0.51	0.05	0.23	0.24	0.05	0.04	
GeoReM	51.87	2.11	13.74	6.53	11.08	0.20	10.48	2.33	0.39	0.24	

Table 4.8: Operating conditions for LA-ICP-MS trace element analysis

Thermo Element 2 ICP-MS	
Cool gas	15.7 $Lmin^{-1}$
Auxiliary gas	1.05-1.20 $Lmin^{-1}$
Sample gas	1.25 $Lmin^{-1}$
RF power	1050-1150 W
UO^+/U^+	$<0.2\%$
ThO^+/Th^+	$<0.8\%$
Analytes	^{29}Si, ^{43}Ca, ^{44}Ca, ^{85}Rb, ^{88}Sr, ^{89}Y, ^{90}Zr, ^{93}Nb, ^{133}Cs, ^{137}Ba, ^{139}La, ^{140}Ce, ^{141}Pr, ^{143}Nd, ^{147}Sm, ^{151}Eu, ^{158}Gd, ^{159}Tb, ^{163}Dy, ^{165}Ho, ^{166}Er, ^{169}Tm,^{174}Yb, ^{175}Lu, ^{178}Hf, ^{181}Ta, ^{232}Th, ^{238}U
Runs/passes	1/10
Samples per peak	100
Mass window	5%
Segment durations	0.05 seconds
Acquisition time	20 seconds

GeoLas 193 nm Excimer laser	
Excitation voltage	~ 24 kV
Laser fluence	10 Jcm^{-2}
Repetition rate	5 Hz
Pulse length	13-20 ns
Mask thickness	0.3 mm (>10 μm craters), 0.1 mm (6 μm and 4 μm craters)

shards were analysed using larger crater diameters of 20 μm to minimize the element fractionation associated with acquisition using smaller crater diameters (Pearce *et al.*, 2011) and to give a better instrument signal and therefore improved limits of detection. Typically $>$ 20 shards were analysed in a tephra sample and, if the shards were of sufficient size, several analyses were undertaken alongside one another to determine compositional homogeneity within each shard. Prior to and after the acquisition of glass analyses, a set of gas blanks (the instrumental contribution to the signal, with no sample in the plasma) and calibration spectra (using NIST 612) were acquired in order to monitor instrument drift during the analytical session (Pearce *et al.*, 2011). Two to three tephra samples were analysed during a run, the acquisition time for each analysis is $\sim$ 20 s with gas blanks obtained immediately prior to each unknown spectra. The MPI-DING

Table 4.9: LA-ICP-MS analytical considerations. Median lower limits of detection (LLD), calculated from all analytical sessions. Average trace element concentrations measured in the ATHO-G reference material throughout all analytical sessions. Two standard deviation on the ATHO-G analyses, and published concentrations from the GeoReM database (Jochum *et al.*, 2006) are shown. All concentrations are in ppm.

	Rb	**Sr**	**Y**	**Zr**	**Nb**	**Cs**	**Ba**	**La**	**Ce**	**Pr**	**Nd**	**Sm**	
LLD	**0.62**	**1.05**	**0.17**	**0.37**	**0.07**	**0.19**	**1.88**	**0.09**	**0.07**	**0.06**	**0.25**	**0.14**	
ATHO-G	66.5	96.4	100	512	63.2	1.08	546	55.7	118	14.4	61.5	14.6	
2 σ	*4.18*	*6.58*	*6.34*	*45.89*	*3.47*	*0.15*	*53.98*	*3.77*	*8.17*	*1.26*	*4.54*	*1.28*	
GeoReM	65.3	94.1	94.5	512	62.4	1.08	547	55.6	121	14.6	60.9	14.2	
	Eu	**Tb**	**Dy**	**Ho**	**Er**	**Tm**	**Yb**	**Lu**	**Hf**	**Ta**	**Pb**	**Th**	**U**
LLD	**0.13**	**0.06**	**0.13**	**0.04**	**0.07**	**0.05**	**0.15**	**0.04**	**0.08**	**0.06**	**0.12**	**0.01**	**0.00**
ATHO-G	2.83	2.64	16.9	3.65	11.2	1.61	10.8	1.62	14.5	4.07	6.09	7.62	2.49
2 σ	*0.35*	*0.27*	*1.59*	*0.35*	*1.07*	*0.21*	*1.05*	*0.20*	*1.29*	*0.33*	*2.00*	*0.67*	*0.58*
GeoReM	2.76	2.51	16.2	3.43	10.3	1.52	10.5	1.54	13.7	3.90	5.67	7.40	2.37

reference material ATHO-G was analysed five times at a 20 μm crater diameters during an analytical session to determine the analytical accuracy. All tephra samples (apart from four trachytic Dendi tephras) analysed as part of this study are rhyolitic, therefore a reference material with a similar compositional matrix was selected. Average analyses of ATHO-G during the analytical sessions are given in Table 4.9, and trace elements were typically determined to within 2 standard deviations of reported concentrations from Jochum *et al.* (2006).

The majority of glass analyses were performed using 20 μm crater diameters, and at this resolution limits of detection were < 0.4 ppm for most elements (Table 4.9). The highly evolved glass compositions analysed here are enriched in incompatible elements, at concentrations well above these LLD's. Limits of detection increase using 10 μm crater diameters to typically < 2 ppm, due a decrease in the ^{29}Si signal to background ratio.

Detection limits are sensitive to instrumental variations, associated with tuning and gas blanks (Pearce *et al.*, 2011). The ^{29}Si blank decreases throughout an analytical session, associated with the warm-up of the ICP-MS (Pearce *et al.*,

2011). Background counts for Sr, Rb, Cs and Ba increase over time, their 'sticky' nature causing them to adhere to the glassware and interface cones of the ICP-MS (Pearce *et al.*, 2011). Thus, detection limits for these analytes are comparatively higher than other elements, at < 1.88 ppm and < 11.3 ppm using 20 μm and 10 μm crater diameters, respectively.

The conversion of data in the form of counts per second (cps) to concentration (ppm) requires the prior determination of SiO_2 concentrations by EPMA. Where available, grain specific SiO_2 concentrations were used as internal standards. However, average SiO_2 concentrations in the Ayelu tephras and Corbetti obsidians were used as internal standards. These samples had previously been analysed for major element concentrations by N. Pearce and G. WoldeGabriel, using EPMA at the University of Toronto and Los Alamos National Laboratory, respectively. Using an Excel spreadsheet; gas blank cps were first subtracted from sample cps and the resulting analyte cps were then divided by the internal standard cps and multiplied by the internal standard concentration obtained by EPMA. The analytical drift during the run was then calculated by dividing the average NIST 612 (Pearce *et al.*, 1997) Si counts obtained from 20 μm crater diameters from the end of the session by those at the start. The analyses are then corrected for this drift and divided by the calibration slopes, this is calculated by taking the average of all the 20 μm or 10 μm NIST 612 acquisitions and dividing each slope by the preferred NIST 612 concentrations. Finally, data was fractionation corrected by dividing element concentrations by the fractionation factor calculated by Pearce *et al.* (2011).

4.4.4.1 Trace element data reduction

Analyses contaminated by mineral inclusions were then filtered from the dataset on the basis of anomalous trace element concentrations, e.g. high Zr and Hf concentrations indicate zircon inclusion, high Ba and Sr (feldspar), high Si counts and low trace element concentrations (quartz) and high Rb and Cs concentrations (mica) (Pearce *et al.*, 2011, 2014).

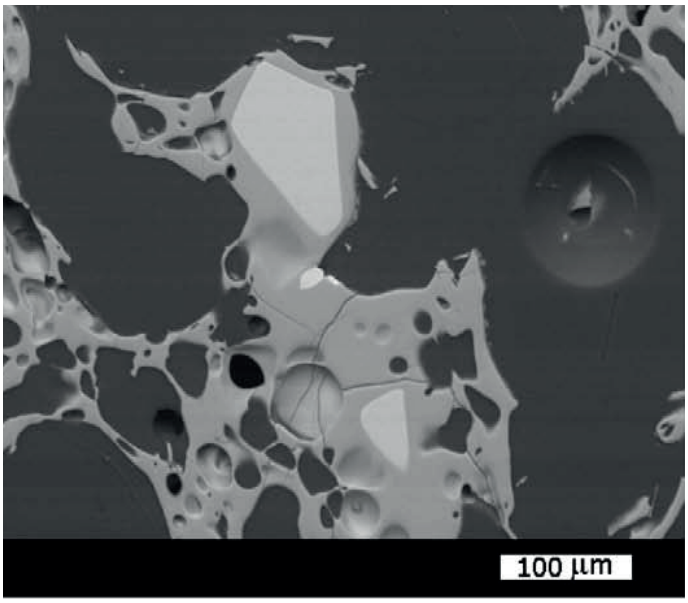

Figure 4.21: Mineral inclusions in glass. Visible or sub surface phenocrysts may contaminate EPMA and LA-ICP-MS analyses. Figure from Tomlinson *et al.* (2010).

4.4.5 Major and trace element data interpretation

The compositions of tephras were compared and differentiated using bi-plots of selected major and trace element concentrations. Generally elements present at lower concentrations in the tephras studied (e.g. Ti, Mn, Mg, Ca, Sr, Cs and Ba) were not included in bi-plots, due to greater associated analytical errors. Potential correlations and geochemical differences were tested using principal component

analysis (PCA) run in Minitab® software. A selection of elements shown to discriminate between the tephras using bi-plots were used to run the PCA. Three principal components were produced by the PCA and these were then plotted on bi-plots to test whether tephras were statistically similar or different. This allowed any compositional similarities and differences between tephras noted from the bi-plots to be statistically tested.

Chapter 5

Characteristics and composition of Holocene Ethiopian tephras

This chapter describes the physical characteristics and Bayesian-modelled age estimates of the tephras identified by this study, from seven lake sediment sequences throughout Ethiopia. The major and trace element compositions of tephra glass shards are also presented in Section 5.4.

The geochemical composition of the tephras studied in each of the lakes is compared and discussed, in order to:

1. Assess glass shard compositional variability throughout the Ethiopian Rift Valley

2. Provide a background and justification for potential tephra correlations explored in Chapters 6 and 7.

5.1 The occurrence and characteristics of tephras in lake sediments from the Ethiopian Highlands

5.1.1 Lake Ashenge tephras

The Ashenge lake sediments contain a total of 9 visible tephra and cryptotephra layers. These are labelled AST-1 to AST-9, (see Table 5.1) and range in age from $15.3 - 0.3$ cal. ka BP, respectively. Four visible tephras (AST-1; 2; 5; 8) occur in the sediments; these are $1 - 2.5$ cm thick and comprised of normally graded, grey-white, fine to coarse volcanic ash (Heiken and Wohletz, 1985). Tephras are typically well to moderately well-sorted; however AST-5 is poorly-sorted. Zirconium counts, measured using XRF core scanning, for the Ashenge sediments are shown in Fig. 5.2. Zirconium counts increase relative to the background sediment counts at depths where visible tephras occur.

Five cryptotephras were identified in the Ashenge stratigraphy on the basis of shard counting (Fig. 5.2). Four cryptotephras (AST-4; 6; 7; 9) are associated with elevated Zr counts measured in the Ashenge sediments. Shard morphologies (page 25) include bubble wall, platy and stretched and fluted pumiceous shards (Figure 5.1). Age estimates for all tephra layers identified in Lake Ashenge, interpolated from a Bayesian depositional model (see Methods, page 122), are reported in Table 5.1. The precision on the tephra ages varies within the age model, from ~ 200 years for AST-1 and AST-2, to nearly ~ 1500 years for AST-9 at the 95.4 % confidence level. The youngest tephra (AST-1) dates to the historic age ($546 - 321$ cal. a BP, $1404 - 1629$ AD). This tephra was deposited following a > 4 ka period where no tephras were identified in the Ashenge sediments. Six tephras (AST-2 to AST-7) are recorded in the Ashenge sediments between $\sim 7.5 - \sim 4.8$ cal. ka BP, giving an average frequency of an eruption every 500

years during this interval. A major sediment hiatus occurs at $\sim 11.8 - \sim 7.6$ cal. ka BP, below which two tephras occur in the sediments between $\sim 15.3 - \sim 13.5$ cal. ka BP. Tephras deposits are not recorded in the Ashenge sediments between ~ 15.3 cal. ka BP and the base of the core at ~ 17 cal. ka BP.

Table 5.1: Characteristics of tephras recorded in the Ashenge and Hayk lake sediments. Cryptotephras are indicated with an asterisk. †Radiocarbon age estimates are provided at the 95.4% confidence interval.

Tephra ID	**Composite depth of the base (cm)**	**Thickness (cm)**	**Description**	**^{14}C age†(cal. a BP)**
Ashenge				
AST-1	12	2	discontinuous layer of grey fine ash	321 – 546
AST-2	439	1	grey fine-coarse ash	4824 – 5041
AST-3*	485	< 1		4975 – 5625
AST-4*	527	< 1		5334 – 5871
AST-5	610	2.5	diffuse layer of grey fine-coarse ash	6348 – 7155
AST-6*	624	< 1		6485 – 7505
AST-7*	635	< 1		6721 – 7578
AST-8	745	1	grey fine-coarse ash	13582 – 14590
AST-9*	758	< 1		13847 – 15332
Hayk				
HT-1*	66	< 1		1626 – 2611
HT-2	109	0.5	discontinuous grey fine-coarse ash	2460 – 2876
HT-3*	119	< 1		2513 – 2929
HT-4	146	0.5	discontinuous grey fine-coarse ash	2792 – 3635
HT-5*	160	< 1		2913 – 3914
HT-6*	169	< 1		3197 – 3981
HT-7*	181	< 1		3835 – 4804
HT-8*	200	< 1		5582 – 7382
HT-9*	268	< 1		8432 – 10514
HT-10*	289	< 1		8903 – 11045
HT-11*	387	< 1		11299 – 11962
HT-12*	462	< 1		12027 – 12952

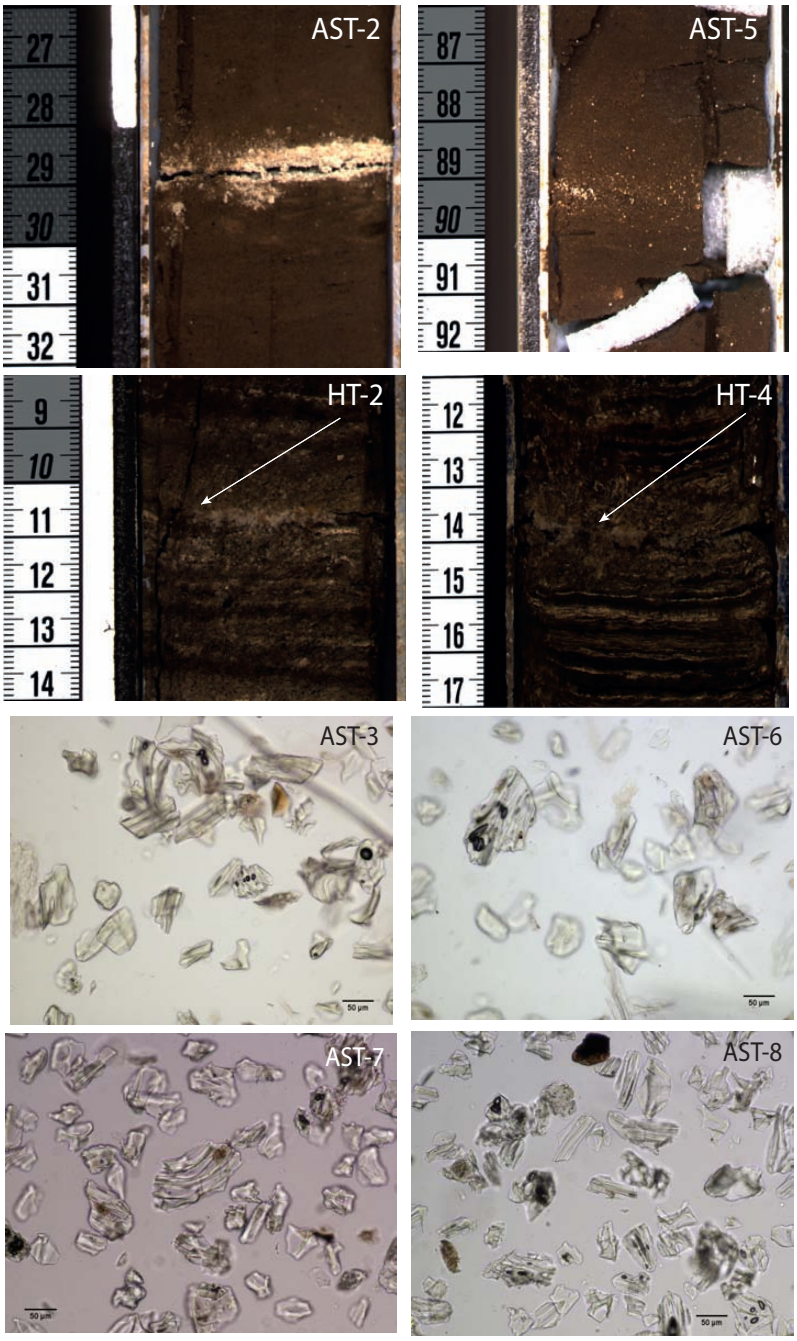

Figure 5.1: Photographs of selected visible tephras in the Lake Ashenge and Hayk sediments, with transmitted light microscope images of glass shards in cryptotephras occuring in the Ashenge core. Microscope image scale = 50 μm.

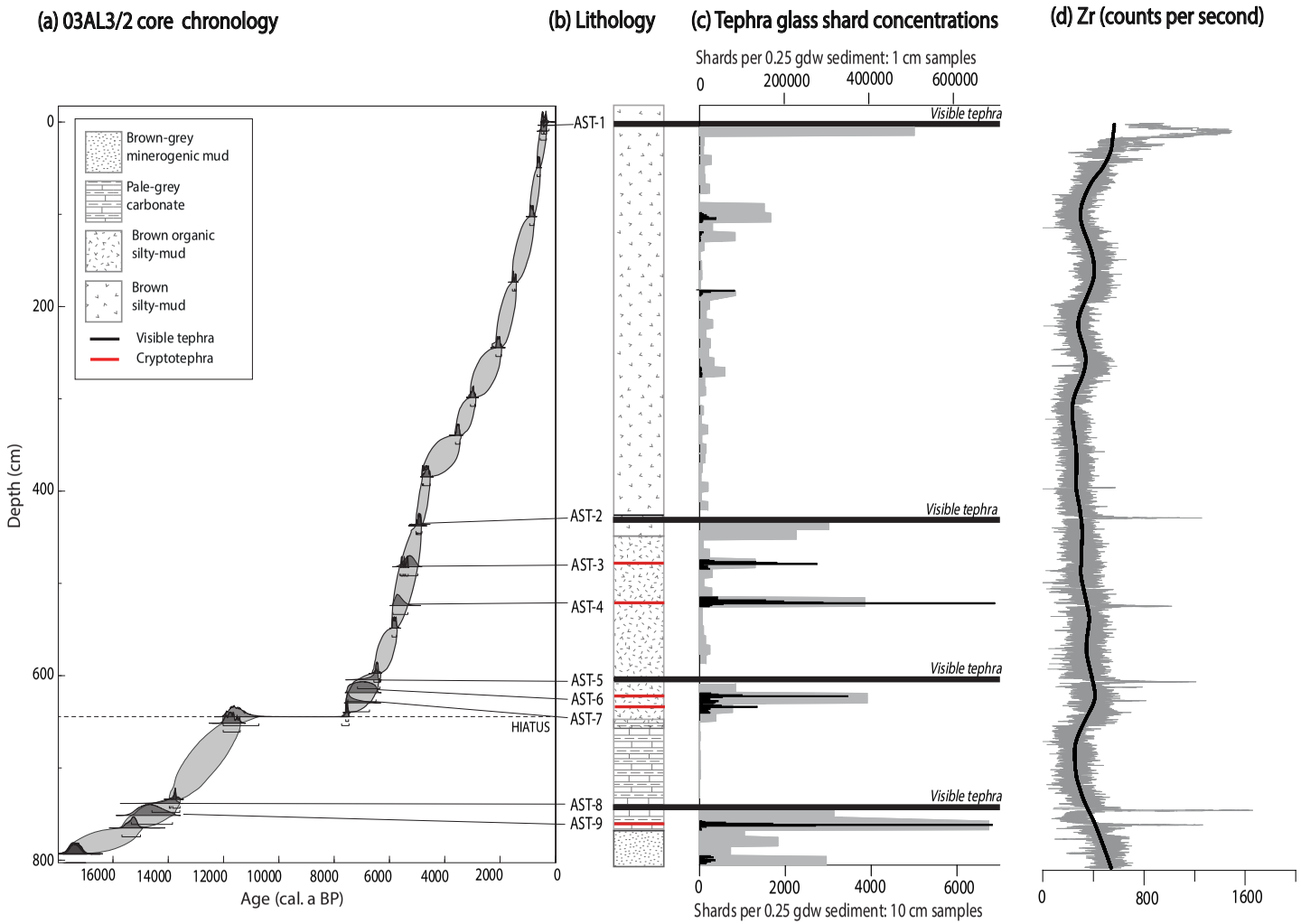

Figure 5.2: Lake Ashenge sediment core 03AL3/2. (a) Bayesian age-depth model (for parameters, see page 122). Grey envelope shows interpolated 95 % confidence interval, between modelled probability density functions (filled) for calibrated radiocarbon dates (unfilled). Interpolated ages for tephra layers AST-1 to AST-9 indicated with horizontal bars. (b) Core lithology, see key, on original depth scale. (c) Tephra shards per gram dry weight (gdw). Grey bars indicate shard concentrations across 10 cm sample intervals, black bars are shard concentrations across 1 cm sample intervals. Cryptotephra samples where not collected from depths where visible tephras occur. (d) Zr counts measured through the stratigraphy.

5.1.2 Lake Hayk tephras

The Lake Hayk sediments contains two visible tephras and ten cryptotephras, these are labelled HT-1 to HT-12 and range in age from $1.6 - 13.0$ cal. ka BP, respectively (Table 5.1). The visible tephras (HT-2 and HT-4) occur as discontinuous $0.5 - 1$ cm thick layers, comprised of grey, well-sorted grey fine to medium ash. Cryptotephras were identified on the basis of shard counts conducted throughout the core sediments (Fig. 5.3). Like the Ashenge cryptotephras, the Hayk cryptotephras contain a range of shard morphologies, including bubble wall, platy and pumiceous shards.

Unfortunately, due to heavy sampling of the core after initial cryptotephra processing, cryptotephras HT-1, HT-3, HT-8 and HT-11 could not be re-sampled for geochemical analysis.

Age ranges for the Hayk tephras, based on Bayesian age modelling of the Hayk sediments (Fig. 5.3), are given in Table 5.1. Precision on the ages of these tephras varies within the age model, ranging from ~ 400 years for HT-2 and HT-3 to ~ 2000 years for HT-8; 9 and HT-10, at the 95.4 % confidence level. Between $\sim 13.0 - \sim 1.6$ cal. ka BP, tephras are recorded in the Hayk archive at a frequency of 1 every < 950 years. Tephras are not recorded between the oldest tephra at ~ 13.0 cal. ka BP and the base of the core at ~ 16.0 cal. yr BP.

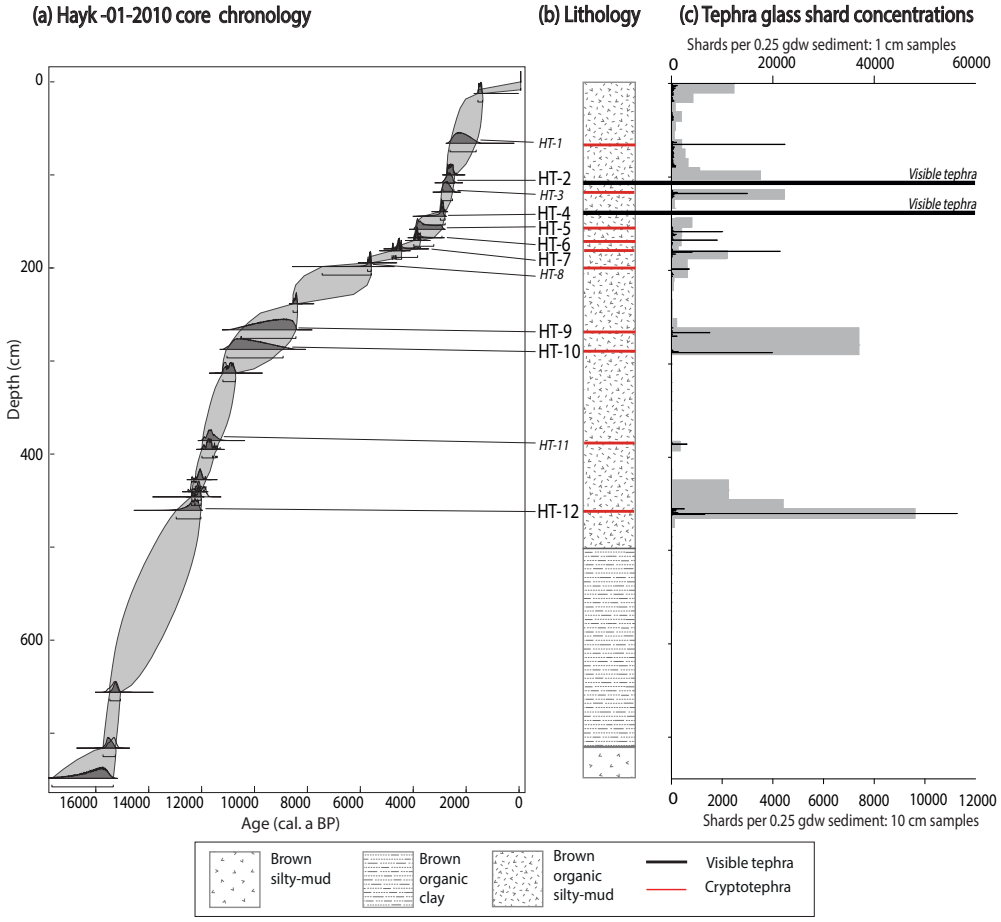

Figure 5.3: Lake Hayk sediment core Hayk-01-2010 (a) Bayesian age model, (b) lithology, (c) tephra shards per gdw sediment. Grey bars are shard concentrations across 10 cm sample regions; black bars are shard concentrations across 1 cm sample regions. Horizontal lines indicate the probability density functions for the Hayk tephras within the age model. Cryptotephra samples were not collected from depths where visible tephras occur. Cryptotephras which could not be analysed are labelled in italics.

5.2 The occurrence and characteristics of tephras in lake sediments from the Yerer-Tullu Wellel Volcano Tectonic Lineament

5.2.1 Lake Dendi tephras

Five visible tephras have been identified within the Lake Dendi sediments, labelled here DT-1 to DT-5 (youngest to oldest). The tephras range in thickness from $1-200$ cm and consist of well-sorted fine-coarse buff coloured ash. However, DT-2 has a uniquely grey colour (see Table 5.2). Glass shards comprising the tephra layers typically possess a range of shard morphologies; including bubble wall, cuspate and 'aero' like pumiceous shards.

The basal, 200 cm thick, tephra (DT-5) is discontinuous and shows evidence of reworking. However, the constituent shards appear vitreous, angular and unaltered (pristine) under transmitted light microscopy (Fig. 5.4).

The tephras range in age from $\sim 10.1-0.7$, on the basis of an unpublished Bayesian age model provided by B. Wagner (University of Cologne).

Table 5.2: Characteristics of tephras recorded in sediments from Lake Dendi.

Tephra ID	**Composite depth of the base (cm)**	**Thickness (cm)**	**Description**	**^{14}C age (cal. yrs BP)**
Dendi				
DT-1	79.8	1	buff fine-coarse ash	~ 650
DT-2	596.2	1	grey fine-coarse ash	~ 6990
DT-3	603.6	1	buff fine-coarse ash	~ 7060
DT-4	894.5	1.5	buff fine-coarse ash	~ 10100
DT-5	1130	200	buff fine-coarse ash, fines upwards ~ 10610	
Hora				
HRT-1	$L6,17$ cm	0.5	grey fine medium ash	
HRT-2	$L8,46$ cm	1	grey fine medium ash	

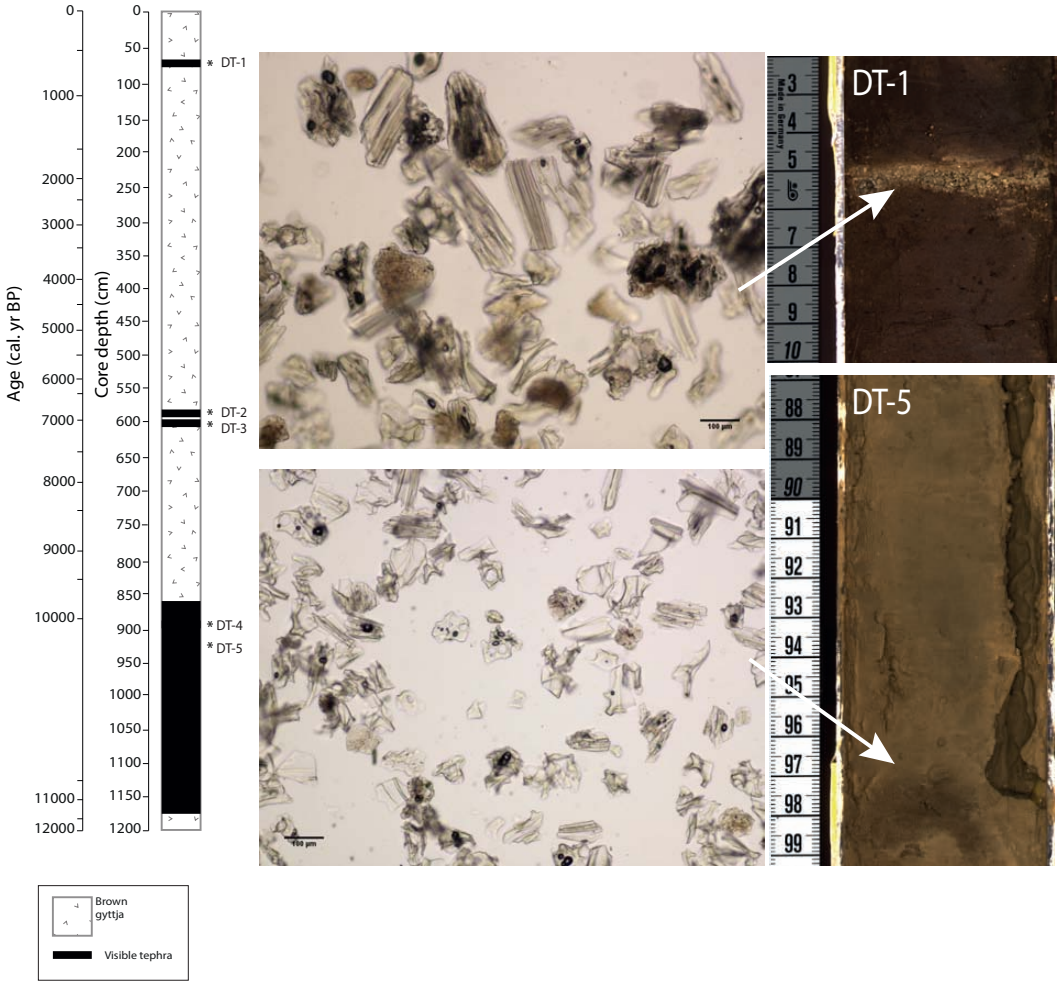

Figure 5.4: Age, occurrence and morphology of visible tephra glass shards in the Dendi sediments. Scale on photographs = 100 μm.

5.2.2 Lake Hora tephras

Two visible tephras occur within the Lake Hora sediment stratigraphy. These tephra deposits are comprised of grey fine-coarse ash and occur as continuous, well-sorted layers of $0.5-1$ cm thickness. The Hora tephras are Holocene, however, due to uncertainties in coring depths and the age model for the Hora lake sediments, the ages of these tephras are unknown. The tephras are referred to here as HRT-1 (occurring in core section L6) and HRT-2 (core section L8).

5.3 The occurrence and characteristics of tephras in lake sediments from the central Main Ethiopian Rift

5.3.1 Lake Tilo

Fourteen visible tephra layers occur within the Tilo lake sediments. These are labelled here TT-1 to TT-14 and range in age from $\sim 0.01-\sim 10.0$ cal. ka BP. The tephras range in thickness from $0.5-48$ cm and are composed of predominantly grey fine to coarse ash; however, TT-8 and TT-12 contain lapilli grain sizes. The tephra layers are typically well-sorted and normally graded, however, TT-1 and TT-5 show reverse grading. Glass shards comprising the tephra layers typically have inflated pumiceous or bubble wall morphologies.

The Bayesian age model for the Tilo sediments is seen in Fig. 5.6 and provides age ranges for the Tilo tephras (see Table 5.3). Precision on the tephra ages varies within the age model; from $\sim 800-900$ years form TT-5, TT-7, TT-8, TT-10 and TT-13 to ~ 1900 years for TT-4 and TT-6. Tephras range in age from

the historic period (TT-1, $1309-50$ cal. a BP, or $641-1900$ AD) to 10180 cal. a BP (TT-14). Tephra layers are recorded frequently throughout the Holocene, averaging a rate of 1 every ~ 700 years.

Table 5.3: Characteristics of tephras recorded in sediments from lakes Awassa, Tilo and Chamo. Cryototephras are identified with an asterisk. †Radiocarbon age estimates are provided at the 95.4% confidence interval.

Tephra ID	**Composite depth of the base (cm)**	**Thickness (cm)**	**Description**	**^{14}C age†(cal. yrs BP)**
Tilo				
TT-1	103	4.5	reverse graded, grey coarse ash	50 – 1309
TT-2	220	20	discontinuous, grey fine-coarse ash	1185 – 2099
TT-3	238	0.5	grey, fine-coarse ash	1252 – 2326
TT-4	272.5	2	grey, fine-coarse ash	1296 – 2489
TT-5	292	5	reverse graded, grey fine-coarse ash	1345 – 2601
TT-6	321	1	grey, fine-coarse ash	1602 – 2701
TT-7	385	1	grey, fine-coarse ash	2346 – 4206
TT-8	427	37	grey coarse ash and lapilli	2352 – 4208
TT-9	588	38	grey coarse ash	3968 – 4853
TT-10	710	30	grey, fine-coarse ash	4697 – 6279
TT-11	763.5	6	grey coarse ash	5063 – 6431
TT-12	915	35	grey coarse ash and lapilli	6144 – 7048
TT-13	1623	5	grey coarse ash	8029 – 8888
TT-14	2272	48	grey-yellow coarse ash	9344 – 10180
Awassa				
AWT-1	253	14	grey coarse ash	1120 – 1540
AWT-2	550	4	grey coarse ash and lapilli	3258 – 4093
AWT-3	818	10	grey coarse ash	5219 – 6318
AWT-4	928	73	grey, fine-coarse ash	5420 – 6571
AWT-5	1087	6	grey, fine-coarse ash	6436 – 7368
AWT-6	1160.5	0.5	grey, fine-coarse ash	$>$ 7499
AWT-7	1189	24	grey, fine-coarse ash	$>$ 7499
Chamo				
CHT-1*	702	$<$ 1 cm		1244 – 2800
CHT-2	1361	1	grey, fine-coarse ash	6299 – 9443

5.3.2 Lake Awassa

Seven visible tephras occur in the Awassa lake sediments, identified in this study as AWT-1 to AWT-7 (youngest to oldest). The tephras range in age from

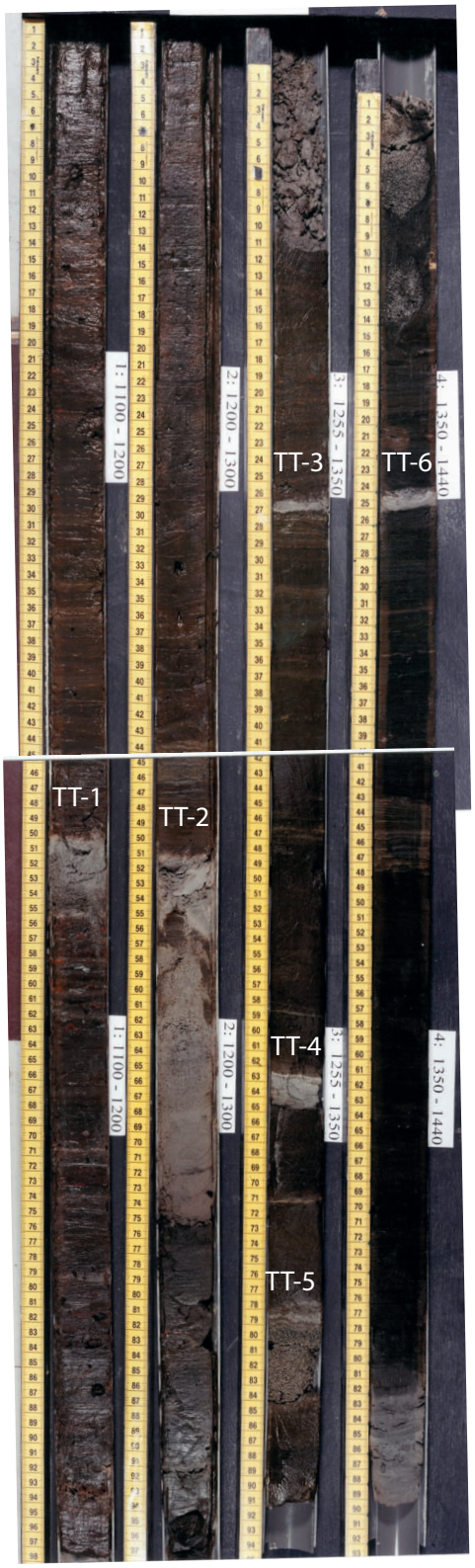

Figure 5.5: Photos of the Tilo tephras TT-1 to TT-6.

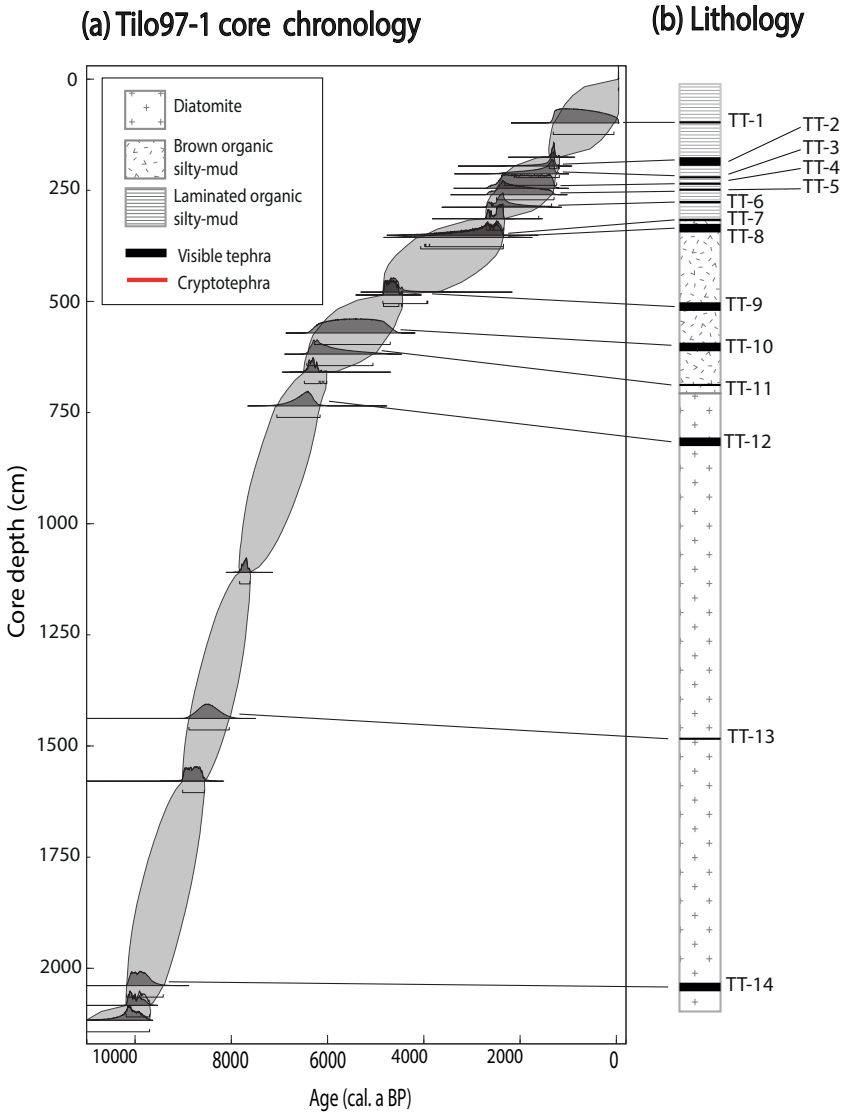

Figure 5.6: Tilo97-1 core, (a) Bayesian age model, using core depths adjusted for the presence of $>$ 0.5 cm thick tephras, (b) core lithology. Core depths include tephras $>$ 0.5 cm thick, horizontal lines indicate the position of these tephras in the age model.

$\sim>7.5-\sim 1.1$ cal. ka BP and from $0.5-73$ cm thick. The Awassa tephras are typically comprised of well-sorted grey fine to coarse ash, except AWT-2 which is comprised of coarse ash to lapilli. The tephras are normally graded, in contrast AWT-5 and AWT-7 show reverse grading. Glass shards in the Awassa tephras show morphologies ranging from pumiceous to bubble wall.

The Bayesian age model (Fig. 5.7) for the Awassa sediments provides age ranges for the Awassa tephras (see Table 5.3), from $>7.5-1.1$ cal. ka BP. The precision of tephra ages varies throughout the Awassa age model, from ~ 400 years for AWT-1 to ~ 1100 years for AWT-3 and AWT-4. It was only possible to calculate the younger age limit for AWT-6 and AWT-7 because sediments below these tephras were not sampled for radiocarbon dating. Tephras AWT-5 and AWT-4 were deposited in rapid succession with ~ 130 years separating their eruption. Longer time intervals separate the eruption of AWT-1; 2 and 3, ranging from $\sim 890-1700$ years. Due to degradation of the Awassa core sediments since its initial study, it was only possible to sample AWT-1, AWT-2 and AWT-4 for compositional analysis as part of this study.

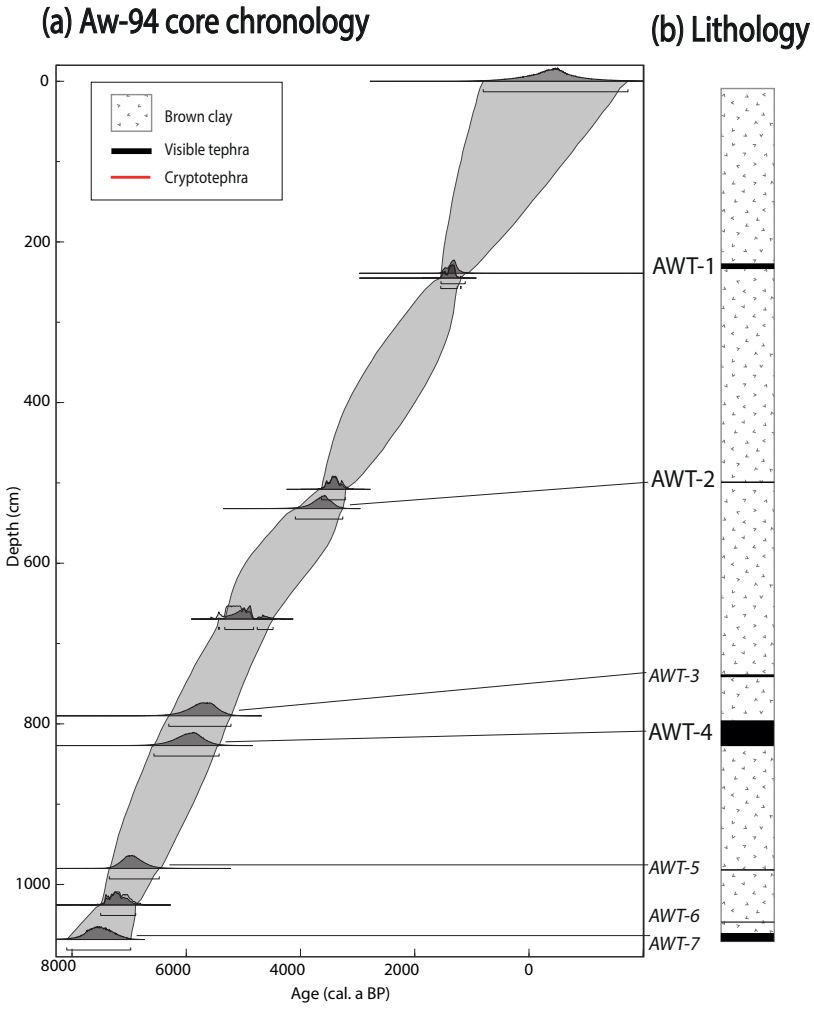

Figure 5.7: Aw-94 core, (a) Bayesian age model, using core depths adjusted for the presence of > 0.5 cm thick tephras, (b) core lithology. Core depths include tephras > 0.5 cm thick. Tephras labelled in italics could not be analysed. Horizontal lines indicate depths of the tephras in the age model.

5.3.3 Lake Chamo

Two tephra layers occur in the Lake Chamo sediments, identified here as CHT-1 and CHT-2, and dated to $\sim 9.4-$ ~ 1.2 cal. ka BP, respectively (see Table 5.3). Glass shards in the two Chamo tephras display bubble wall to pumiceous shards. CHT-1 is a cryptotephra that was identified using glass shard counting and CHT-2 is a 1 cm thick layer composed of well-sorted, fine-coarse grey ash. Due to time constraints and sample availability, cryptotephra counting in core CHA-01-2010 was restricted to the depth interval between $502-920$ cm depth ($0.5-4.5$ cal. ka BP).

Figure 5.8 shows the Bayesian age model for the Chamo core, alongside the core lithology and glass shard concentrations. The precision on the tephra age estimates varies within the Chamo age model, from ~ 300 years for CHT-1 to ~ 4100 years for CHT-2. No tephras were detected between $5.3-1.5$ cal. ka BP in the Chamo sediments.

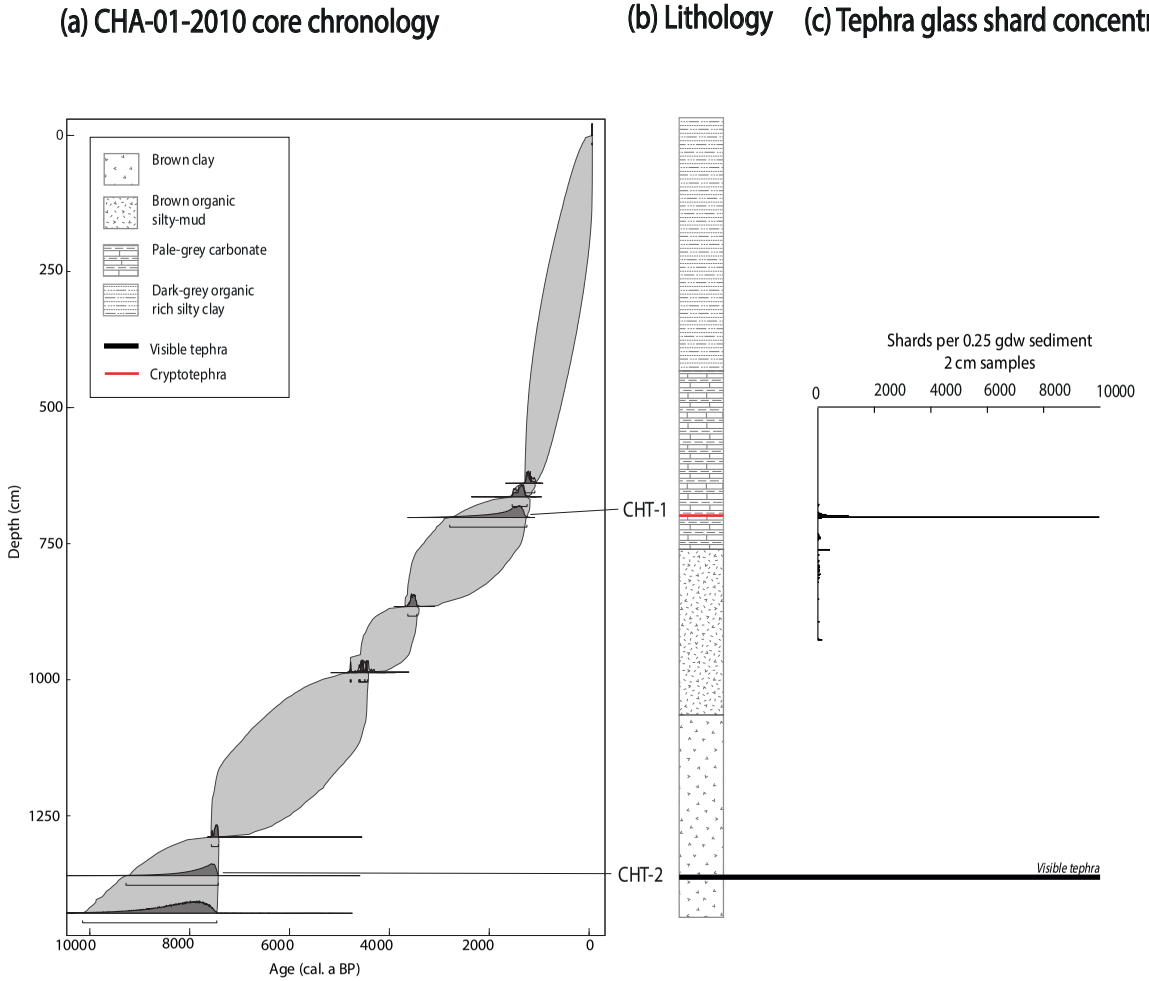

Figure 5.8: CHA-01-2010 core, (a) Bayesian age model, (b) lithology, (c) tephra shards per gdw sediment (d) Zr counts through the stratigraphy. Grey bars are shard concentrations across 10 cm sample regions, black bars are shard concentrations across 1 cm sample regions. Cryptotephra samples were not collected from depths where visible tephras occur. Cryptotephras which could not be analysed are labelled in italics. Horizontal lines indicate the probability density functions for the Chamo tephras.

5.4 The composition of Holocene tephras recorded in Ethiopian lake sediment cores

This section presents the major and trace element composition of glass shards in tephras detected in seven Ethiopian lake sediment cores. Firstly, this section investigates whether the geochemistry of these tephras varies systematically throughout the Ethiopian Rift. Secondly, the composition of the tephras is compared to provide a justification for potential tephra correlations explored in forthcoming chapters. The analytical precision and accuracy on the glass compositions presented in the following section are given on pages 134 and 136.

5.4.1 Petrogenesis and spatial variations in the composition of Holocene tephras from Ethiopia

Defining the control of regional tectonic processes on volcanism is crucial in understanding the evolution of rift zones (Abebe *et al.*, 2007). The composition of volcanic deposits as a function of geographic distribution has been used in numerous studies to shed light on the relationship between magma composition and rifting (e.g. Barberi *et al.*, 1970; Baker *et al.*, 1972; Barberi *et al.*, 1975; Betton and Civetta, 1984; Hart *et al.*, 1989; WoldeGabriel *et al.*, 1990; Abebe *et al.*, 2007). However, studies focussing on the spatial variation of Holocene volcanism remain limited (e.g. Abebe *et al.*, 1998; Adhana, 2014).

Selected glass shard major and trace element concentrations from all tephras, grouped by lake, are shown in Fig. 5.9 and 5.10. Glass shards recorded in sediments from lakes on the rift floor and margins of the surrounding plateaus have a rhyolitic composition, except 3 trachytic shards which occur in the Awassa and Tilo tephras. In contrast, glass shards recorded in sediments from Lake Dendi

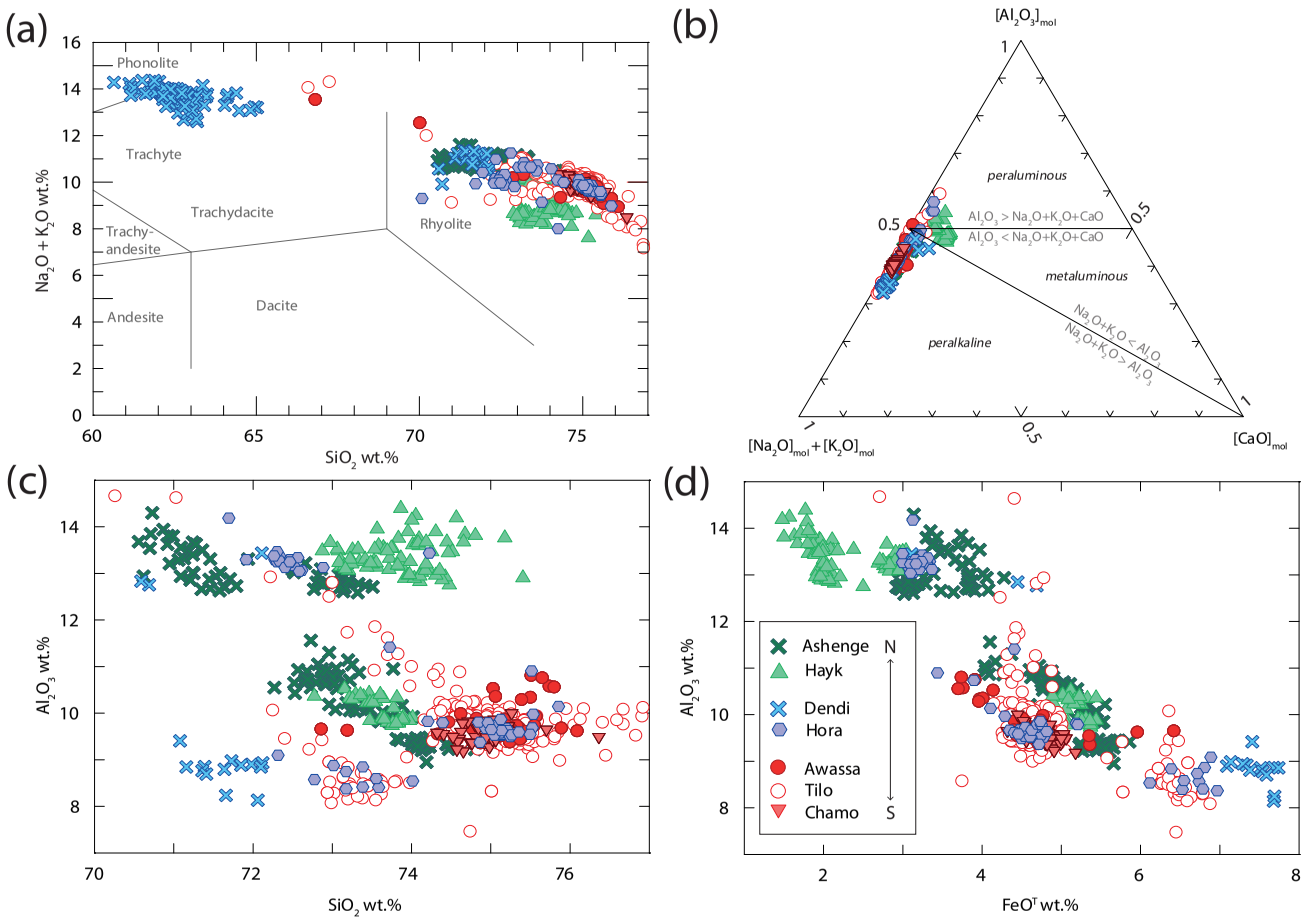

Figure 5.9: Major element composition of glass shards from Holocene Ethiopian Tephras, grouped by lake site. (a) Total alkali silica diagram (Le Bas *et al.*, 1986) showing the composition of all tephra glass shards (b) glass compositions of only rhyolitic shards ($>$ 70 wt.% SiO_2) projected onto a ternary plot of Al_2O_3, ($Na_2O + K_2O$) and CaO (molar proportions), with peraluminous, metaluminous and peralkaline fields shown (Le Bas *et al.*, 1986), (c) and (d) Bi-plots of selected major element concentrations of rhyolitic tephra glass shards only.

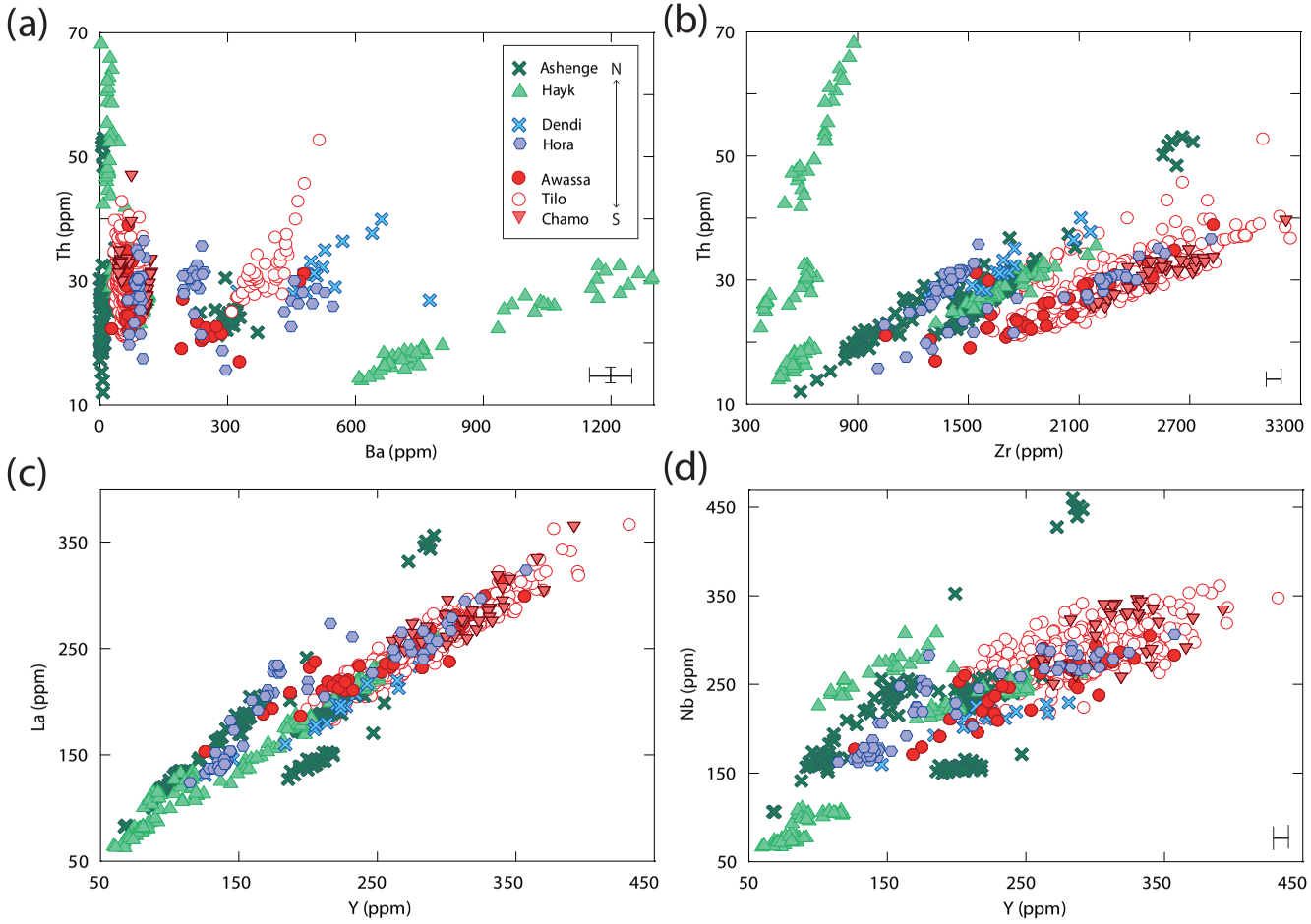

Figure 5.10: Bi-plots of selected trace elements in glass shards from rhyolitic tephras (> 70 wt. % SiO_2) recorded in lakes Ashenge, Hayk, Dendi, Hora, Awassa, Tilo and Chamo. Error bars at the 95 % confidence interval were calculated from repeat analyses of ATHO-G, the rhyolitic MPI-DING standard.

are predominantly phonolitic - trachytic (Fig. 5.9a). The spatial distribution of the tephras is discussed below, in relation to these contrasting compositions.

Rhyolitic tephras

The majority of rhyolitic ($>$ 70 wt.% SiO_2) tephra glass shards can also be classified as peralkaline (Fig. 5.9b). However, some shards from Lakes Hayk, Tilo and Hora have marginally peraluminous and metaluminous compositions.

Bi-variate plots (Fig. 5.10) of incompatible element Y, Zr, La and Th for all rhyolitic tephras show positive linear trends (Fig. 5.10b, c). These elements are excluded from the crystallising mineral assemblages, thus becoming concentrated in the melt as fractional crystallisation proceeds. However, glass shards in the majority of tephras show curvilinear positive Y/Nb trends (Fig. 5.10d), indicating that Nb is becoming progressively less compatible with increasing concentrations of Y. This may be related to the onset of a new phase crystallising during magmatic evolution, in which Nb may be mildy compatible.

Figure 5.11 shows a chondrite-normalised spider diagram (after Thompson, 1982). It is apparent that all rhyolitic tephras have similar trace element patterns, suggesting that they are derived from magmatic sources which are fractionating similar assemblages of minerals. All tephras display negative Ba, K, Sr and Ti anomalies, indicating that their magmatic evolution was dominated by the fractionation of feldspars and Fe-Ti oxides.

Average glass compositions of rhyolitic tephra glass shards from all lakes are projected onto the haplogranite or quartz-albite-orthoclase ternary diagram in Fig. 5.12, following the methods of Blundy and Cashman (2001). All compositions trend away from orthoclase feldspar towards the 50 MPa cotectic, reiterating

that the evolution of these tephras was dominated by fractional crystallisation of orthoclase.

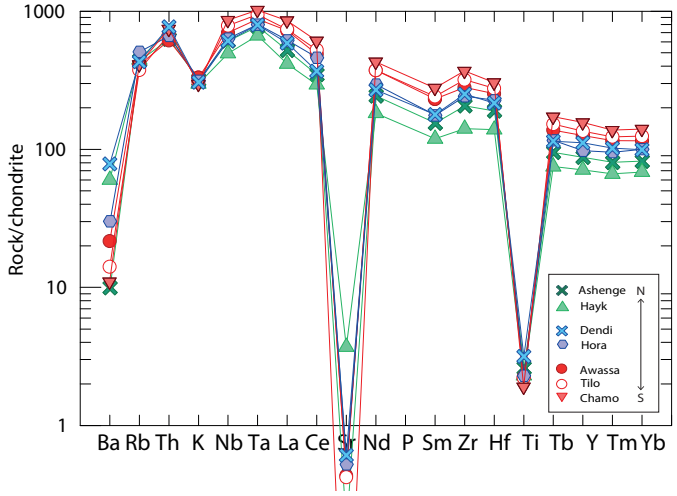

Figure 5.11: Average trace element concentrations of rhyolitic tephra glass shards from all lake sediments studied, normalised to chondrites after Thompson (1982).

Figures 5.10 to 5.12 demonstrate that tephras from lakes Awassa, Tilo and Chamo are more evolved than Ashenge, Hayk, Dendi and Hora tephras. Tephras from the central MER are more depleted in Zr, Hf and HREE and have reached minimum compositions, having evolved through continued fractional crystallisation of orthoclase (Figs. 5.11 and 5.12). However, the Ashenge, Hayk, Hora and Dendi tephras are less evolved and have not reached minimum compositions.

Figure 5.13 shows major and trace element ratios plotted against the latitudes of the lake in which they are recorded. Ratios of Zr/Th in the glass shards show the most systematic and apparent changes, ranging from $49.6 - 92.1$ in lake sediments in the south to $11.5 - 65.7$ in lake sediments to the north (Fig. 5.13f). This indicates that these tephras are derived from different sources, and that the geochemistry of these sources is varying systematically with latitude.

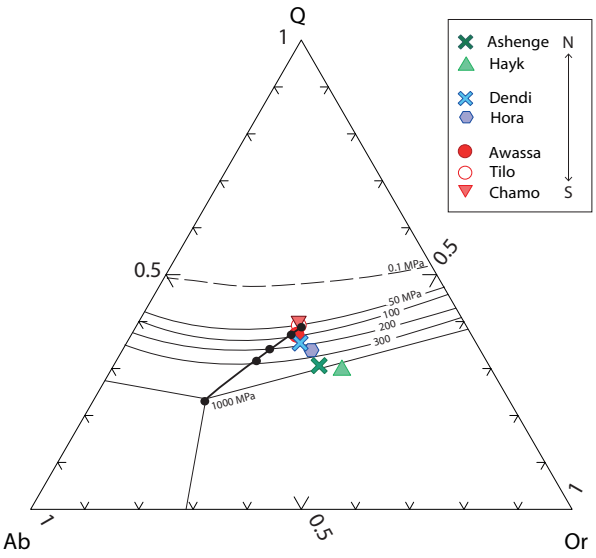

Figure 5.12: Projection of glass composition from rhyolitic tephras recorded in Ethiopian lake sediments onto a Qz-Ab-Or ternary, following methods of Blundy and Cashman (2001). Cotectic lines are from Blundy and Cashman (2001) and minima compositions are from Rollinson (1993).

It is apparent that tephras are broadly more evolved in southern Ethiopian lake archives. There are notable contrasts between the north and south tectonic settings of the lakes. The closest Holocene volcanoes ($<$ 70 km) to lake core sites in northern Ethiopia are located within the Afar Rift, where the highly extended crust is $\sim$ 20 km thick. However, the volcanoes in the Main Ethiopian Rift are located closest ($<$ 40 km) to lake core sites from southern Ethiopia, and here the crust reaches $\sim$ 30 km thick (Dugda *et al.*, 2005). Therefore, volcanoes supplying tephras to southern Ethiopian lakes may have evolved through greater interaction with the underlying crust.

The potential role of crustal assimilation in these tephras is explored further in Figure 5.14. This shows ratios of Rb/Nb versus Ba/Nb in rhyolitic tephra glass shards, with the composition of Precambrian Ethiopian basement rocks plotted for comparison (Peccerillo *et al.*, 1998). Melting of crustal rocks preserves or increases Rb/Nb and Ba/Nb ratios (Watt and Harley, 1993; Beard *et al.*,

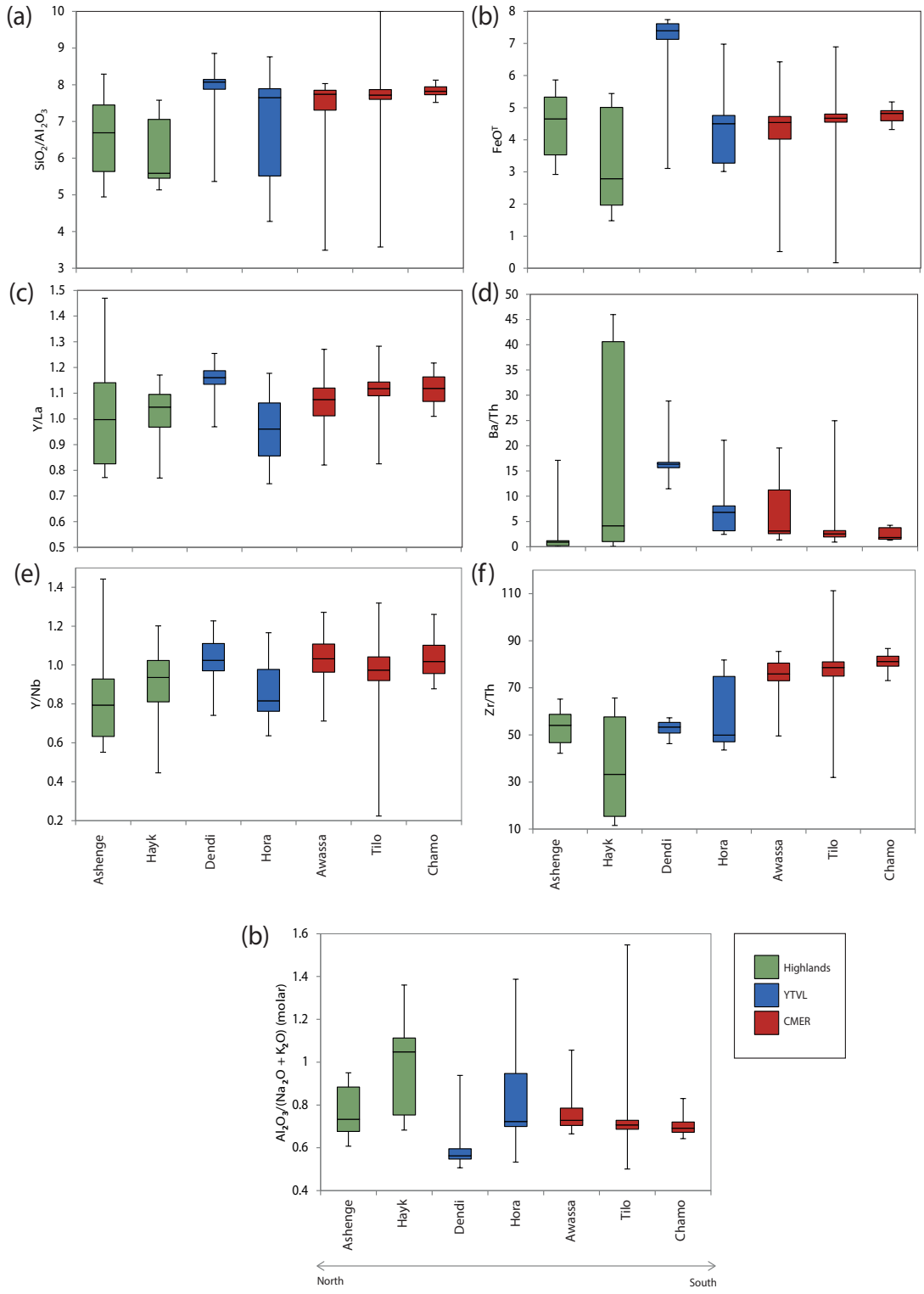

Figure 5.13: Selected major and trace element ratios for all rhyolitic tephra glass shards - ordered from north (left) to south (right).

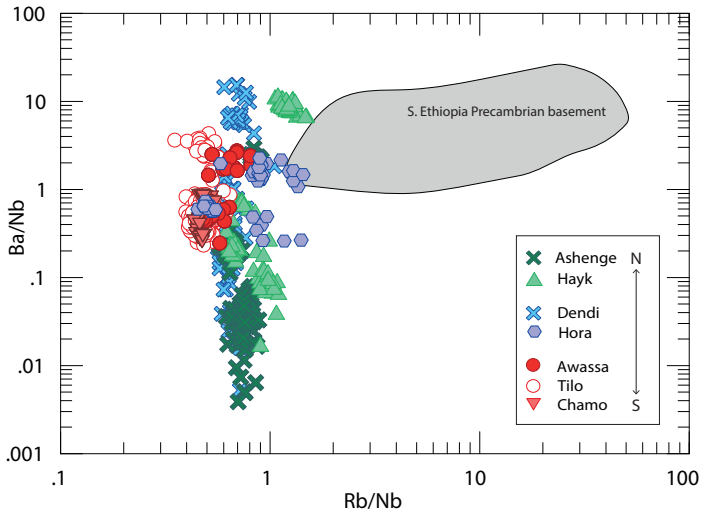

Figure 5.14: Rb/Nb versus Ba/Nb in glass shards from tephras recorded in all lake sediments. Compositions of Precambrian rocks from southern Ethiopia are from Peccerillo *et al.* (1998).

1994; Ayres and Harris, 1997), and they act as indicators of crustal assimilation. However, the composition of glass shards is not systematically influenced by interaction with the crust. One population of Hayk glass shards is more compositionally related to the southern Ethiopian basement rocks than other Hayk glass shards. This population may have been erupted from a volcano in the Afar that lay closer to the rift shoulders, where continental crust may have influenced the composition of the melt.

Broad differences in the geochemistry of tephras throughout Ethiopia cannot simply be related to varying amounts of crustal assimilation in the region. However, further interpretation is hindered by numerous limitations. This study assumes that tephras recorded in these archives are locally derived. Nonetheless, there is the possibility that tephras were erupted from distant volcanoes, and may not represent the composition of local sources. Furthermore, the interpretations made here are based only on glass compositions. Sampling of source volcanoes

and mineral analyses is required to ascertain the full range of compositions erupted.

This study has also generalised regional tectonic processes in the Ethiopian Rift and it is notable that there are smaller scale, basinal, tectonic variations (WoldeGabriel *et al.*, 1990). Macgregor (2015) outlined rifting in Ethiopia did not simply develop from north to south, and indicates that rifting in the central Main Ethiopian Rift commenced before extension in the northern Main Ethiopian Rift. This variation may further determine magma genesis and therefore tephra composition.

Phonolitic-trachytic tephras

The previous discussion has focussed on the predominant rhyolitic tephras from Ethiopian lake sediments. Numerous studies also document the prevalence of silicic compositions in the rift, with minor basalts and a characteristic lack of intermediate composition (Mohr, 1971; Berhe, 1987; Walter *et al.*, 1987; Mohr and Zanettin, 1988; Hart *et al.*, 1989; Peccerillo *et al.*, 2007).

Contrastingly, the thicker crust at the rift shoulders causes basaltic magmas to evolve at high pressures, and here volcanoes erupt trachytic compositions (Gasparon *et al.*, 1993; Peccerillo *et al.*, 2007). Lakes Dendi and Hora are located along the Yerer-Tullu Wellel Volcano Tectonic Lineament (YTVL), on the rift shoulders (Fig. 5.17). The composition of phonolitic-trachytic Dendi tephras is shown in Fig. 5.15, and it is apparent that they, like the rhyolitic tephras, have evolved through fractional crystallisation of feldspars and Fe-Ti oxides. These phonolitic-trachytic tephras have 5% nepheline in the calculated CIPW norm, and are therefore marginally silica-undersaturated. The CIPW norm of these tephras is plotted in Fig. 5.16, demonstrating that they have crystallised out

albite, and as the temperature drops, their melt composition is moving towards the feldspar-nepheline cotectic.

Lake Hora is located $\sim$ 100 km east of Lake Dendi and $<$ 40 km from the Main Ethiopian Rift (Fig. 5.17). The composition of the Hora tephras is, in contrast, silica-oversaturated (see Fig. 5.12). Adhana (2014) documents the change from silica-oversaturated to undersaturated compositions westwards along the YTVL, resulting in a decrease in melting away from the Main Ethiopian Rift. The Yerer-Bishoftu volcanoes and centres in the Main Ethiopian Rift are proximal to Lake Hora, and produce peralkaline rhyolites. Contrastingly, the Wechacha and Wenchi volcanoes, in the vicinity of Lake Dendi, produce silica saturated to marginally undersaturated alkali basalt-trachyte compositions. It is apparent that the Dendi and Hora archives provide effective records of the compositional variation along the YTVL.

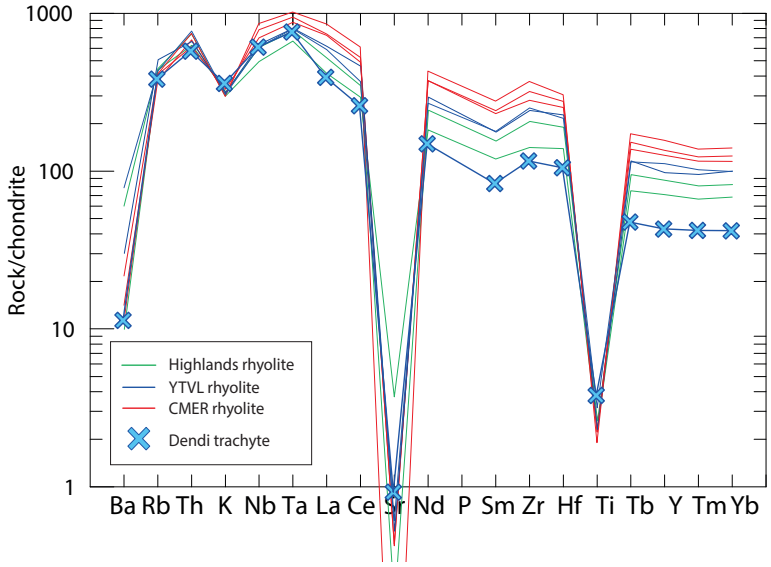

Figure 5.15: Average trace element concentrations in the Dendi phonolitic-trachytic tephra glass shards compared with average compositions of rhyolite glass shards from all other lakes, normalised to chondrites after Thompson (1982).

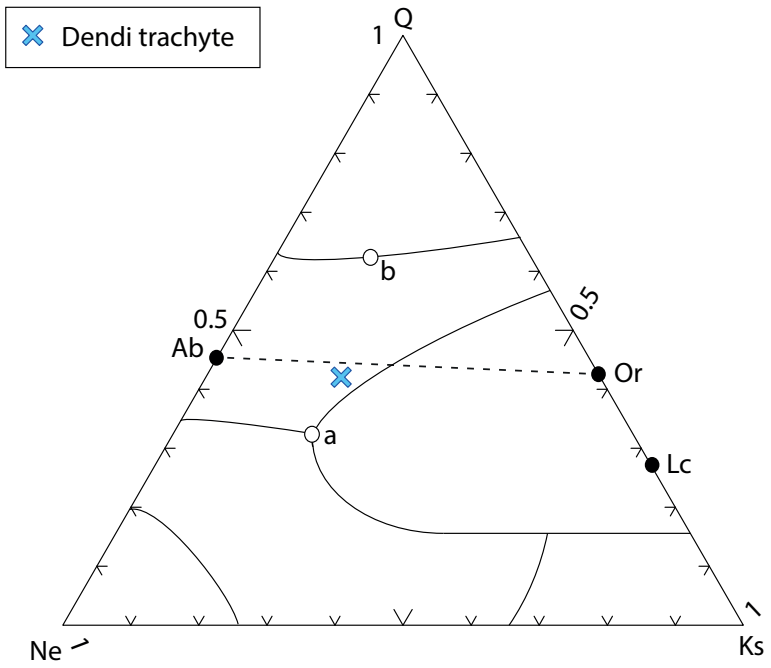

Figure 5.16: Projection of glass composition from phonolitic-trachytic Dendi tephras onto the quartz, nepheline and kalsilite residua system. 1100^{o}C contours are indicated, contours decrease either side of the albite-orthoclase thermal barrier (dashed line). The silica undersaturated Dendi tephras are evolving towards the feldspar-nepheline cotectic (a). Silica oversaturated compositions instead evolve towards the feldspar-quartz cotectic (b).

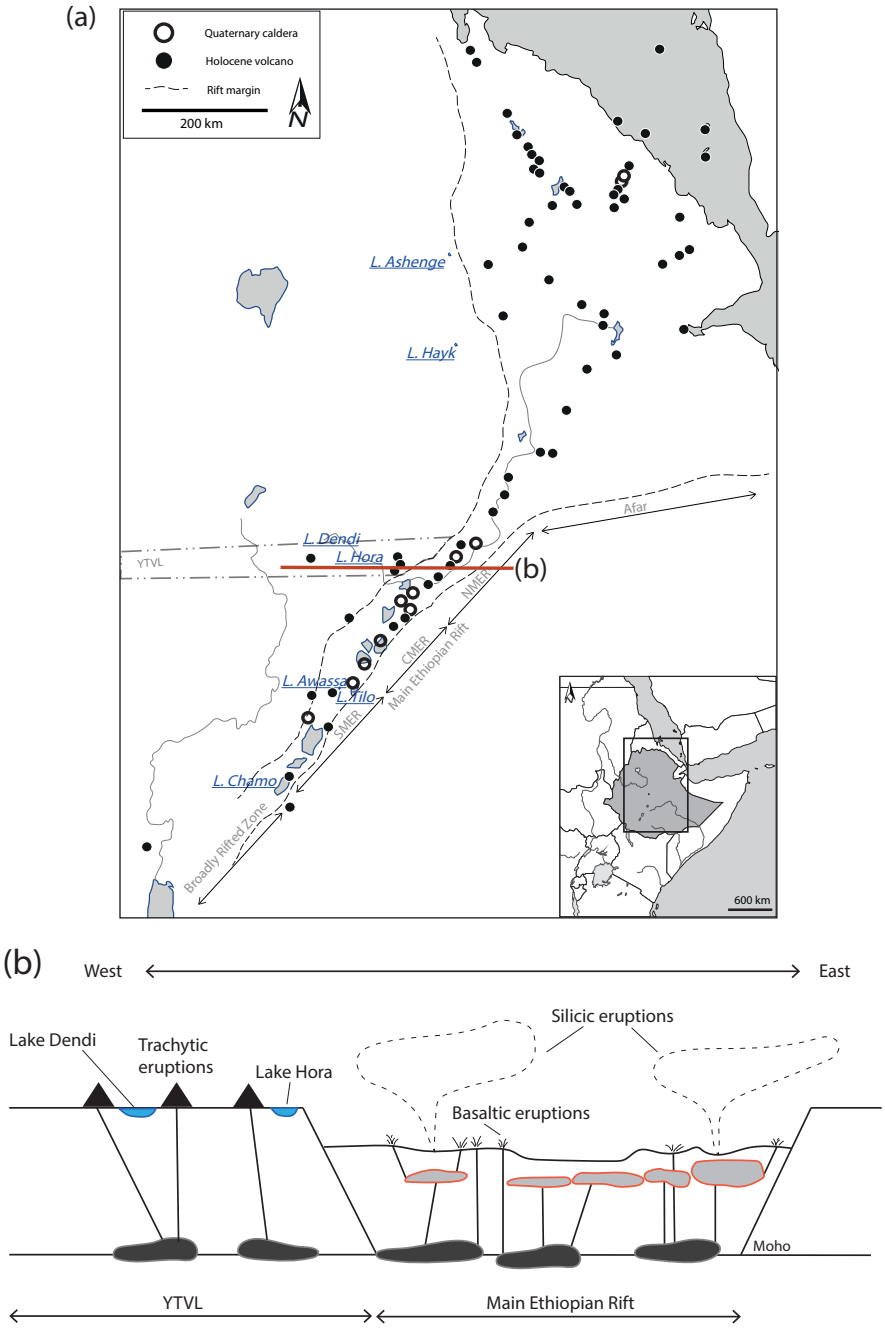

Figure 5.17: (a) Map of Ethiopia showing lake sites and Holocene volcanoes, (b) cross section schematic through the northern Main Ethiopian Rift and Yerer-Tullu Wellel Volcano Tectonic Lineament (YTVL). Red line in (a) shows its approximate location. The distribution of different magmatic types from west to east is shown, basaltic magmas evolve at high pressure to trachytes beneath the rift shoulders, silicic magmas are generated by fractional crystallisations at shallow depths. Figure (b) adapted from Peccerillo *et al.* (2007).

5.4.2 Potential tephra correlations

The previous discussion has demonstrated that Awassa, Tilo and Chamo tephras are more evolved than tephras occurring in archives from the Highlands. These compositional differences are reiterated in Fig. 5.18. Nonetheless, a population of Ashenge and Hayk tephra glass shards have similar Zr/Th ratios ($\approx 53.5 - 65.7$) to some Tilo tephra shards (Zr/Th $\approx 55.9 - 65.2$). However, these Tilo tephra glass shards contain higher Zr, Ba and Th concentrations than the Ashenge and Hayk tephras (Fig. 5.18c, e). The compositional differences between these tephras may be a product of their eruption from a zoned magma chamber. Whilst these Tilo tephras are enriched in incompatible elements, they also contain lower SiO_2 and Al_2O_3 than these Ashenge and Hayk shards. These different fractionation trends indicate these tephras are not co-genetic. Therefore, tephra correlations between these lakes will not be explored in forthcoming chapters.

Section 5.4.1 highlighted that the Dendi trachytic tephras, derived from the western Yerer-Tullu Wellel Volcano Tectonic Lineament (YTVL), are distinct. However, some tephras from the Hora archive (eastern YTVL) have similar Zr/Th ratios ($\approx 63.3 - 81.3$) to the Awassa, Chamo and most Tilo tephra glass shards ($\approx 56.2 - 92.1$, Figs. 5.19e). The composition of these tephras is further compared using a PCA, in Figs. 5.19b, d and f, and affirms that these tephras cannot be distinguished.

Furthermore, the sole rhyolitic Dendi tephra, and a population of Hora glass shards, have similar Zr/Th ratios ($\approx 43.6 - 54.3$) to a population of Ashenge and Hayk tephras (Zr/Th $\approx 42.2 - 65.7$). However, these Hora and Dendi glass shards contain higher Ba, and principal component analysis of their glass compositions reiterates that they are distinct (Fig 5.20d). It is possible that a change in wind direction during an eruption tapping a zoned magma chamber could cause this

large variation in tephra composition. For instance, the zoned Laacher See 12.92 cal. ka BP eruption deposited a spatially variable range of tephra compositions (e.g. Reide *et al.*, 2011).

However, assessment of this requires further sampling of regional tephras and source volcanoes to capture the full compositional range of the eruption. The Hora archive may represent a valuable link between tephra records from the Ethiopian Highlands, and those from the central Main Ethiopian Rift. However, the lack of stratigraphic and chronological control for the Hora tephras limits further investigation of these possible tephra correlations.

To establish regional correlations in Ethiopia, further lake core sites are required. The following chapters will investigate localised tephra correlations. Chapter 6 investigates potential correlations between Ashenge and Hayk (Ethiopian Highlands) and Chapter 7 investigates tephra deposits in the Awassa, Tilo and Chamo (CMER) archives.

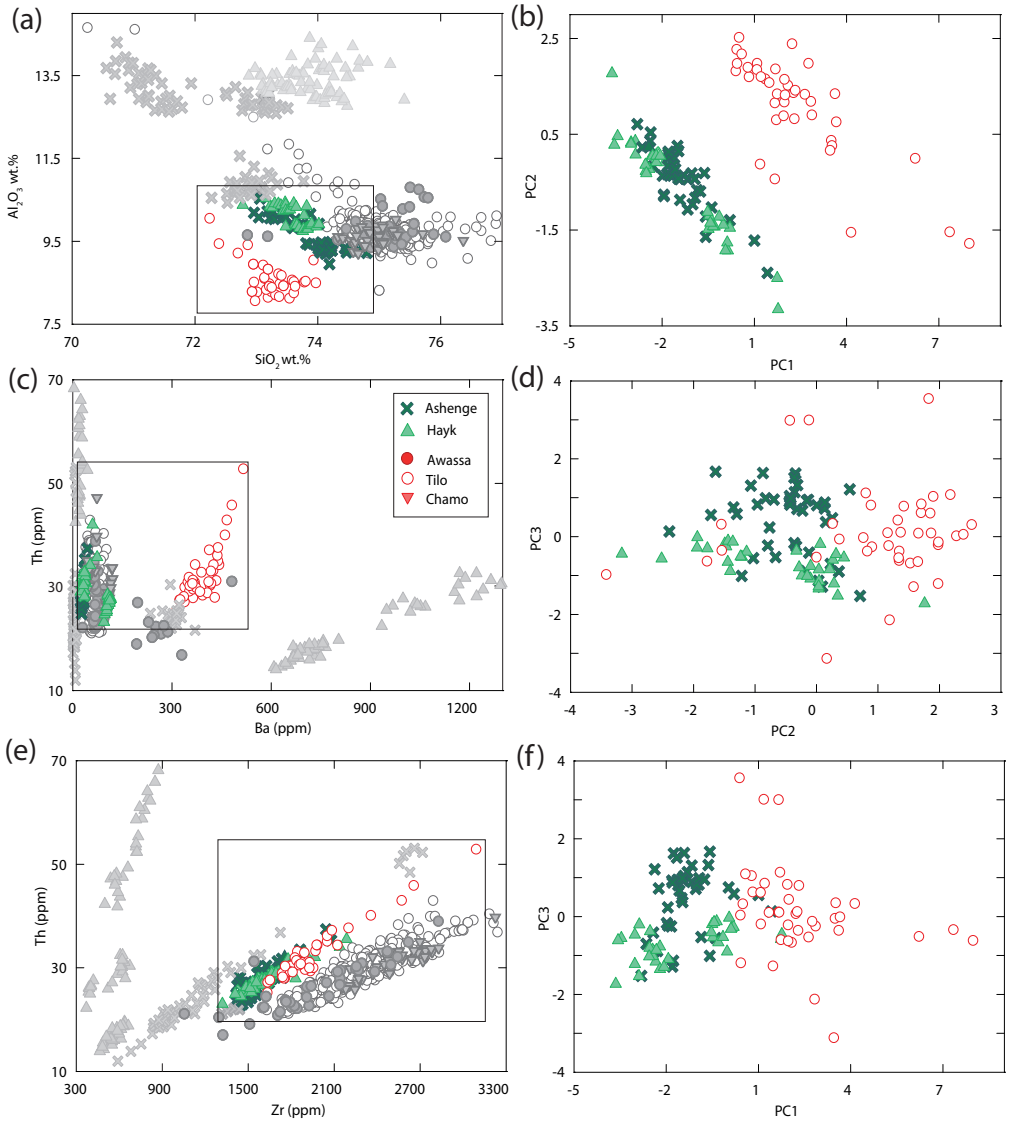

Figure 5.18: (a), (c), (e) Selected major and trace element bi-plots comparing the composition of tephras from lakes Ashenge and Hayk with Awassa, Tilo and Chamo tephras, those shown in grey scale are not included in the principal component analysis. (b), (d), (f) Principal component analysis comparing SiO_2, Al_2O_3, FeO^T, Y, Zr, Nb, Ba, La and Th concentrations in the compositionally similar Ashenge, Hayk and Tilo tephras.

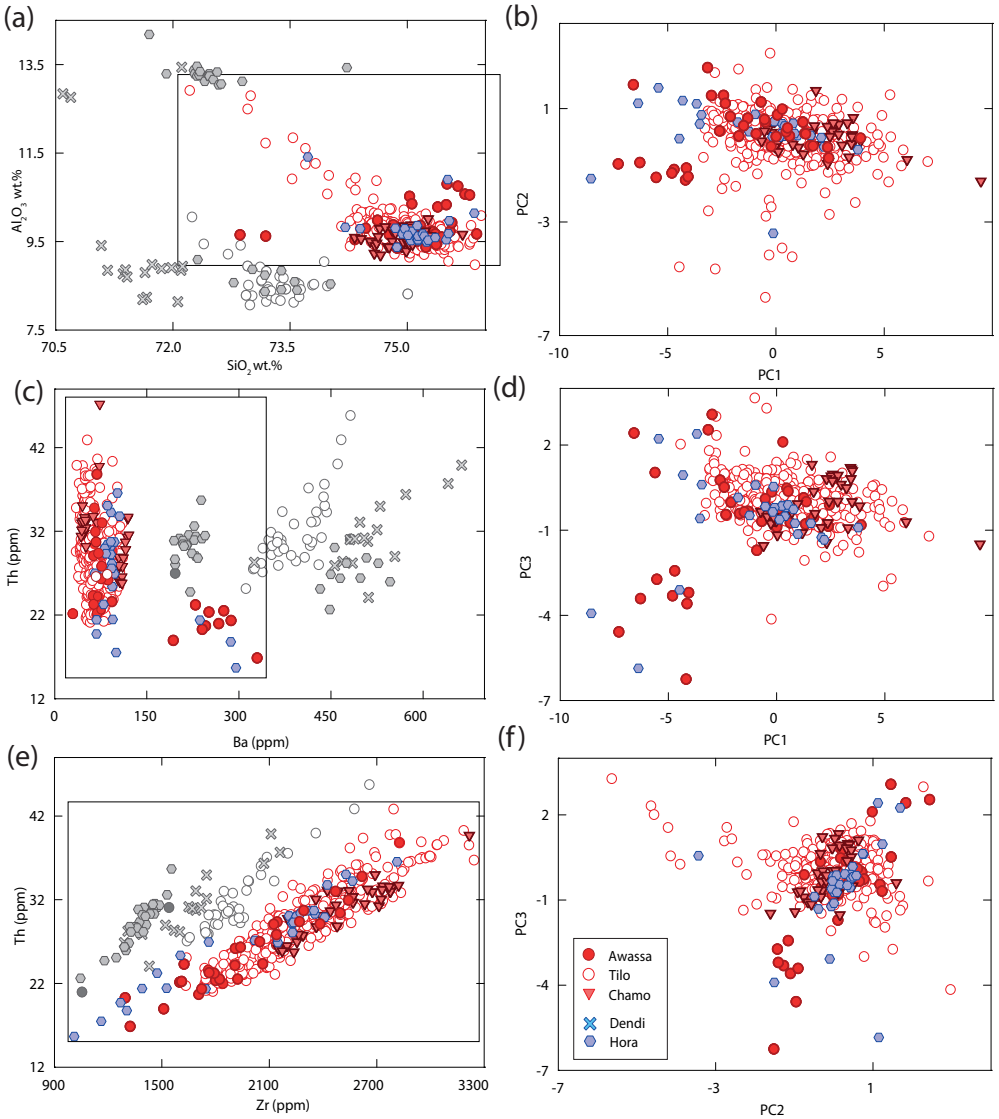

Figure 5.19: (a), (c), (e) Selected major and trace element bi-plots comparing the composition of tephras from lakes Dendi and Hora with Awassa, Tilo and Chamo tephras, those shown in grey scale are not included in the principal component analysis. (b), (d), (f) Principal component analysis comparing SiO_2, Al_2O_3, FeO^T, Y, Zr, Nb, Ba, La and Th concentrations in the compositionally similar Hora, Awassa, Tilo and Chamo glass shards.

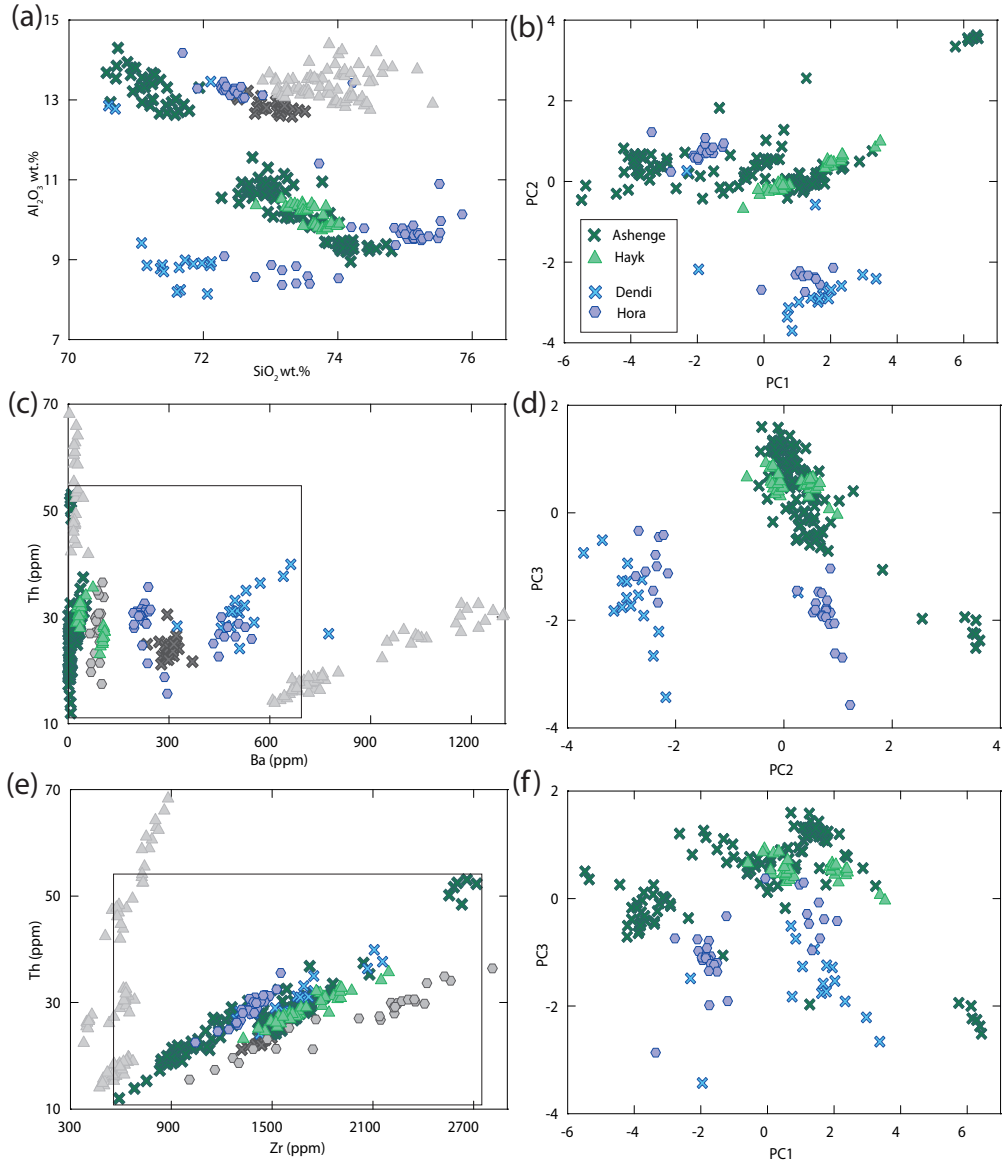

Figure 5.20: (a), (c), (e) Selected major and trace element bi-plots comparing the composition of tephras from lakes Ashenge and Hayk with Dendi and Hora tephras, those shown in grey scale are not included in the principal component analysis. (b), (d), (f) Principal component analysis comparing SiO_2, Al_2O_3, FeO^T, Y, Zr, Nb, Ba, La and Th concentrations in the compositionally similar Ashenge, Hayk, Dendi and Hora tephras.

5.5 Conclusions

This chapter has described the occurrence and physical characteristics of visible and crypto-tephras in the Ashenge, Hayk, Dendi, Hora, Awassa, Tilo and Chamo lake sediments. Bayesian age modelling has provided age ranges for the tephras in the archives. Archives from lakes Ashenge and Hayk, in the Ethiopian Highlands, contain a total of 21 visible and crypto-tephras, which range in age from $15.3 - 0.3$ cal. ka BP. A total of 7 visible tephras occur in the Hora and Dendi lake sediments, from the Yerer-Tullu Wellel Volcano Tectonic Lineament. The depths and ages of the Hora tephras remain unknown, whereas, the Dendi tephras range in age from $10.1 - 0.7$ cal. ka BP. Archives from lakes Awassa, Tilo and Chamo contain 23 visible and crypto-tephras, ranging in age from $10.2 - 0.01$ cal. ka BP.

The major and trace element composition of tephra glass shards has been presented. Tephra glass shards range in composition from minor phonolites and trachytes to predominant peralkaline rhyolites. However, some rhyolitic shards in lakes Hayk, Tilo and Hora are slightly peraluminous or metaluminous.

This section has investigated whether the geochemistry of the Holocene tephras changes systematically in relation to the location of the lake in which the tephras are recorded. Rhyolitic tephras are typically recorded in archives from lakes on the rift floor and the bordering rift escarpments. In contrast, tephras recorded in Lake Dendi are distinctly phonolitic-trachytic. Lake Dendi is located on the rift shoulders, where the trachytic composition of eruptives has been widely reported (Abebe *et al.*, 1995, 1998; Adhana, 2014). On the rift shoulders, mafic magmas pond in the lower crust and undergo high pressure evolution to form trachytic magmas (see Fig. 5.17). However, in the axial rift zone, magmas ascend more rapidly to form large zoned magma chambers, where

fractional crystallisation produces a peralkaline silicic upper layer overlying basalts (Peccerillo *et al.*, 2007). Furthermore, it is apparent that tephras recorded in lake sediments from the central Main Ethiopian Rift (CMER) are broadly more evolved than those recorded in lakes to the north. Extension decreases from the Afar Rift towards the Main Ethiopian Rift and this variation may influence melt production. However, it is likely that localised tectonic variations also influence melt composition. Therefore, further sampling of regional volcanoes coupled with chronological control, is required to further investigate this relationship.

Importantly, this chapter has provided the rationale for the tephra correlations explored in the coming chapters. Many of the tephras have distinct compositions; SiO_2, Al_2O_3, FeO^T, Y, Zr, Nb, Ba, La and Th are particularly useful for their discrimmination. Potential regional tephra correlations have been explored both graphically, using major and trace element bi-plots, and statistically, using principal component analysis. It is apparent that regional tephra correlations cannot be established in Ethiopia at this stage. The Hora archive may provide tephra links between central Ethiopia, and those from the Ethiopian Highlands and the central Main Ethiopian Rift. However, stratigraphic and chronological control for the Hora tephras is required before correlations can be assessed. Therefore, local tephra correlations between lakes Ashenge and Hayk will be explored in Chapter 6. This is followed by an investigation of potential correlations between Awassa, Tilo and Chamo archives in Chapter 7.

Chapter 6

The timing and composition of post-17 ka distal volcanism from the Afar recorded in Lakes Ashenge and Hayk

6.1 Introduction

Tephras recorded in lake sediments from Ashenge and Hayk (Ethiopian Highlands) are investigated in this chapter. Potential tephra correlations between these archives are tested and factors influencing these correlations are considered. These archives also provide an important record of past volcanism. The likely sources for these tephras and the information they provide on past eruption frequency is discussed.

6.2 The composition of the Ashenge and Hayk tephras

6.2.1 The Ashenge tephras

The major and trace element composition of the Ashenge tephra glass shards is given in Table 6.1 and Fig.6.1. The Ashenge tephra glass shards are compositionally distinct and can be divided into three groups based on their varying Y/La and Zr/Th ratios. These ratios may be indicative of three different groups of fractionating magma. The composition of the Ashenge tephras is discussed below in terms of glass shards sharing similar incompatible element ratios, and potentially of co-magmatic origin.

Table 6.1: Selected normalised major element (wt.%) and trace element (ppm) concentrations of glass shards in the Ashenge tephras. These elements have proven particularly useful for discrimination. Average (± st. dev.) concentrations of selected elements which have proved to be useful for correlation are shown here. The range of element concentrations in each tephra is shown in italics, minimum and maximum element concentrations in glass shards from each group of tephras are given in bold.

	Group I					Group II			Group III
	AST-1	**AST-2**	**AST-7**	**AST-8**	**AST-9**	**AST-3**	**AST-4**	**AST-6**	**AST-5**
Age (ka)	0.5 – 0.3	5.0 – 4.8	7.6 – 6.7	14.6 – 13.6	15.3 – 13.8	5.6 – 5.0	5.9 – 5.3	7.5 – 6.5	7.2 – 6.4
SiO_2	71.04 (0.21)	71.25 (0.37)	72.74 (0.83)	72.84 (0.17)	72.82 (0.26)	73.51 (0.29)	74.17 (0.20)	74.25 (0.28)	72.99 (0.34)
	70.71 - 71.36	***70.56*** *- 71.79*	*71.24 -* ***73.77***	*72.57-73.08*	*72.27 - 73.22*	***72.96*** *- 74.02*	*73.81 - 74.57*	*73.99 -* ***74.80***	*71.94 - 73.51*
Al_2O_3	13.58 (0.32)	13.12 (0.43)	11.45 (1.10)	10.89 (0.10)	10.63 (0.09)	10.03 (0.13)	9.33 (0.08)	9.31 (0.15)	12.85 (0.19)
	13.21 - ***14.30***	*12.66 - 13.94*	***10.08*** *- 13.40*	*10.70 - 11.05*	*10.43 - 10.78*	*9.82 -* ***10.22***	*9.20 - 9.48*	***8.95*** *- 9.47*	*12.59 - 13.31*
FeO^T	3.58 (0.21)	3.81 (0.26)	4.08 (0.57)	4.76 (0.14)	4.94 (0.14)	5.37 (0.11)	5.53 (0.53)	5.48 (0.14)	3.11 (0.14)
	3.14 *- 3.84*	*3.30 - 4.28*	*3.18 -* ***5.26***	*4.60-5.03*	*4.75-5.20*	***5.18*** *- 5.55*	*5.23 -* ***5.86***	*5.24 - 5.66*	*2.92 - 3.48*
Na_2O	6.00 (0.17)	6.04 (0.21)	6.30 (0.28)	6.07 (0.16)	6.28 (0.19)	5.82 (0.18)	5.75 (0.17)	5.81 (0.20)	5.57 (0.19)
	5.81 - 6.32	***5.59*** *- 6.47*	*5.87 -* ***7.01***	*5.89-6.35*	*5.89-6.58*	*5.43 -* ***6.26***	*5.47 - 6.07*	***5.40*** *- 6.09*	*5.09 - 6.06*
K_2O	4.80 (0.08)	4.82 (0.12)	4.77 (0.21)	4.45 (0.08)	4.60 (0.08)	4.46 (0.08)	4.42 (0.08)	4.41 (0.06)	4.64 (0.11)
	4.66 - 4.91	*4.52 - 5.00*	*4.57 -* ***5.23***	***4.28*** *- 4.56*	*4.50-4.75*	***4.32 - 4.58***	*4.32 - 4.57*	*4.36 - 4.52*	*4.48 - 4.94*
Y	99.7 (12.4)	109 (23.7)	127 (29.9)	233 (66.9)	153 (14.4)	209 (14.0)	213 (12.3)	223 (21.7)	205 (12.4)
	67.6 *- 113*	*87.8 - 199*	*68.6-170*	*148 -* ***291***	*128-187*	***192*** *- 241*	*193 - 240*	*199 -* ***262***	*186 - 247*
Zr	888 (110)	955 (199)	1240 (265)	2160 (596)	1160 (138)	1650 (107)	1660 (98.2)	1770 (177)	1480 (87.1)
	590 *- 1000*	*753 - 1730*	*681 - 1590*	*1440 -* ***2720***	*876 - 1380*	*1510 - 1860*	***1450*** *- 1860*	*1590 -* ***2080***	*1320 -1780*
Nb	160 (18.9)	172 (43.2)	207 (42.1)	366 (103)	233 (12.3)	226 (8.12)	239 (7.81)	253 (9.88)	157 (4.87)
	106 *- 169*	*141 - 353*	*106 - 256*	*235 -* ***460***	*205 - 253*	***213*** *- 240*	*224 - 257*	*240 -* ***271***	*150 - 171*
Ba	5.30 (3.10)	4.46 (2.70)	3.64 (2.54)	7.44 (3.08)	6.54 (2.27)	30.1 (6.99)	30.9 (2.88)	37.9 (4.97)	303 (24.4)
	2.01 - 10.8	*0.860 -* ***11.7***	***0.560*** *- 7.29*	*1.26 - 11.1*	*3.09 - 11.2*	*25.2 -* ***53.3***	***24.6*** *- 34.6*	*32.8 - 46.6*	*235 - 370*
La	122 (14.8)	133 (28.9)	154 (35.3)	284 (79.8)	181 (15.4)	186 (11.3)	190 (11.1)	197 (21.0)	143 (8.4)
	82.2 *- 134*	*99.7 - 242*	*83.7 - 205*	*187 -* ***356***	*152 - 206*	***171*** *- 208*	*172 - 221*	*176 -* ***246***	*127 - 170*
Ce	230 (28.2)	240 (30.1)	278 (57.2)	502 (132)	263 (25.4)	329 (16.5)	341 (14.9)	371 (25.4)	259 (13.2)
	152 - 250	*196 - 342*	***148*** *- 346*	*335 -* ***619***	*206 - 304*	***306*** *- 361*	*312 - 369*	*344 -* ***427***	*232 - 294*
Hf	22.6 (3.40)	27.3 (13.5)	31.0 (5.99)	55.7 (15.4)	35.4 (3.79)	43.6 (2.48)	43.3 (3.26)	45.3 (4.32)	40.1 (2.90)
	13.7 *- 26.4*	*19.6 -* ***83.3***	*18.1 - 39.0*	*34.3 - 72.4*	*27.5 - 40.9*	*40.0 - 47.5*	***36.0*** *- 49.3*	*40.4 -* ***53.0***	*35.2 - 48.6*
Th	19.2 (2.67)	20.7 (4.19)	24.5 (5.10)	42.5 (11.6)	25.9 (2.87)	28.7 (1.99)	28.9 (1.92)	30.6 (3.54)	24.1 (1.89)
	12.0 *- 21.5*	*15.3 - 36.8*	*13.9 - 32.5*	*27.1 -* ***53.1***	*20.0 - 30.3*	***24.8*** *- 32.2*	*25.7 - 33.5*	*27.0 -* ***37.4***	*21.2 - 30.5*
U	5.42 (0.661)	5.97 (1.22)	6.86 (1.09)	11.2 (3.18)	10.1 (1.31)	6.54 (0.353)	6.65 (0.354)	7.84 (0.241)	5.89 (0.412)
	3.58 *- 5.86*	*4.65 - 10.8*	*4.03 - 8.14*	*7.27 -* ***14.5***	*8.44 - 13.3*	***5.98*** *- 7.33*	*6.05 - 7.29*	*7.48 -* ***8.17***	*5.63 - 6.94*
	$n = 10$	$n = 20$	$n = 12$	$n = 9$	$n = 16$	$n = 14$	$n = 20$	$n = 10$	$n = 10$

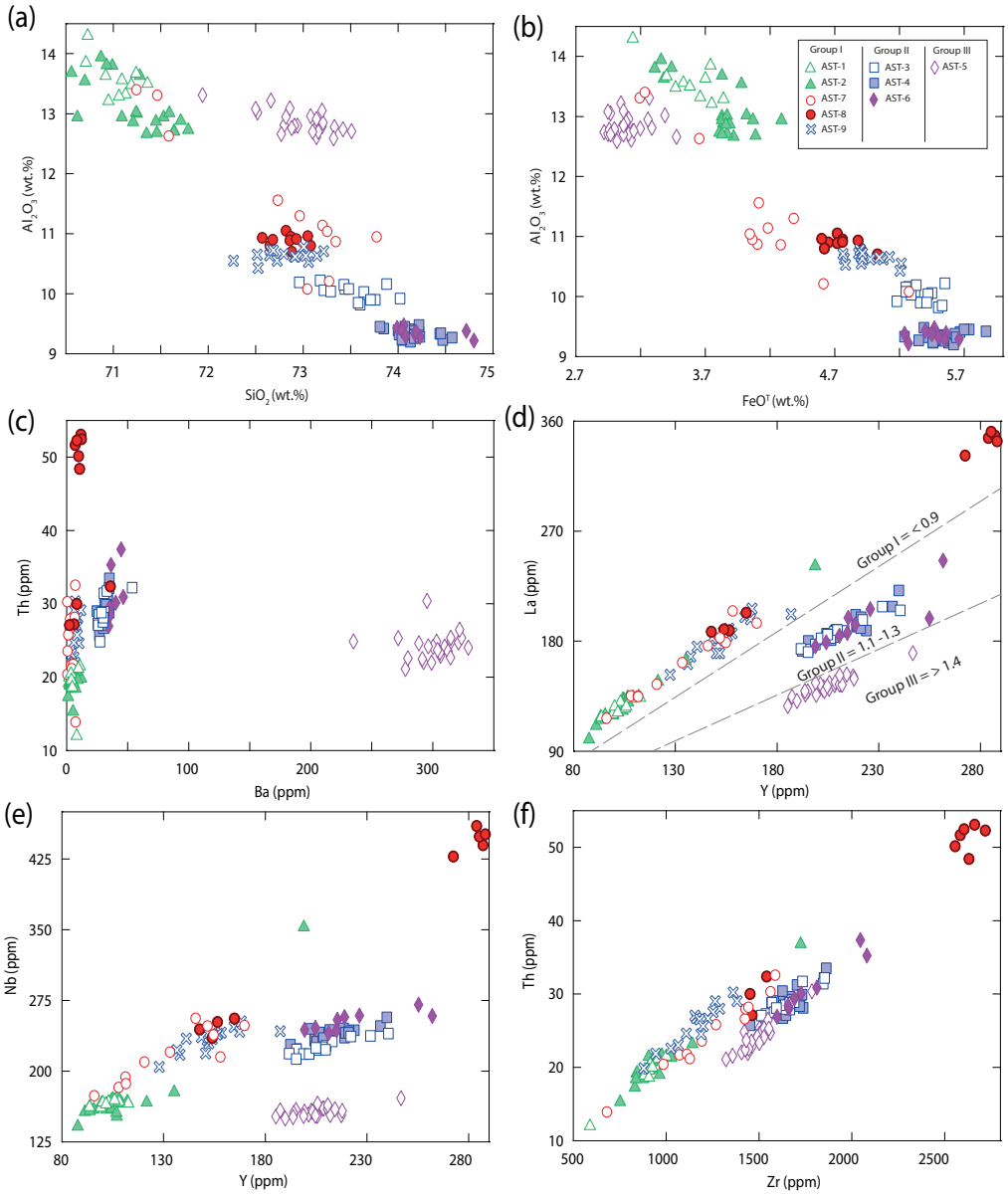

Figure 6.1: Major and trace element composition of single shards from the Ashenge tephras. Incompatible element ratios (d, e, f) divide the Ashenge tephras into three compositional groups.

6.2.1.1 *Group I Ashenge tephras:* AST-1; 2; 7; 8 & 9, Y/La ≈ 0.6 - 0.9

The Group I tephras have a wide range of ages ($\sim 15.30 - \sim 0.3$ cal. ka BP) and tephras of this composition are not recorded in the Ashenge sediments between $\sim 6.2 - \sim 5.0$ cal. ka BP. The younger and older Group I tephras can be distinguished between: AST-1 and AST-2, contain lower SiO_2 and FeO^T concentrations and higher Al_2O_3 concentrations than the older AST-8 and AST-9 (Table 6.1, Fig. 6.1a,b). AST-8 glass shards are compositionally bimodal; one population has a similar composition to other Group I tephras whilst those in the second population are more evolved, containing glass shards with comparatively higher Y, Zr, La and Th concentrations (Fig. 6.1d, e, f). The first tephra recorded after the hiatus in the lake record, AST-7, contains glass shards which cannot be compositionally distinguished from other Group I Ashenge tephra glass shards.

6.2.1.2 *Group II Ashenge tephras:* AST-3; 4 & 6, Y/La ≈ 1.1 - 1.3

Group II Ashenge tephra glass shards (AST-3, 4 and 6) are restricted to the mid-Holocene ($\sim 7.5 - \sim 5.0$ cal. ka BP) sediments. Their glass shards have higher Y/La ratios and contain higher Ba concentrations than Group I tephras (Table 6.1, Fig. 6.1c,d). Group II tephra glass shards contain broadly higher Zr/Th ratios ($\approx 42.3 - 61.8$) when compared to Group I tephra glass shards (Fig. 6.1f). Glass shards in Group II tephras contain the highest SiO_2 and FeO^T and the lowest Al_2O_3 concentrations when compared with other Ashenge tephras (Table 6.1, Fig. 6.1a, b).

The Group II Ashenge tephras have differing glass shard compositions. Glass shards in AST-3 contain lower SiO_2 and higher Al_2O_3 concentrations than AST-4 and AST-6 (Table 6.1, Fig. 6.1a, b).

6.2.1.3 *Group III Ashenge tephras:*, AST-5, Y/La ≈ 1.4 - 1.5

AST-5 ($\sim 7.2- \sim 6.4$ cal. ka BP) has a distinct composition when compared with all other Ashenge tephras and is the sole member of Group III. Glass shards in AST-5 have the highest Y/La and Ba concentrations amongst the Ashenge tephras (Table 6.1, Fig. 6.1c,e). Group III tephra shards have the highest Zr/Th ratios (≈ 57.0 - 65.2) of the other Ashenge tephras. Plots of SiO_2 against Al_2O_3 and FeO^T (Fig. 6.1a, b) concentrations in the Ashenge glass shards show that AST-5 glass shards have distinct major element ratios when compared with other Ashenge glass shards.

6.2.2 The Hayk tephras

The rhyolitic Hayk tephra glass shards separate into five different populations on the basis of their varying Zr/Th ratios. These differing ratios may suggest that the Hayk tephras are derived from five different centres and the composition of these tephras is explored in detail below in relation to these groupings.

6.2.2.1 *Group I Hayk tephras:* HT-2 & 4, Zr/Th ≈ 30.4 - 37.9

Glass shards in Group I tephras (HT-2 and HT-4) are the youngest tephras ($\sim 3.6- \sim 2.5$ cal. ka BP) in the Hayk core to have been analysed and have the differing Zr/Th ratios to older Hayk glass shards.

Group I tephra glass shards contain lower FeO^T concentrations than Hayk Group IV and higher FeO^T concentrations than Hayk Group II, III and V glass shards. Glass shards in the Group I tephras are depleted in Y, Nb, La and Th relative to glass shards in all other Hayk tephras. Glass shards in Group I tephras contain higher Ba concentrations than Group IV and V glass shards and lower Ba concentrations than Group II and III tephra glass shards.

HT-2 and HT-4 tephras cannot be distinguished compositionally; although HT-2 glass shards contain broadly higher Y concentrations than HT-4.

6.2.2.2 *Group II Hayk tephras:* HT-5, Zr/Th ≈ 18.9 - 23.2

The late-Holocene HT-5 ($\sim 3.9 - \sim 2.9$ cal. ka BP) is the sole tephra member of Group II, with a distinct Zr/Th ratio to glass shards in other Hayk tephras. Glass shards in this tephra are distinguished from other Hayk tephras on the basis of their higher Ba concentrations. HT-5 and HT-6 glass shards have broadly lower Y/La ratios (≈ 0.8 - 0.9) when compared with other Hayk tephras (≈ 0.9 - 1.2). However, HT-5 contains higher Y, Zr, La and Ba concentrations than HT-6 glass shards.

6.2.2.3 *Group III Hayk tephras:* HT-6, Zr/Th ≈ 15.1 - 16.9

HT-6 ($4.0 - 3.2$ cal. ka BP) is the only tephra comprising Group III; its glass shards in this tephra contain distinctly lower Zr concentrations than all other Hayk tephras.

6.2.2.4 *Group IV Hayk tephras:* HT-7 & 12, Zr/Th ≈ 55.1 - 65.7

Group IV Hayk tephras (HT-7 and HT-12) are easily distinguished from other Hayk tephras, containing higher FeO^T and Zr and lower Al_2O_3 than other Hayk tephras (Table 6.2, Fig. 6.2b, f). Group IV tephras have the widest ranges of ages ($\sim 13.0 - \sim 3.8$ cal. ka BP) when compared with all other tephra groups recorded in the Hayk sediments.

HT-7 contains higher Zr, La and Th and lower Al_2O_3 and Ba when compared with glass shards in HT-12, the oldest tephra identified in the Hayk sediments (Fig. 6.2a, d, f).

6.2.2.5 *Group V Hayk tephras:* HT-9 & 10, Zr/Th $\approx$ 11.5 - 14.2

Group V tephras (HT-9 and HT-10) are restricted to the early Holocene ($\sim$ 11.0$-$ $\sim$ 8.4 cal. yr BP) section of the Hayk sediments. Their glass shards have distinct Zr/Th ratios when compared with other Hayk tephra glass shards (Table 6.2, Fig. 6.2f). Glass shards in these tephras are more enriched in Th when compared with other Hayk tephras (Fig. 6.2f).

Glass shards in HT-9 can be compositionally distinguished from those in the older HT-10 tephra. Glass shards in HT-9 contain higher Zr, Nb, La and Th than HT-10 (Fig. 6.2c, d, e, f).

Table 6.2: Selected average normalised major element (wt.%) and trace element (ppm) concentrations of glass shards in each of the Hayk tephras. Elements which have proved to be useful for correlation are shown here. The standard deviation the concentration of each element in each tephra is given in brackets, the range of element concentrations in each tephra is given in italics. The minimum and maximum element concentrations in glass shards from each group of tephras are given in bold. Major element concentrations are presented to two decimal places and trace element concentrations are presented to three significant figures, the grain specific compositions for all analytes are given in the supplementary materials.

	Group I		Group II	Group III	Group IV		Group V	
	HT-2	**HT-4**	**HT-5**	**HT-6**	**HT-7**	**HT-12**	**HT-9**	**HT-10**
Age (ka)	2.9 – 2.5	3.6 – 2.8	3.9 – 2.9	4.0 – 3.2	4.8 – 3.8	13.0 – 12.0	10.5 – 8.4	11.0 – 8.9
SiO_2	73.26 (0.17)	73.45 (0.37)	74.31 (0.40)	74.18 (0.27)	73.78 (0.15)	73.44 (0.24)	74.23 (0.37)	73.71 (0.22)
	*73.07 - **75.53***	***72.88** - 74.48*	*73.65 - 75.18*	*73.87 - 74.57*	*73.48 - **74.02***	***72.78** - 73.82*	*73.87 - **75.41***	***73.33** - 74.19*
Al_2O_3	13.28 (0.14)	13.21 (0.18)	13.66 (0.11)	14.03 (0.32)	9.81 (0.05)	10.33 (0.09)	12.98 (0.12)	13.48 (0.21)
	13.14 - 13.52	***12.75 - 13.66***	*13.46 - 13.84*	*13.44 - 14.39*	***9.73** - 9.91*	*10.11 - **10.52***	***12.82** - 13.33*	*13.17 - **13.95***
FeO^T	2.92 (0.13)	2.85 (0.13)	1.88 (0.20)	1.72 (0.15)	5.28 (0.11)	5.13 (0.14)	2.02 (0.08)	2.01 (0.10)
	*2.69 - **3.18***	***2.50** - 3.12*	*1.50 - 2.38*	*1.48 - 1.89*	*5.07 - 5.44*	***4.89 - 5.44***	*1.90 - 2.21*	***1.81** - 2.18*
Na_2O	4.90 (0.17)	4.79 (0.15)	4.34 (0.39)	4.31 (0.12)	5.53 (0.15)	5.46 (0.14)	4.86 (0.41)	4.77 (0.12)
	*4.54 - **5.12***	***4.45** - 5.05*	*3.30 - 4.70*	*4.14 - 4.47*	*5.28 - **5.84***	***5.19** - 5.81*	***3.58 - 5.27***	*4.57 - 4.94*
K_2O	3.64 (0.07)	3.73 (0.10)	4.39 (0.08)	4.47 (0.04)	4.46 (0.07)	4.54 (0.08)	4.81 (0.10)	4.86 (0.07)
	***3.52** - 3.72*	*3.58 - **4.00***	*4.27 - 4.55*	*4.44 - 4.55*	***4.35** - 4.56*	*4.37 - **4.67***	***4.69 - 5.04***	*4.73 - 5.00*
Y	82.4 (5.08)	71.9 (6.20)	109 (8.59)	87.2 (3.57)	245 (16.7)	191 (9.16)	163 (18.7)	122 (14.6)
	*74.3 - **91.3***	***59.3** - 80.5*	*92.8 -118*	*80.9 - 92.1*	*215 - **289***	***170** - 202*	*118 - **198***	***100** - 149*
Zr	609 (31.4)	553 (51.1)	616 (38.9)	401 (14.2)	1870 (127.7)	1560 (90.1)	772 (78.4)	613 (68.6)
	*570 - **670***	***471** - 638*	*528 - 679*	*377 - 425*	*1670 - **2190***	***1330** - 1660*	*576 - **879***	***505** - 739*
Nb	73.8 (2.50)	71.3 (4.37)	103 (3.04)	101 (5.58)	249 (7.86)	220 (5.09)	277 (17.7)	248 (15.5)
	70.5 - 77.7	***65.4 - 81.6***	*95.3 -107*	*92.0 - 109*	*238 - **268***	***210** - 229*	*237 - **307***	***225** - 274*
Ba	733 (37.0)	680 (42.0)	1210 (70.4)	1000 (44.6)	37.6 (10.6)	108 (5.96)	25.0 (10.4)	23.1 (12.7)
	*677 - **805***	***609** - 757*	*1070 - 1320*	*935 - 1050*	***25.2** - 74.8*	*95.6 - **116***	***4.51** - 45.3*	*9.12 - **60.6***
La	82.1 (4.34)	73.2 (6.80)	123 (10.3)	109 (5.42)	224 (16.7)	175 (9.68)	148 (16.7)	115 (9.29)
	*76.9 - **90.6***	***62.7** - 83.0*	*98.5 - 134*	*100 - 115*	*199 - **267***	***153** - 188*	*111 - **181***	***99.5** - 133*
Ce	153 (4.61)	146 (8.58)	213 (16.6)	187 (7.72)	391 (22.9)	349 (15.5)	283 (20.2)	228 (21.6)
	*148 - **164***	***130** - 159*	*175 - 232*	*171 - 195*	*356 - **458***	***309** - 374*	*229 - **321***	***197** - 280*
Hf	17.2 (1.67)	16.1 (1.70)	19.9 (2.05)	13.7 (0.972)	47.0 (3.61)	40.4 (2.09)	30.0 (3.66)	22.9 (2.55)
	*14.3 - **19.9***	***13.3** - 18.8*	*16.4 - 23.7*	*12.3 - 14.8*	*40.4 - **54.3***	***35.6** - 43.0*	*22.2 - **37.1***	***17.2** - 27.0*
Th	17.8 (1.12)	16.7 (1.70)	29.9 (1.96)	25.7 (1.58)	31.2 (1.81)	26.6 (1.40)	59.9 (6.66)	47.2 (3.94)
	*16.1 - **19.6***	***13.9** - 18.9*	*26.0 - 32.5*	*25.7 - 27.6*	*28.0 - **35.5***	***23.0** - 28.3*	*46.0 - **70.4***	***41.9** - 55.4*
U	4.41 (0.311)	4.59 (0.351)	6.08 (0.453)	5.62 (0.382)	7.01 (0.343)	7.40 (0.252)	16.1 (0.913)	15.9 (1.06)
	***3.89** - 4.90*	*3.98 - **5.28***	*5.01 - 6.71*	*4.85 - 5.97*	***6.44 - 7.81***	*7.00 - 7.74*	*15.1 - **18.4***	***14.2** - 17.7*
	$n = 12$	$n = 19$	$n = 15$	$n = 8$	$n = 20$	$n = 18$	$n = 15$	$n = 12$

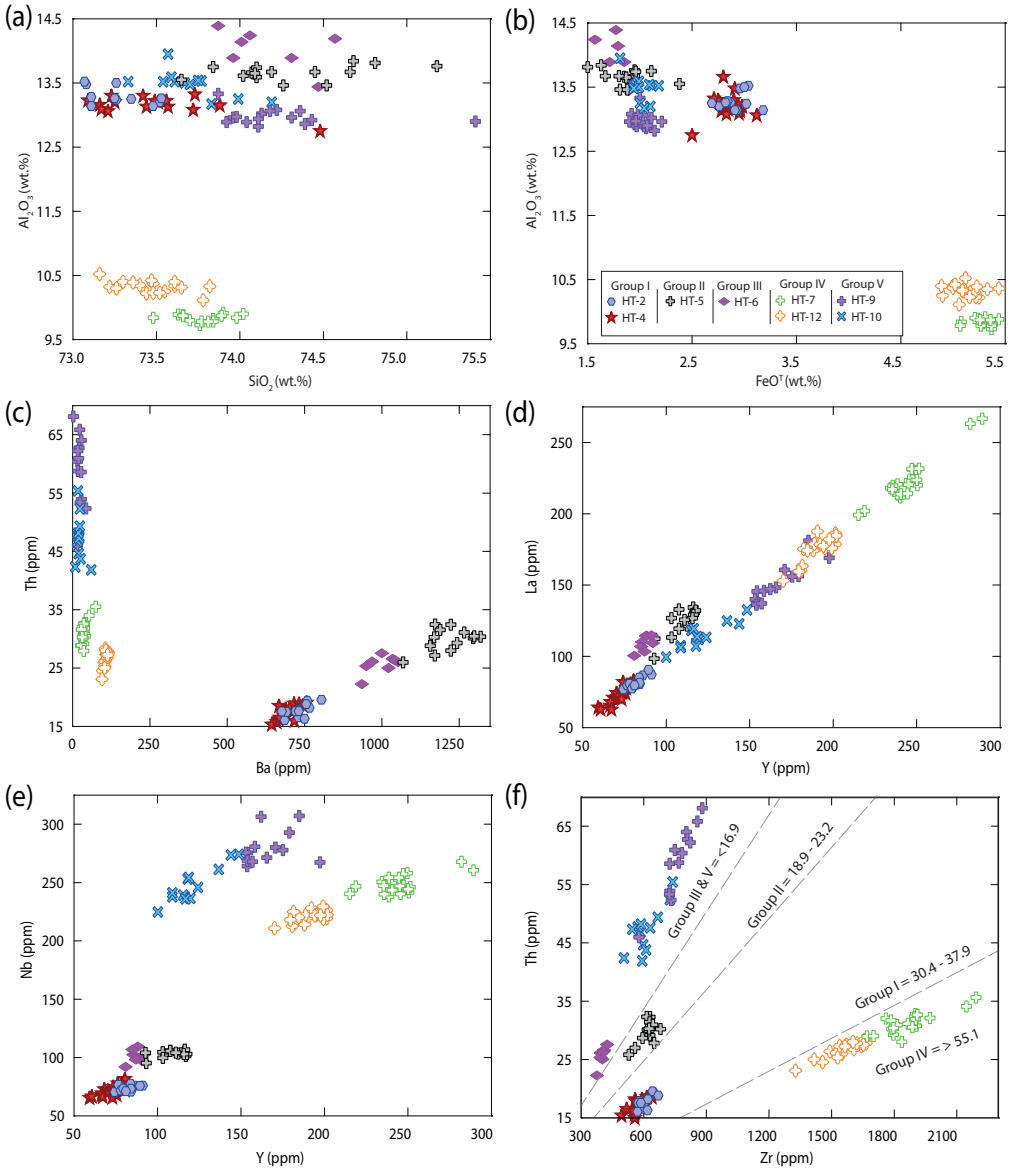

Figure 6.2: Major and trace element composition of single shards from the Hayk tephras. Barium/Th and Zr/Th ratios (c, f) divide the Hayk tephras into five compositional groups.

6.3 Discussion

6.3.1 Tephra correlations between Lake Ashenge and Hayk

The major and trace element composition of the Ashenge and Hayk tephra glass shards is compared in Figs. 6.3 and 6.4 to test whether there are potential tephra correlations between the archives. For the majority of tephra deposits in the Ashenge and Hayk cores, the major and trace element compositions of their component glass shards are distinct. Nonetheless, some tephra deposits within both lakes have glass shards which are compositionally similar.

Hayk Group IV tephras (HT-7 and HT-12) have similar Y/La ($\approx 1.0-1.1$) and Zr/Th ($\approx 55.1-65.7$) ratios to Ashenge Group II (Y/La $\approx 1.1-1.3$, Zr/Th $\approx 53.5-61.8$) tephras (AST-3, AST-4 and AST-6) (Fig. 6.3). Bi-plots of the first three principal components from principal component analysis of Y, Zr, Nb, Ba, La and Th concentrations in the Ashenge and Hayk tephra glass shards are shown in Fig.6.13. This demonstrates that there are statistical similarities between the compositions of the Ashenge Group II and Hayk Group IV glass shards.

HT-7 glass shards are compositionally similar to AST-3 (Fig. 6.4). However, HT-7 is also more evolved than AST-3, containing higher concentrations of SiO_2 and incompatible trace elements and lower concentrations of Al_2O_3 than AST-3. Furthermore, HT-7 ($\sim 4.8-\sim 3.8$ cal. ka BP) is too young to correlate with AST-3 ($\sim 5.6-\sim 5.0$ cal. ka BP). This is consistent with HT-7 and AST-3 being produced by two separate eruptions from the same source, with a time interval between allowing fractional crystallisation of feldspar and ilmenite from the source magma chamber and the subsequent eruption of the more evolved HT-7. Glass shards in HT-12 (Hayk Group IV) have similar incompatible element ratios to the Ashenge Group II tephras. However glass shards in HT-12 are enriched in

Ba (Fig. 6.3c) relative to AST-3, 4 and 6 and HT-12 is too old (13.0 – 12.0 cal. ka BP) to correlate with the Ashenge Group II tephras.

It is apparent that the lake Ashenge and Hayk sediments record different eruptive events; however, glass shards in Ashenge Group II and Hayk Group IV tephras have similar incompatible element ratios, suggesting that they may be derived from the same source. Furthermore, the new age models presented in this study reveal that, of the 9 tephra layers in Lake Ashenge and 12 in Lake Hayk, there is very little temporal overlap. Tephra HT-8, dated to $\sim 7.8 - \sim 5.5$ cal. ka BP, shows the only possible chronological correlation, overlapping within 95.4% confidence intervals with tephra layers AST-4, 5, 6, and 7 ($\sim 7.6 - \sim 5.5$ cal. ka BP). Unfortunately, HT-8 could not be analysed, so the potential for correlation here cannot be tested.

Peralkaline rhyolites erupted from the nearby Dabbahu volcano and elsewhere in the Ethiopian Rift are widely reported to have evolved from parental basalts through fractional crystallisation (Barberi *et al.*, 1975; Peccerillo *et al.*, 2007; Field *et al.*, 2013). To test whether AST-3 and HT-7 could have originated from the same magmatic source, fractional crystallisation, using the older AST-3 as the starting composition, was modelled using Petromodeler version 2 (Ersoy, 2013) (Fig. 6.5). A mineral assemblage dominated by orthoclase and plagioclase with minor aenigmatite, aegirine, ilmenite and olivine was used for the model - based on CIPW Norm values (Cross *et al.*, 1912) calculated using Igpet06 and mineral assemblages observed in peralkaline rhyolites from the Dabbahu volcano (Field *et al.*, 2013). Fig. 6.5 demonstrates that fractional crystallisation of 30% K feldspar, 20% plagioclase, 5 % aenigmatite, 3% aegirine, 2 % olivine and 0.5 % ilmenite could evolve the composition of AST-3 to give a melt with similar Y, La, Nb, Zr and Th concentrations to those in HT-7 glass shards.

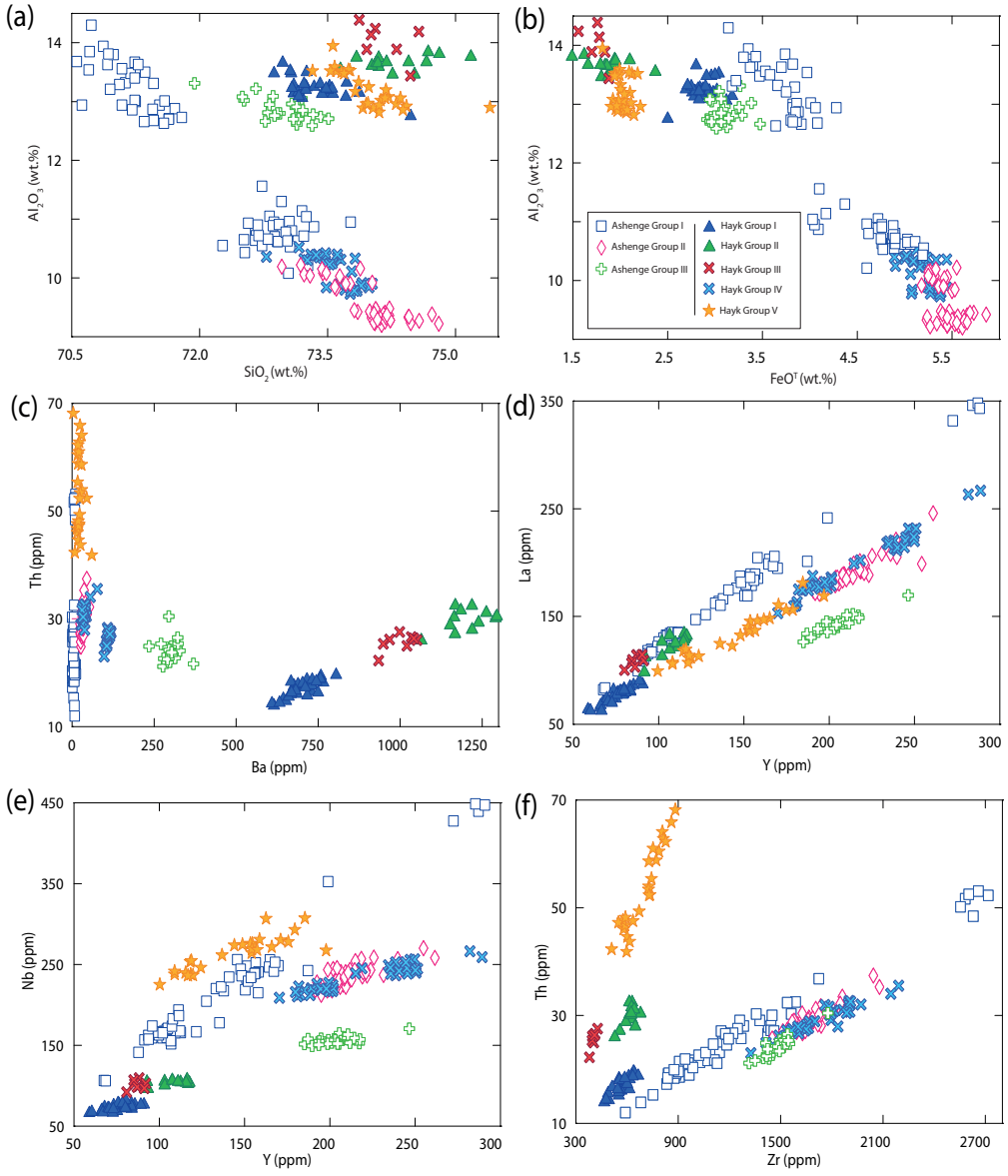

Figure 6.3: Major and trace element bi-plots comparing the composition of the Ashenge and Hayk tephra glass shards

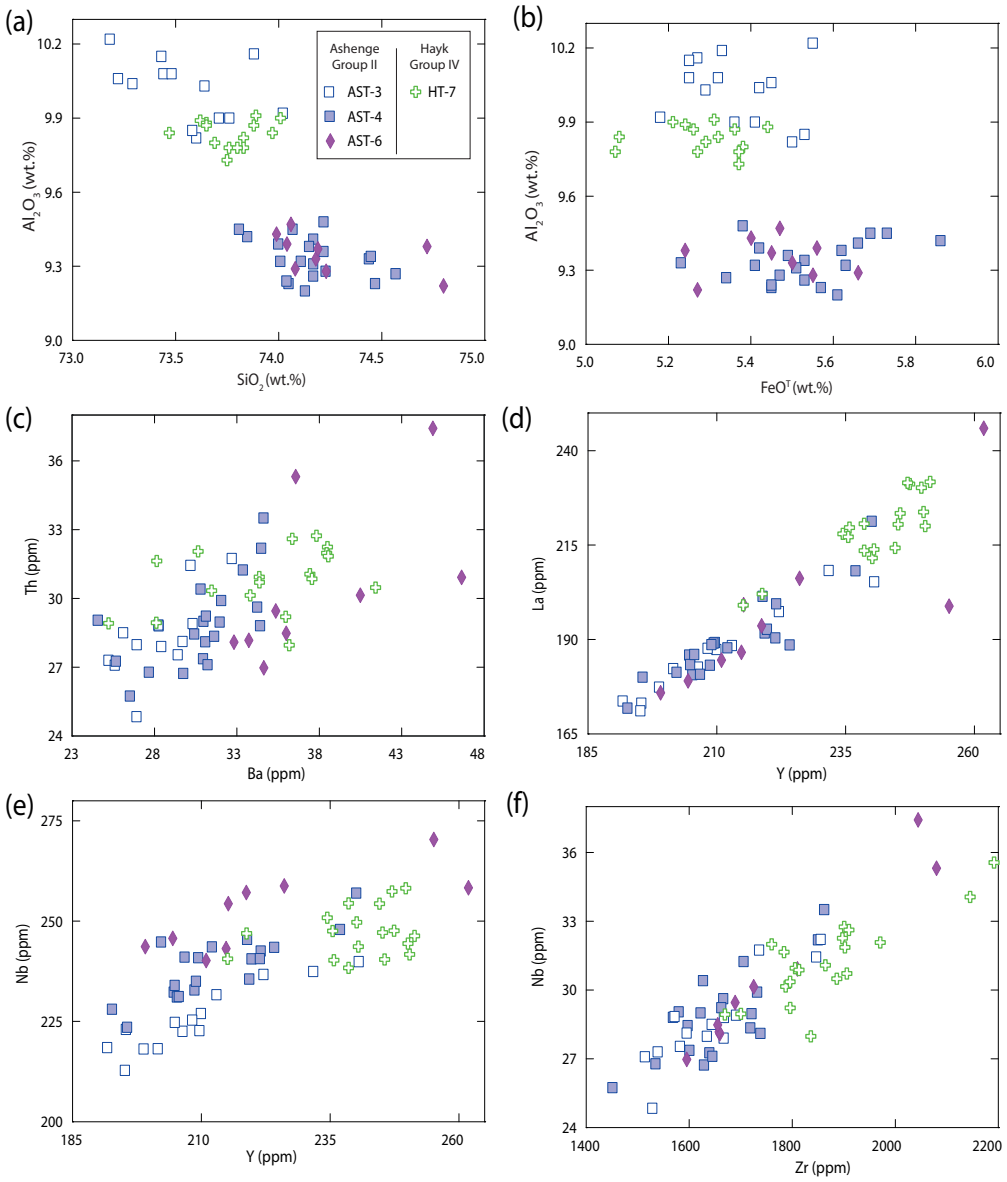

Figure 6.4: Major and trace element bi-plots comparing the composition of HT-7 with Ashenge Group 2 tephras: AST-3; 4; 6. HT-7 has a similar, but more evolved composition than AST-3, containing higher Y, Nb, Zr, SiO_2, Al_2O_3 and lower FeO^T.

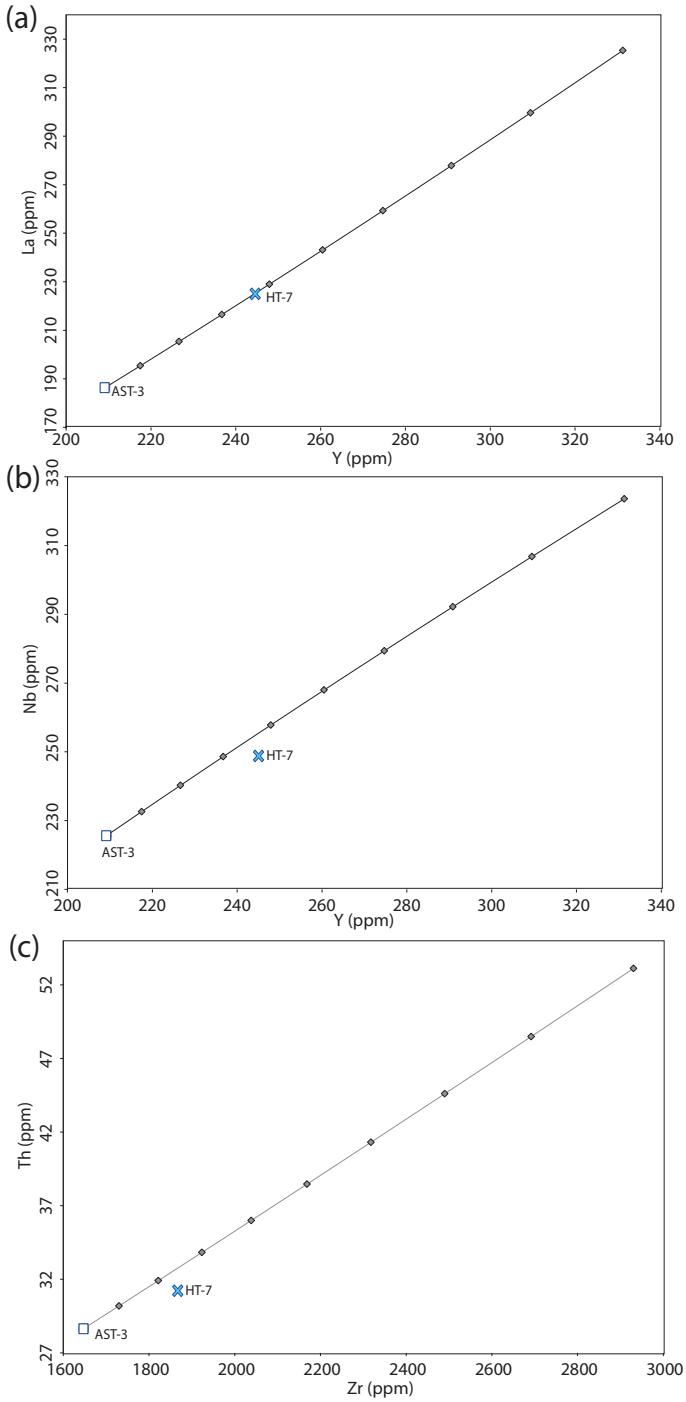

Figure 6.5: Bi-plots showing the average concentrations of selected trace elements in AST-3 and HT-7 tephra glass shards. Lines indicate modelled fractional crystallisation using AST-3 (the older tephra) as a starting composition, with increments indicating 10 % crystallisation. Bulk partition coefficients for trace elements in peralkaline rhyolite melts are from Mahood and Stimac (1990); Pearce (1990) and Ewart and Griffin (1994).

6.3.1.1 The lack of tephra correlations in archives from the Ethiopian Highlands

The lack of correlations between archives collected from lakes < 140 km apart in the Ethiopian Highlands may be related to a number of factors, including eruption magnitude, wind speed and direction, and the grain-size of ejecta (Sparks *et al.*, 1997). The wind direction varies seasonally over Ethiopia (Fig. 6.6) and this will affect the dispersal of tephra and consequently the likelihood of it being preserved in a distal record. During the winter, easterly winds may disperse tephra from volcanoes in the Afar towards the Ethiopian Highlands. In the summer the winds reverse, causing tephra produced in the Afar to be predominantly dispersed to the east. However, these are modern wind regimes and may have been different during the late Quaternary.

Lake Ashenge is located to the north of Lake Hayk and this may determine the type and frequency of tephras received; eruptions from the northern Afar may be supplying the tephras in Lake Ashenge, whilst the tephras recorded in Lake Hayk may be derived from the southern Afar. To deposit a tephra from the same event in these different lakes, a change in wind-direction during the eruption may be required (see Fig. 6.6).

The Nabro (Eritrea) 2011 eruption provides a recent analogue for comparison with potential tephra dispersal during the Holocene. The eruption occurred during June, when the predominant wind direction is away from the Afar Rift, towards the west and the Ethiopian Highlands. Tephra deposited by the eruption was observed throughout the Tigray region, including Lake Ashenge, however tephra was not observed in the Lake Hayk area (A. Asrat 2016, pers. comm., 23rd Feb 2016). Lake Hayk (< 300 km) is located farther away from the Nabro volcano than Lake Ashenge (~ 250 km) and is therefore less likely to receive

tephras. Furthermore, Lake Hayk is located on a more southerly axis from Nabro than Ashenge and therefore tephras are unlikely to be transported by the predominantly easterly winds.

Lake Ashenge is located at a high elevation (2500 m a.s.l.) on the flank of the highlands and close ($<$ 10 km) to the rift margin (see Fig. 6.7). However, Lake Hayk is located within a graben at a comparatively lower elevation (1900 m a.s.l.) and is separated from the Afar Rift to the east by a series of horsts attaining $<$ 2400 m height. Therefore, Lake Ashenge is more exposed to the Afar Rift to the east and is potentially more likely to receive tephra deposits, this is particularly likely if localised eruptions, that do not attain high eruption columns, produced these tephras. The setting of these lakes may therefore determine the frequency and type of tephra layers deposited in each of the archives.

Lakes Ashenge and Hayk are alkaline lakes (pH $\sim 8.8-9$) (Lamb *et al.*, 2007; Marshall *et al.*, 2009). Rhyolitic glass is more soluble in alkali conditions (Mariner and Surdam, 1970) and variations in lake alkalinity through time may therefore determine the preservation of glass shards in the archives. Tephra glass shards observed in the Ashenge and Hayk archives are pristine; however, variable glass preservation during periods of past lake alkalinity may be responsible for the lack of correlations. The glass may have been dissolved or altered by increased alkalinity, and hence the tephras in different archives may no longer compositionally match, limiting the opportunities for correlations.

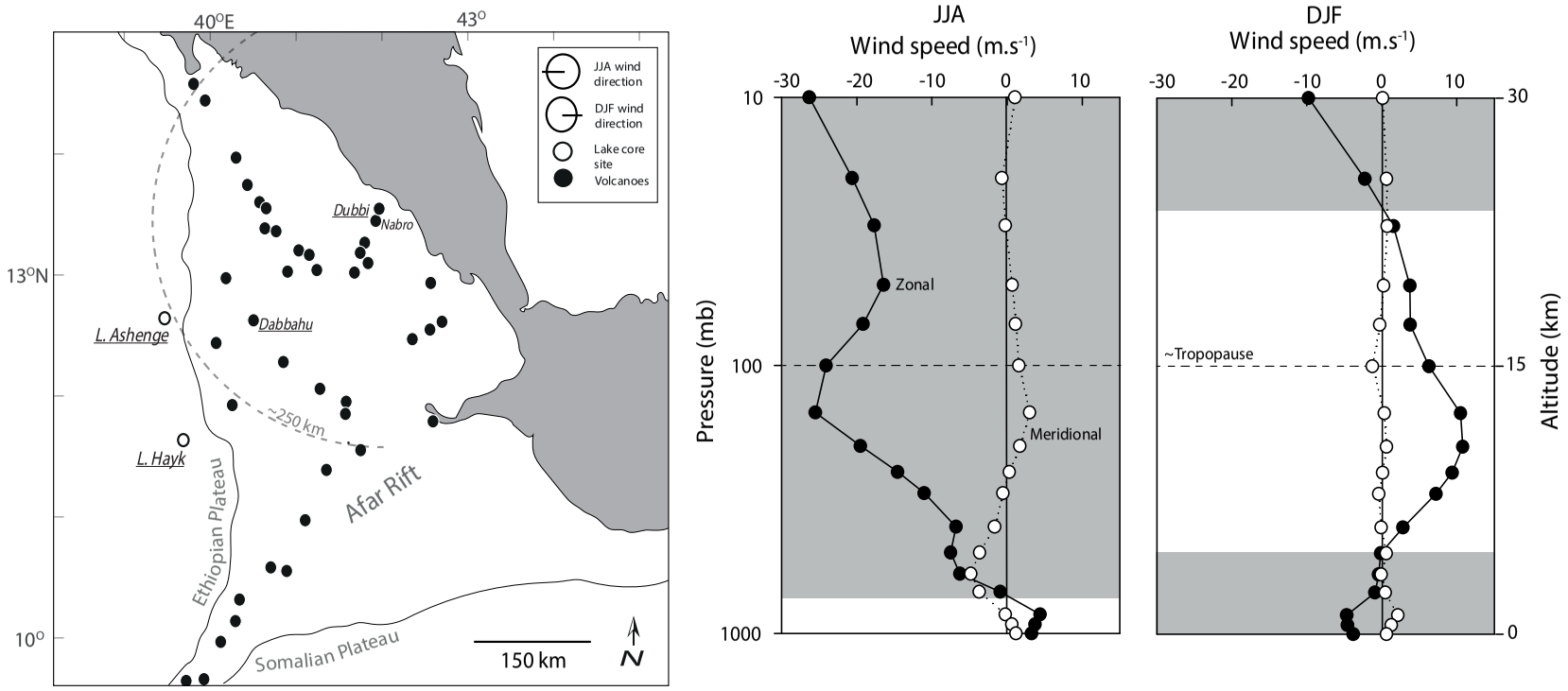

Figure 6.6: (a) Map of the Afar region of northern Ethiopia, showing the location of Lakes Ashenge and Hayk in relation to Holocene volcanoes from (Siebert *et al.*, 2011), volcanoes referred to in the text are labelled. The dashed line deliminates $\sim$ 250 km distance from the Nabro volcano. (b) Profile through atmosphere showing the speed of zonal and meridional winds during the summer and (c) winter monsoon months - after Feakins *et al.* (2007). Wind velocities obtained from the NOAA NCEP CDAS-1 monthly pressure level climatology dataset spanning January 1949 - January 2016 (Kalnay *et al.*, 1996), averaged over $40 - 45^{O}$E, $6 - 15^{O}$N. Negative wind speed values indicate easterly flow of zonal winds and southerly flow of meridional winds. Positive values indicate westerly zonal winds and northerly meridional winds. Grey shading indicates favourable wind trajectories towards from the Afar Rift towards the Ethiopian Highlands in the west. The approximate altitude of the tropopause is given for reference, based on vertical pressure.

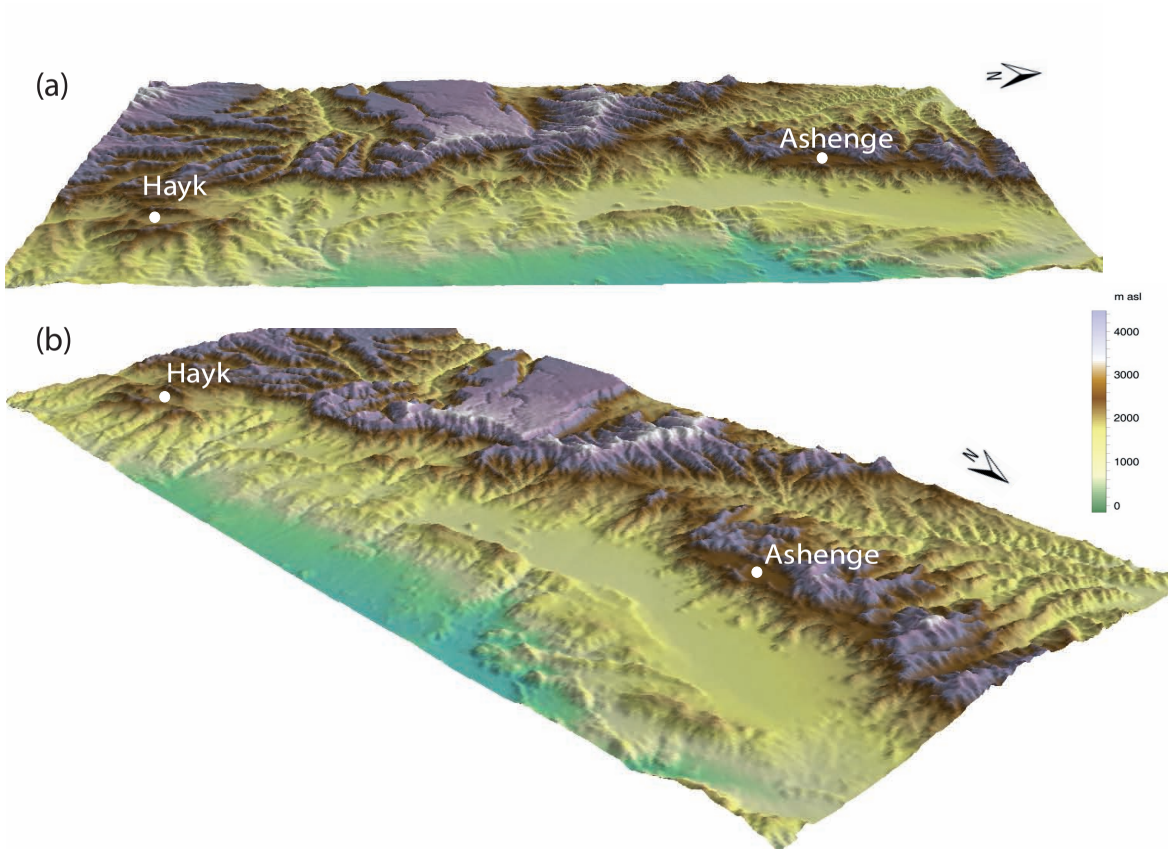

Figure 6.7: 3D elevation model of the topography of areas surrounding Lakes Ashenge and Hayk derived from the NASA SRTM 1 Arc-Second Global dataset (http://earthexplorer.usgs.gov/). (a) The topography of the Afar Rift shoulders viewed from the Afar Rift to the east and the (b) north-east. Lake Ashenge is more open to tephra deposition produced by volcanoes in the Afar Rift.

6.3.2 Eruption tempo and characteristics

The distribution of visible and crypto-tephras in the Ashenge and Hayk stratigraphies gives an insight into the frequency of past eruptions. Table 5.1 shows Bayesian modelled ages of the tephras recorded in the Ashenge and Hayk archives. Thirteen of the total 21 tephras documented in both archives occur at $\sim 7.5- \sim 1.6$ cal. ka BP; potentially reflecting a peak in explosive volcanism during this period. Tephras are recorded frequently in both archives between $\sim 15.3- \sim 1.6$ cal. ka BP, indicating explosive eruptions in this area occurred at an average of every ~ 1000 years during this period. The only recent tephra recorded in the Ashenge and Hayk stratigraphies over the past 1.6 cal. ka BP is the $\sim 0.5- \sim 0.3$ cal. ka BP AST-1, in the Ashenge core.

Selected compositional parameters (major and trace element concentrations and incompatible element ratios) from glass shards in separate tephra groups are plotted against their age in Fig. 6.8. Glass shards from each individual tephra in lakes Ashenge and Hayk occupy a wide compositional range. This compositional heterogeneity suggests that these tephras are derived from evolving or compositionally zoned magma chambers. However, multiple contemporaneous eruptions from different sources may also result in compositional differences in glass shards within a tephra layer.

The Ashenge Group I tephras have a wider range of ages ($\sim 15.3- \sim 0.3$ cal. ka BP) than other tephra compositional groups recorded in the archives. The Ashenge Group I tephras may represent intermittent eruptions from a distant caldera active over a long time period. A lack of documented Ashenge Group I tephras at $\sim 16.7- \sim 13.6$ cal. ka BP and $\sim 4.8- \sim 0.3$ cal. ka BP are potentially associated with periods of repose.

Whilst the similar incompatible element ratios of the Ashenge Group I tephras suggests these tephras have a co-magmatic origin, their tephra glass shards become depleted in SiO_2, FeO^T and Y and enriched in Al_2O_3 concentrations through time. This trend is the opposite to that which would be expected for simple crystal fractionation of a feldspar dominated assemblage. To constrain the petrogenesis of these tephras, detailed mapping and sampling of the potential source volcanoes is required. However, it is apparent that other processes (potentially recharge and/or assimilation) are involved in their petrogenesis.

The fractional crystallisation of Group I Ashenge tephras is modelled in Fig. 6.9, using the oldest tephra (AST-9) as the starting melt composition. Figure 6.9 reiterates that the evolution of the Ashenge Group I tephras is complex. Crystallisation of a mineral assemblage comprised of orthoclase (50 %), plagioclase (15 %), aenigmatite (5 %), clinopyroxene (5 %), olivine (2 %) and ilmenite (0.2 %) will evolve the melt composition from AST-9 towards AST-8. However, it is apparent that fractional crystallisation of this assemblage could not reduce incompatible element concentrations in the melt to subsequently produce AST-7; 2 and 1 compositions.

Other compositional groups (e.g. Hayk Group I and V) recorded in the archives are comprised of eruptions covering relatively short times spans ($<\sim 3$ ka). These tephras are more homogeneous than eruptions depositing the Ashenge Group I tephras, this may be an indication of compositional zoning developing in the magma chambers with relatively longer repose periods. However, the Hayk Group I and V tephra glass shards show enrichment in Y through time when compared to older tephras from the same compositional group. This suggests that the evolution of the Hayk tephras was dominated by fractional crystallisation of feldspar, differing to the Ashenge Group I melt evolution.

Fractional crystallisation of the Hayk Group I and Hayk Group V tephras is modelled in Figs. 6.10 and 6.11, using the oldest tephras from each group as starting compositions. Crystallisation of orthoclase (50 %), plagioclase (15 %), aenigmatite (5 %), clinopyroxene (5 %), olivine (2 %) and ilmenite (1 %) from the Hayk Group I and V melts produces similar compositions to younger tephras from each group. This reinforces the fact that the Hayk Group I and V tephras evolved through crystallisation of a different mineral assemblage to those dominating the evolution of the Ashenge Group I tephras.

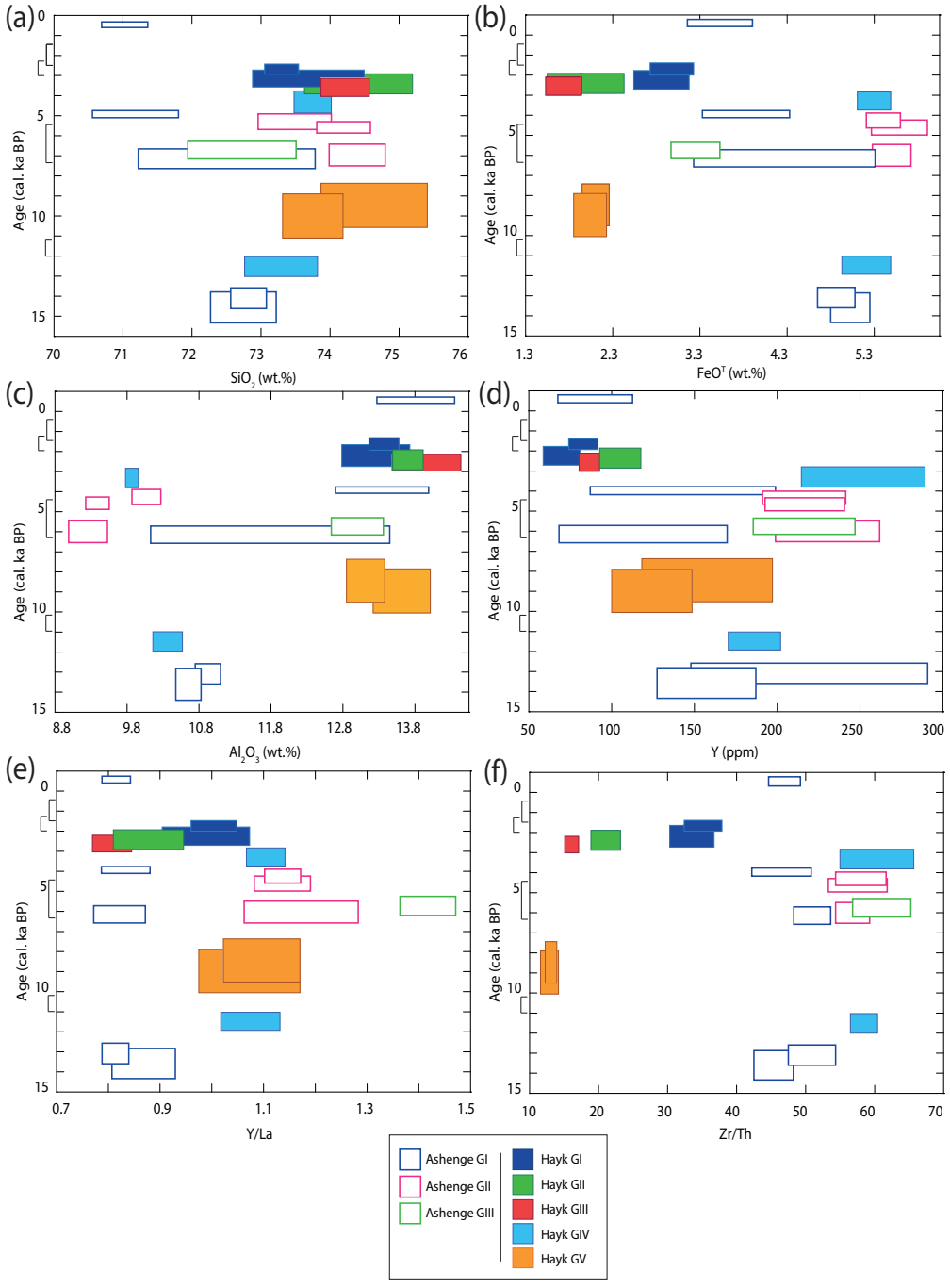

Figure 6.8: Major and trace element concentrations and incompatible element ratios of glass shards in the Ashenge and Hayk tephras plotted against their modelled tephra age. Brackets on the Age axis indicate the age ranges of tephras that were not analysed.

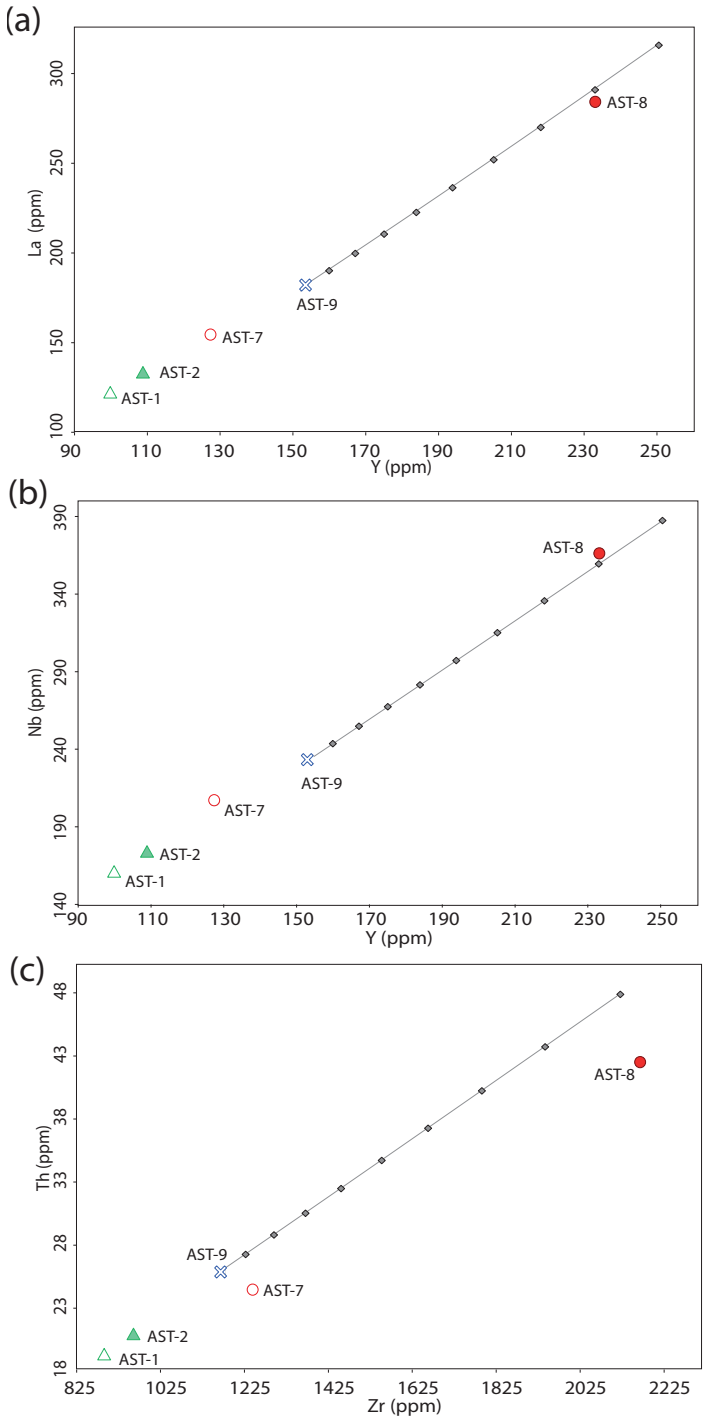

Figure 6.9: Bi-plots showing the average concentrations of selected trace elements in AST-3 and HT-7 tephra glass shards. Lines indicate modelled fractional crystallisation using AST-3 (the older tephra) as a starting composition, with increments indicating 10 % crystallisation. Bulk partition coefficients for trace elements in peralkaline rhyolite melts are from Mahood and Stimac (1990); Pearce (1990) and Ewart and Griffin (1994).

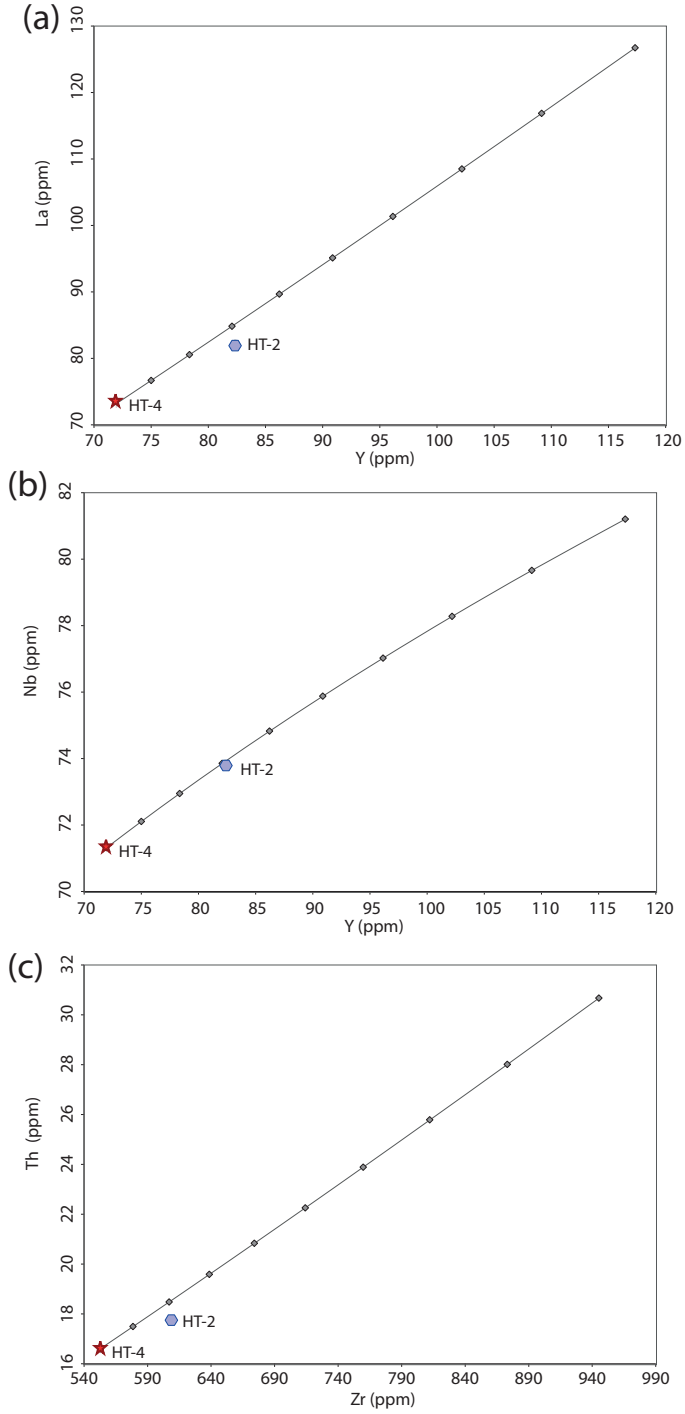

Figure 6.10: Bi-plots showing the average concentrations of selected trace elements in HT-2 and HT-4 tephra glass shards. Lines indicate modelled fractional crystallisation using HT-4 (the older tephra) as a starting composition, with increments indicating 10 % crystallisation. Bulk partition coefficients for trace elements in peralkaline rhyolite melts are from Mahood and Stimac (1990); Pearce (1990) and Ewart and Griffin (1994).

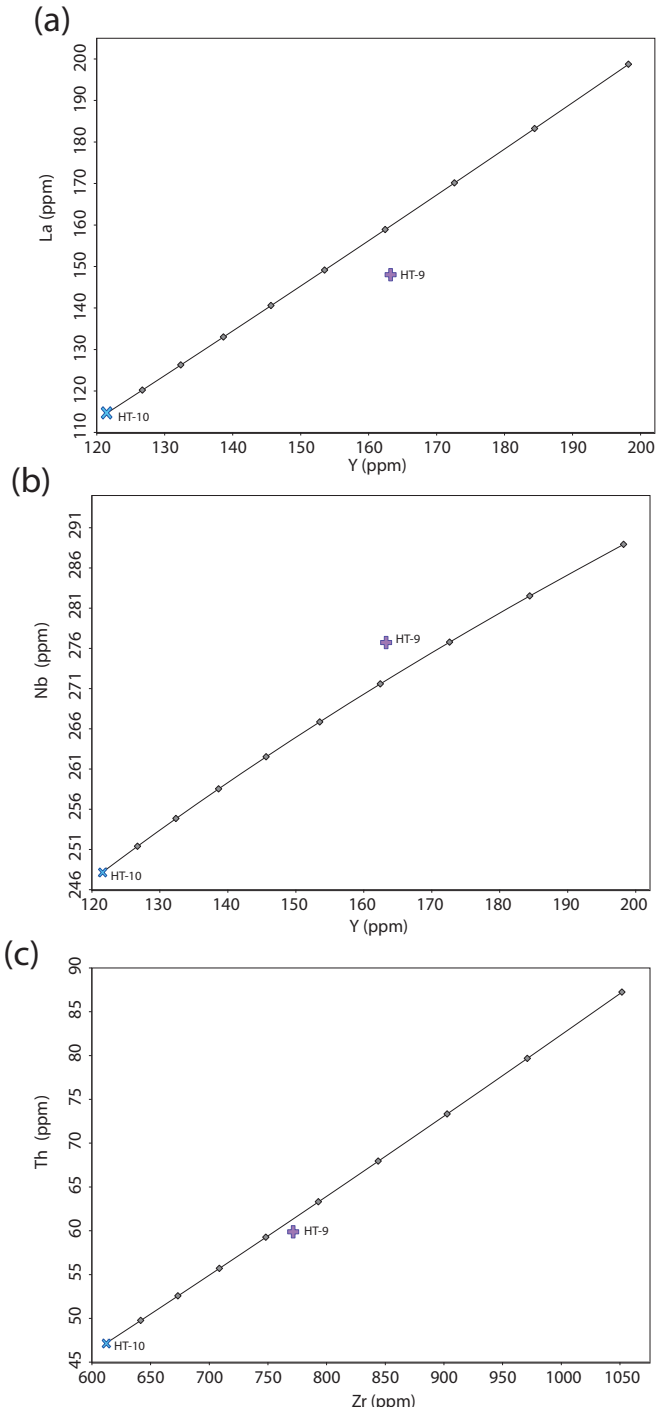

Figure 6.11: Bi-plots showing the average concentrations of selected trace elements in HT-9 and HT-10 tephra glass shards. Lines indicate modelled fractional crystallisation using HT-10 (the older tephra) as a starting composition, with increments indicating 10 % crystallisation. Bulk partition coefficients for trace elements in peralkaline rhyolite melts are from Mahood and Stimac (1990); Pearce (1990) and Ewart and Griffin (1994).

6.3.3 Provenance of the Holocene Lake Ashenge and Hayk tephras

The closest volcanoes to lakes Ashenge and Hayk that are thought to have been active during the Holocene are located to the east in the Afar Rift (Fig. 6.6). Given the lack of correlations between lakes Ashenge and Hayk, it is likely that the tephras recorded in these archives are locally derived.

There is a scarcity of geochemical and chronological data from Holocene volcanic deposits in the Afar Rift. Therefore it is currently not possible to assess correlations with all possible source volcanoes which could have generated tephras deposited in lakes Ashenge and Hayk during the Holocene. The Ashenge and Hayk tephras are compared here with published glass analyses on proximal pumice and obsidians from Dabbahu volcano and new glass analyses on proximal tephra deposits from the Dubbi volcano (Eritrea).

Dabbahu (Boina) (Fig. 6.6) is the closest volcano to Lakes Ashenge and Hayk with published geochemical data. Dabbahu is a Pleistocene - Holocene volcanic massif; its basalt-pantellerite suite having evolved through fractional crystallisation dominated by orthoclase, clinopyroxene and apatite to produce late stage obsidian flows, lava domes and pumice cones at its summit (Barberi *et al.*, 1975; Field *et al.*, 2012). Fission track dates on obsidians from the upper flanks give ages of ~ 44 ka and ~ 1.5 ka and a recent eruption (VEI=3) in 2005 deposited tephra over 100 km^2 (Barberi *et al.*, 1975; Ayele *et al.*, 2007*a*; Ferguson *et al.*, 2010).

Glass analyses of proximal pumice and obsidian samples from Dabbahu (Field *et al.*, 2012) are compared with Ashenge and Hayk tephra glass shard analyses in Fig. 6.12. Dabbahu glass contains similar Y/La ratios (≈ 0.95) to some of the Hayk Group I, IV and V tephra glass shards ($\approx 0.9 - 1.2$). However,

Dabbahu glass contains higher Zr/Th ratios (> 98.8) than the Ashenge and Hayk tephra glass shards (< 65.7). Fig. 6.13 further demonstrates that there is a statistical difference between the composition of the Ashenge and Hayk tephras and the Dabbahu obsidians and pumices. Therefore further sampling and 'side-by-side' analyses of glass from Dabbahu proximal deposits are required to assess the similarity of the incompatible element ratios to those of the Ashenge Group I glass shards.

The uppermost tephra in the Ashenge archive (AST-1, $546 - 321$ cal. a BP) is the only historic tephra documented in the Ashenge and Hayk records. The 1861 eruption of Dubbi (Eritrea, 270 km NE of Ashenge, Fig. 6.6) is reputed to be Africa's largest historic eruption (VEI=3); dispersing volcanic ash 300 km to the west on the Ethiopian Plateau (Wiart and Oppenheimer, 2000). A previous eruption (VEI=2) from Dubbi at 1400 AD may also have occurred (Gouin, 1979) and this is comparable to the modelled date of $1404 - 1629$ AD for AST-1.

Analyses of tephra glass shards from the Dubbi 1861 pyroclastic flow deposits (collected by C. Oppenheimer, University of Cambridge) were analysed as part of this study. The composition of AST-1 glass shards can be broadly compared with those from the 1861 Dubbi tephra, in order to ascertain whether AST-1 was deposited by a possible older eruption from Dubbi (Fig. 6.12). The AST-1 tephra glass shards have similar Zr/Th ratios ($\approx 44.6 - 49.2$) to the Dubbi glass shards ($\approx 43.3 - 52.3$). However, AST-1 glass shards contain lower Al_2O_3 and incompatible element concentrations and higher FeO^T concentrations than the Dubbi 1861 tephra glass shards (Fig. 6.12). Further glass analysis of a wider range of proximal samples from Dubbi is therefore required to investigate the source of AST-1.

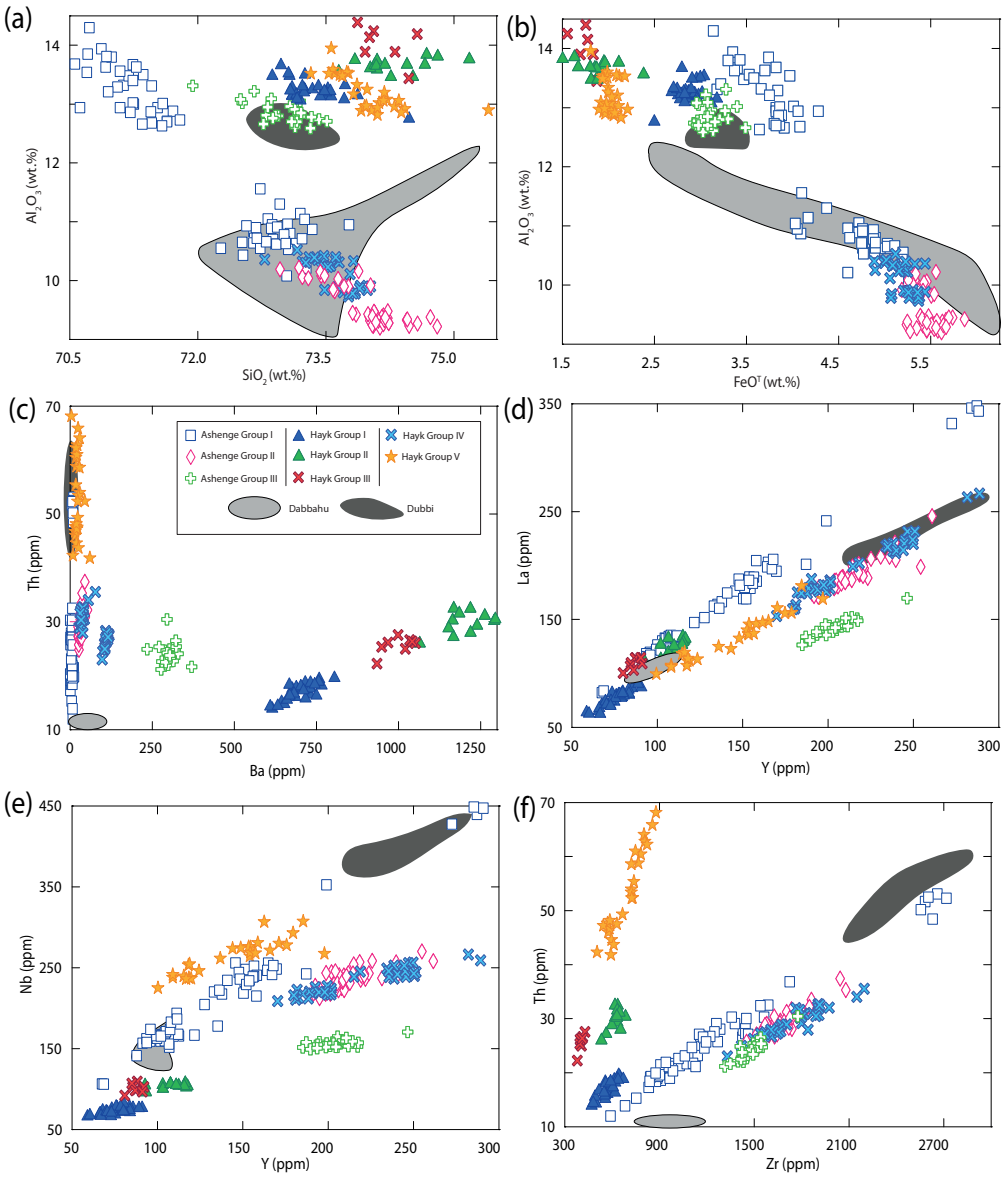

Figure 6.12: Comparison of the composition of Ashenge and Hayk tephras with proximal tephra samples from the Dabbahu and Dubbi volcanoes in the Afar. Glass analyses on pumice and obsidian from Dubbahu are from Field *et al.* (2012), Dubbi proximal samples were analysed as part of this study.

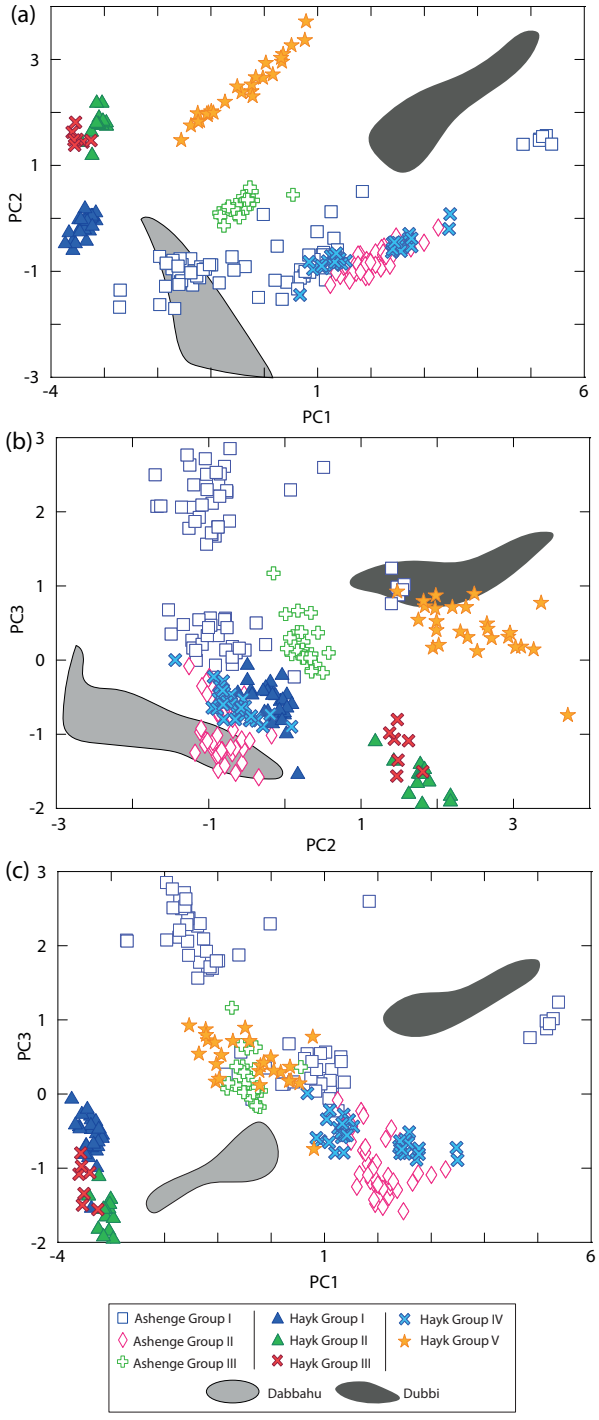

Figure 6.13: Bi plots of the first three principal components from principal component analysis of SiO_2, Al_2O_3, FeO^T, Y, Zr, Nb, Ba, La and Th concentrations of tephras from Ashenge, Hayk, Dabbahu and Dubbi.

6.4 Conclusions

Distal tephras in lake sediment archives from the Ethiopian Highlands provide a < 17 cal. ka BP record of volcanism from the Afar Rift. This section presents an initial late Pleistocene to Holocene tephra framework for the Afar Rift, the first to cover this temporal and spatial range. This is the first instance where cryptotephras have been identified and dated in terrestrial archives from Ethiopia; of the 21 tephra layers across the two study sites, 15 of these were identified as cryptotephra layers. These results highlight the essential contribution of cryptotephra studies to our understanding of past volcanism.

This chapter provides the first database of major and trace element glass compositions for tephras from Ethiopia to cover this temporal range. Glass compositions include comendites, pantellerites and minor peraluminous and metaluminous rhyolites. Between $15.3 - 1.6$ cal. ka BP, explosive eruptions occurred at a frequency of < 1000 years. The majority of tephras were recorded at $\sim 7.5 - \sim 1.6$ cal. ka BP, possibly reflecting a peak in volcanic activity, and the only historically documented tephra layer recorded in the archives occurs at $\sim 0.5 - \sim 0.3$ cal. ka BP. This new tephra framework provides an insight into the volcanic history of the Afar that has important implications for hazard assessments in a region where the record of recent volcanism has remained largely undocumented.

Distinct major and trace element compositions of the lakes Ashenge and Hayk tephras indicate that they record different eruptive events. The lack of correlations between archives collected from < 140 km apart may be associated with numerous factors. It is apparent that, due to the location of both lakes, a change in wind direction during the eruption would be required to disperse tephra produced by eruptions in the Afar Rift towards both lake sites. The topographic

setting of each lake may influence the frequency and type of tephras deposited in each lake. Lake Ashenge is more exposed than Lake Hayk, the latter sheltered from localised eruptions in the Afar Rift by a series of horsts. Both lakes are alkali and, due to the increased solubility of rhyolitic glass in alkaline waters, this may determine the preservation of tephra glass shards and limit opportunities for tephra correlation.

The Ashenge and Hayk tephra glass shards have different incompatible element ratios, indicating they may have been erupted from as many as seven volcanic centres over the past $<$ 15 cal. ka BP, most likely located in the nearby Afar Rift. Some tephras recorded in both lakes have similar incompatible element ratios, suggesting they may represent different eruptive events from the same source. It is apparent that the Ashenge and Hayk melts evolved through fractional crystallisation dominated by feldspar and ilmenite, however, it is likely that other processes including recharge and/or assimilation may have contributed to their evolution. Comparison of the Ashenge and Hayk tephra compositions with glass analyses of proximal deposits from the Dabbahu and Dubbi volcanoes is inconclusive. Further glass analyses of a wider range of proximal samples, combined with chronological control is required to investigate whether these volcanoes may have supplied the Ashenge and Hayk tephras.

Lake sediments have been shown to provide an accessible record of past volcanism from the remote Afar Rift. A greater network of sites must now be studied, which would capture not only the eruption frequency, but also the patterns of dispersal. This approach is, however, challenged by the lack of published major and trace element analyses of tephra glass shards from outcrops proximal to volcanoes in the Afar Rift. Further geochemical characterisation of the regional volcanoes is therefore essential to identify the sources of tephras

recorded in the lakes Ashenge and Hayk sediments as well as those that will be uncovered in future studies.

Chapter 7

The composition, timing and characteristics of post $\sim$ 10 ka eruptions from Corbetti recorded in lakes Awassa, Tilo and Chamo

7.1 Introduction

This chapter explores whether tephras can be correlated between the Awassa, Tilo and Chamo archives. No published glass shard data are available for tephras from nearby volcanic centres. However, comparisons are made here between the composition of tephra layers in Tilo, Awassa and Chamo and obsidians and tephra samples from the Corbetti caldera. This is the first attempt to identify the likely source of these tephra layers and the implications of these findings are discussed with regards to regional volcanic hazards.

7.2 The composition of the Awassa, Tilo and Chamo tephras

7.2.1 The Tilo tephras

The major and trace element composition of the 14 Tilo tephras is given in Table 7.1 and Fig. 7.1. Most of the Tilo tephras are peralkaline rhyolites, and can be further classified as pantellerites (Le Maitre, 2002). These pantelleritic glass shards are comprised of two populations, containing varying FeO^T, Ba, Zr and Th concentrations. Notably, these two glass population have different Zr/Th ratios and this indicates that they are derived from two different volcanic sources (Fig. 7.1f). The composition of the Tilo tephras is discussed below in terms of these two populations.

Table 7.1: Normalised major element (wt.%) and trace element (ppm) concentrations of glass shards in the Tilo tephras. Average ($\pm$ 1 st. dev.) concentrations of selected elements which have proved to be useful for correlation are shown here. The range of element concentrations in each tephra is shown in italics.

	TT-1	**TT-2**	**TT-3**	**TT-4**	**TT-5**	**TT-6**	**TT-7**
Age (ka)	1.3 – 0.5	2.1 – 1.2	2.3 – 1.3	2.5 – 1.3	2.6 – 1.3	2.7 – 1.6	4.2 – 2.3
SiO_2	74.91 (0.55)	74.94 (0.56)	73.38 (0.38)	74.80 (0.24)	74.84 (0.46)	73.35 (0.69)	74.84 (0.23)
	72.99-75.41	*72.95-75.84*	*72.39-73.97*	*74.35-75.31*	*73.69-76.66*	*72.24-75.00*	*74.41-75.22*
Al_2O_3	10.08 (0.75)	9.92 (0.66)	8.57 (0.33)	9.87 (0.14)	9.92 (0.27)	8.57 (0.52)	9.83 (0.12)
	9.56-12.81	*9.39-12.51*	*8.16-9.46*	*9.71-10.24*	*9.65-11.26*	*7.47-10.07*	*9.70-10.16*
FeO^T	4.57 (0.11)	4.56 (0.15)	6.39 (0.25)	4.60 (0.12)	4.64 (0.14)	6.45 (0.26)	4.66 (0.13)
	4.38-4.75	*4.24-4.87*	*5.59-6.79*	*4.39-4.81*	*4.36-4.97*	*5.79-6.89*	*4.43-4.88*
Na_2O	5.31 (0.17)	5.45 (0.19)	6.38 (0.30)	5.38 (0.17)	5.28 (0.39)	6.45 (0.19)	5.39 (0.13)
	4.99-5.58	*4.76-5.79*	*5.79-6.84*	*5.06-5.76*	*3.56-5.70*	*6.12-6.84*	*5.20-5.59*
K_2O	4.48 (0.13)	4.47 (0.10)	4.31 (0.11)	4.48 (0.14)	4.46 (0.08)	4.16 (0.17)	4.43 (0.08)
	4.16-4.68	*4.27-4.66*	*4.09-4.47*	*4.21-4.61*	*4.28-4.63*	*3.76-4.42*	*4.31-4.61*
Y	260 (18.4)	259 (34.2)	265 (45.3)	265 (14.7)	280 (44.2)	231 (17.5)	230 (16.4)
	236-311	*199-346*	*213-377*	*246-296*	*212-395*	*204-274*	*205-268*

Continued on next page

Table 7.1 Continued from previous page

	TT-1	**TT-2**	**TT-3**	**TT-4**	**TT-5**	**TT-6**	**TT-7**
Zr	2110 (131)	2130 (267)	2090 (369)	2110 (121)	2290 (348)	1820 (113)	1880 (118)
	1930-2410	*1630-2720*	*1740-3090*	*1960-2340*	*1770-3190*	*1640-2090*	*1730-2130*
Nb	259 (8.56)	262 (10.7)	286 (36.7)	269 (8.07)	267 (18.4)	274 (15.4)	245 (6.64)
	243-276	*222-279*	*239-356*	*254-286*	*233-337*	*233-301*	*233-260*
Ba	94.4 (5.74)	92.1 (10.0)	438 (29.4)	83.3 (6.95)	82.5 (9.29)	358 (22.8)	57.6 (4.74)
	81.7-107	*71.7-111*	*394-517*	*70.5-94.1*	*56.1-102*	*312-414*	*51.5-71.9*
La	234 (12.5)	234 (24.7)	250 (44.5)	232 (14.0)	245 (33.3)	224 (16.6)	201 (13.8)
	215-259	*193-292*	*204-363*	*214-259*	*191-323*	*198-263*	*181-226*
Hf	52.5 (4.02)	53.5 (6.05)	53.1 (8.53)	56.4 (4.44)	58.0 (8.98)	45.4 (3.46)	46.7 (3.18)
	47.7-63.0	*44.2-65.3*	*44.6-75.1*	*50.6-65.0*	*45.4-80.3*	*38.6-53.7*	*41.1-52.1*
Th	26.4 (1.71)	26.9 (3.39)	35.2 (6.60)	28.1 (2.21)	28.4 (4.08)	30.1 (2.52)	23.1 (1.63)
	24.3-29.7	*21.8-33.4*	*28.0-52.8*	*25.1-32.0*	*22.6-40.3*	*25.1-37.1*	*21.1-26.4*
U	6.32 (0.37)	6.66 (0.857)	7.61 (0.924)	7.42 (0.445)	7.31 (0.583)	7.37 (0.583)	6.58 (0.239)
	5.80-7.29	*4.18-8.60*	*6.15-9.40*	*6.78-8.26*	*5.84-8.16*	*6.44-8.35*	*5.98-6.92*
	$n = 16$	$n = 48$	$n = 18$	$n = 19$	$n = 40$	$n = 23$	$n = 19$

	TT-8	**TT-9**	**TT-10**	**TT-11**	**TT-12**	**TT-13**	**TT-14**
Age (ka)	4.2 – 2.34	4.9 – 4.0	6.3 – 4.7	6.4 – 5.1	7.0 – 6.1	8.9 – 8.0	10.2 – 9.3
SiO_2	74.97 (0.52)	75.18 (0.52)	75.14 (0.49)	75.12 (1.01)	74.82 (0.90)	74.73 (2.14)	75.07 (1.23)
	73.82-76.91	*74.36-75.65*	*74.58-78.39*	*70.25-77.13*	*71.02-78.00*	*66.63-78.05*	*67.28-76.58*
Al_2O_3	9.87 (0.26)	9.69 (0.26)	9.65 (0.22)	9.82 (0.83)	9.93 (0.73)	9.88 (2.04)	9.75 (1.24)
	9.41-11.28	*9.40-10.06*	*8.57-10.26*	*9.25-14.67*	*9.43-14.63*	*9.16-18.28*	*8.99-17.76*
FeO^T	4.67 (0.21)	4.68 (0.21)	4.64 (0.20)	4.62 (0.36)	4.70 (0.16)	4.65 (0.91)	4.58 (0.57)
	4.33-5.78	*4.33-5.02*	*3.76-5.02*	*2.72-5.04*	*4.29-5.05*	*0.94-5.06*	*0.66-4.84*
Na_2O	5.22 (0.53)	5.36 (0.53)	5.43 (0.24)	5.15 (0.69)	5.23 (0.75)	5.51 (0.98)	5.49 (0.34)
	2.73-5.73	*4.86-5.80*	*4.10-5.73*	*2.80-5.99*	*1.81-5.91*	*1.96-6.18*	*3.56-5.91*
K_2O	4.47 (0.09)	4.45 (0.09)	4.48 (0.13)	4.53 (0.26)	4.45 (0.10)	4.65 (0.94)	4.50 (0.56)
	4.20-4.66	*4.25-4.62*	*3.75-4.68*	*4.35-6.01*	*4.13-4.69*	*4.27-8.48*	*4.10-8.40*
Y	264 (23.7)	256 (23.7)	267 (32.9)	310 (32.9)	305 (30.4)	356 (27.8)	291 (20.8)
	218-321	*216-298*	*209-347*	*223-369*	*238-394*	*300-432*	*239-345*
Zr	2120 (184)	2100 (184)	2190 (248)	2440 (238)	2300 (229)	2960 (212)	2410 (164)
	1750-2500	*1740-2400*	*1770-2780*	*1790-2850*	*1790-2800*	*2460-3460*	*2030-2750*
Nb	265 (17.1)	272 (17.1)	276 (13.4)	293 (28.3)	296 (19.1)	335 (13.9)	303 (14.0)
	211-311	*247-289*	*227-297*	*212-330*	*255-330*	*313-361*	*264-335*
Ba	71.4 (8.48)	64.2 (8.48)	67.3 (7.60)	55.9 (13.0)	49.2 (6.33)	55.0 (6.63)	56.4 (6.05)
	59.0-96.68	*51.8-78.8*	*56.4-88.0*	*35.2-96.2*	*35.5-65.8*	*44.6-70.1*	*46.4-74.1*
La	234 (23.4)	233 (23.4)	243 (30.1)	268 (24.7)	268 (24.3)	315 (22.9)	259 (17.8)

Continued on next page

Table 7.1 Continued from previous page

	TT-8	TT-9	TT-10	TT-11	TT-12	TT-13	TT-14
	191-293	*198-266*	*190-311*	*205-310*	*206-323*	*264-367*	*212-302*
Hf	52.4 (5.83)	52.3 (5.83)	54.0 (6.21)	63.7 (8.09)	64.0 (6.51)	73.3 (5.40)	58.2 (4.47)
	39.8-67.1	*41.6-63.5*	*42.4-67.0*	*46.9-78.8*	*46.4-77.8*	*59.9-79.9*	*48.2-72.1*
Th	26.6 (2.89)	26.6 (2.89)	27.5 (3.19)	31.8 (3.71)	31.8 (3.46)	36.6 (2.66)	30.0 (2.02)
	21.2-35.2	*22.0-31.3*	*21.4-34.6*	*23.5-39.8*	*24.6-42.9*	*30.4-40.6*	*25.1-37.2*
U	6.82 (0.597)	6.97 (0.597)	7.07 (0.41)	7.36 (0.75)	7.81 (0.775)	8.30 (0.461)	8.10 (1.35)
	5.20-9.12	*6.22-8.20*	*6.21-7.90*	*5.16-8.70*	*6.40-9.72*	*7.36-9.16*	*6.57-16.3*
	$n = 57$	$n = 59$	$n = 61$	$n = 39$	$n = 58$	$n = 19$	$n = 52$

Concluded

7.2.1.1 Composition of the Tilo Group I tephras

Glass shards in TT-3 ($2.3 - 1.3$ cal. ka BP) and TT-6 ($2.7 - 1.6$ cal. ka BP) contain higher FeO^T and Ba than all other glass shards in the Tilo tephras (Table 7.1, Fig. 7.1b, c). Furthermore, TT-3 and TT-6 have lower Zr/Th ratios ($55.9 - 65.2$) than all other Tilo tephra glass shards ($56.2 - 92.1$, Fig. 7.1f). Glass shards in TT-3 and TT-6 can be distinguished, TT-3 contains higher Ba concentrations than TT-6 (Fig. 7.1b).

7.2.1.2 Composition of the Tilo Group II tephras

The remaining 12 Tilo tephras share similar major and trace element compositions and Y/Zr and Zr/Th ratios (Fig. 7.2), indicating that the may be derived from a shared volcanic source. Barium behaves as a moderately incompatible element in the Tilo tephras, showing positive linear trends when plotted against Th. Figure 7.2f shows that Ba concentrations increase in the Tilo Group II tephras through time, allowing the majority of these tephras to be distinguished. The Tilo Group II tephras are discussed below, in relation to the varying Ba concentrations of their glass shards.

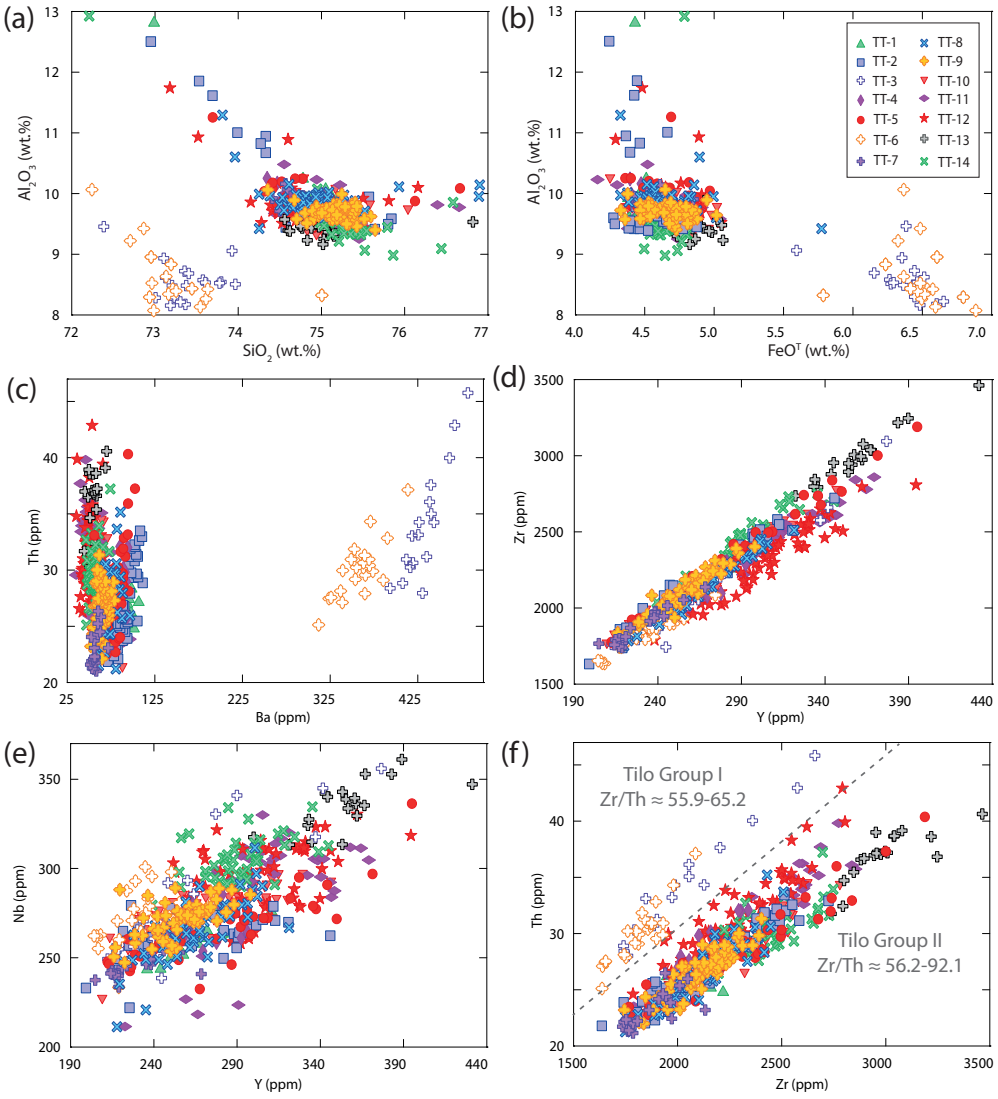

Figure 7.1: Major and trace element compositions of the Tilo tephra glass shards.

The oldest period of volcanism from this source deposited TT-11; 12; 13 and 14 ($10.2 - 5.1$ cal ka BP). Glass shards in these tephras contain the lowest Ba/Th ratios ($\approx 0.9 - 2.4$) amongst the Tilo tephras (Fig. 7.2f). Glass shards in TT-11; 12; 13 and 14 can be broadly distinguished. TT-12 contains lower Y concentrations and TT-13 contains higher FeO^T and Zr than other tephras deposited during this oldest volcanic episode (Fig. 7.1b,d).

The most recent episode of volcanism produced TT-1; 2; 4 and 5 between $2.6 - 0.5$ cal ka BP. Tephra glass shards in these tephras contain higher Ba/Th ratios ($\approx 2.6 - 4.1$) than the majority of glass shards in older tephras (Fig. 7.2f). TT-1 and TT-2 glass shards can be distinguished, containing broadly higher concentrations of Ba than TT-4 and TT-5.

Tephras TT-7; 8; 9 and 10 were deposited between the oldest and youngest volcanic episodes, during $6.3 - 2.3$ cal. ka BP. Glass shards in these tephras have similar Ba/Th ratios ($\approx 1.9 - 3.5$) to tephras produced by younger and older volcanic episodes (Fig. 7.2f). The only tephra which can be distinguished from other tephras deposited during this episode is TT-7, which contains glass shards with comparatively lower Y, Ba and Th concentrations (Fig. 7.2a, e).

7.2.2 Composition of the Awassa tephras

The major and trace element composition of 3 of the total 7 Awassa tephra glass shards is presented in Table 7.3 and Fig. 7.3. The Awassa tephra glass shards are pantelleritic and share similar Y/Zr and Zr/Th ratios (Fig. 7.3d, f), suggesting that they are co-genetic. However, FeO^T, Y, Zr, La, Nb and Th concentrations display inter-eruptive variations and divide the Awassa tephras into three glass populations. Glass shards in AWT-1 ($1.5 - 1.1$ cal. ka BP) contain lower concentrations of Y, Zr and Nb than older Awassa tephras (Fig.

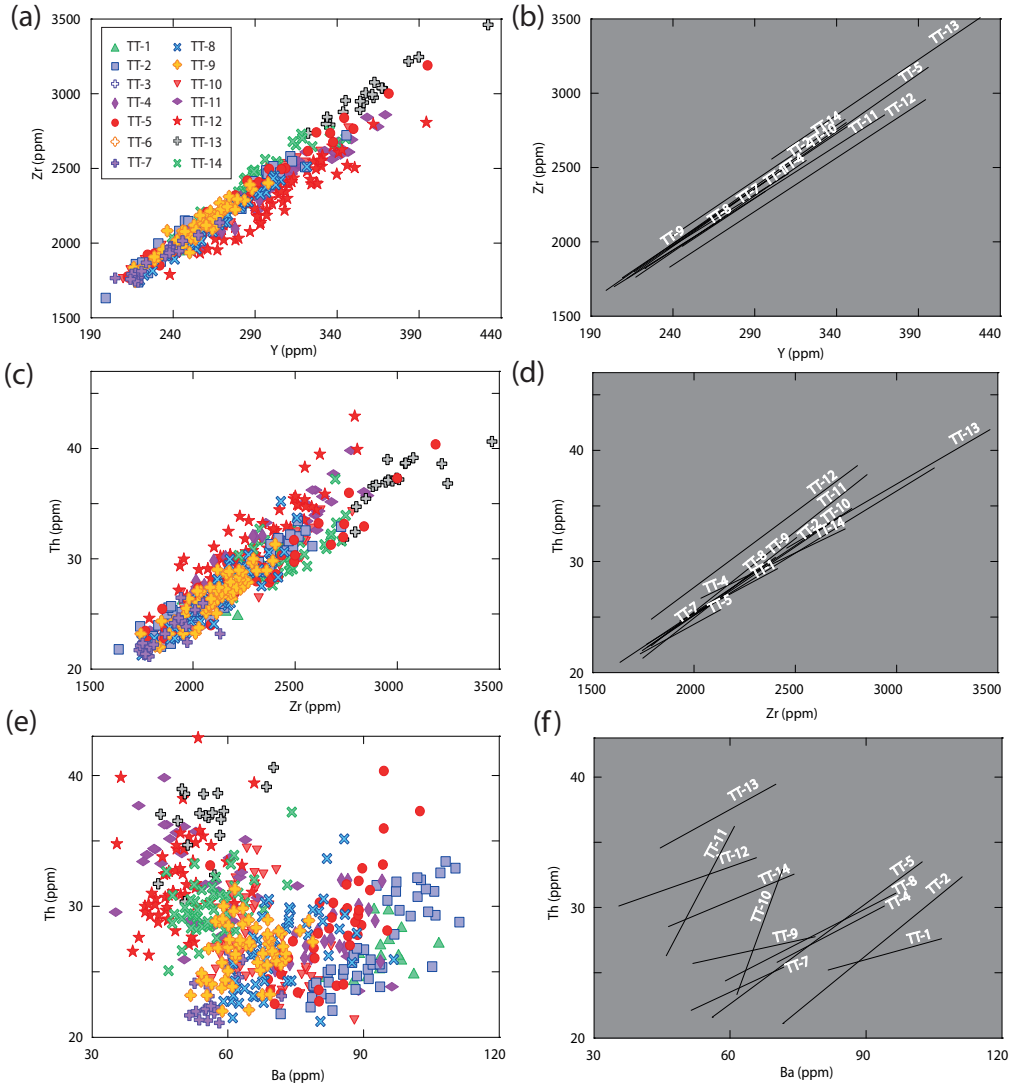

Figure 7.2: Ratios of Y/Zr, Zr/Th and Ba/Th in the Tilo Group II glass shards (see Fig. 7.1f), (b), (d) and (f) linear regression trends through showing the relationship between incompatible element concentrations in the Tilo tephras. The Tilo Group II tephras show similar Y/Zr and Zr/Th element ratios, suggesting they are derived from the same source.

7.3d, e). Glass shards in AWT-1 are bimodal; one glass population contains higher Ba concentrations than other Awassa tephras, whilst other AWT-1 glass shards contain similar Ba concentrations to other Awassa tephras (Fig. 7.3c). AWT-1 contains glass shards which display the widest range of Al_2O_3, FeO^T and Ba concentrations amongst the Awassa tephras (Fig. 7.3b, c). Glass shards in AWT-2 ($4.9 - 3.3$ cal. ka BP) and AWT-4 ($6.6 - 5.4$ cal. ka BP) are compositionally similar, however, AWT-2 contains higher Y concentrations than all other Awassa tephras and lower concentrations of Zr and Th than AWT-2 (Fig. 7.3d, f).

Table 7.3: Normalised major element (wt.%) and trace element (ppm) concentrations of glass shards in the Awassa tephras. Average (± st. dev.) concentrations of selected elements which have proved to be useful for correlation are shown here. The range of element concentrations in each tephra is shown in italics.

	AWT-1	**AWT-2**	**AWT-4**
Age (ka)	1.5 – 1.1	4.9 – 3.3	6.6 – 5.4
SiO_2	74.08 (2.49)	75.42 (0.27)	74.93 (0.34)
	66.81-75.80	*75.09-76.09*	*74.33-75.37*
Al_2O_3	11.12 (2.54)	9.62 (0.14)	9.65 (0.13)
	9.35-19.13	*9.37-9.92*	*9.43-9.88*
FeO^T	4.06 (1.39)	4.60 (0.12)	4.78 (0.23)
	0.52-6.43	*4.41-4.89*	*4.53-5.36*
Na_2O	5.03 (0.68)	5.20 (0.27)	5.23 (0.15)
	3.44-6.17	*4.58-5.59*	*4.97-5.51*
K_2O	5.08 (0.98)	4.47 (0.11)	4.43 (0.14)
	4.26-7.36	*4.34-4.71*	*4.18-4.55*
Y	203 (28.7)	285 (34.0)	294 (26.5)
	126-237	*227-357*	*256-339*
Zr	1620 (236)	2030 (254)	2400 (228)
	1060-1910	*1610-2470*	*2130-2830*
Nb	213 (27.2)	260 (19.0)	278 (16.0)
	171-260	*221-287*	*246-305*
Ba	237 (130)	81.2 (33.0)	69.8 (9.74)
	29.7-481	*62.7-196*	*60.1-94.1*
La	210 (21.3)	251 (25.3)	269 (27.1)
	153-238	*211-299*	*235-316*
Hf	44.1 (4.94)	51.8 (5.61)	63.6 (5.56)
	31.5-52.9	*43.9-62.61*	*56.6-72.3*
Th	22.8 (3.69)	26.5 (3.18)	31.4 (3.46)
	16.9-31.1	*22.2-33.0*	*26.6-38.8*
U	6.43 (1.15)	7.54 (1.82)	8.11 (0.71)
	5.01-8.98	*5.23-13.3*	*7.09-9.11*
	$n = 30$	$n = 28$	$n = 10$

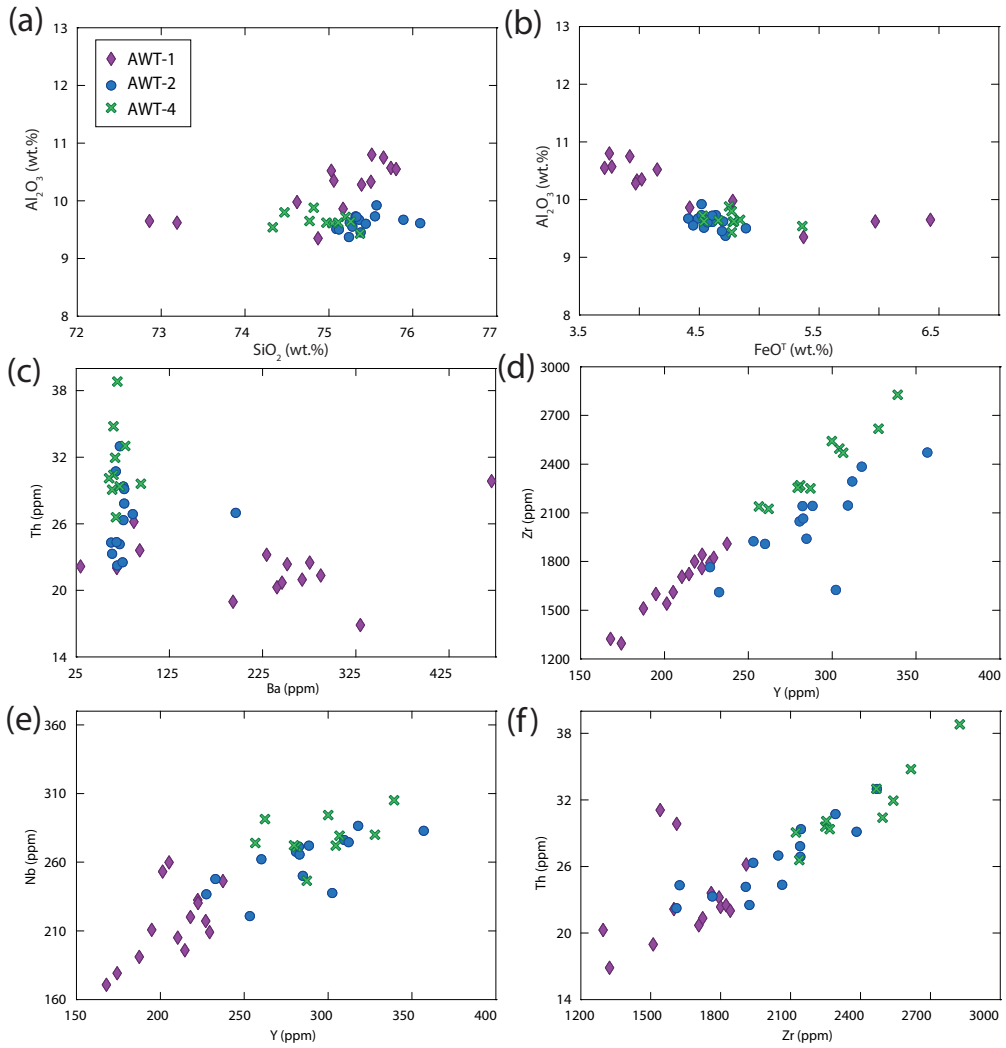

Figure 7.3: Major and trace element compositions of the Awassa tephra glass shards.

7.2.3 Composition of the Chamo tephras

The compositions of glass shards in the 2 Chamo tephras is given in Table 7.4 and Fig. 7.4. The Chamo tephras are pantellerites and have similar Y/Zr and Zr/Th ratios, indicating that they may be derived from a shared volcanic source (Fig. 7.4d, f). Concentrations of Al_2O_3, Nb, Ba and Th show the variation between CHT-1 and CHT-2, enabling them to be distinguished. Glass shards in the younger tephra, CHT-1 ($2.8 - 1.2$ cal. ka BP), contain higher Al_2O_3 and Ba concentrations and lower Zr, Nb and Th concentrations than CHT-2 ($9.4 - 6.3$ cal. ka BP) glass shards (Fig. 7.4a, c, e, f).

Table 7.4: Normalised major element (wt.%) and trace element (ppm) concentrations of glass shards in the Chamo tephras. Average (± st. dev.) concentrations of selected elements which have proved to be useful for correlation are shown here. The range of element concentrations in each tephra is shown in italics.

	CHT-1	**CHT-2**
Age (ka)	2.8 – 1.2	9.4 – 6.3
SiO_2	75.04 (0.26)	74.86 (0.43)
	74.65-75.72	*74.33-76.37*
Al_2O_3	9.74 (0.12)	9.44 (0.12)
	9.50-10.01	*9.19-9.61*
FeO^T	4.63 (0.17)	4.90 (0.14)
	4.32-4.86	*4.56-5.18*
Na_2O	5.29 (0.16)	5.61 (0.41)
	4.87-5.50	*4.06-6.07*
K_2O	4.42 (0.12)	4.33 (0.08)
	4.10-4.56	*4.20-4.47*
Y	302 (34.6)	332 (38.2)
	262-366	*283-452*
Zr	2420 (235)	2700 (324)
	2150-2790	*2360-3760*
Nb	276 (16.3)	333 (13.6)
	250-320	*304-371*
Ba	108 (12.5)	50.6 (8.93)
	68.4-121	*42.7-73.2*
La	283 (26.7)	288 (43.3)
	246-335	*254-436*
Hf	57.4 (5.55)	65.7 (8.10)
	47.2-66.4	*57.7-94.9*
Th	29.3 (2.74)	33.9 (3.74)
	25.8-33.7	*30.2-47.2*
U	6.82 (0.529)	9.06 (0.499)
	5.71-7.54	*7.68-9.93*
	$n = 16$	$n = 19$

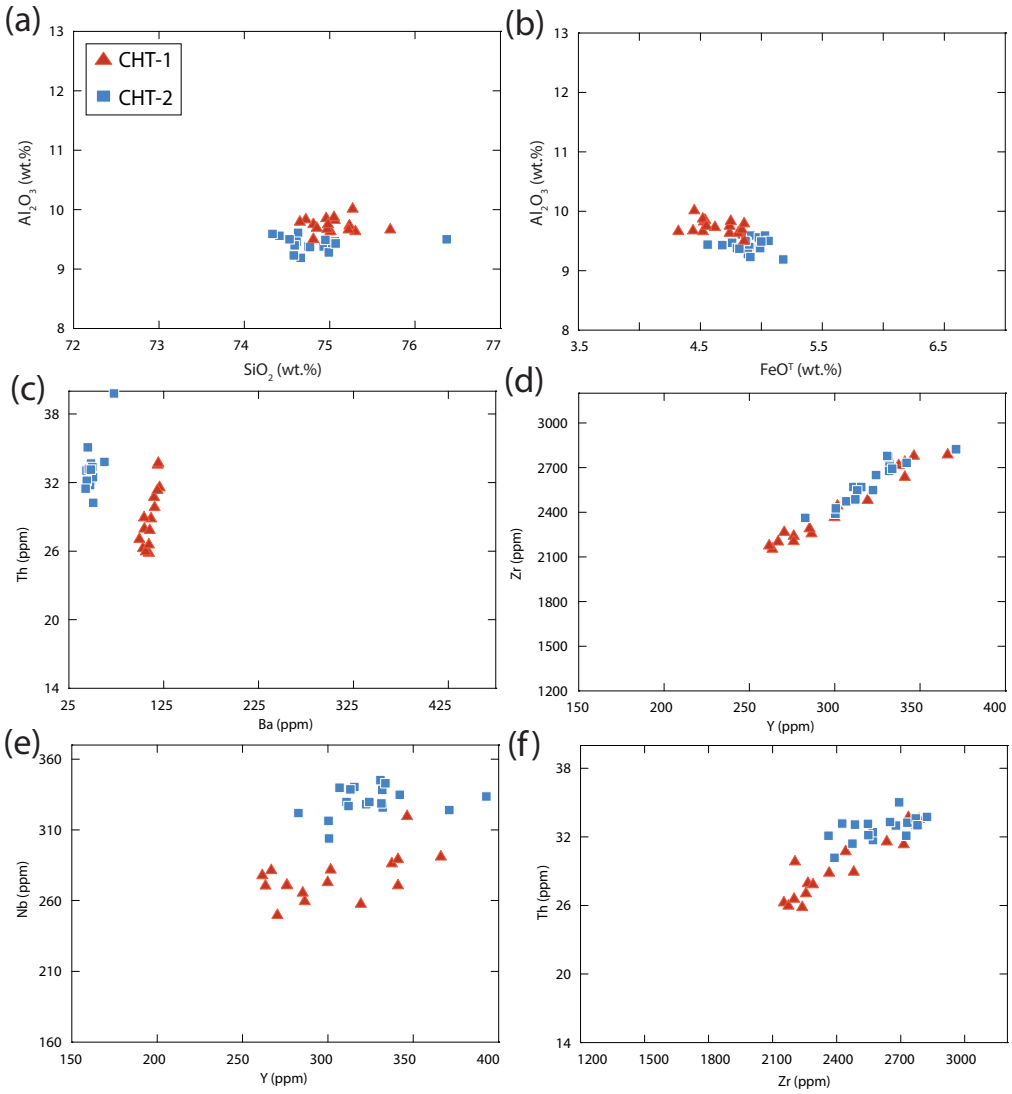

Figure 7.4: Major and trace element compositions of the Chamo tephra glass shards.

7.3 Discussion

7.3.1 Potential tephra correlations

The composition of tephra glass shards from lakes Tilo, Chamo and Awassa is compared in Figs. 7.5 to 7.10, in order to test whether the tephras in these archives can be correlated.

Figure 7.5 indicates that Tilo Group I (TT-3 and TT-6) glass shards are distinct from other tephras recorded in lakes Awassa and Chamo. Notably, TT-3 and TT-6 glass shards contain higher FeO^T and Ba concentrations, lower SiO_2 concentrations and different Zr/Th ratios when compared with all other glass shards (Fig. 7.5a, b, c, f). Glass shards in AWT-1 are also distinct from all other tephras. AWT-1 glass shards contain lower Ba concentrations than the Tilo Group I tephras, but higher Ba concentrations than all other tephra glass shards (Fig. 7.5c).

The Chamo tephras are distinct from the other Awassa (AWT-2 and AWT-4) tephras. The youngest Chamo tephra, CHT-1 ($2.8 - 1.2$ cal. ka BP), contains higher Ba concentrations than AWT-2 and AWT-4. The oldest Chamo tephra, CHT-2 ($9.4 - 6.3$ cal. ka BP), contains lower Ba concentrations than AWT-2 and AWT-4 (Fig. 7.5c). However, both the Chamo tephras and AWT-2 and AWT-4 Awassa tephras have comparable compositions to the Tilo Group II tephras (Fig. 7.5c). Furthermore, these glass shards contain similar major and trace element concentrations and have similar Zr/Th ratios (Fig. 7.5f), suggesting the tephras recorded in these archives may be derived from a shared source.

Nonetheless, there are compositional similarities between the Chamo and Awassa tephras (AWT-2 and AWT-4) and the Group II Tilo tephras. Notably, most of the Chamo and Awassa tephra glass shards have similar Zr/Th ratios

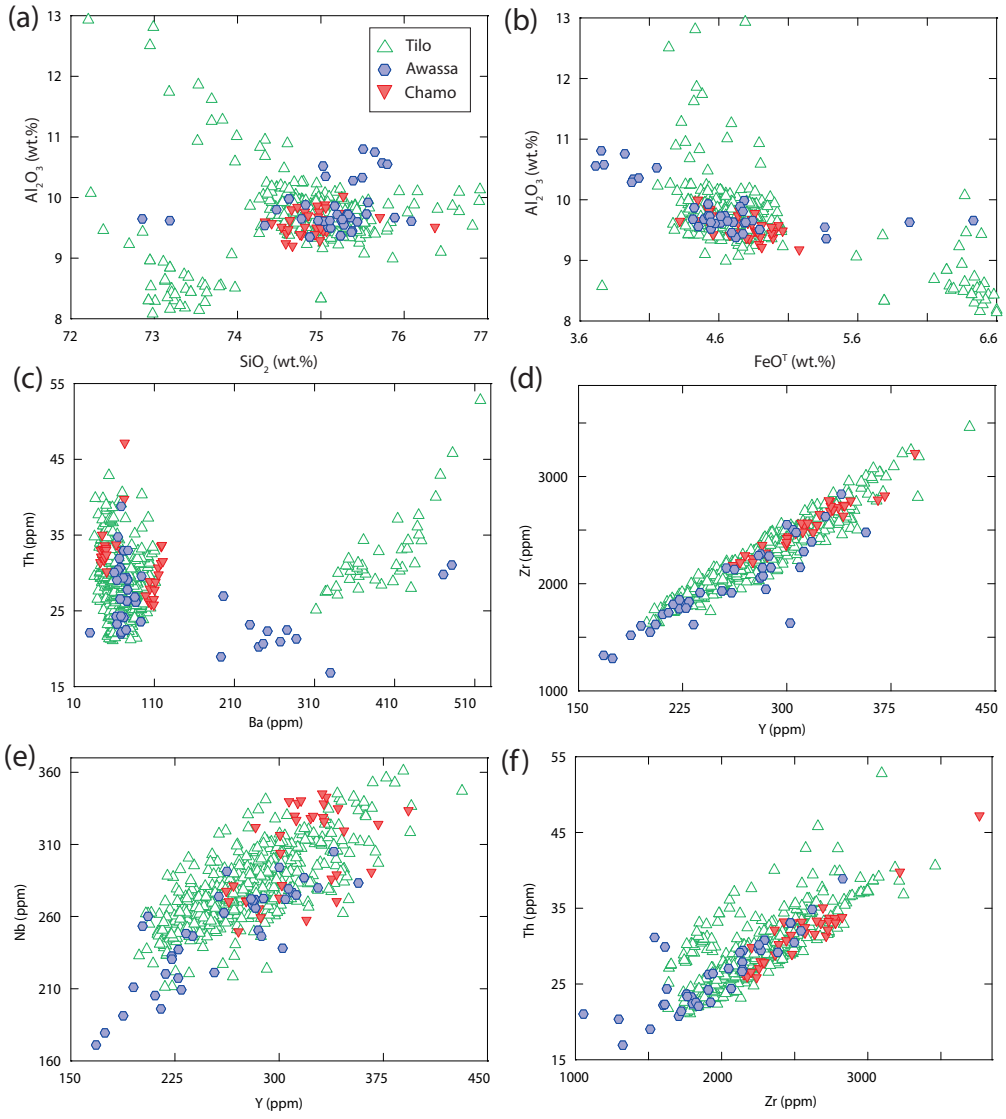

Figure 7.5: Major and trace element compositions of the Awassa, Tilo and Chamo tephra glass shards

($\approx 64.0 - 86.7$) to the Tilo Group II tephras ($\approx 56.2 - 92.1$) , suggesting that the tephras from these different archives may originate from a single source.

Glass shards in CHT-1 have a comparable composition to younger Tilo tephras, TT-1, TT-2, TT-4 and TT-5 ($2.6 - 0.5$ cal. ka BP). However, glass shards in TT-4 contain lower Zr concentrations and TT-4 and TT-5 glass shards have lower Ba concentrations than CHT-1 (Fig. 7.6c, d). It is therefore apparent that CHT-1 has a more comparable composition to TT-1 and TT-2 glass shards. The compositional similarities between these tephras noted using bi-plots are further investigated using principal component analysis in Fig.7.7. This allows the concentrations of SiO_2, Al_2O_3, FeO^T, Y, Zr, Nb, Ba, La and Th in these tephra glass shards to be statistically compared. Figure.7.7b verifies the compositional differences between CHT-1 and TT-4 and TT-5 noted previously, and indicates that TT-1 is compositionally different to CHT-1. On this basis, TT-2 ($2.1 - 1.2$ cal. ka BP) may have been produced by the same eruptive event as CHT-1 ($2.8 - 1.2$ cal. ka BP), and this is supported by their comparable age ranges.

The oldest recorded Chamo tephra, CHT-2, contains glass shards which are compositionally similar to older Tilo Group II tephras (TT-11; 12; 13 and TT-14, $10.2 - 5.1$ cal. ka BP). Further comparison of these tephras (Fig.7.8) shows that TT-14 contains broadly higher SiO_2 and Ba concentrations and lower FeO^T, Y and Th concentrations than CHT-2. TT-12 is also distinct from CHT-2, its glass shards contain comparably lower Al_2O_3 and Th concentrations and higher Y concentrations (Fig.7.8a, c, d). It is not clear whether TT-11 or TT-13 are potential correlatives of CHT-2 based on the major and trace element composition of their glass shards. CHT-2 glass shards are statistically compared with older Tilo Group II tephras in Fig. 7.9, and this suggests that TT-13 ($8.9 - 8.0$ cal. ka BP) has a more comparable composition to CHT-2 ($9.4 - 6.3$ cal. ka BP). These

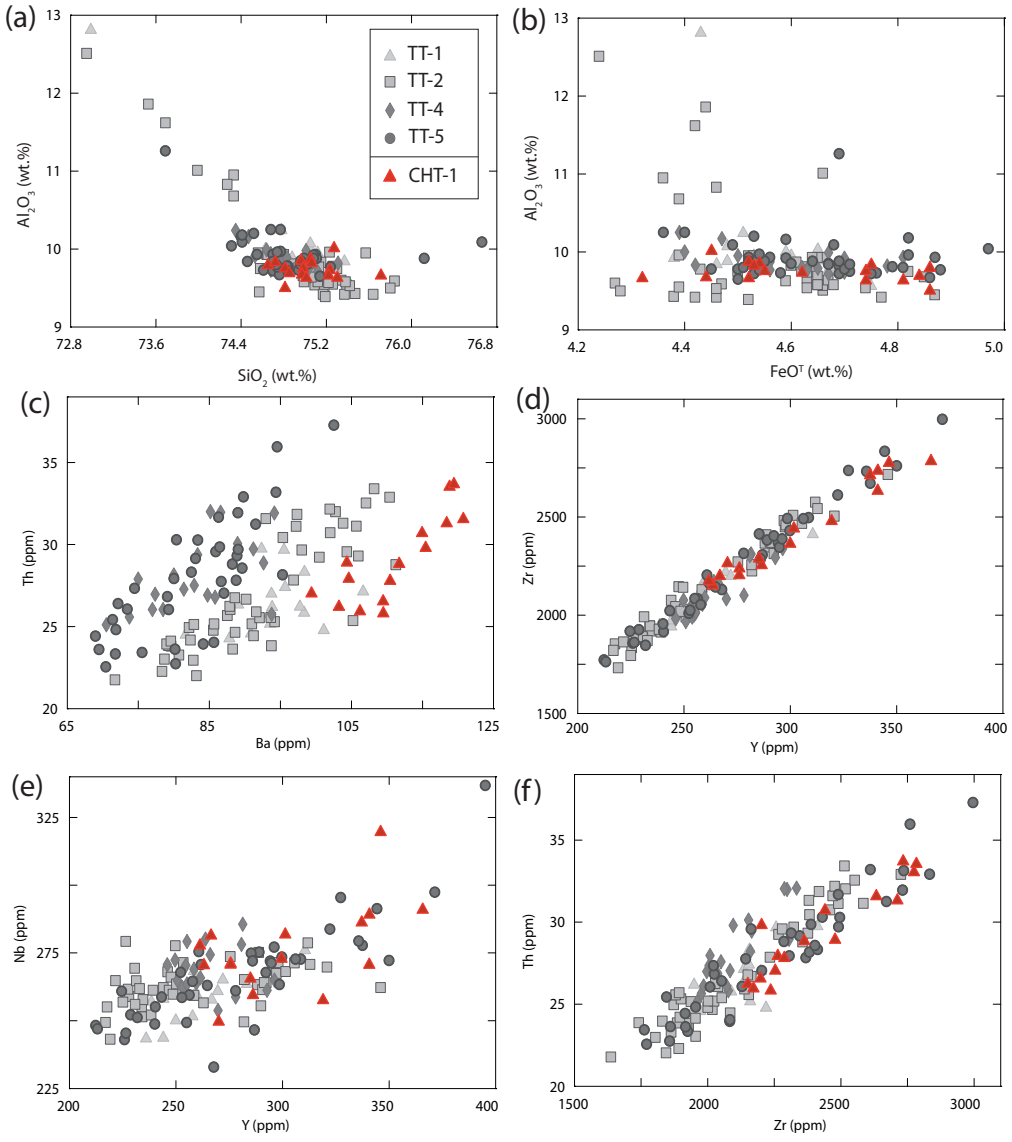

Figure 7.6: Biplots comparing concentrations of selected major and trace elements in the CHT-1 glass shards and TT-1; 2; 4 and TT-5 glass shards.

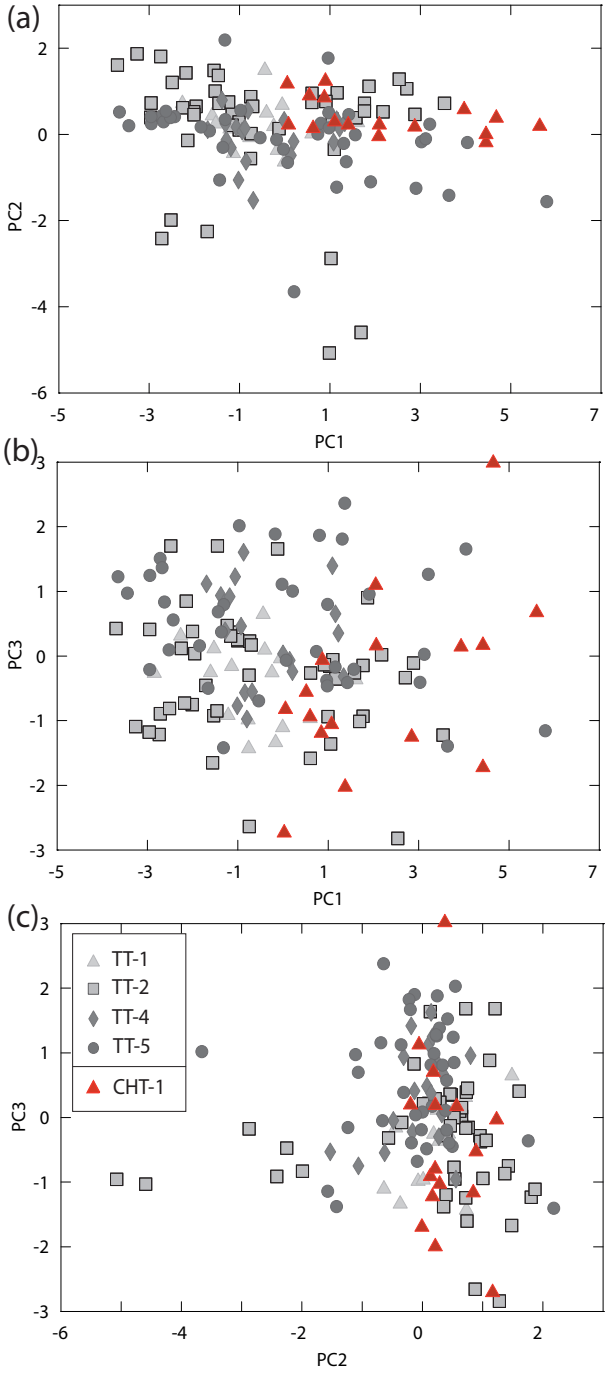

Figure 7.7: Bi-plots of the first three principal components from a principal component analysis of the compositionally similar CHT-1, TT-1; 2; 4 and TT-5 tephra glass shards. SiO_2, Al_2O_3, FeO^T, Y, Zr, Nb, Ba, La and Th are used as variables.

tephras have similar ages, and it is highly likely that CHT-2 is derived from the same source as TT-13. However, this link remains tentative and requires testing with further sampling and glass analysis.

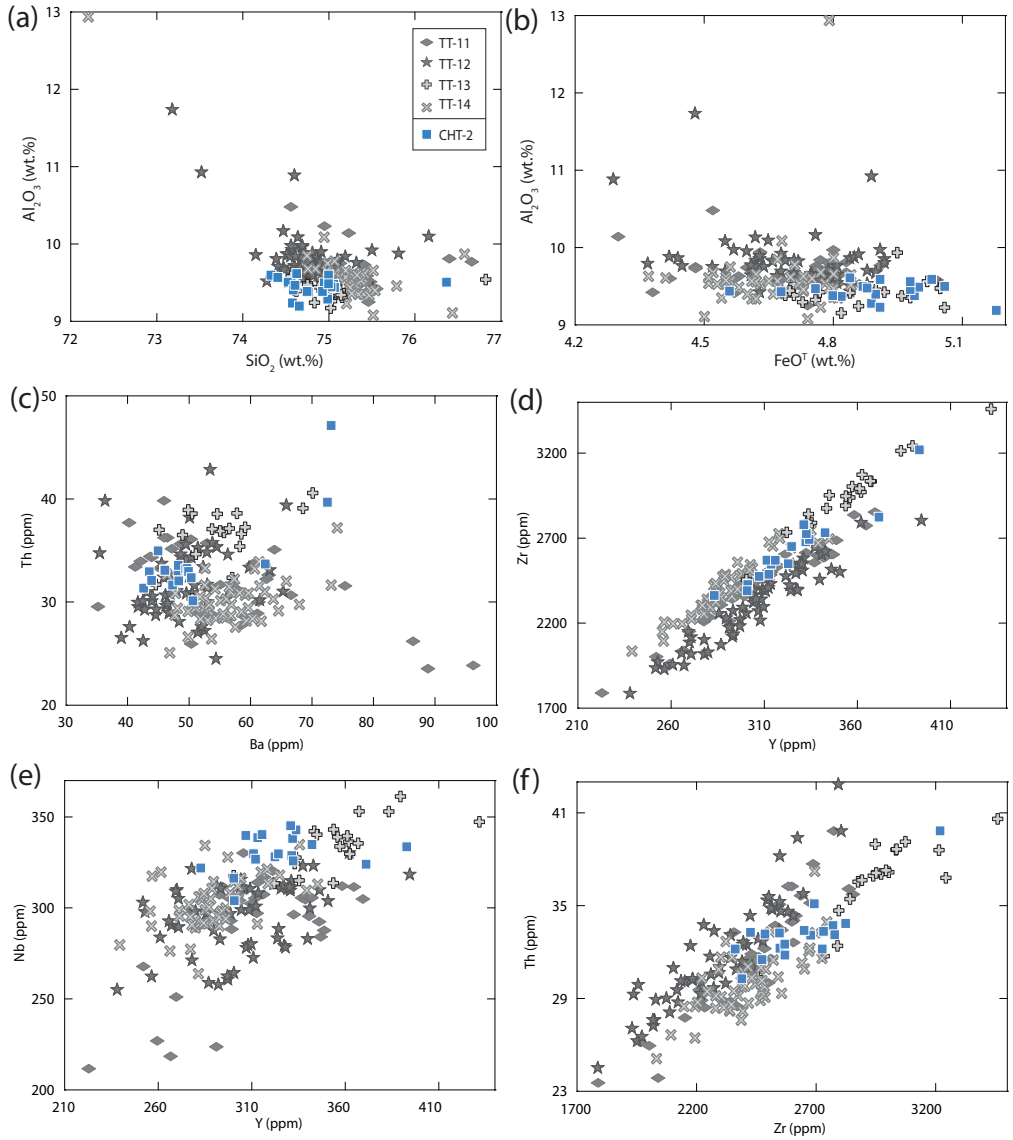

Figure 7.8: Bi-plots showing selected major and trace element compositions of the CHT-2 and TT-11;12;13 and TT-14 glass shards.

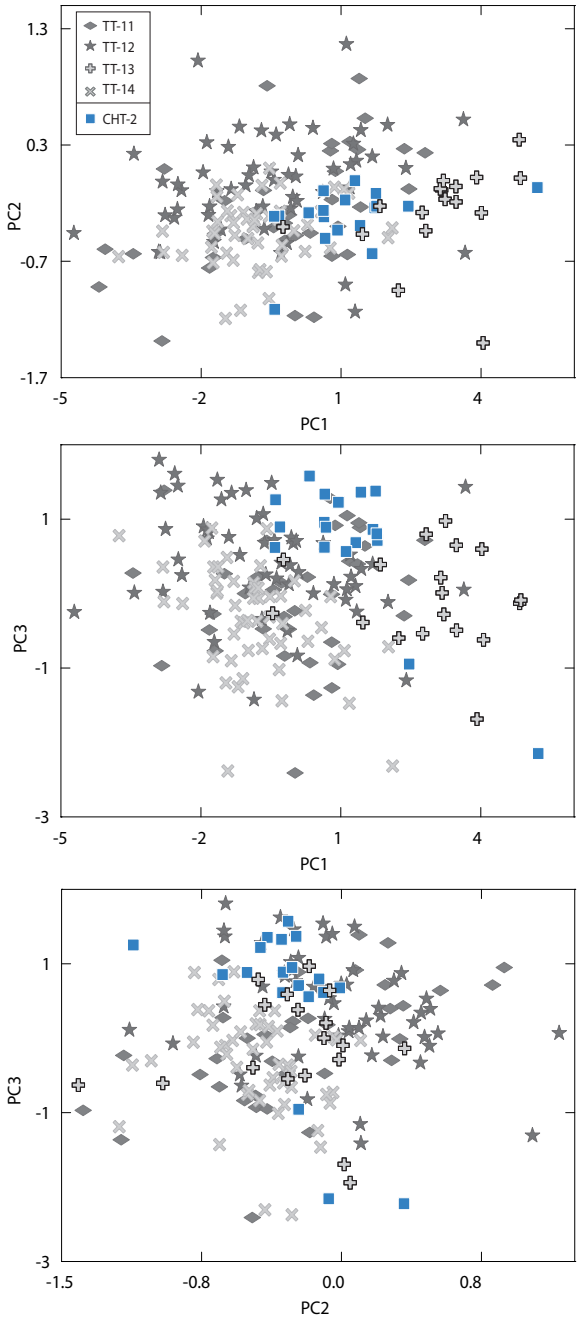

Figure 7.9: Bi-plots of the first three principal components from a principal component analysis of the compositionally similar CHT-2 and TT-11;12;13 tephra glass shards. SiO_2, Al_2O_3, FeO^T, Y, Zr, Nb, Ba, La and Th are used as variables.

The Awassa tephras, AWT-2 and AWT-4 (6.6 – 3.3 cal. ka BP) contain glass shards which have a comparable composition to TT-7; 8; 9 and TT-10 (6.3 – 2.3 cal. ka BP). Glass shards in TT-7 contain lower Y, Nb, Ba and Th concentrations than AWT-2 and AWT-4 (Fig.7.10c, e). The composition of glass shards in AWT-2, AWT-4 and the 6.3 – 2.3 ka Tilo tephras is statistically compared in Fig.7.11. This further demonstrates that TT-7 is compositionally different from AWT-2 and AWT-4, however, no further differences between these tephras are noted. Whilst it is apparent that these tephras are most likely derived from the same source, it is not possible to ascertain which tephras were produced by the same eruptive event and correlate between the Awassa and Tilo archives.

Therefore, it is apparent that the majority of tephras recorded in the Awassa, Tilo and Chamo archives are derived from a shared source. CHT-1 and CHT-2 can be tentatively correlated to TT-2 and TT-13, respectively (see Fig.7.12). The Awassa tephras, AWT-2 and AWT-4 are compositionally similar to TT-8; 9 and TT-10, however, it is not possible to ascertain which of the Tilo tephras are correlatives based on their composition.

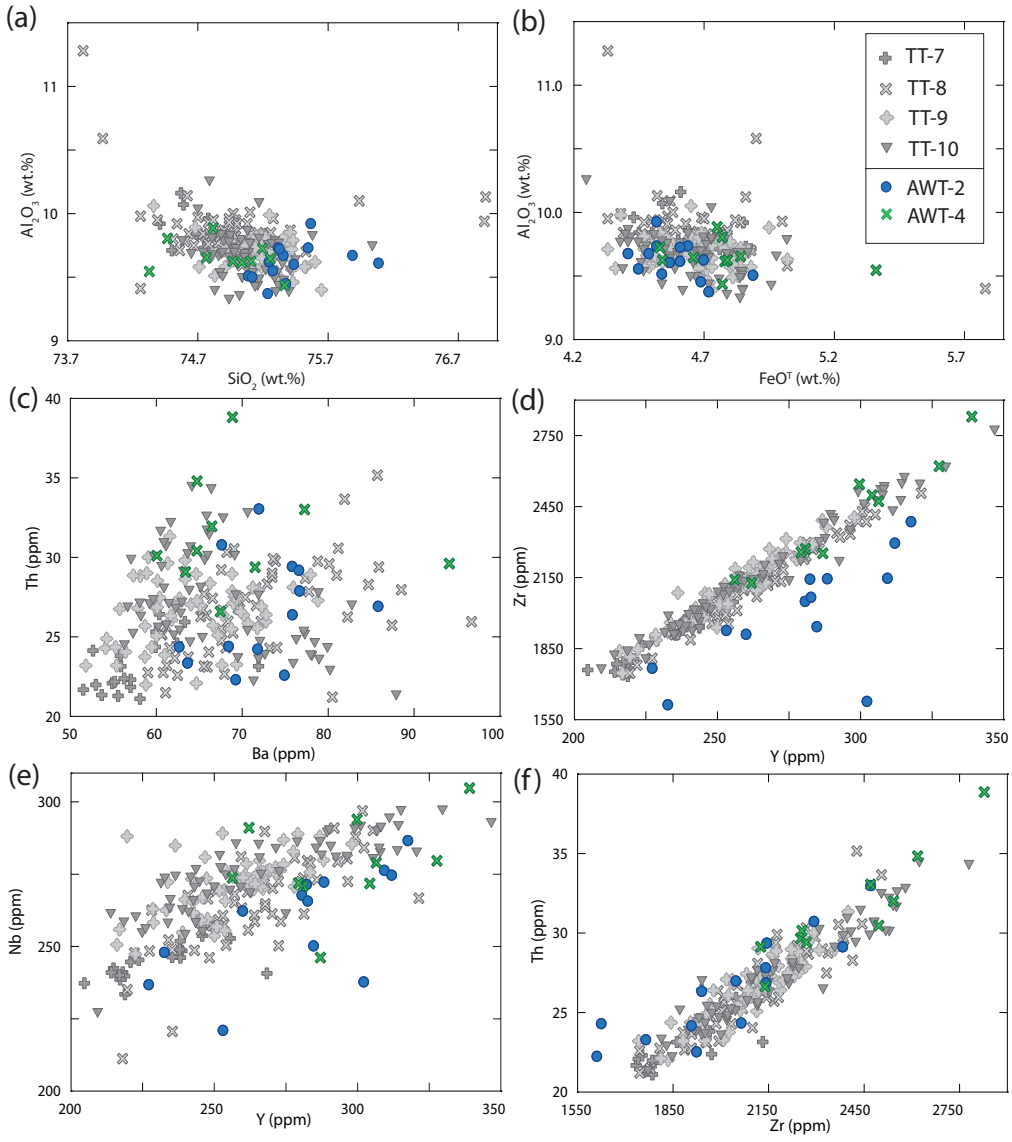

Figure 7.10: Bi-plots showing selected major and trace element concentrations in the AWT-2, AWT-4, and TT-7;8;9 and TT-10 tephra glass shards.

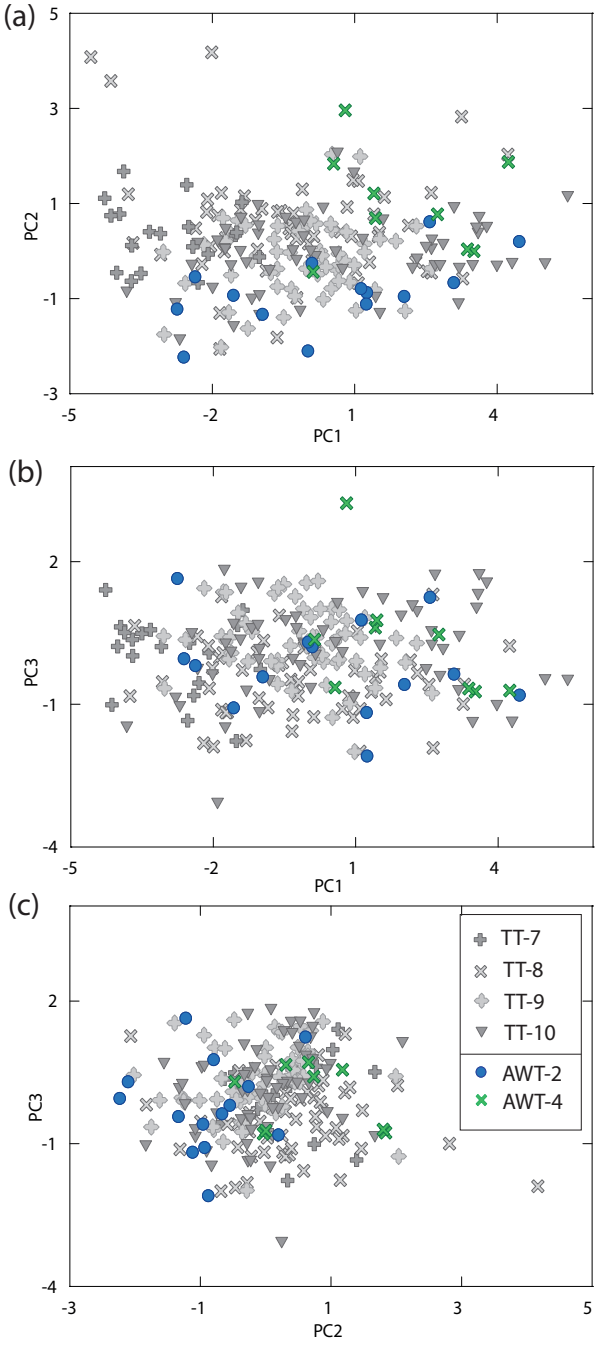

Figure 7.11: Bi-plots of the first three principal components from a principal component analysis of the compositionally similar AWT-2, AWT-4, and TT-7;8;9 and TT-10 tephra glass shards. SiO_2, Al_2O_3, FeO^T, Y, Zr, Nb, Ba, La and Th are used as variables.

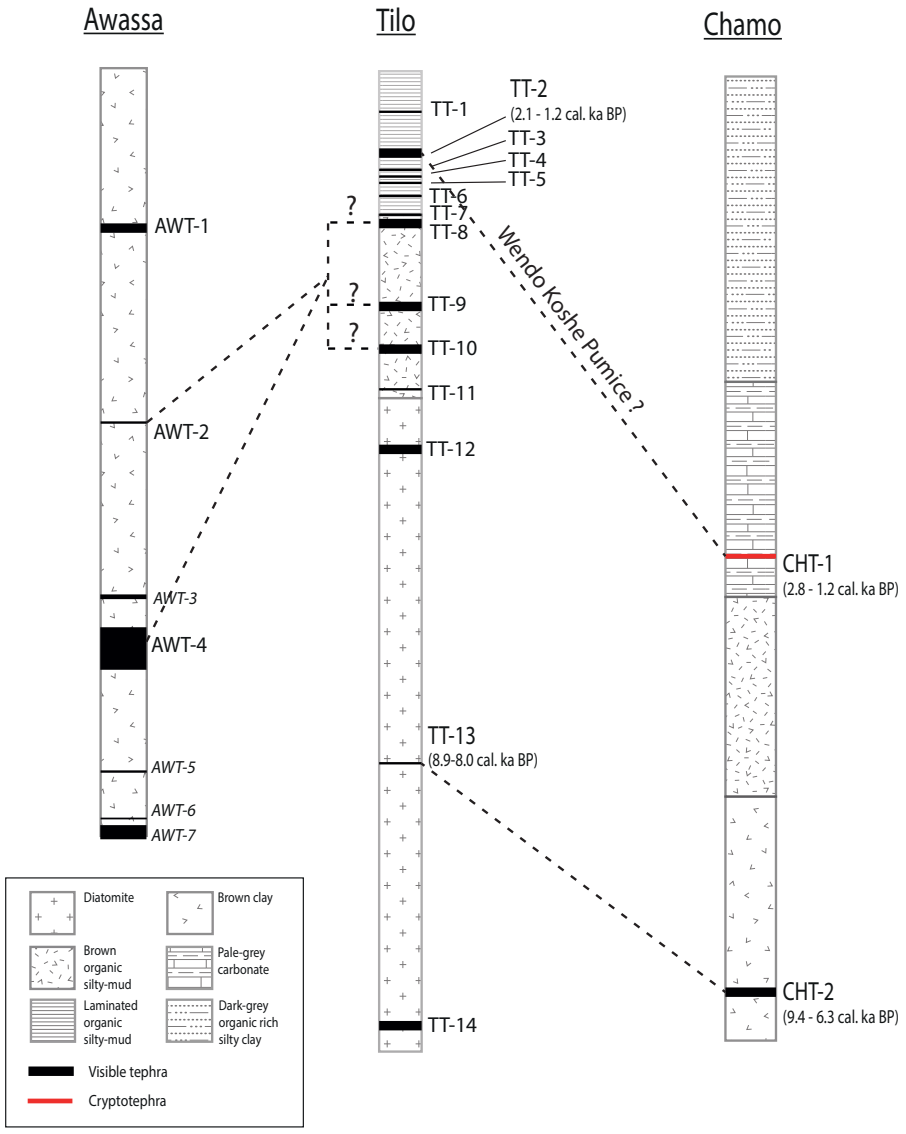

Figure 7.12: Correlations between Awassa, Tilo and Chamo archives. Based on their geochemistry, it is not possible to ascertain whether TT-8; 9 or TT-10 are correlatives of AWT-2 and AWT-4. CHT-1 and TT-2 may represent the latest Wendo Koshe eruption (see page 235).

7.3.2 Provenance of tephras deposited in central MER lakes

Many of the tephras recorded in these archives have similar incompatible element ratios and are therefore potentially derived from one shared source. However, variable incompatible element ratios suggest eruptions from other centres deposited two tephras in Lake Tilo (TT-3 and TT-6) and one tephra in Lake Awassa (AWT-1). Lake Awassa is located within the Corbetti caldera, whilst Lake Tilo is located $<$ 40 km from this centre (Fig.7.13b). Since the collapse of this caldera during the Quaternary, the recent centres Wendo Koshe and Chabbi (Fig.7.13b) have developed on the northern shores of Lake Awassa and are associated with obsidian flows and rhyolitic monotonous pumice deposits. Žáček *et al.* (2014) and Rapprich *et al.* (2016) described the most recent eruption from Wendo Koshe, which dispersed a 10 cm thick pumice lapilli deposit over an area of 1000 km^2. Radiocarbon dates on paleosol underlying the deposit date the eruption to $\sim$ 400 BC (Rapprich *et al.*, 2016). This deposit overlies a yellowish phreatomagmatic tuff. Žáček *et al.* (2014) suggests this originates from Fike Volcano (Fig.7.13a), between lakes Shalla and Abijata, on the basis of field observations.

In order to test if Corbetti is the source for many Awassa, Tilo and Chamo tephras, selected pumice and obsidian samples from the Chabbi volcano and Tilo crater walls have been analysed as part of this study (Fig.7.14). Published whole rock analyses of Holocene obsidian and pumice deposits from the Wendo Koshe volcano, from Rapprich *et al.* (2016) are shown for comparison in (Fig.7.14). These published bulk analyses contain contaminant minerals, and only incompatible element ratios can therefore be compared.

Unfortunately, comparison of the composition of tephras from these archives with other centres in the MER is limited. This is due to the scarcity of published glass analyses and chronological control on proximal samples from volcanoes in

this area. The Pleistocene volcano, Duguna, is located $\sim$ 10 km south of Lake Tilo (Fig.7.13b). This has produced tephra deposits of $>$ 30 m thickness, with reported ages on deposits from the eastern flanks of $430-460$ ka. However, to the author's knowledge, there are no published geochemical data characterising this centre. Published compositions of melt inclusions within obsidians from the Fantale (Taylor *et al.*, 1997) and Boseti (Macdonald *et al.*, 2012) volcanoes (Fig.7.13a) are shown for comparison in Fig.7.14. Although obsidian flows are effusive and do not occur as widespread deposits, their glass composition gives a broad geochemical signature for a volcano.

Glass shards in TT-3 and TT-6 have different Zr/Th ratios to the proximal obsidian samples from Corbetti and are therefore most likely derived from a different volcanic centre (Fig.7.14f). However, further sampling of proximal tephras and obsidians is required to constrain the potential source of TT-3 and TT-6.

Comparison of these tephras with the composition of melt inclusions in obsidians from Fantale show that they are distinct. The Fantale obsidians have different Zr/Th ratios ($\approx 41.9-53.2$) to tephras from the Awassa, Tilo and Chamo archives ($\approx 56.2-92.1$). The Boseti melt inclusions have distinct major element compositions to the Awassa, Tilo and Chamo tephras (Fig.7.14a, b). However, further trace element analysis of glass shards is required to test if this centre could be a source of these tephras.

Obsidian and pumices samples from Chabbi and Wendo Koshe (Rapprich *et al.*, 2016) have similar Zr/Th ratios (Chabbi $\approx 70.3-87.5$, Wendo Koshe $\approx 83.4-97.4$) to Group II Tilo tephras and Awassa and Chamo tephras ($\approx$ $56.2-92.1$). Therefore, it is possible that the majority of Awassa, Tilo and Chamo tephras are derived from centres within the Corbetti caldera. If Corbetti

Table 7.5: Tephra and obsidian samples from selected centres throughout the central Main Ethiopian Rift, used here to determine the potential source of the Tilo tephras.

Sample ID	**Sample area**	**Volcano**	**Sample type**	**Data source**
ST1-NW	Lake Awassa: Shallo Swamp	Corbetti	Pumice	This study
E95003	Lake Awassa: Quarry to east	Corbetti	Obsidian	This study
E95007	Lake Awassa: Shashamene-Awassa road cut	Corbetti	Tephra	This study
E95010	Lake Awassa: Promontory on northern shore	Corbetti	Obsidian	This study
E95011	Lake Awassa: Promontory on northern shore	Corbetti	Weathered obsidian	This study
E95019	Lake Awassa: Hill on northern shore	Corbetti	Obsidian xenoliths	This study
E95025	Lake Tilo: northern shore	Corbetti	Obsidian xenolith	This study
E97003	Lake Tilo: northern shore	Corbetti	Pumice in ignimbrite	This study
B350 - B375	Pre caldera Boseti	Boseti	Obsidian melt inclusions	(Macdonald *et al.*, 2012)
i2B2/o - FiN4	Post caldera Fantale	Fantale	Obsidian melt inclusions	(Taylor *et al.*, 1997)
CO6-IG	Wendo Koshe centre	Corbetti	Pumice bulk analysis	(Rapprich *et al.*, 2016)

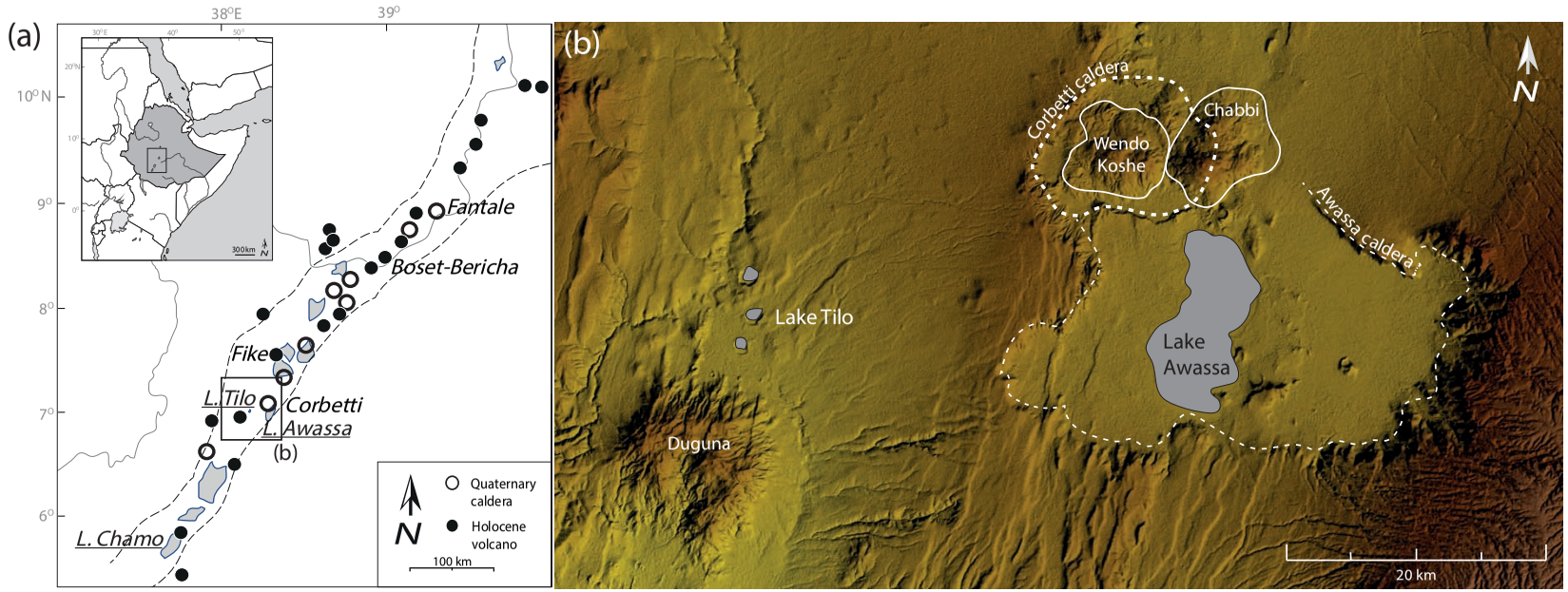

Figure 7.13: Map showing the locations of Corbetti and Fantale in relation to Awassa, Tilo and Chamo, (b) elevation map of the central Main Ethiopian Rift to the surrounding lakes Awassa and Tilo. Note that Lake Awassa drains the older Awassa and younger Corbetti calderas. Recent volcanic centres, Wendo Koshe and Chabbi, have developed on the northern shore of Lake Awassa, within the Corbetti caldera.

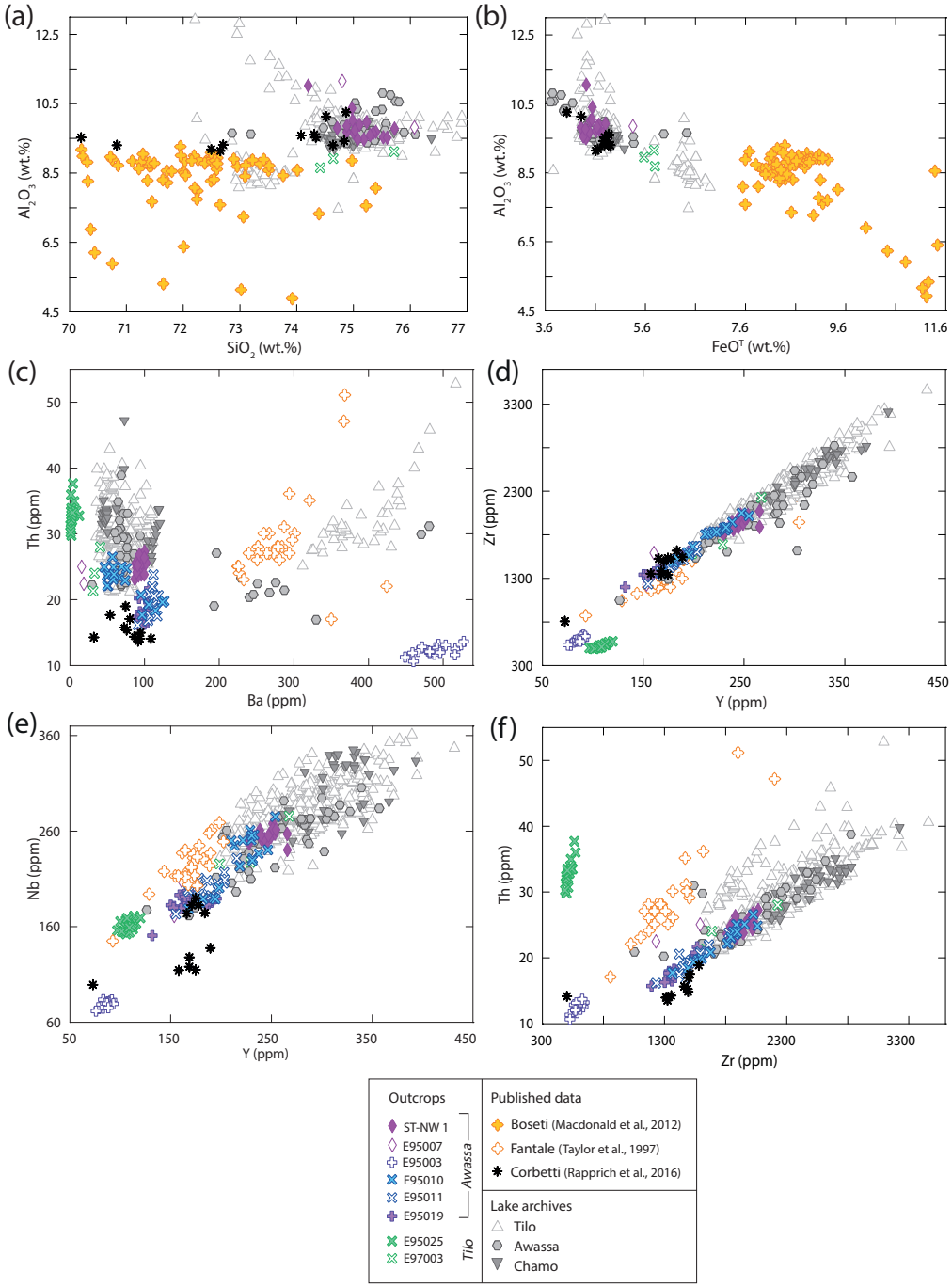

Figure 7.14: Comparison of the composition of tephra glass shards from Awassa, Tilo and Chamo with the composition of outcrop samples from Corbetti, Tilo crater walls and published melt inclusion data on obsidians erupted from Boseti and Fantale volcanoes from Taylor *et al.* (1997); Macdonald *et al.* (2012).

is the source for these tephras, this would explain the thickness (< 48 cm) of the tephras from nearby lake Tilo. Glass analysis of tephras from Corbetti are now required to confirm these correlations. Despite the limitations, these comparisons are the first and best attempt to characterise and correlate these tephras to a source.

An obsidian sample (E95003) from a Quarry to the east of Awassa and obsidian xenolith from the Tilo crater walls (E95025) have distinct compositions (Zr/Th $\approx 43.9 - 50.7$ and $\approx 15.0 - 16.7$, respectively). It is possible that these samples are older and the xenolith could be derived from a different centre, potentially explaining their distinct composition.

The only tephra outcrop sample to have a similar composition to the lakes Awassa, Tilo and Chamo tephras is ST-NW1, collected from the Shalo Swamp ($\sim$ 10 km east of Lake Awassa). The ST-NW1 glass shards have similar Zr/Th ratios ($\approx 71.1 - 82.6$) and compositions to the youngest group of Tilo tephras (TT-1; 2; 4 and TT-5, Zr/Th $\approx 71.6 - 89.6$) and the youngest Chamo tephra (CHT-1; Zr/Th $\approx 73.9 - 86.7$). Glass shards in ST-NW1 contain higher Ba concentrations than TT-4 and TT-5 and have a more comparable composition to TT-1, TT-2 and CHT-1 (Fig. 7.15c). However, CHT-1 glass shards are more evolved than the ST-NW1 glass shards (Fig. 7.15d, e, f). The similarities between the ST-NW1, the youngest Tilo tephras and CHT-1 glass shards are explored further using a PCA in Fig. 7.16. This demonstrates that TT-4 and TT-5 have different compositions to ST-NW1 (Fig. 7.16a, c) and supports the similarities between TT-1 and TT-2 noted previously. It is not possible to clearly identify whether TT-1 or TT-2 are correlatives of ST-NW1. Figure 7.16 reiterates that ST-NW1 and CHT-1 have statistically different compositions, however, the collective compositional fields occupied by ST-NW1 and CHT-1 occupy a broadly similar

area to the TT-2 glass shards. It is possible that ST-NW1 and CHT-1 were produced by the same eruptive event and a change in wind direction during the eruption caused less evolved compositions to be erupted close to the source, at the Shalo Swamp (eastern shores of Lake Awassa), and more evolved compositions to be deposited only at distal locations, at Lake Chamo. This widespread tephra deposit may be the Wendo Koshe pumice, produced by the most recent explosive eruption from Wendo Koshe (Rapprich *et al.*, 2016). If TT-2 is the Wendo Koshe pumice, the older and compositionally distinct TT-3 (Tilo Group I), may be the pyroclastic deposit from Fike Volcano that underlies the Wendo Koshe pumice in the Awassa area. However, further glass analyses of the Wendo Koshe pumice and the Fike Volcano pyroclastic deposits are required to ascertain this.

Therefore, it is possible that many tephras recorded in the Awassa, Tilo and Chamo archives are derived from centres within the Corbetti caldera. However, the source of two Tilo tephras and one Awassa tephra, which have distinct compositions, remains uncertain. To determine the source of these distinct tephras, further detailed field work and glass analyses on proximal tephra samples is required.

7.3.3 The tempo, petrogenesis and characteristics of < 10 ka Corbetti eruptions

The previous section demonstrated that most tephras recorded in lakes Awassa, Tilo and Chamo are potentially derived from the Corbetti caldera. The distribution and frequency of tephra deposits in these archives gives an indication of the frequency of regional eruptions, most likely derived from Corbetti. The Tilo archive preserves the most comprehensive record of regional volcanism. Lake Awassa drains the 1300 km^2 Corbetti caldera, whilst Tilo is a < 1 km diameter,

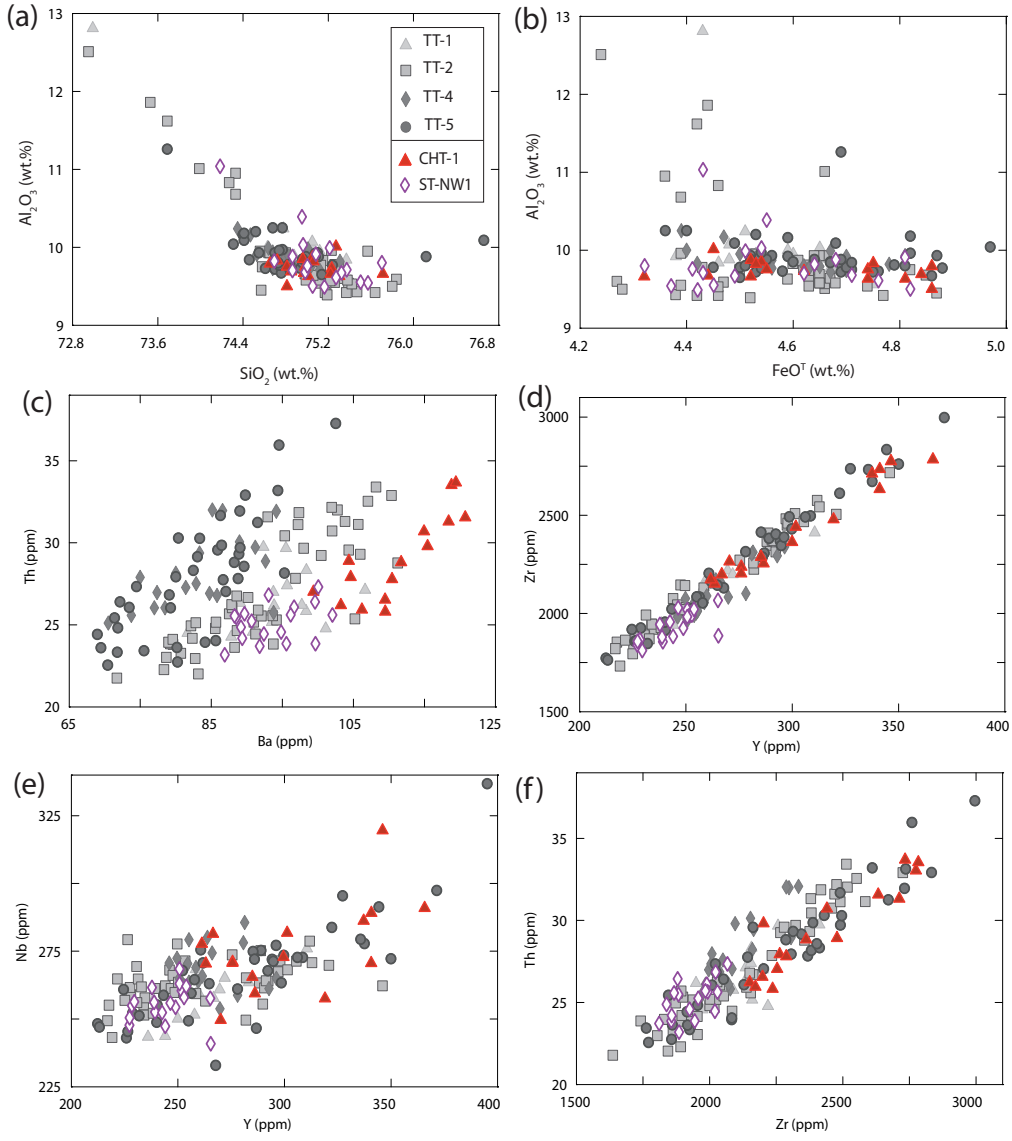

Figure 7.15: Bi-plots comparing concentrations of selected major and trace elements in the ST-NW1, CHT-1, TT-1;2;4 and TT-5 tephra glass shards

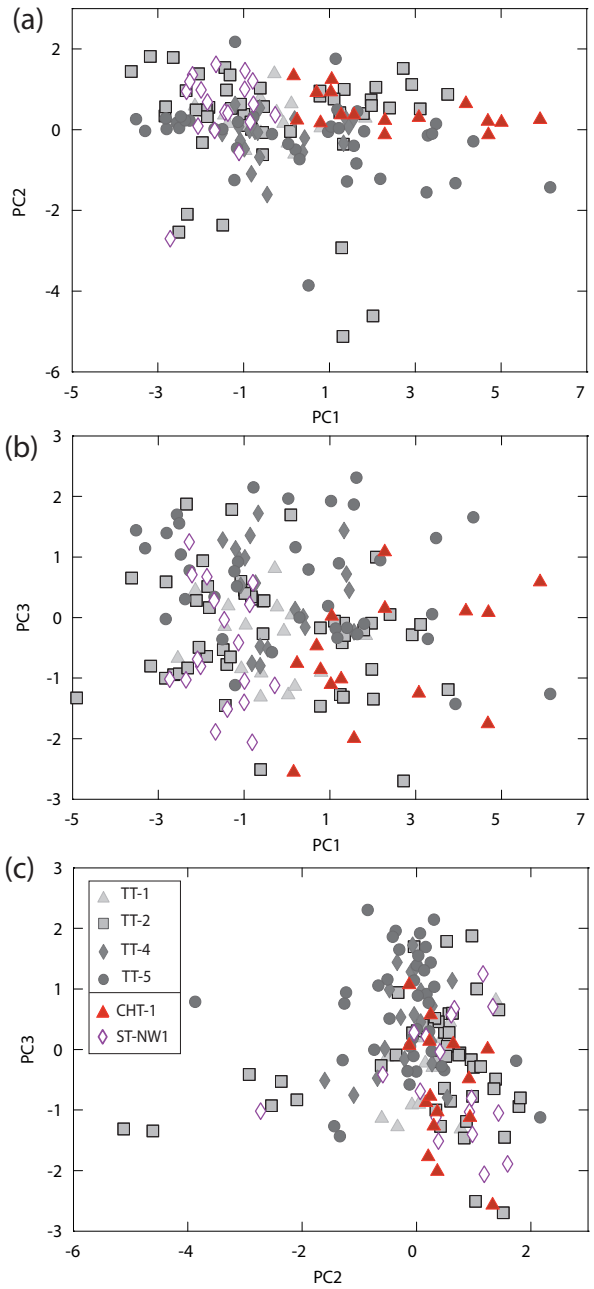

Figure 7.16: Bi-plots of the first three principal components from a principal component analysis of the compositionally similar ST-NW1, CHT-1, TT-1;2;4 and TT-5 tephra glass shards. SiO_2, Al_2O_3, FeO^T, Y, Zr, Nb, Ba, La and Th are used as variables.

steep sided crater lake with no in or out-lets (Fig. 7.13). It is possible that the Awassa tephras cannot be correlated to Tilo tephras because they contain mixed populations, having been reworked and mixed with older tephras within the Awassa catchment. However, tephras deposited in Tilo are most likely primary deposits, and their occurrence and thickness therefore provide an accurate reflection of past eruption frequency, and an indication of eruption explosivity.

The Tilo archive records 12 eruptions which appear to be derived from Corbetti during the past 10.2 ka. Fig. 7.17 shows selected trace element ratios in these 12 tephra deposits against their age ranges, giving an indication of the timing and composition of past eruptions. Many of the Tilo tephras range in thickness from several centimetres to half a metre, at a distance of ~ 40 km from Corbetti, suggesting that numerous recent eruptions from this centre have been highly explosive.

The first Corbetti eruption recorded in the Tilo archive occurred at $10.2 - 9.3$ cal. ka BP, depositing the thickest (48 cm) tephra (TT-14) in the Tilo archive. Following a short period (~ 450 years) during which no tephras were recorded in the Tilo archive, an eruption occurred from Corbetti ($8.9 - 8.0$ cal. ka BP), depositing TT-13 at Lake Tilo and CHT-2 at Lake Chamo (~ 170 km to the south-west). A ~ 980 year period without tephra deposition at Lake Tilo followed, potentially reflecting the longest interval of quiescence at Corbetti over the past ~ 10 ka. However, this could be related to changes in dominant wind direction during this time, or lower preservation potential at Lake Tilo. An explosive eruption from Corbetti followed at $7.0 - 6.1$ cal. ka BP, depositing TT-12 at Lake Tilo. Over the past ~ 7.0 ka, 10 explosive eruptions occurred from the Corbetti caldera and at frequent intervals, averaging one eruption every ~ 700 years. All tephras deposited in the Tilo archive during the past 7.0 ka have overlapping age

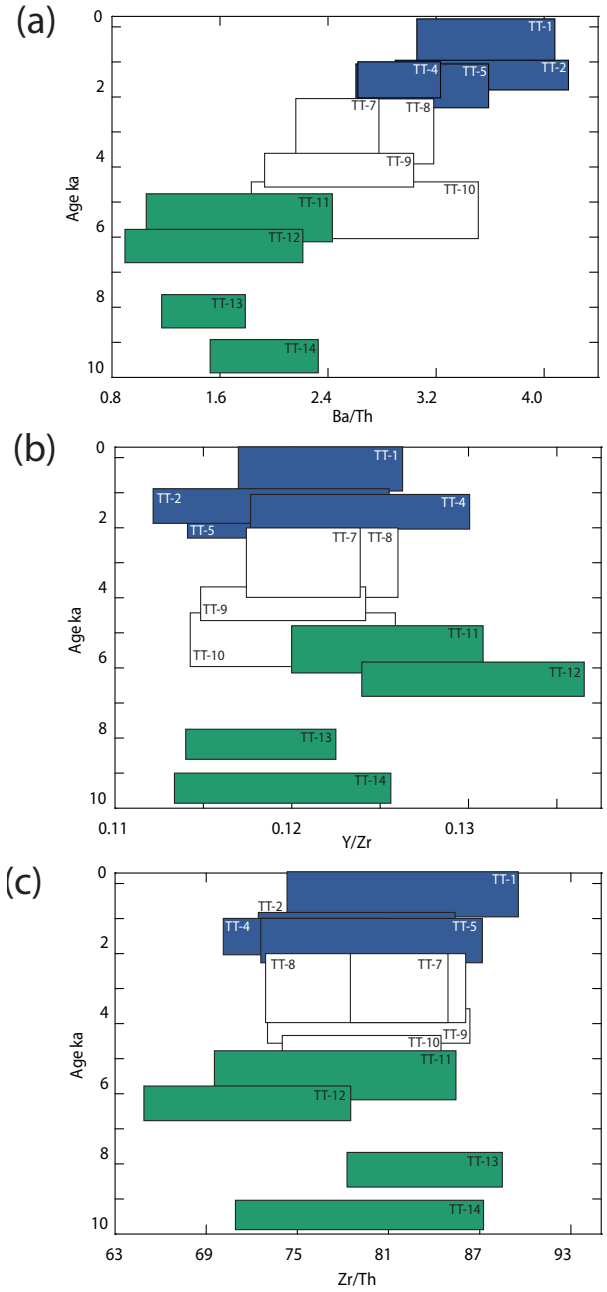

Figure 7.17: Selected trace element ratios in the Tilo Group II tephra glass shards plotted against their age ranges, modelled at the 95.4 % confidence interval. Groups of tephras which have similar compositions and ages are indicated in the same colour.

ranges at 95.4 % confidence intervals. During $\sim 6.3 - 2.3$ ka, three eruptions from Corbetti deposited three, $30 - 37$ cm thick, tephras at Lake Tilo. These tephras were also recorded as reworked deposits in Lake Awassa. The most explosive of recent eruptions from Corbetti, potentially the Wendo Koshe Pumice eruption, deposited the 20 cm thick TT-2 tephra in Lake Tilo at $2.1 - 1.2$ cal. ka BP. The same eruption most likely deposited tephra at Shalo Swamp (east of Lake Awassa) and at Lake Chamo, to the south-west.

The most recent eruption from Corbetti caldera occurred at $1.3 - 0.5$ cal. ka BP ($641 - 1900$ AD), depositing TT-1 in Lake Tilo. This is younger than the most recent 400 BC Wendo Koshe eruption described by Rapprich *et al.* (2016).

Figures 7.5 and 7.17 show that the Awassa and Tilo tephra glass shards have wide intra-eruptive compositional ranges, indicating these tephras originated from an evolving or compositionally zoned magma chamber. In contrast, the Chamo tephras are more homogeneous (Fig. 7.5), although it is possible that only part of the compositional range is represented at distal sites as wind direction can change during an eruption. However, it should be noted that fewer glass shards from the Chamo tephras were analysed. Figure 7.17 shows how the composition of tephras originating from Corbetti has changed over the past 10.2 ka. Concentrations of incompatible elements in the Tilo tephra glass shards remain relatively consistent through time. This may reflect the frequency of the eruptions from Corbetti, with little time between eruptions for fractional crystallisation to evolve the composition. Rapprich *et al.* (2016) also described the uniform geochemistry of the post-caldera eruptives from Corbetti over time. Nonetheless, following the longest period of quiescence recorded in the Tilo archive, erupted glass compositions (TT-12) contain higher concentrations of Y in relation the older TT-13 glass shards. It is apparent that between the eruption

of TT-13 and TT-12, there was sufficient time for fractional crystallisation to cause enrichment of Y in the melt.

Barium concentrations vary the most dramatically in the Tilo tephras, showing an increasing trend through time. However, Fig. 7.17a shows that this relationship is more complex. For instance, TT-11; 12; 13 and 14 ($10.2 - 5.1$ ka) show a progressive depletion in Ba concentrations through time, contrary to the overall trend. During $6.3 - 2.3$ ka, the tephras deposited (TT-7; 8; 9 and 10) have broadly consistent Ba concentrations through time. Recent volcanism, between $2.6 - 0.1$ ka, deposited tephras TT-1; 2; 4 and 5, which are increasingly enriched in Ba through time.

It is apparent that Ba appears to be behaving as an incompatible element in the Tilo tephra glass shards (Fig. 7.1c). This is contrary to the typical compatibility of Ba in feldspars. However, Mahood and Stimac (1990) described the complex behaviour of Ba in peralkaline melts and found that Ba is only weakly compatible in pantellerites. It is therefore possible that Ba may be behaving as a weakly compatible to incompatible element in the pantellerite Tilo tephras.

However, Section 5.4.1 highlighted that the Tilo tephras are highly evolved. Due to the minimum composition of the Tilo tephras, it is possible that they could not undergo further fractional crystallisation.

Assimilation of crustal rocks containing high Ba concentrations could cause its continued enrichment in the Tilo tephras through time. Figure 7.18 models the change in composition of the Tilo tephras through assimilation fractional crystallisation. The southern Ethiopian Precambrian basement rocks contain variable Ba concentrations ($39 - 1730$ ppm), here, the average composition of high-Ba granitoid basement rocks from Peccerillo *et al.* (1998) are used as the assimilant. The model assumes that 8 % of the crustal rocks were melted. The

Tilo tephras are highly evolved and their melt most likely relatively cool and incapable of melting large volumes of crustal rock.

Figure 7.18 shows that assimilation of even high-Ba basement rocks cannot increase Ba concentrations sufficiently to explain the range of compositions exhibited by the Tilo tephras.

The youngest Tilo tephras (TT-1 to TT-5) show the most systematic increase in Ba concentrations through time. However, using the oldest of these tephras (TT-5) as the starting composition, assimilation of the basement still causes modelled Ba concentrations to decrease, rather than increase.

Tephras TT-7; 8; 9 and TT-10 show complex magmatic evolution, with fluctations in Ba concentrations between the eruption of each tephra. These step-like changes may be related to replenishment of the Corbetti magma chamber with less fractionated magma. Figure 7.18b and c shows that concentrations of incompatible elements decrease between the eruption of TT-13 and TT-14 and again TT-13 and TT-12. Fractional crystallisation typically increases these elements in the residual melt, and this pattern may therefore suggest magma recharge played a role in the evolution of these tephras. Sampling of proximal deposits from Corbetti, coupled with mineral analyses and isotope data are required in order to identify the magmatic processes involved in the petrogenesis of the Tilo tephras.

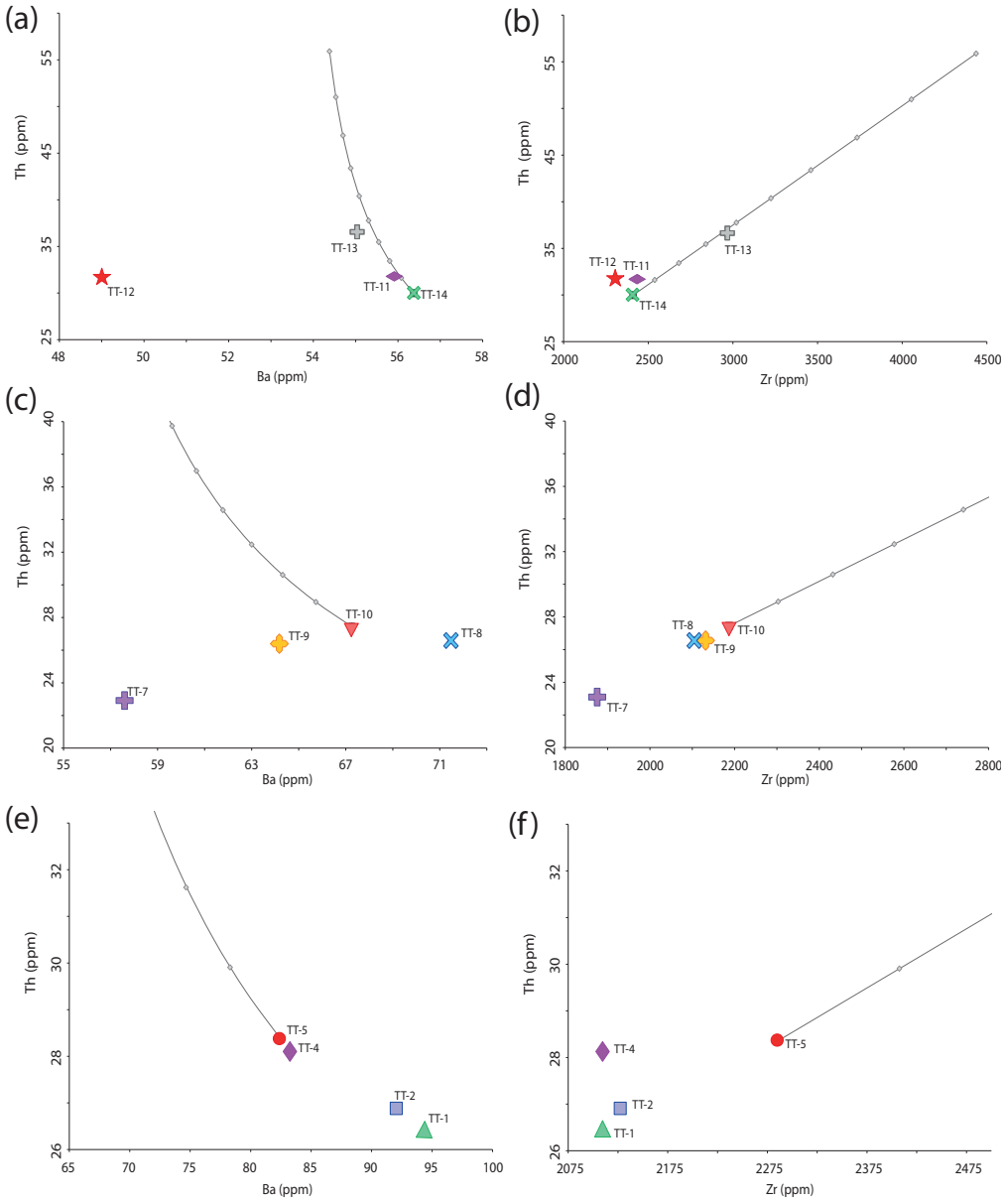

Figure 7.18: Bi-plots showing the average concentrations of selected trace elements in Tilo tephra glass shards. The Tilo tephras are grouped on the basis of their varying Ba concentrations through time (see Fig. 7.17). Lines indicate modelled assimilation fractional crystallisation using the older tephra from each 'episode' as the starting composition, with increments indicating 1 % assimilation of the crust. High-Ba granitoid basement rocks from Peccerillo *et al.* (1998) were used as the assimilant. A mineral assemblage of 20 % orthoclase, 20 % plagioclase, 5 % aenigmatite, 3 % C-pyroxene, 2 % olivine, 0.2 % apatite and 0.1 % ilmenite was used, based on CIPW norm calculations and petrography of Corbetti pyroclastic deposits noted by Di Paola (1971). Bulk partition coefficients for trace elements in peralkaline rhyolite melts are from Mahood and Stimac (1990); Pearce (1990) and Ewart and Griffin (1994).

7.4 Conclusions

Tephras recorded in lake archives from Awassa, Tilo and Chamo provide the first record of Holocene volcanism from the central Main Ethiopian Rift. Twenty three tephras occur in these archives, varying from proximal tephras attaining half a metre in thickness in the Awassa and Tilo archives, to distal < 1 cm tephras in the Chamo archive. A total of ~ 1200 major and trace element analyses on 19 of these tephras have been presented here. Two tephras preserved in the Chamo archive, CHT-2 ($9.4 - 6.3$ cal. ka BP) and CHT-1 ($2.8 - 1.2$ cal. ka BP), are tentatively correlated to two Tilo tephras, respectively TT-13 ($8.9 - 8.0$ cal. ka BP) and TT-2 ($2.0 - 1.2$ cal. ka BP), on the basis of their major and trace element compositions. Furthermore, two Awassa tephras, AWT-4 ($6.6 - 5.4$ cal. ka BP) and AWT-2 ($4.9 - 3.3$ cal ka BP) have similar compositions to TT-8; 9 and TT-10 ($6.3 - 2.3$ cal. ka BP), however it is not possible to ascertain which are correlatives.

The correlation of CHT-2 to TT-13 ties down the chronology for the lower half of the Chamo core, where the radiocarbon dates have greater uncertainties.

The distinct incompatible element ratios of the Awassa, Tilo and Chamo tephras suggest they may have been derived from potentially three volcanic centres. However, many of the Awassa, Tilo and Chamo tephra glass shards have similar incompatible element ratios and compositions, suggesting that one volcanic source may have erupted most of these tephras. Glass analyses of proximal obsidian and tephra samples from Corbetti caldera (located on the northern shores of lake Awassa, < 40 km east of lake Tilo and 170 km north of Lake Chamo) show that this is the most likely source for many Awassa, Tilo and Chamo tephras. It is possible that TT-2 and CHT-1 represent the Wendo Koshe

Pumice, produced by the 400 BC eruption from the Wendi Koshe volcano, inside the Corbetti caldera (Rapprich *et al.*, 2016).

Biggs *et al.* (2011) demonstrated that Corbetti has undergone numerous uplift and subsidence events of $10-15$ cm over the past decade, suggesting that this volcano remains very much active. The hazards posed by this volcano are significant; $570,000$ people live within 5 km of Corbetti and this volcano is listed at the highest risk level in the World Bank report on volcanic hazards in the MER (Siebert *et al.*, 2011; Aspinall *et al.*, 2011). Furthermore, Rapprich *et al.* (2016) suggests that future eruptions from Corbetti could cover nearby Awassa and Shashamene towns in ~ 0.5 m of pumice. The local inhabitants remain unaware of the potential hazards posed by Corbetti and no crisis management plan exists (Rapprich *et al.*, 2016).

This is the first study to date that provides a < 10 ka volcanic history for this volcano, and therefore has important implications for hazards assessments in this area. Twelve of the total 14 tephras deposited in the Tilo archive over the past < 10 ka are potentially derived from Corbetti, averaging an eruption frequency throughout the archive of ~ 1 eruption every 800 years. The latest, historic, eruption may have occurred from Corbetti at $1309-50$ cal. ka BP ($641-1900$ AD). This is younger than the most recent, 400 BC eruption from Wendo Koshe reported by Rapprich *et al.* (2016). The Tilo archive shows that 6 highly explosive eruptions occurred from Corbetti over the past 10 ka. Furthermore, two of these eruptions at $8.9-8.0$ cal. ka BP and as recently as $2.1-1.2$ cal. ka BP were sufficiently powerful to deposit tephra 170 km to the south, at Lake Chamo. It is likely that many of these eruptions from Corbetti during the past < 10 ka deposited additional regional tephra layers, which may be identified in future studies. Identification of these tephras in other locations throughout Ethiopia will

allow more detailed mapping of the dispersal of these tephras from Corbetti and enable the explosivity of these eruptions to be calculated.

The magmatic evolution of tephras derived from Corbetti during the past 10 ka is complex. Potentially due to the frequency of eruptions from Corbetti, fractional crystallisation may not have had time to significantly influence the composition of the Tilo tephras between each eruption. An apparent increase in Ba concentrations in the Tilo tephras through time is not related simply to assimilation of high-Ba basement rocks. Clearly, further field work and proximal sampling of the Corbetti eruptives is required to constrain the petrogenesis of these tephras. It is likely that mineral and isotope analyses will also shed light on the magmatic evolution of the Corbetti tephras.

Finally, this chapter has demonstrated that lake sediments from a range of geographic settings, preserving proximal and cryptotephras, can provide valuable records of past volcanism. The value of these archives for reconstructing past volcanism is dependant on the geographic setting of these lakes. Sediments from Lake Tilo, located in a small closed basin, has provided the most complete record of past volcanism from this area. The archives from the central Main Ethiopian Rift provide an insight into the frequency and magnitude of eruptions from centres that have no volcanic history and pose a high risk. Given the frequency and thickness of previous events recorded in the Tilo archive, it is likely that future eruptions from Corbetti will be highly explosive. Further field work at Corbetti is required to understand the risks posed by this centre, and this is the subject of current investigations by the RiftVolc project (http://www.geos.ed.ac.uk/riftvolc) and the Ethiopian and Czech geological surveys (Rapprich *et al.*, 2013; Žáček *et al.*, 2014; Rapprich *et al.*, 2016).

Chapter 8

Conclusions

8.1 Context

The Ethiopian Rift Valley represents a fascinating natural laboratory where active continental rifting can be observed and associated magmatic and tectonic processes studied. The rift basins have provided desirable conditions for the proliferation of life, and subsequent preservation of fossil remains. Beginning in the 1960s, the Ethiopian Rift Valley has been intensely explored, leading to the discovery of the most comprehensive record of human evolution spanning the past 6 million years (WoldeGabriel *et al.*, 2013). Quaternary tephra deposits, erupted from volcanoes throughout Ethiopia, and inter-bedded within fossiliferous sedimentary sequences at archaeological sites, have assumed paramount importance in providing crucial chronological control for hominin fossils (e.g. Brown, 1982; Pickford *et al.*, 1991; WoldeGabriel *et al.*, 1999; Katoh *et al.*, 2000; Clark *et al.*, 2003; Brown *et al.*, 2006; Haile-Selassie *et al.*, 2007; Campisano and Feibel, 2008; DiMaggio *et al.*, 2008; Saylor *et al.*, 2016).

Volcanic activity continued into the Holocene, and there are currently 65 volcanoes of suspected Holocene age throughout Ethiopia (Siebert *et al.*, 2011). Four volcanoes (Corbetti, Alutu, Bora and Haledebi) in the Main Ethiopian Rift are actively deforming and many more are at fumarolic stage (Biggs *et al.*, 2011; Siebert *et al.*, 2011). Despite this, only 14 volcanoes in the region have a recorded historic eruption and the recent volcanic history of Ethiopia remains largely unconstrained (Siebert *et al.*, 2011). The hazards posed by these volcanoes are underestimated, and the World Bank report on volcanic hazards lists the risk posed by the Main Ethiopian Rift volcanoes at the highest level of uncertainty (Aspinall *et al.*, 2011). Furthermore, towns, cities and industries in the Main Ethiopian Rift are rapidly developing, notably $\sim 570,000$ people live < 5 km from the actively deforming Corbetti volcano (Siebert *et al.*, 2011). The potential for regional volcanoes to erupt without warning is exemplified by the Nabro (2011) eruption from Eritrea. Volcanic ash dispersed by the eruption disrupted international air traffic, and no volcanic monitoring network existed at the time of the eruption, so there was no warning (Lenhardt and Oppenheimer, 2014; Goitom *et al.*, 2015). Projects including the Ethiopia-Afar Geoscientific Lithospheric Experiment (EAGLE), Afar Rift Consortium and RiftVolc have supplied valuable information on past and current volcanism and hazards (e.g. Ayele *et al.*, 2007*b*; Bastow *et al.*, 2011; Keir *et al.*, 2011; Ferguson *et al.*, 2013). However, to date, studies focussing on the Holocene tephra record in Ethiopia remain scarce.

The early stage of regional geological studies, may in part, be related to the logistical challenges of undertaking field work in remote and inhospitable regions, notably the Afar Rift (Wiart and Oppenheimer, 2004). Proximal deposits close to volcanic centres may be buried, eroded or have no clear stratigraphic context and may therefore not provide a comprehensive record of past volcanism

(e.g. Rawson *et al.*, 2015). In contrast, lakes throughout the Ethiopian Rift Valley and surrounding rift shoulders preserve tephras in aggrading systems (White and Riggs, 2001). Thus, sediment archives from these lakes provide more complete records of past volcanism, and provide information on the timing of past eruptions and the inter-relationships between different centres (e.g. Feakins *et al.*, 2007). Lake sediments have good potential for radiocarbon dating and these dates can be used in conjunction with stratigraphic information in Bayesian age models, e.g. OxCal (Bronk Ramsey, 2009*a*), to further constrain the ages of eruptive events (e.g. Rawson *et al.*, 2015).

This study aimed to construct an initial late Pleistocene to Holocene tephra frame work for Ethiopia, using sediment archives collected from lakes throughout the region and a selection of samples from outcrops proximal to volcanoes. This represents the first systematic study of visible and crypto-tephras occurring in Ethiopian lake sediments. This work set out to assess if this lake sediment tephrostratigraphic approach can successfully be applied in this region and whether lake archives provide comprehensive records of volcanism. Specific research questions were asked, including: can tephras in Ethiopian lake archives be correlated? What are the sources for these tephras? What do these deposits tell us about the timing of past eruptions? Answering these questions would give an insight into past eruptions, and therefore provide important information on volcanic hazards associated with future eruptions. Finally, this study set out to investigate the magma genesis of recent volcanism in Ethiopia, and how tectonic setting may influence erupted magma composition, providing valuable information on the evolution of some of the least studied peralkaline volcanoes on Earth (Hutchison *et al.*, 2015).

8.2 A late Pleistocene-Holocene tephrostratigraphy for Ethiopia

This study has successfully presented the first late Pleistocene to Holocene tephrostratigraphy for Ethiopia, constructed using sediment archives from seven lakes: Ashenge and Hayk (Ethiopian Highlands), Dendi and Hora (Yerer-Tullu Welle Volcano Tectonic Lineament) and Awassa, Tilo and Chamo (central Main Ethiopian Rift). This tephra record represents the most detailed account of Holocene volcanism in selected areas of the Ethiopian Rift so far available. This is the first major and trace element single grain glass dataset of Holocene Ethiopian tephras. The dataset will enable the future identification of these tephras in other locations, and provides information on the magmatic evolution of regional peralkaline volcanoes. Bayesian age models have provided an initial indication of eruption recurrence rates in this area, which have important implications for hazard assessments. The implications of this tephra framework, in relation to specific research questions, outlined in Chapter 1, are discussed below and are summarised in Fig. 8.1.

8.2.1 Ethiopian lake archives provide a valuable record of past volcanism

Lake sediment archives have proved a powerful resource for constructing a record of Ethiopian volcanism. This work has investigated lake archives from a range of geographic settings, containing complementary records of both proximal tephras and crypto-tephras. This study has shown that this tephrostratigraphic approach has numerous advantages over studying proximal tephras exposed at volcanoes. Notably, archives from lakes Ashenge, Hayk, Dendi, Hora and Tilo preserve

inter-fingering tephra deposits from multiple volcanoes. This has enabled the timing of past volcanism from a number of centres to be assessed simultaneously. These interpretations would be significantly more challenging based on their proximal counterparts. Furthermore, this regional tephrostratigraphic approach has shown the capacity for developing a regional understanding of the dispersal and explosivity of past eruptions.

This study also demonstrates the considerable potential for future application of this approach elsewhere in Ethiopia. The Hominin Sites and Paleolakes Drilling Project (HSPDP, https://hspdp.asu.edu/) has collected some $2,000$ m of lake sediments, extending back 4 Ma, from locations throughout Ethiopia and Kenya to investigate the palaeoclimatic context of hominin evolution. It is likely that some of the tephras studied here will be identified in late Pleistocene to Holocene sections of these sediments, and this will enable the dispersal of these tephras to be further refined. Lake sediments show potential for refining the tephrostratigraphy and dispersal of Quaternary tephras which have already proved so invaluable for dating east African archaeological sites.

The completeness of lake sediment tephra records depends upon the dispersal of tephras and their subsequent deposition and dispersal at the lake site. This is demonstrated by lakes Ashenge and Hayk, from the Ethiopian Highlands. These lakes are located < 140 km apart, along the rift escarpment and close to volcanoes in the Afar Rift. However, archives from these lakes record different eruptive events. It is possible that local eruptions, potentially from the nearby Afar Rift, dispersed these tephras over only small areas. Futhermore, it is probable that the dispersal of these tephras is largely dependant on wind direction. The dominantly easterly winds provide favourable conditions for tephra dispersal towards lakes Ashenge and Hayk, in the west. However, to record an eruptive event in both

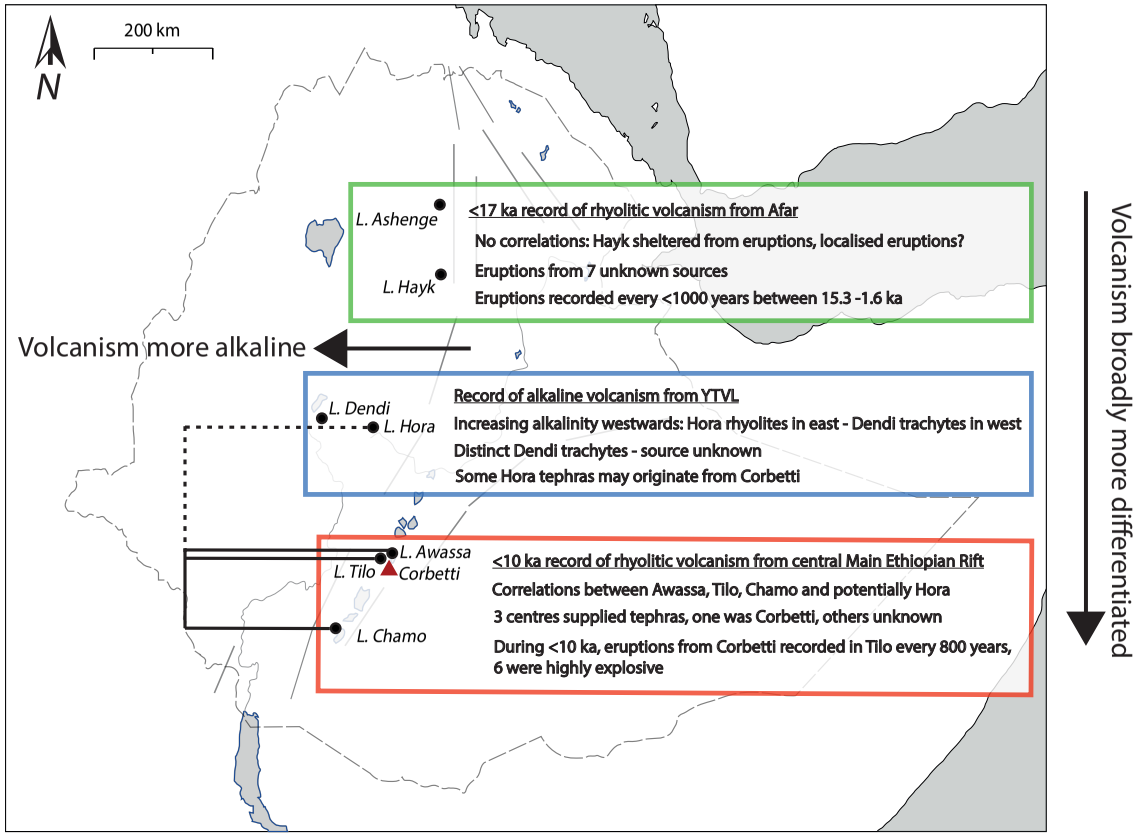

Figure 8.1: Schematic summarising the key findings of this study. Tephra correlations have been established between lakes Awassa, Tilo and Chamo and are most likely derived from Corbetti. These tephras may also be recorded in the Hora archive, however, the ages and depths of the Hora tephras need to be constrained.

archives, a change in wind direction mid-eruption would be required to disperse tephra towards Hayk, located to the south of Ashenge. Ashenge and Hayk are located on the edge of the rift shoulders; however, Hayk is sheltered from volcanoes in the Afar Rift by a series of horsts. Lake Ashenge is, in contrast, more exposed and its surrounding topography may essentially 'funnel' localised volcanic plumes towards the lake basin. These differences may explain why A. Asrat (Addis Ababa University) noted that tephra from the Nabro 2011 eruption was deposited in the vicinity of Lake Ashenge, but not at Lake Hayk (A. Asrat 2016, pers. comm., 23rd Feb 2016). Thus, it is possible that location and basin morphology of these lakes may have limited the potential for an eruption to be simultaneously recorded in both archives. Depsite these challenges, archives from Ashenge and Hayk provide the most comprehensive record of the timing and composition of Holocene eruptions from volcanoes in the Afar so far available.

Archives from the central Main Ethiopian Rift demonstrate that the setting and the lake catchment morphology influence the type and frequency of tephras recorded in sediments. The Tilo and Awassa archives were collected from lakes <40 km apart, and contain proximal tephras of ~ 50 cm thickness. The Tilo archive proved the most comprehensive archive from this region. However tephras in the Awassa archive cannot be directly correlated directly to Tilo tephras. The Awassa tephras contain mixed glass populations, possibly associated with reworking, which explains why these tephras cannot be correlated to individual eruptive events in the Tilo archive. The <1 km diameter, steep sided, Tilo crater lake has no direct in or outflow. However, Lake Awassa has a contrasting morphology, possessing an area of ~ 92 km^2 and draining the 1300 km^2 Corbetti caldera. Tephras deposited within the Awassa catchment may therefore be mixed with older tephras prior to redeposition on the Awassa lake floor. Thus, there

is more potential for the Awassa tephras to be mixed with pre-existing tephra deposits in the Corbetti caldera, prior to their deposition at the lake bed. The Tilo tephras most likely represent primary air-fall deposits, and their thicknesses are potentially a real reflection on the explosivity of past eruptions from Corbetti. Rapprich *et al.* (2016) demonstrate that the volcanic history of Corbetti is difficult to constrain based on proximal deposits. This work shows the significant value of lake sediment archives like Tilo, which provides an accessible record of 12 eruptions from Corbetti during the past 10 ka.

The lake sediment tephrostratigraphic approach can be successfully applied in Ethiopia. This study paves the way for future studies to refine this tephra record spatially and temporally. Nonetheless, the interpretation of past volcanism using tephra records in lake sediments must be considered within the wider context, including variations in lake basin morphology and wind direction. These factors may influence the potential for tephra correlation and have implications for estimations of past eruption frequency and explosivity. This work shows that lakes with smaller drainage basins, located in an exposed setting and down-wind of volcanoes, are more likely to record comprehensive tephra records.

8.2.2 The composition of < 17 ka tephras varies spatially

This study presents a database of the major and trace element glass compositions ($\sim$ 2100 analyses) of 47 visible and crypto-tephras recorded in Ethiopian lake archives. This database will aid the future identification of the tephras at proximal and distal localities. The geochemistry of these tephras also gives an important insight into the magmatic evolution of peralkaline silcic volcanism.

Tephras deposited throughout the Ethiopian Rift are dominantly peralkaline rhyolites (comendites and pantellerites) with minor peraluminous and metalu-

minous rhyolites. Previous studies have shown that silicic rift volcanism is most likely derived from fractional crystallisation of basalts at shallow depth (Walter *et al.*, 1987; Peccerillo *et al.*, 2007; Ukstins Peate *et al.*, 2008; Rooney *et al.*, 2012). The geochemistry of late Pleistocene-Holocene tephras indicates that these have also evolved through fractional crystallisation of an assemblage dominated by K-feldspar and Fe-Ti oxides.

The composition of late Pleistocene-Holocene tephras recorded in Ethiopian archives varies spatially. Tephras recorded in Tilo, Awassa and Chamo lake sediments contain broadly higher concentrations of the incompatible elements, Y, Zr and La than tephras in archives from lakes Ashenge and Hayk. Tephras recorded in central MER lakes are the most highly differentiated rhyolitic tephras investigated in this study, and have reached minimum compositions. It is likely that these variations may be related to the differing tectonic settings of the source volcanoes supplying tephras to different regions of Ethiopia. The closest volcanoes to lakes Hayk and Ashenge are in the Afar Rift ($<$ 70 km). Volcanoes in the central Main Ethiopian Rift are located $<$ 40 km from the Tilo and Awassa lakes. On the basis that these tephras are derived from local volcanoes, there is significantly thinner crust ($\sim$ 20 km) in the Afar than the central Main Ethiopian Rift ($\sim$ 30 km). However, despite these differences, there is no apparent difference in the amount of crustal contamination involved in the petrogenesis of tephras recorded in lake archives throughout Ethiopia. In fact, the role of crustal contamination in the evolution of many of these tephras appears to be negligible. This supports work by Peccerillo *et al.* (2007), who suggest that fractional crystallisation is instead the main cause of magmatic differentiation in this region. However, this work suggests that processes other than fractional crystallisation, potentially recharge, may have influenced the

evolution of Ethiopian 17 ka tephras. Further sampling from regional volcanoes, coupled with Sr isotope analysis of eruptives, is now required to constrain the role of crustal assimilation in the evolution of these tephras more confidently.

Peralkaline silicic volcanism in the axial rift is therefore generated by shallow depth fractional crystallisation of mafic magmas. However, at the rift shoulders, the thicker crust causes magmas to pond at greater depths and evolve through high pressure fractional crystallisation to produce phonolites and trachytes. The off-axis Yerer-Tullu Wellel Volcano Tectonic Lineament (YTVL) is made up of alkaline central volcanoes associated with high pressure evolution. The composition of eruptives along this lineament varies from phonolitic-trachytic on the Sudan border, to peralkaline rhyolites $\sim$ 40 km from Addis Ababa. The Dendi archive was collected from a crater lake along the western YTVL. The Dendi tephras are dominantly phonolitic-trachytic tephras and most likely derived from a nearby alkaline volcano. Contrastingly, the Hora archive was collected from eastern limits of the YTVL, and contains peralkaline rhyolites which may originate from the axial rift or the centres in the eastern YTVL.

This work shows that the composition of late Pleistocene - Holocene tephras varies spatially. The most marked differences are seen between the peralkaline rhyolitic tephras erupted from the axial rift, versus the phonolitic-trachytic tephras erupted from the rift shoulders.

8.2.3 Widespread tephras can be correlated between archives from the central Main Ethiopian Rift

The potential for correlation between tephra layers recorded in lakes along the Ethiopian Rift is directly influenced by the eruption explosivity, tephra dispersal and subsequent depositional processes. This study has successfully established

tephra correlations between lakes Awassa, Tilo and Chamo, in the central Main Ethiopian Rift. It is likely that these <10 ka eruptions were highly explosive and thus dispersed tephras throughout the central Main Ethiopian Rift. Two tephras in the Awassa archive, AWT-4 ($6.6-5.4$ cal. ka BP) and AWT-2 ($4.9-3.3$ cal. ka BP) may correlate to tephras from the Lake Tilo (<40 km from Lake Awassa). However, the Awassa tephras may be reworked and it is not possible to narrow down whether Tilo tephras TT-8; TT-9 or TT-10 ($6.3-2.3$ cal. ka BP) are correlatives. Two tephras were dispersed ~ 170 km to the south of Tilo and recorded in the Chamo archive. Chamo tephra CHT-2 ($9.4-6.3$ cal. ka BP) and CHT-4 ($2.8-1.2$ cal. ka BP) can be tentatively correlated to Tilo tephras TT-13 ($8.9-8.0$ cal. ka BP) and TT-2 ($2.0-1.2$ cal. ka BP), respectively. It is apparent that conditions, including eruption explosivity and wind direction, were favourable for the dispersal of two of these tephras to distal locations, at Chamo. Further sampling of other depths in the Chamo sediments will most likely yield further cryptotephra deposits. Depending on variations in tephra taphonomy and preservation, there is potential for finding these tephras in Holocene sections of the Chew Bahir lake core (~ 150 km SW of Chamo), drilled as part of the Hominin Sites and Paleolakes Drilling Project. These tephras were not dispersed to the Ethiopian Highlands, in the north. Tilo, Awassa and Chamo tephras are geochemically similar to tephras recorded in the Hora archive, to the north. However, the nature of any correlations cannot be futher investigated due to the lack of stratigraphic context and chronological control for the Hora tephras.

Contrastingly, archives from the Ashenge, Hayk (Ethiopian Highlands) and Dendi (Yerer-Tullu Wellel Volcano Tectonic Lineament) lakes cannot be correlated between. Lake Ashenge and Hayk are located ~ 140 km from one another, however, they record different eruptive events. It is probable that this is

related to the contrasting location and basin morphology of these lakes, coupled with the potentially localised nature of the eruptive events. Lake Hayk is sheltered by a series of horsts from volcanoes in the Afar, and this will influence the type and frequency of tephras recorded in these archives. Investigation of further lake archives in the Ethiopian Highlands may identify these tephras in the future. Nonetheless, the Ashenge and Hayk archives provide an important indication of past eruption frequency, most likely from the nearby Afar Rift.

The Dendi tephras have a distinctly phonolitic-trachytic composition and thus cannot be correlated to other archives. These thick, < 2 m, tephras show evidence of reworking, and were most likely erupted from an alkaline centre in the western Yerer-Tullu Wellel Volcano Tectonic Lineament. It is probable that these eruptions were insufficiently explosive to disperse the Dendi tephras over greater areas, explaining why these tephras cannot be correlated. The Dendi archive contains one peralkaline rhyolitic tephra, which is most likely derived from a centre nearer the axial rift, but this cannot be correlated to other archives.

8.2.4 Frequent < 17 ka explosive volcanic eruptions from centres in the Afar and CMER

The initial late Pleistocene-Holocene tephra record presented here provides an insight into the timing of past eruptions and dispersal of tephras in Ethiopia.

The major and trace element composition of widely dispersed tephras from the central Main Ethiopian Rift indicates that they are derived from three different magmatic sources. However, it is likely that a single volcanic source supplied 16 of the 19 tephras studied recorded in the Tilo, Awassa and Chamo archives. Obsidian and tephra samples from the Corbetti caldera (northern shores of Lake Awassa) have been analysed as part of this study. The composition of the many of

tephras recorded in the Tilo, Awassa and Chamo archives is distinguishable from the Corbetti obsidians and tephras. It is likely that Corbetti is the source of these tephras, and the Tilo archive provides a comprehensive record of past volcanism from this centre. Eruptions from Corbetti are recorded in the Tilo archive every ~ 800 years during the past 10 ka, with the most recent explosive eruption recorded at $641-1900$ AD. The thickness and dispersal of these tephras gives an indication that at least 6 eruptions from Corbetti over the past 10 ka were highly explosive. There is good potential for future identification of these widespread tephras in other archives, and this will enable isopachs for these eruptions to be constructed. This is the first systematic study of recent eruptions and deposits from Corbetti, and has important implications for hazard monitoring. Previous work by Biggs *et al.* (2011) and Rapprich *et al.* (2016) shows that Corbetti has experienced Holocene eruptions, and remains active today. However, the volcanic history of Corbetti has remained, until now, poorly constrained and the local inhabitants of Awassa and Shashamene are unaware of the threat Corbetti poses. The record of Corbetti eruptions preserved in archives from the central Main Ethiopian Rift demonstrates that future eruptions may be explosive and cause significant disruption in this area. This tephra record shows that Corbetti poses a significant risk to the $570,000$ local inhabitants, and these hazards must be prepared for.

In the sparsely populated and remote Afar Rift, the risks posed by future eruptions are less severe. Nonetheless, the 2011 eruption of Nabro (Eritrea) caused widespread disruption to air-traffic over the region. Archives from lakes Ashenge and Hayk (Ethiopian highlands) contain 21 visible and crypto-tephras. The tephra record shows that 7 centres, probably located in the nearby Afar Rift, erupted during the past 17 ka. The Ashenge and Hayk archives record

different eruptive-events, however, it is possible that some of the tephras in these archives are derived from a shared source. These tephras provide valuable information about the timing of past eruptions, with one explosive eruption recorded every < 1000 years between $15.3 - 1.6$ cal. ka BP. An historic tephra, AST-1 ($1404 - 1629$ AD), is documented in the Ashenge archive. The only documented regional eruption of a similar age is from Dubbi (Eritrea, 270 km NE of Ashenge) at 1400 AD. The 1861 eruption from this volcano is reputed to be Africa's largest historic eruption. However, comparison of the historic Ashenge tephra with the glass composition of proximal 1861 Dubbi tephra is inconclusive, and further field work, sampling and tephra analysis is required to ascertain if this is the source. Comparison of other Ashenge and Hayk tephras with published glass compositions from the nearby Dabbahu does not definitively indicate this is the source of these eruptions. The seven sources of the Ashenge and Hayk tephras thus remain unknown. A lack of correlations between these lake archives may indicate that these eruptions were not highly explosive. Thus, future eruptions from these centres may not cause significant disruption to local inhabitants, or widespread disruption to air-traffic. Nonetheless, the dispersal of these eruptions may not only be a function of their explosivity, but the topography surrounding each lake. This work demonstrates that numerous centres in the Afar have erupted frequently and their associated risks should not be underestimated.

8.3 Research limitations and further work

Sediment archives from Ethiopian lakes can be used to construct a regional tephrostratigraphy for the late Pleistocene to Holocene. Furthermore, the tephrostratigraphy presented here has provided valuable information on the timing and

style of past eruptions, and magmatic processes. The lake sediment tephrostratigraphic approach used here shows great potential for application to other areas in Ethiopia, in order to build upon this tephra framework.

A greater network of archives from lakes throughout Ethiopia must now be studied. Core sites throughout Ethiopia were selected to ensure a spatially comprehensive record of past volcanism was captured. Expanding this network will increase the likelihood for eruptive events, including from localised eruptions, to be represented in the tephra record. Resolving this tephrostratigraphy at a higher spatial resolution will in turn contribute more information about the timing and dispersal of past eruptions. This will enable isopachs to be constructed and past eruption explosivity to be calculated more confidently. These factors will have important implications for assessing the hazards associated with future eruptions. This works shows that site specific processes may result in the uneven distribution and deposition of tephras. Thus, not all eruptive events may be captured in a single sediment core from a lake. Future tephrostratigraphic investigations of Ethiopian lake archives should therefore use multiple sediment cores from a single lake (Davies, 2015).

This study has demonstrated the essential contribution of cryptotephra studies in developing our understanding of past volcanism in Ethiopia. Further regional cryptotephra studies will increase the potential for tephra correlations and expand the spatial area over which they can be established. More detailed investigation of the Ashenge and Hayk sediments, and sampling of other depths in the Chamo sediments may yield further cryptotephras.

The lake sediment tephrostratigraphic approach used in this study is limited by the lack of published geochemical data for regional source volcanoes. This has hindered the potential for correlation of many tephras to source volcanoes.

This study investigated regional magmatic processes, finding that tephras from southern Ethiopian lakes are typically more evolved. The regional approach adopted in this study has provided a wider context for the petrogenesis of recent volcanism. However, interpretations of magma genesis made using tephra records have significant drawbacks where the source volcanoes cannot be identified. Magma evolution needs to be considered within the context of the tectonic setting of the source volcano. This work assumes that Holocene tephras studied here are locally derived, however, they could be from other locations in the Ethiopian Rift. They may therefore not represent local volcanism and further field work is required. Detailed sampling at these centres, coupled with major and trace element and isotope analysis is the most effective and reliable method for investigating magmatic processes.

Ideally, this work would be improved through using more lake sites, coupled with detailed field work at volcanoes throughout the region. Furthermore, airfall or co-ignimbrite ash deposits at regional volcanic centres need to be thoroughly sampled and geochemically fingerprinted. Detailed field work at source volcanoes has obvious time constraints and, moreover, outcrop samples may be poorly exposed and inaccessible. However, the thickness and dispersal of the tephras presented here gives an initial indication of where potential source regions may be, and where field work could focus. This < 17 ka tephrostratigraphy shows that further field work at Corbetti, and centres in the Afar Rift, is required.

Finally, this study highlights the need for further work to assess hazards associated with future eruptions. Ethiopia is developing rapidly and infrastructure is advancing onto volcanic areas, without consideration of associated hazards. Field work at regional volcanoes and monitoring of these volcanoes will mitigate

these hazards, and this is part of ongoing work by RiftVolc and the Ethiopian and Czech Geological Surveys (e.g. Ayele *et al.*, 2015; Goitom *et al.*, 2015; Hutchison *et al.*, 2015; Keir *et al.*, 2015; Rapprich *et al.*, 2016).

References

Abbott, P. M., Davies, S. M., Austin, W. E. N., Pearce, N. J. G., Hibbert, F. D. 2011. Identification of cryptotephra horizons in a North East Atlantic marine record spanning marine isotope stages 4 and 5a (∼60,000-82,000 a b2k). *Quaternary International*, **246** (1-2), 177–189.

Abbott, P. M., Davies, S. M., Steffensen, J. P., Pearce, N. J. G., Bigler, M., Johnsen, S. J., Seierstad, I. K., Svensson, A., Wastegård, S. 2012. A detailed framework of Marine Isotope Stages 4 and 5 volcanic events recorded in two Greenland ice-cores. *Quaternary Science Reviews*, **36**, 59–77.

Abebe, b., Acocella, V., Korme, T., Ayalew, D. 2007. Quaternary faulting and volcanism in the Main Ethiopian Rift. *Journal of African Earth Sciences*, **48** (2-3), 115–124.

Abebe, T., Mazzarini, F., Innocenti, F., Manetti, P. 1995. The Yerer-Tullu Wellel extensional structure (central Ethiopia): evidences from remote sensing, petrologic and geochronologic data. *In Quantitative Remote Sensing for Science and Application*, volume 1. Firenze, Italy, volume 1, pp. 374 – 376.

Abebe, T., Mazzarini, F., Innocenti, F., Manetti, P. 1998. The Yerer-Tullu Wellel volcanotectonic lineament: a transtensional structure in central Ethiopia and

the associated magmatic activity. *Journal of African Earth Sciences*, **26** (1), 135–150.

Acocella, V., Korme, T., Salvini, F., Funiciello, R. 2002. Elliptic calderas in the Ethiopian Rift: control of pre-existing stuctures. *Journal of Volcanology and Geothermal Research*, **119** (1-4), 189–203.

Adhana, T. A. 2014. The occurrence of a complete continental rift type of volcanic rocks suite along the Yerer-Tullu Wellel Volcano Tectonic Lineament, Central Ethiopia. *Journal of African Earth Sciences*, **99** (2), 374–385.

Alloway, B. V., Larsen, G., Lowe, D. J., Shane, P. A. R., Westgate., J. A. 2007. *Encyclopedia of Quaternary Science*, Elsevier, volume 4, chapter Tephrochronology. pp. 2869–2898.

Ambrose, S. H. 1998. Late Pleistocene human population bottlenecks, volcanic winter, and differentiation of modern humans. *Journal of Human Evolution*, **34** (6), 623–651.

Amelung, F., Oppenheimer, C., Segall, P., Zebker, H. 2000. Ground deformation near Gada 'Ale Volcano, Afar, observed by Radar Interferometry. *Geophysical Research Letters*, **27** (19), 3093–3096.

Anderson, R., Nuhfer, E., Dean, W. 1985. Sinking of volcanic ash in uncompacted sediment in Williams Lake, Washington. *Science*, **225** (4661), 505–508.

Aronson, J. L., Schmitt, T. J., Walter, R. C., Taieb, M., Tiercelin, J. J., Johanson, D. C., Naeser, C. W., Nairn, A. E. M. 1977. New geochronologic and palaeomagnetic data for the hominid-bearing Hadar Formation of Ethiopia. *Nature*, **267** (5609), 323 – 327.

Asfaw, B., Gilbert, W. H., Beyene, Y., Hart, W. K., Renne, P. R., WoldeGabriel, G., Vrba, E. S., White, T. D. 2002. Remains of *Homo erectus* from Bouri, Middle Awash, Ethiopia. *Nature*, **416**, 317–320.

Aspinall, W., Auker, M., Hincks, S., T. Mahony, Nadim, F., Pooley, J., Sparks, R. S. J., Syre, E. 2011. Volcano hazard and exposure in GFDRR priority countries and risk mitigation measures. *In Volcano Risk Study 0100806001-R: Washington, D.C., Global Facility for Disaster Reduction and Recovery*.

Awulachew, S. B. 2006. Characteristics Investigation of physical and bathymetric characteristics of Lakes Abaya and Chamo, Ethiopia, and their management implications. *Lakes & Reservoirs: Research and Management*, **11** (3), 133–140.

Ayele, A., Ebinger, C. J., Van Alstyne, C., Keir, D., Nixon, C. W., Belachew, M., Hammond, J. O. S. 2015. Seismicity of the central Afar rift and implications for Tendaho dam hazards. *In* Wright, T. J., Ayele, A., Ferguson, D. J., Kidane, T., Vye-Brown, C. (eds.) *Magmatic Rifting and Active Volcanism*, volume 420, Geological Society, London, Special Publications.

Ayele, A., Jacques, E., Kassim, M., Kidane, T., Omar, A., Tait, S., Nercessian, A., de Chabalier, J.-B., King, G. 2007*a*. The volcano-seismic crisis in Afar, Ethiopia, starting September 2005. *Earth and Planetary Science Letters*, **255** (1-2), 177–187.

Ayele, A., Stuart, G., Bastow, I. D., Keir, D. 2007*b*. The August 2002 earthquake sequence in north Afar: insights into the neotectonics of the Danakil microplate. *Journal of African Earth Sciences*, **48** (2-3), 70–79.

Ayres, M., Harris, N. 1997. REE fractionation and Nd-isotope disequilibrium during crustal anatexis: constraints from Himalayan leucogranites. *Chemical Geology*, **139** (1-4), 249–269.

Baker, B. H., Mohr, P. A., Williams, L. A. J. 1972. Geology of the Eastern Rift System of Africa. *The Geological Society of America Special Papers*, **136**, 1–67.

Balascio, N. L., Francus, P., Bradley, R. S., Schupack, B. B., Miller, G. H., Kvisvik, B. C., Bakke, J., Thordarson, T. 2015. *Micro-XRF Studies of Sediment Cores*, Springer Netherlands, volume 17, chapter Investigating the Use of Scanning X-Ray Fluorescence to Locate Cryptotephra in Minerogenic Lacustrine Sediment: Experimental Results. pp. 305–324.

Barberi, F., Bonatti, E., Marinelli, G., Varet, J. 1974. Transverse tectonics during the split of a continent: Data from Afar rift. *Tectonophysics*, **23** (1-2), 17–29.

Barberi, F., Borsi, S., Ferrara, G., Marinelli, G., Varet, J. 1970. Relations between tectonics and magmatology in the northern Danakil Depression (Ethiopia). *Philosophical Transactions of the Royal Society of London. Series A, Mathematical and Physical Sciences*, **267** (1181), 293–311.

Barberi, F., Ferrara, C., Santacroce, R., Treuil, M., Varet, J. 1975. A Transitional Basalt-Pantellerite Sequence of Fractional Crystallisation, the Boina Centre (Afar Rift, Ethiopia). *Journal of Petrology*, **16** (1), 22–56.

Barberi, F., Varet, J. 1977. Volcanism of Afar: Small-scale plate tectonics implications. *Geological Society of America Bulletin*, **88** (9), 1251–1266.

Bastow, I. D., Keir, D., Daly, E. 2011. The Ethiopia Afar Geoscientific Lithospheric Experiment (EAGLE): Probing the transition from continental

rifting to incipient seafloor spreading. *In* Beccaluva, L., Bianchini, G., Wilson, M. (eds.) *Volcanism and Evolution of the African Lithosphere*, Geological Society of America Special Paper 478.

Beard, J. S., Lofgren, G. E., Sinha, K., Tollom, R. P. 1994. Partial melting of apatite-bearing charnockite, granulite, and diorite: melt compositions, restite mineralogy, and petrologic implications. *Journal of Geophysical Research*, **99** (B11), 21,591—21,603.

Berhe, S. M. 1987. Geology, geochronology and geodynamic implications of the Cenozoic magmatic province in W and SE Ethiopia. *Journal of Geological Society*, **144** (2), 213–226.

Betton, P. J., Civetta, L. 1984. Strontium and neodymium isotopic evidence for the heterogeneous nature and development of the mantle beneath Afar (Ethiopia). *Earth and Planetary Science Letters*, **71** (1), 59–70.

Biggs, J., Anthony, E. Y., Ebinger, C. J. 2009. Multiple inflation and deflation events at Kenyan volcanoes, East African Rift. *Geological Society of America Bulletin*, **37** (11), 979–982.

Biggs, J., Bastow, I. D., Keir, D., Lewi, E. 2011. Pulses of deformation reveal frequently recurring shallow magmatic activity beneath the Main Ethiopian Rift. *Geochemistry, Geophysics, Geosystems*, **12** (9), 1–11.

Blaauw, M., Christen, J. A. 2011. Flexible paleoclimate age-depth models using an autoregressive gamma process. *Bayesian Analysis*, **6** (3), 457–474.

Blockley, S. P. E., Pyne-O'Donnell, S. D. F., Lowe, J. J., Matthews, I. P., Stone, A., Pollard, A. M., Turney, C. S. M., Molyneux, E. G. 2005. A new and less destructive laboratory procedure for the physical separation of distal

glass tephra shards from sediments. *Quaternary Science Reviews*, **24** (16-17), 1952–1960.

Blundy, J., Cashman, K. 2001. Ascent-driven crystallisation of dacite magmas at Mount St Helens, 1980 - 1986. *Contributions to Mineralogy and Petrology*, **140** (6), 631–650.

Boccaletti, M., Mazzuoli, R., Bonini, M., Trua, T., Abebe, B. 1999. Plio-Quaternary volcanotectonic activity in the northern sector of the Main Ethiopian Rift: relationships with oblique rifting. *Journal of African Earth Sciences*, **29** (4), 679–698.

Bonini, M., Corti, G., Innocenti, F., Manetti, P., Mazzarini, F., Abebe, T., Pecskay, Z. 2005. Evolution of the Main Ethiopian Rift in the frame of Afar and Kenya rifts propagation. *Tectonics*, **24** (1), 1–21.

Bosworth, W., Huchon, P., McClay, K. 2005. The Red Sea and Gulf of Aden Basins. *Journal of African Earth Sciences*, **43** (1-3), 334–378.

Bowen, B. E., Vondra, C. F. 1973. Stratigraphical relationships of the Plio-Pleistocene deposits, East Rudolf, Kenya. *Nature*, **242** (5397), 391–393.

Boygle, J. 1999. Variability of tephra in lake and catchment sediments, Svínavatn, Iceland. *Global and Planetary Change*, **21** (1-3), 129–149.

Bramham-Law, C. W. F., Theurerkauf, M., Lane, C. S., Mangerud, J. 2013. New findings regarding the Saksunarvatn Ash in Germany. *Journal of Quaternary Science*, **28** (3), 248–257.

Brandt, S. A., Fisher, E. C., Hildebrand, E. A., Vogelsang, R., Ambrose, S. H., Lesur, J., Wang, H. 2012. Early MIS 3 occupation of Mochena Borago

Rockshelter, Southwest Ethiopian Highland: Implications for Late Pleistocene archaeology, palaeoenvironments and modern human dispersals. *Quaternary International*, **274**, 38–54.

Brendryen, J., Haflidason, H., Sejrup, H. P. 2010. Norwegian Sea tephrostratigraphy of marine isotope stages 4 and 5: Prospects and problems for tephrochronology in the North Atlantic region. *Quaternary Science Reviews*, **29**, 847–864.

Bronk Ramsey, C. 2009*a*. Bayesian analysis of radiocarbon dates. *Radiocarbon*, **51** (1), 337–360.

Bronk Ramsey, C. 2009*b*. Dealing with outliers and offsets in radiocarbon dating. *Radiocarbon*, **51** (3), 1023–1045.

Brown, F. H. 1969. Observations on the stratigraphy and radiometric age of the "Omo Beds". *Quaternaria*, **11**, 7–14.

Brown, F. H. 1982. Tulu Bor Tuff at Koobi Fora correlated to the Sidi Hakoma Tuff at Hadar. *Nature*, **300**, 631–635.

Brown, F. H., Cerling, T. E. 1982. Stratigraphic significance of the Tulu Bor tuff of the Koobi Fora formation. *Nature*, **299** (5880), 212–215.

Brown, F. H., de Heinzelin, J., Howell, F. C. 1970. Pliocene/Pleistocene formations in the lower Omo basin, southern Ethiopia. *Quaternaria*, **13**, 247–268.

Brown, F. H., Feibel, C. S. 1986. Revision of lithostratigraphic nomenclature in the Koobi Fora region, Kenya. *Journal of the Geological Society*, **143**, 297–310.

Brown, F. H., Haileab, B., McDougall, I. 2006. Sequence of tuffs between the KBS Tuff and the Chari Tuff in the Turkana Basin, Kenya and Ethiopia. *Journal of the Geological Society*, **163**, 185–204.

Brown, F. H., Sarna-Wojcicki, A. M., Meyer, C. E., Haileab, B. 1992. Correlation of Pliocene and Pleistocene tephra layers between the Turkana Basin of East Africa and the Gulf of Aden. *Quaternary International*, **13-14** (6), 453–468.

Brown, F. H., Shuey, R. T., Croes, M. K. 1978. Magnetostratigraphy of the Shungura and Usno Formations, southwestern Ethiopia: new data and comprehensive reanalysis. *Geophysical Journal International*, **54** (3), 519–538.

Bryant, C., Arculus, R., Eggins, S. 1999. Laser ablation-inductively coupled plasma-mass spectrometry and tephras: A new approach to understanding arc-magma genesis. *Geology*, **27** (12), 1119–1122.

Campisano, C., Feibel, C. S. 2008. *The Geology of Early Humans in the Horn of Africa: Geological Society of America Special Paper 446*, The Geological Society of America, chapter Tephrostratigraphy of the Hadar and Busidima Formations at Hadar, Afar Depression, Ethiopia.

Carey, S., Bursik, M. 2015. Chapter 32 - Volcanic Plumes. *In* Sigurdsson, H. (ed.) *The Encyclopedia of Volcanoes (Second Edition)*, Academic Press, Amsterdam. Second edition edition, pp. 571 – 585.

Carter, L., Manighetti, B., Elliot, M., Trustrum, N. 2002. Source, sea level and circulation effects on the sediment flux to the deep ocean over the past 15 ka off eastern New Zealand. *Global and Planetary Change*, **33** (3-4), 339–355.

Caseldine, C. J., Baker, A., Barnes, W. L. 1999. A rapid, non-destructive scanning method for detecting distal tephra layers in peats. *The Holocene*, **9** (5), 635–638.

Cerling, T. E., Brown, F. H. 1982. Tuffaceous marker horizons in the Koobi Fora region and the lower Omo valley. *Nature*, **299**, 216–221.

Cerling, T. E., Brown F. H. amd Cerling, B. W., Curtis, G. H., Drake, R. E. 1979. Preliminary correlations between the Koobi Fora and Shungura Formations, East Africa. *Nature*, **279**, 118–121.

Chernet, T., Hart, W. K., Aronson, J. L., Walter, R. C. 1998. New age constraints on the timing of volcanism and tectonism in the northern Main Ethiopian Rift - southern Afar transition zone (Ethiopia). *Journal of Volcanology and Geothermal Research*, **80** (3-4), 267–280.

Chesner, C. A. 1998. Petrogenesis of the Toba Tuffs, Sumatra, Indonesia. *Journal of Petrology*, **39** (3), 397438.

Clark, J. D., Beyene, Y., WoldeGabriel, G., Hart, W. K., Renne, P. R., Gilbert, H., Defleur, A., Suwa, G., Katoh, S., Ludwig, K. R., Boisserie, J.-R., Asfaw, B., White, T. D. 2003. Stratigraphic, chronological and behavioural contexts of Pleistocene *Homo sapiens* from Middle Awash, Ethiopia. *Nature*, **423**, 747–752.

Corti, G. 2009. Continental rift evolution: From rift initiation to incipient break-up in the Main Ethiopian Rift, East Africa. *Earth-Science Reviews*, **96** (1-2), 1–53.

Corti, G. 2015. The Ethiopian Rift Valley.
URL `http://ethiopianrift.igg.cnr.it/ETHvolcanoes.html`

Coulter, S., Pilcher, Hall, V. A., Plunkett, G., Davies, S. M. 2009. Testing the reliability of the JEOL FEGSEM 6500F electron microprobe for quantitative major element analysis of glass shards from rhyolitic tephra. *Boreas*, **39** (1), 163–169.

Cronin, S. J., Neall, V. E., Palmer, A. S., Stewart, R. B. 1997. Methods of identifying late Quaternary rhyolitic tephras on the ring plains of Ruapehu and Tongariro volcanoes, New Zealand. *New Zealand Journal of Geology and Geophysics*, **40** (2), 175–184.

Cross, W., Iddings, J. P., Pirsson, L. V., Washington, H. S. 1912. Modifications of the Quantitive System of Classification of Igneous Rocks. *The Journal of Geology*, **20** (6), 550–561.

Croudace, I. W., Rindby, A., Rothwell, R. G. 2006. ITRAX: Description and evaluation of a new multi-function X-ray core scanner. *In* Rothwell, R. G. (ed.) *New Techniques in Sediment Core Analysis*, Geological Society of London. pp. 51–63.

Damaschke, M., Sulpizio, R., Zanchetta, Wagner, B., Bohm, A., Nowaczyk, N., Rethemeyer, J., Hilgers, A. 2013. Tephrostratigraphic studies on a sediment core from Lake Prespa in the Balkans. *Climate of the Past*, **9**, 267–287.

Dartevelle, S., Ernst, G. G. J., Stix, J., Bernard, A. 2002. Origin of the Mount Pinatubo climactic eruption cloud: Implications for volcanic hazards and atmospheric impacts. *Geological Society of America Bulletin*, **30** (7), 663–666.

Davidson, A., Rex, D. C. 1980. Age of volcanism and rifting in southwestern Ethiopia. *Nature*, **283**, 657–658.

Davies, S. M. 2015. Cryptotephras: the revolution in correlation and precision dating. *Journal of Quaternary Science*, **30** (2), 114–130.

Davies, S. M., Larsen, G., Wastegård, S., Turney, C. S. M., Valerie, A. H., Coyle, L., Thordarson, T. 2010. Widespread dispersal of Icelandic tephra: how does the Eyjafjöll eruption of 2010 compare to past Icelandic events? *Journal of Quaternary Science*, **25** (5), 605–611.

de Fino, M., La Volpe, L., Lirer, L. 1973. Volcanology and petrology of the Assab Range (Ethiopia). *Bulletin Volcanologique*, **37** (1), 95–110.

de Fontaine, C. S., Kaufman, D. S., Anderson, R. S., Werner, A., Waythomas, C. F., Brown, T. A. 2007. Late Quaternary distal tephra-fall deposits in lacustrine sediments, Kenai Peninsula, Alaska. *Quaternary Research*, **68** (1), 64–78.

de Heinzelin, J., Clark, J. D., White, T., Hart, W., Renne, P., WoldeGabriel, G., Beyene, Y., Vrba, E. 1999. Environment and Behavior of 2.5 - Million - Year -Old Bouri Hominids. *Science*, **284** (5414), 625–629.

Deino, A. L., McBrearty, S. 2002. ^{40}Ar/^{39}Ar dating of the Kapthurin Formation, Baringo, Kenya. *Journal of human evolution*, **42** (1-2), 185–210.

Deino, A. L., Potts, R. 1990. Single-Crystal ^{40}Ar/^{39}Ar Dating of the Olorgesailie Formation, Southern Kenya Rift. *Journal of Geophysical Research*, **95** (B6), 8453–8470.

Deino, A. L., Scott, G. R., Saylor, B., Alene, M., Angelini, J. D., Haile-Selassie, Y. 2010. ^{40}Ar/^{39}Ar dating, paleomagnetism, and tephrochemistry of Pliocene strata of the hominid-bearing Woranso-Mille area, west-central Afar Rift, Ethiopia. *Journal of Human Evolution*, **52** (2), 111–126.

Deino, A. L., Tauxe, L., Monaghan, M., Hill, A. 2002. $^{40}Ar/^{39}Ar$ geochronology and paleomagnetic stratigraphy of the Lukeino and lower Chemeron Formations at Tabarin and Kapcheberek, Tugen Hills, Kenya. *Journal of Human Evolution*, **42** (1-2), 117–140.

deMenocal, P. B., Brown, F. 1999. *The Evolution Neogene Terrestrial Ecosystems in Europe*, Cambridge University Press, chapter Pliocene tephra correlations between East African hominid locations, the Gulf of Aden, and the Arabian Sea. pp. 23–54.

Di Paola, G. M. 1971. Geology of the Corbetti Caldera area (Main Ethiopian Rift Valley). *Bulletin Volcanologique*, **35** (2), 497–506.

Di Paola, G. M. 1972. The Ethiopian Rift Valley (between $7^{o}00'$ and $8^{o}40'$ lat North). *Bulletin Volcanologique*, **36** (4), 517–560.

DiMaggio, E., Campisano, C., Arrowsmith, J. R., Reed, K., Swisher, C. I., Lockwood, C. 2008. *The Geology of Early Humans in the Horn of Africa: Geological Society of America Special Paper 446*, The Geological Society of America, chapter Correlation and stratigraphy of the BKT-2 volcanic complex in west-central Afar, Ethiopia. pp. 163 –177.

Dugda, M. T., Nyblade, A. A., Julia, J., Langston, C. A., Ammon, C. J., Simiyu, S. 2005. Crustal structure in Ethiopian and Kenya from receiver function analysis: Implications for rift development in eastern Africa. *Journal of Geophysical Research*, **110** (B1), 1–15.

Dugmore, A. 1989. Icelandic volcanic ash in Scotland. *Scottish Geographical Magazine*, **105** (3), 168–172.

Eastwood, W. J., Pearce, N. J. G., Westgate, J. A., Perkins, W. T., Lamb, H. F., Roberts, N. 1999. Geochemistry of Santorini tephra in lake sediments from Southwest Turkey. *Global and Planetary Change*, **21** (1-3), 17–29.

Ebinger, C. J., Yemane, T., WoldeGabriel, G., Aronson, J., Walter, R. C. 1993. Late Eocene-Recent volcanism and faulting in the southern main Ethiopian rift. *Journal of the Geological Society*, **150**, 99–108.

Eggins, S. M., Kingsley, L. P. J., Shelley, J. M. G. 1998. Deposition and element fractionation processes during atmospheric pressure laser sampling for analysis by ICP-MS. *Applied Surface Science*, **127-129**, 278–286.

Eissen, J.-P., Juteau, T., Joron, J.-L., Dupre, B., Humler, E., Al'Mukamedov, A. 1989. Petrology and geochemistry of basalts from the Red Sea Axial Rift at 18^o North. *Journal of Petrology*, **30** (4), 791–839.

Ersoy, E. Y. 2013. PETROMODELER (Petrological Modeler): a Microsoft® Excel© spreadsheet program for modelling melting, mixing, crystallization and assimilation processes in magmatic systems. *Turkish Journal of Earth Sciences*, **22**, 115–125.

Ewart, A., Griffin, W. L. 1994. Application of Proton-Microprobe Data to Trace-Element Partitioning in Volcanic-Rocks. *Chemical Geology*, **117** (1-4), 251–284.

Feakins, S. J., Brown, F. H., deMenocal, P. B. 2007. Plio-Pleistocene microtephra in DSDP site 231, Gulf of Aden. *Journal of African Earth Sciences*, **48** (5), 341–352.

Feibel, C. S. 1999. Tephrostratigraphy and geological context in paleoanthropology. *Evolutionary Anthropology: Issues, News, and Reviews*, **8** (3), 87–111.

Feibel, C. S. 2011. A Geological History of the Turkana Basin. *Evolutionary Anthropology*, **20** (6), 206–216.

Ferguson, D., Barnie, T. D., Pyle, D. M., Oppenheimer, C., Yirgu, G., Lewi, E., Kidane, T., Carn, S., Hamling, I. 2010. Recent rift-related volcanism in Afar, Ethiopia. *Earth and Planetary Science Letters*, **292** (3-4), 409–418.

Ferguson, D., Maclennan, J., Bastow, I. D., Pyle, D., Jones, S., Keir, D., Blundy, J., Plank, T., Yirgu, G. 2013. Melting during late-stage rifting in Afar is hot and deep. *Nature*, **499**, 70–73.

Field, L., Blundy, J., Brooker, R. A., Wright, T., Yirgu, G. 2012. Magma storage conditions beneath Dabbahu Volcano (Ethiopia) constrained by petrology, seismicity and satellite geodesy. *Bulletin of Volcanology*, **74**, 981–1004.

Field, L., Blundy, J., Calvert, A., Yirgu, G. 2013. Magmatic history of Dabbahu, a composite volcano in the Afar Rift, Ethiopia. *Geological Society of America Bulletin*, **125** (1-2), 128–147.

Fisher, R., Schminke, H.-U. 1984. *Pyroclastic Rocks*. Springer Berlin Heidelberg.

Gasparon, M., Innocenti, F., Manetti, P., Peccerillo, A., A., T. 1993. Genesis of the Pliocene to Recent bimodal mafic-felsic volcanism in the Debre Zeyt area, central Ethiopia: volcanological and geochemical constraints. *Journal of East African Earth Sciences*, **17** (2), 145–165.

Gehrels, M. J., Newnham, R. M., Lowe, D. J., Wynne, S., Hazell, Z. J., Caseldine, C. J. 2008. Towards rapid assay of cryptotephra in peat cores: Review and evaluation of various methods. *Quaternary International*, **178** (1), 68–84.

George, R., Rogers, N., Kelley, S. 1998. Earliest magmatism in Ethiopia: Evidence for two mantle plumes in one flood basalt province. *Geology*, **26** (10), 923–926.

Ghinassi, M., D'Oriano, F., Benvenuti, M., Awramik, S., Bartolini, C., Fedi, M., Ferrari, G., Papini, M., Sagri, M., Talbot, M. 2012. Shoreline fluctuations of Lake Hayk (northern Ethiopia) during the last 3500 years: Geomorphological, sedimentary, and isotope records. *Palaeogeography, Palaeoclimatology, Palaeoecology*, **365-366**, 209–226.

Gibbons, A. 1993. Pleistocene Population Explosions. *Science*, **262** (5130), 27–28.

Gibson, I. L. 1967. Preliminary account of the volcanic geology of Fantale, Shoa, Ethiopia. *Bulletin of the Geophysical Observatory, Addis Ababa*, **10**, 59–68.

Gibson, I. L. 1969. The structure and volcanic geology of an axial portion of the Main Ethiopian Rift. *Tectonophysics*, **8** (4-6), 561–565.

Gill, R. 2010. *Igneous Rocks and Processes: A Practical Guide*. Wiley-Blackwell.

Giordano, F., D'Antonio, M., Civetta, L., Tonarini, S., Orsi, G., Ayalew, D., Yirgu, G., Dell'Erba, F., Di Vito, M. A., Isaia, R. 2014. Genesis and evolution of mafic and felsic mmagma at Quaternary volcanoes wiwith the Main Ethiopian Rift: Insights from Gedemsa and Fant'Ale complexes. *Lithos*, **188**, 130–144.

Goitom, B., Oppenheimer, C., Hammond, J. S., Grandin, R., Barnie, T., Donovan, A., Ogubazghi, G., Yohannes, E., Kibrom, G., Kendall, J.-M., Carn, S., Fee, D., C, S., Keir, D., Ayele, A., Blundy, J., Hamlyn, J., Wright, T., Berhe, S. 2015. First recorded eruption of Nabro volcano, Eritrea, 2011. *Bulletin of Volcanology*, **77** (85).

Gomez, B., Carter, L., Trustrum, N. A. 2007. A 2400 yr record of natural events and anthropogenic impacts in intercorrelated terrestrial and marine sediment cores: Waipaoa sedimentary system, New Zealand. *Geological Society of America Bulletin*, **119** (11-12), 1415–1432.

Gouin, P. 1979. *Earthquake history of Ethiopia and the Horn of Africa*. Ottawa : International Development Research Centre.

Günther, D., Hattendorf, B. 2005. Solid sample analysis using laser ablation inductively coupled plasma mass spectrometry. *TrAC Trends in Analytical Chemistry*, **24** (3), 255–265.

Haile-Selassie, Y., Deino, A., Saylor, B., Umer, M., Latimer, B. 2007. Preliminary geology and paleontology of new hominid-bearing Pliocene localities in the central Afar region of Ethiopia. *Anthropological Science*, **115** (3), 215–222.

Haileab, B., Brown, F. H. 1992. Turkana Basin-Middle Awash Valley correlations and the age of the Sagantole and Hadar formations. *Journal of Human Evolution*, **22** (6), 453–468.

Haileab, B., Brown, F. H. 1994. Turkana Basin - Middle Awash Valley correlations and the age of the Sagantole and Hadar Formations. *Journal of Human Evolution*, **22** (6), 453–468.

Harangi, S., Mason, P. R. D., Lukács, R. 2005. Correlation and petrogenesis of silicic pyroclastic rocks in the Northern Pannonian Basin, Eastern-Central Europe: In situ trace element data of glass shards and mineral chemical constraints. *Journal of Volcanology and Geothermal Research*, **143** (4), 237–257.

Harris, J. M. 1977. Palaeomagnetic stratigraphy of the Koobi Fora Formation, east of Lake Turkana (Lake Rudolf), Kenya. *Nature*, **268** (5621), 669–670.

Harris, W. C. 1844. *The Highlands of Aethiopia*, volume 1. Longman Brown.

Hart, W. K., Walter, R. C., WoldeGabriel, G. 1992. Tephra sources and correlations in Ethiopia: Application of elemental and neodymium isotope data. *Quaternary International*, **13-14**, 77–86.

Hart, W. K., WoldeGabriel, G., Walter, R. C., Mertzman, S. A. 1989. Basalt Volcanism in Ethiopia: Constraints on Continental Rift and Mantle Interactions. *Journal of Geophysical Research*, **94** (B6), 7731–7748.

Hayward, C. 2011. High spatial resolution electron probe microanalysis of tephras and melt inclusions without beam-induced chemical modification. *The Holocene*, **22** (1), 119–125.

Heiken, G. 1972. Morphology and Petrography of Volcanic Ashes. *Geological Society of America Bulletin*, **83** (7), 1961–1988.

Heiken, G. 1974. *An Atlas of Volcanic Ash*. Technical report, Smithsonian Inst. Press, Washington, United States.

Heiken, G., Wohletz, K. 1985. *Volcanic Ash*. Los Alamos series in basic and applied sciences, University of California Press.

Heiken, G., Wohletz, K. 1991. *Sedimentation in Volcanic Settings*, Society of Economic Paleontologists and Mineralogists, Special Publication, volume 45, chapter Fragmentation processes in explosive volcanic eruptions. pp. 19–26.

Hergenröder, R. 2006. Hydrodynamic sputtering as a possible source for fractionation in LA-ICP-MS. *Journal of Analytical Atomic Spectrometry*, **21**, 517–524.

Hewlitt, G. 2000. The genetic legacy of the Quaternary ice Ages. *Nature*, **405**.

Hodder, A. P. W., de Lange, P. J., Lowe, D. J. 1991. Dissolution and depletion of ferromagnesian minerals from Holocene tephra layers in an acid bog, New Zealand, and implications for tephra correlation. *Journal of Quaternary Science*, **6** (3), 195–208.

Hodgson, D. A., Dyson, C. L., Jones, V. J., Smellie, J. L. 1998. Tephra analysis of sediments from Midge Lake (South Shetland Islands) and Sombre Lake (South Orkney Islands), Antarctica. *Antarctic Science*, **10** (1), 13–20.

Hofmann, C., Courtillot, V., Féraud, G., Rochette, P., Yirgu, G., Ketefo, E., Pik, R. 1997. Timing of the Ethiopian flood basalt event and implications for plume birth and global change. *Nature*, **389**, 838–841.

Hogg, A. G., McCraw, J. D. 1983. Late Quaternary tephras of Coromandel Peninsula, North Island, New Zealand: A mixed peralkaline and calcalkaline tephra sequence. *New Zealand Journal of Geology and Geophysics*, **26**, 163–187.

Howell, C. 1968. Omo research expedition. *Nature*, **219**, 567–572.

Humphreys, M. C. S., Kearns, S. L., Blundy, J. D. 2006. SIMS investigation of electron-beam damage to hydrous, rhyolitic glasses: Implications for melt inclusion analysis. *American Mineralogist*, **91** (4), 667–679.

Hunt, J. B., Hill, P. G. 2001. Tephrological implications of beam size - sample-size effects in electron microprobe analysis of glass shards. *Journal of Quaternary Science*, **16** (2), 105–117.

Hurst, T., Smith, W. 2004. A Monte Carlo methodology for modelling ashfall hazards. *Journal of Volcanology and Geothermal Research*, **138** (3-4), 393–403.

Hutchison, W., Mather, T. A., Pyle, D. M., Biggs, J., Yirgu, G. 2015. Structural controls on fluid pathways in an active rift system: A case study of the Aluto volcanic complex. *Geosphere*, **11** (3), 542–562.

Irvine, T. N., Barager, W. R. A. 1971. A guide to the chemical classification of the common volcanic rocks. *Canadian Journal of Earth Sciences*, **8** (5), 523–548.

Jackson, L. J., Stone, J. R., Cohen, A. S., Yost, C. L. 2015. High-resolution paleoecological records from Lake Malawi show no significant cooling associated with the Mount Toba supereruption at ca. 75 ka. *Geology*, **43** (9), 823–826.

Jenkins, S. F., Magill, C. R., McAneney, K. J. 2007. Multi-stage volcanic events: A statistical investigation. *Journal of Volcanology and Geothermal Research*, **161** (4), 275–288.

Jensen, B. J., Pyne-ODonnell, S., Plunkett, G., Froese, D. G., Hughes, P. D., Sigl, M., McConnell, J. R., Amesbury, M. J., Blackwell, P. G., van den Bogaard, C.,

Buck, C. E., Charman, D. J., Clague, J. J., Valerie, Hall, Koch, J., Mackay, H., Mallon, G., McColl, L., Pilcher, J. R. 2014. Transatlantic distribution of the Alaskan White River Ash. *Geology*, **42** (10), 875–878.

Jochum, K. P., Nohl, U., Herwig, K., Lammel, E., Stoll, B., Hofmann, A. W. 2005. GeoReM: a new geochemical database for reference materials and isotopic standards. *Geostandards and Geoanalytical Research*, **29** (3), 333–338.

Jochum, K. P., Stoll, B., Herwig, K., Willbold, M., Hofmann, A. W., Amini, M., Aarburg, S., Abouchami, W., Hellebrand, E., Mocek, B., Raczek, I., Stracke, A., Alard, O., Bouman, C., Becker, S., Dücking, M., Brätz, H., Klemd, R., de Bruin, D., Canil, D., Cornell, D., de Hoog, C., Dalpé, C., Danyushevsky, L., Eisenhauer, A., Gao, Y., Snow, J. E., Groschopf, N., Günther, D., Latkoczy, C., Guillong, M., Hauri, E. H., Höfer, H. E., Lahaye, Y., Horz, K., Jacob, D. E., Kasemann, S. A., Kent, A. J. R., Ludwig, T., Zack, T., Mason, P. R. D., Meixner, A., Rosner, M., Misawa, K., Nash, B. P., Pfänder, J., Premo, W. R., Sun, W. D., Tiepolo, M., Vannucci, R., Vennemann, T., Wayne, D., Woodhead, J. D. 2006. MPI-DING reference glasses for in situ microanalysis: New reference values for element concentrations and isotope ratios. *Geochemistry, Geophysics, Geosystems*, **7** (2), 1–44.

Jordan, B. R., Sigurdsson, H., Carey, S. N., Rogers, R., Ehrenborg, J. 2007. Geochemical variation along and across the Central American Miocene paleoarc in Honduras and Nicaragua. *Geochimica et Cosmochimica Acta*, **71** (14), 3581–3591.

Julien, P. Y. 1995. *Erosion and Sedimentation*. Cambridge University Press.

Kalb, J. E. 1976. *Rift Valley Research Mission in Ethiopia, Annual report 1976-1977*. Technical report, Ethiopian Ministry of Culture (Addis Ababa).

Kalb, J. E. 1993. Refined Stratigraphy of the Hominid-Bearing Awash Group, Middle Awash Valley, Afar Depression, Ethiopia. *Newsletters on Stratigraphy*, **29** (1), 21–62.

Kalb, J. E. 1995. Fossil elephantoids, Awash paleolake basins, and the Afar triple junction, Ethiopia. *Palaeogeography, Palaeoclimatology, Palaeoecology*, **114** (2-4), 357 – 368.

Kalnay, E., Kanamitsu, M., Kistler, R., Collins, W., Deaven, D., Gandin, L., Iredell, M., Saha, S., White, G., Woolen, J., Zhu, Y., Chelliah, M., Ebisuzaki, W., Higgins, W., Janowiak, J., Mo, K., Ropelewski, C., Wang, J., Leetma, A., Reynolds, R., Jenne, R., Joseph, D. 1996. The NCEP/NCAR 40 year reanalysis project. *Bulletin of the American Meteorological Society*, **77**, 437–471.

Kassa, T. G. 2013. *Holocene environmental history of Lake Chamo, South Ethiopia*. Ph.D. thesis, University of Cologne.

Katoh, S., Nagaoka, S., WoldeGabriel, G., Renne, P., Snow, M. G., Beyene, Y., Suwa, G. 2000. Chronostratigraphy and correlation of the Plio-Pleistocene tephra layers of the Konso Formation, southern Main Ethiopian Rift, Ethiopia. *Quaternary Science Reviews*, **19** (13), 1305–1317.

Kebede, E., Mariam, Z. G., Ahlgren, I. 1994. The Ethiopian Rift Valley lakes: chemical characteristics of a salinity-alkalinity series. *Hydrobiologia*, **288** (1), 1–12.

Kebede, S., Lamb, H. F., Telford, R. J., Leng, M. J., Umer, M. 2002. Lake Groundwater Relationships, Oxygen Isotope Balance and Climate Sensitivity of the Bishoftu Crater Lakes, Ethiopia. *In* Odada, E. O., Olago, D. O. (eds.)

Advances in Global Change Research, volume 12, Springer Netherlands. pp. 261–275.

Keir, D., Bastow, I. D., Corti, G., Mazzarini, F., Rooney, T. O. 2015. The origin of along-rift variations in faulting and magmatism in the Ethiopian Rift. *Tectonics*, **34** (3), 464–477. 2014TC003698.

Keir, D., Belachew, M., Ebinger, C. J., Kendall, J. M., Hammond, J. O. S., Stuart, G. W., Ayele, A., Rowland, J. V. 2011. Mapping the evolving strain field during continental breakup from crustal anisotropy in the Afar Depression. *Nature Communications*, **285** (2), 1–7.

Köninger, S., Stollhofen, H. 2001. *Volcaniclastic sedimentation in lacustrine settings*, Blackwell Science, chapter Environmental and tectonic controls on preservation potential of distal fallout ashes in fluvio-lacustrine settings: the Carboniferous-Permian Saar-Nahe Basin, south western Germany. pp. 263–285.

Kuehn, S. C., Froese, D. G. 2010. Tephra from ice- A simple method to routinely mount, polish, and quantitatively analyze sparse fine particles. *Microscopy and microanalysis : the official journal of Microscopy Society of America, Microbeam Analysis Society, Microscopical Society of Canada*, **16** (2), 218–225.

Kuehn, S. C., Froese, D. G., Shane, P. A. R. 2011. The INTAV intercomparison of electron-beam microanalysis of glass by tephrochronology laboratories: Results and recommendations. *Quaternary International*, **246** (1-2), 19–47.

Kylander, M. E., Lind, E. M., Wastegård, S., Lowemark, L. 2011. Recommendations for using XRF core scanning as a tool in tephrochronology. *The Holocene*, **22** (3), 371–375.

Lamb, A. L. 2000. *Stable Isotope Geochemistry of Lakes Tilo and Awassa, Ethiopia: a Holocene record of volcanic and climatic change*. Ph.D. thesis, University of Wales Aberystwyth.

Lamb, A. L., Leng, M. J., Lamb, H. F., Mohammed, M. U. 2000. A 9000-year oxygen and carbon isotope record of hydrological change in a small Ethiopian crater lake. *The Holocene*, **10** (2), 167–177.

Lamb, A. L., Leng, M. J., Lamb, H. F., Telford, R. J., Mohammed, M. U. 2002*a*. Climatic and non-climatic effects on the $\delta^{18}O$ and $\delta^{13}C$ compositions of Lake Awassa, Ethiopia, during the last 6.5 ka. *Quaternary Science Reviews*, **21** (1-2), 2199–2211.

Lamb, A. L., Leng, M. J., Mohammed, M. U., Lamb, H. F. 2004. Holocene climate and vegetation change in the Main Ethiopian Rift Valley, inferred from the composition (C/N and $\delta^{13}C$) of lacustrine organic matter. *Quaternary Science Reviews*, **23** (7-8), 881–891.

Lamb, H. F., Kebede, S., Leng, M. J., Ricketts, D., Telford, R. J., Umer, M. 2002*b*. Origin and Isotopic Composition of Aragonite Laminae in an Ethiopian Crater Lake. *The East African Great Lakes: Limnology, Palaeolimnology and Biodiversity*, **12**, 487–508.

Lamb, H. F., Leng, M. J., Telford, R. J., Ayenew, T., Umer, M. 2007. Oxygen and carbon isotope composition of authigenic carbonate from an Ethiopian lake: a climate record of the last 2000 years. *The Holocene*, **17** (4), 517–526.

Lane, C. S., Blockley, S. P. E., Magerud, J., Smith, V. C., Lohne, Ø. S., Tomlinson, E. L., Matthews, I. P., Lotter, A. F. 2012. Was the 12.1 ka Icelandic Vedde Ash one of a kind? *Quaternary Science Reviews*, **33**, 87–99.

Lane, C. S., Brauer, A., Blockley, S. P. E., Dulski, P. 2013*a*. Volcanic ash reveals time-transgressive abrupt climate change during the Younger Dryas. *Geology*, **41** (12), 1251–1254.

Lane, C. S., Chorn, B. T., Johnson, T. C. 2013*b*. Ash from the Toba supereruption in Lake Malawi shows no volcanic winter in East Africa at 75 ka. *Proceedings of the National Academy of Sciences of the United States of America*, **110** (20), 8025–8029.

Lane, C. S., Cullen, V. L., White, D., Bramham-Law, C. W. F., Smith, V. C. 2014. Cryptotephra as a dating and correlation tool in archaeology. *Journal of Archaeological Science*, **42**, 42–50.

Langdon, P. G., Caseldine, C. J., Croudace, I. W., Jarvis, S., Wastegård, S., Crowford, T. C. 2011. A chironomid-based reconstruction of summer temperatures in NW Iceland since AD 1650. *Quaternary Research*, **75** (3), 451–460.

Lawson, I. T., Swindles, G. T., Plunkett, G., Greenberg, D. 2012. The spatial distribution of Holocene cryptotephras in north-west Europe since 7 ka: implications for understanding ash fall events from Icelandic eruptions. *Quaternary Science Reviews*, **41**, 57–66.

Le Bas, M. J., Le Maitre, R. W., Streisen, A., Zanettin, B. 1986. A chemical classification of volcanic rocks based on the total alkali-silica diagram. *Journal of Petrology*, **27** (3), 745–750.

Le Maitre, R. W. 2002. *Igneous Rocks: A Classification and Glossary of Terms: Recommendations of the International Union of Geological Sciences Subcommission on the Systematics of Igneous Rocks*. Cambridge University Press.

Leakey, L., Evernden, J., Curtis, G. 1961. Age of Bed I, Olduvai Gorge, Tanganyika. *Nature*, **191**, 478–479.

Lee, M.-Y., C.-H., C., K.-Y., W., Lizuka, Y., Carey, S. 2004. First Toba supereruption revival. *Geology*, **32** (1), 61–64.

Leng, M. J., Lamb, A. L., Lamb, H. F., Telford, R. J. 1999. Palaeoclimatic implications of isotopic data from modern and early Holocene shells of the freshwater snail Melanoides tuberculata, from lakes in the Ethiopian Rift Valley. *Journal of Paleolimnology*, **21**, 97–106.

Leng, M. J., Marshall, J. D. 2004. Palaeoclimate interpretation of stable isotope data from lake sediment archives. *Quaternary Science Reviews*, **23** (7-8), 811–831.

Lenhardt, N., Oppenheimer, C. 2014. *Extreme Natural Hazards, Disaster Risks and Societal Implications*, Cambridge University Press, chapter Volcanism in Africa: geological perspectives, hazards and societal implications. pp. 169–199.

Lowe, D. J. 1985. Application of impulse radar to continuous profiling of tephra-bearing lake sediments and peats: An initial evaluation. *New Zealand Journal of Geology and Geophysics*, **28** (4), 667–674.

Lowe, D. J. 2011. Tephrochronology and its application: A review. *Quaternary Geochronology*, **6** (2), 107–153.

Lowe, D. J., Shane, P. A. R., Alloway, B. V., Newnham, R. M. 2008. Fingerprints and age models for widespread New Zealand tephra marker beds erupted since 30,000 years ago: a framework for NZ-INTIMATE. *Quaternary Science Reviews*, **27** (1-2), 95–126.

Lowe, J., Barton, N., Blockley, S., Ramsey, C. B., Cullen, V. L., Davies, W., Gamble, C., Hardiman, K. G. M., Housley, R., Lane, C. S., Lee, S., Lewis, M., MacLeod, A., Menzies, M., Müller, W., Pollard, M., Price, C., Roberts, A. P., Rohlinge, E. J., Satowa, C., Smith, V. C., Stringer, C. B., Tomlinson, E. L., White, D., Albert, P., Arienzoi, I., Barker, G., Borić, D., Carandente, A., Civetta, L., Ferrier, C., Guadelli, J.-L., Karkanas, P., Koumouzelis, M., Mller, U. C., Orsi, G., Pross, J., Rosi, M., Shalamanov-Korobarq, L., Sirakovr, N., Tzedakiss, P. C. 2012. Volcanic ash layers illuminate the resilience of Neanderthals and early modern humans to natural hazards. *Proceedings of the National Academy of Sciences of the United States of America*, **109** (34), 532537.

Macdonald, R., Bagiński, Ronga, F., Dzierżanowski, M., P. amd Lustrino, Marzoli, A., Melluso, L. 2012. Evidence for extreme fractionation of peralkaline silicic magmas, the Boseti volcanic complex, Main Ethiopian Rift. *Mineralogy and Petrology*, **104** (3), 163–175.

Macgregor, D. 2015. History of the development of the East African Rift System: A series of interpreted maps through time. *Journal of African Earth Sciences*, **101**, 232–252.

Mahood, G. A., Stimac, J. A. 1990. Trace-element partitioning in pantellerites and trachytes. *Geochimica et Cosmochimica Acta*, **54** (8), 2257–2276.

Manville, V., Segschneider, B., White, J. D. L. 2002. Hydrodynamic behaviour of Taupo 1800a pumice: implications for the sedimentology of remobilized pyroclasts. *Sedimentology*, **49** (5), 955–976.

Mariner, R. H., Surdam, R. C. 1970. Alkalinity and formation of zeolites in saline alkaline lakes. *Science*, **170** (3961), 977–980.

Marsh, B. D. 2015. Chapter 8 - Magma Chambers. *In* Sigurdsson, H. (ed.) *The Encyclopedia of Volcanoes (Second Edition)*, Academic Press, Amsterdam. Second edition edition, pp. 185 – 201.

Marshall, M. H. 2006. *Late Pleistocene and Holocene palaeolimnology of Lakes Tana and Ashenge, northern Ethiopia*. Ph.D. thesis, University of Wales Aberystwyth.

Marshall, M. H., Lamb, H. F., Davies, S. J., Leng, M. J., Kubsa, Z., Umer, M., Bryant, C. 2009. Climatic change in northern Ethiopia during the past 17,000 years: A diatom and stable isotope record from Lake Ashenge. *Palaeogeography, Palaeoclimatology, Palaeoecology*, **279** (1-2), 114–127.

McCanta, M. C., Hatfield, R. G., Thomson, B. J., Hook, S. J., Fisher, E. 2015. Identifying cryptotephra units using correlated rapid, non-destructive methods: VSWIR spectroscopy, X-ray fluorescence and magnetic susceptibility. *Geochemistry, Geophysics, Geosystems*, **16** (12), 4029–4056.

McDougall, I. 1985. $^{40}Ar/^{39}Ar$ dating of the hominid-bearing Pliocene-Pleistocene sequence at Koobi Fora, Lake Turkana, northern Kenya. *Geological Society of America Bulletin*, **96** (2), 159–175.

McHenry, L. 2005. Phenocryst composition as a tool for correlating fresh and altered tephra, Bed I, Olduvai Gorge, Tanzania. *Stratigraphy*, **2** (2), 101–115.

Michels, J. W., Tsong, I. S. T., Nelson, C. M. 1983. Obsidian Dating and East African Archeology. *Science*, **219** (4583), 361–366.

Mohr, P., Zanettin, B. 1988. *Continental Flood Basalts*, Kluwer, chapter The Ethiopian Flood Basalt Province. pp. 63–110.

Mohr, P. A. 1971. Ethiopian Rift and Plateaus: Some Volcanic Petrochemical Differences. *Journal of Geophysical Research*, **76** (8), 1967–1983.

Mohr, P. A. 1978. Afar. *Annual Review of Earth and Planetary Sciences*, **6**, 145–172.

Morgan, G. B., London, D. 1996. Optimizing the electron microprobe analysis of hydrous alkali aluminosilicate glasses. *American Mineralogist*, **81** (9-10), 1176–1185.

Morgan, G. B., London, D. 2005. Effect of current density on the electron microprobe analysis of alkali aluminosilicate glasses. *American Mineralogist*, **90**, 1131–1138.

Nagaoka, S., Katoh, S., WoldeGabriel, G., Sato, H., Nakaya, H., Beyene, Y., Suwa, G. 2005. Lithostratigraphy and sedimentary environments of the hominid-bearing Pliocene-Pleistocene Konso Formation in the southern Main Ethiopian Rift, Ethiopia. *Palaeogeography, Palaeoclimatology, Palaeoecology*, **216** (3-4), 333–357.

Namwamba, F. L. 1993. *Tephrostratigraphy of the Chemeron Formation Baringo Basin, Kenya*. Master's thesis, The University of Utah.

Narcisi, B., Petit, J. R., Tiepolo, M. 2006. A volcanic marker (92ka) for dating deep east Antarctic ice cores. *Quaternary Science Reviews*, **25** (21-22), 2682–2687.

NASA. 2011. Earth Observatory - Eruption at Nabro Volcano, Eritrea. URL `http://earthobservatory.nasa.gov/NaturalHazards/view.php?id=50988`

Newhall, C. G., Self, S. 1982. The Volcanic Explosivity Index (VEI): An Estimate of Explosive Magnitude for Historical Volcanism. *Journal of Geophysical Research*, **87** (C2), 1231–1238.

Oppenheimer, C. 2011. *Eruptions that Shook the World.* Cambridge University Press.

Oppenheimer, C., Francis, P. 1997. Remote sensing of heat, lava and fumarole emissions from Erta'Ale volcano, Ethiopia. *International Journal of Remote Sensing*, **18** (8), 1661–1692.

Payne, R. J., Kilfeather, A. A., van der Meer, J. J. M., Blackford, J. J. 2005. Experiments on the taphonomy of tephra in peat. *Suoseura - Finnish Peatland Society*, **56** (4), 147–156.

Pearce, N. J. G. 1990. Zirconium and niobium-bearing ilmenites from the Igaliko dyke swarm, South Greenland. *Mineralogical Magazine*, **54**, 585–588.

Pearce, N. J. G., Abbott, P. M., Martin-Jones, C. M. 2014. Microbeam methods for the analysis of glass in fine-grained tephra deposits: a SMART perspective on current and future trends. *In* Austin, W. E. N., Abbott, P. M., Davies, S. M., Pearce, N. J. G., Wastegård, S. (eds.) *Marine Tephrochronology*, Geological Society of London, Special Publications.

Pearce, N. J. G., Alloway, B. V., Westgate, J. A. 2008. Mid-Pleistocene silicic tephra beds in the Auckland region, New Zealand: Their correlation and origins based on the trace element analyses of single glass shards. *Quaternary International*, **178** (1), 16–43.

Pearce, N. J. G., Bendall, C. A., Westgate, J. A. 2008. Comment on "Some numerical considerations in the geochemical analysis of distal microtephra' by A.M. Pollard, S.P.E. Blockley and C.S. Lane. *Applied Geochemistry*, **23** (10), 1353–1364.

Pearce, N. J. G., Perkins, W. T., Westgate, J. A., Gorton, M. P., Jackson, S. E., Neal, C. R., Chenery, S. P. 1997. A Compilation of New and Published Major and Trace Element Data for NIST SRM 610 and NIST SRM 612 Glass Reference Materials. *Geostandards Newsletter*, **21**, 115–144.

Pearce, N. J. G., Perkins, W. T., Westgate, J. A., Wade, S. C. 2011. Trace-element microanalysis by LA-ICP-MS: The quest for comprehensive chemical characterisation of single, sub- $\sim$10 μm volcanic glass shards. *Quaternary International*, **246** (1-2), 57–81.

Pearce, N. J. G., Westgate, J. A., Gatti, E., Pattan, J. N., Parthiban, G., Achyuthan, H. 2014. Individual glass shard trace element analyses confirm that all known Toba tephra reported from India is from the c. 75-ka Youngest Toba eruption. *Journal of Quaternary Science*, **29** (8), 729–734.

Pearce, N. J. G., Westgate, J. A., Perkins, W. T., Eastwood, W. J., Shane, P. 1999. The application of laser ablation ICP-MS to the analysis of volcanic glass shards from tephra deposits: bulk glass and single shard analysis. *Global and Planetary Change*, **21** (1-3), 151–171.

Peccerillo, A., Donati, C., Santo, A. P., Orlando, A., Yirgu, G., Ayalew, D. 2007. Petrogenesis of silicic peralkaline rocks in the Ethiopian Rift: Geochemical evidence and volcanological Implications. *Journal of African Earth Sciences*, **48** (2-3), 161–173.

Peccerillo, A., Mandefro, B., Solomon, G., Hambisa, G., Beru, H., Tesfaye, K. 1998. The Precambrian rocks from Southern Ethiopia: petrology, geochemistry and their interaction with the recent volcanism from the Ethiopian Rift Valley. *Neues Jahrbuch für Minereralogie, Abhandlungen*, **173**, 237–262.

Perkins, W. T., Pearce, N. J. G. 1995. Mineral microanalysis by laserprobe inductively coupled plasma mass spectrometry. *In* Potts, P. J., Bowles, J. F. W., Reed, S. J. B., Cave, M. R. (eds.) *Microprobe Techniques in the Earth Sciences*, The Mineralogical Society, London.

Persson, C. 1966. Försök till tefrokronologisk datering av några svenska torvmossar. *Geologisku Förenitzgens i Stockholm Förhandlingar*, **88** (3), 361–395.

Pickford, M., Senut, B., Poupeau, G., Brown, F. H., Haileab, B. 1991. Correlation of tephra layers from the Western Rift Valley (Uganda) to the Turkana Basin (Ethiopia/Kenya) and the Gulf of Aden. *Comptes Rendus de L'Academie des Sciences Serie II*, **313**, 223–229.

Pyle, D. M. 1989. The thickness, volume and grainsize of tephra fall deposits. *Bulletin of Volcanology*, **51** (1), 1–15.

Pyle, D. M. 1999. Widely dispersed Quaternary tephra in Africa. *Global and Planetary Change*, **21** (1-3), 95–112.

Rampey, M., Oppenheimer, C., Pyle, D. M., Yirgu, G. 2010. Caldera-forming eruptions of the Quaternary Kone Volcanic Complex, Ethiopia. *Journal of African Earth Sciences*, **58** (1), 51–66.

Rampino, M. R., Ambrose, S. H. 2000. Volcanic winter in the Garden of Eden: the Toba super-eruption and the Late Pleistocene human population crash. *In*

McCoy, F. W., Heiken, G. (eds.) *Volcanic Hazards and Disasters in Human Antiquity*, Special Paper 345, Geological Society of America, chapter 6. pp. 71–82.

Rapprich, V., Čížek, D., Daniel, K., Firdawok, L., Habtamu, B., Hroch, T., Kopačková, V., Málek, J., Malík, J., Mišurec, J., Orgoň, A., Šebesta, J., Šíma, J., Tsigehana, T., Verner, K., Yewubinesh, B. 2013. *Explanation Booklet to the Set of Geoscience maps of Ethiopia at scale 1:50,000, subsheet 0738-C4 Awassa*. Technical report, Czech Geological Survey/Aquatest/Geological Survey of Ethiopia, Praha/Addis Ababa, Czech Republic/Ethiopia.

Rapprich, V., Žáček, V., Verner, K., Erban, V., Goslar, T., Bekele, Y., Legesa, F., Hroch, T., Hejtmánková, P. 2016. Wendo Koshe Pumice: The latest Holocene silicic explosive eruption product of the Corbetti Volcanic System (Southern Ethiopia). *Journal of Volcanology and Geothermal Research*, **310**, 159 – 171.

Rasmussen, T. L., Wastegård, S., Kuijpers, A., van Weering, T. C. E., Heinemeier, J., Thomsen, E. 2003. Stratigraphy and distribution of tephra layers in marine sediment cores from the Faeroe Islands, North Atlantic. *Marine Geology*, **199** (3-4), 263–277.

Rawson, H., Naranjo, J. A., Smith, V. C., Fontijn, K., Pyle, D. M., Mather, T. A., Moreno, H. 2015. The frequency and magnitude of post-glacial explosive eruptions at Volcán Mocho-Choshuenco, southern Chile. *Journal of Volcanology and Geothermal Research*, **299**, 103–129.

Reide, F., Bazely, O., Newton, A. J., Lane, C. S. 2011. A Laacher See-eruption supplement to Tephrabase: Investigating distal tephra fallout dynamics. *Quaternary International*, **246** (1-2), 134–144.

Reimer, P. J., Bard, E., Bayliss, A., Warren Beck, J., Blackwell, P. G., Bronk Ramsey, C., Buck, C. E., Cheng, H., Lawrence Edwards, R., Friedrich, M., Grootes, P. M., Guilderson, T. P., Haflidason, H., Hajdas, I., Hatté, C., Heaton, T. J., Hoffmann, D. L., Hogg, A. G., Hughen, K. A., Kaiser, K. F., Kromer, B., Manning, S. W., Niu, M., Reimer, R. W., Richards, D. A., Marian Scott, E., Southon, J. R., Staff, R. A., Turney, C. S. M., van der Plicht, J. 2013. IntCal13 and Marine13 radiocarbon age calibration curves 0-50,000 years cal BP. *Radiocarbon*, **55** (4), 1869–1887.

Renne, P. R., WoldeGabriel, G., Hart, W. K., Heiken, G., White, T. D. 1999. Chronostratigraphy of the Miocene-Pliocene Sagantole Formation, Middle Awash Valley, Afar rift, Ethiopia. *Geological Society of America Bulletin*, **111** (6), 869–885.

Rogers, N. 2015. Chapter 4 - The Composition and Origin of Magmas. *In* Sigurdsson, H. (ed.) *The Encyclopedia of Volcanoes (Second Edition)*, Academic Press, Amsterdam. Second edition edition, pp. 93 – 112.

Rollinson, H. 1993. *Using Geochemical Data: Evaluation, Presentation, Interpretation*. Geochemistry series, Longman Scientific & Technical.

Rooney, T. O., Hart, W. K., Hall, C. M., Ayalew, D., Ghiorso, M. S., Hidalgo, P., Yirgu, G. 2012. Peralkaline magma evolution and the tephra record in the Ethiopian Rift. *Contributions to Mineralogy and Petrology*, **164** (3), 407–426.

Rose, W. I., Chesner, C. A. 1987. Dispersal of ash in the great Toba eruption, 75 ka. *Geology*, **15** (10), 913–917.

Rose, W. I., Durant, A. J. 2009. Fine ash content of explosive eruptions. *Journal of Volcanology and Geothermal Research*, **186** (1-2), 32–39.

Sarna-Wojcicki, A. M., Meyer, C. E., Roth, P. H., Brown, F. H. 1985. Ages of tuff beds at East African early hominid sites and sediments in the Gulf of Aden. *Nature*, **313**, 306–308.

Sawamura, P., Vernier, J. P., Barnes, J. E., Berkoff, T. A., Welton, E., Alados-Arboledas, L., Navas-Guzmán, F., Pappalardo, G., Mona, L., Madonna, F., Lange, D., Sicard, M., Godin-Beekmann, S., Payen, G., Wang, Z., Hu, S., Tripathi, S. N., Cordoba-Jabonero, C., Hoff, R. M. 2012. Stratospheric AOD after the 2011 eruption of Nabro volcano measured by lidars over the Northern Hemisphere. *Environmental Research Letters*, **7** (3), 1–9.

Saylor, B. Z., Angelini, J., Deino, A., Alene, M., Fournelle, J. H., Haile-Selassie, Y. 2016. Tephrostratigraphy of the Waki-Mille area of the Woranso-Mille paleoanthropological research project, Afar, Ethiopia. *Journal of Human Evolution*, **93**, 25–45.

Shane, P. A., Smith, I. 2000. Geochemical fingerprinting of basaltic tephra deposits in the Auckland Volcanic Field. *New Zealand Journal of Geology & Geophysics*, **43** (4), 569–577.

Shane, P. A. R., Hoverd, J. 2002. Distal record of multi-sourced tephra in Onepoto Basin, Auckland, New Zealand: implications for volcanic chronology, frequency and hazards. *Bulletin of Volcanology*, **64** (7), 441–454.

Shuey, R. T., Brown, F. H., Croes, M. K. 1974. Magnetostratigraphy of the Shungura Formation, southwestern Ethiopia: Fine structure of the lower Matuyama polarity epoch. *Earth and Planetary Science Letters*, **23** (2), 249–260.

Siebert, L., Simkin, T., Kimberly, P. 2011. *Volcanoes of the World: Third Edition*. University of California Press.

Smeds, H. 1964. A Note on Recent Volcanic Activity on the Ethiopian Plateau, as Witnessed by a Rise of the Level of Lake Wonchi 1400 $\pm$ 140 B.P. *Acta Geographica*, **18** (1), 32.

Smith, D. G. W., Westgate, J. A. 1968. Electron probe technique for characterising pyroclastic deposits. *Earth and Planetary Science Letters*, **5**, 313–319.

Smith, V. C., Isaia, R., Pearce, N. J. G. 2011*a*. Tephrostratigraphy and glass compositions of post-15 kyr Campi Flegrei eruptions: implications for eruption history and chronostratigraphic markers. *Quaternary Science Reviews*, **30** (25-26), 3638–3660.

Smith, V. C., Pearce, N. J. G., Matthews, N. E., Westgate, J. A., Petraglia, M. D., Haslam, M., Lane, C. S., Korisettar, R., Pal, J. N. 2011*b*. Geochemical fingerprinting of the widespread Toba tephra using biotite compositions. *Quaternary International*, **246** (1-2), 97–104.

Smith, V. C., Shane, P. A. R., Smith, I. E. M. 2002. Tephrostratigraphy and geochemical fingerprinting of the Mangaone Subgroup tephra beds, Okataina Volcanic Centre, New Zealand. *New Zealand Journal of Geology and Geophysics*, **45** (2), 207–219.

Smith, V. C., Staff, R. A., Blockley, S. P. E., Bronk Ramsey, C., Nakagawa, T., Mark, D. F., Takemura, K., Danhara, T., Suigetsu 2006 Project Members. 2013. Identification and correlation of visible tephras in the Lake Suigetsu SG06 sedimentary archive, Japan: chronostratigraphic markers for synchronising

of east Asian/west Pacific palaeoclimatic records across the last 150 ka. *Quaternary Science Reviews*, **67**, 121–137.

Sørensen, H. 1974. *The Alkaline Rocks*. Wiley-Interscience publication, J. Wiley.

Sparks, R. S. J., Bursik, M. I., Ablay, G. J., Thomas, R. M. E., Carey, S. N. 1992. Sedimentation of tephra by volcanic plumes. Part 2: controls on thickness and grain-size variations of tephra fall deposits. *Bulletin of Volcanology*, **54** (8), 685–695.

Sparks, R. S. J., Bursik, M. I., Carey, S., Gilbert, J. G., Glaze, L. S., Sigurdson, H., Woods, A. 1997. *Volcanic Plumes*. John Wiley & Sons.

Sparks, R. S. J., Walker, G. P. L. 1977. The significance of vitric-enriched air-fall ashes associated with crystal-enriched ignimbrites. *Journal of Volcanology and Geothermal Research*, **2** (4), 329–341.

Swindles, G. T., Lawson, I. T., Savov, I. P., Connor, C. B., Plunkett, G. 2011. A 7000 yr perspective on volcanic ash clouds affecting northern Europe. *Geology*, **39** (9), 887–890.

Sylvester, P. 2008. Matrix effects in Laser Ablation-ICP-MS. *In Mineralogical Association of Canada Short Course 40*. pp. 67–78.

Taieb, M. 1974. *Evolution Quaternaire du Basin de l'Awash, Ethiopia*. Ph.D. thesis, University of Paris.

Takemura, K., Hayashida, A., Okamura, M., Matsouka, H., Ali, M., Kuniko, Y., Torii, M. 2000. Stratigraphy of multiple piston-core sediments for the last 30,000 years from Lake Biwa, Japan. *Journal of Paleolimnology*, **23** (2), 185–199.

Taylor, R. P., Jackson, S. E., Longerich, H. P., Webster, J. D. 1997. In situ trace-element analysis of individual silicate melt inclusions by laser ablation microprobe-inductively coupled plasma-mass spectrometry (LAM-ICP-MS). *Geochimica et Cosmochimica Acta*, **61** (13), 2559–2567.

Telford, R. J. 1998. *Diatom stratigraphies of Lake Awassa and Tilo, Ethiopia: Holocene records of groundwater variability and climate change*. Ph.D. thesis, University of Wales Aberystwyth.

Telford, R. J., Lamb, A. L. 1999. Groundwater-Mediated Response to Holocene Climatic Change Recorded by the Diatom Stratigraphy of an Ethiopian Crater Lake. *Quaternary Research*, **52** (1), 63–75.

Telford, R. J., Lamb, H., Umer, M. 1999. Diatom-derived palaeoconductivity estimates for Lake Awassa, Ethiopia: evidence for pulsed inflows of saline groundwater? *Journal of Paleolimnology*, **21** (4), 409–421.

Thompson, R. N. 1982. Magmatism of the British Tertiary volcanic province. *Scottish Journal of Geology*, **18** (1), 49.

Tomlinson, E. L., Thordarson, T., Müller, W., Thirlwall, M., Menzies, M. A. 2010. Microanalysis of tephra by LA-ICP-MS - Strategies, advantages and limitations assessed using the Thorsmörk ignimbrite (Southern Iceland). *Chemical Geology*, **279** (3-4), 73–89.

Tryon, C., Roach, N., Logan, M. 2008. The Middle Stone Age of the northern Kenyan Rift: age and context of new archaeological sites from the Kapedo Tuffs. *Journal of Human Evolution*, **55** (4), 652–664.

Turner, M. B., Bebbington, M. S., Cronin, S. J., Stewart, R. B. 2009. Merging eruption datasets: building an integrated Holocene eruptive record for Mt Taranaki, New Zealand. *Bulletin of Volcanology*, **71** (8), 903–918.

Turner, M. B., Cronin, S. J., Stewart, R. B., Bebbington, M., Smith, I. E. M. 2008. Using titanomagnetite textures to elucidate volcanic eruption histories. *Geology*, **36** (1), 31–34.

Turney, C. S. M. 1998. Extraction of rhyolitic component of Vedde microtephra from minerogenic lake sediments. *Journal of Paleolimnology*, **19** (2), 199–206.

Ukstins Peate, I., Baker, J. A., Kent, A. J. R., Al-Kadasi, M., Al-Subbary, A., Ayalew, D., Menzies, M. 2003. Correlation of Indian Ocean tephra to individual Oligocene silicic eruptions from Afro-Arabian flood volcanism. *Earth and Planetary Science Letters*, **211** (3-4), 311–327.

Ukstins Peate, I., Kent, A. J. R., Baker, J. A., Menzies, M. A. 2008. Extreme geochemical heterogeneity in Afro-Arabian Oligocene tephras: Preserving fractional crystallization and mafic recharge processes in silicic magma chambers. *Lithos*, **102** (1-2), 260–278.

Venuti, A., Verosub, K. L. 2010. Paleomagnetic record of basaltic volcanism from Pukaki and Onepoto maar lake cores, Auckland Volcanic Field, New Zealand. *New Zealand Journal of Geology and Geophysics*, **53** (1), 71–79.

Vogel, H., Zanchetta, G., Sulpizio, R., Wagner, B., Nowaczyk, N. 2010. A tephrostratigraphic record for the last glacial-interglacial cycle from Lake Ohrid, Albania and Macedonia. *Journal of Quaternary Science*, **25** (3), 320–338.

Žáček, V., Rapprich, V., Aman, Y., Berhanu, B., Čížek, D., Dereje, K., Erban, V., Ezra, T., Firdawok, L., Habtamu, M., Hroch, T., Kopačková, V., P. Kycl, J. M., Mišurec, J., Orgoň, A., Pécskay, Z., Šíma, J., Tarekegu, D., Verner, K. 2014. *Explanation booklet to the Set of Geoscience maps of Ethiopia at a scale 1 : 50,000: sub-sheet 0738-D3 Shashemene*. Technical report, Czech Geological Survey/Aquatest/Geological Survey of Ethiopia, Praha/Addis Ababa, Czech Republic/Ethiopia.

Walker, G. P. L. 1971. Grain-Size Characteristics of Pyroclastic Deposits. *The Journal of Geology*, **79** (6), 696–714.

Walker, G. P. L. 1973. Explosive volcanic eruptions - a new classification scheme. *International Journal of Earth Sciences*, **62** (2), 431–446.

Walter, R. C. 1989. Application and limitation of fission-track geochronology to Quarternary tephras. *Quaternary International*, **1**, 35–46.

Walter, R. C. 1994. Age of Lucy and the First Family: Single-crystal 40Ar/39Ar dating of the Denen Dora and lower Kada Hadar members of the Hadar Formation, Ethiopia. *Geology*, **22** (1), 6–10.

Walter, R. C., Aronson, J. 1993. Age and source of the Sidi Hakoma Tuff, Hadar Formation, Ethiopia. *Journal of Human Evolution*, **25**, 229–240.

Walter, R. C., Hart, W. K., Westgate, J. A. 1987. Petrogenesis of a basalt-rhyolite tephra from the west-central Afar, Ethiopia. *Contributions to Mineralogy and Petrology*, **95** (4), 462–480.

Wastegård, S. 2005. Late Quaternary tephrochronology of Sweden: a review. *Quaternary International*, **130** (1), 49–62.

Wastegård, S., Veres, D., Kliem, P., Hahn, A., Ohlendorf, C., Zolitschka, The PASADO Science Team. 2013. Towards a late Quaternary tephrochronological framework for the southernmost part of South America e the Laguna Potrok Aike tephra record. *Quaternary Science Reviews*, **71**, 81–90.

Watson, E. B. 1979. Zircon saturation in felsic liquids - Experimental results and applications to trace-element geochemistry. *Contributions to Mineralogy and Petrology*, **70** (4), 407–419.

Watt, G. R., Harley, S. L. 1993. Accessory phase controls on the geochemistry of crustal melts and restites produced during water undersaturated partial melting. *Contributions to Mineralogy and Petrology*, **101** (4), 220–231.

Webster, J. D., Taylor, R. P., Bean, C. 1993. Pre-eruptive melt composition and constraints on degassing of a water-rich pantellerite magma, Fantale volcano, Ethiopia. *Contributions to Mineralogy and Petrology*, **114** (1), 53–62.

Westgate, J. A., Pearce, N. J. G., Perkins, W. T., Preece, S. J., Chesner, C. A., Muhammad, R. F. 2013. Tephrochronology of the Toba tuffs: four primary glass populations define the 75-ka Youngest Toba Tuff, northern Sumatra, Indonesia. *Journal of Quaternary Science*, **28** (8), 772–776.

Westgate, J. A., Perkins, W. T., Fuge, R., Pearce, N. J. G., Wintle, A. G. 1994. Trace element analysis of volcanic glass shards by laser ablation inductively coupled plasma mass spectrometry: application to Quaternary tephrochronological studies. *Applied Geochemistry*, **9** (3), 323–355.

White, J. D. L., Riggs, R. 2001. *Volcaniclastic Sedimentation in Lacustrine Settings*, Blackwell Science, chapter Introduction: styles and significance of lacustrine volcaniclastic sedimentation. pp. 1–6.

Wiart, P., Oppenheimer, C. 2000. Largest known historical eruption in Africa: Dubbi volcano, Eritrea, 1861. *Geology*, **28** (4), 291–294.

Wiart, P., Oppenheimer, C. 2004. Large magnitude silicic volcanism in north Afar: the Nabro Volcanic Range and Ma'alalta volcano. *Bulletin of Volcanology*, **67** (2), 99–115.

Wilkinson, P., Mitchell, J. G., Cattermole, P. J., Downie, C. 1986. Volcanic chronology of the Men-Kilimanjaro region, Northern Tanzania. *Journal of the Geological Society*, **143**, 601–605.

WoldeGabriel, G. 1994. Ecological and temporal placement of early Pliocene hominids at Aramis. *Nature*, **371**, 330–333.

WoldeGabriel, G., Aronson, J. L., Walter, R. C. 1990. Geology, geochronology, and rift basin development in the central sector of the Main Ethiopia Rift. *Geological Society of America Bulletin*, **102** (4), 439–458.

WoldeGabriel, G., Endale, T., White, T. D., Thouveny, N., Hart, W. K., Renne, P. R., Asfaw, B. 2013. The role of tephra studies in African paleoanthropology as exemplified by the Sidi Hakoma Tuff. *Journal of African Earth Sciences*, **77**, 41–58.

WoldeGabriel, G., Haile-Selassie, Y., Renne, P. R., Hart, W. K., Ambrose, S. H., Asfaw, B., Heiken, G., White, T. 2001. Geology and palaeontology of the Late Miocene Middle Awash valley, Afar rift, Ethiopia. *Nature*, **412**, 175–178.

WoldeGabriel, G., Hart, W., Katoh, S., Beyene, Y., Suwa, G. 2005. Correlation of Plio-Pleistocene Tephra in Ethiopia and Kenyan rift basins: Temporal calibration of geological features and hominid fossil records. *Journal of Volcanology and Geothermal Research*, **147** (1-2), 81–108.

WoldeGabriel, G., Hart, W. K. 2005. Innovative tephra studies in the East African rift system. *Eos*, **86** (27), 255.

WoldeGabriel, G., Walker, R., Aronson, J. L., Hart, W. 1992. Geochronology and distribution of silicic volcanic rocks of Plio-Pleistocene age from the central sector of the Main Ethiopian Rift. *Quaternary International*, **13-14** (69-76).

WoldeGabriel, G., Walter, R. C., Hart, W. K., Mertzman, J. L., S. A. amd Aronson. 1999. Temporal relations in the geochemical features of felsic volcanism in the central sector of the Main Ethiopian Rift. *Acta Vulcanologica*, **11** (1), 53–67.

Wolfenden, E., Ebinger, C., Yirgub, G., Deino, A., Ayalew, D. 2004. Evolution of the northern Main Ethiopian rift: birth of a triple junction. *Earth and Planetary Science Letters*, **224** (1-2), 213–228.

Woods, A. W., Wohletz, K. 1991. Dimensions and dynamics of co-ignimbrite eruption columns. *Nature*, **350**, 225–227.

Wulf, S., Ott, F., Słowinski, M., Noryókiewicz, A. M., Dröger, N., Martin-Puertas, C., Czymzik, M., Neugebauer, I., Dulski, P., Bourne, A. J., Błaszkiewicz, M., Brauer, A. 2013. Tracing the Laacher See Tephra in the varved sediment record of the Trzechowskie palaeolake in central Northern Poland. *Quaternary Science Reviews*, **76**, 129–139.

Appendices

.1 Sample details

The inventory seen below can be used by future workers to locate samples for further study - contact information is given at the start of this section. Most lake sediment archives used in this study are stored at Aberyswtyth University, however the Dendi records are based at the University of Cologne. Processed Ashenge, Hayk and Chamo sediments, of different densities, are stored at Aberystwyth University and may yield additional cryptotephras through further study. Tephra and obsidian samples from Corbetti and Tilo are housed at Aberystwyth University, whilst Dubbi proximal samples are located at the University of Cambridge. For information regarding the epoxy resin stubs containing tephras for analysis, contact Catherine Martin-Jones (presently at Aberystwyth University).

Contact information

Catherine Martin-Jones	Department of Geography and Earth Sciences, Aberystwyth University	martinjonescatherine@gmail.com
Henry Lamb	Department of Geography and Earth Sciences, Aberystwyth University	hfl@aber.ac.uk
Nick Pearce	Department of Geography and Earth Sciences, Aberystwyth University	njp@aber.ac.uk
Christine Lane	School of Environment, Education and Development, University of Manchester	christine.lane@manchester.ac.uk
Frank Schaebitz	Seminar for Geography, University of Cologne	ape15@uni-koeln.de
Clive Oppenheimer	Department of Geography, University of Cambridge	co200@cam.ac.uk

Lake sediment core details

Site	Core name	c/o	Stored at	Notes
Ashenge	03AL3/2	Henry Lamb	Aberystwyth cold store	5 cm diameter, 1 long split cores in sealed plastic
Hayk	Hayk 2010	Henry Lamb	Aberystwyth cold store	5.8 cm diameter, 1 long split cores in sealed plastic
Dendi	DEN-1 and DEN-2	Frank Schaebitz	Seminar for Geography, Cologne	5.8 cm diameter, 1 long split cores in sealed plastic
Hora	Hora 2001	Henry Lamb	Aberystwyth boat house	5 cm diameter, 1 long split cores in sealed plastic
Awassa	AW-94	Henry Lamb	Aberystwyth boat house	5 cm diameter, 1 long split cores in sealed plastic
Tilo	T-97	Henry Lamb	Aberystwyth boat house	5 cm diameter, 1 long split cores in sealed plastic
Chamo	CHA-01-2010	Frank Schaebitz/Henry Lamb	Aberystwyth cold store	Sediment in 2 x 2 cm oriented cubes

Cryptotephra samples

Site	Core name	c/o	Stored at	Notes
Processed sediment samples in bagged test tubes - labelled according to core depth				
Ashenge	03AL3/2	Henry Lamb	Aberystwyth cold store	Whole core: 10 cm and 1 cm resolution sediment samples, which have been sieved to $> 25\ \mu$m then divided into < 1.95, $1.95 - 2.55$ and > 2.55 g/cm^3 densities. i.e. each sediment section is divided into 3 testubes
Hayk	Hayk 2010	Henry Lamb	Aberystwyth cold store	"
Chamo	CHA-01-2010	Henry Lamb	Aberystwyth cold store	Between 502-920 cm: 2 cm resolution sediment samples, which have been sieved to $> 25\ \mu$m then divided into < 1.95, $1.95 - 2.55$ and > 2.55 g/cm^3 densities. i.e. each sediment section is divided into 3 testubes
Cryptotephra slides for counting, $1.95 - 2.55$ *g/cm*^{3} *separates from the sediments - labelled according to core depth*				
Ashenge	03AL3/2	Henry Lamb	Aberystwyth cold store	Low res samples mounted in canada balsam. High res samples mounted in glycerin jelly, soluble in distilled warm water if further work required
Hayk	Hayk 2010	Henry Lamb	Aberystwyth cold store	Mounted in glycerin jelly, soluble in distilled warm water if further work required
Chamo	CHA-01-2010	Henry Lamb	Aberystwyth cold store	"

Proximal tephra samples

Site	Sample type	Sample label	c/o	Stored at
Corbetti	Obsidian thin section	E95010	Nick Pearce	
	Obsidian thin section	E95011	Nick Pearce	
	Obsidian thin section	E95019	Nick Pearce	
	Obsidian thin section	E95003	Nick Pearce	
	Bagged pumice	E95006	Nick Pearce	Llandinam A5 rock drawers
	Bagged pumice	E95007	Nick Pearce	Llandinam A5 rock drawers
	Auger sample	ST1-NW	Henry Lamb	Aberystwyth boat house
Tilo crater walls	Obsidian xenolith	E95025	Nick Pearce	Llandinam A5 rock drawers
	Bagged pumice	E97003	Nick Pearce	Llandinam A5 rock drawers
Dubbi	Bagged PDC	Dubbi 1861	Clive Oppenheimer	

EPMA/ LA-ICP-MS epoxy resin blocks

Visible and cryptotephras from lake sediment and outcrops mounted in 4 or 6 hole resin blocks, labelled on reverse with letter

EPMA session	Stub label	Sample sites	Tephra IDs	c/o
Feb-14	4 hole no label	Ashenge/ Dendi	AST-5, DT-1, DT-2, DT-3,	Catherine Martin-Jones
	6 hole no label	Ashenge	AST-1, AST-2, AST-8	"
	B	Tilo	TT-3, TT-4, TT-5	"
	C	Tilo	TT-6, TT-7, TT-8	"
	F	Tilo	TT-11, TT-12	"
	H	Tilo	TT-14, AT-1, AT-2, AT-4	"
Aug-14	A	Tilo	TT-1, TT-2	Catherine Martin-Jones
	D	Tilo	TT-8, TT-9	"
	E	Tilo	TT-10, TT-11	"
	G	Tilo	TT-13, TT-14	"
	B2	Corbetti	ST1-SW, ST1-NW, E97003, E97006	"
	C2	Ashenge/Hayk/Corbetti	AST-5, HT-1, HT-2, E95007	"
	D2	Corbetti/Dendi	E95002, DT1-1, DT1-2, DT1-3	"
	A3	Ashenge	AST-3, AST-4, AST-6, AST-7	"
	D3	Ashenge/Awassa/Hora	AST-9, AT-1, AT-2, HRT-1	"
Jun-15	A2	Awassa/Hora	AWT-4, AWT-7, HRT-2	Catherine Martin-Jones
	A	Hayk	HT-1, HT-3, HT-6, HT-10	"
	B	Hayk	HT-5, HT-9, HT-11, HT-12	"
	C	Hayk/Chamo	HT-7, HT-8, CHT-1, CHT-2	"
	D	Mochena Borago	BIS-1, BIS-2, M14 0.27m NW, M14 0.75m NE	"
	E	Dubbi/Mochena Borago	Dubbi 1, Dubbi 2, M14 0.47m SW, TU2	"

.2 Crypotephra glass shard counts

The following table gives glass shard concentrations in Ashenge, Hayk and Chamo lake sediments. Shard counting was first undertaken across continuous 10 cm regions in the sediments. At depths where high glass shard counts were identified, the relevant sections were resampled at a 1 cm resolutions, to identify the exact position of the cryptotephra. The Chamo sediments were only sampled at a 1 cm resolution. Shard counts are recorded per gram dry weight (gdw) sediment. Elevated glass shard counts at the 1 cm resolution, indicating cryptotephra horizons, are indicated in bold.

Tephra glass shard counts in the Ashenge, Hayk and Chamo lake sediments

Ashenge			Hayk			Chamo	
Core depth (cm)	**Shards per gdw 10 cm sample**	**Shards per gdw 1 cm sample**	**Core depth (cm)**	**Shards per gdw 10 cm sample**	**Shards per gdw 1 cm sample**	**Core depth (cm)**	**Shards per gdw 1 cm sample**
10	5000		0	2457	844	680	135
11	5000		1	2457	162	682	70
12	5000		2	2457	1103	684	25
13	5000		3	2457	798	686	28
14	5000		4	2457	247	688	31
15	5000		5	2457	549	690	16
16	5000		6	2457	313	692	63
17	5000		7	2457	333	694	111
18	5000		8	2457	172	696	515
19	5000		9	2457	44	698	1141
20	6250		10	841	314	700	4282
21	6250		11	841	220	702	**39826**
22	6250		12	841	312	704	501
23	6250		13	841	103	706	10
24	6250		14	841	60	708	25
25	6250		15	841	164	710	5
26	6250		16	841	161	712	32
27	6250		17	841	226	714	14
28	6250		18	841	281	716	20
29	6250		19	841	303	718	7
30	5000		20	140		720	22
31	5000		21	140		724	52
32	5000		22	140		726	47
33	5000		23	140		728	62
34	5000		24	140		732	68
35	5000		25	140		734	123
36	5000		26	140		736	183
37	5000		27	140		738	339
38	5000		28	140		740	315
39	5000		29	140		742	71
40	109		30	393	49	744	46
41	109		31	393	66	746	47
42	109		32	393	70	748	4
43	109		33	393	90	750	3
44	109		34	393	131	752	34
45	109		35	393	288	754	8
46	109		36	393	296	756	7
47	109		37	393	102	758	50
48	109		38	393	207	760	1641
49	109		39	393	144	761	26
50	89		40	150		763	9
51	89		41	150		765	24
52	89		42	150		767	57
53	89		43	150		769	131
54	89		44	150		771	16
55	89		45	150		773	28
56	89		46	150		775	38
57	89		47	150		777	13
58	89		48	150		779	132

Continued on next page

Tephra glass shard counts in the Ashenge, Hayk and Chamo lake sediments

Ashenge			Hayk			Chamo	
Core depth (cm)	Shards per gdw 10 cm sample	Shards per gdw 1 cm sample	Core depth (cm)	Shards per gdw 10 cm sample	Shards per gdw 1 cm sample	Core depth (cm)	Shards per gdw 1 cm sample
59	89		49	150		781	99
60	274		50	150		783	46
61	274		51	104		785	60
62	274		52	104		787	124
63	274		53	104		789	161
64	274		54	104		791	224
65	274		55	104		793	84
66	274		56	104		795	202
67	274		57	104		797	182
68	274		58	104		799	136
69	274		59	104		803	344
70	112		60	399	43	805	161
71	112		61	399	26	807	43
72	112		62	399	148	809	188
73	112		63	399	955	811	101
74	112		64	399	148	813	9
75	112		65	399	**22358**	815	5
76	112		66	399	213	817	84
77	112		67	399	104	819	8
78	112		68	399	490	821	1
79	112		69	399	250	823	0
80	125		70	399	391	825	0
81	125		71	529	97	827	0
82	125		72	529	202	829	0
83	125		73	529	269	831	0
84	125		74	529	353	833	0
85	125		75	529	292	835	0
86	125		76	529	148	837	0
87	125		77	529	286	839	0
88	125		78	529	322	841	0
89	125		79	529	420	843	0
90	234		80	644	87	845	1
91	234		81	644	208	847	97
92	234		82	644	245	849	6
93	234		83	644	240	851	36
94	234		84	644	94	853	0
95	234		85	644	205	855	0
96	234		86	644	287	857	0
97	234		87	644	461	859	26
98	234		88	644	816	861	23
99	234		89	644	772	863	0
100	0		90	1109		865	2
101	0		91	1109		867	22
102	0		92	1109		869	0
103	0		93.5	1109		871	0
104	0		94.5	3506		873	0
105	0		95.5	3506		875	0
106	0		96.5	3506		877	0
107	0		97.5	3506		879	0
108	0		98.5	3506		881	0
109	0		99.5	3506		883	0
110	1505		100.5	3506		885	0
111	1505	4765	101.5	3506		887	148
112	1505	8667	102.5	3506		889	0
113	1505	15867	103.5	3506		891	2
114	1505	10462	104.5	3172		893	1
115	1505	20615	105.5	3172		895	0
116	1505	38692	106.5	3172		897	2
117	1505	38000	107.5	3172		899	0
118	1505	4667	108.5	3172		901	4
119	1505	7286	109.5	3172		903	0
120	1659	5571	110.5	3172		905	1
121	1659		111.5	3172		907	0
122	1659		112.5	3172		911	0
123	1659		113.5	4551	10367	913	0
124	1659		114.5	4551	228	915	3
125	1659		115.5	4551	158	917	100
126	1659		116.5	4551	1100	919	544
127	1659		117.5	4551	**14909**	921	2
128	1659		118.5	4551	484	923	3
129	1659		119.5	4551	112		
130	301		120.5	4551	344		
131	301	8429	121.5	4551	101		
132	301	4158	122.5	4551	83		
133	301	3476	123.5	4551			
134	301	706	124.5	2618			
135	301	308	125.5	2618			
136	301	765	126.5	2618			
137	301	1200	127.5	2618			
138	301	692	128.5	2618			
139	301	2125	129.5	2618			
140	825	900	130.5	2618			
141	825		131.5	2618			

Continued on next page

Tephra glass shard counts in the Ashenge, Hayk and Chamo lake sediments

Ashenge			Hayk			Chamo	
Core depth (cm)	Shards per gdw 10 cm sample	Shards per gdw 1 cm sample	Core depth (cm)	Shards per gdw 10 cm sample	Shards per gdw 1 cm sample	Core depth (cm)	Shards per gdw 1 cm sample
142	825		132.5	2618			
143	825		133.5	2618			
144	825		134.5	2618			
145	825		135.5	2618			
146	825		136.5	2618			
147	825		137.5	2618			
148	825		138.5	2618			
149	825		139.5	2618			
150	102		140.5	2618			
151	102		141.5	2618			
152	102		142.5	2618			
153	102		143.5	2618			
154	102		144.5	1549			
155	102		145.5	1549			
156	102		146.5	1549			
157	102		147.5	1549			
158	102		148.5	1549			
159	102		149.5	1549			
160	10		150.5	1549			
161	10		151.5	1549			
162	10		152.5	1549			
163	10		153.5	1549	80		
164	10		154.5	1549	216		
165	10		155.5	422	88		
166	10		156.5	422	120		
167	10		157.5	422	199		
168	10		158.5	422	**9925**		
169	10		159.5	422	108		
170	47		160.5	422	281		
171	47		161.5	422	884		
172	47		162.5	422	629		
173	47		163.5	422	87		
174	47		164.5	356	179		
175	47		165.5	356	78		
176	47		166.5	356	190		
177	47		167.5	356	**8898**		
178	47		168.5	356	56		
179	47		169.5	356	40		
180	51		170.5	356	198		
181	51		171.5	356	89		
182	51		172.5	356	73		
183	51						
184	51		177.5	2161	173		
185	51		178.5	2161	205		
186	51		179.5	2161	**21409**		
187	51		180.5	2161	3920		
188	51		181.5	2161	69		
189	51		182.5	2161	638		
190	19		183.5	2161	63		
191	19		184.5	2161	98		
192	19		185.5	2161	92		
193	19		186.5	2161	26		
194	19		187.5	611			
195	19		188.5	611			
196	19		189.5	611			
197	19		190.5	611			
198	19		191.5	611			
199	19		192.5	611			
200	20		193.5	611			
201	833	82467	194.5	611			
202	833	25786	195.5	611			
203	833	4500	196.5	611			
204	833	7077	197.5	622	19		
205	833	3714	198.5	622	**3446**		
206	833	2056	199.5	622	50		
211	233		200.5	622	47		
212	233		201.5	622	9		
213	233		202.5	622	83		
214	233		203.5	622	182		
215	233		204.5	622	226		
216	233		205.5	622	46		
217	233		206.5	622	182		
218	233		207.5	93			
219	233		208.5	93			
220	233		209.5	93			
221	153		210.5	93			
222	153		211.5	93			
223	153		212.5	77			
224	153		213.5	77			
225	153		214.5	77			
226	153		215.5	77			
227	153		216.5	77			
228	153		217.5	77			

Continued on next page

Tephra glass shard counts in the Ashenge, Hayk and Chamo lake sediments

Ashenge			Hayk			Chamo	
Core depth (cm)	Shards per gdw 10 cm sample	Shards per gdw 1 cm sample	Core depth (cm)	Shards per gdw 10 cm sample	Shards per gdw 1 cm sample	Core depth (cm)	Shards per gdw 1 cm sample
229	153		218.5	77			
230	153		219.5	77			
231	304		220.5	77			
232	304		221.5	77			
233	304		222.5	9			
234	304		223.5	9			
235	304		224.5	9			
236	304		225.5	9			
237	304		226.5	9			
238	304		227.5	9			
239	304		228.5	9			
240	304		229.5	9			
241	146		230.5	9			
242	146		231.5	9			
243	146		232.5	36			
244	146		233.5	36			
245	146		234.5	36			
246	146		235.5	36			
247	146		236.5	36			
248	146		237.5	36			
249	146		238.5	36			
250	146		239.5	36			
251	254		240.5	36			
252	254		241.5	36			
253	254		242.5	23			
254	254		243.5	23			
255	254		244.5	23			
256	254		245.5	23			
257	254		246.5	23			
258	254		247.5	23			
259	254		248.5	23			
260	254		249.5	23			
261	210		250.5	23			
262	210		251.5	23			
263	210		252.5	283			
264	210		253.5	283			
265	210		254.5	283			
266	210		255.5	283			
267	210		256.5	283			
268	210		257.5	283			
269	210		258.5	283			
270	210		259.5	283			
271	339		260.5	283			
272	339		261.5	7390	104		
273	339		264.5	7390	88		
274	339		265.5	7390	102		
275	339		266.5	7390	**7539**		
276	339		267.5	7390	20		
277	339		268.5	7390	123		
278	339		269.5	7390	15		
279	339		270.5	7390	1040		
280	339		280	7390	27		
281	587	2923	281	7390	14		
282	587	3667	282	7390	17		
283	587	4364	283	7390	27		
284	587	4000	284	7390	59		
285	587	2615	285	7390	84		
286	587	3071	286	7390	245		
287	587	5316	287	7390	1182		
288	587	5294	288	7390	**19741**		
289	587	4762	289	7390	11		
290	587	5000	290	2			
291	116		291	2			
292	116		292	2			
293	116		293	2			
294	116		294	2			
295	116		295	2			
296	116		296	2			
297	116		297	2			
298	116		298	2			
299	116		299	2			
300	116		300	2			
301	137		301	2			
302	137		302	5			
303	137		303	5			
304	137		304	5			
305	137		305	5			
306	137		306	5			
307	137		307	5			
308	137		308	5			
309	137		309	5			
310	137		310	5			
311	0		311	5			

Continued on next page

Tephra glass shard counts in the Ashenge, Hayk and Chamo lake sediments

Ashenge			Hayk			Chamo	
Core depth (cm)	Shards per gdw 10 cm sample	Shards per gdw 1 cm sample	Core depth (cm)	Shards per gdw 10 cm sample	Shards per gdw 1 cm sample	Core depth (cm)	Shards per gdw 1 cm sample
312	0		312	5			
313	0		313	6			
314	0		314	6			
315	0		315	6			
316	0		316	6			
317	0		317	6			
318	0		318	6			
319	0		319	6			
320	0		320	6			
321	89		321	6			
322	89		322	6			
323	89		323	6			
324	89		324	6			
325	89		325	6			
326	89		326	6			
327	89		327	6			
328	89		328	6			
329	89		329	6			
330	89		330	6			
331	41		331	9			
332	41		332	9			
333	41		333	9			
334	41		334	9			
335	41		335	9			
336	41		336	9			
337	41		337	9			
338	41		338	9			
339	41		339	9			
340	41		340	9			
341	187		341	6			
342	187		342	6			
343	187		343	6			
344	187		344	6			
345	187		345	6			
346	187		346	6			
347	187		347	6			
348	187		348	6			
349	187		349	6			
350	187		350	6			
351	49		351	6			
352	49		352	6			
353	49		353	2			
354	49		354	2			
355	49		355	2			
356	49		356	2			
357	49		357	2			
358	49		358	2			
359	49		359	2			
360	49		360	2			
361	151		361	2			
362	151		362	2			
363	151		363	2			
364	151		364	11			
365	151		365	11			
366	151		366	11			
367	151		367	11			
368	151		368	11			
369	151		369	11			
370	151		370	11			
371	127		371	11			
372	127		372	11			
373	127		373	11			
374	127		374	7			
375	127		375	7			
376	127		376	7			
377	127		377	7			
378	127		378	7			
379	127		379	7			
380	127		380	7			
381	64		381	7			
382	64		382	336			
383	64		383	336			
384	64		384	336	7		
385	64		385	336	141		
386	64		386	336	**3015**		
387	64		387	336	2		
388	64		388	336	6		
389	64		389	336	8		
390	64		390	336	5		
391	29		392.5	336	10		
392	29		393	336	1		
393	29		394	7			
394	29		395	7			

Continued on next page

Tephra glass shard counts in the Ashenge, Hayk and Chamo lake sediments

Ashenge			Hayk			Chamo	
Core depth (cm)	Shards per gdw 10 cm sample	Shards per gdw 1 cm sample	Core depth (cm)	Shards per gdw 10 cm sample	Shards per gdw 1 cm sample	Core depth (cm)	Shards per gdw 1 cm sample
395	29		396	7			
396	29		397	7			
397	29		398	7			
398	29		399	7			
399	29		400	7			
400	29		401	7			
401	195		402	7			
402	195		403	7			
403	195		404	5			
404	195		405	5			
405	195		406	5			
406	195		407	5			
407	195		408	5			
408	195		409	5			
409	195		410	5			
410	195		411	5			
411	39		412	5			
412	39		413	5			
413	39		414	5			
414	39		415	10			
415	39		416	10			
416	39		417	10			
417	39		418	10			
418	39		419	10			
419	39		420	10			
420	39		421	10			
421	192		422	10			
422	192		423	10			
423	192		424	2235			
424	192		425	2235			
425	192		426	2235			
426	192		427	2235			
427	192		428	2235			
428	192		429	2235			
429	192		430	2235			
430	192		431	2235			
431	2089		432	2235			
432	2089		433	2235			
433	2089		434	2235			
434	2089		435	2235			
435	2089		436	2235			
436	2089		437	2235			
437	2089		438	2235			
438	2089		439	2235			
439	2089		440	2235			
440	2089		441	2235			
441	6250		442	2235			
442	6250		443	2235			
443	6250		444	2235			
444	6250		445	4399			
445	6250		446	4399			
446	6250		447	4399			
447	6250		448	4399			
448	6250		449	4399			
449	6250		450	4399			
450	6250		451	4399			
451	2250		452	4399			
452	2250		453	4399			
453	2250		454	4399			
454	2250		455	4399			
455	2250		455.5	9606	2467		
456	2250		456.5	9606	910		
457	2250		457.5	9606	775		
458	2250		458.5	9606	133		
459	2250		459.5	9606	1078		
460	2250		460.5	9606	**56220**		
461	84		461.5	9606	6540		
462	84		462.5	9606	69		
463	84		463.5	9606	37		
464	84		464.5	9606	12		
465	84		465.5	9606	56		
466	84		466.5	106			
467	84		467.5	106			
468	84		468.5	106			
469	84		469.5	106			
470	84		470.5	106			
471	231		471.5	106			
472	231		472.5	106			
473	231		473.5	106			
474	231		474.5	106			
475	231		475.5	106			
476	231		476.5	6			
477	231		477.5	6			

Continued on next page

Tephra glass shard counts in the Ashenge, Hayk and Chamo lake sediments

Ashenge			Hayk			Chamo	
Core depth (cm)	Shards per gdw 10 cm sample	Shards per gdw 1 cm sample	Core depth (cm)	Shards per gdw 10 cm sample	Shards per gdw 1 cm sample	Core depth (cm)	Shards per gdw 1 cm sample
478	231		478.5	6			
479	231		479.5	6			
480	231		480.5	6			
481	1294	22083	481.5	6			
482	1294	33833	482.5	6			
483	1294	132714	483.5	6			
484	1294	182625	484.5	6			
485	1294	**277250**	485.5	6			
486	1294	8600	486.5	3			
487	1294	18429	487.5	3			
488	1294	16125	488.5	3			
489	1294	19333	489.5	3			
490	1294	23667	490.5	3			
491	293		491.5	3			
492	293		492.5	3			
493	293		493.5	3			
494	293		494.5	3			
495	293		495.5	3			
496	293		496.5	3			
497	293		497.5	2			
498	293		498.5	2			
499	293		499.5	2			
500	293		500.5	2			
501	96		501.5	2			
502	96		502.5	2			
503	96		503.5	2			
504	96		504.5	2			
505	96		505.5	2			
506	96		506.5	2			
507	96		507.5	2			
508	96		508.5	2			
509	96		509.5	2			
510	96		510.5	2			
511	282		511.5	2			
512	282		512.5	2			
513	282		513.5	2			
514	282		514.5	2			
515	282		515.5	2			
516	282		516.5	1			
517	282		517.5	1			
518	282		518.5	1			
519	282		519.5	1			
520	282		520.5	1			
521	3846	42400	521.5	1			
522	3846	22500	522.5	1			
523	3846	42700	523.5	1			
524	3846	155500	524.5	1			
525	3846	198571	525.5	1			
526	3846	291563	526.5	1			
527	3846	**697643**	527.5	1			
528	3846	55583	528.5	1			
529	3846	28833	529.5	1			
530	3846	22923	530.5	1			
531	63		531.5	1			
532	63		532.5	1			
533	63		533.5	1			
534	63		534.5	1			
535	63		535.5	1			
536	63		536.5	2			
537	63		537.5	2			
538	63		538.5	2			
539	63		539.5	2			
540	63		540.5	2			
541	64		541.5	2			
542	64		542.5	2			
543	64		543.5	2			
544	64		544.5	2			
545	64		545.5	2			
546	64		546.5	2			
547	64		547.5	1			
548	64		548.5	1			
549	64		549.5	1			
550	64		550.5	1			
551	90		551.5	1			
552	90		552.5	1			
553	90		553.5	1			
554	90		554.5	1			
555	90		555.5	1			
556	90		556.5	2			
557	90		557.5	2			
558	90		558.5	2			
559	90		559.5	2			
560	90		560.5	2			

Continued on next page

Tephra glass shard counts in the Ashenge, Hayk and Chamo lake sediments

Ashenge			Hayk			Chamo	
Core depth (cm)	Shards per gdw 10 cm sample	Shards per gdw 1 cm sample	Core depth (cm)	Shards per gdw 10 cm sample	Shards per gdw 1 cm sample	Core depth (cm)	Shards per gdw 1 cm sample
561	135		561.5	2			
562	135		562.5	2			
563	135		563.5	2			
564	135		564.5	2			
565	135		565.5	2			
566	135		566.5	2			
567	135		567.5	2			
568	135		568.5	2			
569	135		569.5	2			
570	135		570.5	2			
571	239		571.5	2			
572	239		572.5	2			
573	239		573.5	2			
574	239		574.5	2			
575	239		575.5	2			
576	239		576.5	11			
577	239		577.5	11			
578	239		578.5	11			
579	239		579.5	11			
580	239		580.5	11			
581	151		581.5	11			
582	151		582.5	11			
583	151		583.5	11			
584	151		584.5	11			
585	151		585.5	11			
586	151						
587	151						
588	151						
589	151						
590	151						
591	5000						
592	5000						
593	5000						
594	5000						
595	5000						
596	5000						
597	5000						
598	5000						
599	5000						
600	5000						
601	5000						
602	5000						
603	5000						
604	5000						
605	5000						
606	5000						
607	5000						
608	5000						
609	5000						
610	5000						
611	837						
612	837						
613	837						
614	837						
615	837						
616	837						
617	837						
618	837						
619	837						
620	837						
621	3905	26200					
622	3905	43588					
623	3905	100222					
624	3905	**350345**					
625	3905	53708					
626	3905	17625					
627	3905	24105					
628	3905	18462					
629	3905	43850					
630	3905	37063					
631	3905	33533					
632	766	6619					
633	766	31065					
634	766	51217					
635	766	**135794**					
636	766	9297					
637	766	24621					
638	766	19733					
639	766	9063					
640	766	20917					
641	766	24130					
642	380						
643	380						

Continued on next page

Tephra glass shard counts in the Ashenge, Hayk and Chamo lake sediments

Ashenge			Hayk			Chamo	
Core depth (cm)	Shards per gdw 10 cm sample	Shards per gdw 1 cm sample	Core depth (cm)	Shards per gdw 10 cm sample	Shards per gdw 1 cm sample	Core depth (cm)	Shards per gdw 1 cm sample
644	380						
645	380						
646	380						
647	380						
648	380						
649	380						
650	380						
651	3						
652	3						
653	3						
654	3						
655	3						
656	3						
657	3						
658	3						
659	3						
660	3						
661	11						
662	11						
663	11						
664	11						
665	11						
666	11						
667	11						
668	11						
669	11						
670	11						
671	4						
672	4						
673	4						
674	4						
675	4						
676	4						
677	4						
678	4						
679	4						
680	4						
681	10						
682	10						
683	10						
684	10						
685	10						
686	10						
687	10						
688	10						
689	10						
690	10						
691	12						
692	12						
693	12						
694	12						
695	12						
696	12						
697	12						
698	12						
699	12						
700	12						
701	16						
702	16						
703	16						
704	16						
705	16						
706	16						
707	16						
708	16						
709	16						
710	16						
711	1						
712	1						
713	1						
714	1						
715	1						
716	1						
717	1						
718	1						
719	1						
720	1						
721	3						
722	3						
723	3						
724	3						
725	3						
726	3						

Continued on next page

Tephra glass shard counts in the Ashenge, Hayk and Chamo lake sediments

Ashenge			Hayk			Chamo	
Core depth (cm)	Shards per gdw 10 cm sample	Shards per gdw 1 cm sample	Core depth (cm)	Shards per gdw 10 cm sample	Shards per gdw 1 cm sample	Core depth (cm)	Shards per gdw 1 cm sample
727	3						
728	3						
729	3						
730	3						
731	5005						
732	5005						
733	5005						
734	5005						
735	5005						
736	5005						
737	5005						
738	5005						
739	5005						
740	5005						
741	3130						
742	3130						
743	3130						
744	3130						
745	3130						
746	3130						
747	3130						
748	3130						
749	3130						
750	3130						
754	6741	4648					
755	6741	12214					
756	6741	60925					
757	6741	173216					
758	6741	**691803**					
759	6741	273865					
760	6741	15235					
761	6741	1294					
762	6741	3125					
763	6741	3962					
764	1042						
765	1042						
766	1042						
767	1042						
768	1042						
769	1042						
770	1042						
771	1823						
772	1823						
773	1823						
774	1823						
775	1823						
776	1823						
777	1823						
778	1823						
779	1823						
780	1823						
781	720						
782	720						
783	720						
784	720						
785	720						
786	720						
787	720						
788	720						
789	720						
790	720						
791	2951	25438					
792	2951	32109					
793	2951	10838					
794	2951	17964					
795	2951	36397					
796	2951	25962					
797	2951	16817					
798	2951	15319					
799	2951	12837					
800	2951	14774					

.3 Tephras from the Ethiopian Highlands

This Appendix firstly provides the glass compositions of tephras from the Ethiopian Highlands. In the latter part of this section, the Oxcal code used to make Bayesian age models for the Ashenge and Hayk archives is provided.

.3.1 Major and trace element glass compositions

The following tables give shard-specific major and trace element concentrations in the Ashenge and Hayk tephras. Major and trace element analysis of Dubbi 1861 (collected by C. Oppenheimer, University of Cambridge) proximal deposits are given on page 338. Major elements are presented to 2 decimal places and trace elements to 3 significant figures, for the raw data the reader is referred to the electronic version.

Some major elements (e.g. Cl) were not analysed on all analytical sessions, and these are left blank. All Fe is calculated as FeO^T. Lower limits of detection (LLD) for EPMA analyses are given on page 401. The median LLD for the rhyolitic ATHO-G reference material over all EPMA analytical sessions is given in the following table headings. Most major elements occur at concentrations above the LLD in the Ashenge, Hayk and Dubbi glass shards, except MgO, MnO and P_2O_5 which are present in some shards at very low concentrations.

Trace element analyses were typically undertaken using 20 μm crater diameters, however, †indicates glass shards were analysed using 10 μm crater diameters. Lower limits of detection for LA-ICP-MS analyses are given on page 407. The median LLD concentrations at 20 μm crater diameters of all LA-ICP-MS analytical sessions are given beneath each analyte heading in the following tables. Due to high Sr and Ba concentrations in the gas blanks, coupled

with frequent low sample concentrations, some negative concentrations were measured - these are indicated with a dash.

Analyses of MPI-DING reference materials were used to check the EPMA and LA-ICP-MS calibrations. These analyses are given on page 398, and are ordered by analysis date.

Unnormalised major element concentrations (wt.%) in Ashenge glass shards

Label	Tephra	Analysis date	SiO_2 0.08	TiO_2 0.05	Al_2O_3 0.05	MgO 0.04	FeO^T 0.08	MnO 0.07	CaO 0.04	Na_2O 0.08	K_2O 0.03	P_2O_5 0.10	Cl 0.02	Total
A03AL2/1	AST-1	20/02/14	69.75	0.18	13.20	0.00	3.40	0.11	0.49	5.84	4.76	0.02	0.23	97.97
A03AL2/2	AST-1	20/02/14	68.07	0.27	12.98	0.01	3.38	0.11	0.43	5.58	4.67	0.01	0.24	95.76
A03AL2/3	AST-1	20/02/14	70.56	0.24	13.35	0.00	3.54	0.07	0.34	5.78	4.77	0.05	0.18	98.88
A03AL2/4	AST-1	20/02/14	64.24	0.24	12.02	0.03	3.47	0.09	0.44	5.35	4.28	0.01	0.23	90.40
A03AL2/5	AST-1	20/02/14	69.89	0.24	13.43	0.00	3.65	0.15	0.46	5.91	4.64	0.00	0.17	98.55
A03AL2/6	AST-1	20/02/14	67.69	0.23	12.60	0.00	3.58	0.07	0.44	5.97	4.63	0.00	0.19	95.40
A03AL2/7	AST-1	20/02/14	71.12	0.23	13.65	0.00	3.39	0.06	0.37	6.03	4.78	0.00	0.20	99.83
A03AL2/8	AST-1	20/02/14	70.52	0.21	14.26	0.00	3.13	0.11	0.34	6.30	4.65	0.02	0.16	99.70
A03AL2/9	AST-1	20/02/14	69.58	0.23	13.63	0.02	3.68	0.12	0.48	5.72	4.69	0.03	0.22	98.40
A03AL2/10	AST-1	20/02/14	67.74	0.22	12.69	0.00	3.49	0.06	0.44	5.73	4.68	0.02	0.19	95.24
A03AL2/11	AST-1	20/02/14	67.46	0.19	14.93	0.00	2.54	0.03	0.32	5.37	5.55	0.02	0.14	96.54
03AL2439/1	AST-2	20/02/14	69.67	0.21	12.72	0.01	3.73	0.14	0.37	5.94	4.75	0.03	0.21	97.78
03AL2439/2	AST-2	20/02/14	69.84	0.24	12.58	0.00	3.79	0.12	0.41	5.86	4.68	0.01	0.21	97.75
03AL2439/3	AST-2	20/02/14	70.70	0.25	12.54	0.00	3.81	0.15	0.36	5.84	4.83	0.00	0.21	98.69
03AL2439/4	AST-2	20/02/14	69.98	0.26	13.40	0.00	3.93	0.16	0.43	6.03	4.62	0.00	0.18	98.99
03AL2439/5	AST-2	20/02/14	68.60	0.22	12.39	0.02	3.71	0.11	0.42	5.96	4.69	0.03	0.19	96.34
03AL2439/6	AST-2	20/02/14	69.26	0.26	13.43	0.00	3.75	0.15	0.43	6.04	4.68	0.04	0.12	98.16
03AL2439/7	AST-2	20/02/14	69.25	0.30	12.28	0.02	3.67	0.11	0.37	5.59	4.67	0.02	0.19	96.46
03AL2439/8	AST-2	20/02/14	68.31	0.24	12.43	0.00	3.90	0.07	0.39	5.88	4.64	0.05	0.19	96.10
03AL2439/9	AST-2	20/02/14	70.81	0.25	12.56	0.00	3.77	0.13	0.37	6.28	4.46	0.03	0.19	98.84
03AL2439/10	AST-2	20/02/14	65.35	0.27	11.98	0.00	3.97	0.04	0.40	5.71	4.63	0.00	0.20	92.55
03AL2439/11	AST-2	20/02/14	67.96	0.29	12.21	0.00	3.63	0.14	0.39	5.30	4.68	0.00	0.18	94.77
03AL2439/12	AST-2	20/02/14	67.27	0.26	11.93	0.00	3.84	0.05	0.22	5.74	4.56	0.03	0.23	94.13
03AL2439/14	AST-2	20/02/14	67.95	0.25	12.29	0.01	3.62	0.14	0.40	5.55	4.59	0.00	0.21	95.00
03AL2439/15	AST-2	20/02/14	70.53	0.22	13.49	0.02	3.33	0.12	0.36	5.88	4.80	0.01	0.19	98.95
03AL2439/16	AST-2	20/02/14	66.22	0.24	13.02	0.00	3.13	0.06	0.30	5.72	4.57	0.02	0.15	93.43
03AL2439/17	AST-2	20/02/14	67.37	0.19	12.24	0.00	3.63	0.05	0.41	5.38	4.63	0.00	0.19	94.10
03AL2439/18	AST-2	20/02/14	69.06	0.23	13.42	0.00	3.21	0.10	0.32	6.29	4.46	0.03	0.16	97.29
03AL2439/19	AST-2	20/02/14	69.32	0.28	12.30	0.02	3.80	0.20	0.52	5.95	4.57	0.00	0.20	97.16
03AL2439/20	AST-2	20/02/14	70.96	0.25	12.97	0.00	4.00	0.09	0.38	5.85	4.89	0.03	0.18	99.60
03AL2439/21	AST-2	20/02/14	68.63	0.21	13.36	0.00	3.32	0.15	0.39	5.90	4.66	0.00	0.14	96.76
AST-3_1	AST-3	26/08/14	70.53	0.30	9.85	0.02	5.35	0.18	0.24	5.65	4.25	0.01		96.38
AST-3_3	AST-3	26/08/14	71.28	0.33	9.96	0.00	5.21	0.12	0.29	6.12	4.40	0.00		97.70
AST-3_4	AST-3	26/08/14	70.17	0.30	9.70	0.02	5.01	0.14	0.26	5.67	4.28	0.00		95.55
AST-3_6	AST-3	26/08/14	71.63	0.30	9.82	0.00	5.12	0.14	0.28	5.65	4.47	0.06		97.48
AST-3_7	AST-3	26/08/14	71.57	0.31	9.58	0.00	5.38	0.20	0.30	5.57	4.34	0.01		97.27
AST-3_9	AST-3	26/08/14	69.35	0.33	9.31	0.01	5.09	0.12	0.28	5.52	4.07	0.01		94.08
AST-3_10	AST-3	26/08/14	70.42	0.38	9.67	0.01	5.24	0.18	0.30	5.59	4.36	0.03		96.18
AST-3_12	AST-3	26/08/14	71.67	0.29	9.61	0.03	5.01	0.15	0.26	5.56	4.25	0.00		96.83
AST-3_14	AST-3	26/08/14	72.72	0.28	9.70	0.00	5.43	0.15	0.28	5.74	4.50	0.00		98.81
AST-3_15	AST-3	26/08/14	71.47	0.31	9.59	0.01	5.19	0.16	0.31	5.48	4.36	0.00		96.89
AST-3_16	AST-3	26/08/14	72.19	0.37	9.89	0.00	5.34	0.21	0.31	5.81	4.38	0.01		98.50
AST-3_18	AST-3	26/08/14	70.51	0.30	9.68	0.00	5.11	0.19	0.27	5.69	4.25	0.00		96.01
AST-3_19	AST-3	26/08/14	72.51	0.33	9.87	0.04	5.21	0.22	0.27	5.68	4.31	0.03		98.47
AST-3_20	AST-3	26/08/14	71.00	0.35	9.77	0.03	5.07	0.16	0.28	5.22	4.21	0.01		96.10
AST-4_1	AST-4	26/08/14	72.08	0.34	8.98	0.00	5.42	0.18	0.21	5.78	4.31	0.04		97.34
AST-4_2	AST-4	26/08/14	71.87	0.31	8.94	0.00	5.14	0.19	0.28	5.38	4.27	0.00		96.38
AST-4_3	AST-4	26/08/14	70.34	0.24	8.78	0.01	5.24	0.18	0.27	5.48	4.28	0.00		94.82
AST-4_4	AST-4	26/08/14	71.57	0.37	8.94	0.01	5.27	0.19	0.27	5.56	4.22	0.00		96.41
AST-4_5	AST-4	26/08/14	70.92	0.37	9.06	0.00	5.14	0.15	0.23	5.52	4.18	0.00		95.56
AST-4_6	AST-4	26/08/14	68.95	0.30	8.68	0.00	5.25	0.09	0.29	5.47	4.08	0.04		93.16
AST-4_7	AST-4	26/08/14	71.76	0.29	9.16	0.00	5.55	0.18	0.29	5.46	4.19	0.00		96.89
AST-4_8	AST-4	26/08/14	71.04	0.35	8.86	0.00	5.23	0.20	0.26	5.82	4.18	0.01		95.95
AST-4_9	AST-4	26/08/14	71.11	0.29	9.10	0.00	5.48	0.11	0.26	5.77	4.22	0.00		96.34
AST-4_10	AST-4	26/08/14	71.37	0.34	9.05	0.00	5.44	0.17	0.27	5.26	4.32	0.00		96.22
AST-4_11	AST-4	26/08/14	71.83	0.38	9.06	0.00	5.31	0.08	0.27	5.55	4.27	0.02		96.78
AST-4_12	AST-4	26/08/14	72.38	0.31	9.16	0.00	5.49	0.24	0.28	5.47	4.26	0.04		97.61
AST-4_13	AST-4	26/08/14	68.94	0.29	8.79	0.00	5.47	0.22	0.28	5.29	4.04	0.03		93.36
AST-4_14	AST-4	26/08/14	71.76	0.35	9.11	0.03	5.26	0.16	0.27	5.64	4.40	0.00		96.97
AST-4_15	AST-4	26/08/14	72.90	0.31	9.05	0.01	5.52	0.17	0.29	5.57	4.47	0.06		98.34
AST-4_16	AST-4	26/08/14	72.20	0.30	9.08	0.01	5.27	0.10	0.25	5.89	4.32	0.00		97.42
AST-4_17	AST-4	26/08/14	72.31	0.33	9.06	0.00	5.08	0.24	0.28	5.39	4.44	0.00		97.14
AST-4_18	AST-4	26/08/14	70.18	0.29	8.70	0.00	5.14	0.12	0.23	5.40	4.18	0.00		94.25
AST-4_19	AST-4	26/08/14	72.27	0.34	9.06	0.01	5.37	0.14	0.22	5.46	4.20	0.00		97.07
AST-4_20	AST-4	26/08/14	72.75	0.41	9.13	0.01	5.41	0.15	0.23	5.57	4.42	0.01		98.08
03AL2594/1	AST-5	20/02/14	69.50	0.16	12.06	0.00	2.76	0.04	0.37	5.28	4.28	0.01	0.20	94.66
03AL2594/2	AST-5	20/02/14	70.91	0.22	12.23	0.00	3.04	0.05	0.37	5.48	4.45	0.01	0.20	96.95

Continued on next page

Unnormalised major element concentrations (wt.%) in Ashenge glass shards

Label	Tephra	Analysis date	SiO_2 0.08	TiO_2 0.05	Al_2O_3 0.05	MgO 0.04	FeO^T 0.08	MnO 0.07	CaO 0.04	Na_2O 0.08	K_2O 0.03	P_2O_5 0.10	Cl 0.02	Total
03AL2594/3	AST-5	20/02/14	71.22	0.21	12.50	0.00	3.12	0.06	0.37	5.39	4.59	0.02	0.19	97.67
03AL2594/4	AST-5	20/02/14	67.58	0.21	11.73	0.00	2.74	0.06	0.36	5.08	4.38	0.02	0.21	92.37
03AL2594/5	AST-5	20/02/14	69.23	0.25	12.03	0.01	2.91	0.06	0.29	5.29	4.45	0.02	0.17	94.71
03AL2594/7	AST-5	20/02/14	70.26	0.15	12.30	0.01	3.03	0.02	0.38	5.60	4.44	0.00	0.20	96.40
03AL2594/8	AST-5	20/02/14	70.07	0.24	12.30	0.00	2.93	0.14	0.35	5.00	4.47	0.00	0.21	95.72
03AL2594/10	AST-5	20/02/14	70.61	0.19	12.27	0.01	2.85	0.06	0.36	5.53	4.45	0.00	0.20	96.53
03AL2594/11	AST-5	20/02/14	70.17	0.17	12.31	0.00	2.93	0.12	0.37	5.41	4.52	0.03	0.16	96.20
03AL2594/12	AST-5	20/02/14	72.19	0.20	12.80	0.04	3.07	0.13	0.37	5.25	4.56	0.00	0.18	98.79
03AL2594/13	AST-5	20/02/14	70.21	0.21	12.36	0.00	3.17	0.11	0.37	5.42	4.37	0.03	0.19	96.45
03AL2594/14	AST-5	20/02/14	68.93	0.23	12.02	0.00	2.96	0.18	0.35	5.19	4.22	0.00	0.18	94.26
03AL2594/15	AST-5	20/02/14	70.77	0.18	12.59	0.03	3.17	0.11	0.38	5.37	4.35	0.02	0.21	97.18
03AL2594/16	AST-5	20/02/14	69.79	0.17	12.16	0.01	2.82	0.08	0.36	5.31	4.26	0.00	0.20	95.18
03AL2594/17	AST-5	20/02/14	72.06	0.22	12.72	0.01	3.05	0.09	0.36	5.32	4.51	0.00	0.19	98.51
03AL2594/18	AST-5	20/02/14	69.36	0.22	12.12	0.02	2.84	0.00	0.37	5.32	4.32	0.00	0.19	94.75
03AL2594/19	AST-5	20/02/14	68.59	0.17	11.77	0.03	2.82	0.07	0.39	5.18	4.30	0.03	0.20	93.54
03AL2594/20	AST-5	20/02/14	70.31	0.25	12.15	0.00	2.97	0.08	0.40	4.87	4.42	0.01	0.19	95.64
AST-6_1	AST-6	26/08/14	71.93	0.33	8.67	0.00	5.48	0.10	0.26	5.81	4.37	0.00		96.96
AST-6_2	AST-6	26/08/14	72.72	0.28	8.96	0.00	5.12	0.20	0.20	5.48	4.25	0.00		97.23
AST-6_3	AST-6	26/08/14	73.13	0.29	9.14	0.00	5.46	0.14	0.28	5.61	4.45	0.01		98.52
AST-6_8	AST-6	26/08/14	73.53	0.24	9.28	0.01	5.40	0.17	0.24	5.88	4.32	0.04		99.12
AST-6_10	AST-6	26/08/14	72.89	0.30	9.15	0.01	5.11	0.25	0.26	5.27	4.31	0.00		97.55
AST-6_12	AST-6	26/08/14	71.55	0.26	9.12	0.00	5.23	0.20	0.23	5.88	4.21	0.02		96.70
AST-6_14	AST-6	26/08/14	67.32	0.29	8.61	0.00	4.97	0.17	0.22	5.33	3.97	0.02		90.90
AST-6_15	AST-6	26/08/14	72.50	0.28	9.19	0.01	5.45	0.27	0.26	5.68	4.30	0.00		97.93
AST-6_19	AST-6	26/08/14	70.52	0.27	8.87	0.00	5.23	0.19	0.22	5.57	4.15	0.04		95.06
AST-6_20	AST-6	26/08/14	73.24	0.28	9.18	0.01	5.59	0.20	0.25	5.77	4.34	0.00		98.86
AST-7_2	AST-7	26/08/14	68.90	0.31	9.51	0.01	4.96	0.18	0.24	5.89	4.33	0.01		94.34
AST-7_3	AST-7	26/08/14	66.15	0.21	12.45	0.00	2.99	0.07	0.19	5.97	4.81	0.00		92.86
AST-7_4	AST-7	26/08/14	67.15	0.22	9.97	0.01	3.69	0.16	0.21	5.35	4.25	0.02		91.03
AST-7_5	AST-7	26/08/14	68.80	0.23	10.94	0.00	3.87	0.06	0.25	5.98	4.47	0.00		94.59
AST-7_6	AST-7	26/08/14	66.38	0.27	9.25	0.04	4.16	0.14	0.27	5.79	4.28	0.00		90.60
AST-7_7	AST-7	26/08/14	69.39	0.28	10.46	0.00	3.82	0.15	0.27	5.96	4.40	0.00		94.73
AST-7_11	AST-7	26/08/14	68.62	0.26	10.21	0.00	4.01	0.16	0.22	5.95	4.56	0.01		94.02
AST-7_13	AST-7	26/08/14	67.92	0.14	11.98	0.02	3.46	0.10	0.26	6.65	4.34	0.01		94.89
AST-7_14	AST-7	26/08/14	68.01	0.23	10.08	0.00	3.79	0.14	0.29	5.83	4.36	0.00		92.74
AST-7_16	AST-7	26/08/14	69.17	0.26	10.71	0.01	4.15	0.11	0.28	5.61	4.50	0.01		94.81
AST-7_19	AST-7	26/08/14	67.45	0.21	10.26	0.00	3.85	0.16	0.22	5.67	4.31	0.01		92.14
AST-7_20	AST-7	26/08/14	67.18	0.16	12.51	0.01	2.99	0.04	0.20	5.98	4.91	0.02		94.02
03AL2732/3	AST-8	20/02/14	68.63	0.25	10.41	0.01	4.44	0.17	0.21	5.56	4.30	0.02	0.25	94.25
03AL2732/6	AST-8	20/02/14	70.89	0.24	10.41	0.00	4.89	0.20	0.23	5.94	4.17	0.04	0.28	97.27
03AL2732/8	AST-8	20/02/14	67.95	0.27	10.19	0.01	4.35	0.22	0.22	5.87	4.18	0.00	0.23	93.49
03AL2732/10	AST-8	20/02/14	69.42	0.20	10.32	0.00	4.68	0.02	0.21	6.07	4.33	0.02	0.29	95.56
B03AL2732/1	AST-8	20/02/14	69.98	0.25	10.50	0.00	4.41	0.15	0.25	5.77	4.24	0.00	0.25	95.80
B03AL2732/2	AST-8	20/02/14	70.12	0.30	10.49	0.01	4.58	0.26	0.22	5.68	4.21	0.02	0.26	96.14
B03AL2732/3	AST-8	20/02/14	68.34	0.26	10.29	0.01	4.60	0.09	0.31	5.85	4.17	0.04	0.23	94.17
B03AL2732/6	AST-8	20/02/14	71.10	0.34	10.50	0.00	4.50	0.13	0.21	5.84	4.37	0.03	0.28	97.28
B03AL2732/10	AST-8	20/02/14	69.22	0.27	10.40	0.01	4.52	0.24	0.26	5.62	4.19	0.03	0.22	95.00
B03AL2732/11	AST-8	20/02/14	71.80	0.31	10.74	0.01	4.66	0.15	0.22	5.96	4.46	0.00	0.25	98.56
AST-9_1	AST-9	26/08/14	67.01	0.23	9.76	0.00	4.56	0.19	0.28	5.66	4.19	0.03		91.91
AST-9_2	AST-9	26/08/14	69.90	0.24	10.32	0.00	4.67	0.15	0.27	5.84	4.33	0.02		95.73
AST-9_3	AST-9	26/08/14	67.39	0.28	9.86	0.00	4.37	0.17	0.26	5.42	4.28	0.02		92.04
AST-9_4	AST-9	26/08/14	70.16	0.28	10.21	0.00	4.71	0.14	0.25	5.92	4.40	0.01		96.07
AST-9_5	AST-9	26/08/14	67.94	0.27	9.94	0.00	4.76	0.12	0.26	5.74	4.23	0.04		93.32
AST-9_7	AST-9	26/08/14	65.83	0.24	9.61	0.00	4.73	0.19	0.23	5.93	4.31	0.01		91.09
AST-9_8	AST-9	26/08/14	65.61	0.25	9.43	0.00	4.70	0.24	0.22	5.71	4.30	0.00		90.46
AST-9_9	AST-9	26/08/14	67.04	0.29	9.89	0.01	4.52	0.12	0.24	5.79	4.34	0.00		92.24
AST-9_10	AST-9	26/08/14	66.45	0.22	9.66	0.00	4.32	0.17	0.21	5.62	4.19	0.00		90.85
AST-9_11	AST-9	26/08/14	69.28	0.28	10.22	0.01	4.64	0.15	0.22	6.18	4.34	0.03		95.35
AST-9_12	AST-9	26/08/14	68.48	0.26	10.00	0.00	4.58	0.19	0.26	5.77	4.22	0.02		93.78
AST-9_14	AST-9	26/08/14	67.89	0.28	9.78	0.00	4.43	0.21	0.22	5.87	4.24	0.00		92.93
AST-9_15	AST-9	26/08/14	67.27	0.27	9.85	0.00	4.53	0.09	0.25	6.02	4.31	0.00		92.59
AST-9_16	AST-9	26/08/14	65.84	0.25	9.59	0.00	4.57	0.10	0.26	5.55	4.10	0.02		90.30
AST-9_17	AST-9	26/08/14	65.93	0.21	9.68	0.00	4.58	0.15	0.22	5.94	4.21	0.00		90.92
AST-9_18	AST-9	26/08/14	65.69	0.24	9.53	0.00	4.42	0.08	0.26	5.94	4.10	0.05		90.32

Trace element concentrations (ppm) in Ashenge glass shards

Label	Tephra	Analysis date	Rb 0.62	Sr 1.05	Y 0.17	Zr 0.37	Nb 0.07	Cs 0.19	Ba 1.88	La 0.09	Ce 0.07	Pr 0.06	Nd 0.25	Sm 0.14	Eu 0.13	Tb 0.06	Dy 0.13	Ho 0.04	Er 0.07	Tm 0.05	Yb 0.15	Lu 0.04	Hf 0.08	Ta 0.06	Pb 0.12	Th 0.01	U 0.00
A03AL2/1	AST-1	09/07/14	136	3.36	113	1000	166	1.23	10.8	134	250	30.4	119	23.0	1.88	3.30	19.5	4.25	12.7	1.52	12.9	1.68	23.1	10.5	61.9	21.5	5.76
A03AL2/2	AST-1	09/07/14	134	-	103	915	167	1.27	3.61	130	240	27.9	116	19.7	1.19	2.92	19.1	3.88	12.2	1.66	9.84	1.79	25.0	11.0	25.7	20.5	5.53
A03AL2/3	AST-1	09/07/14	140	2.40	93.6	883	162	1.08	2.32	118	230	27.0	105	18.1	1.01	2.63	17.5	3.84	10.7	1.64	11.0	1.27	22.5	11.4	27.9	18.9	5.63
A03AL2/4	AST-1	09/07/14	133	2.03	108	957	168	1.47	9.64	133	246	28.4	109	24.0	0.86	2.97	22.2	3.98	13.2	1.78	9.81	1.85	26.4	10.9	42.1	21.2	5.54
A03AL2/5	AST-1	09/07/14	134	-	100	909	167	1.01	3.98	126	239	27.7	108	19.2	1.41	3.08	18.1	3.44	11.1	1.39	11.2	1.49	22.3	11.3	23.7	19.6	5.60
A03AL2/6	AST-1	09/07/14	129	-	102	908	165	0.82	4.66	122	237	28.2	106	21.9	1.13	3.10	18.7	3.14	10.5	1.60	10.3	1.77	22.0	9.31	22.6	18.6	5.55
A03AL2/7	AST-1	09/07/14	118	0.87	106	926	169	0.69	2.01	126	231	28.7	112	22.9	0.93	2.88	18.8	3.81	11.6	1.23	10.8	1.59	23.6	11.8	28.1	20.0	5.68
03AL2/8	AST-1	09/07/14	126	-	99.1	886	161	0.96	4.11	120	232	26.3	113	20.9	1.48	2.97	18.5	4.02	10.6	1.41	9.79	1.74	22.9	10.8	23.2	19.7	5.46
03AL2/9	AST-1	09/07/14	131	0.86	105	911	167	1.00	3.61	125	242	29.0	110	20.8	1.08	2.94	18.1	3.80	12.0	1.57	11.3	1.47	24.5	11.5	22.9	19.7	5.86
03AL2/10	AST-1	09/07/14	99.2	1.18	67.6	590	106	0.62	8.22	82	152	18.1	72.0	13.5	0.89	2.14	13.6	2.37	6.46	1.21	6.44	1.14	13.7	6.94	15.2	12.0	3.58
03AL2/11	AST-1	09/07/14	130	0.74	103	916	165	0.81	8.79	124	232	27.5	113	20.7	1.55	3.15	19.2	3.82	11.6	1.16	10.1	1.62	21.6	11.4	22.5	19.8	5.74
03AL2439/1	AST-2	09/07/14	133	1.08	95.7	885	159	0.96	2.53	120	230	26.8	107	20.9	1.46	3.38	20.1	3.97	10.2	1.35	10.5	1.64	23.6	11.0	24.5	19.0	5.91
03AL2439/2	AST-2	09/07/14	135	-	93.6	844	162	0.94	2.47	118	223	26.6	102	20.9	1.06	2.74	16.0	3.98	11.4	1.58	10.2	1.52	23.3	11.3	26.6	19.3	5.50
03AL2439/3	AST-2	09/07/14	140	0.90	112	977	168	0.88	6.19	135	241	28.3	120	20.7	1.61	3.29	18.7	4.29	10.5	1.68	10.9	1.87	25.7	12.3	23.1	21.7	6.00
03AL2439/4	AST-2	09/07/14	133	-	100	889	166	0.86	3.84	122	234	27.1	102	20.4	1.68	3.34	18.1	3.73	10.9	1.31	11.1	1.65	23.6	11.8	26.6	19.3	5.30
03AL2439/5†	AST-2	09/07/14	180	0.12	199	1720	353	1.62	-	241	342	46.9	146	93.1	0.04	6.56	32.7	8.91	21.9	1.53	18.0	2.03	83.3	30.8	23.5	36.8	10.8
03AL2439/6	AST-2	09/07/14	124	0.12	93.7	838	158	0.92	6.95	116	217	25.7	101	19.5	1.25	3.11	17.0	3.48	11.4	1.40	10.2	1.73	21.5	10.6	23.6	18.4	5.68
03AL2439/7	AST-2	09/07/14	134	0.09	102	902	166	1.14	8.65	122	236	27.4	110	21.5	1.21	3.44	20.0	3.46	11.5	2.23	9.75	1.41	21.9	10.4	27.9	19.6	6.10
03AL2439/8	AST-2	09/07/14	114	0.55	87.8	753	141	1.03	4.79	100	196	21.0	87.9	22.3	1.22	2.51	14.2	3.50	9.37	1.54	8.74	1.20	19.6	9.18	19.7	15.3	4.65
03AL2439/9	AST-2	09/07/14	107	1.41	107	959	174	0.88	3.87	134	246	27.8	119	20.8	1.15	3.43	21.2	3.67	12.1	2.06	10.7	1.65	24.8	11.9	23.1	21.2	5.90
03AL2439/10	AST-2	09/07/14	134	-	91.3	832	157	0.86	0.86	111	217	24.6	101	20.1	1.37	3.15	17.1	3.38	10.3	1.30	9.39	1.66	24.3	11.0	22.7	17.3	5.40
03AL2439/11	AST-2	09/07/14	135	0.07	109	959	166	1.20	7.66	135	247	29.0	117	23.3	1.15	3.91	20.0	4.17	12.7	1.49	11.1	1.60	24.4	11.6	23.6	21.2	6.10
03AL2439/12	AST-2	09/07/14	103	9.47	102	922	159	0.81	11.7	122	214	25.8	99.2	17.6	1.30	2.84	19.0	3.99	10.4	1.72	9.33	1.21	22.8	11.4	20.6	19.8	5.77
03AL2439/14	AST-2	09/07/14	139	3.01	135	1140	178	0.84	-	164	278	34.2	135	32.0	1.77	4.56	23.0	5.51	13.4	2.25	15.1	2.12	32.9	13.5	25.6	23.2	5.82
03AL2439/15	AST-2	09/07/14	125	0.19	104	877	160	0.97	4.05	123	227	25.5	112	20.8	0.65	3.04	21.7	4.44	11.4	1.45	11.3	1.93	23.6	11.3	35.9	18.4	5.90
03AL2439/16	AST-2	09/07/14	118	-	107	924	152	1.06	7.77	130	235	26.9	113	19.8	1.04	3.54	18.2	4.65	12.1	1.42	11.3	1.66	23.7	10.9	21.0	20.7	5.09
03AL2439/17	AST-2	09/07/14	135	2.75	122	1030	167	1.01	5.18	147	255	31.3	123	22.7	1.32	3.31	21.0	4.45	14.9	2.19	13.1	1.64	27.6	12.0	21.0	21.3	6.15
03AL2439/18	AST-2	09/07/14	122	0.97	100	841	163	0.67	1.41	119	219	26.1	105	20.0	0.61	2.69	17.2	3.52	10.9	1.65	9.53	1.38	22.1	11.6	22.7	19.2	5.51
03AL2439/19	AST-2	09/07/14	134	-	104	925	170	1.06	4.67	133	249	28.3	119	19.6	1.20	3.23	18.5	5.18	13.3	1.74	10.3	1.59	26.6	11.6	27.8	21.0	6.01
03AL2439/20	AST-2	09/07/14	144	0.25	105	906	171	1.02	4.50	132	253	28.0	114	18.7	1.39	3.28	18.5	4.41	13.2	1.30	12.5	1.84	24.4	11.7	26.1	21.5	6.42
03AL2439/21	AST-2	09/07/14	129	1.79	107	965	156	0.83	5.66	134	249	31.2	120	22.5	1.32	3.09	20.7	4.44	13.0	2.20	11.5	1.49	25.5	10.5	27.6	19.0	5.29
AST-3_1	AST-3	12/01/15	158	14.80	210	1570	227	1.35	28.2	187	342	42.5	181	35.8	3.45	6.32	37.2	7.72	21.2	3.47	23.8	3.23	45.3	17.0	24.8	28.8	6.75
AST-3_3	AST-3	12/01/15	140	1.38	195	1530	213	1.31	26.9	171	306	36.7	147	32.6	3.19	5.14	33.7	6.98	19.9	3.01	18.0	3.26	41.7	15.1	23.9	24.8	6.84
AST-3_4	AST-3	12/01/15	151	2.24	202	1600	218	1.35	29.7	182	324	40.8	164	31.4	3.88	5.89	34.7	7.83	21.2	3.34	20.5	3.20	43.1	16.8	25.3	28.1	6.48
AST-3_5†	AST-3	12/01/15	97.2	8.65	215	1680	180	1.02	21.7	164	258	34.4	145	29.8	3.35	5.42	32.2	7.05	20.4	2.78	17.7	2.80	37.0	12.5	17.4	27.1	4.04
AST-3_6	AST-3	12/01/15	154	11.1	232	1860	237	1.28	53.3	208	353	48.0	201	37.8	4.44	6.24	45.1	9.86	26.0	3.95	24.5	3.50	47.5	17.8	27.4	32.2	7.33
AST-3_7	AST-3	12/01/15	149	2.02	222	1740	237	1.44	32.7	197	342	42.4	187	36.2	4.41	6.39	37.8	9.65	25.6	3.50	25.5	3.84	45.6	17.3	24.7	31.7	6.76
AST-3_9	AST-3	12/01/15	148	2.58	205	1670	225	1.13	28.3	185	319	42.4	170	32.8	3.42	5.63	35.3	8.70	25.1	3.79	21.3	3.41	42.2	16.4	25.0	28.8	6.36
AST-3_10	AST-3	12/01/15	144	2.40	208	1670	225	1.27	28.4	188	333	41.8	185	32.4	3.75	6.52	34.6	8.21	22.6	3.93	22.6	3.45	43.6	17.4	23.3	27.9	6.57
AST-3_12	AST-3	12/01/15	143	1.29	213	1630	232	1.43	26.9	188	331	40.8	171	34.1	4.08	6.24	39.5	7.07	22.0	3.45	19.9	3.24	40.3	16.2	24.1	28.0	6.01
AST-3_14	AST-3	12/01/15	151	3.22	241	1850	240	1.36	30.2	205	361	44.7	191	37.4	4.38	7.08	40.5	8.94	25.3	3.96	23.5	3.29	46.5	17.7	24.6	31.4	6.31
AST-3_15	AST-3	12/01/15	143	0.93	206	1640	223	1.11	26.1	183	321	41.2	179	31.2	4.00	5.90	37.1	8.34	24.7	3.47	23.1	3.69	46.4	16.6	22.8	28.5	6.36
AST-3_16	AST-3	12/01/15	149	1.36	195	1540	223	1.25	25.2	173	314	39.0	157	34.7	4.19	5.33	37.9	7.58	22.0	3.15	21.0	2.86	40.0	16.3	24.9	27.3	6.64
AST-3_18	AST-3	12/01/15	142	0.69	192	1510	219	1.25	25.6	174	312	39.1	162	33.6	3.42	5.43	36.6	7.88	24.3	3.31	20.4	2.93	43.0	15.9	23.8	27.1	6.48
AST-3_19	AST-3	12/01/15	151	1.86	199	1580	218	1.27	29.4	177	312	39.6	167	32.1	3.38	5.50	36.3	7.73	20.9	3.20	20.9	2.81	40.6	15.8	24.7	27.5	5.98
AST-3_20	AST-3	12/01/15	145	3.27	210	1690	223	1.32	30.3	189	337	40.3	179	36.4	3.91	6.15	37.1	8.26	24.3	3.42	22.6	3.20	45.0	15.9	24.4	28.9	6.65
AST-4_1	AST-4	12/01/15	145	1.68	224	1720	243	1.30	32.0	189	347	44.5	181	37.2	4.13	6.27	40.8	8.52	22.9	3.81	21.6	3.60	43.7	18.9	25.8	29.0	6.57

Continued on next page

Trace element concentrations (ppm) in Ashenge glass shards

Label	Tephra	Analysis date	Rb 0.62	Sr 1.05	Y 0.17	Zr 0.37	Nb 0.07	Cs 0.19	Ba 1.88	La 0.09	Ce 0.07	Pr 0.06	Nd 0.25	Sm 0.14	Eu 0.13	Tb 0.06	Dy 0.13	Ho 0.04	Er 0.07	Tm 0.05	Yb 0.15	Lu 0.04	Hf 0.08	Ta 0.06	Pb 0.12	Th 0.01	U 0.00
AST-4_2	AST-4	12/01/15	141	1.55	212	1660	244	1.40	31.1	188	331	41.8	176	34.6	4.79	6.04	40.1	8.12	24.8	3.58	22.8	3.59	44.5	18.3	28.1	29.2	6.61
AST-4_3	AST-4	12/01/15	143	1.32	237	1860	248	1.50	34.6	208	369	48.0	201	37.4	4.33	7.19	40.8	9.09	26.8	3.89	23.5	4.00	45.4	20.0	27.2	33.5	6.96
AST-4_4	AST-4	12/01/15	142	1.78	220	1710	241	1.30	33.4	193	342	41.8	174	39.5	4.13	6.05	38.0	8.54	25.7	3.29	23.4	3.79	46.0	19.2	26.1	31.2	6.23
AST-4_5	AST-4	12/01/15	145	2.05	222	1730	243	1.41	32.1	199	344	43.9	179	41.0	3.85	6.35	42.2	9.01	25.5	3.43	24.4	3.57	49.3	16.1	27.1	29.9	6.16
AST-4_6	AST-4	12/01/15	145	1.62	221	1720	241	1.25	31.6	190	329	41.5	174	34.3	4.25	6.18	37.4	8.61	23.7	2.89	20.6	2.70	41.8	17.0	25.5	28.4	6.30
AST-4_7	AST-4	12/01/15	142	2.72	209	1640	233	1.26	25.7	183	316	40.7	157	35.1	3.53	5.30	36.9	7.45	22.9	3.27	21.9	3.22	38.4	16.7	25.2	27.3	6.05
AST-4_8	AST-4	12/01/15	147	2.73	240	1850	257	1.32	34.5	221	368	48.2	194	44.4	4.56	6.73	43.9	9.46	24.7	3.26	25.1	3.66	47.6	18.1	24.8	32.2	6.92
AST-4_9	AST-4	12/01/15	144	2.42	209	1640	235	1.35	31.2	189	331	41.5	166	35.6	3.81	6.31	40.0	8.32	23.8	3.26	23.2	3.18	42.6	16.5	27.3	27.1	6.66
AST-4_10	AST-4	12/01/15	146	1.82	219	1740	236	1.44	31.1	192	348	41.5	177	35.2	3.58	5.95	40.1	8.40	25.1	3.51	21.8	3.12	44.5	16.1	26.1	28.1	6.62
AST-4_11	AST-4	12/01/15	147	2.48	209	1620	241	1.19	31.0	189	340	40.1	170	37.1	4.44	6.07	38.2	8.38	25.9	2.94	22.7	3.44	45.2	16.8	27.6	29.0	6.97
AST-4_12	AST-4	12/01/15	157	3.00	205	1600	232	1.26	30.4	186	343	43.2	175	34.0	4.59	5.98	37.4	8.18	22.6	3.37	23.7	3.40	43.1	16.8	28.7	28.5	7.24
AST-4_13	AST-4	12/01/15	145	2.06	205	1580	231	1.54	24.6	181	341	42.8	166	36.0	3.98	6.26	38.6	7.96	23.8	3.83	21.1	2.60	41.8	16.6	25.8	29.0	6.77
AST-4_14	AST-4	12/01/15	139	1.73	196	1530	224	1.52	27.7	180	329	39.2	160	35.1	3.48	5.68	35.9	7.81	23.4	3.30	19.9	3.75	39.4	15.5	25.3	26.8	6.54
AST-4_15	AST-4	12/01/15	142	1.87	193	1450	228	1.35	26.5	172	312	37.7	157	31.9	3.85	5.39	34.4	7.38	22.3	2.72	17.7	2.98	36.0	15.5	27.5	25.7	6.61
AST-4_16	AST-4	12/01/15	149	1.43	205	1600	234	1.32	30.9	183	334	42.1	167	38.5	3.74	6.05	36.6	7.55	22.6	2.87	20.3	3.08	40.2	15.7	27.7	27.4	6.79
AST-4_17	AST-4	12/01/15	154	1.33	219	1670	245	1.44	34.2	201	362	46.7	181	39.4	4.52	6.77	38.4	8.77	25.0	3.69	21.3	3.81	46.6	18.2	27.2	29.6	6.54
AST-4_18	AST-4	12/01/15	153	1.98	207	1630	241	1.38	29.7	181	342	41.7	167	37.8	3.99	5.65	41.2	7.70	23.3	3.54	21.7	3.35	42.9	16.2	25.5	26.7	6.16
AST-4_19	AST-4	12/01/15	163	1.96	202	1570	245	1.68	34.4	181	347	40.7	167	35.6	3.85	5.55	36.5	8.04	22.7	3.78	22.9	3.32	41.4	17.5	30.1	28.8	7.29
AST-4_20	AST-4	12/01/15	143	2.37	206	1630	231	1.31	30.8	186	351	44.3	177	37.2	3.78	6.27	41.2	7.97	23.6	3.26	22.9	3.36	46.0	18.3	25.2	30.4	6.91
03AL2594/1	AST-5	10/07/14	135	5.59	218	1560	153	1.38	315	151	263	34.6	145	30.7	2.98	6.08	35.4	8.20	23.6	3.12	22.3	3.32	40.9	12.9	23.4	24.9	6.12
03AL2594/2	AST-5	10/07/14	135	5.42	212	1500	158	1.26	288	145	262	33.4	133	28.8	3.44	5.29	34.6	7.66	23.3	3.48	21.3	3.21	40.7	12.2	23.5	24.6	5.80
03AL2594/3	AST-5	10/07/14	125	4.99	190	1350	150	1.12	370	131	232	29.0	121	25.6	2.97	5.05	30.6	6.73	20.8	2.67	17.5	3.00	35.6	10.7	23.1	21.6	5.36
03AL2594/4	AST-5	10/07/14	137	4.03	204	1430	157	1.32	314	139	258	32.1	132	28.2	3.17	5.25	34.1	7.33	23.3	3.07	22.0	3.46	40.1	12.3	26.3	22.7	5.67
03AL2594/5	AST-5	10/07/14	138	5.43	211	1520	160	1.29	323	145	266	34.8	137	30.0	3.09	5.30	35.5	8.41	25.2	3.39	22.9	3.30	43.4	12.7	24.6	25.4	6.52
03AL2594/7	AST-5	10/07/14	135	4.38	200	1440	157	0.98	279	136	242	31.6	131	27.5	2.53	4.73	31.6	7.23	21.0	3.10	20.2	3.05	41.2	11.9	23.4	22.6	5.43
03AL2594/8	AST-5	10/07/14	139	3.76	212	1520	154	1.24	300	144	256	33.6	137	28.3	3.32	5.03	32.5	7.69	22.1	2.94	21.9	3.10	38.9	11.4	23.2	24.2	5.88
03AL2594/10	AST-5	10/07/14	129	3.89	186	1320	152	1.29	277	127	232	28.5	119	26.6	2.39	4.90	29.7	6.55	19.2	2.76	19.0	2.60	35.2	11.2	21.9	21.2	5.49
03AL2594/11	AST-5	10/07/14	137	4.87	203	1480	157	1.28	309	143	257	33.9	132	29.5	2.92	5.29	34.8	7.69	22.0	3.37	21.2	3.17	36.9	12.1	22.4	24.2	5.66
03AL2594/12	AST-5	10/07/14	135	3.84	206	1460	153	1.15	306	141	247	32.5	129	26.5	3.08	5.33	34.5	7.46	21.7	3.40	22.1	3.00	41.2	11.6	22.9	23.0	5.57
03AL2594/13	AST-5	10/07/14	138	4.56	209	1500	160	1.47	314	144	265	33.3	138	27.3	2.84	5.81	35.3	7.66	24.2	3.45	22.2	3.10	41.5	12.2	23.3	25.4	6.04
03AL2594/14	AST-5	10/07/14	134	3.75	218	1560	158	1.34	321	149	266	34.6	137	30.2	3.40	5.99	38.0	7.48	24.1	3.17	21.8	3.15	41.0	12.0	23.5	24.8	5.61
03AL2594/15	AST-5	10/07/14	136	4.75	195	1420	159	1.18	303	139	253	32.5	132	26.5	2.75	4.98	33.6	7.22	20.7	3.35	20.5	2.89	38.4	12.1	24.1	24.9	6.32
03AL2594/16	AST-5	10/07/14	140	5.33	206	1460	165	1.35	312	146	261	33.8	133	29.5	2.89	5.68	34.9	7.63	20.9	3.14	20.8	3.28	40.1	12.0	24.9	23.6	5.86
03AL2594/17	AST-5	10/07/14	137	4.63	188	1400	158	1.10	292	135	252	31.8	127	29.4	3.15	4.90	31.1	6.62	20.0	3.22	21.2	2.90	39.0	12.1	23.6	22.1	5.95
03AL2594/18	AST-5	10/07/14	132	4.64	203	1440	158	1.31	299	140	254	32.3	131	27.6	3.01	5.41	34.6	6.74	22.6	2.85	19.6	2.97	37.8	10.4	24.6	22.0	5.83
03AL2594/19	AST-5	10/07/14	133	4.14	209	1500	160	1.21	329	147	264	33.4	135	27.5	2.82	5.39	33.1	7.63	23.7	3.26	22.5	3.06	39.9	12.5	23.6	24.1	6.03
03AL2594/20	AST-5	10/07/14	138	2.45	202	1510	154	1.44	235	145	255	31.7	135	26.8	2.44	5.24	34.6	7.94	23.9	3.39	22.8	2.89	42.9	11.9	22.9	24.9	5.96
AST-6_1	AST-6	12/01/15	169	2.54	219	1690	257	1.81	35.3	194	366	44.1	180	36.2	3.94	6.01	39.4	9.02	23.6	3.55	22.4	3.13	41.1	17.7	29.0	29.5	7.58
AST-6_3	AST-6	12/01/15	164	2.21	215	1660	243	1.47	33.7	187	358	41.9	168	28.9	4.28	6.00	37.9	8.13	19.7	3.36	21.3	3.11	42.1	16.9	31.9	28.2	7.82
AST-6_8	AST-6	12/01/15	177	1.55	211	1660	240	1.46	36.0	185	350	41.6	172	35.8	4.04	6.06	38.5	8.11	22.9	3.47	21.9	3.29	44.3	16.6	27.7	28.5	7.81
AST-6_10	AST-6	12/01/15	170	3.02	226	1810	259	1.59	46.6	206	387	45.7	199	35.6	4.38	6.24	42.1	8.84	26.0	3.64	22.3	3.79	48.4	18.9	28.5	30.9	8.17
AST-6_12	AST-6	12/01/15	175	0.74	204	1660	246	1.81	32.8	179	354	42.5	168	32.2	4.04	5.22	36.8	7.85	22.4	3.76	21.8	3.28	40.4	15.8	28.7	28.1	7.76
AST-6_14	AST-6	12/01/15	178	4.22	262	2040	259	1.30	44.9	246	427	52.7	206	43.1	4.09	6.40	52.6	9.91	32.4	4.53	27.3	3.70	53.0	18.8	31.0	37.4	7.48
AST-6_15	AST-6	12/01/15	172	1.29	199	1590	244	1.66	34.6	176	344	39.4	164	34.3	4.23	5.80	35.4	7.52	23.3	3.25	18.8	3.13	43.6	17.4	27.9	27.0	7.74
AST-6_19	AST-6	12/01/15	176	1.95	215	1720	255	1.49	40.5	199	383	42.7	178	34.6	4.05	6.29	38.5	8.44	23.8	3.52	23.9	3.24	44.8	17.2	30.3	30.1	8.06
AST-6_20†	AST-6	12/01/15	156	0.62	255	2080	271	1.49	36.5	199	375	46.1	185	38.4	3.73	7.18	44.3	9.67	26.4	3.68	24.0	3.91	50.1	18.7	31.0	35.3	8.11
AST-7_2	AST-7	12/01/15	150	0.88	155	1420	238	1.29	2.62	179	316	37.0	145	27.3	2.52	4.26	26.0	5.68	16.5	2.64	15.0	2.27	36.8	16.1	31.4	26.6	7.32
AST-7_3	AST-7	12/01/15	91.5	2.11	68.6	681	106	0.51	7.29	84	148	18.3	70.6	12.7	1.40	1.80	12.1	2.42	8.59	1.13	8.32	1.09	18.1	8.89	16.3	13.9	4.03
AST-7_4	AST-7	12/01/15	161	2.56	170	1590	248	1.53	7.18	195	346	40.4	173	31.9	2.19	4.51	29.3	6.90	18.8	3.04	17.5	2.78	36.5	17.9	32.1	32.5	7.61

Continued on next page

Trace element concentrations (ppm) in Ashenge glass shards

Label	Tephra	Analysis date	Rb 0.62	Sr 1.05	Y 0.17	Zr 0.37	Nb 0.07	Cs 0.19	Ba 1.88	La 0.09	Ce 0.07	Pr 0.06	Nd 0.25	Sm 0.14	Eu 0.13	Tb 0.06	Dy 0.13	Ho 0.04	Er 0.07	Tm 0.05	Yb 0.15	Lu 0.04	Hf 0.08	Ta 0.06	Pb 0.12	Th 0.01	U 0.00
AST-7_5	AST-7	12/01/15	136	0.81	112	1130	187	1.06	4.31	135	241	29.0	108	22.5	1.93	3.56	19.9	4.49	13.6	1.78	10.5	1.62	25.7	12.6	24.9	21.2	6.50
AST-7_6	AST-7	12/01/15	168	1.44	152	1440	248	1.28	6.61	183	331	39.3	156	25.4	2.69	4.53	29.8	6.35	17.1	2.51	14.4	2.15	34.8	17.3	31.3	28.2	7.56
AST-7_7	AST-7	12/01/15	152	1.36	133	1270	220	1.30	1.44	162	287	32.5	136	25.4	2.08	4.25	25.1	4.92	15.7	2.07	13.2	1.99	34.2	14.8	31.5	25.8	7.70
AST-7_11	AST-7	12/01/15	158	0.26	121	1190	210	1.39	0.80	145	275	31.9	121	21.4	1.64	3.52	22.6	4.91	12.7	1.85	12.2	1.68	29.3	14.4	32.5	23.6	7.40
AST-7_13	AST-7	12/01/15	138	0.27	108	1070	183	1.23	3.75	135	250	27.7	115	23.5	1.68	3.24	17.9	4.07	12.9	1.88	10.6	1.42	28.6	12.3	31.6	21.7	6.51
AST-7_14	AST-7	12/01/15	142	0.80	111	1110	194	1.30	5.49	135	261	28.8	114	24.0	1.46	3.69	20.7	4.29	12.2	1.60	10.4	1.49	27.7	12.9	27.6	21.7	6.66
AST-7_16	AST-7	12/01/15	132	0.89	95.9	986	174	1.02	0.65	117	229	26.2	108	18.5	1.36	2.96	19.4	4.22	10.5	1.67	9.24	1.86	27.1	12.4	26.6	20.4	5.99
AST-7_19	AST-7	12/01/15	151	0.97	158	1560	215	1.22	0.59	205	334	39.5	156	31.7	3.04	4.60	31.4	6.08	17.2	2.79	15.7	2.39	39.0	14.9	27.9	30.3	6.84
AST-7_20	AST-7	12/01/15	195	0.81	146	1430	256	1.43	2.96	176	323	36.8	153	29.7	2.09	4.12	27.7	6.00	17.2	2.50	16.0	1.79	34.6	17.8	31.4	27.9	8.14
03AL2732/3	AST-8	09/07/14	181	2.62	165	1540	256	1.34	34.7	203	381	42.5	173	31.3	2.71	5.14	35.6	5.88	19.8	2.56	17.0	2.63	43.0	18.2	37.8	32.4	7.48
03AL2732/6	AST-8	09/07/14	166	0.34	157	1440	252	1.26	5.09	189	335	39.1	158	29.1	2.20	4.38	26.0	5.72	18.8	2.54	14.3	1.79	34.3	16.6	30.1	27.2	7.48
03AL2732/8	AST-8	09/07/14	170	-	154	1460	235	1.49	1.26	189	344	39.5	165	34.4	2.84	4.47	28.5	7.33	18.2	2.87	14.7	2.23	37.6	16.6	32.6	27.1	7.27
03AL2732/10	AST-8	09/07/14	165	3.30	148	1450	244	1.63	7.21	187	337	41.3	166	32.2	2.94	4.93	27.9	5.88	17.1	2.55	18.4	2.46	37.6	17.5	33.4	30.0	8.06
B03AL2732/1	AST-8	09/07/14	323	3.41	284	2630	460	2.83	9.62	346	605	71.0	292	59.1	4.71	7.94	51.1	9.28	26.6	3.93	29.1	4.42	69.4	31.2	56.2	48.4	14.5
B03AL2732/2	AST-8	09/07/14	308	0.02	288	2600	451	2.60	11.1	343	603	73.1	306	62.6	4.67	8.20	46.4	8.80	26.5	3.67	30.4	4.60	65.2	31.9	58.6	52.5	13.1
B03AL2732/3	AST-8	09/07/14	312	1.23	291	2720	447	2.59	7.40	356	619	75.6	309	65.3	4.66	8.46	44.4	9.65	26.8	3.35	28.4	4.34	67.6	31.7	55.4	52.3	13.9
B03AL2732/6	AST-8	09/07/14	305	0.57	272	2550	428	2.86	8.81	332	585	69.5	287	58.0	4.74	7.58	46.1	9.76	24.9	3.82	26.5	4.08	66.3	30.9	54.1	50.2	13.9
B03AL2732/10	AST-8	09/07/14	293	0.61	287	2580	440	2.57	5.90	348	593	71.5	298	56.6	4.46	7.98	51.1	9.54	25.2	3.58	31.0	4.32	63.3	31.5	50.2	51.7	13.1
B03AL2732/11	AST-8	09/07/14	303	2.38	285	2660	449	2.52	10.6	351	614	73.7	321	60.8	4.29	8.22	48.5	10.1	27.8	3.95	30.7	4.47	72.4	31.8	52.7	53.1	13.5
AST-9_1	AST-9	09/07/14	177	1.57	150	1020	219	1.48	5.54	169	229	30.3	162	31.8	2.03	3.75	23.1	5.17	16.6	2.14	12.6	2.42	31.9	17.7	34.8	22.6	11.7
AST-9_2	AST-9	09/07/14	192	0.92	138	940	217	1.66	6.32	166	229	29.8	158	32.4	2.10	3.84	23.0	4.84	15.7	2.15	15.0	2.20	30.4	18.2	40.4	21.9	13.3
AST-9_3	AST-9	09/07/14	179	1.15	157	1150	240	1.81	7.20	189	265	33.9	180	35.8	2.51	4.30	25.1	5.74	17.6	2.77	17.3	2.29	37.3	19.2	35.4	27.1	10.5
AST-9_4†	AST-9	09/07/14	173	1.92	187	1360	242	1.45	6.51	201	269	36.7	186	36.5	2.47	4.97	30.1	5.71	18.3	2.43	18.9	2.76	40.0	19.7	35.8	30.3	9.57
AST-9_5	AST-9	09/07/14	175	1.95	156	1180	239	1.46	5.33	184	270	33.8	164	35.3	2.40	4.62	25.6	5.42	17.5	2.07	16.7	2.56	37.0	18.9	36.7	26.6	10.4
AST-9_7	AST-9	09/07/14	165	1.57	136	1060	222	1.44	3.43	160	242	30.9	143	31.5	2.56	3.61	23.0	4.77	16.9	2.34	13.5	2.27	31.7	16.9	31.9	23.1	9.26
AST-9_8	AST-9	09/07/14	178	1.50	141	1110	235	1.47	5.53	175	257	33.5	147	32.4	2.33	3.81	25.0	5.07	16.4	2.30	14.9	2.61	33.8	18.3	35.9	24.7	9.41
AST-9_9	AST-9	09/07/14	176	7.01	154	1200	234	1.58	8.36	186	273	35.7	169	33.0	2.73	4.49	27.0	5.31	17.5	2.22	15.9	2.48	34.5	18.4	74.0	25.7	10.3
AST-9_10	AST-9	09/07/14	177	3.24	164	1280	247	1.51	8.87	199	293	38.0	179	32.7	2.65	4.42	29.6	6.05	17.8	2.36	15.7	2.47	36.3	19.3	45.0	28.1	10.2
AST-9_11	AST-9	09/07/14	168	1.67	151	1160	233	1.42	7.76	180	266	33.6	164	31.7	2.48	4.63	26.6	5.10	18.3	2.30	16.0	2.88	37.8	18.6	33.0	26.8	9.91
AST-9_12	AST-9	09/07/14	177	1.07	167	1260	242	1.51	11.2	197	286	38.0	173	37.8	2.50	4.87	27.8	5.66	17.5	2.36	16.4	2.69	39.1	18.6	35.0	29.1	9.64
AST-9_14	AST-9	09/07/14	173	0.70	158	1250	241	1.73	3.52	186	276	35.8	165	36.0	2.36	4.43	26.8	5.55	17.8	2.31	16.6	2.00	38.6	18.9	30.9	27.6	8.91
AST-9_15	AST-9	09/07/14	169	0.89	128	876	205	1.13	6.41	152	206	26.6	141	31.0	1.98	3.12	19.4	4.07	14.1	1.76	12.4	1.72	27.5	17.0	35.1	20.0	12.2
AST-9_16	AST-9	09/07/14	176	2.13	148	1180	236	1.25	9.67	182	270	32.7	149	34.9	2.68	4.15	23.8	4.66	16.2	2.19	15.0	1.79	32.7	17.7	39.4	24.6	8.44
AST-9_17	AST-9	09/07/14	168	1.17	152	1220	229	1.47	3.09	169	271	33.6	169	32.1	2.29	4.10	25.9	5.16	17.4	2.14	15.9	2.59	37.3	18.2	31.9	26.7	9.17
AST-9_18	AST-9	09/07/14	167	1.06	168	1380	253	1.45	5.83	206	303	38.5	181	37.8	2.45	4.49	31.1	6.30	20.5	2.62	16.6	2.52	40.9	19.4	31.9	29.1	8.78

Unnormalised major element concentrations (wt.%) in Hayk glass shards

Label	Tephra	Analysis date	SiO_2 0.08	TiO_2 0.05	Al_2O_3 0.05	MgO 0.04	FeO^T 0.08	MnO 0.07	CaO 0.04	Na_2O 0.08	K_2O 0.03	P_2O_5 0.10	Cl 0.02	Total
HT-1_2	HT-2	28/08/14	71.70	0.24	13.21	0.13	2.93	0.12	1.45	4.44	3.60	0.03		97.86
HT-1_4	HT-2	28/08/14	70.81	0.26	12.86	0.14	2.76	0.06	1.39	4.96	3.60	0.02		96.86
HT-1_5	HT-2	28/08/14	71.18	0.21	12.88	0.13	2.74	0.08	1.45	4.90	3.62	0.00		97.19
HT-1_7	HT-2	28/08/14	71.31	0.29	12.76	0.12	2.85	0.12	1.36	4.74	3.47	0.04		97.05
HT-1_8	HT-2	28/08/14	70.38	0.26	12.72	0.13	2.58	0.08	1.39	4.90	3.46	0.05		95.96
HT-1_9	HT-2	28/08/14	69.56	0.28	12.50	0.14	2.76	0.05	1.50	4.80	3.54	0.00		95.15
HT-1_12	HT-2	28/08/14	69.90	0.25	12.89	0.13	2.83	0.10	1.42	4.61	3.50	0.01		95.65
HT-1_13	HT-2	28/08/14	71.21	0.30	12.87	0.16	2.93	0.15	1.24	4.79	3.49	0.06		97.20
HT-1_15	HT-2	28/08/14	70.98	0.25	12.75	0.14	2.66	0.10	1.39	4.69	3.57	0.02		96.54
HT-1_18	HT-2	28/08/14	69.98	0.27	12.58	0.14	3.04	0.15	1.38	4.74	3.43	0.01		95.72
HT-1_19	HT-2	28/08/14	71.14	0.32	13.16	0.13	2.96	0.07	1.47	4.64	3.43	0.06		97.36
HT-1_20	HT-2	28/08/14	72.25	0.25	13.02	0.14	2.82	0.10	1.42	4.66	3.59	0.00		98.26
HT-2_1	HT-4	28/08/14	69.61	0.22	12.42	0.18	2.63	0.13	1.35	4.39	3.67	0.02		94.62
HT-2_2	HT-4	28/08/14	70.56	0.28	12.78	0.15	2.79	0.12	1.43	4.48	3.52	0.00		96.10
HT-2_3	HT-4	28/08/14	70.65	0.29	12.64	0.13	2.85	0.06	1.33	4.68	3.52	0.05		96.20
HT-2_4	HT-4	28/08/14	71.15	0.24	12.80	0.15	2.74	0.09	1.41	4.71	3.52	0.01		96.82
HT-2_5	HT-4	28/08/14	70.77	0.24	12.78	0.14	2.60	0.14	1.35	4.39	3.56	0.01		95.99
HT-2_6	HT-4	28/08/14	70.78	0.28	12.67	0.14	2.86	0.17	1.41	4.78	3.62	0.03		96.73
HT-2_7	HT-4	28/08/14	71.06	0.29	13.30	0.13	2.72	0.12	1.38	4.75	3.58	0.03		97.38
HT-2_8	HT-4	28/08/14	71.63	0.26	12.97	0.12	2.62	0.07	1.32	4.71	3.48	0.02		97.20
HT-2_10	HT-4	28/08/14	69.89	0.26	12.44	0.15	2.70	0.03	1.37	4.21	3.56	0.00		94.61
HT-2_11	HT-4	28/08/14	69.54	0.27	12.48	0.11	2.70	0.01	1.39	4.53	3.53	0.03		94.60
HT-2_12	HT-4	28/08/14	70.71	0.29	12.55	0.12	2.71	0.10	1.39	4.48	3.52	0.05		95.92
HT-2_13	HT-4	28/08/14	69.27	0.26	12.45	0.17	2.63	0.05	1.35	4.55	3.45	0.01		94.17
HT-2_14	HT-4	28/08/14	69.55	0.29	12.41	0.10	2.96	0.08	1.38	4.64	3.57	0.01		95.00
HT-2_15	HT-4	28/08/14	69.22	0.24	12.45	0.14	2.80	0.09	1.40	4.59	3.65	0.03		94.60
HT-2_16	HT-4	28/08/14	68.55	0.24	12.35	0.10	2.79	0.07	1.38	4.55	3.51	0.04		93.58
HT-2_17	HT-4	28/08/14	68.78	0.30	12.45	0.13	2.77	0.16	1.39	4.49	3.61	0.03		94.11
HT-2_18	HT-4	28/08/14	69.75	0.29	12.67	0.12	2.62	0.03	1.45	4.81	3.46	0.05		95.25
HT-2_19	HT-4	28/08/14	67.54	0.27	12.50	0.14	2.70	0.11	1.36	4.56	3.47	0.03		92.67
HT-2_20	HT-4	28/08/14	69.23	0.22	11.85	0.08	2.32	0.05	1.10	4.36	3.72	0.03		92.95
HT-5_1	HT-5	30/06/15	70.33	0.15	13.04	0.00	1.53	0.00	0.66	3.99	4.17	0.02	0.27	94.17
HT-5_2	HT-5	30/06/15	70.39	0.13	12.92	0.04	1.58	0.04	0.63	4.28	4.25	0.00	0.27	94.54
HT-5_3	HT-5	30/06/15	70.61	0.11	12.95	0.03	1.82	0.02	0.90	4.34	4.28	0.00	0.23	95.30
HT-5_4	HT-5	30/06/15	71.31	0.17	12.88	0.11	1.73	0.02	0.85	4.19	4.17	0.04	0.23	95.69
HT-5_7	HT-5	30/06/15	70.21	0.19	12.72	0.14	1.78	0.06	0.86	4.16	4.16	0.01	0.24	94.54
HT-5_8	HT-5	30/06/15	69.92	0.14	12.86	0.14	1.84	0.07	0.82	4.35	4.09	0.00	0.24	94.45
HT-5_9	HT-5	30/06/15	70.85	0.16	13.03	0.18	2.29	0.07	0.99	4.29	4.11	0.03	0.20	96.20
HT-5_10	HT-5	30/06/15	71.35	0.16	13.06	0.08	1.86	0.11	0.88	3.41	4.35	0.03	0.27	95.56
HT-5_12	HT-5	30/06/15	71.16	0.15	13.03	0.11	1.85	0.13	0.77	3.12	4.10	0.00	0.24	94.66
HT-5_15	HT-5	30/06/15	70.00	0.14	13.03	0.15	2.00	0.00	0.83	4.31	4.14	0.00	0.19	94.80
HT-5_16	HT-5	30/06/15	70.62	0.13	13.03	0.03	1.42	0.01	0.69	4.05	4.17	0.05	0.21	94.41
HT-5_17	HT-5	30/06/15	70.49	0.18	13.00	0.12	1.76	0.00	0.74	4.47	4.18	0.00	0.22	95.16
HT-5_18	HT-5	30/06/15	69.97	0.14	12.98	0.07	1.85	0.03	0.83	4.18	4.04	0.08	0.25	94.42
HT-5_19	HT-5	30/06/15	70.64	0.14	13.02	0.09	1.78	0.09	0.79	4.32	4.22	0.00	0.25	95.34
HT-5_20	HT-5	30/06/15	70.55	0.17	13.00	0.16	1.71	0.11	0.81	4.28	4.08	0.00	0.23	95.10
HT-6_8	HT-6	29/06/15	69.02	0.11	12.96	0.03	1.72	0.05	0.77	4.08	4.25	0.05	0.27	93.31
HT-6_11	HT-6	29/06/15	67.78	0.13	13.04	0.01	1.44	0.06	0.63	4.09	4.07	0.05	0.23	91.52
HT-6_12	HT-6	29/06/15	69.60	0.11	13.01	0.06	1.60	0.07	0.72	4.04	4.20	0.01	0.24	93.66
HT-6_13	HT-6	29/06/15	68.51	0.14	13.34	0.09	1.64	0.12	0.68	3.88	4.12	0.01	0.21	92.73
HT-6_15	HT-6	29/06/15	69.55	0.12	13.29	0.03	1.68	0.00	0.74	4.15	4.17	0.00	0.25	93.98
HT-6_19	HT-6	29/06/15	71.00	0.15	12.81	0.08	1.80	0.07	0.79	4.10	4.28	0.01	0.25	95.33
HT-6_20	HT-6	29/06/15	69.16	0.12	13.16	0.06	1.37	0.00	0.60	3.84	4.11	0.00	0.31	92.75
HT-7_1	HT-7	30/06/15	71.61	0.31	9.52	0.00	5.13	0.19	0.35	5.32	4.24	0.08	0.22	96.97
HT-7_2	HT-7	30/06/15	69.80	0.31	9.34	0.05	5.05	0.17	0.26	5.42	4.28	0.02	0.30	94.99
HT-7_3	HT-7	30/06/15	71.49	0.33	9.51	0.02	5.22	0.17	0.28	5.36	4.39	0.00	0.25	97.00
HT-7_4	HT-7	30/06/15	72.47	0.32	9.60	0.00	5.17	0.18	0.30	5.49	4.37	0.00	0.24	98.15
HT-7_5	HT-7	30/06/15	68.29	0.34	9.01	0.00	4.97	0.16	0.25	5.15	4.07	0.04	0.31	92.59
HT-7_6	HT-7	30/06/15	71.39	0.35	9.59	0.00	5.08	0.20	0.30	5.39	4.38	0.00	0.27	96.95
HT-7_7	HT-7	30/06/15	71.09	0.26	9.51	0.03	5.00	0.15	0.24	5.31	4.22	0.00	0.23	96.05
HT-7_8	HT-7	30/06/15	72.19	0.36	9.46	0.00	5.27	0.03	0.37	2.35	4.39	0.00	0.27	94.69
HT-7_9	HT-7	30/06/15	69.67	0.26	9.27	0.00	4.78	0.27	0.32	5.10	4.21	0.02	0.27	94.18
HT-7_10	HT-7	30/06/15	71.54	0.39	9.59	0.00	5.14	0.15	0.28	5.11	4.30	0.00	0.31	96.80
HT-7_11	HT-7	30/06/15	71.86	0.34	9.60	0.00	5.12	0.20	0.30	5.16	4.43	0.00	0.25	97.25
HT-7_12	HT-7	30/06/15	71.99	0.33	9.65	0.01	5.32	0.18	0.27	5.31	4.42	0.00	0.25	97.73
HT-7_13	HT-7	30/06/15	68.98	0.28	9.14	0.03	5.02	0.19	0.25	5.26	4.11	0.00	0.25	93.50
HT-7_14	HT-7	30/06/15	71.27	0.32	9.52	0.00	4.92	0.23	0.30	3.02	4.34	0.00	0.25	94.17
HT-7_15	HT-7	30/06/15	69.24	0.34	9.31	0.03	5.10	0.15	0.28	2.09	4.15	0.02	0.35	91.05
HT-7_16	HT-7	30/06/15	71.50	0.31	9.49	0.00	5.36	0.15	0.26	3.17	4.37	0.00	0.27	94.88
HT-7_17	HT-7	30/06/15	71.82	0.29	9.62	0.02	5.23	0.16	0.32	5.42	4.39	0.00	0.22	97.50
HT-7_18	HT-7	30/06/15	71.41	0.30	9.32	0.01	5.00	0.30	0.25	2.10	4.26	0.00	0.31	93.26
HT-7_19	HT-7	30/06/15	72.74	0.37	9.71	0.04	5.33	0.27	0.26	2.45	4.35	0.01	0.25	95.78
HT-7_20	HT-7	30/06/15	72.09	0.37	9.55	0.00	4.95	0.22	0.28	5.71	4.25	0.00	0.24	97.67
HT-9_1	HT-9	29/06/15	70.14	0.12	12.18	0.03	1.84	0.04	0.30	4.63	4.44	0.04	0.47	94.23
HT-9_2	HT-9	29/06/15	70.39	0.13	12.18	0.00	2.04	0.02	0.33	4.92	4.50	0.05	0.44	94.98
HT-9_5	HT-9	29/06/15	69.78	0.15	12.17	0.07	1.86	0.10	0.31	4.97	4.49	0.00	0.49	94.39
HT-9_6	HT-9	29/06/15	70.10	0.15	12.36	0.04	1.81	0.10	0.31	4.46	4.64	0.00	0.48	94.44
HT-9_7	HT-9	29/06/15	70.34	0.15	12.16	0.06	1.94	0.06	0.34	4.38	4.64	0.02	0.46	94.56
HT-9_8	HT-9	29/06/15	69.45	0.16	12.09	0.02	1.91	0.07	0.34	4.85	4.48	0.00	0.42	93.80
HT-9_9	HT-9	29/06/15	70.06	0.12	12.31	0.01	2.00	0.08	0.32	4.74	4.43	0.00	0.45	94.52
HT-9_10	HT-9	29/06/15	68.92	0.14	12.43	0.00	1.86	0.01	0.33	4.58	4.55	0.03	0.44	93.29
HT-9_11	HT-9	29/06/15	70.04	0.15	12.21	0.02	1.79	0.04	0.35	4.61	4.57	0.01	0.46	94.25
HT-9_13	HT-9	29/06/15	69.94	0.17	12.26	0.07	2.09	0.13	0.34	4.63	4.44	0.03	0.47	94.57

Continued on next page

Unnormalised major element concentrations (wt.%) in Hayk glass shards

Label	Tephra	Analysis date	SiO_2 0.08	TiO_2 0.05	Al_2O_3 0.05	MgO 0.04	FeO^T 0.08	MnO 0.07	CaO 0.04	Na_2O 0.08	K_2O 0.03	P_2O_5 0.10	Cl 0.02	Total
HT-9_14	HT-9	29/06/15	69.86	0.12	12.20	0.01	1.91	0.07	0.33	4.80	4.46	0.03	0.49	94.27
HT-9_16	HT-9	29/06/15	70.34	0.17	12.36	0.02	1.92	0.11	0.34	4.29	4.58	0.05	0.42	94.60
HT-9_18	HT-9	29/06/15	70.58	0.10	12.08	0.00	1.94	0.03	0.31	3.35	4.72	0.03	0.45	93.60
HT-9_19	HT-9	29/06/15	69.65	0.11	12.26	0.00	1.86	0.12	0.28	4.63	4.51	0.00	0.48	93.89
HT-9_20	HT-9	29/06/15	69.07	0.18	12.11	0.01	1.83	0.11	0.31	4.77	4.52	0.00	0.47	93.36
HT-10_1	HT-10	29/06/15	68.29	0.15	12.54	0.05	1.80	0.01	0.34	4.47	4.64	0.00	0.49	92.78
HT-10_2	HT-10	29/06/15	68.65	0.13	12.66	0.03	1.98	0.13	0.35	4.56	4.60	0.02	0.50	93.61
HT-10_5	HT-10	29/06/15	68.93	0.17	12.64	0.08	1.83	0.04	0.49	4.27	4.53	0.03	0.42	93.44
HT-10_7	HT-10	29/06/15	68.67	0.15	13.02	0.03	1.69	0.07	0.34	4.31	4.59	0.00	0.46	93.34
HT-10_8	HT-10	29/06/15	69.65	0.14	12.47	0.07	1.89	0.05	0.36	4.52	4.56	0.00	0.44	94.14
HT-10_10	HT-10	29/06/15	70.89	0.15	12.61	0.00	2.00	0.12	0.35	4.46	4.52	0.00	0.46	95.56
HT-10_11	HT-10	29/06/15	68.49	0.09	12.57	0.00	1.94	0.09	0.35	4.30	4.55	0.00	0.49	92.87
HT-10_13	HT-10	29/06/15	68.28	0.13	12.61	0.00	1.85	0.08	0.34	4.45	4.55	0.00	0.49	92.77
HT-10_14	HT-10	29/06/15	67.68	0.10	12.40	0.00	1.83	0.11	0.34	4.47	4.40	0.03	0.50	91.87
HT-10_17	HT-10	29/06/15	67.34	0.13	12.38	0.00	2.00	0.04	0.32	4.51	4.42	0.00	0.44	91.57
HT-10_19	HT-10	29/06/15	67.53	0.13	12.05	0.05	1.86	0.00	0.31	4.52	4.47	0.00	0.55	91.48
HT-10_20	HT-10	29/06/15	68.89	0.14	12.60	0.08	1.81	0.11	0.41	4.43	4.47	0.03	0.48	93.46
HT-12_1	HT-12	30/06/15	71.08	0.37	10.09	0.00	4.85	0.29	0.33	5.33	4.37	0.00	0.26	96.98
HT-12_2	HT-12	30/06/15	69.31	0.29	9.78	0.02	4.72	0.24	0.27	5.19	4.24	0.00	0.27	94.32
HT-12_3	HT-12	30/06/15	71.29	0.32	10.25	0.06	4.99	0.23	0.33	5.31	4.42	0.00	0.24	97.44
HT-12_4	HT-12	30/06/15	72.10	0.34	10.12	0.00	5.00	0.20	0.29	5.36	4.29	0.00	0.23	97.95
HT-12_5	HT-12	30/06/15	70.60	0.35	10.01	0.00	4.83	0.16	0.30	5.17	4.40	0.05	0.22	96.09
HT-12_6	HT-12	30/06/15	69.36	0.29	9.78	0.00	5.04	0.06	0.30	5.00	4.41	0.02	0.24	94.49
HT-12_7	HT-12	30/06/15	71.57	0.27	9.81	0.00	4.91	0.15	0.30	5.24	4.48	0.02	0.26	97.01
HT-12_8	HT-12	30/06/15	71.16	0.29	9.92	0.00	4.74	0.21	0.29	5.45	4.44	0.00	0.26	96.76
HT-12_10	HT-12	30/06/15	69.89	0.33	9.85	0.00	4.86	0.24	0.30	5.35	4.30	0.05	0.27	95.45
HT-12_11	HT-12	30/06/15	71.11	0.37	9.89	0.00	5.08	0.10	0.29	5.21	4.51	0.00	0.27	96.82
HT-12_12	HT-12	30/06/15	70.68	0.29	9.84	0.05	5.02	0.16	0.29	5.27	4.30	0.04	0.25	96.18
HT-12_13	HT-12	30/06/15	71.91	0.30	10.07	0.03	5.05	0.19	0.32	5.07	4.40	0.05	0.26	97.64
HT-12_15	HT-12	30/06/15	69.14	0.34	9.72	0.00	4.92	0.15	0.26	5.23	4.35	0.02	0.25	94.38
HT-12_16	HT-12	30/06/15	70.98	0.26	9.87	0.03	4.98	0.29	0.28	5.19	4.43	0.00	0.23	96.55
HT-12_17	HT-12	30/06/15	69.84	0.34	9.89	0.00	4.98	0.12	0.33	5.18	4.26	0.00	0.26	95.20
HT-12_18	HT-12	30/06/15	72.09	0.37	10.09	0.00	4.97	0.12	0.32	5.18	4.27	0.00	0.26	97.66
HT-12_19	HT-12	30/06/15	70.34	0.34	9.94	0.00	4.67	0.16	0.27	5.22	4.36	0.00	0.27	95.56
HT-12_20	HT-12	30/06/15	71.58	0.33	10.19	0.00	5.35	0.16	0.27	5.71	4.48	0.03	0.26	98.35

Trace element concentrations (ppm) in Hayk glass shards

Label	Tephra	Analysis date	Rb 0.62	Sr 1.05	Y 0.17	Zr 0.37	Nb 0.07	Cs 0.19	Ba 1.88	La 0.09	Ce 0.07	Pr 0.06	Nd 0.25	Sm 0.14	Eu 0.13	Tb 0.06	Dy 0.13	Ho 0.04	Er 0.07	Tm 0.05	Yb 0.15	Lu 0.04	Hf 0.08	Ta 0.06	Pb 0.12	Th 0.01	U 0.00
HT-1_2	HT-2	05/05/15	90.8	129	78.0	597	71.9	0.40	731	80.9	152	17.4	61.5	13.5	2.64	2.19	15.7	3.17	8.70	1.65	7.97	1.25	16.4	5.24	13.3	17.6	4.26
HT-1_4	HT-2	05/05/15	88.4	145	91.3	642	76.0	1.21	805	87.3	157	19.7	78.9	14.0	2.81	2.88	15.5	3.03	9.12	1.65	10.5	1.78	19.2	5.81	15.3	19.6	4.57
HT-1_5	HT-2	05/05/15	85.1	142	83.9	620	77.7	1.13	766	85.1	157	17.8	71.5	16.1	2.78	2.13	14.3	2.73	10.7	1.24	9.59	1.43	17.4	5.66	15.5	18.2	4.11
HT-1_7	HT-2	05/05/15	84.8	178	84.1	618	73.4	0.36	750	81.4	150	17.5	70.7	16.6	1.72	2.75	15.4	3.53	8.49	1.56	7.69	1.41	18.6	5.69	12.2	16.3	3.89
HT-1_8	HT-2	05/05/15	90.3	139	89.5	670	75.8	0.56	756	90.6	154	18.6	66.9	18.2	3.04	2.38	17.1	3.17	10.4	1.43	9.20	1.73	19.9	5.46	13.2	18.8	4.45
HT-1_9	HT-2	05/05/15	81.3	133	81.1	586	71.1	0.77	676	79.8	150	16.5	73.2	14.1	2.40	2.12	12.6	3.30	9.11	1.30	9.16	1.56	17.4	4.98	11.1	17.6	4.05
HT-1_12	HT-2	05/05/15	86.9	132	84.2	599	70.8	0.77	730	80.5	154	17.5	70.9	15.4	2.24	2.14	13.0	2.83	10.2	1.21	8.53	1.48	16.0	5.26	14.4	16.6	4.75
HT-1_13	HT-2	05/05/15	87.1	130	86.0	647	75.9	0.99	758	86.6	164	19.9	77.6	15.7	2.73	2.53	14.6	3.58	8.69	1.48	8.82	1.65	18.9	5.56	12.3	19.4	4.61
HT-1_15	HT-2	05/05/15	85.9	128	80.1	580	72.6	0.75	731	78.2	150	18.4	72.3	13.7	2.10	2.53	16.7	2.67	8.26	1.30	8.27	1.23	15.5	4.85	12.5	17.8	4.27
HT-1_18	HT-2	05/05/15	84.5	122	74.3	570	70.5	0.75	686	76.9	148	17.0	70.9	15.0	2.46	2.09	14.0	2.91	8.87	1.19	8.81	1.27	16.5	4.81	14.4	16.1	4.32
HT-1_19	HT-2	05/05/15	84.4	139	76.6	574	76.7	0.56	720	79.8	150	18.1	63.8	14.0	2.09	2.43	12.8	3.06	9.49	1.23	8.94	1.21	16.6	5.20	13.3	17.6	4.90
HT-1_20	HT-2	05/05/15	91.2	134	79.5	602	73.4	0.63	692	77.5	149	18.5	69.3	15.1	2.79	2.22	13.9	2.88	7.50	1.34	7.79	1.64	14.3	4.72	12.7	17.5	4.76
HT-2_1	HT-4	06/05/15	89.8	122	75.6	557	68.0	0.29	667	74.1	144	15.9	66.5	13.1	2.28	2.38	15.6	3.09	8.26	1.55	8.99	1.23	18.4	4.86	14.1	18.3	4.52
HT-2_2	HT-4	06/05/15	95.3	135	80.5	631	81.6	0.59	757	83.0	158	18.6	73.0	13.9	2.26	2.15	18.0	3.30	9.16	1.68	12.8	1.46	18.8	5.67	16.2	18.9	4.86
HT-2_3	HT-4	06/05/15	88.0	115	70.9	555	70.9	0.88	717	71.5	150	15.8	64.6	16.1	1.91	2.06	12.9	2.56	5.88	1.06	8.14	1.24	14.7	5.16	12.5	15.8	4.62
HT-2_4	HT-4	06/05/15	92.8	123	76.2	605	77.8	1.00	711	77.5	152	17.5	74.6	15.5	2.75	2.22	16.4	3.33	9.05	0.921	9.18	1.28	15.5	5.36	15.4	17.3	5.02
HT-2_5	HT-4	06/05/15	89.4	121	73.3	549	70.3	0.79	669	70.0	140	16.9	65.5	12.3	2.28	1.91	13.0	2.98	7.85	1.27	8.78	1.12	15.4	4.56	13.1	16.3	4.44
HT-2_6	HT-4	06/05/15	90.5	131	78.7	638	77.5	0.83	732	80.9	156	18.1	74.9	11.9	2.37	2.12	13.1	3.28	9.17	1.55	8.91	1.26	16.4	5.13	14.7	18.7	4.51
HT-2_7	HT-4	06/05/15	89.9	124	80.4	590	72.0	0.72	745	82.0	151	18.0	74.8	13.5	2.35	2.44	16.1	2.69	9.68	1.28	8.88	1.36	16.8	5.01	14.4	18.4	4.5
HT-2_8	HT-4	06/05/15	90.9	117	69.7	554	70.9	0.58	658	72.4	145	16.1	62.0	13.3	1.77	2.41	11.9	3.26	6.96	1.09	9.13	1.19	15.4	5.16	15.6	18.1	4.53
HT-2_10	HT-4	06/05/15	92.3	121	74.2	593	71.4	0.89	689	82.1	155	17.4	70.9	18.0	1.77	2.42	11.9	3.17	10.0	1.14	7.92	1.08	17.8	5.70	14.3	17.8	4.64
HT-2_11	HT-4	06/05/15	93.4	130	80.3	614	73.3	0.86	716	82.5	159	17.8	62.0	13.3	2.07	1.99	16.7	3.05	9.52	1.26	8.13	1.16	18.0	5.69	15.6	18.7	4.97
HT-2_12	HT-4	06/05/15	90.1	114	68.1	558	72.8	0.67	666	71.1	143	15.8	65.0	14.2	1.97	2.56	12.4	2.87	8.65	1.07	8.27	1.70	15.9	5.60	15.0	16.0	4.30
HT-2_13	HT-4	06/05/15	98.1	119	73.0	556	65.8	0.38	644	71.1	145	16.4	57.5	12.3	2.01	2.13	12.7	2.57	7.73	1.35	9.26	1.09	18.6	5.51	12.9	15.1	4.42
HT-2_14	HT-4	06/05/15	91.5	106	59.3	471	65.4	0.59	616	64.1	132	15.5	62.3	10.2	1.55	2.05	10.6	2.11	8.14	1.09	6.97	1.17	13.3	4.63	12.5	13.9	4.09
HT-2_15	HT-4	06/05/15	95.6	133	73.6	559	74.9	0.75	702	74.6	153	17.0	68.4	14.4	2.72	2.07	14.0	2.91	7.72	1.37	7.92	1.36	15.8	5.79	16.8	18.0	5.28
HT-2_16	HT-4	06/05/15	86.7	114	66.3	489	68.0	0.87	652	65.4	130	15.2	53.1	8.77	2.40	1.96	10.3	2.20	8.75	1.00	7.85	1.28	16.6	4.76	14.1	14.7	3.98
HT-2_17	HT-4	06/05/15	92.8	114	66.7	498	69.3	0.49	609	68.0	137	15.0	59.5	12.8	2.19	1.77	10.6	2.75	7.44	1.01	7.11	0.98	13.6	4.49	14.3	14.3	4.42
HT-2_18	HT-4	06/05/15	90.6	112	67.2	493	66.3	0.83	660	62.7	138	16.4	58.4	12.5	2.16	1.74	11.8	2.48	7.00	1.06	7.27	1.22	14.5	5.19	13.2	15.6	4.29
HT-2_19	HT-4	06/05/15	93.0	107	60.7	480	66.7	0.85	632	62.9	137	14.9	56.6	11.3	1.33	1.86	12.5	2.20	6.93	1.22	6.83	0.975	14.0	4.34	13.4	14.4	4.51
HT-2_20	HT-4	06/05/15	105	94.1	70.3	517	71.7	0.70	681	74.3	147	18.2	67.4	12.4	1.92	1.94	12.2	2.80	6.96	1.11	8.87	1.22	17.1	5.37	16.5	16.7	5.23
HT-5_1	HT-5	23/07/15	128	44.1	108	630	106	1.01	1220	133	227	25.5	102	19.6	2.21	3.08	20.5	4.40	14.3	1.74	11.6	1.83	19.9	9.70	16.3	32.4	6.54
HT-5_2	HT-5	23/07/15	111	54.5	103	615	105	1.00	1170	127	232	26.5	103	22.9	1.82	2.85	21.0	3.53	12.6	1.51	10.9	1.48	19.2	8.80	19.3	30.3	6.22
HT-5_3	HT-5	23/07/15	118	64.1	112	613	103	0.79	1170	122	212	23.5	86.9	17.6	1.70	2.85	22.4	4.19	10.4	1.51	10.8	1.69	20.2	8.23	17.2	32.5	6.34
HT-5_4	HT-5	23/07/15	114	56.1	103	557	99.7	0.20	1170	113	212	22.6	89.0	17.3	1.54	2.69	17.8	3.60	11.1	1.65	11.2	1.65	18.7	9.23	15.0	27.2	6.41
HT-5_7	HT-5	23/07/15	120	66.2	116	629	105	1.05	1240	134	226	25.7	98.3	17.8	2.76	3.45	21.4	4.53	12.2	1.91	13.5	1.85	20.4	8.77	19.4	29.3	6.10
HT-5_8	HT-5	23/07/15	130	63.3	117	679	101	1.11	1320	131	229	25.3	102	24.2	1.98	3.75	19.4	4.15	14.6	2.02	13.5	2.21	23.7	9.50	21.9	30.4	5.77
HT-5_9	HT-5	23/07/15	104	153	93.3	593	95.3	1.21	1160	112	190	22.6	88.8	21.8	2.88	3.01	19.7	3.13	9.35	2.15	11.4	1.18	16.4	7.62	14.3	28.8	5.91
HT-5_10	HT-5	23/07/15	123	63.4	118	648	103	0.06	1220	132	213	25.5	91.9	19.7	2.35	3.32	20.8	5.17	11.8	2.12	12.7	1.90	20.6	7.73	20.3	28.0	5.76
HT-5_16	HT-5	23/07/15	138	50.2	108	627	106	0.55	1190	119	200	23.5	94.4	23.5	2.66	3.03	19.9	3.91	12.5	1.85	11.5	1.88	20.8	9.37	15.8	31.6	5.91
HT-5_17	HT-5	23/07/15	135	43.2	116	642	107	1.05	1270	129	219	24.8	100	17.7	2.34	3.62	22.1	3.52	13.0	1.73	15.2	1.79	22.2	10.6	16.3	31.1	6.71
HT-5_18	HT-5	23/07/15	131	68.7	116	624	103	0.72	1290	127	223	25.2	95.1	23.5	1.73	3.12	21.4	4.41	14.0	1.85	13.8	1.41	21.2	9.75	16.7	30.1	6.47
HT-5_19	HT-5	23/07/15	137	55.1	111	624	104	0.32	1300	126	216	23.8	93.4	19.1	1.65	3.04	16.5	3.63	12.2	1.61	11.2	1.38	18.8	8.49	17.0	30.5	5.94
HT-5_20	HT-5	23/07/15	117	53.9	92.8	528	104	0.79	1070	98.5	175	20.0	73.5	14.6	1.98	2.15	14.4	3.09	10.5	1.60	10.8	1.69	16.4	7.10	13.6	26.0	5.01
HT-6_8	HT-6	21/07/15	125	45.5	88.2	410	109	0.90	1040	115	195	20.3	84.0	16.7	2.15	2.90	15.4	3.68	10.5	1.23	10.7	1.38	14.7	8.12	14.2	26.6	5.34
HT-6_11	HT-6	21/07/15	122	43.2	88.0	397	99.6	1.09	1050	114	193	21.0	80.9	15.2	1.75	2.50	15.8	3.52	9.92	1.16	9.32	1.32	13.0	8.30	14.5	26.1	5.57
HT-6_12	HT-6	21/07/15	124	45.6	85.5	402	102	0.91	1020	110	189	22.3	83.9	19.8	1.62	2.60	15.7	3.22	10.4	1.44	9.05	1.39	12.7	7.77	14.7	25.0	5.97

Continued on next page

Trace element concentrations (ppm) in Hayk glass shards

Label	Tephra	Analysis date	Rb 0.62	Sr 1.05	Y 0.17	Zr 0.37	Nb 0.07	Cs 0.19	Ba 1.88	La 0.09	Ce 0.07	Pr 0.06	Nd 0.25	Sm 0.14	Eu 0.13	Tb 0.06	Dy 0.13	Ho 0.04	Er 0.07	Tm 0.05	Yb 0.15	Lu 0.04	Hf 0.08	Ta 0.06	Pb 0.12	Th 0.01	U 0.00
HT-6_13	HT-6	21/07/15	128	46.8	85.0	394	107	0.87	969	107	185	20.5	77.8	14.3	1.31	2.60	16.2	2.81	9.10	1.27	8.81	1.37	14.3	7.61	15.2	26.2	5.90
HT-6_15	HT-6	21/07/15	122	43.2	87.1	393	98.3	0.82	950	103	183	20.7	76.9	15.8	1.60	2.73	15.3	3.01	8.89	1.34	10.4	1.56	14.8	8.13	14.4	25.4	5.78
HT-6_19	HT-6	21/07/15	124	41.7	92.1	425	103	1.10	1000	109	191	22.5	79.1	18.9	1.92	2.92	17.5	3.72	10.9	1.51	9.04	1.52	14.5	8.52	15.1	27.6	5.93
HT-6_20	HT-6	21/07/15	119	45.1	91.2	407	96.8	0.79	1040	115	192	21.7	85.4	17.5	1.50	2.19	14.8	3.82	9.24	1.17	9.60	1.16	14.2	7.98	12.8	26.4	5.61
HT-7_1	HT-7	24/07/15	162	-	247	1900	247	1.22	37.8	231	394	48.6	210	41.5	4.56	6.61	41.3	8.63	28.5	3.65	25.7	3.29	52.4	18.5	26.3	32.7	6.59
HT-7_2	HT-7	24/07/15	165	-	250	1900	242	1.43	38.5	220	382	48.6	194	39.9	4.84	6.26	40.7	9.72	26.7	3.88	24.1	3.87	47.2	18.2	27.4	32.2	6.79
HT-7_3	HT-7	24/07/15	171	-	239	1810	238	1.36	34.3	214	385	48.4	194	38.6	4.49	6.33	40.7	8.18	25.2	3.76	23.8	3.51	45.6	18.2	28.4	30.9	7.44
HT-7_4	HT-7	24/07/15	175	-	240	1760	250	1.26	38.4	212	370	46.7	197	39.9	3.63	6.06	42.2	8.48	27.0	3.48	23.9	3.61	43.8	18.3	25.8	32.0	7.1
HT-7_5	HT-7	24/07/15	176	-	250	1910	258	1.81	34.3	230	394	49.7	207	40.2	4.82	6.27	40.9	8.48	27.8	4.22	24.7	4.17	48.6	19.1	28.8	30.7	6.75
HT-7_6	HT-7	24/07/15	168	-	246	1870	240	1.47	37.4	223	382	48.3	185	44.0	4.78	6.60	40.3	8.34	26.7	3.44	23.4	3.29	44.4	17.5	24.9	31.1	6.68
HT-7_7	HT-7	24/07/15	168	-	247	1900	257	1.44	38.5	232	389	49.2	204	39.5	4.61	6.25	42.6	9.28	27.8	4.04	25.5	3.81	51.5	18.6	26.8	31.8	7.2
HT-7_8	HT-7	24/07/15	169	-	219	1670	247	1.38	25.2	202	372	44.1	179	36.0	3.78	5.75	35.6	7.94	23.7	2.94	22.1	3.10	40.4	16.1	27.4	28.9	6.44
HT-7_9	HT-7	24/07/15	171	-	289	2190	261	2.12	74.8	267	458	56.3	239	46.7	4.84	6.75	50.7	10.4	35.2	4.18	30.4	4.51	52.3	20.2	28.6	35.5	7.43
HT-7_10	HT-7	24/07/15	164	-	239	1810	254	1.29	37.5	221	389	48.1	192	38.3	4.49	6.96	40.6	9.21	26.5	3.76	25.4	3.54	48.7	17.7	27.0	30.9	7.27
HT-7_11	HT-7	24/07/15	164	-	251	1970	246	1.68	30.6	232	389	49.4	201	34.4	3.57	6.84	45.0	9.48	28.5	4.00	26.1	3.54	46.4	18.1	24.2	32.0	6.62
HT-7_12	HT-7	24/07/15	166	-	245	1890	247	1.09	41.4	220	388	48.8	197	41.3	3.97	6.77	42.6	9.67	26.8	3.90	24.3	3.40	46.1	17.7	26.6	30.5	6.93
HT-7_13	HT-7	24/07/15	166	-	282	2150	268	2.00	53.4	263	439	57.7	219	46.3	4.60	6.75	47.8	10.5	30.3	4.31	29.6	4.22	54.3	20.3	27.4	34.0	7.81
HT-7_14	HT-7	24/07/15	176	-	234	1800	251	1.32	35.9	218	405	49.3	190	41.7	4.30	6.53	40.5	8.28	26.0	3.80	22.4	3.15	45.1	17.6	26.3	29.2	7.15
HT-7_15	HT-7	24/07/15	157	-	250	1910	244	1.78	36.3	224	394	49.7	189	43.7	4.19	6.93	42.2	10.1	29.1	3.71	24.3	3.39	49.5	18.1	25.9	32.6	7.24
HT-7_16	HT-7	24/07/15	164	-	215	1700	240	1.59	28.1	199	356	42.3	173	35.5	4.24	6.27	36.7	8.01	23.1	3.22	18.2	3.20	43.8	16.3	24.9	28.9	6.85
HT-7_17	HT-7	24/07/15	159	-	236	1780	240	1.30	28.1	220	385	48.4	191	38.4	4.53	6.07	39.0	8.06	25.0	3.76	22.2	3.49	43.3	18.0	25.8	31.6	6.85
HT-7_18	HT-7	24/07/15	157	-	235	1790	247	1.64	33.8	217	371	46.8	197	41.1	5.32	6.03	39.8	8.50	24.5	3.54	24.5	3.70	45.3	18.2	25.9	30.1	6.97
HT-7_19	HT-7	24/07/15	160	-	241	1840	243	1.62	36.1	214	377	47.0	187	41.8	4.67	6.51	39.2	8.67	24.5	3.92	23.9	3.54	47.2	16.9	24.8	28.0	6.98
HT-7_20	HT-7	24/07/15	162	-	245	1800	254	1.31	31.4	214	391	47.4	187	38.3	3.60	6.69	39.7	8.98	25.9	3.66	22.2	3.48	43.6	17.0	26.9	30.3	7.11
HT-9_1	HT-9	23/07/15	257	-	179	856	293	2.24	24.8	156	296	31.8	122	28.0	0.93	4.79	30.0	6.87	19.3	2.78	16.8	2.68	35.4	24.5	34.0	65.9	15.8
HT-9_2	HT-9	23/07/15	251	-	166	783	271	2.06	18.1	148	287	31.9	116	27.6	1.29	4.22	28.4	6.80	18.4	2.86	15.9	2.34	28.9	22.8	33.2	60.5	15.5
HT-9_5	HT-9	23/07/15	258	-	154	766	275	2.32	19.3	146	293	31.9	109	29.4	0.36	3.75	27.2	5.67	16.9	2.99	20.0	2.36	28.2	25.9	34.8	58.8	16.0
HT-9_6	HT-9	23/07/15	251	-	159	748	281	1.75	21.5	146	282	30.6	108	23.1	0.62	4.52	31.9	5.17	16.7	3.16	19.0	2.43	31.3	22.1	34.7	61.0	16.5
HT-9_7	HT-9	23/07/15	255	-	162	803	307	8.23	29.8	147	291	33.5	114	24.6	0.72	3.40	31.2	5.56	19.6	2.47	17.1	2.38	30.8	24.8	39.4	64.1	17.1
HT-9_8	HT-9	23/07/15	245	-	154	724	264	1.88	30.0	137	281	29.0	104	28.0	1.01	4.15	26.0	5.93	15.8	2.38	14.3	2.13	27.5	21.8	30.3	54.0	15.1
HT-9_10	HT-9	23/07/15	276	-	185	879	307	1.32	4.51	181	321	38.8	146	23.4	1.33	4.67	30.6	7.03	19.9	2.65	20.8	3.28	37.1	27.4	35.0	68.2	18.4
HT-9_11	HT-9	23/07/15	238	-	153	730	276	2.65	45.3	140	277	30.0	110	24.0	0.70	4.23	26.9	5.36	13.4	2.42	15.9	2.31	27.1	22.1	33.1	52.4	15.3
HT-9_12	HT-9	23/07/15	243	-	154	722	280	2.26	24.2	140	285	30.1	103	22.3	0.62	4.01	27.3	5.01	16.6	2.54	14.3	2.18	26.9	21.2	31.6	52.4	15.9
HT-9_13	HT-9	23/07/15	259	-	154	722	269	2.79	26.0	136	266	28.4	106	24.5	0.55	3.93	23.4	5.21	16.6	2.11	15.5	2.19	29.8	21.9	33.0	53.4	15.3
HT-9_14	HT-9	23/07/15	262	-	171	809	280	1.81	22.4	161	290	32.5	116	29.4	0.88	3.80	27.1	5.53	18.3	3.03	18.5	2.56	28.4	23.8	35.5	62.8	16.2
HT-9_16	HT-9	23/07/15	285	-	175	822	278	2.68	18.8	156	294	34.5	130	29.2	0.54	5.75	31.0	5.37	16.6	3.31	19.0	2.25	32.5	23.6	33.4	62.3	17.0
HT-9_18†	HT-9	23/07/15	249	-	198	864	267	2.47	42.9	169	277	33.6	106	30.3	-	5.05	33.6	6.97	18.5	1.76	22.0	1.77	31.7	23.8	36.4	70.4	15.9
HT-9_19	HT-9	23/07/15	217	-	118	576	237	2.44	17.1	111	229	23.7	91.1	19.2	-	3.54	20.8	4.45	13.8	1.90	13.0	1.50	22.2	20.4	28.6	46.0	15.1
HT-9_20	HT-9	23/07/15	250	-	157	723	268	2.92	29.2	137	276	30.6	109	26.6	-	4.17	26.3	5.52	14.9	2.13	17.3	2.24	29.1	22.9	32.0	58.6	16.2
HT-10_1	HT-10	21/07/15	244	-	120	597	236	2.17	20.0	112	217	23.4	85.6	19.3	0.29	3.19	21.4	4.28	13.6	1.89	12.4	1.84	22.4	18.4	27.0	44.6	15.0
HT-10_2	HT-10	21/07/15	241	-	100	505	225	1.95	9.12	99.5	197	19.5	69.8	15.6	0.23	2.50	16.0	3.63	11.5	1.67	10.9	1.44	17.2	16.6	32.8	42.3	14.2
HT-10_5	HT-10	21/07/15	235	6.91	109	593	238	2.30	60.6	107	205	22.9	83.8	17.6	0.50	2.91	18.5	4.20	11.0	1.75	12.8	1.79	20.9	18.4	33.0	41.9	15.7
HT-10_7	HT-10	21/07/15	240	-	124	611	246	2.26	26.2	113	222	23.4	82.3	18.6	0.61	3.82	21.2	3.93	11.9	1.82	14.1	1.97	23.6	18.7	33.2	43.7	14.4
HT-10_8	HT-10	21/07/15	240	-	118	584	253	2.07	16.0	107	222	23.2	86.2	21.1	0.39	3.47	21.5	4.48	11.4	2.09	12.7	1.80	22.0	19.2	33.0	46.7	16.9
HT-10_10	HT-10	21/07/15	263	-	115	571	239	2.39	16.8	118	234	26.3	86.5	18.5	0.34	2.93	17.7	4.36	13.0	2.07	12.8	1.80	21.5	20.4	35.8	47.7	16.5
HT-10_11	HT-10	21/07/15	266	-	149	725	274	2.42	24.0	133	280	29.8	106	23.7	0.43	3.79	24.5	5.13	18.1	2.40	14.4	2.21	26.1	23.4	35.3	52.3	16.2
HT-10_13	HT-10	21/07/15	245	-	144	739	274	2.51	17.7	123	240	25.8	96.5	20.6	0.50	4.03	25.4	5.07	15.0	2.19	16.2	2.16	27.0	22.1	34.5	55.4	17.1
HT-10_14	HT-10	21/07/15	255	-	117	631	236	2.30	22.2	119	229	26.1	79.5	17.5	0.43	3.47	23.9	4.69	14.6	2.00	13.1	1.74	23.6	18.6	39.6	47.5	15.6
HT-10_17	HT-10	21/07/15	249	-	109	545	241	2.52	21.1	106	214	25.9	86.7	18.5	0.03	3.21	20.3	4.11	14.0	1.78	13.7	2.05	24.0	19.6	32.7	47.3	15.6

Continued on next page

Trace element concentrations (ppm) in Hayk glass shards

Label	Tephra	Analysis date	Rb 0.62	Sr 1.05	Y 0.17	Zr 0.37	Nb 0.07	Cs 0.19	Ba 1.88	La 0.09	Ce 0.07	Pr 0.06	Nd 0.25	Sm 0.14	Eu 0.13	Tb 0.06	Dy 0.13	Ho 0.04	Er 0.07	Tm 0.05	Yb 0.15	Lu 0.04	Hf 0.08	Ta 0.06	Pb 0.12	Th 0.01	U 0.00
HT-10_19	HT-10	21/07/15	265	-	119	586	254	3.49	19.3	114	232	23.2	95.1	20.9	0.49	2.81	19.8	4.38	13.4	2.04	12.1	1.80	22.5	21.2	38.8	48.2	17.7
HT-10_20	HT-10	21/07/15	256	-	137	667	261	2.20	23.7	125	245	26.8	108	20.5	0.93	3.35	21.8	4.96	12.3	2.43	14.2	1.85	24.3	20.6	33.1	49.4	16.2
HT-12_1	HT-12	23/07/15	158	2.2	183	1490	214	1.51	108	175	346	40.2	150	31.0	4.55	5.06	34.2	7.31	18.9	2.90	20.8	2.69	37.5	16.2	26.8	26.3	7.67
HT-12_2	HT-12	23/07/15	164	-	191	1640	220	1.32	110	188	371	42.0	172	34.8	5.04	5.72	37.3	7.48	24.0	2.92	21.6	3.27	41.5	15.8	25.9	27.2	7.32
HT-12_3	HT-12	23/07/15	155	-	188	1550	214	1.08	103	174	332	38.7	162	35.1	4.32	5.20	35.1	7.15	21.5	3.23	20.6	3.18	40.8	15.7	28.4	25.9	7.44
HT-12_4	HT-12	23/07/15	168	-	181	1460	212	1.35	97.1	160	334	37.9	150	31.4	3.82	4.90	30.7	7.23	21.6	2.93	20.2	2.91	38.6	15.0	28.0	24.5	7.01
HT-12_5	HT-12	23/07/15	162	-	189	1600	222	1.62	113	179	348	41.5	160	32.9	5.06	5.52	36.4	7.41	22.3	3.42	20.6	2.99	42.0	17.5	28.4	27.7	7.63
HT-12_6	HT-12	23/07/15	165	-	202	1650	226	1.30	106	186	374	42.0	156	35.8	4.55	5.98	35.8	6.84	19.8	3.29	23.4	2.96	42.1	16.4	27.3	28.3	7.00
HT-12_7	HT-12	23/07/15	160	-	185	1520	220	1.56	104	174	355	40.9	164	30.0	4.51	5.72	31.6	7.09	21.4	2.98	20.2	2.71	41.2	16.3	30.5	26.1	7.63
HT-12_8	HT-12	23/07/15	156	-	202	1610	219	1.28	112	179	356	40.5	165	32.3	4.66	5.35	32.6	7.45	23.9	3.06	21.4	2.93	41.6	16.4	28.4	26.7	7.24
HT-12_10	HT-12	23/07/15	168	-	192	1660	227	1.44	115	178	356	40.8	165	34.3	5.25	6.04	36.1	7.58	20.7	3.04	20.2	2.86	41.9	15.0	28.1	27.7	7.56
HT-12_11	HT-12	23/07/15	163	-	195	1540	222	1.36	109	176	348	37.8	162	30.0	4.17	5.80	31.6	6.72	21.0	2.76	19.7	2.69	42.0	17.0	29.3	27.3	7.38
HT-12_12	HT-12	23/07/15	161	-	200	1570	218	1.19	115	182	353	41.4	169	34.2	4.84	5.30	37.1	7.29	22.6	3.29	21.0	3.02	40.6	16.1	27.0	27.5	7.61
HT-12_13	HT-12	23/07/15	155	-	182	1530	224	1.52	104	163	337	37.9	152	32.5	4.03	5.03	33.8	6.79	20.3	2.98	19.1	2.86	38.8	15.4	27.4	25.3	7.29
HT-12_15	HT-12	23/07/15	162	-	202	1650	222	1.59	116	185	357	44.7	175	40.0	5.17	5.60	37.0	6.68	21.4	3.08	19.5	3.32	43.0	16.2	26.0	27.5	7.74
HT-12_16	HT-12	23/07/15	150	-	199	1620	229	1.29	112	176	356	40.6	172	35.4	4.35	5.60	36.9	7.48	24.5	3.38	21.0	3.14	41.8	16.0	29.0	27.7	7.06
HT-12_17	HT-12	23/07/15	159	-	195	1600	221	1.42	108	178	364	41.9	166	33.7	5.09	6.09	33.7	7.31	22.9	3.32	19.7	3.03	39.5	15.8	28.9	28.0	7.03
HT-12_18	HT-12	23/07/15	162	-	198	1560	221	1.28	113	182	347	39.7	166	32.2	3.79	4.96	35.2	7.17	22.6	2.67	21.4	2.96	41.4	14.9	28.0	27.2	7.69
HT-12_19	HT-12	23/07/15	163	-	180	1420	217	1.66	104	160	334	36.4	148	30.8	4.06	4.99	31.4	6.83	21.9	2.85	18.3	2.53	36.8	16.2	30.7	25	7.45
HT-12_20	HT-12	23/07/15	179	-	170	1330	210	1.42	95.6	153	309	34.0	132	28.8	3.85	4.90	28.4	5.79	20.0	2.35	18.4	2.21	35.6	13.5	29.2	23.0	7.38

Unnormalised major element concentrations (wt.%) in Dubbi 1861 tephra glass shards

Label	Tephra	Analysis date	SiO_2 0.08	TiO_2 0.05	Al_2O_3 0.05	MgO 0.04	FeO^T 0.08	MnO 0.07	CaO 0.04	Na_2O 0.08	K_2O 0.03	P_2O_5 0.10	Cl 0.02	Total
Dubbi_1_1	Dubbi 1861	03/07/15	68.56	0.16	11.66	0.02	2.68	0.09	0.25	5.34	4.18	0.01	0.33	93.29
Dubbi_1_4	Dubbi 1861	03/07/15	67.57	0.10	11.50	0.00	3.04	0.08	0.27	5.11	4.24	0.01	0.34	92.27
Dubbi_1_5	Dubbi 1861	03/07/15	68.56	0.21	11.88	0.00	2.91	0.09	0.27	5.34	4.09	0.00	0.32	93.67
Dubbi_1_6	Dubbi 1861	03/07/15	68.74	0.18	11.93	0.01	2.97	0.00	0.29	5.27	4.06	0.00	0.34	93.80
Dubbi_1_7	Dubbi 1861	03/07/15	67.43	0.17	11.53	0.00	3.00	0.07	0.30	5.34	4.15	0.01	0.37	92.37
Dubbi_1_9	Dubbi 1861	03/07/15	68.13	0.15	11.71	0.01	2.84	0.05	0.30	5.01	4.26	0.00	0.34	92.81
Dubbi_1_10	Dubbi 1861	03/07/15	61.56	0.42	16.22	0.00	6.64	0.29	2.25	5.05	6.37	0.02	0.04	98.84
Dubbi_1_11	Dubbi 1861	03/07/15	67.72	0.18	11.62	0.00	2.84	0.17	0.30	4.93	4.12	0.00	0.36	92.23
Dubbi_1_12	Dubbi 1861	03/07/15	68.23	0.20	11.63	0.00	3.02	0.03	0.30	5.36	4.29	0.00	0.34	93.38
Dubbi_1_13	Dubbi 1861	03/07/15	68.46	0.17	11.60	0.04	3.30	0.11	0.25	5.46	4.17	0.00	0.34	93.90
Dubbi_1_15	Dubbi 1861	03/07/15	67.60	0.21	12.03	0.02	2.99	0.09	0.27	4.93	4.32	0.00	0.36	92.81
Dubbi_1_17	Dubbi 1861	03/07/15	67.76	0.16	11.61	0.00	3.01	0.11	0.27	5.17	4.23	0.03	0.39	92.74
Dubbi_1_18	Dubbi 1861	03/07/15	68.07	0.14	11.65	0.00	2.93	0.00	0.26	4.91	4.21	0.00	0.36	92.55
Dubbi_1_20	Dubbi 1861	03/07/15	68.56	0.11	11.55	0.00	3.10	0.13	0.29	2.74	4.30	0.04	0.39	91.19
Dubbi_1/2_7	Dubbi 1861	03/07/15	66.49	0.15	11.71	0.00	3.05	0.05	0.39	5.35	4.08	0.01	0.31	91.58

Trace element concentrations (ppm) in Dubbi 1861 tephra glass shards

Label	Tephra	Analysis date	Rb 0.62	Sr 1.05	Y 0.17	Zr 0.37	Nb 0.07	Cs 0.19	Ba 1.88	La 0.09	Ce 0.07	Pr 0.06	Nd 0.25	Sm 0.14	Eu 0.13	Tb 0.06	Dy 0.13	Ho 0.04	Er 0.07	Tm 0.05	Yb 0.15	Lu 0.04	Hf 0.08	Ta 0.06	Pb 0.12	Th 0.01	U 0.00
Dubbi_1_1	Dubbi 1861	28/07/15	199	-	255	2410	390	1.76	3.00	239	397	49.5	190	37.0	1.58	7.44	47.4	9.20	27.8	3.91	25.8	4.13	68.0	30.2	36.3	52.5	11.9
Dubbi_1_4	Dubbi 1861	28/07/15	193	-	232	2220	368	1.06	2.95	220	382	45.1	178	39.4	1.58	6.74	43.0	7.84	24.2	3.42	22.3	2.82	60.6	25.3	47.8	45.4	14.2
Dubbi_1_5	Dubbi 1861	28/07/15	185	-	221	2170	377	1.44	4.31	211	356	42.8	170	33.7	1.99	5.86	43.8	7.28	23.8	3.50	22.2	2.60	55.5	26.6	37.6	47.2	10.9
Dubbi_1_6	Dubbi 1861	28/07/15	193	-	211	2070	376	1.34	1.77	204	371	43.8	165	33.3	1.38	6.52	39.3	7.82	24.7	3.36	20.5	3.05	52.4	27.9	37.3	44.4	10.6
Dubbi_1_7	Dubbi 1861	28/07/15	198	-	225	2200	383	1.46	0.14	211	374	44.5	175	35.9	1.39	6.40	40.7	8.50	24.9	3.48	21.4	3.16	58.4	27.8	41.0	45.9	11.6
Dubbi_1_9	Dubbi 1861	28/07/15	196	-	209	2110	390	1.63	1.56	211	390	45.5	167	38.1	1.54	7.08	40.4	8.03	23.8	3.06	21.2	2.79	54.4	28.2	41.0	46.9	11.1
Dubbi_1_10	Dubbi 1861	28/07/15	47.5	-	77.5	695	105	0.06	545	199	334	40.0	158	22.7	3.49	2.42	19.2	3.44	8.59	1.12	8.90	1.35	19.2	6.3	10.7	13.3	2.85
Dubbi_1_11	Dubbi 1861	28/07/15	197	-	226	2250	402	1.56	8.10	221	385	45.2	179	37.7	1.28	6.32	40.1	8.98	25.5	3.40	22.8	2.82	57.8	28.5	36.9	49.1	11.8
Dubbi_1_12†	Dubbi 1861	28/07/15	183	-	302	3050	431	1.44	-	269	421	56.1	206	53.2	1.32	8.55	50.1	10.7	29.7	4.23	25.7	4.01	81.8	33.3	35.8	63.2	10.5
Dubbi_1_13	Dubbi 1861	28/07/15	196	-	248	2420	402	1.64	4.51	238	415	49.4	201	39.0	1.79	6.31	46.7	9.14	23.2	3.97	24.6	3.46	65.2	28.6	38.9	51.1	11.8
Dubbi_1_15†	Dubbi 1861	28/07/15	192	-	302	3220	430	1.04	1.20	306	458	60.9	230	48.3	1.58	9.24	58.0	10.3	31.2	3.62	33.3	4.74	90.5	36.9	36.1	71.2	10.8
Dubbi_1_17	Dubbi 1861	28/07/15	210	-	251	2440	388	1.05	5.77	236	404	46.8	187	39.9	1.72	7.44	49.8	9.53	24.1	4.01	27.7	3.47	69.9	32.6	51.4	55.9	12.0
Dubbi_1_18	Dubbi 1861	28/07/15	193	-	222	2270	382	1.42	3.29	210	367	43.1	174	36.1	1.06	6.4	42.8	8.42	24.4	3.52	22.4	3.22	56.9	28.2	35.2	46.7	11.0
Dubbi_1_20†	Dubbi 1861	28/07/15	197	-	347	3550	519	1.59	2.37	332	491	62.8	243	52.6	1.69	9.63	68.1	12.7	33.3	5.62	36.5	5.28	107	43.9	37.3	81.9	11.1
Dubbi_1/2_7	Dubbi 1861	28/07/15	193	-	185	1820	365	1.62	-	188	350	41.3	149	32.5	1.38	6.2	32.5	6.15	20.0	2.56	19.6	2.50	49.5	24.6	43.2	41.4	11.1

.3.2 Bayesian age models

The following pages show the OxCal (Bronk Ramsey, 2009*b*) code used to generate the Ashenge and Hayk Bayesian age models. These P_sequence models allow for more flexible modelling of the data to the IntCal13 calibration curve. Statistical outliers were included in the model, but given less weighting. Two models were run either side of a sedimentary hiatus at 650 cm depth in the Ashenge archive. The core depths are corrected for the presence of > 0.5 cm thick tephras, which are assumed to have been deposited instantaneously. Tephra age ranges were then extracted from the age model using the *Date* function.

Ashenge

Ashenge OxCal script

Two P_sequence models, above and below a sedimentary hiatus at 650 cm, with outlier analysis

```
Options()
{
 BCAD=FALSE;
 PlusMinus=FALSE;
};
Plot()
{
 Sequence("Ashenge")
 {
 P_Sequence("Ashenge1",1,0.5,U(-2,2))
 {
  Boundary()
  {
  z=793.5;
  };
  R_Date("SUERC-6273",14309,123)
  {
  z=793;
  };
  R_Date("SUERC-6270",12810,99)
  {
  z=765;
  };
  Date("AST9")
  {
  z=751.5;
  };
  Date("AST8")
  {
  z=738.5;
  };
  R_Date("Beta analytic 739.5",11920,40)
  {
  z=734;
  };
  R_Date("SUERC-6269",10127,66)
  {
  z=651.5;
  };
  Boundary("hiatus_start")
  {
  z=644.55;
  };
 };
 P_Sequence("Ashenge2",1,0.5,U(-2,2))
 {
  Boundary("hiatus")
  {
  z=644.5;
  };
  R_Combine("SUERC-7439/SUERC-7178")
  {
  R_Date("SUERC-7439",6622,40);
  R_Date("SUERC-7178",6696,40);
  z=640;
  };
  Date("AST7")
  {
  z=629.5;
  };
  Date("AST6")
  {
  z=618.5;
  };
  Date("AST5")
  {
  z=604.5;
  };
  R_Date("SUERC-29481",5671,39)
  {
  z=597.5;
  };
  R_Date("SUERC-6268",5063,34)
  {
  z=548.5;
  };
  Date("AST4")
  {
  z=524;
  };
  R_Date("SUERC-6266",4714,30)
  {
  Outlier( );
  z=482.5;
  };
  Date("AST3")
  {
  z=482;
  };
  R_Date("SUERC-29480",4361,38)
  {
  z=437.5;
  };
  Date("AST2")
  {
  z=436;
  };
  R_Date("SUERC-29479",4143,38)
  {
  z=384.5;
  };
  R_Date("SUERC-29478",3298,35)
  {
  z=339.5;
  };
  R_Date("SUERC-6265",2865,28)
  {
  z=298.5;
  };
  R_Date("SUERC-29477",2082,37)
  {
  z=244.5;
  };
  R_Date("SUERC-6264",1609,22)
  {
  z=173.5;
  };
  R_Date("SUERC-29476",923,35)
  {
  z=102.5;
  };
  R_Date("SUERC-6263",618,31)
  {
  z=49.5;
  };
  Date("AST1")
  {
  z=10;
  };
  R_Date("SUERC-29473",377,37)
  {
  z=3.5;
  };
  Boundary()
  {
  z=0;
  };
 };
};
```

OxCal output

	Unmodelled (BP)		Modelled (BP)	
Boundary			509	234
R_Date SUERC-29473	508	316	506	316
AST1			545	322
R_Date SUERC-6263	658	549	658	550
R_Date SUERC-29476	925	762	927	777
R_Date SUERC-6264	1554	1415	1553	1415
R_Date SUERC-29477	2146	1950	2150	1951
R_Date SUERC-6265	3070	2882	3069	2883
R_Date SUERC-29478	3610	3450	3611	3450
R_Date SUERC-29479	4826	4550	4808	4527
AST2			5041	4831
R_Date SUERC-29480	5039	4850	5039	4852
AST3			5627	4974
R_Date SUERC-6266	5581	5324	5581	5324
AST4			5878	5332
R_Date SUERC-6268	5907	5735	5907	5741
R_Date SUERC-29481	6560	6323	6564	6324
AST5			7160	6347
AST6			7505	6484
AST7			7577	6720
R_Combine SUERC-7439/SUERC-7178	7582	7484	7581	7478
Boundary hiatus			7725	7463
P_Sequence Ashenge2	-2	2	-1.52819	-0.98019
Boundary hiatus_start			12018	10718
R_Date SUERC-6269	12021	11404	12013	11397
R_Date Beta analytic 739.5	13944	13567	13961	13575
AST8			14593	13583
AST9			15335	13848
R_Date SUERC-6270	15671	14967	15675	15005
R_Date SUERC-6273	17793	17070	17711	16975
Boundary			17779	16963
P_Sequence Ashenge1	-2	2	-1.34794	-0.55594

OxCal age model

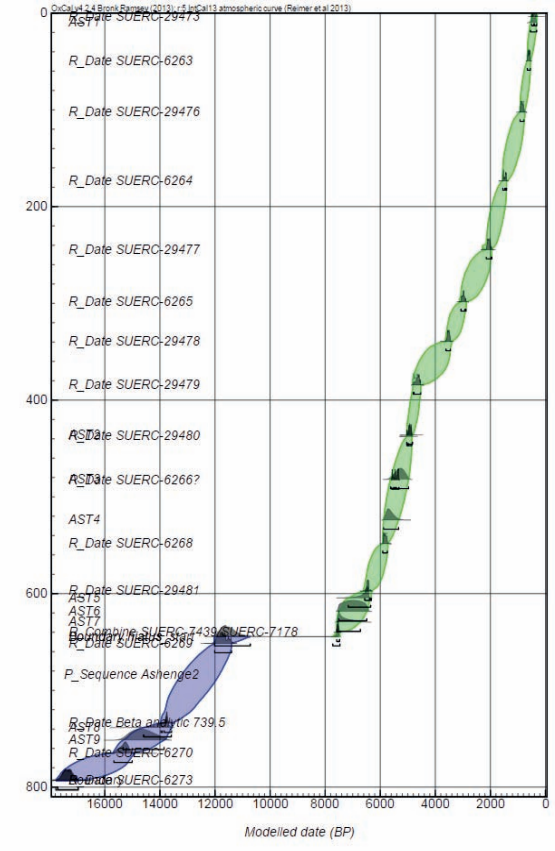

Hayk

Hayk OxCal script
P_sequence model, with outlier analysis

```
Options()
{
 BCAD=FALSE;
 PlusMinus=FALSE;
};
Plot()
{
 Outlier_Model("General",T(5),U(0,4),"t");
 P_Sequence("",1,0.1,U(-2,2))
 {
  Boundary()
  {
   z=748.5;
  };
  R_Date("14c 14",12873,60)
  {
   Outlier(0.05);
   z=716;
  };
  R_Date("14c 13",12846,67)
  {
   Outlier(0.05);
   z=656;
  };
  Date("HT12")
  {
   z=460.5;
  };
  R_Date("14c 12",10254,62)
  {
   Outlier(0.05);
   z=446;
  };
  R_Date("14c 11",10393,46)
  {
   Outlier(0.05);
   z=440.5;
  };
  R_Date("14c 10",10287,45)
  {
   Outlier(0.05);
   z=427.5;
  };
  R_Date("14c 9",10102,44)
  {
   Outlier(0.05);
   z=395;
  };
  Date("HT11")
  {
   z=385.5;
  };
  R_Date("14c 8",9643,79)
  {
   Outlier(0.05);
   z=313;
  };
  Date("HT10")
  {
   z=287.5;
  };
  Date("HT9")
  {
   z=266.5;
  };
  R_Date("14c 7",7650,45)
  {
   Outlier(0.05);
   z=238.5;
  };
  Date("HT8")
  {
   z=198.5;
  };
  R_Date("14c 6",4914,35)
  {
   Outlier(0.05);
   z=194.5;
  };
  R_Date("14c 5",4068,33)
  {
   Outlier(0.05);
   z=181.5;
  };
  Date("HT7")
  {
   z=179.5;
  };
  R_Date("14c 4",3563,36)
  {
   Outlier(0.05);
   z=170.5;
  };
  Date("HT6")
  {
   z=167.5;
  };
  Date("HT5")
  {
   z=158.5;
  };
  Date("HT4")
  {
   z=144.5;
  };
  R_Date("14c 3",2795,31)
  {
   Outlier(0.05);
   z=139.5;
  };
  Date("HT3")
  {
   z=118.5;
  };
  Date("HT2")
  {
   z=108.5;
  };
  R_Date("14c 2",2485,32)
  {
   Outlier(0.05);
   z=100;
  };
  Date("HT1")
  {
   z=66;
  };
  R_Date("14c 1",1583,32)
  {
   Outlier(0.05);
   z=12.5;
  };
  Boundary(Date(N(2010,1)))
  {
   z=0;
  };
 };
};
```

OxCal output

	Unmodelled (BP)		Modelled (BP)	
	from	to	from	to
Boundary(N(2010,1))	-57	-61	-57	-61
R_Date 14c 1	1545	1404	1568	-63
HT1			2617	1607
R_Date 14c 2	2729	2433	2729	2432
HT2			2876	2461
HT3			2930	2518
R_Date 14c 3	2965	2795	2973	2795
HT4			3635	2793
HT5			3910	2914
HT6			3983	3236
R_Date 14c 4	3971	3724	3973	3723
HT7			4803	3834
R_Date 14c 5	4802	4438	4803	4436
R_Date 14c 6	5716	5592	5719	5590
HT8			7240	5582
R_Date 14c 7	8540	8385	8543	8380
HT9			10510	8433
HT10			11046	8906
R_Date 14c 8	11205	10749	11196	10717
HT11			11963	11298
R_Date 14c 9	11971	11404	11985	11414
R_Date 14c 10	12379	11829	12237	11837
R_Date 14c 11	12516	12060	12369	12018
R_Date 14c 12	12378	11757	12384	12026
HT12			12954	12028
R_Date 14c 13	15599	15120	15468	15066
R_Date 14c 14	15616	15158	15728	15259
Boundary			17692	15349
P_Sequence(1,0.1,U(-2,2))	-2	2	-1.46283	-1.21883
U(0,4)	3.99E-17	4	5.38E-17	3.68
T(5)	-2.65	2.65		
Outlier_Model General			-1577	551

OxCal age model

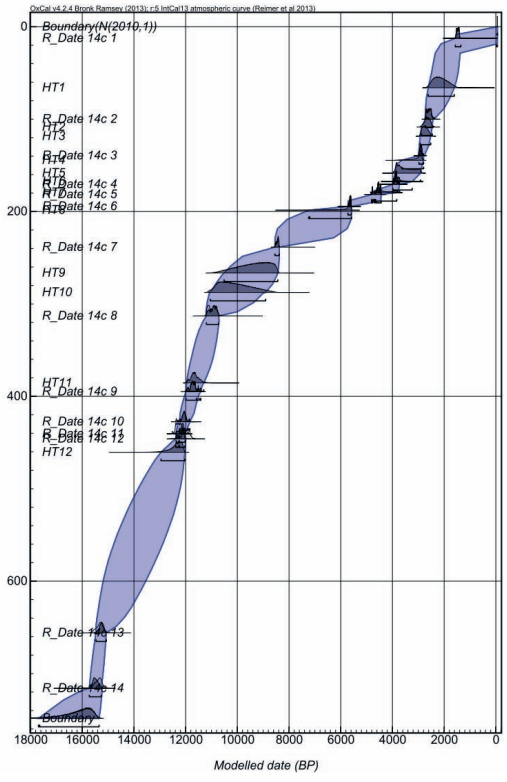

.4 Tephras from the YTVL

The following Appendix provides the major and trace element glass compositions of glass shards in tephras from the lakes Hora and Dendi sediments. At the end of this Appendix, the age model for the Dendi archive is provided.

.4.1 Major and trace element glass compositions

Shard specific major and trace element concentrations in the Hora and Dendi tephras are given in the following tables. Major element data is presented to 2 decimal places, and trace element data is presented to 3 significant figures. Major element conncentrations presented are unnormalised.

Some major elements (e.g. Cl) were not analysed on all analytical sessions, and all Fe is calculated as FeO^T. The median LLD for the rhyolitic ATHO-G reference material over all EPMA analytical sessions is given in the following table headings, full details of the limits of detection are on page 401. In some shards MgO and P_2O_5 are below the limit of detection, all other elements are present at concentrations above the LLD.

Most glass shards were analysed for trace elements using 20 μm crater diameters, however, †indicates analyses using 10 μm crater diameters. LA-ICP-MS lower limits of detection (LLD) are given on page 407. For comparison, median LLD concentrations at 20 μm crater diameters of all LA-ICP-MS analytical sessions are given in the following table headings. Some low Sr and Ba sample concentrations, coupled with high concentrations of these analytes in the gas blank, caused negative concentrations to be measured. These negative values are indicated with a dash. Analyses of MPI-DING reference materials

were used to check EPMA and LA-ICP-MS accuracy. These analyses are given on page 398, and are ordered by analysis date.

Unnormalised major element concentrations (wt.%) in Hora tephra glass shards

Label	Tephra	Analysis date	SiO_2 0.08	TiO_2 0.05	Al_2O_3 0.05	MgO 0.04	FeO^T 0.08	MnO 0.07	CaO 0.04	Na_2O 0.08	K_2O 0.03	P_2O_5 0.10	Cl 0.02	Total
HRT_2_1	HRT-1	29/06/15	72.62	0.18	9.31	0.00	4.31	0.28	0.17	4.91	4.17	0.00	0.18	96.14
HRT_2_2	HRT-1	29/06/15	72.53	0.25	9.41	0.00	4.41	0.13	0.20	5.06	4.35	0.08	0.25	96.66
HRT_2_3	HRT-1	29/06/15	71.26	0.26	9.03	0.00	4.54	0.27	0.13	4.93	4.22	0.00	0.21	94.84
HRT_2_4	HRT-1	29/06/15	70.48	0.29	8.97	0.00	4.42	0.17	0.17	4.89	4.21	0.00	0.20	93.79
HRT_2_5	HRT-1	29/06/15	71.48	0.20	9.08	0.00	4.47	0.17	0.16	5.07	4.29	0.00	0.21	95.13
HRT_2_6	HRT-1	29/06/15	73.33	0.25	9.43	0.00	4.25	0.29	0.14	5.17	4.44	0.00	0.22	97.51
HRT_2_7	HRT-1	29/06/15	72.56	0.25	9.28	0.02	4.52	0.21	0.15	4.88	4.38	0.00	0.23	96.46
HRT_2_8	HRT-1	29/06/15	71.68	0.25	9.13	0.02	4.54	0.18	0.17	4.97	4.26	0.00	0.23	95.41
HRT_2_10	HRT-1	29/06/15	69.08	0.24	8.64	0.00	4.37	0.19	0.18	5.10	4.23	0.00	0.23	92.27
HRT_2_11	HRT-1	29/06/15	72.56	0.22	9.40	0.01	4.53	0.13	0.16	5.04	4.43	0.00	0.19	96.67
HRT_2_12	HRT-1	29/06/15	73.04	0.27	9.27	0.00	4.50	0.26	0.20	5.21	4.35	0.00	0.22	97.32
HRT_2_13	HRT-1	29/06/15	71.55	0.22	9.03	0.00	4.28	0.22	0.20	5.02	4.36	0.00	0.20	95.09
HRT_2_14	HRT-1	29/06/15	70.48	0.24	8.91	0.00	4.25	0.14	0.15	4.64	4.31	0.00	0.22	93.34
HRT_2_15	HRT-1	29/06/15	72.40	0.23	9.27	0.00	4.26	0.21	0.18	5.11	4.45	0.00	0.24	96.35
HRT_2_16	HRT-1	29/06/15	72.96	0.23	9.24	0.03	4.48	0.24	0.15	4.97	4.40	0.00	0.23	96.92
HRT_2_17	HRT-1	29/06/15	70.34	0.23	9.07	0.05	4.36	0.17	0.18	4.93	4.28	0.02	0.22	93.87
HRT_2_18	HRT-1	29/06/15	72.65	0.23	9.25	0.00	4.31	0.23	0.19	4.96	4.30	0.01	0.28	96.41
HRT_2_19	HRT-1	29/06/15	68.35	0.23	10.57	0.48	4.10	0.09	0.20	4.42	4.06	0.00	0.20	92.70
HRT_2_20	HRT-1	29/06/15	69.14	0.23	9.25	0.00	3.75	0.21	0.18	3.89	4.30	0.00	0.19	91.14
HRT_2B_1	HRT-1	29/06/15	71.20	0.26	12.81	0.00	3.09	0.21	0.41	5.34	4.57	0.00	0.15	98.05
HRT_2B_2	HRT-1	29/06/15	69.34	0.25	12.75	0.07	3.21	0.08	0.39	5.05	4.63	0.00	0.17	95.93
HRT_2B_3	HRT-1	29/06/15	69.29	0.28	12.57	0.09	2.96	0.09	0.41	5.09	4.60	0.00	0.18	95.55
HRT_2B_4	HRT-1	29/06/15	67.32	0.23	15.74	0.14	2.98	0.19	0.41	4.62	4.32	0.00	0.13	96.10
HRT_2B_5	HRT-1	29/06/15	71.35	0.27	13.16	0.07	3.15	0.15	0.37	5.22	4.73	0.00	0.15	98.62
HRT_2B_6	HRT-1	29/06/15	71.35	0.26	13.07	0.06	3.28	0.11	0.40	5.26	4.74	0.00	0.15	98.67
HRT_2B_7	HRT-1	29/06/15	69.99	0.21	12.82	0.08	2.91	0.12	0.35	5.07	4.81	0.07	0.17	96.60
HRT_2B_8	HRT-1	29/06/15	71.60	0.27	13.13	0.02	3.10	0.18	0.39	5.22	4.67	0.07	0.17	98.81
HRT_2B_9	HRT-1	29/06/15	69.32	0.27	13.71	0.03	3.03	0.10	0.40	5.04	4.56	0.02	0.19	96.68
HRT_2B_10	HRT-1	29/06/15	70.77	0.27	13.18	0.06	2.95	0.11	0.36	5.19	4.77	0.03	0.18	97.86
HRT_2B_11	HRT-1	29/06/15	71.98	0.31	13.02	0.07	3.16	0.09	0.40	2.99	4.78	0.00	0.17	96.97
HRT_2B_12	HRT-1	29/06/15	70.68	0.21	12.99	0.07	3.09	0.20	0.36	4.96	4.66	0.01	0.18	97.40
HRT_2B_13	HRT-1	29/06/15	71.24	0.30	13.06	0.08	3.26	0.18	0.38	5.21	4.60	0.00	0.19	98.48
HRT_2B_14	HRT-1	29/06/15	69.03	0.26	12.43	0.06	3.05	0.09	0.34	4.86	4.43	0.00	0.16	94.71
HRT_2B_15	HRT-1	29/06/15	70.95	0.23	12.95	0.07	3.05	0.11	0.37	5.47	4.57	0.00	0.15	97.90
HRT_2B_16	HRT-1	29/06/15	69.28	0.29	12.45	0.04	2.97	0.10	0.30	5.20	4.66	0.00	0.17	95.44
HRT_2B_17	HRT-1	29/06/15	67.09	0.21	12.15	0.10	3.13	0.10	0.36	4.81	4.55	0.02	0.13	92.66
HRT_2B_18	HRT-1	29/06/15	71.16	0.25	13.16	0.09	3.27	0.09	0.42	5.07	4.74	0.03	0.15	98.46
HRT_2B_19	HRT-1	29/06/15	70.98	0.28	13.11	0.03	3.20	0.20	0.40	5.60	4.69	0.02	0.17	98.69
HRT_2B_20	HRT-1	29/06/15	68.77	0.27	12.56	0.03	3.02	0.17	0.44	4.80	4.67	0.01	0.15	94.89
HRT-4_1	HRT-2	26/08/14	71.76	0.15	8.19	0.02	6.38	0.37	0.15	6.32	4.17	0.01		97.52
HRT-4_10	HRT-2	26/08/14	68.33	0.12	8.59	0.00	6.52	0.31	0.23	6.17	4.21	0.00		94.49
HRT-4_11	HRT-2	26/08/14	73.67	0.25	9.72	0.01	4.19	0.21	0.21	4.87	4.38	0.00		97.52
HRT-4_13	HRT-2	26/08/14	71.33	0.23	9.77	0.00	3.56	0.12	0.18	1.32	4.51	0.00		91.01
HRT-4_14	HRT-2	26/08/14	69.93	0.11	8.49	0.00	6.53	0.30	0.20	5.98	4.22	0.00		95.76
HRT-4_15	HRT-2	26/08/14	72.06	0.15	8.42	0.00	6.43	0.38	0.23	6.24	4.04	0.02		97.97
HRT-4_16	HRT-2	26/08/14	71.63	0.14	8.20	0.01	6.83	0.30	0.16	6.53	4.09	0.00		97.88
HRT-4_17	HRT-2	26/08/14	68.60	0.22	9.07	0.02	4.81	0.18	0.20	5.12	4.21	0.00		92.44
HRT-4_18	HRT-2	26/08/14	71.38	0.21	8.23	0.00	5.92	0.27	0.22	6.09	4.11	0.00		96.42
HRT-4_19	HRT-2	26/08/14	73.57	0.25	9.63	0.00	4.63	0.28	0.19	5.28	4.46	0.00		98.28
HRT-4_2	HRT-2	26/08/14	70.37	0.14	8.29	0.00	6.53	0.28	0.19	6.70	4.18	0.01		96.68
HRT-4_20	HRT-2	26/08/14	71.62	0.19	9.35	0.01	4.54	0.17	0.24	5.11	4.27	0.02		95.52
HRT-4_3	HRT-2	26/08/14	70.48	0.21	10.17	0.00	3.22	0.11	0.17	4.45	4.52	0.00		93.32
HRT-4_4	HRT-2	26/08/14	70.05	0.22	8.43	0.00	6.11	0.29	0.18	5.99	4.17	0.01		95.45
HRT-4_5	HRT-2	26/08/14	72.92	0.23	9.57	0.00	4.61	0.10	0.19	5.04	4.40	0.00		97.06
HRT-4_6	HRT-2	26/08/14	70.49	0.17	8.42	0.01	6.49	0.29	0.19	6.05	4.22	0.00		96.33
HRT-4_7	HRT-2	26/08/14	73.21	0.27	9.63	0.00	5.13	0.16	0.15	5.06	4.78	0.00		98.40
HRT-4_8	HRT-2	26/08/14	71.93	0.18	8.24	0.00	6.67	0.33	0.20	6.46	3.99	0.01		98.01
HRT-4_9	HRT-2	26/08/14	67.62	0.18	8.69	0.03	4.35	0.23	0.16	4.83	4.08	0.00		90.16

Trace element concentrations (ppm) in Hora tephra glass shards

Label	Tephra	Analysis date	Rb 0.62	Sr 1.05	Y 0.17	Zr 0.37	Nb 0.07	Cs 0.19	Ba 1.88	La 0.09	Ce 0.07	Pr 0.06	Nd 0.25	Sm 0.14	Eu 0.13	Tb 0.06	Dy 0.13	Ho 0.04	Er 0.07	Tm 0.05	Yb 0.15	Lu 0.04	Hf 0.08	Ta 0.06	Pb 0.12	Th 0.01	U 0.00
HRT_2_1	HRT-1	20/07/15	140	-	300	2350	281	1.48	91.5	273	579	67.4	263	52.5	6.93	8.97	55.8	10.9	38.7	3.89	28.7	4.51	57.6	19.9	45.5	30.7	8.38
HRT_2_2	HRT-1	20/07/15	141	-	275	2230	271	1.04	93.1	247	509	59.2	241	49.7	5.90	8.56	50.8	10.0	27.9	3.89	26.9	4.17	54.2	18.7	49.1	28.1	7.57
HRT_2_3	HRT-1	20/07/15	142	-	287	2310	283	1.26	97.3	260	569	66.7	275	58.3	6.34	8.29	51.3	12.4	32.7	4.86	32.0	4.29	57.9	20.2	50.4	30.7	8.67
HRT_2_4	HRT-1	20/07/15	133	-	263	2150	267	1.16	97.3	242	542	59.0	254	51.2	6.23	9.25	49.3	10.6	31.6	4.80	30.1	4.59	53.1	19.8	47.7	26.9	7.89
HRT_2_5	HRT-1	20/07/15	141	-	303	2420	286	1.57	106	279	605	64.6	278	59.4	7.54	9.80	55.4	12.1	35.5	4.45	32.1	4.91	65.1	21.0	47.8	33.7	8.81
HRT_2_6	HRT-1	20/07/15	139	-	246	2020	258	1.32	80.9	227	496	60.8	217	43.2	6.86	8.50	48.5	10.4	29.6	3.80	26.6	4.18	51.1	18.5	51.0	27.1	8.27
HRT_2_7	HRT-1	20/07/15	150	-	261	2140	290	0.98	92.8	249	560	57.5	240	49.4	6.51	7.59	44.3	10.3	29.4	3.80	25.0	4.17	53.9	18.7	49.4	27.5	7.96
HRT_2_8	HRT-1	20/07/15	141	-	273	2270	266	0.91	86.1	254	528	57.0	248	57.0	6.93	9.45	54.6	10.8	32.2	4.39	32.5	4.49	59.4	19.1	49.4	30.4	7.86
HRT_2_10	HRT-1	20/07/15	155	-	357	2810	306	1.49	102	324	605	71.3	312	67.6	5.50	9.87	59.7	13.5	39.3	6.15	37.2	5.49	74.0	23.7	51.0	36.5	8.70
HRT_2_11	HRT-1	20/07/15	128	-	288	2250	266	0.94	83.7	250	531	60.4	264	43.4	7.05	7.59	58.0	10.5	31.5	4.86	32.3	3.92	55.5	18.3	44.1	30.0	7.55
HRT_2_12	HRT-1	20/07/15	133	-	283	2250	293	2.02	81.1	245	504	58.1	241	47.9	6.72	8.95	58.3	10.4	34.8	4.11	27.6	4.32	57.7	20.4	47.9	29.8	8.50
HRT_2_13	HRT-1	20/07/15	141	-	303	2410	269	1.21	81.5	267	556	63.6	266	52.7	6.49	10.3	56.6	11.5	30.6	5.37	31.2	4.36	59.1	18.9	47.7	29.9	7.84
HRT_2_14	HRT-1	20/07/15	149	-	313	2530	279	1.92	86.0	295	591	67.0	277	51.7	8.37	9.32	58.4	11.8	34.2	4.40	32.4	5.19	62.3	22.4	48.4	35.0	8.53
HRT_2_15	HRT-1	20/07/15	139	-	283	2230	288	1.32	91.5	240	500	59.4	239	49.1	7.52	7.72	51.0	11.3	28.7	4.24	30.4	3.73	56.0	18.6	45.5	29.2	7.59
HRT_2_16	HRT-1	20/07/15	143	-	283	2230	268	1.12	83.6	266	542	62.0	252	50.9	6.55	8.53	57.0	10.9	33.7	4.15	26.8	4.23	57.5	18.2	47.8	29.3	7.67
HRT_2_17	HRT-1	20/07/15	144	-	267	2210	287	1.25	90.6	265	551	62.8	247	47.1	6.80	7.33	53.5	10.7	31.1	4.21	26.7	4.43	62.2	19.5	47.7	30.0	7.48
HRT_2_18	HRT-1	20/07/15	138	-	324	2560	286	1.04	91.8	297	602	68.9	292	60.2	7.49	10.5	64.2	12.5	33.0	5.12	32.1	4.07	65.6	22.7	47.1	34.2	7.50
HRT_2_19	HRT-1	20/07/15	147	-	293	2350	268	1.29	89.0	257	543	61.4	246	54.7	6.60	8.10	55.2	10.8	31.0	4.94	32.5	4.47	61.4	18.4	46.1	30.3	8.05
HRT_2_20	HRT-1	20/07/15	118	-	211	1740	203	1.21	236	205	416	48.2	189	37.9	4.74	5.97	37.9	7.88	21.4	3.34	21.3	3.17	43.2	13.6	33.8	21.3	5.21
HRT_2B_1	HRT-1	20/07/15	148	-	125	1360	165	0.99	196	133	227	27.7	100	21.3	1.92	3.70	21.0	4.73	15.3	1.95	14.5	2.42	35.7	11.8	38.2	28.6	1.96
HRT_2B_2	HRT-1	20/07/15	155	-	134	1410	170	1.17	229	137	237	26.8	113	19.3	1.98	3.28	22.3	4.37	14.9	2.26	16.0	2.18	38.1	12.5	40.4	29.0	1.81
HRT_2B_3	HRT-1	20/07/15	150	-	141	1430	173	1.30	215	145	245	29.8	106	21.7	2.26	3.26	23.2	5.26	15.7	2.20	16.7	2.46	35.4	12.7	37.6	30.3	2.60
HRT_2B_4	HRT-1	20/07/15	147	-	129	1370	162	1.28	196	137	225	27.0	104	21.1	1.75	3.51	23.6	4.86	14.6	2.47	15.7	2.49	36.8	11.9	38.4	28.0	1.76
HRT_2B_5	HRT-1	20/07/15	152	-	144	1490	178	1.05	230	153	255	30.1	120	25.5	2.00	3.76	23.2	5.32	14.9	2.47	16.0	2.44	38.0	12.4	37.5	31.3	2.85
HRT_2B_6	HRT-1	20/07/15	151	-	143	1480	168	1.26	203	153	247	30.0	117	21.3	2.17	3.58	24.8	4.94	17.0	2.25	15.8	2.49	36.5	12.8	38.1	31.1	3.03
HRT_2B_7	HRT-1	20/07/15	156	-	140	1460	173	1.08	216	145	243	28.6	109	19.1	1.68	3.59	22.9	5.38	15.4	1.95	15.8	2.76	37.3	12.9	43.2	30.3	4.00
HRT_2B_8	HRT-1	20/07/15	147	-	137	1410	164	0.99	209	141	237	28.6	98.7	20.2	1.52	3.75	23.4	5.26	15.9	2.65	15.9	2.32	38.3	12.2	35.9	30.8	1.86
HRT_2B_9	HRT-1	20/07/15	153	-	144	1530	175	0.90	227	154	247	31.4	114	22.0	2.43	4.15	22.4	5.71	16.4	2.54	16.9	2.38	39.7	13.1	38.1	32.6	1.54
HRT_2B_10	HRT-1	20/07/15	151	-	141	1460	174	1.18	218	142	244	27.8	113	20.7	1.80	3.60	25.9	6.07	16.0	2.79	17.3	2.39	41.0	12.9	39.6	31.5	2.14
HRT_2B_11	HRT-1	20/07/15	164	-	135	1450	177	1.09	245	144	255	29.6	104	17.9	1.56	3.86	22.5	4.95	15.5	2.23	16.5	2.25	39.6	12.8	40.5	31.4	2.49
HRT_2B_12	HRT-1	20/07/15	147	-	128	1350	167	0.77	233	137	233	26.9	97.0	18.6	2.27	3.46	20.7	4.61	14.2	2.33	15.3	2.61	35.7	11.9	38.7	28.7	2.16
HRT_2B_13	HRT-1	20/07/15	150	-	132	1370	173	0.89	224	137	235	27.4	100	21.8	2.01	3.76	21.1	4.76	14.7	2.09	16.2	2.25	36.5	12.9	36.4	29.3	2.21
HRT_2B_14	HRT-1	20/07/15	153	-	135	1390	168	1.16	211	139	246	28.5	103	22.1	2.06	3.39	23.9	5.05	15.2	2.64	15.4	2.30	36.3	12.7	39.6	30.2	2.00
HRT_2B_15	HRT-1	20/07/15	148	-	138	1420	169	1.27	209	138	242	28.1	105	20.1	1.82	3.57	23.1	4.87	14.9	2.72	15.0	2.64	38.9	12.6	35.1	30.4	3.59
HRT_2B_16	HRT-1	20/07/15	152	-	136	1370	174	1.00	194	136	234	28.3	101	18.9	1.97	3.74	22.8	4.87	14.6	2.17	15.3	2.38	35.8	13.0	36.5	30.8	2.52
HRT_2B_17	HRT-1	20/07/15	154	-	139	1450	187	0.92	227	146	268	31.3	111	18.5	2.60	3.51	22.7	5.88	15.4	2.34	17.1	2.51	38.4	13.6	38.4	30.9	3.38
HRT_2B_18	HRT-1	20/07/15	135	-	114	1180	162	1.05	221	124	220	24.2	90.5	19.3	1.93	3.22	19.4	4.08	12.5	2.08	14.1	2.27	30.7	11.0	37.1	24.7	3.39
HRT_2B_19	HRT-1	20/07/15	154	-	153	1550	174	1.18	239	158	266	32.4	123	20.9	2.33	3.87	26.8	6.04	16.3	2.47	19.1	2.94	42.3	14.1	40.8	35.7	5.90
HRT_2B_20	HRT-1	20/07/15	160	-	139	1400	178	1.19	240	141	253	28.8	108	22.9	1.97	3.99	23.9	4.90	15.0	2.26	15.5	2.52	37.8	14.4	40.4	31.1	3.72
HRT-4_1	HRT-2	13/01/15	339	6.48	175	1290	254	2.11	498	228	474	49.9	216	36.3	7.45	6.36	34.9	8.18	22.4	3.03	19.4	3.21	42.1	17.6	60.5	26.4	11.9
HRT-4_10	HRT-2	13/01/15	235	7.27	178	1400	245	1.53	475	227	424	48.0	215	36.7	6.63	5.41	33.9	8.58	24.7	2.81	21.1	3.37	44.4	19.6	47.9	28.1	10.8
HRT-4_11	HRT-2	13/01/15	197	8.78	200	1470	216	1.25	79.6	219	442	50.4	212	39.7	4.51	6.29	36.5	8.44	26.8	3.79	23.8	3.48	42.3	16.0	46.9	23.2	8.74

Continued on next page

Trace element concentrations (ppm) in Hora tephra glass shards

Label	Tephra	Analysis date	Rb 0.62	Sr 1.05	Y 0.17	Zr 0.37	Nb 0.07	Cs 0.19	Ba 1.88	La 0.09	Ce 0.07	Pr 0.06	Nd 0.25	Sm 0.14	Eu 0.13	Tb 0.06	Dy 0.13	Ho 0.04	Er 0.07	Tm 0.05	Yb 0.15	Lu 0.04	Hf 0.08	Ta 0.06	Pb 0.12	Th 0.01	U 0.00
HRT-4_13	HRT-2	13/01/15	260	4.45	164	1300	192	1.24	287	192	377	43.4	185	33.2	4.45	5.89	32.4	7.93	23.8	3.21	20.0	3.08	39.9	13.6	51.4	18.7	6.77
HRT-4_14	HRT-2	13/01/15	221	6.27	175	1320	246	1.29	450	208	422	46.1	191	36.9	6.01	5.30	30.4	7.17	22.9	3.22	21.0	2.64	40.5	16.2	46.8	26.8	9.86
HRT-4_15	HRT-2	13/01/15	225	8.45	159	1250	248	1.61	432	201	412	44.2	184	33.7	6.29	5.93	30.0	7.58	22.4	2.58	18.8	3.08	38.6	15.9	49.8	25.1	10.1
HRT-4_16	HRT-2	13/01/15	250	7.60	180	1410	283	1.48	456	228	473	52.6	222	39.6	7.07	6.69	36.6	9.09	25.0	3.31	24.2	3.47	45.0	19.5	64.5	30.0	12.8
HRT-4_17	HRT-2	13/01/15	194	6.63	171	1390	225	1.82	68.3	211	425	48.2	216	36.7	4.74	7.27	37.5	8.73	27.5	3.36	23.1	3.22	43.5	15.6	64.4	21.4	9.54
HRT-4_18	HRT-2	13/01/15	200	7.01	171	1290	224	1.17	465	206	402	44.1	184	37.8	6.22	5.28	33.8	8.22	21.6	2.59	21.0	3.21	40.6	17.5	45.8	26.3	9.29
HRT-4_19	HRT-2	13/01/15	190	3.13	199	1530	229	1.59	94.5	212	424	49.2	212	41.7	4.96	6.14	36.6	8.69	22.0	3.85	21.5	3.82	41.6	14.2	47.2	21.4	7.21
HRT-4_2	HRT-2	13/01/15	308	9.91	178	1320	250	1.91	508	233	463	52.9	220	39.3	6.48	6.26	37.8	8.93	24.3	3.01	22.4	3.70	44.2	19.2	54.7	28.8	13.2
HRT-4_20	HRT-2	13/01/15	345	6.24	216	1600	245	2.90	93.9	273	528	59.1	267	47.3	5.70	7.85	41.5	11.4	32.4	4.03	27.3	4.15	56.8	18.3	63.1	25.3	11.3
HRT-4_3	HRT-2	13/01/15	230	6.24	133	1010	178	1.80	295	152	345	37.3	159	26.2	4.40	4.70	24.6	6.45	18.0	2.19	15.9	2.30	32.4	11.9	43.6	15.6	7.04
HRT-4_4	HRT-2	13/01/15	267	4.61	144	1050	206	1.45	448	182	380	40.3	173	31.8	5.31	6.06	27.8	7.13	17.8	2.41	18.4	2.84	35.1	15.6	47.9	22.6	10.2
HRT-4_5	HRT-2	13/01/15	256	4.54	169	1270	219	2.01	68.1	205	444	47.5	211	37.4	4.18	5.70	33.7	8.06	21.6	2.67	20.8	3.56	40.7	15.6	53.3	19.7	9.71
HRT-4_6	HRT-2	13/01/15	247	8.00	175	1300	219	1.91	546	234	429	46.6	199	35.2	6.47	6.65	33.2	8.26	20.9	2.95	22.6	3.40	42.2	16.4	47.7	25.9	9.82
HRT-4_7	HRT-2	13/01/15	199	3.94	146	1160	206	1.69	100	173	394	39.9	168	32.4	4.63	5.02	28.7	7.21	19.1	2.37	18.4	2.75	35.4	14.8	42.4	17.5	9.30
HRT-4_8	HRT-2	13/01/15	348	5.92	178	1330	242	1.96	527	235	450	50.5	222	34.7	5.73	6.36	34.4	8.38	25.1	3.16	21.9	3.42	44.9	19.0	53.3	28.1	12.2
HRT-4_9	HRT-2	13/01/15	242	3.18	232	1760	262	1.95	65.3	261	521	58.2	251	47.6	5.89	7.98	45.1	10.9	30.4	3.94	27.9	4.64	55.0	19.1	61.1	26.9	11.0

Unnormalised major element concentrations (wt.%) in Dendi tephra glass shards

Label	Tephra	Analysis date	SiO_2 0.08	TiO_2 0.05	Al_2O_3 0.05	MgO 0.04	FeO^T 0.08	MnO 0.07	CaO 0.04	Na_2O 0.08	K_2O 0.03	P_2O_5 0.10	Cl 0.02	Total
DT1-1_1	DT1-1	28/08/14	68.34	0.37	12.34	0.20	4.53	0.20	1.07	5.36	4.23	0.03		96.67
DT1-1_11	DT1-1	28/08/14	67.14	0.30	8.31	0.01	6.85	0.23	0.29	6.16	3.95	0.03		93.28
DT1-1_12	DT1-1	28/08/14	68.90	0.29	8.54	0.00	6.97	0.32	0.30	6.25	3.97	0.00		95.54
DT1-1_13	DT1-1	28/08/14	66.28	0.36	8.23	0.04	7.13	0.28	0.31	6.33	3.87	0.01		92.85
DT1-1_14	DT1-1	28/08/14	69.27	0.20	12.91	0.08	2.98	0.19	0.42	5.23	4.78	0.01		96.07
DT1-1_15	DT1-1	28/08/14	70.01	0.27	8.67	0.00	6.90	0.24	0.34	6.71	4.24	0.04		97.44
DT1-1_16	DT1-1	28/08/14	70.24	0.32	9.29	0.03	7.33	0.29	0.41	6.73	4.17	0.01		98.81
DT1-1_17	DT1-1	28/08/14	70.37	0.30	8.75	0.01	7.65	0.25	0.38	6.95	4.16	0.06		98.90
DT1-1_18	DT1-1	28/08/14	70.05	0.32	8.59	0.01	7.31	0.30	0.34	6.01	4.22	0.01		97.15
DT1-1_2	DT1-1	28/08/14	69.11	0.33	12.57	0.07	4.36	0.21	0.76	5.96	4.39	0.14		97.91
DT1-1_20	DT1-1	28/08/14	69.18	0.25	8.66	0.00	6.88	0.30	0.34	6.72	4.07	0.04		96.45
DT1-1_3	DT1-1	28/08/14	70.90	0.28	8.71	0.00	7.49	0.28	0.37	6.92	4.36	0.04		99.34
DT1-1_4	DT1-1	28/08/14	69.63	0.27	7.87	0.00	7.42	0.24	0.33	6.71	4.13	0.03		96.63
DT1-1_5	DT1-1	28/08/14	69.56	0.35	8.47	0.00	7.40	0.23	0.31	6.85	4.19	0.06		97.40
DT1-1_7	DT1-1	28/08/14	67.19	0.36	8.25	0.00	6.92	0.37	0.38	6.29	4.02	0.00		93.79
DT1-1_9	DT1-1	28/08/14	65.44	0.27	7.52	0.02	7.02	0.35	0.33	6.41	3.95	0.01		91.32
DT1-2_1	DT1-2	28/08/14	54.67	0.45	15.83	0.19	5.14	0.23	0.76	7.72	5.17	0.02		90.18
DT1-2_10	DT1-2	28/08/14	60.59	0.38	16.84	0.22	5.08	0.20	0.76	8.29	5.23	0.07		97.66
DT1-2_11	DT1-2	28/08/14	60.96	0.29	16.99	0.21	5.14	0.22	0.72	8.42	5.38	0.02		98.35
DT1-2_12	DT1-2	28/08/14	61.14	0.37	16.78	0.17	5.10	0.26	0.70	8.34	5.18	0.08		98.12
DT1-2_13	DT1-2	28/08/14	60.51	0.33	16.59	0.21	4.92	0.25	0.71	8.34	5.25	0.05		97.13
DT1-2_14	DT1-2	28/08/14	59.83	0.36	16.88	0.18	5.09	0.18	0.81	8.21	5.22	0.03		96.78
DT1-2_15	DT1-2	28/08/14	61.33	0.39	16.78	0.18	5.03	0.24	0.78	8.38	5.40	0.03		98.54
DT1-2_16	DT1-2	28/08/14	62.26	0.32	17.35	0.16	4.56	0.23	0.66	8.44	5.29	0.03		99.31
DT1-2_17	DT1-2	28/08/14	60.85	0.36	16.38	0.20	5.39	0.23	0.76	7.85	5.20	0.03		97.25
DT1-2_18	DT1-2	28/08/14	59.48	0.39	16.77	0.18	4.82	0.23	0.74	8.22	5.32	0.06		96.22
DT1-2_19	DT1-2	28/08/14	56.86	0.36	16.38	0.19	5.01	0.17	0.70	7.83	5.00	0.06		92.53
DT1-2_2	DT1-2	28/08/14	57.69	0.37	16.68	0.18	5.09	0.24	0.69	8.30	5.14	0.04		94.41
DT1-2_20	DT1-2	28/08/14	56.46	0.38	16.32	0.16	4.94	0.24	0.77	7.89	5.11	0.04		92.31
DT1-2_3	DT1-2	28/08/14	58.70	0.38	16.62	0.17	4.65	0.18	0.74	7.84	5.23	0.07		94.57
DT1-2_4	DT1-2	28/08/14	59.67	0.32	16.51	0.17	5.41	0.25	0.76	8.30	5.11	0.05		96.55
DT1-2_5	DT1-2	28/08/14	59.95	0.39	16.83	0.19	4.97	0.20	0.77	8.41	5.23	0.07		97.01
DT1-2_6	DT1-2	28/08/14	59.71	0.36	16.70	0.22	5.02	0.24	0.77	7.84	5.18	0.04		96.09
DT1-2_7	DT1-2	28/08/14	59.85	0.30	16.86	0.16	4.65	0.20	0.71	8.00	5.35	0.01		96.08
DT1-2_8	DT1-2	28/08/14	60.68	0.38	16.64	0.17	4.88	0.27	0.75	8.07	5.21	0.03		97.08
DT1-2_9	DT1-2	28/08/14	62.39	0.19	18.10	0.09	2.54	0.12	0.59	7.73	5.56	0.03		97.35
DT1-3_1	DT1-3	28/08/14	63.00	0.62	17.51	0.46	3.97	0.14	1.21	7.38	5.50	0.15		99.93
DT1-3_10	DT1-3	28/08/14	63.14	0.37	16.58	0.13	4.57	0.27	0.63	8.42	5.28	0.04		99.45
DT1-3_11	DT1-3	28/08/14	63.18	0.32	16.56	0.12	4.89	0.23	0.61	8.29	5.31	0.03		99.56
DT1-3_12	DT1-3	28/08/14	64.18	0.26	17.14	0.09	3.93	0.16	0.51	8.22	5.54	0.06		100.09
DT1-3_13	DT1-3	28/08/14	59.88	0.37	16.02	0.13	4.97	0.23	0.63	8.27	5.14	0.03		95.67
DT1-3_14	DT1-3	28/08/14	62.97	0.65	17.82	0.44	4.18	0.13	1.26	7.13	5.59	0.15		100.31
DT1-3_15	DT1-3	28/08/14	62.58	0.58	17.70	0.42	3.80	0.19	1.17	7.05	5.44	0.13		99.06
DT1-3_16	DT1-3	28/08/14	61.04	0.37	15.27	0.25	6.77	0.31	0.87	8.77	4.87	0.07		98.60
DT1-3_17	DT1-3	28/08/14	61.44	0.33	16.39	0.13	4.93	0.24	0.67	8.40	5.00	0.04		97.56
DT1-3_18	DT1-3	28/08/14	60.89	0.34	16.21	0.12	5.33	0.23	0.61	8.43	5.24	0.04		97.45
DT1-3_19	DT1-3	28/08/14	63.98	0.38	16.59	0.11	4.71	0.21	0.61	8.14	5.15	0.04		99.92
DT1-3_2	DT1-3	28/08/14	62.97	0.29	16.52	0.15	5.19	0.22	0.69	8.65	5.20	0.03		99.91
DT1-3_20	DT1-3	28/08/14	62.05	0.31	16.26	0.12	5.21	0.24	0.71	8.46	4.91	0.08		98.35
DT1-3_21	DT1-3	28/08/14	61.01	0.29	15.72	0.21	5.39	0.29	0.68	8.52	4.93	0.03		97.09
DT1-3_22	DT1-3	28/08/14	65.28	0.24	17.91	0.08	2.91	0.08	0.61	7.69	5.56	0.04		100.41
DT1-3_3	DT1-3	28/08/14	62.23	0.32	16.49	0.15	4.95	0.18	0.64	8.45	5.11	0.01		98.53
DT1-3_4	DT1-3	28/08/14	62.35	0.62	17.91	0.44	3.93	0.16	1.17	7.40	5.52	0.10		99.60
DT1-3_5	DT1-3	28/08/14	61.51	0.35	16.32	0.14	5.91	0.16	0.70	8.55	5.03	0.05		98.71
DT1-3_6	DT1-3	28/08/14	61.24	0.26	16.21	0.14	4.94	0.22	0.72	7.89	4.96	0.03		96.59
DT1-3_7	DT1-3	28/08/14	61.99	0.29	16.27	0.10	5.04	0.25	0.67	8.50	4.98	0.03		98.13
DT1-3_8	DT1-3	28/08/14	62.71	0.62	17.50	0.42	3.92	0.20	1.17	7.12	5.52	0.12		99.31
DT1-3_9	DT1-3	28/08/14	63.57	0.21	16.67	0.13	4.08	0.19	0.82	8.04	4.84	0.04		98.60
DEN12A/1	DT-1	21/02/14	64.11	0.13	18.62	0.05	1.78	0.07	0.79	7.47	5.58	0.03		98.72
DEN12A/10	DT-1	21/02/14	61.51	0.38	16.71	0.19	5.10	0.13	0.73	7.98	5.23	0.07		98.31
DEN12A/11	DT-1	21/02/14	61.85	0.48	16.54	0.20	5.41	0.27	0.82	8.53	5.22	0.05		99.62
DEN12A/12	DT-1	21/02/14	61.22	0.27	16.40	0.12	5.28	0.19	0.68	9.22	4.91	0.03		98.72
DEN12A/13	DT-1	21/02/14	60.91	0.37	16.64	0.16	4.76	0.11	0.74	8.02	5.15	0.05		97.18
DEN12A/14	DT-1	21/02/14	61.34	0.34	16.32	0.20	5.15	0.25	0.74	8.10	5.09	0.03		97.84
DEN12A/15	DT-1	21/02/14	59.02	0.32	15.69	0.18	4.71	0.24	0.75	8.13	4.92	0.08		94.33
DEN12A/16	DT-1	21/02/14	60.87	0.35	16.12	0.18	5.04	0.25	0.80	8.14	5.08	0.04		97.13
DEN12A/17	DT-1	21/02/14	64.48	0.20	18.81	0.06	1.97	0.06	0.82	8.07	4.94	0.00		99.49
DEN12A/18	DT-1	21/02/14	62.06	0.36	16.65	0.21	4.98	0.22	0.76	8.20	5.11	0.03		98.83
DEN12A/19	DT-1	21/02/14	61.50	0.39	16.69	0.22	4.83	0.17	0.84	8.13	5.22	0.03		98.27
DEN12A/2	DT-1	21/02/14	60.73	0.42	16.36	0.21	4.88	0.27	0.81	8.31	5.18	0.03		97.47
DEN12A/20	DT-1	21/02/14	61.68	0.37	16.44	0.19	4.94	0.18	0.72	8.28	5.28	0.04		98.41
DEN12A/3	DT-1	21/02/14	61.56	0.44	16.07	0.20	5.54	0.23	0.79	8.19	5.04	0.06		98.43
DEN12A/4	DT-1	21/02/14	61.60	0.40	16.38	0.19	4.73	0.13	0.72	8.01	5.13	0.06		97.60
DEN12A/5	DT-1	21/02/14	60.96	0.48	15.98	0.24	6.28	0.33	0.85	8.93	5.06	0.07		99.52
DEN12A/6	DT-1	21/02/14	61.80	0.36	16.34	0.20	5.17	0.16	0.81	8.44	4.96	0.04		98.55
DEN12A/7	DT-1	21/02/14	60.13	0.46	15.70	0.25	6.21	0.21	0.76	8.44	5.03	0.08		97.62
DEN12A/8	DT-1	21/02/14	61.34	0.35	16.52	0.19	5.08	0.17	0.73	8.24	5.16	0.02		98.07
DEN12A/9	DT-1	21/02/14	61.84	0.35	16.70	0.19	5.27	0.24	0.74	7.91	5.24	0.06		98.82
DEN12C/1	DT-2	21/02/14	58.88	0.44	14.74	0.17	5.73	0.26	0.72	8.17	4.63	0.04		94.08
DEN12C/11	DT-2	21/02/14	62.20	0.16	17.46	0.00	0.80	0.00	0.07	7.46	2.69	0.03		90.89
DEN12C/12	DT-2	21/02/14	57.47	0.38	14.48	0.19	5.98	0.30	0.70	7.78	4.57	0.07		92.19
DEN12C/13	DT-2	21/02/14	61.33	0.44	15.29	0.18	6.49	0.25	0.78	8.76	4.70	0.09		98.57
DEN12C/15	DT-2	21/02/14	61.15	0.37	15.46	0.12	5.51	0.27	0.71	8.46	4.86	0.05		97.21

Continued on next page

Unnormalised major element concentrations (wt.%) in Dendi tephra glass shards

Label	Tephra	Analysis date	SiO_2 0.08	TiO_2 0.05	Al_2O_3 0.05	MgO 0.04	FeO^T 0.08	MnO 0.07	CaO 0.04	Na_2O 0.08	K_2O 0.03	P_2O_5 0.10	Cl 0.02	Total
DEN12C/16	DT-2	21/02/14	59.52	0.35	14.87	0.14	6.35	0.24	0.69	8.49	4.78	0.08		95.79
DEN12C/18	DT-2	21/02/14	59.61	0.41	14.48	0.15	5.93	0.23	0.78	4.71	4.76	0.05		91.40
DEN12C/19	DT-2	21/02/14	60.43	0.38	14.78	0.16	5.94	0.24	0.72	8.81	4.62	0.03		96.40
DEN12C/2	DT-2	21/02/14	59.78	0.36	15.30	0.10	4.51	0.11	0.58	8.21	5.13	0.06		94.35
DEN12C/20	DT-2	21/02/14	61.13	0.39	15.15	0.14	6.68	0.28	0.70	8.85	4.71	0.05		98.38
DEN12C/20	DT-2	21/02/14												
DEN12C/3	DT-2	21/02/14	56.34	0.32	15.72	0.19	4.13	0.16	0.68	7.58	4.90	0.05		90.43
DEN12C/5	DT-2	21/02/14	60.39	0.42	15.10	0.16	6.23	0.13	0.81	8.37	4.75	0.04		96.72
DEN12C/6	DT-2	21/02/14	60.14	0.37	15.20	0.17	5.94	0.28	0.79	7.66	4.73	0.03		95.63
DEN12C/7	DT-2	21/02/14	61.50	0.36	15.02	0.15	6.17	0.31	0.72	8.47	4.63	0.03		97.64
DEN12C/8	DT-2	21/02/14	61.82	0.37	15.23	0.14	6.72	0.32	0.71	9.02	4.80	0.05		99.47
DEN12B/1	DT-3	21/02/14	60.25	0.37	15.16	0.17	6.06	0.25	0.79	8.65	4.82	0.06		96.85
DEN12B/10	DT-3	21/02/14	59.55	0.34	16.36	0.20	4.81	0.22	0.69	8.73	4.95	0.04		96.19
DEN12B/11	DT-3	21/02/14	60.52	0.47	15.10	0.13	6.19	0.21	0.75	8.86	4.83	0.03		97.36
DEN12B/12	DT-3	21/02/14	59.94	0.38	14.82	0.11	6.20	0.26	0.76	8.22	4.67	0.03		95.68
DEN12B/13	DT-3	21/02/14	61.37	0.47	15.42	0.19	5.80	0.25	0.79	8.13	4.62	0.08		97.37
DEN12B/14	DT-3	21/02/14	60.13	0.58	16.92	0.30	4.37	0.28	0.98	7.29	5.51	0.13		96.62
DEN12B/15	DT-3	21/02/14	59.76	0.34	16.47	0.12	4.79	0.22	0.70	8.22	4.83	0.02		95.81
DEN12B/17	DT-3	21/02/14	59.78	0.39	14.79	0.17	5.76	0.24	0.74	8.45	4.73	0.04		95.33
DEN12B/18	DT-3	21/02/14	59.80	0.49	16.47	0.31	4.15	0.17	0.87	7.61	5.09	0.10		95.28
DEN12B/19	DT-3	21/02/14	59.28	0.67	14.83	0.43	6.92	0.22	0.85	8.29	5.03	0.17		96.94
DEN12B/2	DT-3	21/02/14	56.56	0.72	14.38	0.93	6.27	0.27	2.60	7.06	4.03	0.18		93.15
DEN12B/20	DT-3	21/02/14	61.22	0.39	15.11	0.14	6.35	0.23	0.74	8.17	4.76	0.08		97.47
DEN12B/3	DT-3	21/02/14	59.35	0.42	14.45	0.18	6.36	0.29	0.73	9.11	4.68	0.08		95.92
DEN12B/4	DT-3	21/02/14	60.57	0.40	14.96	0.16	6.19	0.17	0.79	8.72	4.86	0.04		97.11
DEN12B/5	DT-3	21/02/14	59.30	0.45	14.94	0.20	6.33	0.27	0.74	9.22	4.64	0.06		96.41
DEN12B/6	DT-3	21/02/14	62.59	0.27	17.16	0.06	2.87	0.08	0.63	7.91	5.53	0.04		97.23
DEN12B/7	DT-3	21/02/14	56.07	0.30	16.13	0.18	3.97	0.19	0.69	7.40	4.95	0.01		90.23
DEN12B/9	DT-3	21/02/14	65.93	0.33	7.54	0.01	7.36	0.33	0.34	6.13	3.78	0.05		92.06

Trace element concentrations (ppm) in Dendi tephra glass shards

Label	Tephra	Analysis date	Rb 0.62	Sr 1.05	Y 0.17	Zr 0.37	Nb 0.07	Cs 0.19	Ba 1.88	La 0.09	Ce 0.07	Pr 0.06	Nd 0.25	Sm 0.14	Eu 0.13	Tb 0.06	Dy 0.13	Ho 0.04	Er 0.07	Tm 0.05	Yb 0.15	Lu 0.04	Hf 0.08	Ta 0.06	Pb 0.12	Th 0.01	U 0.00
DT1-1_1†	DT1-1	07/05/15	156	6.62	266	2110	217	1.26	663	212	311	42.3	185	40.0	6.50	7.47	57.0	9.21	25.9	4.39	28.1	4.50	56.0	18.4	37.3	39.9	5.82
DT1-1_11	DT1-1	07/05/15	150	3.08	235	1750	211	1.84	525	206	332	42.6	189	36.6	5.96	6.95	41.8	8.87	25.7	3.15	23.1	3.67	43.6	15.2	39.3	32.2	6.44
DT1-1_12	DT1-1	07/05/15	150	6.19	228	1720	210	1.54	489	195	328	42.5	172	34.5	6.51	5.95	40.2	7.85	23.9	4.00	20.4	3.78	41.7	15.7	35.2	31.1	6.09
DT1-1_13	DT1-1	07/05/15	149	6.63	223	1690	211	1.55	497	196	328	40.4	177	37.0	7.07	6.89	40.2	8.20	25.0	3.55	23.8	3.11	42.3	16.7	38.3	33.1	6.42
DT1-1_14	DT1-1	07/05/15	141	2.60	126	1310	170	1.13	325	130	236	26.5	97.2	20.6	1.80	2.88	21.3	4.30	12.9	2.16	13.7	1.96	33.7	12.8	35.0	28.3	6.22
DT1-1_15†	DT1-1	07/05/15	144	-	265	2070	227	1.41	572	219	315	44.4	171	44.9	7.32	7.16	52.6	9.00	32.8	4.35	29.8	4.55	48.0	16.9	35.8	36.4	6.46
DT1-1_16	DT1-1	07/05/15	144	7.80	205	1520	201	1.05	554	173	306	37.9	162	33.7	6.30	5.65	33.2	7.31	22.3	2.82	19.1	3.45	41.8	15.3	34.9	29.0	6.11
DT1-1_17	DT1-1	07/05/15	152	5.85	221	1690	215	1.59	510	197	332	41.8	175	39.7	7.68	5.91	41.6	8.28	23.6	3.45	22.7	3.22	43.0	16.3	36.2	30.8	6.37
DT1-1_18	DT1-1	07/05/15	148	4.52	214	1600	225	1.57	485	179	306	37.8	159	30.7	6.47	5.75	37.1	7.81	21.9	3.46	19.3	3.03	40.0	15.6	34.1	28.2	6.57
DT1-1_2	DT1-1	07/05/15	125	30.5	146	1290	159	0.85	776	145	242	28.9	124	21.7	3.76	2.96	24.6	4.70	17.9	2.23	15.1	1.92	33.8	11.1	33.7	26.9	5.24
DT1-1_20†	DT1-1	07/05/15	150	7.64	281	2160	229	1.41	641	232	320	43.6	175	39.1	8.58	7.12	63.1	9.72	33.9	3.22	25.0	6.10	57.7	18.6	37.6	37.7	5.46
DT1-1_3	DT1-1	07/05/15	157	4.55	206	1570	211	1.44	469	177	315	37.8	160	35.6	5.95	5.41	35.3	7.09	22.3	3.53	20.6	3.23	36.4	14.3	36.3	28.4	6.33
DT1-1_4	DT1-1	07/05/15	139	3.55	184	1390	192	1.10	456	159	283	35.0	144	30.9	5.46	4.73	34.0	6.94	20.5	3.23	17.7	2.98	35.3	14.2	34.7	27.9	5.98
DT1-1_5	DT1-1	07/05/15	154	4.86	224	1650	220	1.24	504	192	344	41.1	183	37.6	6.57	5.96	35.2	7.48	23.9	3.11	20.1	3.25	42.0	15.8	39.0	31.2	6.27
DT1-1_7	DT1-1	07/05/15	153	-	243	1750	219	1.33	530	216	359	45.8	209	46.5	7.86	6.57	42.9	9.34	27.7	4.20	23.2	3.84	38.1	16.7	39.8	35.0	6.51
DT1-1_9	DT1-1	07/05/15	151	4.13	224	1670	230	1.45	481	196	340	41.9	173	38.7	6.62	5.97	41.2	7.57	23.9	3.40	20.8	3.69	42.8	16.2	38.5	31.0	6.53
DT1-2_1	DT1-2	07/05/15	133	0.88	76.7	723	207	1.03	9.45	112	217	22.4	85.8	14.0	0.72	1.99	14.0	3.09	7.71	1.25	7.22	1.41	17.9	13.8	20.8	21.7	5.39
DT1-2_10	DT1-2	07/05/15	85.8	1.23	52.9	547	139	0.64	32.8	74.1	141	14.4	51.4	10.1	0.93	1.41	9.31	2.04	6.57	0.83	5.76	0.84	16.2	11.0	13.3	16.0	4.48
DT1-2_11	DT1-2	07/05/15	124	0.92	69.3	700	188	1.01	15.3	105	188	19.7	79.9	11.3	0.69	1.80	12.2	2.62	7.34	1.10	7.55	1.09	17.1	12.7	17.0	20.0	5.75
DT1-2_12	DT1-2	07/05/15	118	2.30	79.8	800	225	1.40	14.1	126	222	21.8	91.8	14.7	0.82	2.18	15.1	3.04	9.26	1.34	9.79	1.17	17.1	15.4	20.9	22.2	5.93
DT1-2_13	DT1-2	07/05/15	141	-	82.4	839	212	1.31	7.70	125	232	23.8	85.0	15.6	0.68	2.47	12.9	3.26	8.85	1.36	8.36	1.19	19.9	14.7	18.6	24.1	6.18
DT1-2_14	DT1-2	07/05/15	133	1.08	79.1	795	211	0.77	12.8	118	219	23.3	83.2	14.7	1.25	2.14	13.7	2.58	8.28	1.33	7.75	1.08	19.3	14.4	16.9	24.3	5.57
DT1-2_15	DT1-2	07/05/15	134	-	83.9	838	214	1.00	10.2	128	227	24.6	97.6	16.2	1.30	2.42	15.0	2.93	9.77	1.20	8.78	1.54	19.0	14.5	20.4	24.3	6.03
DT1-2_16	DT1-2	07/05/15	140	-	84.9	845	220	1.12	5.36	127	229	23.5	91.8	20.0	1.14	2.34	15.9	3.04	8.31	1.27	8.57	1.49	20.6	16.2	18.2	24.9	6.32
DT1-2_17	DT1-2	07/05/15	129	-	86.4	855	227	1.50	5.16	128	233	25.1	90.2	14.7	1.62	2.13	14.5	3.15	9.54	1.70	7.98	1.43	19.9	15.9	20.8	25.2	6.30
DT1-2_18	DT1-2	07/05/15	130	2.43	74.5	764	212	1.06	65.6	112	215	22.7	81.8	15.7	0.86	1.99	14.5	2.97	9.43	1.22	7.86	1.20	19.6	14.4	18.9	23.6	5.94
DT1-2_19	DT1-2	07/05/15	133	3.19	89.2	858	219	1.34	9.42	132	246	23.8	91.3	19.4	1.13	2.39	16.7	2.77	8.41	1.50	10.1	1.58	20.8	17.2	20.1	26.1	6.61
DT1-2_2	DT1-2	07/05/15	115	0.41	80.8	792	222	1.11	10.4	127	240	23.5	85.4	16.1	0.92	2.48	12.3	2.95	7.98	1.49	8.27	1.35	20.4	14.1	19.9	23.4	5.99
DT1-2_20	DT1-2	07/05/15	133	0.95	76.7	777	210	1.15	7.96	118	214	22.6	83.3	13.1	0.97	2.31	11.4	2.84	8.08	1.02	8.27	1.09	18.2	13.9	21.0	21.9	5.62
DT1-2_3	DT1-2	07/05/15	114	0.86	71.6	748	196	0.96	13.9	106	196	21.6	79.3	14.1	1.09	1.92	13.4	2.41	8.09	1.17	6.89	1.49	18.5	12.5	19.5	20.0	5.22
DT1-2_4	DT1-2	07/05/15	146	-	86.8	874	236	1.37	3.63	136	245	27.0	99.9	19.6	0.84	2.65	14.8	3.11	9.57	1.44	9.88	1.74	20.5	16.4	22.7	26.4	6.58
DT1-2_5	DT1-2	07/05/15	144	2.02	77.4	773	208	1.27	9.72	120	219	21.9	87.0	20.0	0.72	2.47	13.4	2.92	9.60	1.56	8.76	1.44	20.6	15.3	20.5	24.6	5.81
DT1-2_6	DT1-2	07/05/15	132	-	81.8	798	214	1.23	7.59	123	216	22.8	83.6	14.9	0.88	2.51	13.7	2.87	8.14	1.41	9.35	1.07	18.6	15.5	19.4	22.2	5.95
DT1-2_7	DT1-2	07/05/15	128	-	87.6	886	215	0.99	7.43	128	222	24.5	91.0	18.1	0.78	2.71	16.3	3.30	8.56	1.18	9.82	1.29	22.5	14.8	18.9	25.3	5.95
DT1-2_8	DT1-2	07/05/15	135	-	82.9	829	217	1.10	8.18	125	225	23.3	89.0	15.4	1.10	2.36	14.6	2.91	7.74	1.62	9.15	1.34	19.1	15.0	18.5	24.3	6.05
DT1-2_9	DT1-2	07/05/15	147	-	90.0	915	246	1.41	5.75	133	248	25.6	102	16.5	0.85	2.38	15.8	3.31	10.5	1.51	8.95	1.26	19.7	16.9	22.2	25.8	7.07
DT1-3_1	DT1-3	06/05/15	75.8	73.9	40.5	389	110	0.49	798	65.2	120	14.2	53.6	8.5	2.91	1.43	7.38	1.77	4.07	0.70	3.95	0.41	8.93	8.35	9.70	11.4	2.53
DT1-3_10	DT1-3	06/05/15	164	-	98.0	1050	262	1.38	0.76	149	267	28.7	107	21.8	1.08	2.95	18.2	3.28	13.6	2.02	10.8	1.52	27.3	18.9	22.7	29.3	7.33
DT1-3_11	DT1-3	06/05/15	188	-	108	1120	284	1.60	0.88	162	288	30.6	113	21.3	0.70	2.97	18.6	3.97	12.5	1.93	10.5	1.84	27.0	19.5	25.2	33.0	7.89
DT1-3_12	DT1-3	06/05/15	163	-	92.6	1010	256	1.39	1.41	135	253	26.4	102	15.9	0.91	2.54	18.3	3.21	11.6	1.68	9.75	1.73	24.3	17.5	21.9	29.6	7.04
DT1-3_13	DT1-3	06/05/15	159	2.87	99.9	1090	263	1.77	21.1	154	275	28.6	108	22.0	0.98	3.30	17.8	3.83	11.4	1.72	9.78	1.82	27.5	19.0	22.9	31.9	7.28
DT1-3_14	DT1-3	06/05/15	80.1	59.6	47.5	429	114	0.42	633	78.8	141	15.6	65.5	11.3	2.53	1.59	9.19	1.98	5.93	0.82	6.11	0.70	11.2	7.87	10.0	12.6	2.78

Continued on next page

Trace element concentrations (ppm) in Dendi tephra glass shards

Label	Tephra	Analysis date	Rb 0.62	Sr 1.05	Y 0.17	Zr 0.37	Nb 0.07	Cs 0.19	Ba 1.88	La 0.09	Ce 0.07	Pr 0.06	Nd 0.25	Sm 0.14	Eu 0.13	Tb 0.06	Dy 0.13	Ho 0.04	Er 0.07	Tm 0.05	Yb 0.15	Lu 0.04	Hf 0.08	Ta 0.06	Pb 0.12	Th 0.01	U 0.00
DT1-3_15	DT1-3	06/05/15	80.1	48.2	41.7	402	107	0.30	560	65.9	123	13.3	51.1	9.00	2.32	1.27	7.81	1.38	4.73	0.49	4.48	0.57	9.83	7.92	10.4	10.8	2.75
DT1-3_16	DT1-3	06/05/15	173	-	112	1200	288	1.57	-	169	307	33.7	114	21.9	1.24	3.14	19.4	4.86	12.3	1.92	12.3	2.00	29.6	19.7	24.0	34.2	8.30
DT1-3_17	DT1-3	06/05/15	155	-	95.0	953	251	1.01	23.4	144	277	25.6	102	17.7	0.26	2.72	16.8	4.11	10.5	1.42	10.4	1.77	25.2	17.6	18.1	26.6	6.38
DT1-3_18	DT1-3	06/05/15	179	-	91.6	962	263	1.47	7.05	132	254	26.2	101	19.5	0.73	2.82	15.5	3.46	10.3	1.53	10.3	1.63	22.0	17.5	24.8	27.0	7.12
DT1-3_19	DT1-3	06/05/15	156	-	101	1070	274	1.04	5.20	148	287	31.0	112	20.6	0.53	2.99	14.0	3.49	11.6	1.35	12.6	1.36	24.0	20.5	24.8	29.5	7.57
DT1-3_2	DT1-3	06/05/15	157	-	92.2	985	246	1.34	4.44	140	250	27.4	99.7	19.5	0.47	2.39	15.0	3.54	9.94	1.42	10.1	1.50	26.8	18.5	21.2	26.9	6.48
DT1-3_20	DT1-3	06/05/15	164	-	89.6	963	253	1.24	8.96	140	274	28.3	94.9	17.8	1.12	2.76	15.7	3.43	9.70	1.72	10.5	1.27	23.1	19.1	20.5	27.7	7.52
DT1-3_21	DT1-3	06/05/15	171	-	106	1140	294	1.57	1.37	165	304	32.2	113	21.4	0.61	3.04	20.2	3.81	11.6	1.73	11.8	1.80	27.2	20.9	24.0	31.7	8.25
DT1-3_22	DT1-3	06/05/15	125	1.27	59.5	607	165	0.69	10.9	92.4	174	18.1	72.1	11.1	1.06	1.51	10.7	2.38	7.91	1.12	7.46	1.42	18.9	10.7	16.3	17.8	4.60
DT1-3_3	DT1-3	06/05/15	158	-	93.6	962	251	1.55	4.08	139	260	29.1	95.1	18.0	0.96	2.74	16.8	3.81	10.6	1.32	10.1	1.65	23.5	17.2	19.9	27.4	6.68
DT1-3_4	DT1-3	06/05/15	74.6	74.7	37.2	383	109	0.15	-	60.1	117	12.7	47.9	6.80	1.95	0.85	7.03	1.31	4.97	0.46	4.55	0.85	9.87	7.78	9.40	10.8	2.68
DT1-3_5	DT1-3	06/05/15	160	-	90.9	970	253	1.34	8.05	134	249	26.5	94.6	19.5	0.91	2.47	16.2	2.94	11.1	1.36	9.89	1.49	24.0	17.3	21.5	26.7	6.53
DT1-3_6	DT1-3	06/05/15	151	-	93.2	975	246	1.57	11.0	131	247	26.0	100	18.2	0.96	3.07	15.9	3.23	10.0	1.37	10.6	1.78	24.1	16.9	18.2	25.8	6.31
DT1-3_7	DT1-3	06/05/15	151	-	92.7	950	248	1.27	2.58	138	265	26.5	93.1	15.7	0.99	2.06	16.1	3.56	10.8	1.50	10.7	1.57	24.1	16.9	18.6	27.6	6.42
DT1-3_8	DT1-3	06/05/15	79.9	62.2	37.7	380	105	0.38	661	63.6	117	11.9	46.6	8.90	1.41	1.08	7.06	1.57	5.42	0.58	5.42	0.70	9.51	7.07	10.8	11.1	2.56
DT1-3_9	DT1-3	06/05/15	101	-	76.0	822	208	0.48	16.0	115	216	24.2	76.7	16.6	0.59	1.73	13.7	3.04	10.5	1.24	9.45	1.16	18.3	15.8	16.0	23.8	5.97
DEN12A/1	DT-1	10/07/14	91.3	4.11	43.4	421	113	0.68	100	66.7	108	11.6	44.5	9.80	0.91	1.10	7.92	1.87	6.04	0.96	4.45	0.70	10.6	8.22	13.3	11.9	3.11
DEN12A/10	DT-1	10/07/14	133	-	89.2	896	209	1.03	11.1	132	218	24.3	91.8	14.8	0.62	2.61	16.5	3.37	10.5	1.65	10.0	1.93	23.4	16.1	17.4	25.8	5.83
DEN12A/11	DT-1	10/07/14	136	1.88	72.7	741	178	1.25	29.7	107	178	20.7	73.0	13.6	0.97	2.17	13.3	2.92	7.48	1.01	8.84	1.25	17.9	13.8	17.6	20.6	4.43
DEN12A/12	DT-1	10/07/14	198	-	110	1200	277	1.87	0.54	167	271	30.9	111	18.8	0.80	3.22	22.1	4.49	12.9	1.96	12.7	2.01	33.1	21.4	23.2	34.5	7.57
DEN12A/13	DT-1	10/07/14	137	-	82.7	827	204	0.86	7.31	121	205	22.2	77.8	12.6	0.93	2.44	13.1	3.03	8.99	1.20	7.76	1.08	21.4	16.0	17.3	22.9	5.48
DEN12A/14	DT-1	10/07/14	135	-	92.2	933	218	0.93	12.7	134	226	25.2	92.6	15.7	1.24	2.65	15.3	3.51	10.8	1.66	10.7	1.44	22.7	17.2	18.0	26.5	5.75
DEN12A/15	DT-1	10/07/14	133	1.12	95.0	949	220	1.23	13.9	137	216	24.6	94.2	18.3	0.90	2.69	18.3	3.48	10.8	1.70	9.35	1.32	24.3	17.3	18.4	27.1	5.64
DEN12A/16	DT-1	10/07/14	136	-	81.3	851	202	1.12	18.4	118	199	21.7	82.7	14.6	0.95	2.25	15.7	3.28	11.9	1.26	9.20	1.45	20.0	16.1	18.0	22.5	5.35
DEN12A/17	DT-1	10/07/14	143	-	93.2	981	226	1.13	3.08	139	228	25.9	93.1	19.0	0.77	2.66	16.3	3.43	11.4	1.92	11.0	1.87	26.1	17.1	19.7	26.7	5.98
DEN12A/18	DT-1	10/07/14	137	-	87.7	928	219	1.04	10.4	130	217	23.9	89.8	15.3	1.19	2.73	15.8	3.51	9.66	1.74	10.3	1.67	23.3	16.5	18.9	24.8	5.82
DEN12A/19	DT-1	10/07/14	135	-	90.2	928	201	1.20	16.7	139	202	23.6	90.2	21.5	0.72	2.32	16.0	3.26	9.52	1.63	8.90	1.51	21.9	14.9	17.9	24.8	5.06
DEN12A/2	DT-1	10/07/14	131	1.92	88.5	862	205	1.24	11.3	130	211	25.0	90.0	17.9	1.47	2.71	15.2	3.40	9.17	1.35	8.80	1.48	22.6	15.4	16.9	23.9	4.92
DEN12A/20	DT-1	10/07/14	139	-	84.5	893	209	1.28	5.77	126	210	23.7	91.4	15.3	1.14	2.25	16.9	3.22	8.16	1.39	10.4	1.33	22.2	16.0	17.4	24.5	5.61
DEN12A/3	DT-1	10/07/14	114	-	86.1	861	204	0.95	7.23	122	200	23.8	87.9	17.2	0.92	2.66	14.2	3.18	8.58	1.47	9.92	1.68	21.4	15.7	17.4	25.6	5.65
DEN12A/4	DT-1	10/07/14	125	-	88.8	914	206	0.98	8.43	131	208	26.0	90.5	15.3	1.15	2.23	15.9	3.73	11.1	1.91	8.62	1.43	21.4	15.6	17.8	24.7	5.03
DEN12A/5	DT-1	10/07/14	112	-	108	1040	241	0.85	11.7	154	246	28.3	115	18.2	0.96	2.72	18.7	4.20	11.5	2.01	12.3	1.81	28.1	17.6	16.7	29.1	5.62
DEN12A/6	DT-1	10/07/14	110	-	86.9	888	207	0.95	17.5	125	201	24.6	88.3	13.7	0.93	2.58	14.2	3.68	10.4	1.51	10.3	1.24	25.9	15.9	16.1	26.3	5.57
DEN12A/7	DT-1	10/07/14	123	1.43	93.6	1090	214	1.13	29.2	126	203	25.2	83.4	18.1	0.75	2.58	17.6	3.29	11.2	1.45	10.8	1.56	26.7	16.9	16.5	27.8	5.63
DEN12A/8	DT-1	10/07/14	140	1.00	86.5	866	213	1.10	4.63	128	201	24.5	84.7	15.9	0.88	2.47	14.6	3.15	10.0	1.32	9.37	1.46	22.1	14.8	18.2	25.1	5.32
DEN12A/9	DT-1	10/07/14	131	-	90.5	895	204	0.89	7.07	128	205	23.8	86.1	15.6	0.98	2.57	17.5	2.95	8.91	1.64	9.50	1.55	24.0	16.1	16.3	25.0	4.91
DEN12C/1†	DT-2	10/07/14	142	6.03	98.4	501	206	1.55	42.1	151	243	25.3	114	15.1	2.03	2.32	18.4	4.49	9.66	2.00	8.05	0.75	18.8	14.1	18.2	24.8	4.47
DEN12C/11†	DT-2	10/07/14	150	12.8	145	749	270	1.12	15.0	203	330	40.6	141	21.5	1.92	2.95	24.6	5.29	19.0	1.64	15.3	3.42	29.9	15.7	19.8	34.5	6.29
DEN12C/12†	DT-2	10/07/14	126	-	98.7	537	204	0.69	9.93	146	240	26.8	113	19.9	1.50	2.89	18.4	4.03	13.2	1.48	8.43	1.13	21.8	12.5	17.6	27.1	4.67
DEN12C/13	DT-2	10/07/14	124	7.88	89.1	732	206	0.92	70.0	136	221	26.0	98.9	20.1	1.68	2.91	17.7	3.47	8.30	1.39	9.14	1.35	18.6	13.6	15.6	21.8	5.07
DEN12C/15	DT-2	10/07/14	120	5.66	80.8	747	201	0.92	65.8	128	226	25.0	98.1	17.6	2.04	2.50	15.7	3.75	8.66	1.26	9.45	1.24	17.5	15.7	17.2	22.1	5.63
DEN12C/16†	DT-2	10/07/14	132	-	95.6	490	212	1.27	9.34	157	259	27.9	106	19.7	0.91	3.09	15.5	4.89	6.37	1.72	13.4	1.72	23.2	15.2	17.7	27.3	5.41
DEN12C/18†	DT-2	10/07/14	120	45.4	76.5	429	174	0.99	-	114	200	23.2	113	17.8	3.39	2.50	13.4	4.81	9.47	1.40	9.60	1.45	17.5	11.4	15.0	22.9	3.90
DEN12C/19	DT-2	10/07/14	133	-	85.3	725	211	0.84	21.4	130	230	24.8	103	18.9	1.96	2.78	15.7	3.50	9.62	1.39	9.31	1.14	18.1	15.0	19.8	22.5	4.75

Continued on next page

Trace element concentrations (ppm) in Dendi tephra glass shards

Label	Tephra	Analysis date	Rb 0.62	Sr 1.05	Y 0.17	Zr 0.37	Nb 0.07	Cs 0.19	Ba 1.88	La 0.09	Ce 0.07	Pr 0.06	Nd 0.25	Sm 0.14	Eu 0.13	Tb 0.06	Dy 0.13	Ho 0.04	Er 0.07	Tm 0.05	Yb 0.15	Lu 0.04	Hf 0.08	Ta 0.06	Pb 0.12	Th 0.01	U 0.00
DEN12C/2	DT-2	10/07/14	134	9.75	84.8	842	227	1.28	57.0	149	228	26.8	114	22.2	1.69	2.74	16.3	3.48	11.2	1.53	8.21	1.30	22.0	17.3	18.8	20.4	4.58
DEN12C/20A	DT-2	10/07/14	137	5.00	78.0	703	210	1.04	55.6	128	224	25.2	92.6	17.1	1.74	2.85	15.2	3.03	8.86	1.14	8.67	1.22	17.5	15.0	21.3	22.0	5.98
DEN12C/20B†	DT-2	10/07/14	155	8.03	98.4	511	235	0.74	60.8	159	249	31.8	104	20.4	1.30	2.05	18.0	2.67	10.3	1.99	6.28	2.17	18.0	18.3	19.8	27.9	6.39
DEN12C/3†	DT-2	10/07/14	187	-	120	904	290	1.51	1.39	178	304	30.6	145	19.3	0.33	3.83	17.0	4.71	14.7	1.94	12.9	2.28	36.8	22.5	20.4	42.9	6.53
DEN12C/5†	DT-2	10/07/14	122	1.88	84.8	476	184	1.21	49.5	130	221	28.8	100	15.2	0.94	2.79	21.4	3.94	13.0	1.26	7.91	1.28	22.0	15.2	13.6	25.3	4.76
DEN12C/6†	DT-2	10/07/14	134	8.55	129	684	222	0.27	24.2	181	295	32.4	122	24.2	2.48	4.25	29.3	6.00	11.8	1.34	16.2	3.14	36.6	19.7	15.9	30.0	4.51
DEN12C/7	DT-2	10/07/14	142	3.57	72.4	656	209	1.32	6.03	120	209	22.3	91.4	15.4	1.28	2.62	15.1	2.74	8.63	1.38	8.05	1.28	16.2	14.4	20.3	20.5	6.47
DEN12C/8†	DT-2	10/07/14	148	-	87.9	446	221	0.53	0.93	152	250	26.0	104	15.3	0.76	2.83	12.4	2.85	13.5	1.10	6.87	2.07	18.0	14.2	15.9	22.9	5.48
DEN12B/1	DT-3	10/07/14	116	12.3	62.3	564	187	0.90	138	98.4	177	19.8	73.5	11.4	1.09	1.75	11.4	2.40	6.39	1.06	6.15	0.79	13.7	11.7	14.9	15.4	4.52
DEN12B/10	DT-3	10/07/14	164	1.92	86.9	921	276	1.53	2.82	147	255	27.5	106	16.8	0.96	2.47	14.9	3.55	9.78	1.67	9.59	1.62	23.1	18.8	23.0	29.6	7.67
DEN12B/11	DT-3	10/07/14	122	1.22	96.6	825	219	0.98	19.3	143	229	28.2	112	19.1	1.19	2.27	13.3	3.73	9.27	1.31	7.27	1.26	19.1	15.3	16.7	23.0	4.98
DEN12B/12	DT-3	10/07/14	123	3.70	87.6	757	219	0.82	36.3	136	226	27.7	96.3	18.7	1.61	2.53	16.0	3.70	11.0	1.28	9.10	1.49	19.7	15.5	17.8	24.2	5.21
DEN12B/13	DT-3	10/07/14	135	11.0	95.4	841	237	1.28	79.0	154	251	29.7	109	21.9	1.76	3.00	16.6	4.23	10.2	1.91	11.3	1.53	23.2	16.9	19.4	25.9	6.46
DEN12B/14	DT-3	10/07/14	115	9.92	45.4	441	141	0.57	119	80.0	144	16.2	61.5	9.80	1.55	1.23	10.4	2.07	6.19	0.72	4.98	0.70	11.0	9.75	13.2	14.6	3.56
DEN12B/15†	DT-3	10/07/14	167	-	107	644	267	0.77	9.45	152	260	30.2	131	16.9	0.89	2.87	18.9	4.50	11.9	1.76	9.90	1.29	25.6	16.7	18.6	32.5	7.47
DEN12B/17	DT-3	10/07/14	125	3.39	91.9	765	214	1.01	43.7	142	243	27.9	115	21.2	2.31	2.88	16.7	3.43	10.8	1.75	10.5	1.03	20.5	15.0	18.0	23.2	5.73
DEN12B/18	DT-3	10/07/14	126	3.86	61.7	635	178	0.86	27.3	107	173	20.5	73.4	14.4	1.20	1.60	12.3	3.23	6.09	1.26	7.67	0.95	15.6	13.7	15.4	20.3	5.01
DEN12B/19	DT-3	10/07/14	131	14.4	82.6	671	204	1.02	432	133	228	25.9	96.9	17.6	1.99	2.53	16.3	3.51	9.67	1.44	8.10	1.22	16.5	14.2	18.7	21.5	5.17
DEN12B/2	DT-3	10/07/14	73.6	137	80.2	452	123	0.72	722	95.2	189	24.2	104	20.4	5.09	2.87	15.0	3.11	8.77	1.14	7.70	1.06	11.7	7.68	11.2	12.3	2.81
DEN12B/20	DT-3	10/07/14	128	-	107	568	227	0.84	15.9	154	258	31.2	109	20.5	1.86	3.19	16.2	3.72	11.2	2.04	12.1	1.39	21.6	15.6	16.2	26.8	5.14
DEN12B/3	DT-3	10/07/14	132	4.92	83.9	737	221	0.98	53.7	135	231	25.2	96.5	18.3	1.47	2.29	16.0	3.26	9.57	1.38	8.07	1.30	18.4	14.3	20.1	22.6	5.41
DEN12B/4	DT-3	10/07/14	123	9.55	83.6	776	242	1.09	14.6	133	242	27.2	92.1	18.3	1.41	2.47	16.2	3.43	9.14	1.51	8.22	1.41	20.0	16.3	19.9	23.2	5.83
DEN12B/5	DT-3	10/07/14	125	7.89	79.4	692	209	1.07	74.6	128	217	24.7	96.9	16.8	1.27	2.28	13.5	2.71	8.83	1.06	7.66	1.22	18.8	13.5	16.9	21.4	4.61
DEN12B/6	DT-3	10/07/14	64.8	1.04	22.9	210	62.4	0.12	53.1	37.4	63.6	7.20	27.4	6.50	1.31	0.58	5.03	0.77	2.83	0.43	2.06	0.30	5.02	3.68	6.51	6.40	1.65
DEN12B/7	DT-3	10/07/14	192	1.43	88.2	1070	270	1.67	0.14	136	240	27.0	96.8	17.5	0.60	2.29	14.3	3.08	9.42	1.30	9.42	1.34	26.2	18.2	26.1	33.5	8.41
DEN12B/9	DT-3	10/07/14	136	11.2	198	1430	218	1.39	511	165	289	36.4	156	33.9	5.99	5.11	33.4	7.74	20.9	3.00	20.5	2.90	36.5	14.7	28.2	24.1	5.55

.4.2 Bayesian age models

Bernd Wagner (University of Cologne) provided the Bayesian age model for the Dendi sediments seen below. The model was generated using Bacon software (Blaauw and Christen, 2011), providing approximate ages for the Dendi tephras. Due to the uncertainities over coring depths and chronology, this study did not produce an age model for the Hora archive.

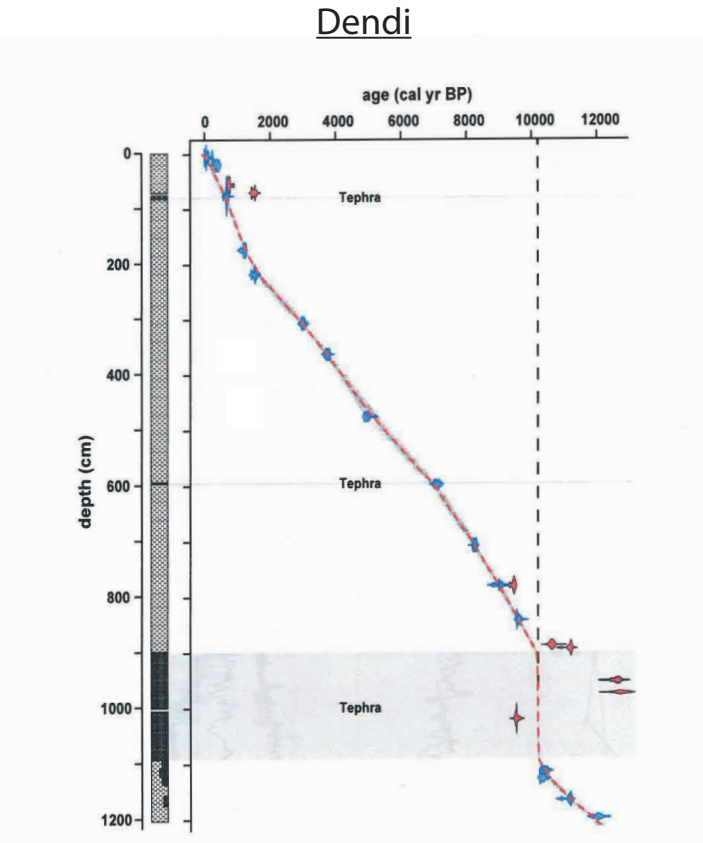

.5 Tephras from the central MER

This Appendix gives the major and trace element composition of tephras recorded in the central Main Ethiopian Rift lake sediments from Awassa, Tilo and Chamo. The composition of tephra and obsidian samples from the Corbetti caldera are

also given. The Bayesian age models for Awassa, Tilo and Chamo archives are presented at the end of this section.

.5.1 Major and trace element glass compositions

The following tables present shard specific major and trace element glass compositions, major elements are presented to 2 decimal places and trace elements are presented to 3 significant figures.

Some major elements (e.g. Cl) were not analysed on all analytical sessions, and all Fe is calculated as FeO^T. Calculated limits of detection for all EPMA sessions are given on page 401. The median LLD for the rhyolitic ATHO-G reference material over all EPMA analytical sessions is given in the following table headings. Most major elements are present at concentrations above these limits of detection, however, concentrations of MgO and P_2O_5 are below the LLD in many shards.

Trace element analyses were typically undertaken using 20 μm crater diameters, however, †indicates glass shards were analysed using 10 μm crater diameters. Lower limits of detection (LLD) for LA-ICP-MS analyses are given on page 407. The median LLD concentrations at 20 μm crater diameters of all LA-ICP-MS analytical sessions are given beneath each analyte heading in the following tables. Due to high Sr and Ba concentrations in the gas blanks, coupled with frequent low sample concentrations, some negative concentrations were measured - these are indicated with a dash. Analyses of MPI-DING reference materials were used to check the EPMA and LA-ICP-MS calibrations. These analyses are given on page 398, and are ordered by analysis date.

Unnormalised major element concentrations (wt.%) in Tilo tephra glass shards

Label	Tephra	Analysis date	SiO_2 0.08	TiO_2 0.05	Al_2O_3 0.05	MgO 0.04	FeO^T 0.08	MnO 0.07	CaO 0.04	Na_2O 0.08	K_2O 0.03	P_2O_5 0.10	Cl 0.02	Total
TT97-1_1	TT-1	26/08/14	73.68	0.22	9.50	0.00	4.58	0.23	0.16	5.27	4.50	0.01		98.16

Continued on next page

Unnormalised major element concentrations (wt.%) in Tilo tephra glass shards

Label	Tephra	Analysis date	SiO_2 0.08	TiO_2 0.05	Al_2O_3 0.05	MgO 0.04	FeO^T 0.08	MnO 0.07	CaO 0.04	Na_2O 0.08	K_2O 0.03	P_2O_5 0.10	Cl 0.02	Total
TT97-1_10	TT-1	26/08/14	73.82	0.24	9.64	0.00	4.37	0.20	0.18	5.07	4.41	0.01		97.94
TT97-1_12	TT-1	26/08/14	73.62	0.21	9.75	0.02	4.50	0.26	0.17	5.05	4.41	0.00		98.00
TT97-1_13	TT-1	26/08/14	74.15	0.22	9.71	0.00	4.64	0.18	0.20	5.18	4.42	0.01		98.71
TT97-1_14	TT-1	26/08/14	74.36	0.24	9.82	0.00	4.63	0.22	0.18	5.46	4.40	0.00		99.31
TT97-1_15	TT-1	26/08/14	70.49	0.24	12.37	0.00	4.27	0.11	0.14	4.81	4.10	0.03		96.57
TT97-1_16	TT-1	26/08/14	68.84	0.24	9.13	0.02	4.03	0.27	0.14	5.13	4.16	0.05		92.00
TT97-1_17	TT-1	26/08/14	73.57	0.21	9.69	0.00	4.39	0.20	0.20	5.28	4.51	0.00		98.06
TT97-1_18	TT-1	26/08/14	73.96	0.23	9.88	0.00	4.58	0.22	0.16	5.03	4.47	0.03		98.56
TT97-1_19	TT-1	26/08/14	73.52	0.30	9.85	0.00	4.53	0.18	0.20	5.39	4.55	0.00		98.52
TT97-1_2	TT-1	26/08/14	71.71	0.24	9.82	0.00	4.32	0.24	0.21	5.03	4.32	0.01		95.89
TT97-1_20	TT-1	26/08/14	73.21	0.25	9.82	0.02	4.37	0.21	0.17	5.02	4.47	0.02		97.56
TT97-1_4	TT-1	26/08/14	74.97	0.26	9.51	0.00	4.73	0.20	0.20	5.41	4.13	0.02		99.42
TT97-1_5	TT-1	26/08/14	74.37	0.25	9.73	0.00	4.50	0.15	0.22	5.41	4.34	0.00		98.97
TT97-1_6	TT-1	26/08/14	73.67	0.24	9.60	0.00	4.59	0.19	0.19	5.14	4.60	0.00		98.22
TT97-1_8	TT-1	26/08/14	74.03	0.22	9.82	0.00	4.47	0.18	0.18	5.41	4.36	0.02		98.69
TT97-2A_1	TT-2	26/08/14	73.18	0.23	9.73	0.02	4.57	0.22	0.14	5.42	4.53	0.02		98.04
TT97-2A_10	TT-2	26/08/14	72.30	0.23	9.15	0.00	4.49	0.21	0.16	5.30	4.31	0.02		96.16
TT97-2A_13	TT-2	26/08/14	73.10	0.23	9.56	0.00	4.72	0.17	0.17	5.60	4.47	0.00		98.02
TT97-2A_14	TT-2	26/08/14	73.25	0.23	9.75	0.00	4.55	0.17	0.16	5.68	4.34	0.00		98.12
TT97-2A_15	TT-2	26/08/14	73.08	0.27	9.75	0.01	4.44	0.17	0.20	5.56	4.53	0.00		98.01
TT97-2A_16	TT-2	26/08/14	72.20	0.23	9.59	0.00	4.49	0.13	0.20	5.31	4.38	0.00		96.52
TT97-2A_18	TT-2	26/08/14	73.57	0.22	9.64	0.02	4.55	0.27	0.20	5.32	4.43	0.01		98.23
TT97-2A_19	TT-2	26/08/14	71.78	0.22	9.40	0.00	4.48	0.16	0.16	5.31	4.23	0.00		95.74
TT97-2A_2	TT-2	26/08/14	72.70	0.19	9.46	0.00	4.53	0.20	0.16	5.37	4.16	0.00		96.78
TT97-2A_3	TT-2	26/08/14	73.39	0.26	9.55	0.00	4.52	0.14	0.18	5.46	4.28	0.01		97.79
TT97-2A_4	TT-2	26/08/14	74.08	0.25	9.55	0.00	4.78	0.16	0.14	5.30	4.32	0.02		98.61
TT97-2A_5	TT-2	26/08/14	70.01	0.22	10.31	0.03	4.11	0.22	0.18	5.05	4.05	0.01		94.19
TT97-2A_6	TT-2	26/08/14	74.41	0.24	9.81	0.00	4.58	0.26	0.20	5.40	4.56	0.00		99.46
TT97-2A_8	TT-2	26/08/14	72.26	0.28	10.53	0.00	4.34	0.15	0.21	5.25	4.27	0.00		97.29
TT97-2A_9	TT-2	26/08/14	70.47	0.29	9.17	0.01	4.37	0.17	0.16	5.26	4.16	0.01		94.05
TT97-2B_1	TT-2	26/08/14	73.69	0.27	9.67	0.00	4.44	0.23	0.17	5.24	4.43	0.00		98.14
TT97-2B_10	TT-2	26/08/14	67.54	0.21	8.56	0.00	4.41	0.23	0.17	5.24	4.21	0.00		90.58
TT97-2B_12	TT-2	26/08/14	72.51	0.20	9.60	0.00	4.23	0.15	0.18	5.36	4.14	0.02		96.39
TT97-2B_13	TT-2	26/08/14	72.84	0.27	9.24	0.01	4.25	0.20	0.21	5.40	4.37	0.00		96.78
TT97-2B_14	TT-2	26/08/14	71.76	0.27	10.31	0.00	4.24	0.19	0.20	5.40	4.17	0.00		96.54
TT97-2B_15	TT-2	26/08/14	73.46	0.23	9.15	0.00	4.29	0.19	0.15	5.22	4.42	0.00		97.12
TT97-2B_16	TT-2	26/08/14	72.75	0.30	9.58	0.00	4.35	0.23	0.25	4.59	4.23	0.00		96.27
TT97-2B_17	TT-2	26/08/14	75.07	0.23	9.49	0.00	4.42	0.23	0.19	5.11	4.23	0.01		98.99
TT97-2B_18	TT-2	26/08/14	73.75	0.30	9.40	0.00	4.18	0.24	0.19	5.40	4.43	0.00		97.89
TT97-2B_19	TT-2	26/08/14	73.96	0.24	9.68	0.00	4.53	0.17	0.20	5.24	4.38	0.02		98.41
TT97-2B_2	TT-2	26/08/14	74.42	0.26	9.59	0.00	4.59	0.23	0.18	5.40	4.57	0.03		99.26
TT97-2B_20	TT-2	26/08/14	74.10	0.23	9.65	0.02	4.59	0.27	0.19	5.56	4.48	0.00		99.10
TT97-2B_3	TT-2	26/08/14	72.96	0.23	9.22	0.01	4.31	0.15	0.20	5.25	4.40	0.00		96.74
TT97-2B_4	TT-2	26/08/14	70.43	0.22	12.08	0.00	4.10	0.19	0.18	5.08	4.25	0.03		96.55
TT97-2B_7	TT-2	26/08/14	73.19	0.26	9.15	0.00	4.25	0.17	0.16	5.34	4.45	0.01		96.98
TT97-2B_8	TT-2	26/08/14	72.44	0.17	9.05	0.00	4.29	0.24	0.18	5.43	4.29	0.02		96.11
TT97-2B_9	TT-2	26/08/14	69.95	0.24	10.41	0.00	4.41	0.18	0.21	4.94	4.18	0.02		94.55
TT97-2C_1	TT-2	26/08/14	71.14	0.30	11.47	0.00	4.29	0.15	0.21	4.85	4.32	0.01		96.74
TT97-2C_10	TT-2	27/08/14	70.25	0.23	8.78	0.03	4.23	0.21	0.17	5.33	4.20	0.02		93.44
TT97-2C_11	TT-2	27/08/14	69.91	0.21	8.88	0.00	4.31	0.21	0.16	5.24	4.15	0.03		93.10
TT97-2C_13	TT-2	27/08/14	73.37	0.21	9.47	0.00	4.54	0.24	0.19	5.33	4.39	0.00		97.74
TT97-2C_14	TT-2	27/08/14	72.79	0.27	9.12	0.00	4.11	0.21	0.21	5.09	4.22	0.00		96.03
TT97-2C_15	TT-2	27/08/14	73.61	0.22	9.37	0.00	4.56	0.22	0.20	5.31	4.38	0.00		97.87
TT97-2C_16	TT-2	27/08/14	74.01	0.19	9.44	0.00	4.58	0.20	0.20	5.42	4.46	0.03		98.51
TT97-2C_17	TT-2	27/08/14	70.39	0.26	9.04	0.01	4.31	0.19	0.17	5.26	4.19	0.02		93.85
TT97-2C_18	TT-2	27/08/14	72.79	0.29	9.25	0.00	4.49	0.21	0.17	5.12	4.24	0.00		96.57
TT97-2C_19	TT-2	27/08/14	73.15	0.20	9.39	0.03	4.55	0.27	0.19	5.24	4.42	0.01		97.46
TT97-2C_2	TT-2	26/08/14	67.60	0.23	8.64	0.00	4.22	0.17	0.17	4.90	4.21	0.01		90.15
TT97-2C_20	TT-2	27/08/14	70.75	0.24	8.87	0.00	4.49	0.25	0.19	5.14	4.20	0.00		94.12
TT97-2C_4	TT-2	26/08/14	67.40	0.25	10.62	0.03	4.04	0.21	0.19	4.72	3.99	0.01		91.47
TT97-2C_5	TT-2	26/08/14	74.21	0.25	9.64	0.00	4.37	0.25	0.20	5.23	4.46	0.00		98.60
TT97-2C_7	TT-2	26/08/14	72.64	0.24	9.40	0.00	4.34	0.14	0.17	5.24	4.30	0.00		96.48
TT97-2C_8	TT-2	27/08/14	71.37	0.24	9.03	0.00	4.48	0.16	0.17	5.01	4.19	0.00		94.67
TT973/1	TT-3	21/02/14	69.02	0.23	8.13	0.00	6.14	0.25	0.17	5.98	4.22	0.02	0.22	94.39
TT973/10	TT-3	21/02/14	71.22	0.20	8.20	0.01	6.04	0.22	0.21	5.79	4.11	0.00	0.28	96.28
TT973/11	TT-3	21/02/14	71.97	0.18	8.39	0.02	6.13	0.30	0.17	6.15	4.17	0.02	0.31	97.82
TT973/12	TT-3	21/02/14	72.30	0.18	8.86	0.00	5.47	0.17	0.16	6.02	4.35	0.01	0.27	97.80
TT973/13	TT-3	21/02/14	70.97	0.13	7.92	0.00	6.38	0.38	0.17	6.43	4.02	0.02	0.31	96.74
TT973/14	TT-3	21/02/14	70.88	0.18	8.03	0.00	6.24	0.31	0.20	6.40	4.27	0.03	0.24	96.78
TT973/15	TT-3	21/02/14	72.64	0.18	8.40	0.00	6.36	0.34	0.17	6.31	4.29	0.01	0.28	98.99
TT973/16	TT-3	21/02/14	70.77	0.15	8.43	0.00	6.21	0.29	0.19	5.94	4.23	0.01	0.25	96.47
TT973/17	TT-3	21/02/14	71.19	0.16	7.94	0.00	6.30	0.36	0.17	6.64	4.12	0.02	0.36	97.27
TT973/18	TT-3	21/02/14	71.04	0.13	8.21	0.00	6.06	0.27	0.20	5.95	4.11	0.01	0.30	96.29
TT973/19	TT-3	21/02/14	71.38	0.15	8.10	0.00	6.64	0.31	0.16	6.69	4.00	0.01	0.33	97.76
TT973/2	TT-3	21/02/14	71.90	0.17	8.06	0.00	6.52	0.21	0.19	6.58	4.13	0.02	0.30	98.09
TT973/20	TT-3	21/02/14	72.19	0.16	8.54	0.02	6.05	0.27	0.22	6.34	4.24	0.04	0.26	98.34
TT973/3	TT-3	21/02/14	73.06	0.16	8.47	0.00	6.35	0.34	0.21	6.68	4.25	0.01	0.26	99.79
TT973/4	TT-3	21/02/14	68.35	0.13	7.92	0.01	6.00	0.29	0.18	5.36	4.11	0.00	0.27	92.62
TT973/5	TT-3	21/02/14	69.55	0.16	9.09	0.01	6.13	0.28	0.21	6.14	4.22	0.02	0.26	96.07
TT973/7	TT-3	21/02/14	71.89	0.19	8.34	0.00	6.31	0.38	0.16	5.92	4.19	0.00	0.28	97.66
TT973/8	TT-3	21/02/14	71.52	0.18	8.74	0.00	6.21	0.25	0.22	6.12	4.28	0.02	0.27	97.82
TT974/1	TT-4	21/02/14	74.35	0.24	9.76	0.00	4.76	0.20	0.20	5.33	4.41	0.02	0.20	99.49
TT974/10	TT-4	21/02/14	73.95	0.30	9.65	0.02	4.34	0.21	0.17	4.97	4.33	0.00	0.25	98.20
TT974/12	TT-4	21/02/14	72.13	0.26	9.54	0.00	4.37	0.24	0.18	5.16	4.28	0.02	0.23	96.40
TT974/13	TT-4	21/02/14	73.30	0.23	9.76	0.00	4.42	0.25	0.18	5.38	4.43	0.00	0.21	98.15

Continued on next page

Unnormalised major element concentrations (wt.%) in Tilo tephra glass shards

Label	Tephra	Analysis date	SiO_2 0.08	TiO_2 0.05	Al_2O_3 0.05	MgO 0.04	FeO^T 0.08	MnO 0.07	CaO 0.04	Na_2O 0.08	K_2O 0.03	P_2O_5 0.10	Cl 0.02	Total
TT974/14	TT-4	21/02/14	72.33	0.21	9.42	0.02	4.47	0.18	0.21	5.10	4.30	0.00	0.20	96.45
TT974/15	TT-4	21/02/14	73.82	0.23	9.81	0.00	4.65	0.21	0.18	5.55	4.38	0.00	0.21	99.04
TT974/16	TT-4	21/02/14	72.32	0.23	9.48	0.00	4.47	0.21	0.19	5.22	4.40	0.04	0.20	96.76
TT974/17	TT-4	21/02/14	73.66	0.28	9.86	0.01	4.34	0.18	0.21	5.41	4.54	0.01	0.18	98.69
TT974/18	TT-4	21/02/14	74.11	0.23	9.58	0.00	4.61	0.18	0.18	5.25	4.29	0.02	0.21	98.66
TT974/19	TT-4	21/02/14	73.50	0.16	9.78	0.02	4.58	0.22	0.18	4.96	4.39	0.00	0.20	97.99
TT974/2	TT-4	21/02/14	70.99	0.24	9.24	0.01	4.39	0.27	0.15	4.96	4.21	0.01	0.22	94.69
TT974/20	TT-4	21/02/14	71.60	0.19	9.31	0.00	4.35	0.16	0.21	5.11	4.29	0.01	0.19	95.42
TT974/3	TT-4	21/02/14	71.45	0.26	9.75	0.00	4.28	0.22	0.17	5.22	4.38	0.03	0.19	95.94
TT974/4	TT-4	21/02/14	67.34	0.23	9.27	0.00	3.98	0.24	0.20	5.03	4.03	0.04	0.21	90.56
TT974/5	TT-4	21/02/14	73.43	0.25	9.75	0.01	4.72	0.17	0.21	5.14	4.35	0.04	0.18	98.24
TT974/6	TT-4	21/02/14	73.68	0.24	9.60	0.03	4.64	0.20	0.20	5.33	4.53	0.01	0.19	98.67
TT974/7	TT-4	21/02/14	72.79	0.26	9.60	0.02	4.44	0.22	0.19	5.24	4.38	0.00	0.22	97.35
TT974/8	TT-4	21/02/14	73.82	0.23	9.60	0.02	4.63	0.20	0.19	5.34	4.28	0.02	0.24	98.56
TT974/9	TT-4	21/02/14	73.47	0.25	9.61	0.00	4.57	0.24	0.19	5.66	4.14	0.00	0.16	98.30
TT975A/1	TT-5	21/02/14	72.16	0.21	9.43	0.00	4.34	0.21	0.19	5.34	4.32	0.00	0.21	96.41
TT975A/10	TT-5	21/02/14	66.75	0.20	10.20	0.00	4.25	0.15	0.16	4.66	3.96	0.01	0.25	90.59
TT975A/11	TT-5	21/02/14	73.92	0.23	9.77	0.00	4.49	0.19	0.19	5.04	4.40	0.02	0.17	98.44
TT975A/12	TT-5	21/02/14	74.14	0.26	9.89	0.00	4.50	0.18	0.20	5.27	4.44	0.04	0.22	99.15
TT975A/13	TT-5	21/02/14	73.94	0.26	9.74	0.02	4.33	0.15	0.15	3.43	4.22	0.00	0.20	96.45
TT975A/14	TT-5	21/02/14	73.27	0.19	9.64	0.02	4.43	0.14	0.18	5.12	4.32	0.00	0.23	97.56
TT975A/15	TT-5	21/02/14	72.32	0.22	9.45	0.01	4.54	0.10	0.17	5.29	4.36	0.00	0.18	96.64
TT975A/16	TT-5	21/02/14	72.35	0.24	9.46	0.01	4.30	0.23	0.18	5.34	4.33	0.03	0.23	96.69
TT975A/17	TT-5	21/02/14	72.97	0.27	9.72	0.02	4.42	0.24	0.22	5.55	4.31	0.00	0.16	97.87
TT975A/18	TT-5	21/02/14	73.61	0.19	9.72	0.03	4.65	0.22	0.18	5.63	4.40	0.01	0.21	98.86
TT975A/19	TT-5	21/02/14	73.44	0.24	9.55	0.02	4.61	0.20	0.21	5.40	4.43	0.02	0.20	98.32
TT975A/2	TT-5	21/02/14	73.10	0.20	9.50	0.00	4.65	0.15	0.17	5.37	4.44	0.02	0.18	97.78
TT975A/20	TT-5	21/02/14	70.69	0.23	9.66	0.02	4.37	0.08	0.18	5.19	4.38	0.02	0.20	95.02
TT975A/3	TT-5	21/02/14	72.94	0.26	9.47	0.02	4.46	0.17	0.20	5.23	4.37	0.03	0.18	97.32
TT975A/4	TT-5	21/02/14	71.24	0.25	9.29	0.00	4.54	0.21	0.20	5.44	4.13	0.00	0.17	95.48
TT975A/5	TT-5	21/02/14	71.73	0.25	9.38	0.00	4.68	0.17	0.19	4.96	4.34	0.05	0.22	95.98
TT975A/6	TT-5	21/02/14	73.49	0.23	9.65	0.00	4.57	0.20	0.18	5.09	4.34	0.00	0.17	97.91
TT975A/7	TT-5	21/02/14	73.39	0.19	9.56	0.01	4.62	0.18	0.20	5.32	4.41	0.00	0.20	98.08
TT975A/8	TT-5	21/02/14	73.02	0.23	9.45	0.00	4.75	0.28	0.17	5.24	4.32	0.02	0.19	97.67
TT975A/9	TT-5	21/02/14	73.20	0.22	9.62	0.03	4.59	0.18	0.18	5.31	4.45	0.00	0.21	98.00
TT975AB/1	TT-5	21/02/14	70.67	0.26	9.68	0.00	4.29	0.22	0.20	5.13	4.18	0.00	0.20	94.84
TT975AB/10	TT-5	21/02/14	73.06	0.19	9.38	0.01	4.38	0.14	0.18	5.38	4.28	0.00	0.23	97.23
TT975AB/11	TT-5	21/02/14	71.03	0.25	9.60	0.00	4.75	0.13	0.15	5.14	4.36	0.00	0.17	95.58
TT975AB/12	TT-5	21/02/14	73.85	0.21	9.84	0.00	4.76	0.20	0.19	5.08	4.44	0.01	0.22	98.81
TT975AB/13	TT-5	21/02/14	74.85	0.19	9.72	0.00	4.57	0.16	0.17	3.92	4.55	0.01	0.18	98.33
TT975AB/14	TT-5	21/02/14	74.09	0.27	9.75	0.02	4.46	0.15	0.18	5.13	4.38	0.02	0.24	98.68
TT975AB/15	TT-5	21/02/14	73.53	0.25	9.62	0.01	4.69	0.16	0.15	5.21	4.19	0.00	0.20	98.00
TT975AB/16	TT-5	21/02/14	73.24	0.21	9.68	0.00	4.48	0.21	0.15	4.99	4.39	0.00	0.20	97.55
TT975AB/17	TT-5	21/02/14	67.78	0.22	9.29	0.00	3.95	0.20	0.17	4.69	4.09	0.01	0.25	90.65
TT975AB/18	TT-5	21/02/14	73.11	0.27	9.59	0.00	4.70	0.17	0.18	5.13	4.48	0.00	0.20	97.83
TT975AB/19	TT-5	21/02/14	73.15	0.22	10.04	0.02	4.31	0.19	0.19	5.23	4.39	0.00	0.22	97.96
TT975AB/2	TT-5	21/02/14	72.37	0.21	9.81	0.04	4.55	0.29	0.16	5.31	4.31	0.01	0.20	97.26
TT975AB/20	TT-5	21/02/14	73.81	0.24	9.69	0.02	4.53	0.18	0.19	5.17	4.44	0.00	0.20	98.47
TT975AB/3	TT-5	21/02/14	70.93	0.26	9.70	0.03	4.60	0.14	0.16	5.04	4.22	0.01	0.24	95.32
TT975AB/4	TT-5	21/02/14	73.68	0.21	9.80	0.00	4.80	0.24	0.17	5.28	4.22	0.00	0.23	98.65
TT975AB/5	TT-5	21/02/14	71.47	0.23	9.28	0.00	4.31	0.14	0.17	4.90	4.26	0.00	0.23	95.00
TT975AB/6	TT-5	21/02/14	74.02	0.22	9.75	0.04	4.63	0.29	0.19	5.41	4.35	0.01	0.18	99.08
TT975AB/7	TT-5	21/02/14	72.65	0.25	9.57	0.00	4.54	0.19	0.19	4.91	4.35	0.01	0.20	96.88
TT975AB/8	TT-5	21/02/14	73.77	0.25	9.65	0.00	4.44	0.21	0.20	5.39	4.32	0.00	0.18	98.41
TT975AB/9	TT-5	21/02/14	71.76	0.23	9.32	0.00	4.34	0.15	0.19	5.40	4.25	0.03	0.23	95.88
TT976/1	TT-6	21/02/14	66.87	0.14	9.32	0.00	5.90	0.30	0.20	5.79	3.74	0.01	0.31	92.56
TT976/10	TT-6	21/02/14	69.37	0.22	8.81	0.02	6.04	0.32	0.19	6.19	3.88	0.04	0.35	95.43
TT976/11	TT-6	21/02/14	72.74	0.17	7.27	0.00	6.29	0.41	0.17	6.12	3.88	0.02	0.27	97.34
TT976/12	TT-6	21/02/14	70.95	0.22	8.38	0.00	6.18	0.28	0.20	6.23	4.29	0.01	0.29	97.03
TT976/13a	TT-6	21/02/14	74.17	0.10	8.24	0.02	5.73	0.18	0.08	6.38	3.72	0.02	0.25	98.89
TT976/14	TT-6	21/02/14	70.66	0.17	8.14	0.01	6.31	0.34	0.24	6.21	4.15	0.01	0.28	96.52
TT976/15	TT-6	21/02/14	70.02	0.21	7.87	0.00	6.19	0.32	0.19	6.07	3.96	0.02	0.28	95.13
TT976/16	TT-6	21/02/14	71.62	0.19	8.20	0.00	6.40	0.29	0.18	5.99	4.14	0.01	0.25	97.27
TT976/17	TT-6	21/02/14	70.89	0.16	8.09	0.00	6.31	0.28	0.18	6.51	4.18	0.02	0.28	96.89
TT976/18a	TT-6	21/02/14	71.53	0.17	8.64	0.00	6.10	0.37	0.19	6.19	4.28	0.02	0.25	97.74
TT976/19a	TT-6	21/02/14	72.08	0.18	8.28	0.00	6.30	0.36	0.19	6.34	4.13	0.00	0.30	98.15
TT976/20a	TT-6	21/02/14	68.50	0.16	8.42	0.00	6.21	0.33	0.17	5.89	3.89	0.00	0.33	93.91
TT976/3	TT-6	21/02/14	72.31	0.20	8.29	0.01	6.39	0.33	0.21	6.57	4.11	0.00	0.30	98.72
TT976/4a	TT-6	21/02/14	70.96	0.20	8.07	0.00	6.61	0.34	0.16	6.66	3.93	0.03	0.33	97.30
TT976/5	TT-6	21/02/14	70.91	0.21	7.85	0.00	6.37	0.31	0.20	6.21	4.06	0.00	0.32	96.43
TT976/6	TT-6	21/02/14	71.25	0.24	7.89	0.00	6.72	0.34	0.19	6.48	4.18	0.00	0.33	97.62
TT976/7	TT-6	21/02/14	71.19	0.21	8.32	0.00	6.34	0.41	0.21	6.46	4.12	0.01	0.29	97.58
TT976/9	TT-6	21/02/14	69.23	0.17	8.96	0.00	6.16	0.23	0.17	5.82	3.95	0.02	0.31	95.02
TT977/1	TT-7	21/02/14	70.79	0.25	9.43	0.00	4.20	0.20	0.17	5.21	4.21	0.00	0.20	94.67
TT977/11	TT-7	21/02/14	72.33	0.23	9.52	0.01	4.49	0.23	0.22	5.19	4.19	0.00	0.17	96.57
TT977/12	TT-7	21/02/14	72.80	0.28	9.49	0.00	4.77	0.19	0.19	5.46	4.30	0.01	0.21	97.72
TT977/13	TT-7	21/02/14	72.42	0.18	9.78	0.00	4.41	0.21	0.18	5.40	4.30	0.01	0.20	97.09
TT977/14	TT-7	21/02/14	71.84	0.20	9.29	0.01	4.42	0.16	0.17	5.22	4.26	0.01	0.19	95.77
TT977/15	TT-7	21/02/14	72.75	0.25	9.41	0.00	4.46	0.21	0.21	5.06	4.31	0.01	0.19	96.85
TT977/16	TT-7	21/02/14	73.08	0.19	9.63	0.04	4.67	0.19	0.17	5.34	4.29	0.04	0.21	97.84
TT977/17	TT-7	21/02/14	73.07	0.32	9.57	0.00	4.63	0.12	0.19	5.07	4.45	0.03	0.18	97.62
TT977/18	TT-7	21/02/14	72.30	0.17	9.36	0.00	4.59	0.19	0.19	5.11	4.32	0.01	0.22	96.46
TT977/19	TT-7	21/02/14	71.68	0.21	9.33	0.02	4.66	0.25	0.19	5.00	4.32	0.02	0.20	95.89
TT977/2	TT-7	21/02/14	72.56	0.23	9.45	0.00	4.44	0.22	0.18	5.07	4.23	0.00	0.21	96.60
TT977/20	TT-7	21/02/14	71.16	0.23	9.37	0.00	4.24	0.16	0.16	5.31	4.39	0.00	0.21	95.24

Continued on next page

Unnormalised major element concentrations (wt.%) in Tilo tephra glass shards

Label	Tephra	Analysis date	SiO_2 0.08	TiO_2 0.05	Al_2O_3 0.05	MgO 0.04	FeO^T 0.08	MnO 0.07	CaO 0.04	Na_2O 0.08	K_2O 0.03	P_2O_5 0.10	Cl 0.02	Total
TT977/3	TT-7	21/02/14	72.66	0.21	9.47	0.00	4.50	0.18	0.18	5.22	4.18	0.00	0.23	96.83
TT977/4	TT-7	21/02/14	73.30	0.23	9.63	0.03	4.58	0.15	0.17	5.22	4.36	0.02	0.24	97.94
TT977/5	TT-7	21/02/14	73.56	0.23	9.63	0.00	4.61	0.30	0.18	5.29	4.39	0.00	0.19	98.37
TT977/6	TT-7	21/02/14	70.02	0.20	9.16	0.00	4.19	0.06	0.19	4.94	4.17	0.00	0.18	93.09
TT977/7	TT-7	21/02/14	72.98	0.27	9.94	0.00	4.52	0.23	0.16	5.29	4.26	0.00	0.22	97.86
TT977/8	TT-7	21/02/14	72.00	0.22	9.60	0.00	4.69	0.21	0.16	5.40	4.29	0.00	0.19	96.76
TT977/9	TT-7	21/02/14	72.82	0.25	9.48	0.01	4.47	0.19	0.20	5.14	4.21	0.04	0.21	97.02
TT97-8_1	TT-8	27/08/14	72.81	0.26	9.71	0.00	4.57	0.23	0.16	5.19	4.54	0.00		97.48
TT97-8_10	TT-8	27/08/14	71.99	0.28	9.27	0.01	4.39	0.19	0.21	4.98	4.16	0.00		95.46
TT97-8_11	TT-8	27/08/14	72.09	0.22	9.27	0.01	4.47	0.16	0.16	5.07	4.30	0.00		95.75
TT97-8_12	TT-8	27/08/14	74.42	0.24	9.67	0.01	4.63	0.24	0.18	5.36	4.33	0.00		99.06
TT97-8_13	TT-8	27/08/14	72.45	0.29	9.31	0.01	4.41	0.20	0.16	4.90	4.20	0.00		95.93
TT97-8_14	TT-8	27/08/14	71.31	0.19	9.33	0.00	4.16	0.12	0.17	5.10	4.37	0.00		94.75
TT97-8_15	TT-8	27/08/14	73.38	0.26	9.70	0.00	4.46	0.18	0.18	5.18	4.38	0.03		97.75
TT97-8_16	TT-8	27/08/14	74.05	0.28	9.70	0.02	4.51	0.10	0.16	4.97	4.42	0.00		98.20
TT97-8_17	TT-8	27/08/14	73.36	0.23	9.43	0.00	4.47	0.16	0.16	5.29	4.31	0.04		97.46
TT97-8_18	TT-8	27/08/14	70.91	0.29	9.49	0.00	4.59	0.24	0.14	5.35	4.31	0.00		95.33
TT97-8_19	TT-8	27/08/14	71.65	0.21	9.33	0.00	4.53	0.18	0.15	4.93	4.34	0.02		95.34
TT97-8_2	TT-8	27/08/14	72.33	0.34	9.16	0.00	5.63	0.22	0.41	5.06	4.26	0.00		97.41
TT97-8_3	TT-8	27/08/14	73.60	0.30	9.79	0.00	4.61	0.25	0.19	5.25	4.20	0.01		98.21
TT97-8_4	TT-8	27/08/14	73.59	0.30	9.68	0.00	4.60	0.23	0.15	5.40	4.41	0.01		98.39
TT97-8_5	TT-8	27/08/14	73.00	0.28	9.32	0.00	4.89	0.22	0.18	5.10	4.27	0.00		97.27
TT97-8_6	TT-8	27/08/14	73.12	0.24	9.60	0.02	4.57	0.21	0.17	5.12	4.47	0.00		97.53
TT97-8_7	TT-8	27/08/14	73.99	0.24	9.69	0.00	4.48	0.25	0.14	5.10	4.53	0.02		98.44
TT97-8_8	TT-8	27/08/14	72.60	0.26	9.43	0.02	4.47	0.24	0.16	5.25	4.39	0.00		96.82
TT97-8_9	TT-8	27/08/14	71.77	0.28	9.10	0.00	4.47	0.26	0.16	4.98	4.30	0.02		95.35
TT978A/1	TT-8	21/02/14	70.52	0.17	9.29	0.00	4.51	0.19	0.22	4.83	4.22	0.00	0.21	94.14
TT978A/11	TT-8	21/02/14	69.06	0.19	10.55	0.00	4.05	0.16	0.20	4.94	4.17	0.00	0.22	93.56
TT978A/12	TT-8	21/02/14	72.37	0.20	9.45	0.00	4.58	0.19	0.15	5.34	4.17	0.00	0.21	96.67
TT978A/13	TT-8	21/02/14	71.47	0.25	9.33	0.01	4.46	0.32	0.14	5.22	4.29	0.00	0.21	95.70
TT978A/14	TT-8	21/02/14	71.30	0.22	9.33	0.01	4.47	0.17	0.18	4.95	4.24	0.00	0.21	95.07
TT978A/15	TT-8	21/02/14	69.92	0.23	9.11	0.00	4.58	0.21	0.21	5.17	4.18	0.00	0.16	93.76
TT978A/16	TT-8	21/02/14	72.66	0.24	9.64	0.00	4.36	0.20	0.18	5.08	4.33	0.01	0.18	96.90
TT978A/17	TT-8	21/02/14	72.29	0.24	9.52	0.03	4.56	0.18	0.22	2.56	4.17	0.02	0.19	93.99
TT978A/18	TT-8	21/02/14	69.79	0.24	9.04	0.00	4.37	0.21	0.21	4.87	4.11	0.00	0.17	93.01
TT978A/19	TT-8	21/02/14	70.87	0.23	9.15	0.00	4.57	0.19	0.19	5.19	4.18	0.00	0.21	94.79
TT978A/2	TT-8	21/02/14	70.32	0.21	9.31	0.00	4.04	0.11	0.16	4.90	4.10	0.04	0.22	93.41
TT978A/20	TT-8	21/02/14	72.96	0.22	9.45	0.00	4.59	0.23	0.16	5.35	4.37	0.02	0.20	97.56
TT978A/3	TT-8	21/02/14	71.56	0.21	9.33	0.02	4.39	0.17	0.18	5.25	4.28	0.03	0.19	95.61
TT978A/4	TT-8	21/02/14	70.01	0.24	9.26	0.00	4.22	0.23	0.21	4.86	4.10	0.02	0.20	93.35
TT978A/5	TT-8	21/02/14	70.49	0.26	9.47	0.00	4.33	0.18	0.20	5.44	4.34	0.00	0.22	94.93
TT978A/7	TT-8	21/02/14	71.52	0.21	9.51	0.00	4.31	0.22	0.25	3.72	4.23	0.00	0.21	94.19
TT978A/8	TT-8	21/02/14	70.46	0.21	9.11	0.01	4.58	0.21	0.15	2.53	4.18	0.00	0.19	91.63
TT978A/9	TT-8	21/02/14	69.81	0.30	10.00	0.03	4.63	0.25	0.19	4.73	4.26	0.00	0.19	94.38
TT978B/1	TT-8	21/02/14	70.73	0.23	9.31	0.00	4.45	0.17	0.19	5.14	4.19	0.00	0.23	94.63
TT978B/10	TT-8	21/02/14	71.85	0.25	9.52	0.00	4.64	0.13	0.18	4.91	4.19	0.00	0.21	95.87
TT978B/11	TT-8	21/02/14	72.51	0.24	9.56	0.02	4.50	0.26	0.18	5.24	4.44	0.00	0.19	97.15
TT978B/12	TT-8	21/02/14	72.51	0.22	9.31	0.01	4.31	0.15	0.20	4.98	4.27	0.01	0.20	96.18
TT978B/13	TT-8	21/02/14	73.29	0.20	9.61	0.00	4.68	0.17	0.18	5.53	4.41	0.00	0.17	98.25
TT978B/14	TT-8	21/02/14	73.11	0.24	9.54	0.00	4.59	0.13	0.21	5.41	4.27	0.04	0.23	97.76
TT978B/15	TT-8	21/02/14	73.27	0.30	9.62	0.00	4.45	0.12	0.18	5.27	4.46	0.00	0.20	97.87
TT978B/16	TT-8	21/02/14	71.13	0.22	9.46	0.00	4.32	0.26	0.14	5.05	4.26	0.01	0.22	95.06
TT978B/17	TT-8	21/02/14	72.89	0.23	9.57	0.00	4.38	0.28	0.18	5.42	4.38	0.00	0.18	97.51
TT978B/18	TT-8	21/02/14	74.08	0.24	9.83	0.04	4.42	0.20	0.19	5.37	4.48	0.00	0.21	99.07
TT978B/19	TT-8	21/02/14	72.48	0.22	9.38	0.00	4.51	0.14	0.20	5.25	4.21	0.02	0.19	96.60
TT978B/2	TT-8	21/02/14	68.59	0.22	8.99	0.03	4.08	0.22	0.16	4.76	4.04	0.00	0.24	91.32
TT978B/20	TT-8	21/02/14	73.19	0.23	9.94	0.00	4.44	0.28	0.19	5.25	4.33	0.01	0.22	98.08
TT978B/3	TT-8	21/02/14	73.04	0.24	9.61	0.00	4.65	0.31	0.21	5.33	4.43	0.00	0.22	98.03
TT978B/4	TT-8	21/02/14	73.27	0.28	9.78	0.00	4.28	0.12	0.16	5.18	4.46	0.01	0.21	97.73
TT978B/5	TT-8	21/02/14	72.35	0.23	9.54	0.00	4.49	0.17	0.16	5.15	4.41	0.00	0.20	96.70
TT978B/6	TT-8	21/02/14	73.27	0.25	9.76	0.00	4.55	0.25	0.16	5.56	4.33	0.00	0.17	98.30
TT978B/7	TT-8	21/02/14	71.91	0.18	9.59	0.03	4.38	0.16	0.20	5.08	4.02	0.00	0.21	95.75
TT978B/8	TT-8	21/02/14	72.12	0.27	9.46	0.00	4.35	0.20	0.18	5.16	4.40	0.00	0.19	96.32
TT978B/9	TT-8	21/02/14	74.35	0.22	9.77	0.00	4.76	0.26	0.20	5.05	4.51	0.01	0.19	99.32
TT97-9A_1	TT-9	27/08/14	74.07	0.23	9.55	0.00	4.79	0.24	0.19	5.34	4.38	0.00		98.79
TT97-9A_10	TT-9	27/08/14	70.80	0.16	9.04	0.00	4.53	0.18	0.17	5.09	4.15	0.01		94.14
TT97-9A_11	TT-9	27/08/14	70.22	0.25	8.94	0.03	4.37	0.15	0.21	5.13	4.15	0.00		93.45
TT97-9A_12	TT-9	27/08/14	72.72	0.21	9.45	0.02	4.66	0.22	0.21	5.12	4.27	0.01		96.88
TT97-9A_13	TT-9	27/08/14	72.95	0.27	9.46	0.00	4.65	0.23	0.19	5.16	4.31	0.03		97.23
TT97-9A_14	TT-9	27/08/14	70.94	0.24	9.11	0.00	4.44	0.10	0.20	5.01	4.17	0.02		94.23
TT97-9A_15	TT-9	27/08/14	72.15	0.22	9.43	0.01	4.33	0.20	0.18	4.96	4.21	0.00		95.69
TT97-9A_16	TT-9	27/08/14	71.08	0.24	9.07	0.02	4.61	0.18	0.17	4.99	4.28	0.00		94.64
TT97-9A_17	TT-9	27/08/14	71.47	0.20	9.47	0.00	4.74	0.18	0.18	5.11	4.32	0.04		95.69
TT97-9A_18	TT-9	27/08/14	69.61	0.28	8.98	0.00	4.31	0.28	0.15	5.00	4.20	0.00		92.80
TT97-9A_19	TT-9	27/08/14	69.78	0.22	9.44	0.03	4.37	0.19	0.19	5.35	4.26	0.01		93.83
TT97-9A_2	TT-9	27/08/14	72.86	0.24	9.39	0.03	4.57	0.21	0.16	5.27	4.28	0.00		97.01
TT97-9A_20	TT-9	27/08/14	70.18	0.22	9.02	0.02	4.69	0.19	0.21	4.87	4.09	0.00		93.50
TT97-9A_3	TT-9	27/08/14	70.36	0.26	9.18	0.00	4.47	0.18	0.17	4.98	4.28	0.00		93.87
TT97-9A_4	TT-9	27/08/14	72.68	0.22	9.50	0.00	4.49	0.19	0.18	5.06	4.40	0.00		96.71
TT97-9A_5	TT-9	27/08/14	70.45	0.21	9.18	0.00	4.39	0.17	0.19	4.93	4.13	0.00		93.66
TT97-9A_6	TT-9	27/08/14	73.75	0.22	9.53	0.03	4.60	0.19	0.15	5.46	4.30	0.00		98.24
TT97-9A_7	TT-9	27/08/14	73.25	0.23	9.57	0.00	4.43	0.17	0.17	5.33	4.27	0.01		97.42
TT97-9A_8	TT-9	27/08/14	71.12	0.19	9.08	0.00	4.45	0.22	0.18	5.11	4.15	0.02		94.52
TT97-9A_9	TT-9	27/08/14	72.90	0.25	9.45	0.00	4.67	0.21	0.15	5.32	4.37	0.00		97.33
TT97-9B_1	TT-9	27/08/14	71.94	0.24	8.93	0.01	4.49	0.21	0.18	4.88	4.20	0.02		95.09

Continued on next page

Unnormalised major element concentrations (wt.%) in Tilo tephra glass shards

Label	Tephra	Analysis date	SiO_2 0.08	TiO_2 0.05	Al_2O_3 0.05	MgO 0.04	FeO^T 0.08	MnO 0.07	CaO 0.04	Na_2O 0.08	K_2O 0.03	P_2O_5 0.10	Cl 0.02	Total
TT97-9B_10	TT-9	27/08/14	71.10	0.28	8.97	0.00	4.54	0.22	0.16	5.00	4.09	0.02		94.39
TT97-9B_11	TT-9	27/08/14	72.07	0.24	9.14	0.00	4.50	0.16	0.16	5.13	4.16	0.00		95.56
TT97-9B_12	TT-9	27/08/14	72.88	0.24	9.14	0.00	4.56	0.09	0.16	5.29	4.25	0.01		96.62
TT97-9B_13	TT-9	27/08/14	70.55	0.19	9.11	0.00	4.58	0.29	0.16	4.87	4.15	0.00		93.90
TT97-9B_14	TT-9	27/08/14	74.11	0.26	9.59	0.00	4.75	0.27	0.19	5.36	4.53	0.00		99.07
TT97-9B_15	TT-9	27/08/14	74.21	0.22	9.57	0.00	4.53	0.24	0.16	5.36	4.41	0.01		98.71
TT97-9B_16	TT-9	27/08/14	73.92	0.26	9.54	0.01	4.79	0.20	0.18	5.11	4.35	0.00		98.35
TT97-9B_17	TT-9	27/08/14	73.06	0.25	9.34	0.00	4.69	0.24	0.18	5.42	4.34	0.00		97.53
TT97-9B_18	TT-9	27/08/14	72.97	0.24	9.36	0.02	4.34	0.20	0.14	5.23	4.31	0.02		96.84
TT97-9B_19	TT-9	27/08/14	73.36	0.27	9.33	0.00	4.25	0.24	0.19	5.38	4.47	0.00		97.50
TT97-9B_2	TT-9	27/08/14	73.33	0.24	9.42	0.00	4.42	0.28	0.20	5.68	4.25	0.00		97.81
TT97-9B_20	TT-9	27/08/14	71.28	0.23	9.19	0.03	4.35	0.28	0.17	4.94	4.27	0.00		94.73
TT97-9B_3	TT-9	27/08/14	70.65	0.26	8.99	0.00	4.24	0.21	0.18	4.79	4.13	0.00		93.45
TT97-9B_5	TT-9	27/08/14	73.09	0.24	9.46	0.01	4.44	0.10	0.14	5.12	4.32	0.01		96.93
TT97-9B_6	TT-9	27/08/14	73.20	0.22	9.39	0.00	4.74	0.21	0.17	5.50	4.52	0.02		97.97
TT97-9B_7	TT-9	27/08/14	73.94	0.26	9.40	0.00	4.78	0.22	0.20	5.58	4.42	0.01		98.81
TT97-9B_8	TT-9	27/08/14	72.92	0.25	9.41	0.00	4.19	0.25	0.18	5.29	4.30	0.01		96.79
TT97-9B_9	TT-9	27/08/14	69.96	0.21	9.14	0.04	4.35	0.15	0.18	5.33	3.98	0.02		93.35
TT97-9C_1	TT-9	27/08/14	73.71	0.30	9.59	0.00	4.43	0.16	0.19	5.37	4.28	0.03		98.05
TT97-9C_10	TT-9	27/08/14	73.82	0.22	9.80	0.01	4.30	0.24	0.18	5.21	4.33	0.00		98.10
TT97-9C_11	TT-9	27/08/14	72.66	0.26	9.41	0.01	4.46	0.22	0.20	5.17	4.22	0.01		96.61
TT97-9C_12	TT-9	27/08/14	74.19	0.25	9.69	0.00	4.62	0.25	0.19	4.78	4.38	0.04		98.39
TT97-9C_13	TT-9	27/08/14	74.69	0.24	9.67	0.00	4.54	0.21	0.20	5.30	4.51	0.00		99.36
TT97-9C_14	TT-9	27/08/14	69.87	0.19	8.82	0.00	4.34	0.15	0.16	5.07	4.18	0.00		92.77
TT97-9C_15	TT-9	27/08/14	73.60	0.18	9.56	0.00	4.64	0.17	0.19	5.31	4.39	0.00		98.04
TT97-9C_16	TT-9	27/08/14	71.72	0.24	9.10	0.04	4.24	0.17	0.16	4.91	4.39	0.00		94.97
TT97-9C_17	TT-9	27/08/14	73.05	0.25	9.48	0.01	4.38	0.20	0.19	5.04	4.24	0.00		96.84
TT97-9C_18	TT-9	27/08/14	73.27	0.24	9.34	0.00	4.61	0.18	0.17	5.27	4.34	0.03		97.45
TT97-9C_19	TT-9	27/08/14	74.16	0.18	9.51	0.00	4.43	0.20	0.22	5.47	4.18	0.00		98.35
TT97-9C_2	TT-9	27/08/14	71.04	0.26	9.23	0.00	4.53	0.09	0.16	4.79	4.22	0.04		94.36
TT97-9C_20	TT-9	27/08/14	73.10	0.22	9.27	0.00	4.35	0.21	0.13	5.12	4.37	0.00		96.78
TT97-9C_3	TT-9	27/08/14	72.34	0.22	9.29	0.00	4.55	0.16	0.17	5.03	4.41	0.05		96.22
TT97-9C_4	TT-9	27/08/14	73.09	0.22	9.45	0.00	4.51	0.23	0.18	5.00	4.34	0.00		97.02
TT97-9C_5	TT-9	27/08/14	71.15	0.21	9.27	0.00	4.22	0.15	0.17	5.11	4.11	0.01		94.40
TT97-9C_6	TT-9	27/08/14	74.06	0.22	9.55	0.01	4.39	0.23	0.16	5.37	4.22	0.00		98.20
TT97-9C_7	TT-9	27/08/14	73.71	0.28	9.56	0.02	4.60	0.26	0.16	4.95	4.36	0.00		97.88
TT97-9C_8	TT-9	27/08/14	72.47	0.20	9.31	0.00	4.63	0.25	0.19	5.22	4.24	0.00		96.51
TT97-9C_9	TT-9	27/08/14	73.21	0.26	9.48	0.00	4.71	0.15	0.19	5.01	4.39	0.03		97.43
TT97-10A_1	TT-10	27/08/14	72.79	0.24	9.38	0.00	4.33	0.19	0.15	5.18	4.38	0.02		96.66
TT97-10A_10	TT-10	27/08/14	71.32	0.23	8.96	0.00	4.47	0.20	0.16	5.34	4.19	0.01		94.89
TT97-10A_11	TT-10	27/08/14	70.34	0.24	8.99	0.00	4.26	0.14	0.15	4.96	4.12	0.03		93.23
TT97-10A_12	TT-10	27/08/14	72.02	0.28	9.34	0.01	4.26	0.18	0.19	5.07	4.27	0.00		95.62
TT97-10A_13	TT-10	27/08/14	73.12	0.25	9.23	0.00	4.51	0.20	0.16	5.42	4.17	0.05		97.12
TT97-10A_14	TT-10	27/08/14	72.52	0.18	9.03	0.01	4.68	0.22	0.19	5.43	4.47	0.04		96.76
TT97-10A_15	TT-10	27/08/14	74.42	0.18	9.60	0.00	4.49	0.19	0.20	5.37	4.38	0.00		98.82
TT97-10A_16	TT-10	27/08/14	71.74	0.21	8.94	0.02	4.61	0.12	0.18	5.10	4.20	0.03		95.15
TT97-10A_17	TT-10	27/08/14	73.91	0.27	9.28	0.01	4.88	0.18	0.19	5.30	4.33	0.00		98.36
TT97-10A_18	TT-10	27/08/14	72.94	0.28	9.35	0.00	4.54	0.20	0.17	5.27	4.40	0.00		97.14
TT97-10A_19	TT-10	27/08/14	73.41	0.23	9.23	0.00	4.64	0.21	0.19	5.21	4.30	0.00		97.42
TT97-10A_2	TT-10	27/08/14	71.98	0.21	9.09	0.02	4.63	0.17	0.18	5.12	4.34	0.02		95.76
TT97-10A_20	TT-10	27/08/14	72.94	0.24	9.38	0.01	4.44	0.25	0.15	5.28	4.48	0.00		97.17
TT97-10A_3	TT-10	27/08/14	73.72	0.27	9.63	0.01	4.65	0.15	0.14	5.33	4.36	0.00		98.27
TT97-10A_4	TT-10	27/08/14	73.84	0.22	9.59	0.00	4.33	0.31	0.18	5.22	4.42	0.00		98.10
TT97-10A_5	TT-10	27/08/14	71.07	0.26	8.87	0.00	4.53	0.19	0.15	5.30	4.35	0.00		94.73
TT97-10A_6	TT-10	27/08/14	71.95	0.24	9.12	0.00	4.19	0.23	0.16	5.17	4.32	0.02		95.41
TT97-10A_7	TT-10	27/08/14	71.27	0.21	9.22	0.00	4.46	0.17	0.24	5.15	4.31	0.02		95.06
TT97-10A_8	TT-10	27/08/14	73.12	0.15	9.37	0.00	4.57	0.29	0.16	5.22	4.26	0.02		97.15
TT97-10A_9	TT-10	27/08/14	72.74	0.20	9.78	0.00	4.61	0.21	0.21	5.38	4.26	0.00		97.38
TT97-10B_1	TT-10	27/08/14	73.72	0.31	9.68	0.00	4.96	0.22	0.16	5.45	4.32	0.01		98.85
TT97-10B_10	TT-10	27/08/14	73.51	0.24	9.37	0.00	4.75	0.29	0.19	5.36	4.48	0.00		98.18
TT97-10B_11	TT-10	27/08/14	72.12	0.22	9.34	0.00	4.50	0.27	0.18	5.36	4.29	0.02		96.30
TT97-10B_12	TT-10	27/08/14	71.47	0.19	8.91	0.02	4.39	0.19	0.18	5.17	4.37	0.02		94.91
TT97-10B_13	TT-10	27/08/14	71.72	0.28	9.28	0.00	4.60	0.25	0.18	5.30	4.26	0.01		95.87
TT97-10B_15	TT-10	27/08/14	71.12	0.21	9.10	0.00	4.32	0.24	0.17	5.37	4.17	0.00		94.71
TT97-10B_16	TT-10	27/08/14	73.34	0.32	9.64	0.01	4.30	0.28	0.20	5.09	4.50	0.01		97.69
TT97-10B_17	TT-10	27/08/14	72.05	0.19	9.15	0.00	4.65	0.18	0.19	5.17	4.31	0.02		95.92
TT97-10B_18	TT-10	27/08/14	74.07	0.22	9.61	0.00	4.56	0.20	0.20	5.41	4.51	0.00		98.78
TT97-10B_19	TT-10	27/08/14	73.67	0.22	9.52	0.01	4.59	0.24	0.16	5.31	4.39	0.00		98.10
TT97-10B_2	TT-10	27/08/14	70.78	0.22	8.96	0.00	4.40	0.15	0.15	5.37	4.25	0.04		94.34
TT97-10B_20	TT-10	27/08/14	71.20	0.19	9.16	0.02	4.48	0.19	0.17	5.24	4.27	0.03		94.94
TT97-10B_3	TT-10	27/08/14	71.33	0.19	9.79	0.00	4.05	0.18	0.16	5.38	4.28	0.02		95.38
TT97-10B_4	TT-10	27/08/14	74.22	0.26	9.41	0.00	4.41	0.20	0.20	5.42	4.41	0.03		98.56
TT97-10B_5	TT-10	27/08/14	74.91	0.27	9.60	0.02	4.64	0.21	0.21	4.04	4.61	0.01		98.50
TT97-10B_6	TT-10	27/08/14	72.97	0.27	9.47	0.00	4.57	0.24	0.18	5.46	4.44	0.03		97.63
TT97-10B_7	TT-10	27/08/14	73.95	0.16	9.55	0.02	4.53	0.19	0.19	5.40	4.53	0.02		98.53
TT97-10B_8	TT-10	27/08/14	72.13	0.18	9.16	0.01	4.67	0.18	0.21	5.41	4.37	0.00		96.31
TT97-10B_9	TT-10	27/08/14	73.55	0.23	9.50	0.00	4.72	0.22	0.20	5.54	4.30	0.00		98.25
TT97-10C_1	TT-10	27/08/14	72.01	0.22	9.15	0.00	4.39	0.16	0.14	5.48	4.14	0.04		95.74
TT97-10C_10	TT-10	27/08/14	73.47	0.22	9.55	0.00	4.39	0.28	0.16	5.35	4.59	0.00		98.01
TT97-10C_11	TT-10	27/08/14	74.27	0.23	9.66	0.00	4.32	0.15	0.19	5.06	4.37	0.01		98.27
TT97-10C_12	TT-10	27/08/14	73.34	0.21	9.58	0.00	4.68	0.24	0.16	5.22	4.50	0.00		97.91
TT97-10C_13	TT-10	27/08/14	71.13	0.18	9.16	0.00	4.72	0.23	0.20	5.07	4.22	0.00		94.91
TT97-10C_14	TT-10	27/08/14	74.09	0.24	9.67	0.01	4.36	0.28	0.20	5.36	4.37	0.00		98.57
TT97-10C_15	TT-10	27/08/14	72.19	0.18	9.25	0.00	4.49	0.27	0.18	5.41	4.27	0.01		96.25
TT97-10C_16	TT-10	27/08/14	74.56	0.25	9.67	0.00	4.52	0.14	0.16	5.32	4.45	0.03		99.10

Continued on next page

Unnormalised major element concentrations (wt.%) in Tilo tephra glass shards

Label	Tephra	Analysis date	SiO_2 0.08	TiO_2 0.05	Al_2O_3 0.05	MgO 0.04	FeO^T 0.08	MnO 0.07	CaO 0.04	Na_2O 0.08	K_2O 0.03	P_2O_5 0.10	Cl 0.02	Total
TT97-10C_17	TT-10	27/08/14	73.06	0.24	9.58	0.02	4.59	0.15	0.16	5.43	4.40	0.02		97.65
TT97-10C_18	TT-10	27/08/14	73.82	0.26	9.60	0.00	4.64	0.25	0.16	4.88	4.39	0.05		98.05
TT97-10C_19	TT-10	27/08/14	71.23	0.20	7.79	0.02	3.41	0.18	0.26	4.35	3.40	0.02		90.86
TT97-10C_2	TT-10	27/08/14	73.74	0.28	9.67	0.00	4.44	0.18	0.16	5.45	4.44	0.03		98.39
TT97-10C_20	TT-10	27/08/14	68.53	0.22	9.20	0.00	4.17	0.17	0.20	4.71	3.97	0.00		91.17
TT97-10C_21	TT-10	27/08/14	74.06	0.23	9.54	0.00	4.65	0.25	0.19	5.25	4.51	0.00		98.69
TT97-10C_22	TT-10	27/08/14	67.70	0.20	8.76	0.00	4.40	0.19	0.20	4.83	4.11	0.03		90.41
TT97-10C_3	TT-10	27/08/14	73.74	0.24	9.69	0.00	4.57	0.16	0.14	5.56	4.37	0.00		98.48
TT97-10C_4	TT-10	27/08/14	73.71	0.24	9.62	0.00	4.47	0.30	0.15	5.41	4.44	0.02		98.36
TT97-10C_5	TT-10	27/08/14	73.40	0.30	9.53	0.00	4.75	0.29	0.20	5.32	4.53	0.01		98.33
TT97-10C_6	TT-10	27/08/14	73.28	0.27	9.18	0.00	4.42	0.17	0.20	5.38	4.38	0.00		97.29
TT97-10C_7	TT-10	27/08/14	71.20	0.23	9.08	0.00	4.21	0.19	0.21	5.25	4.09	0.03		94.49
TT97-10C_8	TT-10	27/08/14	72.84	0.26	9.15	0.02	4.72	0.22	0.17	5.43	4.48	0.05		97.34
TT97-10C_9	TT-10	27/08/14	73.48	0.25	9.55	0.00	4.29	0.19	0.16	5.51	4.39	0.01		97.83
TT97-11_1	TT-11	27/08/14	72.99	0.23	9.29	0.00	4.61	0.28	0.20	5.09	4.37	0.02		97.08
TT97-11_10	TT-11	27/08/14	71.49	0.22	9.16	0.00	4.49	0.23	0.18	5.02	4.30	0.03		95.12
TT97-11_11	TT-11	27/08/14	71.40	0.23	9.07	0.01	4.63	0.22	0.22	5.10	4.23	0.00		95.11
TT97-11_12	TT-11	27/08/14	70.47	0.20	9.14	0.00	4.48	0.20	0.18	5.15	4.21	0.01		94.06
TT97-11_13	TT-11	27/08/14	71.91	0.21	9.06	0.01	4.49	0.13	0.19	4.94	4.30	0.01		95.27
TT97-11_14	TT-11	27/08/14	71.88	0.18	9.14	0.01	4.46	0.23	0.15	4.96	4.20	0.05		95.28
TT97-11_15	TT-11	27/08/14	70.68	0.28	9.04	0.00	4.30	0.28	0.19	4.93	4.13	0.00		93.82
TT97-11_16	TT-11	27/08/14	73.81	0.21	9.38	0.00	4.59	0.19	0.18	5.49	4.40	0.00		98.25
TT97-11_17	TT-11	27/08/14	72.91	0.22	9.35	0.00	4.67	0.20	0.20	5.25	4.33	0.01		97.13
TT97-11_18	TT-11	27/08/14	71.87	0.18	8.81	0.00	4.51	0.19	0.19	5.27	4.21	0.00		95.23
TT97-11_19	TT-11	27/08/14	71.90	0.19	9.17	0.00	4.61	0.27	0.14	3.26	4.25	0.02		93.79
TT97-11_2	TT-11	27/08/14	71.47	0.20	8.92	0.00	4.44	0.24	0.21	5.14	4.41	0.00		95.05
TT97-11_20	TT-11	27/08/14	73.52	0.19	9.46	0.00	4.70	0.17	0.18	5.43	4.48	0.00		98.14
TT97-11_3	TT-11	27/08/14	72.98	0.21	9.16	0.00	4.54	0.27	0.19	5.30	4.22	0.00		96.87
TT97-11_4	TT-11	27/08/14	71.43	0.28	9.14	0.00	4.36	0.16	0.17	5.40	4.36	0.01		95.30
TT97-11_5	TT-11	27/08/14	70.25	0.22	9.21	0.00	4.51	0.19	0.20	5.17	4.26	0.03		94.03
TT97-11_6	TT-11	27/08/14	72.41	0.22	9.02	0.00	4.20	0.16	0.15	5.31	4.37	0.00		95.85
TT97-11_7	TT-11	27/08/14	71.56	0.19	9.10	0.00	4.59	0.23	0.16	5.34	4.36	0.00		95.55
TT97-11_8	TT-11	27/08/14	73.72	0.22	9.19	0.00	4.47	0.20	0.18	5.36	4.31	0.01		97.66
TT97-11_9	TT-11	27/08/14	72.82	0.22	9.19	0.01	4.34	0.21	0.18	3.01	4.41	0.03		94.42
TT9711B/1	TT-11	21/02/14	72.82	0.23	9.46	0.01	4.49	0.27	0.18	5.31	4.32	0.01	0.23	97.34
TT9711B/10	TT-11	21/02/14	70.86	0.27	9.04	0.00	4.16	0.19	0.17	5.08	4.21	0.00	0.23	94.20
TT9711B/11	TT-11	21/02/14	71.43	0.18	9.26	0.00	4.61	0.24	0.19	5.09	4.33	0.02	0.24	95.58
TT9711B/12	TT-11	21/02/14	71.10	0.21	9.23	0.02	4.39	0.10	0.18	5.13	4.32	0.00	0.23	94.91
TT9711B/13	TT-11	21/02/14	71.09	0.20	9.23	0.00	4.57	0.25	0.20	5.45	4.27	0.00	0.24	95.49
TT9711B/14	TT-11	21/02/14	72.63	0.22	9.40	0.00	4.61	0.24	0.21	5.02	4.26	0.02	0.23	96.84
TT9711B/15	TT-11	21/02/14	70.07	0.11	14.64	0.00	2.72	0.06	0.08	5.98	5.99	0.02	0.09	99.74
TT9711B/16	TT-11	21/02/14	70.02	0.27	9.84	0.03	4.25	0.10	0.20	4.78	4.18	0.04	0.21	93.92
TT9711B/17	TT-11	21/02/14	73.11	0.24	9.63	0.00	4.67	0.21	0.19	5.20	4.42	0.00	0.20	97.89
TT9711B/18	TT-11	21/02/14	73.01	0.22	9.38	0.00	4.62	0.16	0.20	3.46	4.25	0.00	0.26	95.56
TT9711B/19	TT-11	21/02/14	70.54	0.22	9.15	0.02	4.21	0.23	0.18	4.92	4.19	0.02	0.23	93.90
TT9711B/2	TT-11	21/02/14	73.09	0.32	9.98	0.01	4.06	0.16	0.21	4.97	4.57	0.00	0.16	97.53
TT9711B/20	TT-11	21/02/14	73.10	0.17	9.36	0.00	4.93	0.23	0.18	5.13	4.42	0.01	0.24	97.77
TT9711B/3	TT-11	21/02/14	71.21	0.19	9.20	0.00	4.52	0.09	0.21	4.58	4.19	0.02	0.24	94.46
TT9711B/4	TT-11	21/02/14	72.60	0.24	9.39	0.00	4.52	0.22	0.18	2.64	4.18	0.00	0.22	94.19
TT9711B/5	TT-11	21/02/14	73.10	0.22	9.44	0.00	4.35	0.21	0.17	4.93	4.25	0.04	0.23	96.94
TT9711B/7	TT-11	21/02/14	72.47	0.20	9.43	0.00	4.60	0.18	0.16	5.13	4.24	0.00	0.20	96.62
TT9711B/8	TT-11	21/02/14	70.56	0.20	9.40	0.00	4.38	0.20	0.20	5.20	4.14	0.01	0.22	94.51
TT9711B/9	TT-11	21/02/14	73.93	0.26	9.97	0.00	4.23	0.23	0.16	4.85	4.49	0.00	0.15	98.27
TT9712A/1	TT-12	21/02/14	73.69	0.21	9.48	0.00	4.60	0.27	0.16	5.48	4.24	0.03	0.25	98.40
TT9712A/10	TT-12	21/02/14	69.51	0.24	8.97	0.01	4.38	0.28	0.20	4.99	4.22	0.00	0.25	93.05
TT9712A/11	TT-12	21/02/14	72.59	0.19	9.46	0.02	4.65	0.29	0.19	3.85	4.31	0.00	0.20	95.75
TT9712A/12	TT-12	21/02/14	69.49	0.28	11.15	0.00	4.25	0.23	0.20	4.99	4.11	0.00	0.25	94.96
TT9712A/13	TT-12	21/02/14	71.84	0.17	9.18	0.00	4.58	0.21	0.18	2.53	4.25	0.00	0.21	93.14
TT9712A/14	TT-12	21/02/14	71.79	0.18	9.38	0.00	4.44	0.21	0.17	5.40	4.21	0.02	0.23	96.04
TT9712A/15	TT-12	21/02/14	70.24	0.20	8.77	0.00	4.30	0.19	0.16	4.80	4.13	0.00	0.23	93.03
TT9712A/16	TT-12	21/02/14	69.73	0.21	8.92	0.00	4.49	0.28	0.18	5.16	4.20	0.01	0.19	93.37
TT9712A/17	TT-12	21/02/14	70.31	0.18	9.23	0.00	4.43	0.19	0.17	5.12	4.05	0.01	0.23	93.93
TT9712A/18	TT-12	21/02/14	72.64	0.22	9.29	0.00	4.44	0.23	0.17	2.85	4.23	0.03	0.22	94.32
TT9712A/19	TT-12	21/02/14	67.93	0.23	8.79	0.00	4.33	0.25	0.22	4.98	4.11	0.00	0.21	91.04
TT9712A/2	TT-12	21/02/14	71.03	0.18	9.26	0.03	4.22	0.20	0.20	5.24	4.24	0.00	0.23	94.83
TT9712A/20	TT-12	21/02/14	72.66	0.14	9.62	0.00	4.72	0.23	0.21	5.43	4.31	0.00	0.20	97.51
TT9712A/3	TT-12	21/02/14	72.83	0.20	9.43	0.00	4.77	0.08	0.19	5.40	4.26	0.00	0.22	97.38
TT9712A/4	TT-12	21/02/14	71.27	0.17	9.14	0.00	4.84	0.25	0.16	5.59	4.29	0.02	0.22	95.94
TT9712A/5	TT-12	21/02/14	71.20	0.21	9.14	0.01	4.54	0.24	0.17	5.00	4.21	0.02	0.22	94.96
TT9712A/6	TT-12	21/02/14	72.80	0.21	9.39	0.00	4.60	0.20	0.19	5.62	4.26	0.01	0.21	97.48
TT9712A/7	TT-12	21/02/14	71.10	0.19	9.23	0.00	4.54	0.24	0.19	5.51	4.24	0.00	0.23	95.46
TT9712A/8	TT-12	21/02/14	71.24	0.20	9.28	0.00	4.58	0.27	0.18	5.18	4.29	0.04	0.23	95.49
TT9712A/9	TT-12	21/02/14	71.87	0.23	9.32	0.00	4.72	0.20	0.19	5.11	4.37	0.00	0.23	96.25
TT9712B/1	TT-12	21/02/14	67.87	0.20	8.66	0.01	4.31	0.20	0.23	4.74	3.97	0.00	0.21	90.40
TT9712B/10	TT-12	21/02/14	71.89	0.22	9.39	0.00	4.62	0.17	0.20	5.23	4.19	0.00	0.22	96.15
TT9712B/11	TT-12	21/02/14	71.60	0.26	9.25	0.01	4.34	0.24	0.16	5.10	4.18	0.01	0.20	95.35
TT9712B/13	TT-12	21/02/14	72.06	0.22	9.32	0.00	4.53	0.12	0.14	5.34	4.25	0.01	0.24	96.23
TT9712B/14	TT-12	21/02/14	72.46	0.20	9.36	0.00	4.61	0.22	0.20	5.58	4.18	0.00	0.21	97.03
TT9712B/15	TT-12	21/02/14	70.97	0.18	9.50	0.00	4.67	0.16	0.16	5.08	4.23	0.03	0.22	95.19
TT9712B/16	TT-12	21/02/14	72.82	0.19	9.57	0.00	4.69	0.20	0.18	4.23	4.34	0.00	0.22	96.45
TT9712B/17	TT-12	21/02/14	71.15	0.14	9.40	0.00	4.40	0.25	0.17	5.05	4.25	0.00	0.17	94.98
TT9712B/18	TT-12	21/02/14	71.83	0.22	9.51	0.01	4.28	0.21	0.17	5.40	4.52	0.03	0.20	96.37
TT9712B/19	TT-12	21/02/14	72.25	0.17	9.26	0.00	4.62	0.20	0.18	5.26	4.39	0.01	0.24	96.56
TT9712B/2	TT-12	21/02/14	71.57	0.24	9.22	0.01	4.41	0.16	0.15	5.28	4.29	0.02	0.23	95.58
TT9712B/20	TT-12	21/02/14	70.94	0.20	10.54	0.00	4.71	0.27	0.15	5.29	4.17	0.00	0.20	96.49

Continued on next page

Unnormalised major element concentrations (wt.%) in Tilo tephra glass shards

Label	Tephra	Analysis date	SiO_2 0.08	TiO_2 0.05	Al_2O_3 0.05	MgO 0.04	FeO^T 0.08	MnO 0.07	CaO 0.04	Na_2O 0.08	K_2O 0.03	P_2O_5 0.10	Cl 0.02	Total
TT9712B/3	TT-12	21/02/14	72.61	0.18	9.48	0.02	4.76	0.16	0.17	5.66	4.32	0.00	0.23	97.58
TT9712B/4	TT-12	21/02/14	71.18	0.22	9.47	0.00	4.44	0.23	0.17	5.64	4.39	0.00	0.26	96.00
TT9712B/5	TT-12	21/02/14	73.78	0.22	9.29	0.00	4.76	0.16	0.20	5.52	4.27	0.00	0.23	98.43
TT9712B/6	TT-12	21/02/14	72.52	0.21	9.44	0.00	4.56	0.21	0.21	5.75	4.28	0.00	0.20	97.39
TT9712B/7	TT-12	21/02/14	73.49	0.21	9.38	0.01	4.77	0.25	0.21	5.71	4.35	0.02	0.21	98.61
TT9712B/8	TT-12	21/02/14	71.80	0.18	9.30	0.00	4.63	0.18	0.21	5.41	4.35	0.00	0.22	96.29
TT9712B/9	TT-12	21/02/14	72.60	0.21	9.24	0.00	4.73	0.27	0.16	5.29	4.11	0.00	0.24	96.84
TT9712C/10	TT-12	21/02/14	71.61	0.23	9.36	0.00	4.41	0.22	0.16	5.02	4.37	0.02	0.22	95.62
TT9712C/11	TT-12	21/02/14	69.23	0.24	9.45	0.02	4.42	0.17	0.17	4.85	4.17	0.00	0.22	92.96
TT9712C/12	TT-12	21/02/14	73.69	0.32	9.61	0.00	4.57	0.20	0.18	5.26	4.45	0.00	0.22	98.51
TT9712C/13	TT-12	21/02/14	73.41	0.21	9.77	0.03	4.61	0.23	0.20	5.36	4.40	0.00	0.22	98.45
TT9712C/14	TT-12	21/02/14	71.60	0.27	9.57	0.00	4.38	0.15	0.18	5.16	4.35	0.02	0.20	95.87
TT9712C/15	TT-12	21/02/14	69.75	0.30	9.25	0.01	4.26	0.17	0.15	3.41	4.06	0.01	0.21	91.59
TT9712C/16	TT-12	21/02/14	72.43	0.24	9.45	0.02	4.21	0.20	0.21	5.17	4.31	0.00	0.20	96.44
TT9712C/17	TT-12	21/02/14	72.77	0.23	9.46	0.04	4.31	0.18	0.25	1.69	4.17	0.00	0.20	93.30
TT9712C/18	TT-12	21/02/14	74.11	0.29	9.88	0.02	4.56	0.22	0.19	5.20	4.50	0.01	0.23	99.22
TT9712C/19	TT-12	21/02/14	73.95	0.26	9.68	0.00	4.61	0.19	0.20	4.86	4.39	0.02	0.19	98.35
TT9712C/2	TT-12	21/02/14	71.63	0.22	9.47	0.00	4.23	0.15	0.25	5.30	4.31	0.01	0.19	95.75
TT9712C/20	TT-12	21/02/14	70.78	0.24	9.34	0.01	4.42	0.25	0.15	5.12	4.33	0.02	0.22	94.87
TT9712C/3	TT-12	21/02/14	71.81	0.23	9.47	0.00	4.45	0.24	0.17	5.25	4.47	0.02	0.22	96.32
TT9712C/4	TT-12	21/02/14	71.63	0.25	9.28	0.07	4.30	0.17	0.19	4.84	4.15	0.00	0.21	95.10
TT9712C/5	TT-12	21/02/14	70.98	0.29	9.59	0.04	4.32	0.13	0.18	5.02	4.36	0.00	0.18	95.10
TT9712C/6	TT-12	21/02/14	68.98	0.23	14.21	0.00	4.30	0.14	0.18	4.86	4.02	0.01	0.22	97.13
TT9712C/7	TT-12	21/02/14	72.96	0.23	10.65	0.00	4.20	0.20	0.18	4.92	4.27	0.00	0.21	97.81
TT9712C/8	TT-12	21/02/14	71.11	0.25	9.38	0.00	4.71	0.20	0.17	5.37	4.19	0.00	0.23	95.59
TT9712C/9	TT-12	21/02/14	72.84	0.20	9.59	0.00	4.54	0.21	0.21	5.32	4.38	0.02	0.22	97.54
TT97-13_1	TT-13	27/08/14	71.27	0.16	8.70	0.01	4.58	0.24	0.15	5.78	4.08	0.02		95.00
TT97-13_10	TT-13	27/08/14	68.13	0.11	8.75	0.01	4.59	0.23	0.14	5.39	4.04	0.00		91.38
TT97-13_11	TT-13	27/08/14	71.73	0.22	8.90	0.00	4.40	0.20	0.16	3.61	4.17	0.00		93.37
TT97-13_12	TT-13	27/08/14	71.17	0.22	8.78	0.01	4.81	0.24	0.19	5.56	4.11	0.03		95.11
TT97-13_13	TT-13	27/08/14	73.72	0.22	9.30	0.00	4.85	0.19	0.16	5.90	4.25	0.01		98.59
TT97-13_14	TT-13	27/08/14	66.59	0.01	18.27	0.00	0.94	0.08	0.01	5.59	8.47	0.00		99.94
TT97-13_15	TT-13	27/08/14	71.52	0.18	9.05	0.04	4.69	0.17	0.18	5.77	4.09	0.00		95.69
TT97-13_16	TT-13	27/08/14	70.92	0.21	8.74	0.00	4.60	0.24	0.18	5.26	4.36	0.01		94.52
TT97-13_17	TT-13	27/08/14	71.96	0.17	8.90	0.01	4.53	0.21	0.15	5.41	4.38	0.04		95.75
TT97-13_18	TT-13	27/08/14	71.50	0.15	8.92	0.00	4.74	0.21	0.15	5.46	4.09	0.00		95.24
TT97-13_19	TT-13	27/08/14	72.03	0.17	9.17	0.00	4.57	0.24	0.19	1.81	4.11	0.00		92.29
TT97-13_2	TT-13	27/08/14	70.79	0.18	8.98	0.00	4.78	0.23	0.22	5.38	4.14	0.00		94.70
TT97-13_20	TT-13	27/08/14	72.15	0.23	9.08	0.03	4.54	0.22	0.17	5.63	4.67	0.01		96.72
TT97-13_3	TT-13	27/08/14	70.34	0.15	8.79	0.00	4.41	0.15	0.16	5.39	4.24	0.00		93.62
TT97-13_4	TT-13	27/08/14	73.00	0.20	9.20	0.00	4.65	0.21	0.15	5.59	4.47	0.02		97.49
TT97-13_6	TT-13	27/08/14	72.84	0.20	9.14	0.00	4.70	0.23	0.19	5.38	4.35	0.03		97.05
TT97-13_7	TT-13	27/08/14	71.44	0.20	8.87	0.00	4.53	0.19	0.15	5.56	4.12	0.02		95.06
TT97-13_8	TT-13	27/08/14	71.50	0.14	8.99	0.00	4.75	0.17	0.15	5.93	4.19	0.00		95.82
TT97-13_9	TT-13	27/08/14	70.90	0.19	8.94	0.01	4.44	0.18	0.21	5.58	4.13	0.00		94.57
TT97-14A_1	TT-14	27/08/14	71.09	0.23	9.08	0.02	4.27	0.20	0.17	5.38	4.21	0.01		94.67
TT97-14A_10	TT-14	27/08/14	70.32	0.21	9.04	0.00	4.34	0.22	0.15	5.41	4.08	0.00		93.78
TT97-14A_11	TT-14	27/08/14	71.09	0.20	9.12	0.00	4.37	0.20	0.17	5.12	4.27	0.00		94.53
TT97-14A_12	TT-14	27/08/14	71.64	0.21	9.22	0.02	4.49	0.22	0.16	3.33	4.22	0.04		93.55
TT97-14A_13	TT-14	27/08/14	70.15	0.13	8.94	0.00	4.26	0.25	0.21	5.44	4.11	0.00		93.48
TT97-14A_14	TT-14	27/08/14	70.69	0.17	9.01	0.00	4.27	0.16	0.15	5.07	4.18	0.04		93.72
TT97-14A_15	TT-14	27/08/14	70.79	0.20	9.08	0.00	4.46	0.13	0.16	5.35	4.12	0.00		94.30
TT97-14A_16	TT-14	27/08/14	71.07	0.16	9.02	0.00	4.46	0.25	0.17	5.32	4.21	0.00		94.66
TT97-14A_17	TT-14	27/08/14	71.79	0.24	8.50	0.02	4.40	0.22	0.14	5.34	3.96	0.02		94.63
TT97-14A_18	TT-14	27/08/14	70.81	0.19	9.32	0.01	4.42	0.19	0.20	5.41	4.12	0.05		94.72
TT97-14A_19	TT-14	27/08/14	70.48	0.25	9.12	0.00	4.50	0.25	0.18	5.25	4.24	0.00		94.26
TT97-14A_2	TT-14	27/08/14	69.94	0.15	9.40	0.02	4.37	0.18	0.17	5.00	4.10	0.00		93.31
TT97-14A_20	TT-14	27/08/14	69.70	0.18	9.00	0.00	4.21	0.24	0.17	5.48	4.12	0.00		93.11
TT97-14A_3	TT-14	27/08/14	71.40	0.20	9.09	0.01	4.39	0.24	0.19	5.40	4.10	0.03		95.05
TT97-14A_4	TT-14	27/08/14	71.12	0.21	9.03	0.04	4.31	0.17	0.19	5.18	4.17	0.03		94.45
TT97-14A_6	TT-14	27/08/14	69.52	0.15	8.78	0.00	4.47	0.20	0.19	4.93	4.05	0.00		92.30
TT97-14A_8	TT-14	27/08/14	71.37	0.20	9.14	0.00	4.47	0.16	0.17	5.23	4.32	0.01		95.07
TT97-14A_9	TT-14	27/08/14	70.83	0.18	9.01	0.00	4.47	0.23	0.13	4.93	4.24	0.00		94.02
TT97-14B_1	TT-14	28/08/14	70.64	0.20	8.85	0.00	4.44	0.10	0.16	5.27	4.21	0.00		93.87
TT97-14B_10	TT-14	28/08/14	71.85	0.22	9.11	0.00	4.43	0.26	0.20	5.29	4.31	0.00		95.67
TT97-14B_11	TT-14	28/08/14	69.09	0.18	8.76	0.00	4.28	0.23	0.22	4.91	4.02	0.03		91.71
TT97-14B_13	TT-14	28/08/14	71.68	0.21	9.10	0.02	4.57	0.19	0.18	5.40	4.22	0.00		95.57
TT97-14B_14	TT-14	28/08/14	70.91	0.16	9.06	0.00	4.51	0.18	0.15	4.80	4.09	0.04		93.90
TT97-14B_15	TT-14	28/08/14	71.44	0.21	8.98	0.01	4.56	0.15	0.17	5.20	4.19	0.00		94.90
TT97-14B_17	TT-14	28/08/14	71.19	0.17	9.08	0.00	4.16	0.12	0.16	5.53	4.12	0.00		94.54
TT97-14B_18	TT-14	28/08/14	69.55	0.16	9.03	0.00	4.23	0.22	0.17	5.06	4.33	0.00		92.75
TT97-14B_19	TT-14	28/08/14	70.76	0.18	8.95	0.00	4.28	0.25	0.17	5.24	4.15	0.01		93.99
TT97-14B_2	TT-14	28/08/14	70.65	0.22	8.84	0.00	4.40	0.21	0.19	5.21	4.16	0.02		93.90
TT97-14B_20	TT-14	28/08/14	70.84	0.17	8.96	0.00	4.24	0.20	0.16	5.27	4.15	0.01		94.02
TT97-14B_3	TT-14	28/08/14	70.58	0.19	8.48	0.01	4.43	0.20	0.17	5.20	4.18	0.01		93.46
TT97-14B_5	TT-14	28/08/14	72.79	0.17	9.08	0.01	4.54	0.21	0.23	4.82	4.20	0.00		96.05
TT97-14B_6	TT-14	28/08/14	71.72	0.23	9.11	0.00	4.43	0.16	0.18	5.22	4.21	0.00		95.26
TT97-14B_8	TT-14	28/08/14	71.35	0.23	9.07	0.00	4.49	0.15	0.20	5.14	4.25	0.00		94.88
TT97-14C_1	TT-14	28/08/14	71.23	0.27	8.80	0.00	4.36	0.16	0.17	5.17	4.21	0.00		94.38
TT97-14C_10	TT-14	28/08/14	71.43	0.19	8.87	0.01	4.55	0.24	0.16	5.29	4.12	0.03		94.90
TT97-14C_11	TT-14	28/08/14	70.28	0.21	8.74	0.02	4.34	0.18	0.18	5.10	4.04	0.00		93.09
TT97-14C_12	TT-14	28/08/14	70.63	0.21	8.41	0.00	4.16	0.12	0.19	4.61	4.07	0.00		92.40
TT97-14C_13	TT-14	28/08/14	71.60	0.22	9.04	0.02	4.30	0.17	0.20	5.25	4.17	0.00		94.98
TT97-14C_14	TT-14	28/08/14	71.33	0.17	9.03	0.00	4.37	0.20	0.15	5.12	4.21	0.01		94.59
TT97-14C_15	TT-14	28/08/14	71.86	0.16	8.90	0.00	4.33	0.15	0.19	5.38	4.32	0.01		95.30

Continued on next page

Unnormalised major element concentrations (wt.%) in Tilo tephra glass shards

Label	Tephra	Analysis date	SiO_2 0.08	TiO_2 0.05	Al_2O_3 0.05	MgO 0.04	FeO^T 0.08	MnO 0.07	CaO 0.04	Na_2O 0.08	K_2O 0.03	P_2O_5 0.10	Cl 0.02	Total
TT97-14C_16	TT-14	28/08/14	71.08	0.20	8.71	0.00	4.50	0.20	0.16	5.41	4.22	0.01		94.51
TT97-14C_17	TT-14	28/08/14	67.18	0.00	17.73	0.00	0.66	0.00	0.00	5.90	8.39	0.00		99.86
TT97-14C_18	TT-14	28/08/14	69.58	0.21	8.88	0.00	4.03	0.17	0.14	5.22	4.06	0.02		92.30
TT97-14C_19	TT-14	28/08/14	68.60	0.18	8.52	0.01	4.21	0.16	0.15	5.26	4.21	0.02		91.31
TT97-14C_20	TT-14	28/08/14	69.32	0.18	8.61	0.01	4.22	0.21	0.18	4.93	4.10	0.00		91.76
TT97-14C_3	TT-14	28/08/14	71.20	0.20	9.15	0.00	4.59	0.17	0.16	5.27	4.19	0.03		94.96
TT97-14C_4	TT-14	28/08/14	71.19	0.18	8.95	0.02	4.41	0.18	0.20	5.20	4.17	0.02		94.53
TT97-14C_5	TT-14	28/08/14	66.79	0.18	11.96	0.02	4.43	0.18	0.38	4.76	3.79	0.00		92.50
TT97-14C_6	TT-14	28/08/14	70.74	0.21	8.90	0.00	4.51	0.13	0.20	5.26	4.04	0.02		94.01
TT97-14C_7	TT-14	28/08/14	71.09	0.21	8.98	0.00	4.34	0.22	0.21	5.51	4.18	0.01		94.74
TT97-14C_8	TT-14	28/08/14	71.44	0.17	8.85	0.00	4.56	0.29	0.20	5.21	4.08	0.00		94.81
TT97-14C_9	TT-14	28/08/14	71.53	0.18	9.31	0.03	4.49	0.16	0.15	5.16	4.26	0.00		95.29

Trace element concentrations (ppm) in Tilo tephra glass shards

Label	Tephra	Analysis date	Rb 0.62	Sr 1.05	Y 0.17	Zr 0.37	Nb 0.07	Cs 0.19	Ba 1.88	La 0.09	Ce 0.07	Pr 0.06	Nd 0.25	Sm 0.14	Eu 0.13	Tb 0.06	Dy 0.13	Ho 0.04	Er 0.07	Tm 0.05	Yb 0.15	Lu 0.04	Hf 0.08	Ta 0.06	Pb 0.12	Th 0.01	U 0.00
TT97-1_1	TT-1	14/01/15	117	3.28	267	2160	258	0.88	98.4	238	424	54.6	216	44.3	5.78	7.55	47.3	10.3	29.7	3.83	25.2	3.85	51.7	17.7	37.8	28.3	6.32
TT97-1_10	TT-1	14/01/15	118	4.09	255	2070	261	1.04	98.4	234	435	53.2	226	44.5	6.50	7.72	48.5	9.02	26.7	3.94	25.2	3.73	52.9	17.6	41.7	25.8	6.39
TT97-1_12	TT-1	14/01/15	120	4.39	244	1970	258	0.94	90.9	221	409	51.4	207	42.3	5.74	6.83	39.5	8.78	25.2	3.51	24.4	3.81	47.7	16.8	38.1	24.6	6.38
TT97-1_13	TT-1	14/01/15	119	3.50	236	1930	243	1.22	87.8	215	395	48.9	194	38.5	5.54	6.65	37.3	8.30	24.8	3.66	24.1	3.29	48.1	16.9	36.3	24.3	5.98
TT97-1_14	TT-1	14/01/15	122	2.45	239	1950	257	1.24	93.9	215	411	50.3	215	42.2	5.21	7.76	42.3	8.95	26.0	3.71	23.1	3.92	49.5	16.5	39.4	26.2	6.75
TT97-1_15	TT-1	14/01/15	127	4.21	244	1940	244	1.25	81.7	219	410	49.2	212	43.2	5.33	6.95	43.2	9.18	27.5	3.47	23.9	3.75	49.4	17.4	37.4	24.5	6.34
TT97-1_16	TT-1	14/01/15	117	3.20	272	2200	265	1.15	93.8	241	436	56.3	241	48.6	6.49	7.66	45.9	9.37	28.6	3.83	27.1	3.41	54.2	17.4	38.2	27.0	6.39
TT97-1_17	TT-1	14/01/15	120	3.26	283	2260	264	1.29	95.5	250	436	56.8	244	49.9	6.01	9.01	47.3	10.1	29.9	4.01	29.8	4.13	56.9	20.3	36.6	29.7	6.62
TT97-1_18	TT-1	14/01/15	127	3.27	270	2220	261	0.98	101	243	435	56.2	238	51.3	6.31	7.31	47.2	10.3	28.5	4.35	25.4	3.76	55.0	16.9	39.5	24.8	5.86
TT97-1_19	TT-1	14/01/15	115	4.51	258	2090	252	1.07	93.4	228	413	55.3	222	47.9	5.96	7.39	42.6	10.0	25.4	3.73	24.6	3.44	51.0	16.7	35.8	25.8	6.11
TT97-1_2	TT-1	14/01/15	118	5.33	258	2140	268	1.22	107	243	447	57.1	242	48.3	5.71	7.86	49.7	9.74	28.8	4.46	25.3	3.95	56.7	18.4	42.0	27.1	6.45
TT97-1_20	TT-1	14/01/15	114	4.13	259	2160	260	0.90	93.6	239	430	54.5	237	50.9	4.91	7.15	47.3	9.64	26.8	3.85	24.9	4.23	51.0	18.7	37.3	25.2	5.80
TT97-1_4	TT-1	14/01/15	123	5.37	258	2130	265	0.99	89.1	236	429	55.0	236	45.5	5.97	7.64	48.2	9.03	27.5	4.42	26.7	4.22	51.6	18.1	42.4	26.3	6.42
TT97-1_5†	TT-1	14/01/15	110	3.86	311	2410	276	1.07	92.3	259	442	54.5	235	46.9	6.15	7.72	53.0	10.9	29.9	3.67	27.0	4.13	63.0	18.5	34.7	29.7	6.10
TT97-1_6	TT-1	14/01/15	123	3.64	260	2150	259	0.92	95.7	232	430	54.4	233	46.3	5.89	7.64	47.3	10.2	28.0	3.74	27.8	3.60	53.6	18.1	39.0	27.4	6.02
TT97-1_8	TT-1	14/01/15	123	4.63	250	2020	250	1.12	97.8	229	417	51.6	226	38.7	6.58	6.71	43.1	8.98	26.4	3.64	25.9	4.20	48.3	17.5	42.0	26.2	7.29
TT97-2A_1	TT-2	14/01/15	123	3.62	239	1920	261	1.01	79.6	211	421	50.9	209	44.4	4.70	7.51	38.3	8.17	27.1	3.60	23.0	3.54	47.9	16.3	42.1	23.8	6.23
TT97-2A_10	TT-2	15/01/15	124	4.11	282	2260	250	1.04	100	261	452	60.2	327	54.2	6.76	8.39	47.6	10.7	28.6	4.65	29.0	3.95	63.2	17.5	37.6	29.3	6.10
TT97-2A_13	TT-2	15/01/15	126	4.22	250	2150	278	1.34	88.5	240	458	53.1	222	50.5	5.62	6.98	47.1	9.91	27.6	4.22	26.8	3.87	51.6	19.0	39.0	26.8	7.21
TT97-2A_14	TT-2	15/01/15	127	4.24	275	2280	274	1.29	104	255	468	58.6	244	52.3	6.63	8.11	51.1	9.80	30.8	4.22	30.0	4.29	57.6	19.7	37.9	29.6	6.73
TT97-2A_15	TT-2	15/01/15	118	6.75	258	2140	259	1.14	91.6	238	435	54.0	214	50.7	5.62	7.48	45.0	8.69	29.0	3.61	24.4	3.94	53.2	16.8	34.0	25.9	5.69
TT97-2A_16	TT-2	15/01/15	127	3.63	247	2150	266	1.36	93.6	230	427	54.7	232	48.1	5.81	8.04	45.7	9.90	27.5	3.95	28.1	3.77	51.4	18.0	38.8	25.6	6.92
TT97-2A_18	TT-2	15/01/15	119	4.08	250	2040	264	1.19	87.9	230	440	53.7	218	46.9	5.61	7.10	47.9	9.57	29.0	4.16	26.5	3.97	53.3	18.6	38.9	26.1	6.84
TT97-2A_19	TT-2	15/01/15	119	4.50	244	2080	262	1.37	91.2	229	439	53.3	216	45.3	5.05	7.00	44.6	8.68	27.2	3.80	25.8	3.65	55.3	17.8	41.6	24.5	6.65
TT97-2A_2	TT-2	14/01/15	124	2.95	247	2020	261	1.11	85.6	231	438	53.8	213	45.7	5.11	7.78	42.8	9.67	27.0	3.99	24.8	3.46	47.9	17.9	43.2	25.2	6.80
TT97-2A_3	TT-2	14/01/15	125	3.78	234	1930	258	0.94	88.2	220	425	51.1	213	42.7	4.94	6.74	38.3	7.96	25.0	3.26	22.6	3.18	48.8	17.1	33.4	23.7	6.60
TT97-2A_4	TT-2	14/01/15	127	7.38	228	1890	259	1.30	78.3	209	409	48.3	211	41.4	5.18	6.90	37.6	9.08	24.4	3.43	23.5	3.31	48.4	17.5	41.8	22.3	6.87
TT97-2A_5	TT-2	14/01/15	125	3.67	234	1950	255	1.05	78.6	213	405	51.7	210	41.6	5.59	6.39	40.7	8.79	24.5	3.64	23.2	3.66	46.7	16.5	44.2	23.1	6.19
TT97-2A_6	TT-2	14/01/15	129	4.52	253	2020	271	1.41	88.6	228	428	53.4	228	43.9	6.31	8.37	43.6	9.51	27.3	4.19	24.9	4.14	50.3	17.5	44.8	24.7	6.97
TT97-2A_8	TT-2	14/01/15	129	4.29	251	2000	261	1.22	85.5	222	430	52.5	226	46.5	5.54	7.79	45.8	8.90	26.1	3.42	24.3	3.21	51.8	17.3	39.2	24.8	6.31
TT97-2A_9	TT-2	14/01/15	129	3.73	238	1940	252	0.98	82.8	217	419	52.0	208	42.0	5.35	5.73	42.3	7.76	26.5	3.23	22.3	3.63	48.6	17.1	39.6	25.2	6.50
TT97-2B_1	TT-2	15/01/15	128	3.74	227	1880	262	1.44	93.7	215	424	51.1	204	37.7	5.28	6.96	42.3	8.80	26.4	3.86	22.4	3.00	49.9	16.6	43.0	23.9	7.23
TT97-2B_10	TT-2	15/01/15	131	5.11	233	1880	262	1.26	92.0	221	468	54.7	216	49.8	6.48	6.99	42.0	8.81	27.1	4.57	24.5	3.43	53.4	18.4	47.6	25.6	7.65
TT97-2B_12	TT-2	15/01/15	130	3.07	218	1860	255	1.05	80.7	201	409	48.8	198	40.4	5.16	6.90	40.1	9.18	24.4	3.33	23.2	3.66	46.3	16.6	40.7	23.3	7.29
TT97-2B_13	TT-2	15/01/15	130	4.86	282	2230	265	1.25	96.8	264	491	59.3	268	54.4	5.95	8.75	54.7	10.3	31.1	4.79	29.6	4.18	57.1	18.7	42.3	27.9	6.79
TT97-2B_14	TT-2	15/01/15	122	3.29	231	1890	256	1.25	82.3	215	426	52.0	201	42.3	5.49	6.93	40.2	8.66	26.7	3.18	24.4	3.43	48.1	17.0	42.0	24.2	6.65
TT97-2B_15	TT-2	15/01/15	127	3.87	225	1800	257	1.11	82.7	206	421	48.2	194	42.6	5.28	6.39	41.6	8.11	25.9	3.64	23.5	3.54	46.7	16.5	40.1	23.0	6.66
TT97-2B_16	TT-2	15/01/15	134	3.65	231	2000	265	1.18	90.9	218	430	53.0	216	45.2	5.55	7.33	45.6	9.01	26.5	3.71	26.8	3.50	49.7	17.2	43.5	25.2	7.53
TT97-2B_17	TT-2	15/01/15	125	3.59	219	1740	243	1.30	79.2	202	399	46.8	193	43.3	5.82	5.97	40.4	7.86	23.6	3.24	23.3	3.56	46.5	16.0	44.0	23.9	6.86
TT97-2B_18	TT-2	15/01/15	130	4.46	246	2050	268	1.19	105	230	448	53.8	223	47.7	5.65	8.06	50.9	9.21	28.5	3.71	27.0	4.18	50.6	17.4	43.8	25.4	6.65
TT97-2B_19	TT-2	15/01/15	130	3.72	234	1950	251	1.03	79.5	218	422	50.8	216	45.9	6.39	6.92	45.1	8.62	25.1	3.53	22.6	3.42	48.2	16.4	40.0	24.2	6.61
TT97-2B_2	TT-2	15/01/15	133	3.19	217	1830	249	1.22	78.9	202	404	47.9	198	42.1	4.61	6.72	42.2	7.91	26.1	3.40	24.0	3.03	46.3	17.2	41.5	24.0	7.22

Continued on next page

Trace element concentrations (ppm) in Tilo tephra glass shards

Label	Tephra	Analysis date	Rb 0.62	Sr 1.05	Y 0.17	Zr 0.37	Nb 0.07	Cs 0.19	Ba 1.88	La 0.09	Ce 0.07	Pr 0.06	Nd 0.25	Sm 0.14	Eu 0.13	Tb 0.06	Dy 0.13	Ho 0.04	Er 0.07	Tm 0.05	Yb 0.15	Lu 0.04	Hf 0.08	Ta 0.06	Pb 0.12	Th 0.01	U 0.00
TT97-2B_20	TT-2	15/01/15	139	4.13	248	2030	260	1.17	87.8	226	452	54.0	228	48.3	5.95	7.03	49.0	9.58	27.2	3.46	25.8	3.67	50.0	17.5	41.7	26.3	7.63
TT97-2B_3	TT-2	15/01/15	146	3.02	226	1890	279	1.38	87.5	213	448	49.2	204	44.3	6.17	6.20	42.0	8.30	25.8	4.02	23.7	3.78	47.1	18.2	51.6	25.7	8.60
TT97-2B_4	TT-2	15/01/15	128	2.85	199	1630	233	1.36	71.7	193	399	47.9	182	39.2	4.77	6.64	33.7	7.78	23.3	3.26	20.1	3.14	44.2	15.2	42.3	21.8	6.75
TT97-2B_7	TT-2	15/01/15	148	3.95	230	1900	269	1.38	94.1	214	431	51.7	213	44.7	6.08	7.02	46.3	8.81	24.3	3.33	24.3	3.58	49.1	16.4	44.8	25.3	7.65
TT97-2B_8	TT-2	15/01/15	138	2.74	221	1870	265	1.34	82.1	209	430	49.9	217	46.0	4.36	6.47	38.4	9.10	25.1	3.55	23.2	3.45	52.6	16.5	41.8	25.0	7.11
TT97-2B_9	TT-2	15/01/15	130	5.53	290	2350	256	1.16	111	269	491	63.9	256	49.3	7.28	7.72	52.0	10.4	35.7	4.65	30.9	4.24	61.0	18.5	41.7	28.8	7.11
TT97-2C_1	TT-2	15/01/15	122	5.07	291	2380	264	1.07	104	255	464	54.9	262	52.1	6.17	8.52	52.7	11.3	30.1	4.36	29.2	4.63	63.7	19.9	40.1	31.3	7.68
TT97-2C_10	TT-2	15/01/15	124	5.53	346	2720	262	1.44	110	292	485	65.1	304	59.5	8.33	8.85	60.4	13.0	35.2	4.36	27.2	4.56	65.3	21.1	33.7	32.9	6.27
TT97-2C_11	TT-2	15/01/15	127	5.91	292	2320	264	0.96	98.0	244	466	53.9	257	48.9	6.08	7.25	53.0	10.5	31.4	4.14	28.9	3.81	56.1	19.0	37.2	29.7	7.43
TT97-2C_13	TT-2	15/01/15	132	4.24	263	2160	257	3.85	90.1	227	439	49.8	235	45.7	5.74	7.34	43.8	10.2	28.1	3.56	26.3	3.60	53.8	17.5	42.9	26.7	6.89
TT97-2C_14	TT-2	15/01/15	131	5.51	313	2550	271	1.42	107	271	502	62.2	290	53.5	7.71	9.00	65.1	13.4	31.2	4.94	33.5	4.43	62.4	22.6	39.2	32.6	6.78
TT97-2C_15	TT-2	15/01/15	126	4.22	288	2370	263	1.09	106	250	468	57.6	258	51.3	6.98	7.37	52.5	10.6	29.5	4.15	28.9	4.05	57.8	18.4	35.8	29.3	6.70
TT97-2C_16	TT-2	15/01/15	126	4.04	298	2460	269	0.94	102	259	476	57.6	269	54.9	6.26	7.97	57.0	12.0	29.8	4.52	31.5	4.11	58.0	20.7	35.3	30.8	6.32
TT97-2C_17	TT-2	15/01/15	126	4.44	297	2490	267	1.20	97.2	252	469	58.5	276	53.0	6.70	7.93	52.8	11.5	30.8	4.50	29.2	4.81	59.0	19.9	37.6	31.1	6.95
TT97-2C_18	TT-2	15/01/15	130	4.84	312	2580	279	1.11	106	270	490	59.2	280	54.9	7.29	7.90	58.1	11.6	31.4	4.41	32.9	4.59	65.0	19.5	35.4	31.2	6.93
TT97-2C_19	TT-2	15/01/15	125	4.37	305	2470	271	1.36	102	261	486	57.6	272	58.4	6.51	8.56	57.9	11.9	31.6	4.41	30.3	4.32	61.4	20.2	40.5	32.2	7.34
TT97-2C_2	TT-2	15/01/15	128	3.18	321	2510	270	1.34	108	274	498	61.9	280	56.3	7.81	8.83	56.8	13.1	30.1	5.03	30.0	4.38	63.7	21.1	41.3	33.4	7.11
TT97-2C_20	TT-2	15/01/15	126	4.40	298	2470	271	1.24	92.9	260	471	57.7	277	54.3	7.16	8.07	54.0	12.3	32.6	3.84	29.2	4.27	56.9	19.6	36.9	31.6	6.89
TT97-2C_4	TT-2	15/01/15	125	6.27	301	2520	268	1.21	103	265	481	60.1	275	58.4	6.08	8.05	54.8	12.1	32.7	4.40	32.7	4.62	60.3	20.5	36.0	32.0	6.60
TT97-2C_5	TT-2	15/01/15	122	4.00	290	2380	262	0.80	95.3	258	475	56.4	254	48.5	6.43	7.31	51.1	11.3	31.3	4.14	29.4	4.09	56.1	19.3	39.4	30.5	6.85
TT97-2C_7	TT-2	15/01/15	130	4.94	289	2420	275	1.15	97.3	263	487	57.1	263	51.9	7.11	7.61	54.2	11.2	32.5	4.01	32.2	3.74	60.9	19.3	39.1	31.9	7.04
TT97-2C_8	TT-2	15/01/15	108	3.88	225	1840	222	0.83	83.1	195	390	44.5	209	38.9	4.78	5.59	39.3	8.17	24.3	3.44	22.4	2.88	45.3	14.7	36.2	22.0	5.77
TT973/1	TT-3	16/07/14	115	13.4	245	1740	239	1.17	394	206	353	45.5	192	40.8	6.51	6.65	38.8	7.55	21.6	2.99	19.9	3.38	46.8	15.9	31.1	28.4	6.15
TT973/10	TT-3	16/07/14	121	8.30	241	1860	261	0.74	412	225	378	48.0	208	39.7	7.40	7.16	41.2	8.17	24.9	3.60	23.7	3.26	46.6	18.1	32.3	31.0	6.84
TT973/11	TT-3	16/07/14	123	6.30	219	1740	255	1.08	408	204	360	46.2	196	42.8	6.58	6.37	35.6	8.08	25.2	3.44	20.8	3.31	47.5	18.2	34.2	28.9	6.97
TT973/12	TT-3	16/07/14	160	9.88	278	2200	331	1.27	440	273	470	59.6	255	55.6	7.43	8.39	49.9	10.6	30.4	4.34	27.8	4.19	55.5	21.8	44.9	37.6	8.96
TT973/13	TT-3	16/07/14	149	8.76	338	2580	318	1.15	467	322	498	65.8	273	63.8	10.2	9.49	57.6	11.4	34.2	4.67	33.9	4.84	60.9	22.4	43.0	42.9	8.57
TT973/14	TT-3	16/07/14	131	6.56	261	2050	293	1.23	440	247	411	53.5	220	51.4	7.97	7.11	46.9	9.39	26.2	3.84	25.4	3.97	51.4	19.8	36.3	35.0	7.57
TT973/15	TT-3	16/07/14	131	8.86	271	2130	273	1.45	427	255	412	53.9	228	50.2	7.93	7.70	48.2	10.6	29.2	4.62	27.4	3.79	54.2	18.8	38.1	34.3	7.02
TT973/16	TT-3	16/07/14	120	6.10	228	1790	256	0.87	417	212	373	46.7	208	40.9	7.08	6.68	41.5	8.18	25.4	3.32	21.3	3.48	48.1	18.6	33.4	30.3	7.37
TT973/17	TT-3	16/07/14	150	9.04	342	2660	345	1.14	482	308	532	69.6	293	62.1	10.0	9.37	57.5	12.4	35.9	4.81	31.8	5.01	70.8	24.7	45.3	45.8	9.34
TT973/18	TT-3	16/07/14	129	6.25	234	1850	271	1.09	419	223	398	49.5	205	43.0	7.25	6.76	41.6	8.82	26.4	3.65	20.9	3.92	47.3	19.5	35.5	33.1	8.07
TT973/19	TT-3	16/07/14	153	21.9	290	2360	341	1.27	461	283	501	63.8	269	51.2	10.2	9.00	51.8	11.4	32.7	4.44	28.5	3.98	58.6	24.7	45.3	40.0	9.40
TT973/2	TT-3	16/07/14	143	7.18	377	3090	356	1.85	517	363	496	71.7	320	52.3	9.36	11.1	71.3	15.0	49.2	6.72	44.0	6.92	75.1	29.8	46.8	52.8	7.59
TT973/20	TT-3	16/07/14	125	8.88	231	1890	266	1.16	420	225	388	49.3	212	41.5	6.41	6.52	42.7	7.81	26.5	3.66	23.1	3.48	44.6	19.4	37.0	30.7	6.93
TT973/3	TT-3	16/07/14	126	6.18	253	1990	267	0.93	444	240	412	52.0	234	48.0	8.82	7.22	44.8	9.00	28.4	4.25	27.8	4.25	52.3	19.6	35.9	34.3	7.22
TT973/4	TT-3	16/07/14	115	6.25	213	1760	249	0.85	430	206	355	45.4	190	38.1	6.36	6.35	37.8	7.89	23.2	3.49	23.2	3.23	46.2	17.4	27.1	28.0	6.67
TT973/5	TT-3	16/07/14	137	8.26	249	1970	292	1.05	426	243	420	52.8	214	42.1	7.40	7.31	45.0	9.21	26.0	4.11	25.7	4.17	48.4	20.3	38.7	33.2	7.77
TT973/7	TT-3	16/07/14	131	8.22	265	2050	286	0.80	439	247	411	53.8	232	45.8	7.52	7.21	47.6	8.97	30.3	4.55	25.8	3.91	53.1	20.3	34.8	36.1	7.58
TT973/8	TT-3	16/07/14	114	9.22	242	1900	253	0.76	435	219	363	47.6	211	44.3	7.82	7.28	42.1	9.27	25.1	3.65	22.6	3.38	48.6	18.5	33.7	31.2	7.07
TT974/1	TT-4	16/07/14	130	3.67	260	2090	264	1.36	77.3	228	437	53.3	234	44.9	6.26	7.59	46.0	9.99	28.1	3.90	26.6	4.42	52.2	18.7	40.4	27.0	6.90
TT974/10	TT-4	16/07/14	133	4.02	259	2050	269	1.20	82.8	226	434	59.2	231	44.9	6.01	8.28	44.6	9.75	29.7	4.61	28.5	4.09	55.5	17.5	44.1	27.6	7.68
TT974/12	TT-4	16/07/14	140	3.66	266	2160	274	1.26	88.9	235	458	54.2	232	48.6	6.13	7.98	48.3	9.97	31.5	4.27	31.3	4.06	60.2	20.4	44.6	30.1	7.78
TT974/13	TT-4	16/07/14	140	5.18	264	2170	280	1.34	83.3	238	455	58.9	247	49.2	6.16	8.00	49.9	11.1	34.4	4.26	30.5	4.70	57.8	19.5	44.9	29.4	7.67

Continued on next page

Trace element concentrations (ppm) in Tilo tephra glass shards

Label	Tephra	Analysis date	Rb 0.62	Sr 1.05	Y 0.17	Zr 0.37	Nb 0.07	Cs 0.19	Ba 1.88	La 0.09	Ce 0.07	Pr 0.06	Nd 0.25	Sm 0.14	Eu 0.13	Tb 0.06	Dy 0.13	Ho 0.04	Er 0.07	Tm 0.05	Yb 0.15	Lu 0.04	Hf 0.08	Ta 0.06	Pb 0.12	Th 0.01	U 0.00
TT974/14	TT-4	16/07/14	134	1.19	278	2100	259	1.20	91.1	238	453	59.3	253	51.4	6.24	7.81	53.8	11.3	34.2	3.78	28.9	4.41	53.9	19.8	42.4	29.8	6.95
TT974/15	TT-4	16/07/14	134	2.70	253	2040	262	1.24	85.8	214	434	54.3	226	45.8	5.67	8.06	43.4	10.2	32.1	4.08	28.2	3.76	59.6	18.9	44.7	26.8	7.52
TT974/16	TT-4	16/07/14	136	3.98	255	2000	270	1.33	84.7	221	429	54.0	224	48.5	6.36	7.95	51.8	11.3	30.2	3.61	26.1	4.12	54.1	18.4	42.5	27.0	7.91
TT974/17	TT-4	16/07/14	137	3.88	255	2010	279	1.31	81.4	222	430	53.5	225	51.0	6.96	7.72	45.4	9.50	30.8	3.99	29.7	4.44	57.5	18.8	45.5	27.3	7.62
TT974/18	TT-4	16/07/14	135	3.38	246	1980	271	1.24	73.7	224	422	53.7	219	50.0	5.98	7.11	45.6	10.1	29.4	3.58	26.7	3.72	51.2	17.4	42.3	25.6	6.85
TT974/19	TT-4	16/07/14	137	6.43	254	1990	269	1.48	76.9	219	441	53.5	227	45.0	5.83	7.01	44.3	9.37	30.1	3.93	26.0	4.03	53.3	17.7	42.2	26.1	7.91
TT974/2	TT-4	16/07/14	130	5.93	296	2340	265	1.10	85.1	259	466	63.0	281	54.1	7.23	8.27	52.5	11.7	36.0	4.74	32.4	4.32	63.5	20.3	42.3	32.0	7.19
TT974/20	TT-4	16/07/14	146	3.93	281	2300	278	1.39	94.1	251	464	59.8	256	56.0	6.73	8.86	58.0	10.4	34.5	4.21	32.9	5.25	64.9	21.2	49.9	32.0	8.26
TT974/3	TT-4	16/07/14	127	1.46	270	2080	254	1.11	93.7	229	426	54.1	236	49.0	5.08	7.68	47.6	11.8	26.3	4.60	28.3	3.96	57.7	18.6	40.2	25.8	6.83
TT974/4	TT-4	16/07/14	128	4.50	262	2160	266	1.41	80.0	232	438	55.7	232	45.2	6.52	7.40	51.0	9.89	30.3	3.85	26.3	3.32	51.4	18.5	40.8	28.2	7.37
TT974/5	TT-4	16/07/14	130	7.88	293	2290	261	0.73	86.6	258	455	59.3	253	55.1	6.54	9.00	54.9	11.1	33.3	4.19	30.4	4.67	64.0	20.4	42.1	32.0	6.78
TT974/6	TT-4	16/07/14	132	5.30	250	2070	272	0.81	78.4	219	430	54.6	236	48.6	5.64	7.51	43.2	8.74	28.4	3.79	29.6	3.67	54.4	18.6	42.8	26.1	7.42
TT974/7	TT-4	16/07/14	131	3.21	255	2010	264	1.40	74.9	216	433	52.9	234	51.2	5.60	8.10	42.8	9.82	30.4	4.17	27.9	4.20	52.3	18.8	41.9	27.9	7.14
TT974/8	TT-4	16/07/14	145	5.97	282	2310	286	1.19	92.6	249	465	60.1	261	54.7	7.10	8.60	51.1	10.5	35.4	4.41	31.6	4.04	56.6	20.9	42.9	28.9	7.96
TT974/9	TT-4	16/07/14	141	6.26	251	1960	265	1.34	70.5	222	426	51.2	218	43.3	5.38	7.09	43.9	9.28	28.7	4.32	25.9	4.61	50.6	18.7	44.6	25.1	7.16
TT975A/1	TT-5	18/07/14	154	5.20	255	2090	249	2.20	85.6	227	417	52.7	242	45.6	5.61	7.52	45.7	9.05	29.8	3.64	24.9	4.36	54.0	17.1	75.6	24.0	5.84
TT975A/10	TT-5	18/07/14	131	4.10	278	2320	261	1.59	88.8	250	480	59.0	265	53.3	6.56	8.11	53.2	10.7	32.0	4.57	26.3	3.79	62.8	18.3	43.9	29.3	7.24
TT975A/11	TT-5	18/07/14	129	2.96	227	1860	245	1.08	80.1	204	437	49.5	207	45.9	5.71	6.44	45.2	9.54	26.0	3.72	22.8	3.25	49.3	16.5	41.2	23.6	7.36
TT975A/12	TT-5	18/07/14	136	2.42	258	2060	264	0.97	72.1	222	472	55.3	223	48.9	5.69	7.95	44.8	8.98	28.9	4.28	26.3	3.62	52.5	17.5	45.0	26.4	7.98
TT975A/13	TT-5	18/07/14	138	3.58	253	2030	258	1.09	79.0	226	458	53.6	232	46.9	5.99	7.82	49.9	9.41	29.1	3.82	25.8	3.60	54.2	17.3	44.9	26.8	8.00
TT975A/14	TT-5	18/07/14	123	5.56	240	1960	249	1.11	71.8	208	424	46.2	218	37.2	4.76	7.40	43.6	9.74	25.3	3.76	24.9	3.23	48.1	16.6	43.9	24.8	7.05
TT975A/15	TT-5	18/07/14	131	3.13	256	2090	259	1.37	84.1	228	443	53.3	221	40.6	5.65	7.50	48.0	9.59	28.1	4.54	25.1	3.93	52.2	17.4	39.5	23.9	7.31
TT975A/16	TT-5	18/07/14	131	3.30	265	2150	263	1.15	86.6	233	458	54.9	234	48.2	6.76	7.85	52.9	10.5	29.4	4.14	27.2	4.31	51.4	18.2	43.5	27.8	7.08
TT975A/17	TT-5	18/07/14	130	5.52	262	2170	270	1.15	85.8	246	478	57.5	244	53.0	7.03	8.81	57.9	11.2	29.6	4.17	29.6	4.31	58.0	19.0	46.5	29.6	7.99
TT975A/18	TT-5	18/07/14	137	4.34	261	2210	275	1.18	87.0	242	475	55.1	236	45.1	6.50	8.12	48.7	12.0	30.2	4.54	27.8	4.16	55.9	18.8	45.8	27.0	7.96
TT975A/19	TT-5	18/07/14	140	4.06	225	1920	261	1.37	69.4	203	426	47.2	202	43.9	5.12	6.56	40.1	9.06	25.9	3.73	24.5	3.37	47.8	15.6	41.9	23.6	7.28
TT975A/2	TT-5	18/07/14	137	4.19	229	1930	252	1.34	71.7	207	426	50.4	223	41.8	5.33	6.92	45.9	8.83	29.1	3.26	25.4	3.77	47.0	17.4	45.0	23.3	8.04
TT975A/20	TT-5	18/07/14	142	5.21	243	2020	258	1.34	74.4	232	468	55.2	240	51.0	5.60	8.04	49.1	9.79	29.1	4.03	26.7	4.02	50.6	18.1	44.2	27.3	7.51
TT975A/3	TT-5	18/07/14	138	2.98	240	1920	255	1.11	68.9	213	442	49.4	213	42.9	5.10	6.52	46.1	8.83	27.7	4.43	24.1	3.76	49.8	16.2	44.3	24.4	7.68
TT975A/4	TT-5	18/07/14	124	3.20	226	1860	243	1.16	80.2	210	411	48.8	202	40.3	4.84	6.96	42.3	8.46	24.8	3.72	23.1	2.93	46.4	15.8	39.5	22.7	6.61
TT975A/5	TT-5	18/07/14	138	4.11	286	2290	272	0.98	88.2	249	501	58.2	244	49.7	6.34	9.03	53.9	12.0	34.1	4.23	27.2	3.68	57.4	19.8	47.1	28.8	7.27
TT975A/6	TT-5	18/07/14	139	3.88	232	1850	251	1.09	71.3	207	423	47.2	216	44.4	5.34	7.79	43.1	8.96	25.3	3.75	24.6	3.64	49.1	16.1	47.0	25.4	7.22
TT975A/7	TT-5	18/07/14	131	2.95	212	1770	248	1.15	70.4	191	397	44.2	183	36.5	4.58	6.24	40.7	8.07	23.0	3.07	21.9	3.25	45.5	15.6	45.4	22.6	6.60
TT975A/8	TT-5	18/07/14	130	4.80	252	2010	268	1.13	79.2	231	473	52.6	227	52.3	6.03	7.71	45.2	9.43	29.9	4.62	26.8	3.64	51.8	17.8	47.0	26.0	7.67
TT975A/9	TT-5	18/07/14	127	1.86	213	1760	247	1.14	75.5	194	419	48.7	197	39.1	5.23	6.72	40.0	8.96	22.7	3.89	22.4	3.39	45.4	15.6	46.2	23.4	6.93
TT975AB/1	TT-5	18/07/14	132	8.20	299	2490	263	1.06	89.0	263	458	59.4	267	55.1	6.98	8.84	59.2	12.8	33.2	4.83	31.2	4.28	60.4	17.3	41.0	29.7	6.69
TT975AB/10	TT-5	18/07/14	132	5.06	296	2390	277	1.06	86.4	267	483	59.2	264	52.9	6.82	9.45	56.8	10.7	33.5	4.70	30.4	4.09	61.6	19.3	38.2	29.9	7.07
TT975AB/11	TT-5	18/07/14	127	3.48	289	2380	275	1.63	95.3	264	470	60.8	250	54.6	7.08	8.97	50.2	11.1	34.5	5.16	28.3	4.72	62.9	19.5	40.4	28.2	6.59
TT975AB/12	TT-5	18/07/14	128	3.16	300	2430	273	1.40	80.3	257	458	57.7	249	47.8	6.83	8.46	51.6	11.4	33.8	4.20	29.5	4.80	59.1	19.2	38.1	30.3	7.52
TT975AB/13	TT-5	18/07/14	138	4.91	294	2370	272	1.09	88.7	257	465	57.7	246	49.6	6.10	8.23	52.5	10.8	34.0	4.75	29.0	4.31	59.7	18.6	36.8	27.8	7.19
TT975AB/14	TT-5	18/07/14	128	3.58	309	2500	272	1.03	83.3	265	470	61.9	261	54.3	6.08	9.85	56.9	12.6	33.3	4.88	30.6	4.18	64.8	18.5	39.2	30.3	7.29
TT975AB/15	TT-5	18/07/14	132	6.17	336	2730	279	1.48	88.9	284	492	67.8	291	57.5	7.48	9.75	63.6	12.6	35.3	5.25	33.3	5.04	74.7	19.3	45.1	31.9	7.45
TT975AB/16	TT-5	18/07/14	113	3.05	268	2130	233	1.16	73.4	225	401	54.7	216	48.0	5.37	7.76	47.3	10.0	29.6	3.96	26.7	4.31	56.2	16.1	37.9	26.1	5.95
TT975AB/17	TT-5	18/07/14	138	6.77	350	2760	272	1.07	94.5	287	500	67.2	301	63.1	8.58	9.51	59.2	13.0	36.4	4.66	32.8	5.09	69.5	20.4	39.7	36.0	7.66

Continued on next page

Trace element concentrations (ppm) in Tilo tephra glass shards

Label	Tephra	Analysis date	Rb 0.62	Sr 1.05	Y 0.17	Zr 0.37	Nb 0.07	Cs 0.19	Ba 1.88	La 0.09	Ce 0.07	Pr 0.06	Nd 0.25	Sm 0.14	Eu 0.13	Tb 0.06	Dy 0.13	Ho 0.04	Er 0.07	Tm 0.05	Yb 0.15	Lu 0.04	Hf 0.08	Ta 0.06	Pb 0.12	Th 0.01	U 0.00
TT975AB/18	TT-5	18/07/14	140	4.36	344	2840	291	1.26	89.7	293	507	67.8	286	59.2	8.67	10.1	63.6	12.8	37.9	5.10	37.3	4.93	73.1	21.0	41.0	32.9	8.00
TT975AB/19	TT-5	18/07/14	144	4.48	372	3000	297	1.16	102	323	549	77.9	318	67.8	7.35	10.6	71.0	14.5	43.4	6.71	35.2	5.67	80.3	23.1	44.0	37.3	8.16
TT975AB/2	TT-5	18/07/14	130	3.21	306	2490	272	1.02	86.2	272	476	61.3	258	49.9	7.19	8.93	59.5	12.5	33.7	4.58	31.0	5.12	63.0	18.4	37.7	31.7	7.19
TT975AB/20	TT-5	18/07/14	140	4.31	322	2610	284	1.26	94.3	283	503	65.1	278	53.8	7.25	9.86	62.9	13.6	36.7	4.97	34.3	4.64	66.0	21.4	44.5	33.2	7.81
TT975AB/3	TT-5	18/07/14	143	6.01	327	2740	295	1.52	56.1	286	505	66.5	277	61.1	7.17	9.27	59.3	12.5	35.4	5.66	34.2	4.79	67.6	22.2	48.8	33.1	8.05
TT975AB/4	TT-5	18/07/14	124	3.17	287	2310	246	1.08	80.0	245	430	56.2	234	47.0	5.94	8.35	49.2	10.8	32.5	4.79	28.5	4.04	53.1	17.7	39.2	27.9	6.30
TT975AB/5†	TT-5	18/07/14	147	10.7	395	3190	337	1.84	94.5	319	502	69.1	276	57.0	9.28	12.00	71.6	16.2	47.2	5.96	45.0	8.58	77.7	27.3	42.7	40.3	8.01
TT975AB/6	TT-5	18/07/14	132	3.94	292	2410	268	1.07	89.6	260	476	59.3	252	53.2	7.61	7.84	50.7	12.0	31.3	4.09	29.1	4.53	56.6	17.6	39.8	28.6	6.81
TT975AB/7	TT-5	18/07/14	127	5.59	295	2350	271	1.26	83.0	260	459	58.9	253	52.1	6.80	8.24	54.5	11.0	29.9	3.83	27.6	5.23	61.9	19.4	40.8	29.2	7.04
TT975AB/8	TT-5	18/07/14	138	3.60	338	2670	278	1.33	91.5	291	515	66.5	279	60.8	7.35	9.69	58.9	12.3	38.9	4.96	34.3	4.02	65.1	20.1	40.1	31.2	7.63
TT975AB/9	TT-5	18/07/14	136	3.53	285	2420	275	0.80	82.4	251	474	59.4	231	47.4	6.72	8.68	54.9	10.7	34.1	4.65	28.2	4.55	58.2	18.3	39.3	28.3	7.29
TT976/1	TT-6	11/07/14	142	9.82	274	2090	280	1.07	414	263	452	58.9	243	50.4	8.05	8.30	47.8	9.79	29.2	4.24	26.4	3.95	53.7	21.3	37.8	37.1	7.65
TT976/10	TT-6	11/07/14	137	7.34	228	1820	277	1.19	339	222	397	50.1	193	43.2	6.94	6.46	39.3	7.66	24.4	3.25	20.9	3.06	46.5	18.0	40.6	30.0	7.65
TT976/11	TT-6	11/07/14	126	4.05	208	1640	263	0.87	312	200	360	43.1	174	40.2	6.27	5.59	34.1	6.84	22.6	2.95	18.6	2.83	38.6	16.3	30.2	25.1	6.44
TT976/12	TT-6	11/07/14	132	8.31	206	1650	262	0.82	324	198	366	44.9	179	37.1	6.23	6.42	36.6	7.64	21.6	2.96	19.6	3.15	40.4	18.1	32.7	27.5	7.17
TT976/13a	TT-6	11/07/14	132	7.66	239	1870	295	1.20	363	230	409	52.9	207	43.2	6.74	6.81	38.7	8.09	24.7	3.49	22.3	3.08	46.7	19.5	37.1	30.7	8.35
TT976/13b	TT-6	11/07/14	136	6.16	237	1810	279	1.11	386	225	410	50.3	208	45.9	7.39	6.78	40.3	8.36	23.1	3.91	22.1	3.38	44.3	17.8	32.6	29.1	7.96
TT976/14	TT-6	11/07/14	123	7.85	207	1640	255	0.96	339	199	355	43.1	183	35.8	5.38	5.84	36.1	7.34	22.1	2.74	20.4	2.65	40.2	17.0	31.9	27.1	6.81
TT976/15	TT-6	11/07/14	124	5.92	204	1660	262	0.96	326	202	374	45.2	177	36.7	6.05	5.82	36.2	7.82	22.2	2.95	21.2	2.66	42.4	16.2	34.2	27.6	7.01
TT976/16	TT-6	11/07/14	125	7.10	219	1760	260	1.03	355	208	382	47.9	194	39.3	6.76	5.99	38.4	8.26	22.5	2.76	20.7	2.95	47.8	18.5	35.3	30.2	7.01
TT976/17	TT-6	11/07/14	131	8.10	232	1800	265	0.71	354	224	371	47.3	190	39.1	7.43	5.47	40.0	8.58	23.0	3.14	21.5	3.18	44.7	18.2	31.5	29.2	6.92
TT976/18a	TT-6	11/07/14	140	6.34	255	1930	281	1.10	370	235	412	53.1	216	42.4	7.28	6.56	41.3	8.62	24.8	3.28	23.5	3.63	46.5	18.4	36.5	31.0	7.70
TT976/18b	TT-6	11/07/14	138	7.70	229	1840	293	1.11	364	228	416	51.2	210	46.4	6.64	6.95	41.9	8.33	25.0	3.69	21.7	3.16	46.8	19.1	38.3	31.3	7.92
TT976/19a	TT-6	11/07/14	128	5.49	218	1740	270	0.99	337	210	373	45.7	177	37.6	6.25	6.14	39.7	8.00	23.2	3.07	20.2	3.24	44.3	18.2	36.8	28.1	7.05
TT976/19b	TT-6	11/07/14	137	6.81	235	1860	275	1.35	370	231	408	53.0	207	47.3	6.63	7.18	36.5	8.30	24.9	3.41	22.1	3.39	44.7	18.6	39.0	30.4	7.25
TT976/20a	TT-6	11/07/14	135	6.46	236	1880	283	0.95	349	224	404	49.0	204	43.9	7.26	5.97	39.6	8.72	26.2	3.46	22.6	3.32	46.1	19.3	36.5	31.0	7.33
TT976/20b	TT-6	11/07/14	135	7.30	224	1830	287	0.85	353	221	407	50.5	204	43.4	6.40	6.57	43.2	7.95	25.0	3.51	22.6	3.32	48.8	18.8	37.4	31.9	8.11
TT976/3	TT-6	11/07/14	155	7.54	249	1900	273	1.42	365	237	409	50.6	202	38.6	5.99	5.94	39.3	8.66	23.7	3.62	21.5	3.94	44.1	16.8	34.3	29.6	6.55
TT976/4a	TT-6	11/07/14	159	7.86	251	1980	298	1.27	371	251	441	53.9	226	48.3	7.93	6.90	44.9	8.90	24.7	3.41	24.9	3.55	49.6	20.2	44.5	34.3	8.35
TT976/4b	TT-6	11/07/14	146	7.32	235	1870	301	1.14	352	231	424	52.0	213	43.2	7.18	7.22	42.7	8.15	23.5	3.72	23.3	3.55	46.4	19.9	42.1	30.9	8.25
TT976/5	TT-6	11/07/14	135	9.84	242	1930	270	1.47	374	235	396	54.5	189	39.0	7.86	6.94	42.8	8.66	22.9	3.37	22.3	2.83	45.5	17.4	35.4	29.9	6.86
TT976/6	TT-6	11/07/14	129	4.19	227	1800	271	0.99	363	228	403	50.3	211	44.7	6.84	6.73	40.0	8.78	23.6	3.36	21.5	3.20	47.1	19.0	36.1	30.2	7.45
TT976/7	TT-6	11/07/14	129	5.63	247	1900	274	0.93	390	240	406	53.1	219	43.6	7.63	6.30	43.9	9.05	25.2	3.67	23.5	3.46	48.6	19.1	34.8	32.8	7.15
TT976/9	TT-6	11/07/14	118	8.02	219	1750	233	0.80	365	213	368	47.6	201	40.6	6.48	5.93	32.5	9.13	24.7	3.44	22.6	3.20	40.3	16.2	32.5	27.9	6.64
TT977/1	TT-7	11/07/14	132	4.57	268	2130	241	1.59	71.9	226	410	51.4	229	46.5	5.88	7.31	45.4	9.63	25.6	3.54	22.9	3.58	46.1	16.2	38.6	23.2	6.68
TT977/11	TT-7	11/07/14	130	2.16	214	1750	241	1.31	57.0	194	395	47.1	187	41.1	4.53	6.19	39.4	7.93	23.3	3.69	22.2	3.47	44.3	15.1	38.5	22.3	6.60
TT977/12	TT-7	11/07/14	125	0.87	205	1760	237	1.10	55.6	181	384	43.7	181	40.9	4.99	6.28	37.0	8.20	22.6	3.33	19.5	3.14	43.4	15.2	38.1	21.3	6.74
TT977/13	TT-7	11/07/14	127	3.03	217	1740	240	1.17	54.9	185	372	45.5	182	40.3	4.17	5.94	39.2	8.47	22.6	3.42	20.2	3.23	43.9	15.1	41.6	22.1	6.61
TT977/14	TT-7	11/07/14	126	2.96	215	1790	242	1.04	53.0	194	391	47.3	190	42.2	5.10	6.87	39.2	7.90	24.2	3.32	21.4	3.05	46.2	15.5	39.6	22.0	6.25
TT977/15	TT-7	11/07/14	123	2.90	218	1790	241	1.34	58.1	187	385	45.1	185	39.5	4.38	6.32	39.7	8.56	24.8	3.19	22.3	3.18	45.6	16.5	37.1	21.1	6.65
TT977/16	TT-7	11/07/14	122	3.65	219	1730	240	1.00	51.5	188	379	45.8	181	40.8	4.58	6.02	37.6	8.26	22.3	3.41	19.8	3.19	41.1	14.2	37.4	21.7	6.31
TT977/17	TT-7	11/07/14	125	3.89	221	1810	245	1.31	55.2	198	382	47.4	203	43.7	4.72	6.91	39.0	8.86	25.9	3.73	22.0	3.08	48.0	16.4	39.4	22.2	6.68
TT977/18	TT-7	11/07/14	125	2.83	246	2010	254	0.90	60.0	214	400	50.9	211	51.7	5.92	7.11	47.9	9.74	27.0	3.32	25.5	3.62	50.8	16.7	36.8	25.3	6.76
TT977/19	TT-7	11/07/14	125	3.93	244	1940	260	1.07	60.4	215	413	51.6	207	44.4	5.73	7.09	46.9	9.07	28.7	3.88	24.8	3.47	50.3	17.1	38.1	26.4	6.90

Continued on next page

Trace element concentrations (ppm) in Tilo tephra glass shards

Label	Tephra	Analysis date	Rb 0.62	Sr 1.05	Y 0.17	Zr 0.37	Nb 0.07	Cs 0.19	Ba 1.88	La 0.09	Ce 0.07	Pr 0.06	Nd 0.25	Sm 0.14	Eu 0.13	Tb 0.06	Dy 0.13	Ho 0.04	Er 0.07	Tm 0.05	Yb 0.15	Lu 0.04	Hf 0.08	Ta 0.06	Pb 0.12	Th 0.01	U 0.00
TT977/2	TT-7	11/07/14	127	3.46	256	2050	253	1.23	63.3	226	438	53.9	218	48.9	5.39	7.71	43.6	9.47	26.6	3.97	24.5	3.77	52.1	18.8	38.4	25.9	6.83
TT977/20	TT-7	11/07/14	124	2.78	238	1970	246	1.14	55.8	207	404	48.7	208	42.6	5.29	6.89	46.0	8.79	27.4	3.44	22.5	3.58	50.4	17.0	35.8	23.8	6.47
TT977/3	TT-7	11/07/14	129	2.87	238	1940	252	1.13	59.9	206	398	48.1	206	43.0	5.56	6.76	42.4	9.09	26.0	3.66	23.7	3.53	48.6	16.0	37.3	24.4	6.40
TT977/4	TT-7	11/07/14	125	3.56	224	1860	245	1.18	55.9	195	376	45.5	204	43.4	4.85	6.76	40.7	8.56	27.3	3.36	21.5	3.43	48.0	16.8	35.4	23.1	6.48
TT977/5	TT-7	11/07/14	127	2.81	235	1910	246	0.99	52.6	205	395	48.8	200	48.7	6.08	7.03	42.9	7.82	23.5	3.87	23.7	3.22	45.3	17.6	36.9	24.1	6.78
TT977/6	TT-7	11/07/14	130	2.41	239	1970	249	1.05	56.3	213	403	48.2	206	46.2	5.40	6.77	42.0	9.00	24.9	3.93	21.8	3.42	50.8	16.5	51.3	22.4	6.60
TT977/7	TT-7	11/07/14	122	2.79	238	1930	249	1.09	62.4	206	392	48.7	211	46.0	5.57	7.05	40.9	8.75	27.9	3.51	23.3	3.75	46.2	15.9	36.4	24.6	6.42
TT977/8	TT-7	11/07/14	124	2.23	217	1790	239	1.07	57.0	193	390	46.7	187	40.6	5.00	5.86	39.1	8.75	24.6	3.86	20.6	3.14	45.4	16.1	37.3	21.9	6.92
TT977/9	TT-7	11/07/14	128	2.94	219	1770	233	1.03	53.7	183	377	44.6	188	39.0	4.77	6.16	41.4	7.44	24.9	3.37	21.8	3.14	41.8	15.4	37.6	21.3	5.98
TT97-8_1	TT-8	15/01/15	128	3.77	286	2270	273	1.10	81.0	252	462	59.5	248	52.7	6.21	8.47	48.5	10.3	29.4	4.53	27.7	4.50	54.5	19.8	42.1	28.9	6.83
TT97-8_10	TT-8	15/01/15	133	3.98	299	2390	288	1.24	80.1	263	502	63.9	259	57.9	6.18	8.21	53.4	10.3	33.1	4.49	29.4	4.16	55.2	19.1	39.1	29.6	7.32
TT97-8_11	TT-8	15/01/15	133	3.93	259	2100	281	1.20	67.7	230	438	53.3	212	47.8	5.53	7.86	43.8	10.2	28.5	3.53	25.8	4.11	51.4	19.3	45.8	26.7	6.60
TT97-8_12	TT-8	15/01/15	130	4.58	282	2280	280	1.19	77.3	257	478	58.3	247	51.6	5.70	8.48	49.5	10.4	31.6	4.15	28.3	3.94	56.5	19.7	44.2	28.7	6.92
TT97-8_13	TT-8	15/01/15	137	4.85	302	2450	297	1.07	81.2	275	521	64.9	269	54.4	6.89	8.33	53.6	11.9	31.3	4.23	31.7	4.57	61.2	21.3	43.9	30.6	7.12
TT97-8_14	TT-8	15/01/15	131	4.62	305	2420	290	1.29	84.7	276	507	62.7	259	58.0	6.57	9.50	53.4	11.2	33.0	4.78	30.3	4.57	58.0	20.2	42.9	28.3	6.71
TT97-8_15	TT-8	15/01/15	129	3.72	281	2240	274	1.23	77.8	252	466	59.4	236	52.5	6.69	8.00	51.3	10.6	28.5	4.20	27.4	4.25	56.4	20.3	40.3	27.8	6.92
TT97-8_16	TT-8	15/01/15	130	3.98	278	2240	281	1.17	67.6	252	463	58.1	239	47.7	5.43	8.34	49.0	10.5	30.9	4.07	27.9	4.21	60.5	19.7	43.1	29.2	7.45
TT97-8_17	TT-8	15/01/15	131	5.46	296	2370	280	1.18	69.1	261	486	62.4	260	54.8	6.77	8.68	52.8	10.5	32.9	4.80	29.2	4.16	58.9	19.7	39.3	30.5	6.39
TT97-8_18	TT-8	15/01/15	128	4.41	321	2510	267	1.01	81.9	293	500	64.5	294	62.4	7.22	10.0	57.5	12.9	36.4	5.96	31.6	4.54	64.5	19.7	39.8	33.7	7.13
TT97-8_19	TT-8	15/01/15	128	4.45	292	2340	291	1.21	73.5	264	504	60.9	233	53.0	6.52	8.44	54.4	11.1	30.1	4.79	26.0	4.07	59.5	18.3	41.1	28.8	6.72
TT97-8_2	TT-8	15/01/15	100	5.80	218	1750	211	0.78	80.5	197	361	45.8	185	41.1	4.95	6.49	36.1	7.75	22.5	3.52	22.5	2.87	40.8	14.7	29.1	21.2	5.20
TT97-8_3	TT-8	15/01/15	131	4.65	293	2320	279	1.04	73.5	260	473	60.2	243	51.7	7.10	9.42	51.3	11.2	30.7	3.95	29.1	4.38	58.4	19.2	41.0	29.0	6.60
TT97-8_4	TT-8	15/01/15	120	4.76	280	2230	272	0.93	88.5	247	454	57.8	233	55.1	6.13	8.53	49.8	10.5	29.1	4.25	27.1	4.04	56.2	19.4	39.8	28.0	6.29
TT97-8_5	TT-8	15/01/15	128	3.75	302	2390	284	0.99	78.8	270	493	61.5	255	57.0	6.85	8.04	50.4	11.3	31.9	4.50	29.2	4.51	59.3	19.1	37.6	29.8	6.78
TT97-8_6	TT-8	15/01/15	129	5.04	257	2080	268	1.28	82.3	233	442	52.9	221	46.4	6.32	7.05	46.2	9.16	26.6	3.81	24.6	3.65	51.3	17.9	44.6	26.2	6.29
TT97-8_7	TT-8	15/01/15	127	3.19	265	2140	272	1.04	96.7	237	448	55.6	224	48.1	5.71	7.53	46.8	9.65	27.2	4.17	26.8	3.65	51.8	18.4	40.0	26.0	6.64
TT97-8_8	TT-8	15/01/15	127	4.84	270	2140	270	1.12	71.6	229	437	54.8	222	51.6	5.85	8.45	47.6	10.3	27.9	3.76	26.9	3.86	54.1	19.2	44.4	27.0	6.89
TT97-8_9	TT-8	15/01/15	131	8.35	272	2230	273	1.10	72.9	246	464	57.4	236	47.3	5.79	8.58	46.6	9.77	29.3	3.80	27.5	3.77	49.9	19.5	40.9	28.3	7.10
TT978A/1	TT-8	16/07/14	134	4.80	248	2000	246	0.97	61.2	214	406	49.4	209	42.2	5.48	6.96	40.6	9.54	22.4	3.26	22.7	3.62	45.3	14.4	34.1	23.2	5.52
TT978A/11	TT-8	16/07/14	110	5.29	235	1910	221	1.08	60.8	210	386	46.7	195	40.5	5.36	6.74	39.5	7.48	23.9	3.28	25.2	3.28	45.2	17.1	38.0	22.8	5.75
TT978A/12	TT-8	16/07/14	135	3.63	235	1910	249	1.19	62.2	210	414	50.7	201	40.2	5.38	7.40	41.3	8.94	25.8	3.89	24.0	3.55	49.4	17.4	41.1	23.7	6.96
TT978A/13	TT-8	16/07/14	131	2.85	262	2100	256	1.39	65.4	236	445	57.5	224	50.3	5.43	8.17	47.3	10.4	30.1	4.39	27.1	4.35	49.7	19.0	42.3	26.7	7.36
TT978A/14	TT-8	16/07/14	129	6.36	296	2330	272	1.30	70.4	260	482	60.9	255	50.7	7.76	8.48	49.8	11.3	31.8	4.40	28.6	4.15	59.6	17.5	40.5	27.5	6.66
TT978A/15	TT-8	16/07/14	132	6.82	301	2430	311	1.39	85.7	286	563	70.6	276	56.3	8.10	8.86	66.1	13.7	38.4	5.34	34.4	5.21	67.1	20.7	50.9	35.2	9.12
TT978A/16	TT-8	16/07/14	133	3.57	250	1950	257	1.15	68.1	216	434	51.6	212	49.0	5.90	6.70	43.9	9.77	25.7	3.87	25.8	3.46	47.3	17.1	44.5	24.3	6.99
TT978A/17	TT-8	16/07/14	133	3.55	264	2100	259	1.36	66.1	230	454	55.4	217	46.8	5.59	7.58	47.8	10.5	27.0	4.02	27.3	3.61	48.6	15.5	35.7	24.0	6.06
TT978A/18	TT-8	16/07/14	133	2.91	268	2120	265	1.18	71.6	236	462	56.8	231	47.6	5.82	8.08	47.4	10.6	31.5	4.21	27.9	3.82	50.5	18.4	43.7	28.1	7.45
TT978A/19	TT-8	16/07/14	136	3.36	248	2050	266	1.17	69.7	226	451	55.7	221	47.4	5.90	7.91	47.0	10.6	26.7	4.33	27.7	4.06	52.4	18.5	46.1	26.7	7.25
TT978A/2	TT-8	16/07/14	133	4.29	267	2180	290	1.41	73.6	240	469	57.4	248	47.4	7.21	7.98	51.6	9.94	29.5	4.27	27.7	4.36	56.7	19.5	45.3	29.9	7.63
TT978A/20	TT-8	16/07/14	129	3.61	219	1750	235	1.34	62.5	191	384	45.3	180	44.5	4.99	6.03	38.8	8.28	24.4	3.28	21.8	2.93	41.1	14.7	43.5	22.6	6.35
TT978A/3	TT-8	16/07/14	132	1.48	254	1950	250	1.49	65.5	208	421	49.7	196	46.6	5.53	6.64	44.6	9.25	28.2	4.25	22.5	3.72	46.9	15.4	35.6	23.2	6.10
TT978A/4	TT-8	16/07/14	141	3.35	250	2050	269	1.27	60.6	221	451	55.3	213	44.0	5.82	7.66	48.1	9.29	26.1	3.86	23.9	3.59	51.1	17.2	48.4	25.2	7.66
TT978A/5	TT-8	16/07/14	129	3.75	222	1780	248	1.21	61.1	192	390	48.3	189	37.0	5.05	6.50	37.6	8.68	21.2	3.20	22.3	3.33	39.8	15.0	40.3	21.5	6.55
TT978A/7	TT-8	16/07/14	142	3.61	241	1890	268	1.40	67.9	216	440	52.3	197	45.1	5.66	7.09	41.3	8.68	25.4	3.81	24.4	3.44	42.1	16.6	42.6	22.7	7.23

Continued on next page

Trace element concentrations (ppm) in Tilo tephra glass shards

Label	Tephra	Analysis date	Rb 0.62	Sr 1.05	Y 0.17	Zr 0.37	Nb 0.07	Cs 0.19	Ba 1.88	La 0.09	Ce 0.07	Pr 0.06	Nd 0.25	Sm 0.14	Eu 0.13	Tb 0.06	Dy 0.13	Ho 0.04	Er 0.07	Tm 0.05	Yb 0.15	Lu 0.04	Hf 0.08	Ta 0.06	Pb 0.12	Th 0.01	U 0.00
TT978A/8	TT-8	16/07/14	142	3.82	228	1880	263	1.30	63.7	205	422	49.7	191	38.8	5.93	6.16	39.5	9.11	22.2	3.00	24.0	3.80	47.1	16.6	44.0	23.7	7.11
TT978A/9	TT-8	16/07/14	129	2.87	249	2010	257	1.27	68.4	220	434	54.1	212	48.3	5.83	7.62	44.8	9.63	24.0	4.24	25.1	3.57	51.7	17.4	41.1	26.0	6.40
TT978B/1	TT-8	16/07/14	131	3.49	248	1960	258	0.87	65.9	216	412	49.6	212	45.5	5.50	6.31	43.2	8.54	25.6	3.43	23.3	3.38	46.8	16.6	34.8	23.1	6.19
TT978B/10	TT-8	16/07/14	132	4.24	281	2300	261	1.62	73.9	252	477	60.5	245	53.1	7.20	8.74	52.2	10.7	31.2	4.27	27.2	4.42	57.3	18.6	40.9	29.8	6.79
TT978B/11	TT-8	16/07/14	131	3.61	253	2010	258	1.02	60.7	221	429	50.8	218	44.4	6.00	6.73	43.3	9.72	27.5	3.86	22.8	4.14	47.8	16.9	45.2	25.1	6.42
TT978B/12	TT-8	16/07/14	133	4.46	272	2130	250	1.03	65.2	241	425	56.7	225	41.9	6.02	7.21	48.7	10.2	27.2	4.05	26.2	3.91	52.2	18.0	36.3	26.3	6.11
TT978B/13	TT-8	16/07/14	138	3.84	261	2120	269	1.15	65.6	235	461	57.2	221	49.4	6.15	7.52	47.9	10.0	28.6	4.49	26.0	3.56	51.4	18.6	43.5	27.7	7.00
TT978B/14	TT-8	16/07/14	129	2.26	251	2050	259	1.16	67.5	222	441	53.5	211	45.0	5.79	7.07	46.1	9.28	29.3	3.66	25.4	3.78	53.2	18.1	41.7	25.5	6.86
TT978B/15	TT-8	16/07/14	131	3.95	267	2170	272	1.39	85.9	244	468	57.4	241	53.1	7.03	8.36	50.6	11.2	33.1	4.52	30.8	4.63	58.7	20.1	40.7	29.4	7.64
TT978B/16	TT-8	16/07/14	134	2.81	270	2170	261	1.08	87.4	232	454	58.4	226	50.2	6.14	7.52	44.6	9.73	29.7	4.56	24.3	4.04	49.9	17.9	43.0	25.7	6.74
TT978B/17	TT-8	16/07/14	133	3.47	227	1810	248	1.06	59.0	199	407	47.2	193	46.1	5.12	6.33	42.2	9.55	25.7	3.66	23.0	3.30	47.1	16.6	38.1	22.8	6.99
TT978B/18	TT-8	16/07/14	128	2.29	250	1990	255	1.41	61.6	220	424	52.6	211	44.6	5.56	6.70	44.1	9.81	28.0	3.99	25.5	3.76	50.0	17.2	38.4	24.3	6.25
TT978B/19	TT-8	16/07/14	133	5.22	283	2270	279	1.36	68.2	248	494	61.0	249	55.1	6.37	8.70	52.8	11.4	31.9	4.49	29.5	4.78	60.6	19.2	43.4	30.3	7.60
TT978B/2	TT-8	16/07/14	133	3.69	264	2070	261	1.29	68.9	221	448	55.7	217	45.5	5.71	8.30	45.2	9.61	27.4	4.00	26.9	3.69	52.6	18.5	42.2	25.3	7.19
TT978B/20	TT-8	16/07/14	133	2.63	253	1990	261	1.32	65.8	224	434	52.7	217	47.1	5.89	8.38	45.5	9.19	28.6	3.64	25.7	4.37	49.9	18.5	42.6	26.4	7.08
TT978B/3	TT-8	16/07/14	134	8.40	245	2040	256	1.40	73.2	206	406	50.5	210	46.2	5.52	7.05	44.5	9.01	27.1	3.64	26.0	3.59	46.8	17.6	45.8	24.3	6.42
TT978B/4	TT-8	16/07/14	125	3.67	234	1920	252	1.21	74.0	213	412	50.4	196	44.0	6.14	6.92	42.9	9.70	27.7	4.03	22.8	3.87	49.2	16.8	40.2	24.3	6.71
TT978B/5	TT-8	16/07/14	131	3.07	273	2180	259	1.16	72.2	234	463	55.9	233	48.2	6.20	8.43	46.9	10.2	27.8	4.31	25.4	4.15	49.6	17.4	40.4	26.0	6.92
TT978B/6	TT-8	16/07/14	128	1.72	243	1970	249	1.18	67.6	211	416	49.6	200	42.0	5.29	7.74	43.9	8.78	26.3	3.84	24.5	3.67	49.5	16.7	38.7	24.8	6.89
TT978B/7	TT-8	16/07/14	128	5.28	268	2120	264	1.24	69.5	232	456	54.6	229	47.3	5.53	8.08	46.8	10.3	27.1	3.98	26.6	4.08	54.9	17.7	40.0	26.8	6.89
TT978B/8	TT-8	16/07/14	133	6.93	259	2160	263	1.49	66.6	234	471	57.4	239	47.7	6.80	7.08	49.3	10.5	29.8	4.22	31.6	3.90	55.1	18.4	42.9	27.4	7.17
TT978B/9	TT-8	16/07/14	132	3.06	257	2010	265	1.36	61.2	224	443	52.2	212	44.6	5.81	7.39	46.0	9.75	28.1	3.90	27.2	3.80	53.6	19.1	42.2	25.6	6.70
TT97-9A_1	TT-9	15/01/15	137	4.26	262	2140	272	1.33	72.2	230	461	56.4	226	48.3	5.45	7.76	47.6	9.36	28.2	4.23	26.1	4.07	52.0	18.4	46.7	26.9	7.16
TT97-9A_10	TT-9	15/01/15	129	5.14	261	2120	275	1.27	68.9	234	450	55.8	231	44.2	5.94	7.22	43.2	10.1	27.0	3.97	26.0	3.55	51.5	18.5	42.3	27.1	7.06
TT97-9A_11	TT-9	15/01/15	131	4.17	265	2180	275	1.35	71.9	245	476	58.4	225	48.7	5.97	7.76	49.2	9.99	28.7	4.03	27.2	4.03	51.3	19.3	41.6	27.9	7.50
TT97-9A_12	TT-9	15/01/15	135	4.78	261	2190	272	1.32	72.8	238	465	55.3	221	45.2	6.57	7.25	49.1	9.42	28.3	4.36	26.2	3.48	52.8	17.8	44.6	26.4	7.38
TT97-9A_13	TT-9	15/01/15	132	3.16	254	2090	276	1.22	67.7	230	457	55.4	217	45.2	5.60	7.17	42.6	9.85	26.8	3.82	26.0	3.92	54.0	16.9	45.4	26.4	7.35
TT97-9A_14	TT-9	15/01/15	139	3.91	258	2140	274	1.41	69.8	232	466	55.3	225	45.6	5.76	7.56	44.1	9.63	29.2	4.14	25.2	3.57	53.3	19.1	42.9	26.6	6.88
TT97-9A_15	TT-9	15/01/15	138	2.93	247	2060	281	1.23	71.8	229	450	54.5	218	45.4	5.24	7.52	45.3	10.1	23.6	4.16	27.2	3.54	49.7	18.0	49.8	25.6	7.17
TT97-9A_16	TT-9	15/01/15	126	14.4	245	1980	259	1.58	70.2	235	437	53.1	231	44.8	5.51	7.77	41.9	8.56	25.1	3.66	24.2	3.38	48.1	18.2	44.5	26.4	6.76
TT97-9A_17	TT-9	15/01/15	134	3.65	274	2250	287	1.15	71.2	249	481	58.7	232	49.3	6.92	7.82	51.1	11.5	29.4	3.51	27.0	4.39	55.0	18.7	43.1	28.1	7.34
TT97-9A_18	TT-9	15/01/15	131	4.96	274	2310	279	1.26	77.9	257	495	60.7	247	52.7	5.56	8.62	50.2	10.8	32.6	4.18	28.1	4.42	55.6	19.8	43.3	28.9	7.50
TT97-9A_19	TT-9	15/01/15	135	4.18	271	2250	278	1.11	69.1	250	479	60.3	231	52.3	5.50	8.56	51.6	10.7	29.1	4.22	26.1	4.09	52.8	17.8	41.4	27.6	7.05
TT97-9A_2	TT-9	15/01/15	135	4.19	242	2010	273	1.10	69.3	218	431	51.9	214	43.7	5.57	6.71	40.4	8.57	23.5	4.02	24.6	3.28	48.1	16.8	40.1	23.3	6.69
TT97-9A_20	TT-9	15/01/15	134	3.13	264	2090	270	1.22	72.8	235	445	56.6	217	47.2	6.44	7.41	47.2	10.1	26.1	3.83	25.4	3.61	51.8	18.5	41.6	26.0	7.00
TT97-9A_3	TT-9	15/01/15	138	3.77	240	1950	266	1.37	67.6	217	443	52.7	204	44.1	5.62	6.90	42.4	8.92	25.2	3.46	24.6	3.60	47.8	16.8	43.9	23.3	6.70
TT97-9A_4	TT-9	15/01/15	130	2.86	252	2080	270	1.26	66.6	224	453	55.2	209	46.3	5.95	7.90	46.5	9.81	26.5	4.22	25.4	3.69	50.1	17.5	44.9	25.7	7.44
TT97-9A_5	TT-9	15/01/15	134	3.27	278	2230	283	1.12	75.9	248	477	59.4	236	47.1	6.32	7.82	49.7	10.5	31.2	3.72	27.9	4.10	56.3	19.7	42.4	28.1	7.61
TT97-9A_6	TT-9	15/01/15	132	4.41	247	2080	274	1.22	70.7	232	449	55.8	217	43.5	6.16	7.58	45.3	9.60	26.7	4.01	26.2	3.82	51.6	18.1	71.3	25.9	7.11
TT97-9A_7	TT-9	15/01/15	136	2.38	254	2060	270	1.12	67.2	229	445	54.4	210	47.4	6.54	7.21	41.4	9.78	27.4	3.72	23.2	3.71	50.7	17.4	45.5	25.1	6.99
TT97-9A_8	TT-9	15/01/15	134	3.16	266	2160	280	1.24	78.8	236	480	53.9	219	52.4	5.39	8.04	48.4	10.6	27.7	3.87	27.5	4.44	55.2	18.1	44.0	27.3	8.14
TT97-9A_9	TT-9	15/01/15	132	4.14	243	1970	262	1.16	68.7	216	436	51.5	201	43.6	5.91	7.06	38.9	8.80	24.5	3.75	24.5	3.56	47.7	17.2	43.6	25.5	7.09
TT97-9B_1	TT-9	16/01/15	110	3.96	254	2030	256	1.21	61.8	230	441	50.9	229	49.6	4.99	7.31	46.1	8.37	27.3	3.89	23.1	4.12	52.1	17.0	38.8	26.1	6.52
TT97-9B_10	TT-9	16/01/15	140	4.50	236	2080	285	1.34	62.7	235	472	55.1	262	46.4	5.71	7.86	47.4	11.0	27.7	3.79	26.3	3.81	54.6	20.1	46.0	27.4	8.20

Continued on next page

Trace element concentrations (ppm) in Tilo tephra glass shards

Label	Tephra	Analysis date	Rb 0.62	Sr 1.05	Y 0.17	Zr 0.37	Nb 0.07	Cs 0.19	Ba 1.88	La 0.09	Ce 0.07	Pr 0.06	Nd 0.25	Sm 0.14	Eu 0.13	Tb 0.06	Dy 0.13	Ho 0.04	Er 0.07	Tm 0.05	Yb 0.15	Lu 0.04	Hf 0.08	Ta 0.06	Pb 0.12	Th 0.01	U 0.00
TT97-9B_11	TT-9	16/01/15	126	4.54	253	2120	289	1.41	61.7	239	478	56.9	240	45.4	5.33	7.32	45.9	9.25	27.6	3.82	26.8	3.45	53.1	17.6	40.1	26.4	7.14
TT97-9B_12	TT-9	16/01/15	120	2.80	254	2040	266	0.98	64.1	224	431	53.4	228	44.5	5.23	6.92	42.1	9.56	24.8	4.02	23.6	3.81	51.1	18.3	38.3	27.1	7.39
TT97-9B_13	TT-9	16/01/15	121	2.97	266	2110	273	1.23	60.2	238	452	54.5	226	52.1	6.01	7.24	44.4	10.3	27.4	4.00	26.2	3.56	50.9	18.2	40.4	25.1	6.89
TT97-9B_14	TT-9	16/01/15	130	3.88	248	2030	260	1.21	58.7	217	433	54.6	229	43.2	5.96	7.28	46.7	8.90	27.7	3.89	25.6	3.68	49.5	17.9	40.9	23.8	6.59
TT97-9B_15	TT-9	16/01/15	119	2.81	222	1850	247	1.15	55.2	204	409	48.4	193	42.5	5.35	7.41	43.3	8.11	22.6	2.87	24.3	2.97	46.3	16.8	38.7	24.4	6.62
TT97-9B_16	TT-9	16/01/15	136	4.19	233	1930	263	0.96	54.1	214	443	49.5	205	42.5	6.06	7.08	40.8	8.79	24.8	3.54	23.9	4.02	47.0	17.8	44.3	24.3	7.43
TT97-9B_17	TT-9	16/01/15	121	3.79	229	1880	258	1.12	55.4	210	402	48.5	212	41.8	5.45	6.62	41.0	8.23	21.3	3.28	22.8	3.27	49.4	16.2	40.3	23.2	6.67
TT97-9B_18	TT-9	16/01/15	126	4.54	229	1910	263	1.25	59.5	219	430	49.5	219	46.0	5.61	6.89	40.5	8.67	24.5	3.88	26.8	3.47	51.2	16.5	39.4	24.4	6.72
TT97-9B_19	TT-9	16/01/15	130	4.12	234	1960	272	1.29	54.2	213	423	52.9	212	37.4	6.52	7.00	43.6	8.78	28.4	3.29	24.5	3.45	48.4	16.6	40.6	24.9	6.86
TT97-9B_2	TT-9	16/01/15	114	6.38	250	1940	254	1.04	56.4	220	422	49.8	214	48.8	5.44	7.22	46.0	8.81	26.0	3.94	23.9	3.48	46.8	16.7	40.1	24.1	6.44
TT97-9B_20	TT-9	16/01/15	125	4.61	269	2200	276	1.17	65.1	243	464	59.0	255	46.9	6.30	7.80	50.0	10.8	28.0	4.39	28.7	4.08	53.3	18.6	39.5	27.0	7.30
TT97-9B_3	TT-9	16/01/15	124	3.98	268	2270	276	1.11	68.8	242	459	56.1	245	50.5	6.36	8.04	47.1	9.98	26.9	4.12	28.6	3.96	52.0	18.7	38.4	27.9	6.76
TT97-9B_5	TT-9	16/01/15	119	3.01	246	2080	267	1.16	58.7	230	440	52.0	230	42.9	5.28	7.38	43.8	9.77	28.3	3.99	26.1	3.58	49.8	17.6	40.0	25.7	6.88
TT97-9B_6	TT-9	16/01/15	117	3.98	239	1950	255	1.02	61.0	217	416	50.8	220	47.7	5.95	7.14	41.9	8.85	25.4	3.47	24.0	3.88	47.6	16.0	41.2	23.9	6.64
TT97-9B_7	TT-9	16/01/15	123	6.05	251	2030	257	1.29	59.9	232	442	53.9	226	49.4	6.26	6.96	48.3	10.5	27.2	3.60	26.2	3.89	54.8	18.2	41.2	26.9	7.75
TT97-9B_8	TT-9	16/01/15	119	4.98	216	1840	251	1.19	58.8	198	397	46.2	193	38.9	5.22	6.18	39.5	8.01	21.0	3.23	21.5	2.88	41.6	15.0	38.7	22.0	6.75
TT97-9B_9	TT-9	16/01/15	122	3.33	217	1740	256	1.15	51.8	200	403	47.9	207	39.5	5.15	6.59	37.7	7.75	23.8	3.91	22.7	3.04	45.8	16.5	43.1	23.2	6.87
TT97-9C_1	TT-9	16/01/15	118	5.09	263	2210	272	0.95	60.4	241	446	56.1	238	45.9	5.84	7.18	47.5	9.33	26.3	4.45	26.6	4.17	53.5	18.8	36.5	27.5	6.22
TT97-9C_10	TT-9	16/01/15	126	7.10	278	2220	271	1.95	68.8	257	471	60.3	250	53.5	6.02	8.37	51.7	10.3	29.6	4.88	28.3	3.85	55.7	18.7	42.5	29.0	6.73
TT97-9C_11	TT-9	16/01/15	129	4.28	256	2190	274	1.08	60.1	235	450	55.5	237	44.9	6.82	8.08	45.5	10.1	30.6	4.09	25.6	4.36	56.5	18.4	43.3	26.9	6.36
TT97-9C_12	TT-9	16/01/15	124	4.76	267	2180	276	1.25	57.3	241	456	57.2	245	47.4	7.39	7.56	52.0	10.3	27.9	4.31	27.7	3.67	57.0	19.7	38.7	28.9	7.17
TT97-9C_13	TT-9	16/01/15	128	4.08	243	2020	266	1.14	62.5	223	436	52.4	229	44.3	5.79	7.75	43.9	9.31	25.6	3.88	26.3	3.72	49.6	16.4	37.4	27.1	6.59
TT97-9C_14	TT-9	16/01/15	122	4.59	260	2120	274	1.38	58.9	241	460	57.5	226	49.2	6.44	8.14	48.7	10.4	27.5	3.87	27.9	3.98	53.4	18.9	41.9	29.0	7.12
TT97-9C_15	TT-9	16/01/15	125	3.02	266	2170	271	1.30	60.1	243	445	55.1	230	47.9	6.18	8.04	51.0	10.1	29.7	4.07	26.6	4.15	55.4	18.9	36.9	28.5	6.81
TT97-9C_16	TT-9	16/01/15	129	2.87	279	2290	289	1.23	59.1	257	480	62.2	249	52.8	6.12	7.53	51.2	10.5	30.6	4.67	28.5	5.07	60.2	18.4	35.7	30.0	7.28
TT97-9C_17	TT-9	16/01/15	129	4.59	298	2400	286	0.98	61.6	264	489	61.6	256	53.5	6.06	8.65	57.6	11.9	32.4	4.84	29.8	4.80	61.1	20.2	63.7	31.3	7.13
TT97-9C_18	TT-9	16/01/15	127	4.26	273	2240	277	1.18	58.1	250	457	58.3	256	49.8	5.89	7.85	46.2	11.0	31.2	4.30	27.7	4.12	57.9	19.4	36.6	28.8	6.75
TT97-9C_19	TT-9	16/01/15	126	2.45	261	2130	279	1.26	57.8	238	458	55.9	231	46.3	6.42	7.51	47.1	9.99	28.5	4.20	27.1	4.19	52.2	17.9	38.0	26.8	6.99
TT97-9C_2	TT-9	16/01/15	119	4.15	287	2390	288	1.15	63.4	266	490	60.4	260	50.4	7.32	8.20	50.3	11.1	31.6	4.04	31.3	4.09	60.1	19.9	36.7	29.8	6.49
TT97-9C_20	TT-9	16/01/15	114	4.28	220	1810	288	1.14	64.6	203	411	50.2	196	41.7	5.34	5.80	42.5	9.42	26.3	3.59	21.4	3.10	45.5	15.4	39.9	22.1	6.36
TT97-9C_3	TT-9	16/01/15	121	4.95	288	2360	280	1.01	64.6	257	467	60.8	257	52.5	6.46	8.83	51.6	10.9	29.1	4.09	31.3	4.98	63.5	20.4	36.2	29.0	6.48
TT97-9C_4	TT-9	16/01/15	125	4.19	258	2130	273	0.89	55.7	233	438	52.2	217	40.7	5.37	7.14	45.1	9.68	27.6	4.53	24.5	3.62	52.9	18.8	34.0	26.8	6.73
TT97-9C_5	TT-9	16/01/15	118	4.00	269	2220	277	1.31	66.2	247	470	56.0	242	48.5	6.47	8.36	47.8	9.95	29.2	4.47	27.2	3.84	58.1	18.5	39.4	28.4	6.55
TT97-9C_6	TT-9	16/01/15	122	4.05	283	2290	276	1.14	61.3	246	462	57.8	246	50.2	5.90	8.12	52.9	11.0	31.6	4.35	31.6	3.84	52.0	18.9	38.7	29.6	7.01
TT97-9C_7	TT-9	16/01/15	124	4.82	267	2130	270	1.12	69.3	240	432	53.8	223	48.7	6.19	7.63	47.5	9.62	26.5	4.03	25.4	4.00	53.0	17.5	35.6	27.4	6.43
TT97-9C_8	TT-9	16/01/15	124	4.72	272	2230	275	1.18	64.7	248	457	58.7	233	47.0	5.95	8.41	47.5	10.4	28.5	3.79	27.8	3.73	56.7	18.0	38.4	27.3	6.71
TT97-9C_9	TT-9	16/01/15	123	3.43	264	2160	272	1.18	63.3	239	451	55.9	227	45.8	5.64	7.79	50.7	10.2	28.5	4.07	28.5	4.12	52.7	17.8	37.4	28.7	6.98
TT97-10A_1	TT-10	19/01/15	124	4.45	314	2550	292	1.04	65.9	290	478	62.9	271	56.6	7.38	8.35	57.9	12.4	36.6	4.67	29.2	4.88	65.1	20.6	42.1	32.7	6.21
TT97-10A_10	TT-10	19/01/15	132	4.88	296	2360	281	1.44	63.2	265	467	59.9	254	53.3	6.56	7.63	54.0	11.4	30.5	4.42	30.0	4.38	62.7	20.1	49.3	29.2	7.18
TT97-10A_11	TT-10	19/01/15	135	5.56	330	2620	297	1.40	64.2	300	520	66.2	274	64.7	6.59	10.0	52.9	12.0	36.6	4.87	32.1	4.77	64.3	22.2	42.5	34.6	7.45
TT97-10A_12	TT-10	19/01/15	136	4.76	315	2580	297	1.12	70.7	297	528	68.3	287	61.6	7.88	10.3	59.5	12.6	37.4	5.14	33.4	5.06	66.8	21.7	45.7	32.9	7.62
TT97-10A_13	TT-10	19/01/15	132	5.11	299	2520	291	1.85	66.0	274	506	65.1	271	57.7	7.52	8.32	57.1	11.7	34.7	4.59	28.5	4.39	60.5	21.5	43.4	30.2	7.28
TT97-10A_14	TT-10	19/01/15	134	4.62	311	2440	295	1.31	66.2	288	506	61.5	265	58.5	7.01	9.27	54.5	11.9	30.9	4.20	31.2	4.52	59.4	20.5	48.4	31.5	7.43
TT97-10A_15	TT-10	19/01/15	129	3.55	301	2470	292	1.07	57.1	267	475	59.9	249	53.1	6.04	8.15	52.5	11.2	28.8	4.34	29.0	3.79	55.1	18.9	41.0	30.0	6.30

Continued on next page

Trace element concentrations (ppm) in Tilo tephra glass shards

Label	Tephra	Analysis date	Rb 0.62	Sr 1.05	Y 0.17	Zr 0.37	Nb 0.07	Cs 0.19	Ba 1.88	La 0.09	Ce 0.07	Pr 0.06	Nd 0.25	Sm 0.14	Eu 0.13	Tb 0.06	Dy 0.13	Ho 0.04	Er 0.07	Tm 0.05	Yb 0.15	Lu 0.04	Hf 0.08	Ta 0.06	Pb 0.12	Th 0.01	U 0.00
TT97-10A_16	TT-10	19/01/15	132	4.96	289	2420	290	1.22	60.7	266	480	61.9	247	50.7	6.31	8.07	50.9	10.7	30.5	4.68	28.4	4.77	57.4	19.2	42.2	29.5	6.89
TT97-10A_17	TT-10	19/01/15	140	3.90	308	2540	292	1.08	66.0	272	497	64.0	254	59.5	6.84	8.92	56.3	11.3	32.4	4.44	28.0	4.73	61.9	20.4	41.8	31.8	7.43
TT97-10A_18	TT-10	19/01/15	128	4.08	290	2410	291	1.31	59.8	272	478	62.3	251	57.3	6.31	8.76	50.9	11.1	32.1	4.67	30.0	4.26	58.8	19.7	41.7	30.2	6.95
TT97-10A_19	TT-10	19/01/15	130	3.72	285	2310	284	0.91	63.7	259	474	59.0	245	53.5	6.13	8.22	52.3	10.1	31.4	4.25	28.2	4.31	58.3	20.0	38.5	30.3	7.41
TT97-10A_2	TT-10	19/01/15	131	4.52	308	2500	284	0.96	67.8	279	485	64.3	274	60.4	7.86	8.69	59.5	11.6	37.0	4.96	33.7	4.37	61.9	21.5	43.8	32.6	6.91
TT97-10A_20	TT-10	19/01/15	132	5.40	291	2400	285	1.31	60.9	269	472	61.3	256	54.1	6.53	8.97	51.3	11.5	32.9	4.26	29.4	4.47	60.7	20.3	42.7	31.0	7.18
TT97-10A_3	TT-10	19/01/15	128	4.22	307	2530	290	1.13	69.2	276	484	61.3	258	57.7	6.75	9.13	57.3	11.4	33.6	4.40	30.6	4.38	60.4	20.9	39.7	30.2	6.66
TT97-10A_4	TT-10	19/01/15	127	4.95	321	2550	283	1.06	60.6	281	483	63.7	272	54.8	6.92	9.34	58.4	12.7	32.7	4.40	30.9	4.39	64.5	21.7	41.2	31.7	6.85
TT97-10A_5	TT-10	19/01/15	131	5.53	308	2530	283	1.30	61.7	282	500	66.4	266	55.3	6.70	9.37	55.4	12.0	33.3	4.81	28.6	4.32	62.9	22.1	40.0	32.3	6.53
TT97-10A_6	TT-10	19/01/15	129	4.12	314	2480	283	1.17	61.2	274	494	63.5	275	56.0	6.83	8.92	55.3	10.6	33.2	4.77	31.4	4.84	60.4	20.5	39.7	30.8	7.19
TT97-10A_7	TT-10	19/01/15	131	4.15	347	2780	293	1.68	66.5	311	508	68.3	306	59.2	7.19	10.5	58.4	13.5	38.9	5.39	34.7	6.30	67.0	23.8	42.8	34.4	6.37
TT97-10A_8	TT-10	19/01/15	124	3.73	305	2480	281	0.92	64.0	270	475	62.4	268	52.4	6.79	8.53	54.8	10.7	33.5	4.69	28.9	4.48	55.6	19.9	39.8	30.8	6.62
TT97-10A_9	TT-10	19/01/15	125	4.00	287	2320	282	0.98	62.9	253	456	56.5	238	49.3	5.93	8.39	48.8	10.5	31.2	4.13	26.0	4.01	55.2	18.5	37.3	26.6	6.39
TT97-10B_1	TT-10	19/01/15	138	3.68	272	2210	284	1.24	62.3	243	450	56.2	228	48.2	5.76	7.84	46.4	10.1	30.8	4.28	27.1	3.81	53.6	19.8	41.6	26.9	7.17
TT97-10B_10	TT-10	19/01/15	135	3.29	243	2020	266	1.34	56.4	225	434	50.1	218	45.6	5.79	7.07	42.9	9.11	26.0	3.33	23.6	3.90	48.0	16.6	41.1	24.6	7.04
TT97-10B_11	TT-10	19/01/15	137	4.50	254	2100	275	1.16	59.3	235	452	54.3	223	49.5	6.02	7.53	47.9	9.20	27.7	3.92	29.0	4.10	55.4	17.9	57.1	27.2	7.29
TT97-10B_12	TT-10	19/01/15	137	4.74	273	2240	276	1.11	78.9	257	474	60.2	236	55.2	6.79	7.70	50.7	10.4	33.7	3.84	28.1	4.01	55.4	17.5	43.5	27.9	6.95
TT97-10B_13	TT-10	19/01/15	130	3.13	275	2140	262	0.89	61.5	253	465	58.6	237	45.6	6.19	8.29	49.4	10.0	30.9	4.65	26.5	3.34	48.2	18.2	41.5	27.2	7.01
TT97-10B_15	TT-10	19/01/15	136	4.02	266	2210	275	1.39	58.1	252	459	56.8	232	53.2	6.19	7.08	49.8	10.2	31.1	3.87	26.8	4.04	55.0	18.0	40.0	27.2	7.12
TT97-10B_16	TT-10	19/01/15	119	3.50	209	1770	227	1.20	88.0	204	376	46.6	193	41.5	5.03	6.30	41.0	8.08	24.4	3.05	23.6	3.38	44.1	15.2	33.0	21.4	6.29
TT97-10B_17	TT-10	19/01/15	135	3.93	266	2170	281	1.38	60.9	261	474	54.8	240	50.0	6.40	7.97	49.9	10.0	29.4	3.78	27.2	3.95	54.4	19.2	44.2	28.2	7.33
TT97-10B_18	TT-10	19/01/15	139	3.60	256	2110	270	1.15	60.3	237	440	55.9	216	43.6	5.82	7.51	46.9	9.23	28.6	3.64	25.3	3.56	52.9	18.1	43.4	25.7	6.98
TT97-10B_19	TT-10	19/01/15	140	2.94	266	2150	286	1.12	58.3	247	456	56.1	242	48.3	6.72	7.16	49.2	9.82	28.3	3.58	26.3	4.19	56.5	18.7	47.5	26.4	7.35
TT97-10B_2	TT-10	19/01/15	134	3.85	287	2380	287	1.20	65.7	278	500	63.1	255	58.8	7.24	8.50	49.8	11.0	32.7	4.20	30.1	4.51	61.2	20.1	45.8	29.9	7.26
TT97-10B_20	TT-10	19/01/15	127	4.85	240	2000	254	1.29	79.0	228	425	53.1	220	42.3	5.46	7.52	40.7	9.11	24.9	3.70	24.5	3.80	47.2	16.2	45.5	23.7	6.70
TT97-10B_3	TT-10	19/01/15	121	3.86	244	1970	258	1.38	65.4	218	423	50.0	206	45.1	5.28	6.77	45.1	8.90	26.8	3.66	24.5	3.43	49.1	16.9	40.4	25.0	6.74
TT97-10B_4	TT-10	19/01/15	126	4.66	246	2030	255	1.20	57.4	227	432	52.5	216	46.9	5.61	7.62	48.5	9.27	26.7	3.89	25.3	3.85	53.0	17.8	42.3	25.3	6.90
TT97-10B_5	TT-10	19/01/15	140	5.72	279	2230	286	1.28	63.9	252	477	57.6	245	48.5	6.09	8.32	49.4	11.0	30.2	4.42	27.0	3.90	57.1	18.5	44.5	28.0	7.70
TT97-10B_6	TT-10	19/01/15	134	4.15	259	2140	271	1.23	59.7	231	447	55.7	213	45.5	6.22	7.68	40.7	8.99	28.4	3.80	24.7	4.11	52.1	17.4	44.4	27.4	6.57
TT97-10B_7	TT-10	19/01/15	139	2.57	263	2150	269	1.32	56.7	245	459	56.9	235	51.3	6.29	8.01	48.2	9.57	27.1	3.72	25.3	3.80	51.3	18.2	43.5	27.0	7.66
TT97-10B_8	TT-10	19/01/15	139	5.67	292	2220	281	1.55	65.2	256	478	59.0	242	55.0	6.86	8.17	51.8	9.91	29.9	3.76	28.6	4.17	51.2	19.0	43.5	28.2	7.80
TT97-10B_9	TT-10	19/01/15	137	3.62	252	2110	278	1.00	62.8	232	444	53.6	219	49.9	5.37	7.37	45.4	9.08	27.7	3.77	25.0	3.40	50.1	17.6	44.3	25.5	7.14
TT97-10C_1	TT-10	19/01/15	127	3.96	233	1990	274	1.21	64.0	210	439	52.4	209	42.4	5.37	7.15	45.2	9.70	25.4	3.52	24.4	3.70	49.6	17.8	50.3	24.8	7.90
TT97-10C_10	TT-10	19/01/15	132	4.73	245	2050	273	1.39	62.1	226	457	53.4	214	42.3	5.14	6.95	47.0	9.03	27.5	4.23	23.6	3.92	48.6	17.4	46.2	25.2	7.56
TT97-10C_11	TT-10	19/01/15	131	4.35	214	1830	262	1.06	80.3	190	409	47.9	196	38.9	5.42	6.42	40.2	8.14	23.0	3.41	22.7	3.23	44.1	16.0	48.2	23.0	6.84
TT97-10C_12	TT-10	19/01/15	129	3.76	235	1920	266	1.09	78.0	212	437	51.0	207	43.9	5.86	6.85	43.8	9.27	25.4	3.49	24.0	3.81	48.5	16.6	44.0	24.0	7.21
TT97-10C_13	TT-10	19/01/15	133	4.23	231	1920	272	1.14	78.2	219	423	51.4	214	43.6	5.50	6.85	43.3	9.57	26.2	3.74	23.9	3.43	47.4	16.6	45.6	23.9	7.08
TT97-10C_14	TT-10	19/01/15	134	5.49	218	1850	259	1.17	71.4	197	431	44.1	195	38.9	5.28	6.42	39.0	8.05	22.3	3.30	21.2	2.99	42.4	15.5	45.1	22.3	6.80
TT97-10C_15	TT-10	19/01/15	136	5.20	252	2080	282	1.18	61.2	225	474	54.1	224	49.4	5.98	7.21	46.4	9.53	26.2	3.93	25.0	3.78	52.5	17.7	45.7	25.8	7.68
TT97-10C_16	TT-10	19/01/15	129	4.33	226	1870	256	1.43	77.3	206	424	48.3	200	40.7	5.33	7.00	43.8	8.52	25.3	3.61	24.3	3.74	45.8	17.3	44.0	25.3	7.35
TT97-10C_17	TT-10	19/01/15	139	4.83	242	2020	274	1.03	72.1	221	461	50.7	211	44.6	5.74	6.71	41.3	9.08	27.7	3.64	25.3	3.52	50.1	17.4	45.1	24.8	7.03
TT97-10C_18	TT-10	19/01/15	135	4.38	241	1930	262	1.24	78.5	205	447	51.3	204	42.4	5.27	6.96	43.5	8.60	26.4	4.06	22.8	3.19	49.6	17.3	51.3	24.7	7.09
TT97-10C_19	TT-10	19/01/15	138	6.77	258	2160	286	1.25	69.3	223	459	54.1	228	46.2	5.27	7.22	47.4	9.77	27.9	3.76	25.7	4.08	53.0	19.2	45.1	27.7	7.49
TT97-10C_2	TT-10	19/01/15	133	4.13	236	1960	275	1.18	70.7	211	442	51.2	208	43.8	5.39	6.55	44.1	8.36	25.3	3.62	23.5	3.57	49.6	17.6	48.1	25.5	7.62

Continued on next page

Trace element concentrations (ppm) in Tilo tephra glass shards

Label	Tephra	Analysis date	Rb 0.62	Sr 1.05	Y 0.17	Zr 0.37	Nb 0.07	Cs 0.19	Ba 1.88	La 0.09	Ce 0.07	Pr 0.06	Nd 0.25	Sm 0.14	Eu 0.13	Tb 0.06	Dy 0.13	Ho 0.04	Er 0.07	Tm 0.05	Yb 0.15	Lu 0.04	Hf 0.08	Ta 0.06	Pb 0.12	Th 0.01	U 0.00
TT97-10C_20	TT-10	19/01/15	131	4.42	239	1950	263	1.03	80.0	214	418	48.5	205	42.6	5.34	6.87	43.2	8.47	26.8	3.84	23.1	3.23	46.9	16.9	47.1	24.4	6.68
TT97-10C_21	TT-10	19/01/15	124	5.70	225	1810	255	1.17	76.0	205	408	48.3	196	40.0	5.13	7.01	44.6	8.63	25.4	4.27	21.5	3.02	46.8	17.2	60.3	23.4	6.63
TT97-10C_22	TT-10	19/01/15	138	6.92	244	1940	277	1.22	82.8	228	464	54.3	231	47.5	6.33	7.62	45.8	9.73	28.4	3.79	24.4	3.99	52.6	17.8	52.9	27.1	7.84
TT97-10C_3	TT-10	19/01/15	133	5.43	223	1900	260	1.21	72.7	203	424	48.9	195	38.9	5.57	7.12	43.8	8.49	25.8	3.42	22.6	3.60	48.3	15.8	47.2	24.0	6.67
TT97-10C_4	TT-10	19/01/15	122	4.14	257	2110	277	1.19	72.0	230	454	52.6	231	48.2	5.70	7.54	47.1	9.97	28.4	4.39	26.6	4.02	53.9	17.5	47.3	27.7	6.86
TT97-10C_5	TT-10	19/01/15	127	3.62	248	2020	268	1.10	76.3	217	448	51.4	218	45.2	5.38	7.61	45.6	9.21	25.8	4.22	24.8	3.59	53.3	17.0	43.4	24.9	6.91
TT97-10C_6	TT-10	19/01/15	127	3.96	234	1950	264	1.22	69.5	206	424	50.2	205	43.9	5.18	6.74	42.3	9.15	26.2	3.67	23.5	3.41	48.5	17.1	43.2	23.8	6.89
TT97-10C_7	TT-10	19/01/15	122	5.70	250	2100	271	1.19	63.0	228	462	52.8	228	44.9	5.78	7.37	44.0	10.1	28.3	3.66	26.2	3.90	51.2	17.6	48.3	27.3	7.32
TT97-10C_8	TT-10	19/01/15	125	4.90	234	1940	258	1.03	72.0	208	412	47.5	193	41.1	5.00	6.31	38.4	8.92	24.7	3.69	24.2	3.55	45.3	16.1	43.1	23.7	6.74
TT97-10C_9	TT-10	19/01/15	147	3.03	243	1990	271	0.91	77.2	217	439	51.9	212	46.4	6.07	6.92	45.3	9.14	25.7	3.39	25.0	3.54	49.1	17.8	44.8	25.5	7.06
TT97-11_1	TT-11	19/01/15	137	4.20	298	2430	306	1.33	53.7	260	492	58.9	246	54.6	5.88	8.17	51.1	11.1	32.9	4.91	27.7	4.20	60.3	20.9	47.3	31.3	7.53
TT97-11_10	TT-11	19/01/15	153	10.2	313	2510	297	4.06	75.4	273	493	62.0	259	57.8	7.03	8.70	55.6	12.2	31.9	4.62	32.2	4.12	64.1	20.5	60.1	31.6	7.17
TT97-11_11	TT-11	19/01/15	137	4.19	280	2230	289	1.29	56.5	249	466	56.5	235	52.5	6.25	7.94	47.9	10.8	31.0	4.25	27.2	4.30	58.8	20.2	45.3	28.4	7.29
TT97-11_12	TT-11	19/01/15	144	3.85	294	2370	312	1.38	52.5	265	495	57.6	246	46.2	6.74	8.75	53.8	10.8	31.8	3.99	28.1	4.35	57.7	19.2	50.7	28.5	7.06
TT97-11_13	TT-11	19/01/15	141	4.01	278	2210	297	1.15	58.8	239	461	54.9	230	50.3	6.18	7.34	49.2	9.99	30.1	3.88	26.1	3.77	56.4	19.0	45.9	28.7	7.28
TT97-11_14	TT-11	19/01/15	142	4.92	313	2480	314	1.32	62.6	275	503	60.2	261	54.3	6.85	8.52	58.5	12.1	33.7	4.11	30.7	4.29	62.4	21.7	49.5	32.2	7.62
TT97-11_15	TT-11	19/01/15	139	9.73	277	2220	300	1.38	61.1	244	468	57.3	230	51.6	6.03	7.46	49.8	10.6	31.2	4.13	27.8	4.19	53.4	20.0	44.1	28.9	7.58
TT97-11_16	TT-11	19/01/15	140	5.05	312	2460	305	1.35	57.9	268	491	62.4	250	56.5	6.56	8.10	55.5	11.7	32.9	4.28	29.4	4.98	61.0	21.2	44.5	31.2	7.76
TT97-11_17	TT-11	19/01/15	128	11.7	252	2000	268	1.22	50.4	229	431	51.4	211	47.2	5.96	6.99	45.6	9.85	27.4	3.69	25.4	3.72	51.4	17.3	49.9	25.9	6.85
TT97-11_18	TT-11	19/01/15	144	5.57	317	2530	317	1.30	60.4	282	532	63.1	262	60.2	7.28	9.26	60.0	11.8	33.6	4.67	29.8	4.35	64.9	22.0	47.0	33.7	7.53
TT97-11_19	TT-11	19/01/15	141	4.20	310	2460	302	1.27	55.1	272	496	60.9	259	53.6	7.12	8.47	56.9	11.9	31.7	4.95	27.9	4.40	61.0	21.6	45.8	31.7	7.11
TT97-11_2	TT-11	19/01/15	138	5.18	321	2610	320	1.20	63.0	285	521	64.8	272	61.6	7.20	9.59	56.6	11.7	33.7	4.90	31.8	4.52	62.0	20.5	43.1	32.6	7.16
TT97-11_20	TT-11	19/01/15	145	4.72	305	2410	309	1.15	53.4	262	496	59.4	252	55.6	7.02	9.00	51.3	11.2	32.8	4.56	30.6	4.24	60.7	20.7	47.5	31.5	7.83
TT97-11_3	TT-11	19/01/15	137	3.74	314	2500	307	1.25	61.3	263	501	61.5	254	53.9	6.74	8.67	56.1	12.1	34.1	4.64	29.5	4.77	60.0	20.9	47.0	30.0	7.57
TT97-11_4	TT-11	19/01/15	134	3.68	299	2410	293	1.33	56.8	263	490	60.0	247	50.2	6.64	8.57	50.6	10.4	30.6	5.08	28.3	4.27	59.2	20.7	64.0	31.2	7.44
TT97-11_5	TT-11	19/01/15	135	3.50	287	2310	294	1.17	51.5	247	472	55.1	233	48.8	6.29	7.92	50.8	10.0	29.2	4.44	25.9	3.86	55.4	19.6	46.2	28.9	7.39
TT97-11_6	TT-11	19/01/15	141	5.25	316	2550	307	1.38	63.9	283	514	65.3	257	64.6	7.37	9.18	58.2	11.6	34.0	5.04	32.3	4.46	64.5	22.2	47.3	35.1	7.28
TT97-11_7	TT-11	19/01/15	138	3.96	303	2430	304	1.16	57.2	267	499	60.2	254	52.2	6.97	8.73	53.5	11.7	33.9	4.20	30.3	4.18	61.1	20.3	45.1	31.9	7.58
TT97-11_8	TT-11	19/01/15	137	4.81	293	2340	307	1.12	53.7	253	473	58.0	252	48.1	6.91	8.02	51.6	10.4	32.1	4.26	28.8	4.40	60.0	20.2	45.4	28.8	7.24
TT97-11_9	TT-11	19/01/15	140	5.17	306	2450	330	1.76	66.6	284	529	66.2	259	57.5	6.33	9.28	55.1	12.1	33.7	4.89	28.3	4.74	60.8	20.3	45.2	30.7	7.99
TT9711B/1	TT-11	22/07/14	138	3.53	341	2680	295	1.68	47.2	287	502	67.0	281	56.2	7.47	9.16	62.2	12.9	34.4	5.27	35.0	5.03	73.1	20.5	41.8	35.2	7.78
TT9711B/10	TT-11	22/07/14	109	4.67	260	1960	227	0.75	86.4	225	389	51.8	218	43.3	6.00	8.12	44.7	9.90	27.4	3.47	26.2	3.24	51.8	16.8	29.9	26.2	5.35
TT9711B/11	TT-11	22/07/14	134	4.14	332	2610	296	1.20	43.9	284	507	66.2	280	54.3	7.32	10.2	61.5	13.2	36.8	5.03	35.3	5.48	69.8	21.9	41.9	34.3	7.56
TT9711B/12	TT-11	22/07/14	139	3.48	342	2640	305	1.48	48.7	287	525	69.4	290	60.0	7.08	10.5	65.3	12.6	38.8	4.79	32.8	5.24	77.0	23.4	40.3	35.6	8.70
TT9711B/13	TT-11	22/07/14	108	7.72	291	2210	224	1.52	35.2	236	408	54.6	238	49.2	5.97	8.60	55.1	10.8	33.2	4.50	28.7	4.83	63.4	17.7	32.4	29.6	6.51
TT9711B/14	TT-11	22/07/14	140	4.76	365	2770	312	1.55	45.9	306	545	72.8	307	61.4	7.56	10.8	64.4	13.1	42.5	6.04	39.8	5.48	78.8	25.7	43.8	39.8	7.83
TT9711B/15	TT-11	22/07/14	130	6.17	346	2600	292	1.27	43.7	288	519	65.6	290	55.4	8.25	9.22	64.0	13.5	40.1	6.04	35.6	5.32	73.6	21.2	39.8	34.4	7.70
TT9711B/16	TT-11	22/07/14	132	4.06	299	2360	288	1.34	45.3	267	489	65.2	264	51.9	6.09	9.62	55.4	11.9	36.3	5.07	34.2	5.03	65.2	21.3	43.2	33.3	7.58
TT9711B/17	TT-11	22/07/14	141	3.48	337	2560	306	0.99	41.3	279	508	64.2	282	56.7	7.30	8.91	52.4	12.9	36.5	5.69	33.6	5.06	68.9	21.0	39.4	33.4	7.97
TT9711B/18	TT-11	22/07/14	135	4.95	339	2600	305	1.41	42.1	289	514	65.8	299	56.1	7.35	10.2	65.1	12.9	36.7	4.73	32.6	5.28	67.0	20.8	39.5	34.0	8.22
TT9711B/19	TT-11	22/07/14	148	8.35	347	2600	284	2.04	49.8	285	498	65.1	276	56.7	6.61	9.12	61.1	13.0	37.6	5.06	32.9	6.04	67.4	20.9	40.5	34.0	7.42
TT9711B/2	TT-11	22/07/14	103	5.03	223	1790	212	0.73	88.9	205	370	47.7	207	39.1	4.93	6.61	41.3	9.74	26.3	3.67	23.9	3.41	46.9	15.1	27.1	23.5	5.44
TT9711B/20	TT-11	22/07/14	136	3.64	342	2580	306	1.41	46.1	287	515	66.5	284	60.8	7.98	9.75	62.3	12.8	39.0	5.77	34.4	4.72	71.2	22.6	39.8	36.2	7.31
TT9711B/3	TT-11	22/07/14	140	5.36	358	2840	312	1.43	50.3	310	561	73.7	310	61.0	8.34	9.57	62.0	13.7	40.7	5.73	36.1	5.72	74.4	22.2	44.6	36.1	7.98

Continued on next page

Trace element concentrations (ppm) in Tilo tephra glass shards

Label	Tephra	Analysis date	Rb 0.62	Sr 1.05	Y 0.17	Zr 0.37	Nb 0.07	Cs 0.19	Ba 1.88	La 0.09	Ce 0.07	Pr 0.06	Nd 0.25	Sm 0.14	Eu 0.13	Tb 0.06	Dy 0.13	Ho 0.04	Er 0.07	Tm 0.05	Yb 0.15	Lu 0.04	Hf 0.08	Ta 0.06	Pb 0.12	Th 0.01	U 0.00
TT9711B/4	TT-11	22/07/14	119	4.91	270	2150	251	1.03	58.5	236	427	54.9	228	46.2	6.14	8.52	48.2	11.2	29.7	4.75	26.9	3.98	57.0	16.4	33.4	27.8	6.29
TT9711B/5	TT-11	22/07/14	140	5.53	369	2850	305	1.91	52.9	305	537	73.9	302	57.3	7.11	10.6	72.4	14.6	43.8	5.26	34.8	5.25	78.5	22.4	46.9	35.7	8.16
TT9711B/7	TT-11	22/07/14	108	5.45	267	2040	218	0.85	96.2	226	392	48.9	213	44.9	5.79	7.95	46.8	10.1	28.5	3.59	25.7	3.83	53.6	15.6	28.9	23.9	5.16
TT9711B/8	TT-11	22/07/14	136	4.73	339	2600	306	1.27	46.5	299	531	68.8	290	57.5	7.92	10.2	65.7	13.3	38.3	4.94	38.1	5.16	76.4	21.6	44.5	36.2	7.89
TT9711B/9	TT-11	22/07/14	155	3.75	349	2690	288	1.62	40.3	284	515	67.1	281	59.3	7.77	9.72	63.5	13.8	39.8	6.08	32.5	5.09	75.4	22.6	43.9	37.7	8.06
TT9712A/1	TT-12	22/07/14	142	4.21	312	2410	301	1.37	46.4	278	503	65.4	263	61.8	7.05	10.2	56.9	12.0	33.0	5.23	30.2	5.18	68.9	21.8	44.4	32.5	7.33
TT9712A/10	TT-12	22/07/14	140	3.52	329	2550	311	1.43	51.4	293	529	69.7	285	59.0	8.14	10.3	60.3	13.3	39.2	6.14	34.4	5.19	70.2	23.7	45.7	35.3	7.58
TT9712A/11	TT-12	22/07/14	137	4.21	304	2370	312	1.15	50.5	267	516	64.3	269	59.0	7.01	9.14	57.5	11.5	34.3	4.17	31.0	4.58	65.5	22.6	46.2	30.9	7.84
TT9712A/12	TT-12	22/07/14	139	3.24	309	2340	299	1.59	50.9	268	501	64.4	266	54.1	7.10	9.52	55.1	11.7	33.3	5.50	32.9	4.91	62.9	22.3	49.3	31.7	8.04
TT9712A/13	TT-12	22/07/14	144	4.48	341	2610	300	1.45	50.4	295	534	68.8	290	66.9	7.45	9.90	64.4	14.0	40.3	5.59	35.0	5.09	72.6	24.0	43.9	34.4	7.73
TT9712A/14	TT-12	22/07/14	140	3.49	286	2260	297	1.32	53.0	262	505	61.9	260	50.0	7.03	8.82	52.9	11.8	32.2	5.10	29.8	4.33	62.7	21.1	46.4	31.8	7.68
TT9712A/15	TT-12	22/07/14	138	2.67	299	2300	297	1.40	46.2	274	523	61.4	271	55.8	7.01	8.98	53.3	12.0	36.7	4.71	33.0	4.62	62.6	22.1	44.6	30.7	8.05
TT9712A/16	TT-12	22/07/14	143	3.78	313	2430	308	1.65	48.0	273	515	66.7	277	52.3	7.00	8.70	57.0	11.7	35.2	5.07	33.0	4.83	63.0	21.5	42.2	31.1	8.08
TT9712A/17	TT-12	22/07/14	142	4.35	326	2550	311	1.29	52.3	287	536	67.4	281	55.5	6.66	10.2	61.1	12.1	35.3	5.13	33.0	5.10	67.7	22.7	42.3	33.5	8.07
TT9712A/18	TT-12	22/07/14	142	5.69	331	2510	310	1.39	52.9	288	529	68.2	289	59.5	7.44	10.4	56.5	13.0	41.5	5.22	33.8	5.02	68.4	22.3	46.7	34.9	7.65
TT9712A/19	TT-12	22/07/14	149	8.87	343	2620	323	3.12	65.8	303	592	74.7	292	64.1	7.60	10.6	60.5	14.3	38.7	4.96	37.6	5.92	76.4	24.1	59.7	39.4	7.97
TT9712A/2	TT-12	22/07/14	137	6.30	337	2650	323	1.07	53.8	313	573	74.3	299	62.8	8.29	10.9	65.6	14.4	36.6	6.37	36.2	5.32	71.6	24.0	40.7	35.8	8.44
TT9712A/20	TT-12	22/07/14	146	4.40	304	2320	316	1.50	41.7	266	500	63.3	250	51.3	7.19	8.55	49.2	12.3	34.6	5.26	30.5	3.85	63.6	20.6	44.5	30.0	7.19
TT9712A/3	TT-12	22/07/14	137	2.60	309	2400	311	1.39	47.9	274	502	63.6	265	52.9	6.79	9.54	55.9	12.3	34.1	4.79	29.5	4.22	61.6	20.9	40.8	31.1	8.00
TT9712A/4	TT-12	22/07/14	135	3.22	290	2230	288	1.30	45.6	261	474	60.4	254	53.9	6.79	8.19	60.3	12.2	40.1	4.92	29.6	4.55	65.5	21.6	48.3	33.8	7.27
TT9712A/5	TT-12	22/07/14	134	7.16	331	2550	311	1.44	48.7	293	535	69.6	279	55.2	7.19	10.5	57.0	13.9	36.0	5.30	60.5	4.55	73.2	22.9	51.6	34.7	8.37
TT9712A/6	TT-12	22/07/14	140	3.83	330	2550	311	1.39	50.1	298	532	72.1	289	63.6	6.79	10.8	63.9	13.3	41.4	5.54	35.8	6.24	71.8	24.5	47.3	38.2	8.35
TT9712A/7	TT-12	22/07/14	140	3.10	331	2580	315	1.47	56.3	296	531	68.9	285	63.6	7.16	10.2	62.5	13.8	39.2	5.70	31.0	4.99	73.5	23.7	45.1	34.7	8.19
TT9712A/8	TT-12	22/07/14	143	4.47	304	2390	299	1.40	46.9	271	490	63.7	268	55.8	7.59	9.41	55.1	12.7	35.8	5.12	32.0	4.34	59.6	21.7	44.4	30.9	7.66
TT9712A/9	TT-12	22/07/14	141	5.50	322	2480	313	1.44	48.4	284	529	67.7	273	55.4	6.86	9.03	57.7	13.5	36.9	5.44	35.2	5.00	65.6	21.1	45.5	32.7	7.92
TT9712B/1	TT-12	22/07/14	141	4.54	269	2150	309	1.08	43.9	247	508	58.8	245	52.8	6.45	9.11	54.6	11.1	33.3	4.31	29.0	3.99	57.0	19.8	46.0	30.1	8.69
TT9712B/10	TT-12	22/07/14	141	3.58	270	2090	310	1.52	48.4	251	497	58.8	239	47.8	7.04	9.25	53.9	11.3	32.9	4.66	28.0	4.41	65.0	21.2	50.6	28.1	8.11
TT9712B/11	TT-12	22/07/14	123	3.91	238	1790	255	1.24	54.4	206	411	49.5	204	48.5	5.32	7.43	44.0	9.29	27.9	3.69	23.0	3.41	46.4	17.3	38.5	24.6	6.75
TT9712B/13	TT-12	22/07/14	138	3.65	261	1960	284	1.42	46.5	224	466	59.0	242	50.2	6.01	8.16	48.4	10.3	33.5	4.84	29.2	4.25	61.1	19.7	44.7	29.9	8.54
TT9712B/14	TT-12	22/07/14	148	4.05	252	1940	303	1.49	42.8	237	485	56.7	217	46.2	5.82	8.41	48.7	10.1	29.5	4.34	26.2	3.99	54.2	21.3	43.5	29.3	9.05
TT9712B/15	TT-12	22/07/14	140	4.33	271	2120	305	1.43	41.7	253	502	58.4	251	57.9	6.58	8.17	52.8	11.2	32.0	4.09	29.7	4.06	61.8	21.1	46.8	29.6	8.77
TT9712B/16	TT-12	22/07/14	145	2.94	293	2280	311	1.62	59.8	275	523	59.6	261	51.8	6.65	8.71	54.3	11.4	39.9	5.15	32.5	4.31	66.5	20.6	50.5	33.4	8.59
TT9712B/17	TT-12	22/07/14	144	6.05	362	2790	330	1.41	53.4	317	574	75.3	310	67.7	11.9	12.3	65.7	12.9	42.8	6.70	40.8	6.01	73.8	26.2	51.9	42.9	9.72
TT9712B/18	TT-12	22/07/14	129	3.10	256	1930	262	1.31	51.4	235	470	54.9	230	46.7	6.58	7.88	49.0	9.58	31.1	4.03	28.7	3.93	54.7	17.8	40.6	27.1	7.19
TT9712B/19	TT-12	22/07/14	149	2.01	291	2180	312	1.31	45.9	262	517	62.7	259	56.5	6.98	10.1	57.2	11.3	34.4	4.75	32.0	4.70	62.3	21.9	49.3	32.4	8.89
TT9712B/2	TT-12	22/07/14	144	4.90	278	2100	322	1.39	43.2	262	524	62.0	258	51.3	6.13	8.81	51.5	10.2	34.6	4.61	30.1	4.68	60.1	22.1	49.3	31.0	9.65
TT9712B/20	TT-12	22/07/14	140	5.07	327	2500	312	1.30	54.5	297	561	70.0	284	60.1	8.11	9.65	64.1	12.6	38.0	5.97	33.5	5.98	69.3	22.5	45.7	35.4	9.11
TT9712B/3	TT-12	22/07/14	142	5.51	293	2140	297	1.52	42.5	255	499	60.0	254	48.1	7.22	8.72	51.1	11.8	31.5	4.41	28.5	4.57	57.0	20.7	44.9	30.2	8.82
TT9712B/4	TT-12	22/07/14	142	4.71	280	2030	298	1.38	46.8	255	539	62.0	255	49.3	6.84	9.34	53.4	11.4	32.7	4.45	31.4	4.48	61.0	21.2	49.4	29.0	8.61
TT9712B/5	TT-12	22/07/14	142	3.56	253	1970	298	1.37	39.0	232	476	52.9	223	48.4	6.06	8.25	44.9	10.8	31.5	4.36	25.5	4.01	52.5	20.1	44.7	26.6	8.22
TT9712B/6	TT-12	22/07/14	136	3.07	271	2020	290	1.33	52.0	245	482	55.2	231	53.0	5.88	7.88	56.1	11.6	30.2	4.75	28.0	4.38	57.0	21.0	51.1	27.7	8.02
TT9712B/7	TT-12	22/07/14	139	3.33	266	2030	293	2.08	40.3	235	491	55.5	235	49.0	5.80	7.29	46.7	12.1	31.5	4.16	29.6	4.32	53.1	20.3	48.5	27.6	8.43
TT9712B/8	TT-12	22/07/14	138	4.61	306	2340	311	1.79	63.1	274	533	64.9	264	54.8	6.63	10.3	60.1	11.7	38.7	5.25	32.4	4.71	64.6	21.6	45.0	33.1	8.34
TT9712B/9	TT-12	22/07/14	141	4.68	267	1950	290	0.87	42.5	233	466	55.0	237	46.2	5.20	7.27	49.1	10.4	30.3	4.08	25.7	4.38	51.7	17.8	45.1	26.3	7.49

Continued on next page

Trace element concentrations (ppm) in Tilo tephra glass shards

Label	Tephra	Analysis date	Rb 0.62	Sr 1.05	Y 0.17	Zr 0.37	Nb 0.07	Cs 0.19	Ba 1.88	La 0.09	Ce 0.07	Pr 0.06	Nd 0.25	Sm 0.14	Eu 0.13	Tb 0.06	Dy 0.13	Ho 0.04	Er 0.07	Tm 0.05	Yb 0.15	Lu 0.04	Hf 0.08	Ta 0.06	Pb 0.12	Th 0.01	U 0.00
TT9712C/10	TT-12	22/07/14	133	1.99	324	2430	283	1.47	48.7	273	511	65.1	292	55.4	7.31	8.90	58.1	11.9	37.2	4.68	30.7	4.50	67.2	20.2	35.0	34.4	6.89
TT9712C/11	TT-12	22/07/14	129	6.12	327	2400	279	0.94	49.6	275	501	66.6	283	47.3	7.13	8.67	52.3	10.2	32.4	4.75	31.4	4.37	66.4	19.8	35.6	30.9	6.67
TT9712C/12	TT-12	22/07/14	132	6.68	287	2080	259	1.62	46.8	241	451	57.7	255	51.8	5.40	7.86	52.7	10.6	32.4	3.83	27.4	3.99	57.6	18.8	36.7	29.0	7.39
TT9712C/13	TT-12	22/07/14	127	2.15	278	2020	271	1.17	52.6	234	446	55.0	233	49.8	6.38	7.97	49.1	9.89	30.3	3.93	27.3	4.82	56.1	17.9	35.7	27.3	6.82
TT9712C/14	TT-12	22/07/14	126	4.93	328	2400	278	1.27	47.0	281	525	64.7	296	65.1	7.32	10.1	60.0	12.8	36.7	5.12	33.1	5.06	63.0	20.8	34.7	32.7	7.23
TT9712C/15	TT-12	22/07/14	132	2.48	297	2190	263	1.23	56.0	254	457	58.7	253	56.5	6.87	8.60	51.3	9.89	33.1	3.62	29.7	4.15	61.7	18.7	34.0	30.3	6.77
TT9712C/16	TT-12	22/07/14	135	5.50	340	2460	283	1.48	49.5	291	491	67.4	307	62.9	7.66	9.28	62.4	11.4	34.1	5.43	29.8	5.83	63.6	21.0	37.9	32.9	7.03
TT9712C/17	TT-12	22/07/14	154	4.16	394	2810	318	1.39	36.3	323	566	76.7	326	65.6	7.19	11.0	67.5	13.4	43.5	7.31	36.7	6.01	77.8	22.8	48.8	39.9	8.18
TT9712C/18	TT-12	22/07/14	128	3.88	308	2220	280	1.08	44.7	257	461	57.3	265	56.4	6.55	8.20	55.6	11.5	30.8	4.06	33.4	4.53	64.1	19.8	36.0	29.3	7.15
TT9712C/19	TT-12	22/07/14	132	7.79	297	2220	261	2.23	53.0	249	431	57.3	254	46.2	6.45	8.47	53.8	11.6	33.8	4.69	28.7	4.25	63.7	19.6	37.7	30.1	6.40
TT9712C/2	TT-12	22/07/14	132	5.27	311	2390	273	1.33	52.9	273	479	63.4	274	55.9	7.21	9.63	59.7	11.4	34.5	6.64	32.5	5.26	67.0	19.4	37.4	31.4	6.80
TT9712C/20	TT-12	22/07/14	130	6.70	351	2500	304	1.43	49.5	299	519	67.3	295	65.0	8.02	10.4	65.9	13.1	38.4	5.57	35.9	4.64	75.0	21.1	38.2	35.6	7.24
TT9712C/3	TT-12	22/07/14	135	3.26	310	2300	280	1.05	65.3	265	476	62.8	264	57.0	6.78	9.42	61.3	11.6	34.9	4.73	33.7	4.70	68.1	19.6	39.3	31.1	7.09
TT9712C/4	TT-12	22/07/14	132	4.89	324	2400	289	1.28	50.0	272	497	65.0	279	54.0	7.32	9.59	58.9	12.7	39.2	5.29	31.9	5.05	68.1	21.4	41.1	32.5	7.54
TT9712C/5	TT-12	22/07/14	127	4.45	307	2270	278	1.30	46.2	267	468	60.4	271	53.8	6.91	8.67	57.6	11.9	35.2	5.80	30.0	5.36	61.4	19.2	34.5	29.7	7.15
TT9712C/6	TT-12	22/07/14	122	3.63	300	2260	264	1.14	44.1	261	453	60.3	261	53.7	6.39	9.41	54.2	11.4	29.6	4.22	31.0	4.66	61.5	18.0	34.6	30.6	7.09
TT9712C/7	TT-12	22/07/14	124	3.53	292	2180	258	1.23	61.5	251	438	57.4	249	51.3	6.47	8.42	55.8	10.9	35.2	4.00	28.7	4.43	63.7	18.0	35.6	30.2	6.42
TT9712C/8	TT-12	22/07/14	139	6.14	346	2520	310	1.24	35.5	291	519	66.9	292	55.9	7.00	9.36	63.0	12.5	41.5	5.38	32.8	4.72	69.5	21.7	41.5	34.8	7.74
TT9712C/9	TT-12	22/07/14	126	4.36	293	2120	283	1.47	44.6	244	469	57.0	256	53.5	6.64	8.47	50.5	10.8	35.2	4.38	30.5	4.03	59.7	19.2	36.4	28.8	7.12
TT97-13_1	TT-13	20/01/15	147	6.83	362	2970	336	1.47	45.1	311	540	71.9	292	58.2	7.83	8.90	69.1	12.7	39.0	4.92	37.6	4.40	73.5	25.4	52.2	37.0	8.35
TT97-13_10	TT-13	20/01/15	147	9.59	345	2950	340	1.40	53.8	316	546	71.3	293	59.3	7.41	10.2	67.8	13.7	37.5	5.52	35.4	5.18	74.6	24.5	55.2	37.1	8.19
TT97-13_11	TT-13	20/01/15	139	11.6	334	2840	327	1.43	58.3	302	521	68.5	284	58.2	7.82	10.0	60.7	12.3	38.9	5.35	35.3	5.14	70.9	23.5	47.8	35.4	8.13
TT97-13_12	TT-13	20/01/15	149	5.01	343	2880	342	1.34	48.9	306	542	71.0	300	62.8	7.71	10.0	63.3	12.7	39.5	5.61	33.6	5.04	75.3	23.7	92.3	36.5	8.48
TT97-13_13	TT-13	20/01/15	141	3.72	333	2800	324	1.31	51.1	294	514	66.5	287	55.0	7.84	10.0	59.2	12.2	35.6	5.49	34.0	5.13	69.9	22.5	45.3	34.7	8.13
TT97-13_14	TT-13	20/01/15	132	3.79	322	2740	313	1.31	44.6	287	496	64.5	268	52.9	6.82	9.12	59.5	12.7	35.2	4.87	30.6	4.45	64.2	21.2	41.0	31.7	7.52
TT97-13_15	TT-13	20/01/15	146	5.52	356	2940	339	1.64	55.1	313	540	72.7	289	59.6	8.39	10.1	64.2	13.3	37.1	5.57	36.3	5.25	69.9	24.7	56.8	36.9	8.40
TT97-13_16	TT-13	20/01/15	134	3.73	335	2790	315	1.47	57.0	294	509	66.6	279	55.4	7.76	9.50	56.9	12.0	35.5	5.08	34.5	4.63	66.3	21.8	42.1	32.4	7.36
TT97-13_17	TT-13	20/01/15	144	5.04	383	3220	353	1.57	54.6	344	578	79.0	326	66.7	8.17	10.8	70.1	13.8	41.3	5.96	38.5	5.99	79.3	25.3	44.9	38.6	8.44
TT97-13_18	TT-13	20/01/15	147	4.59	367	3040	353	1.41	50.5	319	553	73.6	304	67.5	7.20	10.5	65.6	13.5	37.9	5.85	37.8	5.51	77.4	25.4	48.1	38.6	8.57
TT97-13_19	TT-13	20/01/15	147	4.76	367	3040	335	1.36	57.8	334	555	74.9	326	64.0	9.02	9.86	65.1	13.8	41.0	6.18	36.7	5.57	78.4	25.7	49.5	38.7	8.54
TT97-13_2	TT-13	20/01/15	137	9.63	354	2890	313	2.35	58.5	318	538	73.9	309	63.1	8.89	9.54	59.5	12.8	38.8	5.72	37.6	5.03	73.2	24.1	42.4	36.7	8.66
TT97-13_20	TT-13	20/01/15	160	8.24	389	3240	361	1.62	55.7	342	581	77.5	324	64.5	8.14	10.1	66.4	14.1	42.0	5.21	36.5	5.60	74.4	24.6	48.7	36.8	8.74
TT97-13_3	TT-13	20/01/15	134	4.25	300	2460	317	1.35	50.5	264	487	63.6	259	49.7	6.37	8.57	55.8	10.7	33.8	4.54	29.7	4.07	59.9	21.4	52.9	30.4	7.56
TT97-13_4	TT-13	20/01/15	177	3.90	357	3010	334	1.78	56.6	312	548	74.7	299	62.1	8.16	10.4	66.7	13.3	39.9	5.82	36.6	5.30	77.3	25.0	51.7	37.2	8.32
TT97-13_6	TT-13	20/01/15	141	4.17	361	2990	339	0.93	59.1	319	555	73.9	311	59.7	8.37	10.6	69.8	13.7	38.7	5.77	40.3	5.34	76.5	24.1	47.6	37.3	7.85
TT97-13_7	TT-13	20/01/15	145	5.71	432	3460	347	1.68	70.1	367	594	82.0	337	72.4	9.93	10.9	73.7	14.3	43.0	5.62	41.3	5.92	79.9	24.5	79.4	40.6	9.16
TT97-13_8	TT-13	20/01/15	149	11.7	354	2950	343	1.25	49.9	313	543	70.9	308	64.3	7.93	9.73	65.6	13.2	38.5	5.44	37.7	5.51	73.3	25.0	50.9	39.0	8.78
TT97-13_9	TT-13	20/01/15	135	6.44	362	3080	329	2.70	68.5	333	557	74.8	317	62.7	8.34	11.2	71.6	14.6	41.9	5.89	37.9	5.58	78.9	24.7	54.0	39.1	8.48
TT97-14A_1	TT-14	20/01/15	130	3.02	303	2540	304	1.13	52.7	265	469	60.6	258	55.4	7.79	8.42	56.6	10.9	34.8	4.53	31.3	4.58	61.2	21.3	42.2	30.4	8.16
TT97-14A_10	TT-14	20/01/15	140	4.97	285	2400	299	1.28	61.8	248	463	56.3	247	48.9	5.89	7.56	48.9	10.2	31.5	4.17	27.9	4.16	55.4	19.9	46.6	28.2	7.16
TT97-14A_11	TT-14	20/01/15	136	4.94	293	2470	290	1.50	55.6	256	483	59.0	242	52.6	6.77	8.66	51.0	10.6	33.6	4.42	28.5	3.82	56.9	19.6	41.5	28.9	8.23
TT97-14A_12	TT-14	20/01/15	138	4.34	283	2420	304	1.06	56.8	247	464	60.9	237	47.0	7.10	7.78	48.2	10.6	33.1	4.04	25.6	3.29	54.0	19.1	42.6	28.7	7.32
TT97-14A_13	TT-14	20/01/15	150	9.06	318	2730	321	1.94	61.5	281	523	66.3	268	53.2	7.37	9.06	56.4	11.9	33.5	4.23	28.8	4.39	66.5	21.4	50.2	31.6	7.67
TT97-14A_14	TT-14	20/01/15	133	3.67	289	2470	293	1.38	55.1	263	479	61.6	246	51.7	6.94	7.34	50.7	10.6	33.3	4.70	29.4	4.11	60.2	19.6	45.7	30.1	7.28

Continued on next page

Trace element concentrations (ppm) in Tilo tephra glass shards

Label	Tephra	Analysis date	Rb 0.62	Sr 1.05	Y 0.17	Zr 0.37	Nb 0.07	Cs 0.19	Ba 1.88	La 0.09	Ce 0.07	Pr 0.06	Nd 0.25	Sm 0.14	Eu 0.13	Tb 0.06	Dy 0.13	Ho 0.04	Er 0.07	Tm 0.05	Yb 0.15	Lu 0.04	Hf 0.08	Ta 0.06	Pb 0.12	Th 0.01	U 0.00
TT97-14A_15	TT-14	20/01/15	141	4.45	315	2650	320	1.38	58.2	278	516	63.2	250	52.7	6.95	8.68	56.9	10.2	30.9	4.34	30.0	4.77	59.2	21.0	44.4	30.9	7.81
TT97-14A_16	TT-14	20/01/15	156	4.20	288	2470	305	1.67	52.5	252	497	59.8	224	50.3	6.34	8.11	48.7	10.4	30.1	4.33	29.4	4.22	57.6	20.0	47.9	29.4	8.54
TT97-14A_17	TT-14	20/01/15	142	7.45	290	2490	314	1.71	56.9	256	472	59.4	242	51.7	6.48	8.23	48.8	9.40	29.5	4.19	27.6	3.39	54.1	20.3	48.6	29.8	7.39
TT97-14A_18	TT-14	20/01/15	143	2.36	287	2380	291	1.44	64.6	258	476	59.6	234	46.6	7.28	7.89	52.6	10.3	28.2	3.94	26.8	3.86	57.9	19.3	46.0	29.2	7.70
TT97-14A_19	TT-14	20/01/15	136	5.23	319	2700	313	1.22	60.7	290	528	64.0	273	58.0	7.60	9.17	57.9	12.2	35.9	4.68	34.2	4.87	69.0	21.7	45.7	33.2	16.3
TT97-14A_2	TT-14	20/01/15	139	5.13	280	2340	293	1.28	53.0	246	467	57.7	232	48.3	6.35	8.17	46.9	9.99	30.2	4.10	25.8	3.94	56.9	18.5	80.5	28.2	7.57
TT97-14A_20	TT-14	20/01/15	140	4.13	296	2560	300	1.22	52.4	268	484	60.7	244	48.6	5.94	8.04	54.7	11.0	32.1	4.34	27.9	4.73	55.3	19.7	40.8	29.3	7.93
TT97-14A_3	TT-14	20/01/15	148	4.83	299	2490	308	1.61	59.7	265	487	61.2	249	52.9	6.88	9.14	52.1	11.3	33.3	5.52	32.7	4.33	60.9	21.5	55.5	30.9	7.56
TT97-14A_4	TT-14	20/01/15	136	5.41	301	2490	306	1.55	58.5	263	483	60.2	241	51.1	6.60	8.12	51.0	10.2	29.0	4.27	28.8	4.12	55.4	20.9	44.2	29.0	7.56
TT97-14A_6	TT-14	20/01/15	137	2.44	285	2390	334	1.44	57.6	254	478	58.4	256	51.2	7.38	8.24	48.4	10.8	31.7	4.17	29.7	4.30	58.0	20.3	43.9	27.6	7.64
TT97-14A_8	TT-14	20/01/15	133	4.82	284	2430	292	1.12	56.1	257	500	60.7	245	47.3	6.82	8.97	54.3	10.8	29.8	4.02	29.7	4.44	56.1	19.4	43.6	30.3	7.95
TT97-14A_9	TT-14	20/01/15	128	4.57	313	2680	291	1.47	57.4	276	485	63.3	276	55.7	7.46	8.94	53.9	11.7	33.3	4.86	31.6	4.75	61.3	20.6	39.8	32.2	6.85
TT97-14B_1	TT-14	20/01/15	148	5.84	301	2400	314	1.41	67.9	272	526	65.3	268	55.8	7.36	9.03	56.7	11.8	33.5	4.94	31.7	4.48	56.8	21.0	49.6	29.8	7.97
TT97-14B_10	TT-14	20/01/15	145	4.48	262	2200	320	1.64	54.4	243	491	60.5	243	50.8	6.57	8.44	54.3	9.70	30.6	4.58	27.6	4.10	55.5	20.1	51.8	28.5	9.05
TT97-14B_11	TT-14	20/01/15	143	13.0	256	2150	298	1.43	56.0	229	466	56.8	230	49.5	5.75	7.75	43.4	9.61	29.8	4.18	25.8	4.10	48.2	18.8	65.0	28.5	8.80
TT97-14B_13	TT-14	20/01/15	150	3.57	239	2030	279	1.55	46.9	212	458	52.4	205	43.1	4.95	6.76	41.3	8.23	25.9	3.24	24.1	3.50	49.3	17.9	45.9	25.1	8.06
TT97-14B_14	TT-14	20/01/15	147	2.26	271	2250	298	1.28	51.1	239	497	58.4	233	54.1	7.06	7.89	58.0	10.1	31.0	4.21	28.0	4.40	59.2	21.1	48.9	29.4	8.54
TT97-14B_15	TT-14	20/01/15	145	3.39	282	2280	306	1.29	53.3	249	494	60.4	245	50.0	6.33	8.05	47.8	9.83	29.1	4.04	29.2	4.04	54.0	19.6	45.6	29.1	7.93
TT97-14B_17	TT-14	20/01/15	147	4.16	277	2280	295	1.38	51.9	252	473	57.7	236	48.3	6.76	7.80	52.8	10.7	28.1	4.05	29.3	3.86	54.7	19.2	42.4	28.3	7.77
TT97-14B_18	TT-14	20/01/15	141	5.85	296	2400	294	1.49	59.1	268	515	61.1	251	54.0	6.65	8.63	52.4	11.0	33.5	4.90	29.9	4.11	57.6	20.5	45.3	30.7	8.62
TT97-14B_19	TT-14	20/01/15	147	4.45	280	2320	289	1.66	60.4	243	475	59.1	240	46.8	6.25	7.44	51.2	8.99	27.1	3.89	28.0	4.49	57.0	19.0	42.7	28.4	7.69
TT97-14B_2	TT-14	20/01/15	148	16.3	257	2210	317	1.79	47.7	242	486	57.3	242	52.3	5.96	8.41	51.8	9.83	29.2	4.29	27.8	3.90	56.6	19.0	53.4	28.7	9.31
TT97-14B_20	TT-14	20/01/15	147	6.85	256	2090	290	1.45	49.8	231	464	54.0	223	46.2	6.12	7.31	44.8	9.31	28.9	3.85	25.4	3.86	51.7	18.8	48.4	26.6	8.49
TT97-14B_3	TT-14	20/01/15	152	3.69	284	2320	308	1.83	46.4	258	508	61.8	249	50.1	7.58	8.42	51.7	10.6	31.8	4.18	30.2	4.27	55.7	21.6	55.2	32.7	9.30
TT97-14B_5	TT-14	20/01/15	155	23.5	289	2450	310	1.16	50.5	253	509	60.4	242	49.8	6.99	8.52	48.2	10.6	33.6	4.41	29.9	4.25	58.2	20.3	52.3	29.9	8.79
TT97-14B_6	TT-14	20/01/15	147	4.42	283	2350	306	0.98	55.5	250	487	58.6	244	49.3	7.00	8.16	50.6	10.7	32.0	4.47	27.1	4.40	57.5	20.3	49.4	28.6	8.27
TT97-14B_8	TT-14	20/01/15	136	4.92	266	2200	276	1.33	53.7	227	454	52.5	218	44.5	6.79	7.14	44.4	10.1	29.5	3.80	25.8	3.41	54.2	18.3	41.5	26.4	6.72
TT97-14C_1	TT-14	20/01/15	141	3.35	287	2350	300	1.27	52.6	258	490	60.9	245	52.0	7.03	9.11	52.5	10.6	33.0	4.38	29.6	3.80	58.7	21.5	44.9	31.6	8.19
TT97-14C_10	TT-14	20/01/15	142	5.00	304	2520	316	1.13	56.5	275	518	62.6	261	50.4	6.91	8.49	55.1	11.3	31.9	4.47	27.4	4.24	62.3	21.4	40.8	31.5	7.78
TT97-14C_11	TT-14	20/01/15	137	4.49	301	2470	305	1.25	56.8	268	511	63.6	261	59.3	6.44	8.62	55.7	11.7	32.8	4.26	31.4	4.12	58.0	21.8	43.1	31.0	7.99
TT97-14C_12	TT-14	20/01/15	137	4.47	271	2220	295	1.40	63.7	252	460	56.0	239	48.9	6.29	7.68	50.1	9.88	31.8	4.47	25.2	3.83	56.5	19.8	54.8	30.3	7.90
TT97-14C_13	TT-14	20/01/15	137	5.27	302	2420	304	1.43	62.3	269	492	60.7	258	52.3	6.83	8.45	50.6	10.4	32.4	5.03	29.7	4.26	60.0	20.5	43.6	31.0	7.90
TT97-14C_14	TT-14	20/01/15	137	4.00	294	2390	298	1.40	53.3	260	481	59.1	261	51.3	5.87	8.34	53.4	10.8	29.2	3.99	28.4	3.72	57.6	19.5	39.8	29.7	6.57
TT97-14C_15	TT-14	20/01/15	137	4.20	293	2360	297	1.27	59.6	259	476	58.4	264	53.1	6.14	8.66	52.8	11.9	32.8	4.29	29.0	4.16	56.1	20.1	41.2	29.4	7.80
TT97-14C_16	TT-14	20/01/15	141	3.88	336	2750	335	1.61	61.4	302	562	71.9	289	61.5	8.12	9.92	58.9	12.8	37.5	5.18	35.9	4.96	72.1	24.0	43.9	33.9	8.46
TT97-14C_17	TT-14	20/01/15	135	3.66	303	2510	312	1.36	52.6	272	517	62.7	275	58.5	7.84	9.26	55.2	12.2	33.6	4.66	30.9	4.98	63.9	22.5	41.8	33.3	9.21
TT97-14C_18	TT-14	20/01/15	128	4.29	277	2300	277	1.15	73.1	253	465	59.0	244	52.5	6.72	8.09	50.7	10.7	31.2	4.00	30.4	3.89	60.4	19.8	37.5	31.6	6.88
TT97-14C_19	TT-14	20/01/15	129	6.49	293	2390	295	1.20	51.8	261	476	59.1	256	50.8	6.91	8.40	51.5	10.8	33.9	4.47	26.8	4.02	56.0	20.4	52.0	30.5	7.27
TT97-14C_20	TT-14	20/01/15	134	6.73	345	2700	313	1.67	74.1	300	530	69.4	295	61.5	8.04	10.0	63.1	13.1	37.2	5.73	35.3	5.42	69.0	23.2	39.5	37.2	7.62
TT97-14C_3	TT-14	20/01/15	125	4.26	281	2290	264	1.24	47.8	256	446	60.8	253	51.5	7.34	8.16	54.0	11.2	30.3	4.28	27.7	4.65	58.5	19.8	41.0	30.8	9.75
TT97-14C_4	TT-14	20/01/15	140	9.55	297	2480	328	2.05	53.2	279	524	64.0	266	53.0	6.87	9.13	52.4	10.3	32.3	4.78	30.0	4.07	57.2	21.2	47.1	29.2	7.48
TT97-14C_5	TT-14	20/01/15	131	5.91	278	2250	290	1.25	48.1	248	472	57.6	242	45.4	6.21	8.48	52.2	10.3	31.7	5.04	28.0	4.19	54.8	19.8	41.2	29.4	7.58
TT97-14C_6	TT-14	20/01/15	151	3.40	276	2300	302	1.58	49.8	247	474	56.3	243	49.4	6.08	8.78	47.3	9.21	28.6	4.07	26.9	4.14	57.0	19.8	54.2	29.1	8.34
TT97-14C_7	TT-14	20/01/15	134	3.99	339	2670	309	1.59	65.8	295	526	68.7	291	56.3	7.47	9.35	54.4	11.8	35.9	4.97	29.2	4.63	63.9	22.5	40.1	32.0	7.19

Continued on next page

Trace element concentrations (ppm) in Tilo tephra glass shards

Label	Tephra	Analysis date	Rb	Sr	Y	Zr	Nb	Cs	Ba	La	Ce	Pr	Nd	Sm	Eu	Tb	Dy	Ho	Er	Tm	Yb	Lu	Hf	Ta	Pb	Th	U
			0.62	**1.05**	**0.17**	**0.37**	**0.07**	**0.19**	**1.88**	**0.09**	**0.07**	**0.06**	**0.25**	**0.14**	**0.13**	**0.06**	**0.13**	**0.04**	**0.07**	**0.05**	**0.15**	**0.04**	**0.08**	**0.06**	**0.12**	**0.01**	**0.00**
TT97-14C_8	TT-14	20/01/15	144	5.02	325	2640	318	1.53	54.2	280	506	63.4	261	54.1	6.26	8.54	54.6	11.5	32.1	4.55	30.5	4.70	62.2	20.5	40.7	31.3	7.66
TT97-14C_9	TT-14	20/01/15	140	5.13	282	2340	306	1.22	59.3	253	481	58.0	243	49.2	6.49	8.09	51.2	9.97	33.2	4.29	28.1	3.97	60.4	19.2	41.6	28.2	7.90

Unnormalised major element concentrations (wt.%) in Awassa tephra glass shards

Label	Tephra	Analysis date	SiO_2 0.08	TiO_2 0.05	Al_2O_3 0.05	MgO 0.04	FeO^T 0.08	MnO 0.07	CaO 0.04	Na_2O 0.08	K_2O 0.03	P_2O_5 0.10	Cl 0.02	Total
AT-1_1	AWT-1	26/08/14	71.52	0.24	9.95	0.00	3.50	0.14	0.23	4.21	4.56	0.00		94.35
AT-1_11	AWT-1	26/08/14	72.30	0.26	10.27	0.01	3.74	0.17	0.17	4.26	4.39	0.00		95.57
AT-1_12	AWT-1	26/08/14	71.11	0.26	10.17	0.00	3.54	0.13	0.20	4.27	4.47	0.03		94.18
AT-1_13	AWT-1	26/08/14	74.66	0.26	10.42	0.02	3.72	0.15	0.19	4.70	4.46	0.00		98.57
AT-1_14	AWT-1	26/08/14	74.33	0.24	9.75	0.00	4.37	0.21	0.19	5.25	4.54	0.00		98.89
AT-1_15	AWT-1	26/08/14	71.13	0.26	8.88	0.01	5.10	0.25	0.22	4.86	4.29	0.00		94.99
AT-1_16	AWT-1	26/08/14	72.00	0.22	9.82	0.00	3.79	0.20	0.22	4.90	4.35	0.00		95.51
AT-1_18	AWT-1	26/08/14	69.94	0.06	15.07	0.03	2.15	0.04	0.07	5.43	7.08	0.02		99.91
AT-1_3	AWT-1	26/08/14	69.93	0.18	9.57	0.01	3.69	0.19	0.18	4.71	4.16	0.00		92.63
AT-1_4	AWT-1	26/08/14	71.57	0.30	9.41	0.01	5.83	0.31	0.29	5.76	4.31	0.00		97.78
AT-1_5	AWT-1	26/08/14	66.45	0.01	19.03	0.00	0.52	0.00	0.01	6.13	7.32	0.00		99.47
AT-1_6	AWT-1	26/08/14	67.56	0.18	8.95	0.05	5.96	0.33	0.27	5.48	3.95	0.00		92.72
AT-1_7	AWT-1	26/08/14	68.73	0.22	9.64	0.02	3.81	0.12	0.21	4.29	4.56	0.02		91.61
AT-1_8	AWT-1	26/08/14	74.25	0.26	9.93	0.00	4.75	0.16	0.19	5.09	4.86	0.00		99.50
AT-1_9	AWT-1	26/08/14	69.62	0.23	9.60	0.00	3.73	0.21	0.21	3.19	5.94	0.02		92.76
AT-2_1	AWT-2	26/08/14	71.66	0.17	9.16	0.00	4.47	0.27	0.18	5.09	4.19	0.03		95.23
AT-2_11	AWT-2	26/08/14	72.42	0.20	9.33	0.02	4.33	0.22	0.19	4.98	4.16	0.00		95.86
AT-2_12	AWT-2	26/08/14	71.31	0.18	9.37	0.01	4.27	0.17	0.22	4.68	4.17	0.01		94.37
AT-2_13	AWT-2	26/08/14	71.15	0.19	8.92	0.01	4.42	0.26	0.20	4.91	4.28	0.04		94.38
AT-2_15	AWT-2	26/08/14	71.98	0.28	9.09	0.00	4.36	0.24	0.19	4.33	4.10	0.01		94.60
AT-2_16	AWT-2	26/08/14	71.37	0.23	9.16	0.00	4.18	0.26	0.17	5.10	4.22	0.02		94.70
AT-2_17	AWT-2	26/08/14	73.09	0.23	9.31	0.01	4.32	0.24	0.17	4.73	4.21	0.00		96.31
AT-2_18	AWT-2	26/08/14	71.91	0.24	9.15	0.00	4.35	0.16	0.18	4.84	4.49	0.01		95.32
AT-2_19	AWT-2	26/08/14	71.69	0.20	9.26	0.00	4.42	0.21	0.20	4.93	4.26	0.00		95.18
AT-2_2	AWT-2	26/08/14	70.61	0.25	8.80	0.00	4.43	0.18	0.19	5.25	4.12	0.04		93.86
AT-2_3	AWT-2	26/08/14	70.05	0.22	8.89	0.01	4.14	0.27	0.17	5.02	4.27	0.02		93.05
AT-2_4	AWT-2	26/08/14	71.26	0.23	9.02	0.00	4.64	0.19	0.17	5.15	4.20	0.00		94.85
AT-2_8	AWT-2	26/08/14	70.82	0.22	9.14	0.00	4.34	0.20	0.18	4.74	4.32	0.06		94.02
AT-2_9	AWT-2	26/08/14	70.02	0.23	8.87	0.00	4.24	0.23	0.20	5.17	4.27	0.02		93.26
AWT_2002_1	AWT-4	29/06/15	72.31	0.20	9.55	0.00	4.59	0.18	0.15	5.09	4.29	0.05	0.24	96.65
AWT_2002_2	AWT-4	29/06/15	73.36	0.27	9.66	0.03	4.70	0.21	0.17	5.42	4.41	0.02	0.25	98.51
AWT_2002_3	AWT-4	29/06/15	72.91	0.20	9.12	0.05	4.62	0.22	0.19	4.81	4.41	0.00	0.22	96.74
AWT_2002_4	AWT-4	29/06/15	73.26	0.28	9.38	0.02	4.67	0.21	0.20	4.93	4.42	0.02	0.24	97.63
AWT_2002_5	AWT-4	29/06/15	72.34	0.27	9.35	0.00	4.36	0.19	0.23	5.06	4.16	0.00	0.26	96.20
AWT_2002_6	AWT-4	29/06/15	71.32	0.22	9.13	0.00	4.31	0.21	0.20	5.05	4.27	0.02	0.22	94.95
AWT_2002_7	AWT-4	29/06/15	73.32	0.22	9.39	0.06	4.54	0.23	0.28	5.05	4.09	0.03	0.22	97.42
AWT_2002_8	AWT-4	29/06/15	72.94	0.21	9.42	0.02	4.72	0.17	0.18	5.23	4.40	0.00	0.26	97.56
AWT_2002_9	AWT-4	29/06/15	71.78	0.23	9.21	0.09	5.17	0.28	0.51	4.98	4.03	0.04	0.23	96.56
AWT_2002_10	AWT-4	29/06/15	71.67	0.24	9.20	0.00	4.57	0.23	0.18	4.96	4.35	0.00	0.21	95.60

Trace element concentrations (ppm) in Awassa tephra glass shards

Label	Tephra	Analysis date	Rb 0.62	Sr 1.05	Y 0.17	Zr 0.37	Nb 0.07	Cs 0.19	Ba 1.88	La 0.09	Ce 0.07	Pr 0.06	Nd 0.25	Sm 0.14	Eu 0.13	Tb 0.06	Dy 0.13	Ho 0.04	Er 0.07	Tm 0.05	Yb 0.15	Lu 0.04	Hf 0.08	Ta 0.06	Pb 0.12	Th 0.01	U 0.00
AT-1_1	AWT-1	13/01/15	138	5.28	168	1320	171	1.04	330	188	348	42.3	187	33.1	3.76	5.15	31.0	7.11	21.4	2.97	18.6	2.82	36.4	13.0	32.1	16.9	5.85
AT-1_11	AWT-1	13/01/15	134	7.93	227	1790	217	0.96	229	211	392	48.7	213	41.5	6.04	6.51	42.3	9.45	27.5	3.72	22.6	3.90	48.4	15.4	31.9	23.2	5.42
AT-1_12	AWT-1	13/01/15	114	5.53	187	1510	191	0.87	193	209	375	46.7	202	37.3	5.23	5.74	32.3	7.80	23.1	3.15	20.5	2.90	42.9	13.8	31.3	19.0	5.01
AT-1_13	AWT-1	13/01/15	254	5.97	174	1300	179	1.56	240	194	380	44.4	197	34.5	4.73	6.01	34.8	8.50	24.4	2.93	19.7	3.11	41.7	14.0	41.4	20.3	7.25
AT-1_14	AWT-1	13/01/15	148	4.02	237	1910	246	1.32	86.9	234	440	53.9	239	47.1	6.25	7.73	42.7	10.1	27.8	4.07	24.8	3.91	52.9	17.9	40.9	26.2	7.35
AT-1_15	AWT-1	13/01/15	122	0.74	195	1600	211	1.15	29.7	187	336	41.7	178	37.3	4.61	5.33	37.7	8.02	22.4	2.98	19.4	3.24	44.0	13.9	30.1	22.2	5.54
AT-1_16	AWT-1	13/01/15	111	4.79	229	1820	209	1.03	276	221	408	48.7	214	43.0	4.81	6.15	42.6	8.70	24.7	3.74	22.5	3.45	46.5	16.0	31.5	22.5	5.40
AT-1_18	AWT-1	13/01/15	129	3.68	223	1840	230	1.14	68.6	213	393	48.2	201	43.5	4.74	7.09	36.3	8.51	23.8	3.43	21.6	3.56	43.4	15.3	37.1	22.0	6.03
AT-1_3	AWT-1	13/01/15	176	7.79	201	1540	253	1.05	481	232	428	50.9	208	39.6	6.80	6.73	37.6	8.56	24.2	3.52	22.3	3.25	44.4	18.6	58.8	31.1	8.98
AT-1_4	AWT-1	13/01/15	144	3.42	126	1050	177	0.86	267	153	272	31.6	147	25.0	4.18	4.40	23.6	5.52	15.8	2.40	13.9	2.26	31.5	13.0	88.7	21.0	6.52
AT-1_5	AWT-1	13/01/15	180	7.49	205	1610	260	1.31	471	238	437	51.9	224	39.7	7.64	6.63	39.2	9.31	27.1	3.52	20.5	3.28	45.8	18.6	39.9	29.8	8.63
AT-1_6	AWT-1	13/01/15	154	5.76	218	1800	220	1.20	251	215	411	49.4	205	42.3	5.26	6.72	40.4	9.37	25.1	3.43	23.0	3.69	46.6	15.9	40.8	22.4	6.48
AT-1_7	AWT-1	13/01/15	138	4.90	210	1710	205	1.04	246	210	379	46.8	191	39.6	4.02	6.46	35.8	8.61	25.9	3.17	20.6	3.41	43.6	14.2	36.1	20.7	5.87
AT-1_8	AWT-1	13/01/15	149	3.86	222	1760	232	1.29	93.3	220	404	49.7	219	43.1	5.41	6.59	41.4	8.00	25.6	3.30	21.7	3.54	48.0	15.6	41.0	23.6	6.55
AT-1_9	AWT-1	13/01/15	126	7.36	215	1720	196	1.27	287	219	399	50.7	206	39.6	4.52	6.81	36.9	8.80	25.7	3.48	22.3	3.56	45.8	14.9	34.3	21.3	5.63
AT-2_1	AWT-2	13/01/15	142	4.75	285	1940	250	1.22	75.8	265	403	55.6	255	64.9	6.29	7.67	46.6	10.2	28.2	3.41	27.1	5.04	52.7	18.7	46.0	26.3	8.48
AT-2_11	AWT-2	13/01/15	137	3.22	260	1910	262	1.22	71.8	232	403	52.2	243	49.2	6.15	6.80	44.4	9.19	27.0	4.16	23.5	3.95	47.3	16.9	43.9	24.2	6.77
AT-2_12†	AWT-2	13/01/15	144	6.21	302	1620	238	1.61	62.7	238	317	42.0	238	62.5	4.99	7.02	48.9	8.93	27.3	5.05	31.0	4.57	54.3	18.7	55.0	24.3	13.3
AT-2_13	AWT-2	13/01/15	138	5.51	282	2140	272	3.18	76.7	252	482	56.2	257	51.5	7.67	6.13	47.9	11.9	30.1	4.89	27.9	4.32	62.6	21.1	57.5	27.8	7.25
AT-2_15†	AWT-2	13/01/15	140	2.78	283	2060	266	1.67	68.4	232	426	47.3	233	42.4	5.27	6.76	48.3	9.80	22.8	3.97	26.1	3.58	47.5	18.3	40.8	24.3	6.89
AT-2_16	AWT-2	13/01/15	140	4.00	288	2140	272	1.50	85.8	268	461	59.1	269	54.0	6.76	8.81	49.2	10.1	27.9	5.01	29.7	4.16	55.1	18.6	42.6	26.9	6.46
AT-2_17	AWT-2	13/01/15	118	4.72	227	1760	237	1.03	63.6	219	391	47.8	215	42.6	5.43	7.12	40.0	8.48	25.5	3.34	22.6	3.32	43.9	15.8	38.5	23.3	6.47
AT-2_18	AWT-2	13/01/15	137	5.50	318	2380	287	1.04	76.6	282	469	62.5	280	53.3	6.82	8.91	54.5	11.7	32.2	4.04	29.0	4.57	58.0	20.3	43.8	29.1	7.33
AT-2_19	AWT-2	13/01/15	113	2.89	253	1920	221	1.29	74.9	228	373	49.6	237	42.3	4.84	7.79	42.6	9.28	24.3	4.06	23.4	3.32	44.1	13.9	33.1	22.5	5.23
AT-2_2	AWT-2	13/01/15	136	3.57	233	1610	248	1.10	69.2	211	354	45.5	227	47.4	4.34	6.51	39.8	7.79	23.6	3.23	20.7	3.58	45.6	18.1	50.5	22.2	8.01
AT-2_3†	AWT-2	13/01/15	140	5.63	309	2150	276	1.60	75.8	269	409	52.6	255	60.0	7.68	8.32	54.1	10.6	31.3	4.44	26.3	4.21	54.2	21.6	45.9	29.4	7.00
AT-2_4†	AWT-2	13/01/15	142	7.50	312	2290	275	1.10	67.6	273	435	56.7	278	57.3	5.38	7.13	51.8	10.5	32.6	4.47	32.8	4.47	51.1	19.1	42.1	30.7	8.27
AT-2_8†	AWT-2	13/01/15	143	8.06	357	2470	283	2.75	71.9	299	459	63.7	323	50.6	7.46	7.86	54.5	11.7	30.9	3.95	32.9	4.60	58.6	20.4	36.9	33.0	6.84
AT-2_9	AWT-2	13/01/15	136	4.12	281	2050	268	1.52	196	250	417	56.5	258	50.2	6.68	7.09	45.8	9.83	27.9	4.09	27.2	4.03	50.7	18.4	45.1	27.0	7.29
AWT_2002_1	AWT-4	20/07/15	142	-	328	2620	280	1.68	64.7	300	577	68.1	283	59.2	9.03	10.0	62.1	12.8	40.9	5.59	34.6	4.87	70.2	22.2	47.7	34.8	8.11
AWT_2002_2	AWT-4	20/07/15	126	-	287	2250	246	0.99	94.1	244	475	56.2	252	48.8	5.62	6.78	49.4	9.96	33.8	4.81	31.2	4.45	61.5	18.2	45.8	29.6	7.65
AWT_2002_3	AWT-4	20/07/15	155	-	339	2830	305	1.53	68.9	316	608	73.7	302	66.2	6.91	10.8	70.8	13.4	39.7	5.70	38.8	5.96	72.3	24.5	54.8	38.8	9.04
AWT_2002_4	AWT-4	20/07/15	139	-	304	2500	272	1.39	64.7	280	528	67.1	278	64.3	7.87	8.68	58.8	11.6	35.4	5.37	35.4	4.43	65.8	19.6	46.5	30.4	7.22
AWT_2002_5	AWT-4	20/07/15	145	-	300	2540	294	2.23	66.5	281	559	67.7	289	53.8	6.38	9.41	57.9	12.0	37.4	5.69	31.0	5.01	62.0	21.6	48.3	32.0	8.85
AWT_2002_6	AWT-4	20/07/15	147	-	307	2470	279	1.20	77.2	282	565	65.7	273	56.4	6.92	8.91	61.2	12.1	34.0	4.30	32.9	4.84	69.2	21.8	50.6	33.0	9.11
AWT_2002_7	AWT-4	20/07/15	130	-	256	2140	274	1.42	67.4	236	502	53.4	236	44.2	7.04	7.63	51.5	10.3	26.2	4.35	29.6	4.33	56.6	18.8	45.0	26.6	7.09
AWT_2002_8	AWT-4	20/07/15	143	-	281	2270	271	1.35	71.5	261	546	60.5	267	51.4	7.23	7.96	52.7	10.5	30.5	4.50	30.8	4.05	62.8	20.0	47.5	29.4	7.88
AWT_2002_9	AWT-4	20/07/15	143	-	262	2130	291	0.97	63.4	235	493	54.4	241	47.0	5.87	7.97	49.1	9.72	30.8	3.94	28.0	3.91	58.3	18.4	46.3	29.1	8.16
AWT_2002_10	AWT-4	20/07/15	130	-	279	2250	272	0.82	60.1	258	543	59.0	254	49.5	7.26	8.61	49.0	10.8	32.8	5.04	29.3	4.14	57.5	20.0	47.1	30.1	7.99

Unnormalised major element concentrations (wt.%) in Chamo tephra glass shards

Label	Tephra	Analysis date	SiO_2 0.08	TiO_2 0.05	Al_2O_3 0.05	MgO 0.04	FeO^T 0.08	MnO 0.07	CaO 0.04	Na_2O 0.08	K_2O 0.03	P_2O_5 0.10	Cl 0.02	Total
CHA_L4_344_10	CHT-1	30/06/15	70.01	0.18	9.13	0.00	4.43	0.20	0.15	5.09	4.18	0.00	0.22	93.58
CHA_L4_344_11	CHT-1	30/06/15	72.67	0.20	9.55	0.00	4.40	0.24	0.15	5.26	4.27	0.00	0.19	96.95
CHA_L4_344_12	CHT-1	30/06/15	73.72	0.21	9.53	0.00	4.53	0.13	0.19	5.21	4.25	0.00	0.21	97.99
CHA_L4_344_13	CHT-1	30/06/15	72.19	0.21	9.27	0.00	4.34	0.27	0.14	5.02	4.29	0.00	0.24	95.98
CHA_L4_344_14	CHT-1	30/06/15	70.39	0.24	9.12	0.01	4.55	0.20	0.17	4.98	4.14	0.00	0.25	94.05
CHA_L4_344_15	CHT-1	30/06/15	71.82	0.26	9.44	0.01	4.57	0.24	0.21	5.09	4.24	0.04	0.19	96.12
CHA_L4_344_16	CHT-1	30/06/15	68.72	0.21	8.86	0.00	4.07	0.21	0.17	4.95	4.11	0.01	0.35	91.66
CHA_L4_344_17	CHT-1	30/06/15	72.16	0.26	9.48	0.00	4.34	0.22	0.18	5.02	4.29	0.00	0.20	96.14
CHA_L4_344_18	CHT-1	30/06/15	73.53	0.20	9.39	0.03	4.19	0.17	0.16	5.29	3.98	0.00	0.17	97.12
CHA_L4_344_19	CHT-1	30/06/15	69.09	0.29	9.06	0.04	4.50	0.17	0.17	4.73	4.18	0.06	0.27	92.55
CHA_L4_344_2	CHT-1	30/06/15	71.85	0.22	9.19	0.00	4.52	0.20	0.18	4.91	4.10	0.01	0.24	95.42
CHA_L4_344_20	CHT-1	30/06/15	72.86	0.24	9.48	0.05	4.42	0.26	0.18	5.10	4.35	0.00	0.24	97.18
CHA_L4_344_4	CHT-1	30/06/15	70.84	0.19	8.99	0.06	4.60	0.17	0.18	5.10	4.32	0.00	0.23	94.69
CHA_L4_344_5	CHT-1	30/06/15	73.04	0.25	9.55	0.00	4.41	0.15	0.17	5.36	4.16	0.00	0.22	97.31
CHA_L4_344_6	CHT-1	30/06/15	71.63	0.25	9.53	0.00	4.24	0.12	0.20	4.63	4.28	0.00	0.29	95.17
CHA_L4_344_8	CHT-1	30/06/15	71.31	0.19	9.16	0.00	4.58	0.17	0.17	4.99	4.28	0.01	0.23	95.06
CHA_L12_44_1	CHT-2	30/06/15	69.92	0.16	8.94	0.00	4.57	0.16	0.13	5.04	4.06	0.00	0.24	93.23
CHA_L12_44_11	CHT-2	30/06/15	68.60	0.18	8.59	0.00	4.40	0.20	0.17	5.30	3.85	0.01	0.27	91.56
CHA_L12_44_12	CHT-2	30/06/15	70.56	0.17	8.74	0.01	4.60	0.22	0.16	5.25	4.13	0.00	0.26	94.09
CHA_L12_44_13	CHT-2	30/06/15	71.61	0.17	9.01	0.01	4.35	0.23	0.17	5.32	4.23	0.07	0.27	95.45
CHA_L12_44_14	CHT-2	30/06/15	72.05	0.17	9.04	0.01	4.81	0.28	0.16	5.41	4.16	0.00	0.29	96.39
CHA_L12_44_15	CHT-2	30/06/15	70.84	0.19	8.77	0.00	4.66	0.28	0.21	5.50	4.25	0.00	0.28	94.99
CHA_L12_44_16	CHT-2	30/06/15	70.50	0.18	8.85	0.00	4.39	0.14	0.17	5.36	4.04	0.00	0.26	93.92
CHA_L12_44_17	CHT-2	30/06/15	71.79	0.17	8.93	0.02	4.58	0.17	0.14	3.82	4.14	0.00	0.24	94.00
CHA_L12_44_18	CHT-2	30/06/15	70.92	0.19	9.04	0.00	4.82	0.24	0.18	5.49	4.01	0.00	0.27	95.16
CHA_L12_44_19	CHT-2	30/06/15	71.39	0.16	8.94	0.01	4.60	0.20	0.18	5.56	4.12	0.03	0.29	95.47
CHA_L12_44_2	CHT-2	30/06/15	70.39	0.19	8.90	0.01	4.58	0.15	0.11	5.21	4.07	0.01	0.24	93.86
CHA_L12_44_20	CHT-2	30/06/15	72.37	0.10	9.16	0.00	4.82	0.15	0.17	5.37	4.11	0.02	0.29	96.56
CHA_L12_44_3	CHT-2	30/06/15	71.98	0.24	9.27	0.00	4.67	0.24	0.18	5.32	4.29	0.00	0.27	96.45
CHA_L12_44_4	CHT-2	30/06/15	70.92	0.12	8.99	0.00	4.73	0.13	0.19	5.67	4.03	0.02	0.25	95.05
CHA_L12_44_5	CHT-2	30/06/15	70.92	0.13	8.73	0.00	4.92	0.21	0.14	5.42	4.14	0.07	0.30	94.99
CHA_L12_44_6	CHT-2	30/06/15	70.71	0.13	9.08	0.00	4.74	0.28	0.16	5.46	4.13	0.06	0.28	95.04
CHA_L12_44_7	CHT-2	30/06/15	71.04	0.13	9.17	0.00	4.81	0.17	0.13	5.68	4.17	0.00	0.28	95.58
CHA_L12_44_8	CHT-2	30/06/15	71.89	0.21	9.07	0.00	4.56	0.23	0.12	5.24	4.18	0.00	0.28	95.78
CHA_L12_44_9	CHT-2	30/06/15	71.36	0.18	8.99	0.00	4.68	0.18	0.17	5.81	4.02	0.00	0.28	95.67

Trace element concentrations (ppm) in Chamo tephra glass shards

Label	Tephra	Analysis date	Rb 0.62	Sr 1.05	Y 0.17	Zr 0.37	Nb 0.07	Cs 0.19	Ba 1.88	La 0.09	Ce 0.07	Pr 0.06	Nd 0.25	Sm 0.14	Eu 0.13	Tb 0.06	Dy 0.13	Ho 0.04	Er 0.07	Tm 0.05	Yb 0.15	Lu 0.04	Hf 0.08	Ta 0.06	Pb 0.12	Th 0.01	U 0.00
CHA_L4_344_10	CHT-1	24/07/2015	133	-	300	2360	273	0.98	112	282	524	65.6	250	56.1	6.82	59.9	8.11	45.8	11.2	31.1	4.29	29.6	3.89	60.4	19.9	37.8	28.8
CHA_L4_344_11	CHT-1	24/07/2015	131	-	263	2150	270	0.84	103	246	471	58.7	237	49.3	5.78	49.5	7.51	49.2	9.45	29.1	4.20	25.2	4.44	51.4	18.9	37.0	26.2
CHA_L4_344_12	CHT-1	24/07/2015	138	-	262	2170	278	0.88	106	257	486	57.4	241	49.3	6.04	47.6	7.23	47.4	9.82	30.6	3.98	27.6	3.64	54.3	17.6	42.3	26.0
CHA_L4_344_13	CHT-1	24/07/2015	146	-	267	2200	281	1.47	109	259	475	56.9	240	49.2	7.42	53.1	8.03	47.4	9.99	29.1	4.19	24.8	4.07	54.1	17.3	40.8	26.6
CHA_L4_344_14	CHT-1	24/07/2015	141	-	366	2790	291	0.99	119	335	577	69.9	307	58.9	8.27	65.5	10.1	60.1	12.7	37.2	4.93	30.1	6.49	62.7	21.1	39.8	33.5
CHA_L4_344_15	CHT-1	24/07/2015	141	-	337	2710	286	0.99	118	319	538	68.3	292	61.4	7.36	57.7	9.18	55.5	11.8	33.3	5.12	30.2	4.46	62.4	19.7	37.3	31.3
CHA_L4_344_16	CHT-1	24/07/2015	139	-	341	2740	289	1.20	119	295	505	65.3	268	56.5	8.01	63.7	8.97	56.2	12.1	35.2	5.22	32.2	4.76	64.6	20.2	38.8	33.7
CHA_L4_344_17	CHT-1	24/07/2015	129	-	286	2260	259	0.88	99.3	270	477	58.4	234	50.6	6.41	51.1	8.01	46.5	10.1	28.8	4.16	27.8	3.92	51.8	18.2	33.7	27.0
CHA_L4_344_18	CHT-1	24/07/2015	118	-	270	2270	250	0.53	105	248	438	56.7	228	48.7	5.74	54.2	8.13	47.0	9.77	29.7	4.05	25.0	3.64	55.9	17.3	35.7	27.9
CHA_L4_344_19	CHT-1	24/07/2015	141	-	319	2480	258	1.32	104	285	477	62.8	258	51.0	6.38	60.4	9.92	57.9	12.9	30.5	4.47	27.7	4.82	55.6	18.2	41.8	28.9
CHA_L4_344_2	CHT-1	24/07/2015	125	-	276	2240	271	0.93	109	264	494	63.5	255	50.8	5.92	50.5	8.16	44.6	10.1	28.1	3.67	25.8	4.10	47.2	18.2	38.1	25.8
CHA_L4_344_20	CHT-1	24/07/2015	129	-	285	2290	265	1.23	110	265	482	61.8	238	53.6	6.81	57.5	8.73	50.6	9.43	31.6	3.76	26.5	3.77	55.5	17.6	37.5	27.8
CHA_L4_344_4	CHT-1	24/07/2015	148	-	346	2780	320	1.51	68.4	315	585	70.4	278	56.4	7.72	60.4	9.07	57.9	11.9	33.0	4.86	31.8	4.97	66.4	20.6	45.3	33.0
CHA_L4_344_5	CHT-1	24/07/2015	133	1.14	302	2440	282	1.09	115	296	519	65.1	269	55.1	6.63	53.8	8.94	53.6	11.1	33.1	4.57	31.0	4.36	56.1	19.3	41.8	30.7
CHA_L4_344_6	CHT-1	24/07/2015	132	-	276	2200	271	1.23	115	273	505	60.9	249	51.2	7.02	56.9	8.67	51.1	10.4	31.1	4.17	29.9	4.36	55.1	19.0	41.1	29.8
CHA_L4_344_8	CHT-1	24/07/2015	143	-	341	2640	271	1.12	121	308	522	67.7	282	59.1	7.40	68.7	9.20	63.5	10.3	34.1	5.01	31.6	5.68	65.0	19.2	43.2	31.6
CHA_L12_44_1	CHT-2	24/07/2015	153	-	393	3220	334	0.87	72.6	365	637	85.0	368	68.7	9.18	76.3	10.7	69.6	14.1	38.4	5.73	39.9	5.85	74.0	24.4	48.9	39.8
CHA_L12_44_11	CHT-2	24/07/2015	151	-	371	2820	324	1.20	62.5	305	566	74.9	313	73.8	7.85	65.6	9.73	60.1	12.9	36.9	5.30	33.9	4.63	61.9	22.2	49.2	33.8
CHA_L12_44_12	CHT-2	24/07/2015	159	-	332	2680	338	1.53	43.6	280	554	65.2	291	54.3	6.86	59.6	9.18	57.2	11.8	36.3	5.03	35.0	4.93	61.9	21.3	55.9	33.0
CHA_L12_44_13	CHT-2	24/07/2015	161	-	316	2570	340	1.61	50.4	259	532	62.8	269	59.4	7.28	57.1	9.18	56.0	11.6	31.6	4.83	30.0	4.30	62.3	21.0	51.2	32.4
CHA_L12_44_14	CHT-2	24/07/2015	161	-	313	2550	339	1.73	46.1	275	568	69.5	276	56.1	8.14	64.3	8.59	55.7	12.4	35.0	4.95	31.1	4.98	60.9	23.0	55.2	33.2
CHA_L12_44_15	CHT-2	24/07/2015	150	-	322	2550	328	1.42	44.0	268	539	65.8	271	54.4	7.28	60.0	8.97	54.4	11.9	34.0	4.99	33.4	4.37	63.5	20.7	52.1	32.2
CHA_L12_44_16	CHT-2	24/07/2015	156	-	324	2650	330	1.30	49.7	276	549	67.0	261	50.2	7.34	59.5	9.31	58.4	11.7	33.4	4.89	32.4	4.61	62.3	22.1	52.6	33.3
CHA_L12_44_17	CHT-2	24/07/2015	151	-	283	2360	322	1.55	43.9	256	520	63.3	265	55.5	7.06	56.7	8.85	54.5	11.5	34.9	4.99	31.7	4.55	59.1	21.2	50.8	32.1
CHA_L12_44_18	CHT-2	24/07/2015	164	-	334	2690	343	1.16	45.0	276	552	67.6	276	57.7	8.26	62.1	8.53	59.3	12.9	37.0	5.08	34.4	4.95	67.9	22.8	54.7	35.1
CHA_L12_44_19	CHT-2	24/07/2015	163	-	307	2470	340	1.47	42.7	263	526	63.1	257	53.3	5.79	52.2	8.00	52.0	11.4	32.5	4.91	29.3	4.25	61.3	20.8	51.7	31.4
CHA_L12_44_2	CHT-2	24/07/2015	162	-	452	3760	371	1.66	73.2	436	749	99.8	438	97.0	12.2	88.7	14.0	82.0	18.7	51.2	7.59	52.3	7.02	94.9	29.1	59.7	47.2
CHA_L12_44_20	CHT-2	24/07/2015	157	-	312	2490	327	1.51	48.2	277	542	67.4	289	55.9	7.50	63.8	9.39	60.4	12.2	35.1	4.50	31.4	4.74	63.7	22.5	51.9	33.1
CHA_L12_44_3	CHT-2	24/07/2015	155	-	332	2730	326	1.55	48.4	288	557	64.4	285	60.9	7.08	56.5	9.40	58.9	12.2	32.8	4.48	31.6	4.62	64.0	21.7	50.8	32.1
CHA_L12_44_4	CHT-2	24/07/2015	160	0.89	342	2730	335	1.60	49.5	289	587	70.0	291	64.1	7.36	66.8	9.74	65.3	12.2	37.0	5.47	35.1	4.79	70.4	22.8	55.3	33.3
CHA_L12_44_5	CHT-2	24/07/2015	156	-	331	2770	329	1.49	48.3	288	575	69.3	295	62.7	7.06	62.2	9.95	58.3	11.9	34.3	5.11	31.6	4.69	67.0	22.6	54.1	33.6
CHA_L12_44_6	CHT-2	24/07/2015	143	-	300	2390	316	1.53	50.7	261	548	64.6	259	54.0	7.12	54.8	9.29	53.9	11.8	33.1	3.91	32.7	4.14	57.7	19.8	51.2	30.2
CHA_L12_44_7	CHT-2	24/07/2015	154	-	331	2780	345	1.47	50.0	285	549	67.9	284	55.0	6.92	65.9	9.25	54.9	11.8	34.9	4.69	32.4	4.84	67.6	22.4	51.9	33.1
CHA_L12_44_8	CHT-2	24/07/2015	149	0.94	301	2430	304	1.38	46.0	254	526	61.6	264	56.8	6.90	57.8	9.27	56.4	10.5	33.4	4.56	30.6	4.96	65.0	21.2	52.3	33.2
CHA_L12_44_9	CHT-2	24/07/2015	156	-	311	2570	330	1.18	47.4	277	552	65.1	263	59.5	6.26	55.3	9.29	56.9	11.0	33.1	4.89	32.4	4.36	62.2	21.9	55.5	31.7

The major and trace element composition of tephras and obsidian samples from the Corbetti caldera are given in the following two tables. Obsidian samples E950010, E950011, E950019 and E950025 were analysed for only trace elements. Average silica concentrations, determined previously by N. Pearce (Aberystwyth University) using EPMA at the University of Toronto, were used as internal standards for LA-ICP-MS analysis.

Limits of detection for all EPMA sessions are given on page 401, the median limits of detection for ATHO-G are given for comparison in the following table headings. Most major elements are present at concentrations above these limits of detection, however, concentrations of MgO and P_2O_5 are below the LLD in many shards.

Trace element analyses were typically undertaken using 20 μm crater diameters, however, †indicates glass shards were analysed using 10 μm crater diameters. Lower limits of detection (LLD) for LA-ICP-MS analyses are given on page 407. The median LLD concentrations at 20 μm crater diameters of all LA-ICP-MS analytical sessions are given beneath each analyte heading in the following tables. Due to high Sr and Ba concentrations in the gas blanks, coupled with frequent low sample concentrations, some negative concentrations were measured - these are indicated with a dash. Analyses of MPI-DING reference materials were used to check the EPMA and LA-ICP-MS calibrations. These analyses are given on page 398, and are ordered by analysis date.

Unnormalised major element concentrations (wt.%) in tephra and obsidian samples from Corbetti

Label	Tephra	Analysis date	SiO_2 0.08	TiO_2 0.05	Al_2O_3 0.05	MgO 0.04	FeO[1] 0.08	MnO 0.07	CaO 0.04	Na_2O 0.08	K_2O 0.03	P_2O_5 0.10	Cl 0.02	Total
STNW-1_1	ST-NW1	28/08/14	74.45	0.26	9.41	0.01	4.39	0.20	0.20	5.24	4.44	0.00		98.60
STNW-1_10	ST-NW1	28/08/14	73.82	0.28	9.32	0.00	4.34	0.25	0.17	5.54	4.47	0.01		98.21
STNW-1_11	ST-NW1	28/08/14	74.30	0.26	9.57	0.02	4.36	0.25	0.15	5.25	4.39	0.01		98.56
STNW-1_12	ST-NW1	28/08/14	73.64	0.22	9.78	0.00	4.42	0.18	0.17	5.19	4.27	0.04		97.91
STNW-1_13	ST-NW1	28/08/14	73.59	0.25	9.44	0.00	4.39	0.20	0.18	5.31	4.30	0.04		97.70
STNW-1_14	ST-NW1	28/08/14	71.10	0.29	10.58	0.01	4.25	0.18	0.17	5.14	4.11	0.01		95.84
STNW-1_16	ST-NW1	28/08/14	73.81	0.28	9.53	0.02	4.63	0.20	0.18	5.35	4.39	0.01		98.42

Continued on next page

Unnormalised major element concentrations (wt.%) in tephra and obsidian samples from Corbetti

Label	Tephra	Analysis date	SiO_2 0.08	TiO_2 0.05	Al_2O_3 0.05	MgO 0.04	FeO^T 0.08	MnO 0.07	CaO 0.04	Na_2O 0.08	K_2O 0.03	P_2O_5 0.10	Cl 0.02	Total
STNW-1_17	ST-NW1	28/08/14	73.30	0.26	9.81	0.00	4.43	0.32	0.26	5.07	4.31	0.00		97.77
STNW-1_18	ST-NW1	28/08/14	73.83	0.21	9.42	0.01	4.66	0.15	0.22	5.18	4.38	0.00		98.07
STNW-1_19	ST-NW1	28/08/14	74.34	0.25	9.63	0.00	4.59	0.27	0.19	5.54	4.46	0.02		99.28
STNW-1_2	ST-NW1	28/08/14	72.38	0.24	9.16	0.00	4.65	0.18	0.18	5.25	4.36	0.04		96.44
STNW-1_20	ST-NW1	28/08/14	74.19	0.23	9.79	0.00	4.64	0.13	0.19	5.34	4.58	0.00		99.09
STNW-1_3	ST-NW1	28/08/14	70.10	0.21	9.72	0.01	4.25	0.22	0.19	4.69	4.10	0.03		93.52
STNW-1_5	ST-NW1	28/08/14	67.88	0.29	8.92	0.00	4.22	0.19	0.21	5.04	4.09	0.02		90.86
STNW-1_6	ST-NW1	28/08/14	74.57	0.25	9.65	0.00	4.25	0.21	0.20	5.07	4.26	0.03		98.50
STNW-1_7	ST-NW1	28/08/14	72.43	0.21	9.14	0.00	4.19	0.20	0.16	5.08	4.43	0.00		95.84
STNW-1_8	ST-NW1	28/08/14	72.33	0.25	9.54	0.00	4.64	0.16	0.17	4.93	4.29	0.02		96.34
STNW-1_9	ST-NW1	28/08/14	73.60	0.28	9.58	0.00	4.33	0.23	0.18	5.57	4.35	0.00		98.13
E95007_13	E95007	28/08/14	69.92	0.24	10.44	0.05	3.35	0.13	0.22	4.27	4.86	0.00		93.49
E95007_3	E95007	28/08/14	70.31	0.32	9.10	0.02	4.96	0.20	0.21	3.35	3.96	0.01		92.45
E97003_1	E95003	28/08/14	68.21	0.36	7.95	0.03	5.32	0.28	0.17	4.81	4.55	0.00		91.67
E97003_3	E95003	28/08/14	71.25	0.40	8.54	0.01	5.33	0.29	0.18	5.10	4.38	0.00		95.47
E97003_9	E95003	28/08/14	72.20	0.24	8.72	0.05	5.51	0.24	0.17	3.84	4.39	0.02		95.38

Trace element concentrations (ppm) in tephra and obsidian samples from Corbetti

Label	Tephra	Analysis date	Rb 0.62	Sr 1.05	Y 0.17	Zr 0.37	Nb 0.07	Cs 0.19	Ba 1.88	La 0.09	Ce 0.07	Pr 0.06	Nd 0.25	Sm 0.14	Eu 0.13	Tb 0.06	Dy 0.13	Ho 0.04	Er 0.07	Tm 0.05	Yb 0.15	Lu 0.04	Hf 0.08	Ta 0.06	Pb 0.12	Th 0.01	U 0.00
STNW-1_1	ST-NW1	21/01/15	127	2.76	251	2020	269	1.04	92.5	224	421	52.5	210	45.4	5.38	7.33	46.1	8.98	27.1	3.50	25.7	4.10	51.3	17.9	43.8	24.4	6.71
STNW-1_10	ST-NW1	21/01/15	120	4.05	266	1880	241	2.21	87.0	204	394	49.0	207	43.1	4.85	6.41	40.0	9.11	26.6	3.53	24.6	3.94	51.6	16.2	38.3	23.2	6.71
STNW-1_11	ST-NW1	21/01/15	130	4.93	252	1990	261	1.25	96.7	222	422	53.6	228	44.7	5.83	7.70	46.6	9.21	28.4	3.90	26.9	3.55	52.3	17.9	41.5	26.1	6.78
STNW-1_12	ST-NW1	21/01/15	123	6.37	265	2060	258	1.27	100	238	430	56.1	241	43.8	5.10	8.29	46.1	9.79	29.2	4.04	28.0	3.94	50.6	18.0	40.0	27.3	6.63
STNW-1_13	ST-NW1	21/01/15	126	4.11	244	1880	248	1.20	88.6	210	420	48.2	202	48.2	5.63	6.41	41.5	8.73	27.8	3.84	24.6	3.48	47.3	15.5	37.3	25.5	6.43
STNW-1_14	ST-NW1	21/01/15	126	4.22	228	1840	248	1.36	89.2	197	393	49.0	198	42.5	4.95	6.58	39.8	8.65	26.3	3.59	22.4	3.24	48.9	16.2	40.8	24.8	6.32
STNW-1_16	ST-NW1	21/01/15	128	2.51	229	1860	255	1.54	88.3	213	413	49.9	205	39.2	4.62	6.91	41.4	8.74	27.6	3.72	25.5	3.19	47.8	18.0	39.2	25.5	7.17
STNW-1_17	ST-NW1	21/01/15	127	4.05	240	1850	253	1.27	95.6	208	412	49.4	205	42.3	5.18	6.95	43.1	9.87	24.4	3.43	23.0	3.90	47.4	17.0	41.8	23.8	6.66
STNW-1_18	ST-NW1	21/01/15	125	3.92	230	1810	257	1.40	91.9	201	413	51.4	213	41.9	5.88	6.81	39.7	8.60	26.5	3.91	23.3	3.07	49.4	17.5	41.5	23.7	7.04
STNW-1_19	ST-NW1	21/01/15	120	4.03	249	1920	255	1.16	94.9	220	416	51.6	226	42.9	5.08	6.28	44.0	9.13	29.1	3.39	25.5	3.81	50.0	18.3	38.1	24.5	7.44
STNW-1_2	ST-NW1	21/01/15	121	3.52	228	1850	251	1.02	89.4	201	394	46.8	203	37.8	5.17	6.33	41.3	8.70	24.6	4.12	21.7	3.40	48.5	16.2	39.0	24.2	6.50
STNW-1_20	ST-NW1	21/01/15	127	4.3	253	1990	258	1.04	96.2	231	437	51.8	224	47.6	5.51	7.30	45.3	8.96	27.6	3.77	26.1	3.63	52.4	17.4	37.5	25.6	7.06
STNW-1_3	ST-NW1	21/01/15	126	5.31	251	1980	263	1.21	89.8	224	419	50.6	221	48.2	5.27	7.22	43.3	9.42	24.6	3.92	27.1	3.53	50.7	17.8	42.0	25.7	6.45
STNW-1_5	ST-NW1	21/01/15	122	4.66	243	1950	253	0.92	90.8	210	408	49.8	203	46.4	5.45	6.77	45.5	9.64	27.8	3.25	25.4	3.45	50.2	16.6	41.7	25.2	6.09
STNW-1_6	ST-NW1	21/01/15	125	4.37	254	2020	262	1.11	93.1	229	459	53.7	236	47.9	5.88	7.79	47.0	9.22	29.8	3.93	27.7	3.94	54.8	19.0	42.5	26.8	6.97
STNW-1_7	ST-NW1	21/01/15	129	5.92	238	1940	262	1.56	99.7	208	412	49.2	214	44.8	5.04	6.98	44.3	8.61	24.6	3.50	24.6	3.49	46.5	16.8	43.9	23.8	6.43
STNW-1_8	ST-NW1	21/01/15	121	4.48	247	2030	256	1.85	102	228	453	54.3	235	47.1	5.70	7.24	44.1	9.32	31.0	3.92	25.0	3.77	58.2	18.1	40.0	25.6	6.46
STNW-1_9	ST-NW1	21/01/15	128	8.63	239	1880	256	1.15	99.7	220	414	49.6	211	45.2	6.01	7.44	44.3	8.27	28.6	2.93	24.5	3.33	51.7	17.7	50.7	26.4	8.71
E95007_13	E95007	21/01/15	152	-	161	1590	208	0.95	16.1	186	351	43.2	166	33.4	2.84	4.77	29.0	5.98	18.4	2.64	16.9	2.34	40.6	15.3	37.2	25.0	5.77
E95007_3	E95007	21/01/15	109	0.22	153	1230	171	0.56	19.0	154	298	36.1	151	28.9	3.19	4.79	30.1	5.66	15.8	2.46	15.7	2.06	36.9	13.2	25.1	22.4	5.63
E97003_1†	E95003	21/01/15	125	4.34	229	1690	228	0.75	33.4	180	369	37.5	179	39.2	4.60	5.31	48.1	8.87	24.7	3.42	20.1	2.61	42.7	16.0	34.3	24.0	6.04
E97003_3	E95003	21/01/15	107	1.82	198	1580	226	1.00	31.6	169	334	40.9	168	34.5	4.33	5.21	37.7	7.31	21.9	2.99	20.1	3.19	42.3	13.9	29.3	21.2	5.59
E97003_9†	E95003	21/01/15	122	8.82	267	2230	276	2.04	41.0	217	408	50.6	229	44.5	6.10	7.35	62.0	9.29	27.4	4.64	26.5	3.29	51.6	16.7	31.5	27.9	6.52
E95003	E95003	28/10/14	101	2.16	89.5	635	82.0	0.91	517	68.5	45.6	19.2	76.9	14.5	1.92	2.70	16.4	3.30	9.76	1.65	8.83	1.37	17.9	6.09	38.1	12.5	3.87
E95003	E95003	28/10/14	97.1	2.15	90.7	644	81.0	0.89	525	71.3	38.4	18.6	69.9	18.1	2.32	2.67	17.2	4.00	9.06	1.78	8.83	1.43	18.8	5.25	34.1	13.2	3.79
E95003	E95003	28/10/14	101	2.72	88.3	619	79.1	1.21	494	68.2	49.7	19.5	74.8	17.9	1.75	2.62	15.0	3.53	9.98	1.48	9.21	1.33	17.2	5.10	34.3	13.2	4.16
E95003	E95003	28/10/14	104	2.33	91.1	590	83.1	1.20	492	69.8	61.3	19.1	76.7	15.3	2.02	2.69	15.2	3.51	9.14	1.53	9.87	1.35	16.7	5.08	39.0	12.6	3.91
E95003	E95003	28/10/14	97.9	2.15	87.0	582	81.3	1.10	480	65.0	51.7	18.3	75.0	17.6	2.19	2.49	16.7	2.95	9.13	1.18	8.74	1.41	16.3	5.47	36.2	12.2	3.77
E95003	E95003	28/10/14	96.4	2.75	82.2	581	74.7	1.18	488	61.0	47.7	16.4	70.2	15.2	2.15	2.43	12.5	2.97	9.23	1.22	9.59	1.33	15.1	5.57	35.6	11.7	3.61
E95003	E95003	28/10/14	91.6	1.88	78.1	527	74.2	0.84	449	59.5	50.4	16.3	69.1	14.0	1.74	2.05	12.4	2.85	8.49	1.23	8.42	1.11	15.2	5.30	31.9	11.3	3.86
E95003	E95003	28/10/14	99.2	1.4	87.9	581	80.5	1.26	497	69.3	57.3	18.7	72.7	17.0	2.14	2.55	15.8	3.47	9.46	1.25	8.67	1.25	17.8	5.17	34.4	12.3	3.94
E95003	E95003	28/10/14	91.4	2.09	83.8	573	79.8	1.03	482	65.1	54.0	17.9	68.9	16.2	2.23	2.50	15.7	2.51	8.44	1.46	8.36	1.23	17.9	5.35	37.4	12.0	4.05
E95003	E95003	28/10/14	96.1	2.57	82.9	573	78.3	1.19	467	72.6	66.3	17.3	74.2	16.5	1.72	2.14	16.1	3.29	9.26	1.43	8.44	1.44	16.5	4.87	39.5	12.2	4.09
E95003	E95003	28/10/14	94.2	1.93	80.8	563	78.6	1.11	472	64.5	63.2	18.3	73.0	15.7	1.99	2.28	14.1	2.81	8.22	1.26	8.91	1.47	16.4	5.48	37.8	12.8	3.94
E95003	E95003	28/10/14	98.5	1.76	82.5	580	83.5	0.99	459	61.9	42.1	18.0	63.7	15.9	2.51	2.33	13.2	3.22	9.16	0.96	7.76	1.14	15.5	5.23	33.9	11.9	3.65
E95003	E95003	28/10/14	85.4	1.03	75.3	528	71.5	1.04	461	62.8	67.0	17.6	69.2	13.3	1.78	2.65	13.7	2.88	8.53	1.32	8.58	1.04	15.2	5.15	32.8	10.6	3.89
E95003	E95003	28/10/14	98.6	1.34	86.8	579	79.3	1.11	504	70.3	71.0	18.7	74.2	16.3	1.88	2.50	15.1	3.28	8.54	1.45	8.60	1.10	16.1	5.11	36.0	13.1	4.97
E95003	E95003	28/10/14	107	1.65	84.4	586	79.5	1.14	516	69.7	72.1	18.2	71.3	18.5	1.96	2.54	14.6	3.55	9.72	1.28	8.57	1.21	15.4	5.86	35.1	11.6	3.98
E95003	E95003	28/10/14	96.1	2.17	92.4	628	79.2	1.29	528	77.2	76.9	19.6	82.9	19.2	2.16	2.47	15.6	3.55	10.2	1.32	10.1	1.55	21.2	6.03	34.8	13.7	4.50
E95003	E95003	28/10/14	106	2.25	86.2	579	79.2	1.35	482	74.3	78.5	18.8	79.9	17.8	2.42	2.34	15.0	2.88	9.71	1.46	10.0	1.49	19.0	5.28	36.3	12.1	4.10
E95003	E95003	28/10/14	101	2.16	87.5	572	75.0	1.05	496	79.6	97.0	19.2	72.7	17.3	1.51	2.18	13.2	2.77	9.42	1.09	8.88	1.15	17.0	5.56	34.5	12.0	3.88
E950019	E950019	29/10/14	106	3.37	186	1510	185	0.60	112	177	72.2	42.5	163	33.8	4.51	5.65	33.5	6.82	20.2	2.76	18.1	2.78	38.0	13.3	33.3	19.4	4.76

Continued on next page

Trace element concentrations (ppm) in tephra and obsidian samples from Corbetti

Label	Tephra	Analysis date	Rb 0.62	Sr 1.05	Y 0.17	Zr 0.37	Nb 0.07	Cs 0.19	Ba 1.88	La 0.09	Ce 0.07	Pr 0.06	Nd 0.25	Sm 0.14	Eu 0.13	Tb 0.06	Dy 0.13	Ho 0.04	Er 0.07	Tm 0.05	Yb 0.15	Lu 0.04	Hf 0.08	Ta 0.06	Pb 0.12	Th 0.01	U 0.00
E950019	E950019	29/10/14	95.2	5.09	192	1560	187	0.74	109	187	62.1	44.4	179	34.0	4.17	5.50	31.3	7.00	21.1	3.03	17.8	3.05	38.7	12.7	30.2	19.7	4.85
E950019	E950019	29/10/14	112	2.92	191	1570	185	0.79	106	184	71.9	43.4	169	36.7	4.42	5.21	33.8	7.50	21.5	2.68	20.5	2.80	41.7	13.5	31.9	21.7	5.18
E950019	E950019	29/10/14	92.6	4.78	186	1550	181	0.88	92.6	193	84.6	45.5	170	35.3	5.03	5.63	35.5	7.11	19.7	2.98	18.7	2.72	41.1	12.6	34.0	20.2	4.73
E950019	E950019	29/10/14	102	3.99	188	1560	183	0.76	108	186	73.7	41.2	167	35.6	4.45	5.00	35.0	6.88	20.0	2.64	19.1	3.03	35.1	12.9	31.5	20.8	5.31
E950019	E950019	29/10/14	101	3.65	196	1610	189	0.81	107	193	77.4	43.4	182	37.5	4.36	5.33	35.1	7.44	21.0	2.56	19.8	2.54	38.5	13.0	33.9	20.3	4.94
E950019	E950019	29/10/14	102	2.66	186	1550	183	0.75	105	190	78.2	42.7	175	37.8	4.67	5.50	33.0	6.62	20.3	2.74	18.6	3.02	37.3	13.8	34.6	19.6	5.57
E950019	E950019	29/10/14	97.8	2.33	165	1360	183	0.65	104	160	82.4	38.9	158	28.8	4.24	4.26	28.1	5.76	17.1	2.6	15.5	2.40	32.0	11.3	30.6	16.5	4.72
E950019	E950019	29/10/14	105	2.98	165	1380	188	0.88	102	160	80.0	40.2	161	32.3	3.85	5.04	31.8	6.65	18.6	2.41	16.9	2.37	33.5	11.5	34.4	18.3	5.05
E950019	E950019	29/10/14	103	2.46	164	1360	180	0.78	99.9	156	73.3	38.1	147	28.8	3.79	4.72	24.8	6.05	16.3	2.27	16.6	2.67	30.3	10.9	31.5	17.1	5.76
E950019	E950019	29/10/14	89.8	3.72	154	1300	180	0.69	99.0	170	91.5	39.6	153	31.0	3.77	4.70	26.8	6.31	16.6	2.43	16.7	1.92	33.0	11.3	31.5	16.3	4.88
E950019	E950019	29/10/14	67.6	3.66	132	1200	150	0.33	95.5	133	66.2	34.5	123	26.1	3.38	3.72	24.9	5.01	14.9	1.91	16.1	2.15	31.3	10.8	27.8	15.7	4.85
E950019	E950019	29/10/14	85.5	3.27	159	1340	192	0.60	96.7	155	59.5	39.1	137	30.5	3.72	4.33	27.3	5.81	17.5	2.24	16.1	2.44	34.9	12.0	30.9	17.6	5.30
E950019	E950019	29/10/14	132	2.07	164	1410	193	0.90	93.8	171	91.4	41.7	154	33.8	4.21	4.76	31.6	6.45	19.0	2.66	17.6	2.62	34.0	12.3	37.8	18.1	5.42
E950019	E950019	29/10/14	131	3.93	165	1360	191	1.02	89.8	166	94.4	40.7	155	33.2	4.46	4.97	29.1	6.72	15.5	2.70	16.8	2.42	32.6	11.4	36.6	17.4	5.05
E950019	E950019	29/10/14	98.1	2.11	151	1340	182	1.01	100	151	82.3	37.0	140	30.7	3.74	4.88	27.6	6.08	17.9	2.39	17.1	2.36	33.7	11.8	31.9	18.0	4.91
E950019	E950019	29/10/14	120	2.21	171	1430	193	0.70	100	166	90.6	42.6	152	29.8	4.01	4.92	30.1	5.81	16.8	2.56	17.9	2.80	36.0	12.5	34.6	18.0	5.67
E950019	E950019	29/10/14	119	2.64	161	1370	178	0.74	94.9	151	104	36.9	147	30.0	4.00	4.53	28.1	5.97	16.2	2.71	16.4	2.24	30.0	12.0	36.1	17.3	5.45
E950019	E950019	29/10/14	96.3	2.12	153	1330	179	0.85	95.5	149	95.7	37.0	140	26.9	3.11	3.79	25.4	5.54	14.7	2.12	14.6	2.39	31.8	10.9	30.9	17.7	4.82
E950011	E950011	29/10/14	113	2.94	202	1660	205	0.91	112	192	165	47.3	192	39.4	5.37	6.20	37.3	7.88	21.0	2.86	22.0	3.22	40.9	14.3	36.9	21.9	5.96
E950011	E950011	29/10/14	106	5.46	215	1830	231	1.01	112	217	156	49.1	219	43.9	5.38	7.34	41.1	8.78	24.6	3.52	22.5	3.36	50.0	15.7	38.4	23.8	6.37
E950011	E950011	29/10/14	117	1.71	203	1660	216	1.00	110	196	169	49.3	215	39.2	5.21	5.94	39.5	7.86	24.1	3.30	20.7	3.32	42.2	14.5	36.8	22.0	6.20
E950011	E950011	29/10/14	130	2.46	203	1600	208	0.89	116	183	166	43.5	191	37.3	4.98	5.74	36.4	7.30	20.5	3.13	20.4	3.46	41.1	12.7	35.9	20.5	5.80
E950011	E950011	29/10/14	102	4.25	197	1590	204	1.01	106	200	172	48.2	197	41.9	4.99	6.28	36.8	7.42	24.3	3.09	20.0	3.16	40.8	13.9	37.1	20.9	6.00
E950011	E950011	29/10/14	97.9	3.22	196	1590	199	0.95	119	183	173	48.2	180	36.8	5.32	6.02	34.8	7.47	22.2	2.87	19.7	3.11	38.5	12.9	31.7	20.7	5.75
E950011	E950011	29/10/14	128	1.84	186	1530	208	0.85	117	175	164	42.2	174	34.3	3.91	5.44	34.2	6.53	21.1	2.94	19.2	2.63	37.8	13.1	35.1	19.8	5.96
E950011	E950011	29/10/14	117	1.66	177	1470	198	0.78	111	172	170	41.5	174	34.7	4.27	5.66	35.4	7.09	21.6	3.24	18.6	3.01	39.5	13.5	36.9	19.7	6.42
E950011	E950011	29/10/14	124	3.53	168	1380	196	0.83	105	161	165	39.8	163	33.3	5.00	4.89	31.0	6.50	17.7	2.92	17.9	2.61	36.0	12.1	35.9	17.7	6.21
E950011	E950011	29/10/14	110	1.55	181	1470	199	0.97	105	171	176	41.9	161	32.9	4.35	5.10	32.1	6.42	18.7	2.91	18.3	2.36	33.6	12.3	33.7	16.8	5.63
E950011	E950011	29/10/14	108	1.82	167	1370	198	0.95	107	161	171	38.7	170	34.3	4.32	4.97	31.5	6.50	19.3	2.85	17.8	2.48	35.9	12.8	36.8	17.6	5.84
E950011	E950011	29/10/14	120	3.93	178	1490	210	0.83	112	176	152	42.0	171	34.9	4.45	5.62	34.4	7.02	19.3	2.76	19.3	2.99	37.3	13.7	41.6	19.2	6.60
E950011	E950011	29/10/14	99.1	2.94	155	1230	173	0.57	90.9	142	153	35.1	151	32.3	3.84	4.53	27.1	5.98	16.9	2.39	17.2	2.41	30.8	10.9	35.7	16.2	4.89
E950011	E950011	29/10/14	112	3.07	178	1440	193	0.97	113	166	173	41.8	166	34.6	4.21	5.15	32.8	6.93	19.3	2.69	19.0	2.86	37.1	13.4	35.0	18.3	5.06
E950011	E950011	29/10/14	104	2.51	180	1450	186	0.94	114	172	176	41.2	167	36.7	4.85	5.62	34.7	7.50	19.2	2.97	19.7	2.85	34.2	13.0	38.0	18.7	6.30
E950011	E950011	29/10/14	124	1.73	190	1510	192	1.05	105	181	192	44.4	179	35.8	4.40	5.63	32.6	6.93	19.3	2.69	18.8	2.86	38.4	11.9	34.7	19.3	6.02
E950011	E950011	29/10/14	113	3.95	176	1420	189	0.80	117	164	183	40.3	157	33.3	4.16	4.95	32.9	6.38	19.8	2.26	17.7	2.35	34.6	11.6	34.2	17.5	5.55
E950011	E950011	29/10/14	119	2.01	176	1420	205	1.01	113	170	196	42.0	175	37.7	4.80	5.21	33.9	7.51	19.5	3.06	19.9	2.90	35.6	13.5	36.3	20.6	6.99
E950010	E950010	30/10/14	129	4.80	232	1870	231	1.27	66.2	215	242	53.6	219	42.7	5.86	6.61	40.6	9.03	27.0	3.49	24.1	3.35	44.2	16.0	43.4	23.4	6.13
E950010	E950010	30/10/14	111	3.91	199	1670	201	0.80	94.9	195	211	47.9	189	36.1	5.23	5.66	37.2	7.64	21.4	3.39	20.3	3.21	40.5	13.7	35.6	20.8	5.08
E950010	E950010	30/10/14	119	4.74	219	1840	223	1.11	73.8	210	235	51.9	211	37.8	5.28	6.66	40.5	8.51	23.1	3.54	23.2	3.34	43.3	14.1	39.9	22.9	5.93
E950010	E950010	30/10/14	105	3.93	180	1490	185	1.05	114	177	203	42.4	168	34.1	4.56	5.52	33.2	6.84	20.2	2.91	18.9	3.03	36.4	12.3	34.0	18.4	5.07
E950010	E950010	30/10/14	103	4.60	193	1600	190	0.92	126	192	225	46.8	183	36.0	4.79	5.57	35.1	6.96	20.5	2.83	19.1	2.59	40.0	12.3	34.5	19.8	4.68
E950010	E950010	30/10/14	100	4.71	195	1570	189	0.82	124	186	195	45.9	178	35.1	4.57	5.24	35.9	6.83	21.1	3.23	20.4	3.00	38.0	12.9	32.3	19.6	4.57
E950010	E950010	30/10/14	122	4.17	247	2060	240	0.96	75.4	237	265	55.9	222	46.2	5.72	6.67	42.9	8.38	26.4	3.89	23.9	3.41	51.8	16.8	44.2	24.8	7.21
E950010	E950010	30/10/14	142	5.40	238	1950	236	1.05	69.3	230	281	55.0	215	43.4	5.50	6.68	42.9	8.46	25.6	3.78	24.7	3.45	49.3	15.4	42.5	25.0	6.13

Continued on next page

Trace element concentrations (ppm) in tephra and obsidian samples from Corbetti

Label	Tephra	Analysis date	Rb 0.62	Sr 1.05	Y 0.17	Zr 0.37	Nb 0.07	Cs 0.19	Ba 1.88	La 0.09	Ce 0.07	Pr 0.06	Nd 0.25	Sm 0.14	Eu 0.13	Tb 0.06	Dy 0.13	Ho 0.04	Er 0.07	Tm 0.05	Yb 0.15	Lu 0.04	Hf 0.08	Ta 0.06	Pb 0.12	Th 0.01	U 0.00
E950010	E950010	30/10/14	145	4.86	254	2020	275	1.31	56.6	234	302	58.1	237	48.2	6.15	7.11	42.7	9.26	25.8	3.83	27.2	3.73	49.0	16.7	55.0	26.5	8.27
E950010	E950010	30/10/14	136	4.81	230	1880	261	1.00	49.3	212	255	52.1	218	42.9	6.13	6.67	42.5	8.33	25.3	3.61	23.5	3.11	45.3	14.8	48.0	23.7	6.87
E950010	E950010	30/10/14	140	3.37	231	1860	251	1.19	52.0	212	267	52.7	219	46.5	5.70	6.72	39.4	8.52	24.1	3.14	23.0	3.14	47.5	16.9	53.4	23.9	8.08
E950010	E950010	30/10/14	135	4.09	214	1820	245	1.09	51.1	195	245	50.1	205	40.1	4.79	6.13	41.2	8.22	21.8	3.47	21.6	3.20	45.7	15.4	49.5	22.1	6.91
E950010	E950010	30/10/14	132	5.11	233	1890	256	1.22	58.1	222	248	53.6	203	45.3	5.02	6.32	43.2	8.14	25.1	3.52	23.5	3.26	47.5	16.4	46.0	25.0	6.90
E950010	E950010	30/10/14	139	4.25	211	1810	250	1.11	49.9	205	260	50.7	208	41.2	4.84	5.79	39.3	8.21	24.6	3.52	21.8	3.19	49.9	14.3	50.0	22.1	6.31
E950010	E950010	30/10/14	151	3.29	231	1880	255	1.22	46.0	213	250	53.5	208	46.1	5.08	6.24	39.2	8.22	24.3	3.39	23.5	3.40	46.1	16.0	50.0	25.0	7.26
E950010	E950010	30/10/14	141	2.55	222	1840	250	1.35	57.5	210	260	56.0	207	45.1	5.46	5.43	42.0	8.08	24.3	3.32	22.0	3.48	43.3	14.7	50.7	23.1	7.64
E950010	E950010	30/10/14	120	3.81	232	1890	229	1.06	58.7	219	240	52.4	208	40.6	4.95	6.40	38.9	8.26	23.7	3.35	23.1	3.75	47.1	15.6	39.2	23.9	6.37
E950010	E950010	30/10/14	105	3.06	168	1360	179	0.74	96.5	164	199	40.9	153	34.8	4.21	4.96	29.0	6.12	16.5	2.33	16.3	2.74	32.9	11.5	35.6	17.7	4.41
E950010	E950010	30/10/14	109	2.75	183	1540	189	1.04	105	184	216	43.4	174	37.3	4.51	5.15	30.0	6.79	20.6	2.92	18.9	2.81	37.9	12.4	37.1	19.3	5.22
E950025	E950025	30/10/14	292	1.48	116	563	163	1.79	3.77	59.6	62.8	15.3	53.4	14.2	0.13	2.86	19.7	4.45	12.2	1.68	12.1	1.93	23.8	13.1	40.3	37.7	10.3
E950025	E950025	30/10/14	222	1.18	114	535	171	1.62	5.34	61.4	92.1	14.3	50.0	13.8	0.10	2.78	19.3	4.39	12.4	1.69	12.0	1.49	22.7	13.3	40.5	34.9	9.77
E950025	E950025	30/10/14	215	0.52	106	510	166	1.50	2.57	56.2	58.2	13.6	44.6	12.9	0.04	2.41	18.5	3.54	10.3	1.82	11.3	1.50	22.2	12.2	41.8	32.1	9.28
E950025	E950025	30/10/14	213	-	97.2	498	156	1.39	1.66	51.1	61.9	12.2	46.1	12.6	0.09	2.48	15.6	3.60	10.2	1.65	11.9	1.59	18.3	12.0	38.7	29.8	8.84
E950025	E950025	30/10/14	206	0.62	100	493	165	1.57	0.30	53.6	60.4	13.9	46.3	12.0	-	2.71	16.4	3.43	10.0	1.43	10.1	1.59	19.8	12.5	41.4	31.3	9.23
E950025	E950025	30/10/14	207	-	104	497	154	1.61	1.33	52.2	58.3	12.5	41.6	11.5	0.06	2.43	18.3	3.85	10.1	1.38	11.3	1.41	19.9	13.0	39.2	31.9	8.95
E950025	E950025	30/10/14	225	5.12	108	519	167	1.30	12.0	69.7	159	15.6	52.3	12.8	0.20	2.69	17.4	3.95	12.1	1.72	11.5	1.61	20.2	11.9	42.1	32.8	9.52
E950025	E950025	30/10/14	203	0.38	106	513	160	1.56	0.77	53.4	57.0	13.3	47.7	13.7	0.02	2.77	15.8	3.77	12.0	1.37	11.1	1.45	20.1	12.7	37.9	30.7	9.49
E950025	E950025	30/10/14	205	-	106	495	152	1.47	1.55	52.3	63.4	12.8	46.1	12.1	0.10	2.47	16.5	3.94	11.8	1.78	10.8	1.63	20.6	12.5	40.4	32.4	9.15
E950025	E950025	30/10/14	214	-	108	511	163	1.45	4.89	54.7	57.1	13.3	50.5	14.1	0.32	2.52	15.7	3.66	10.7	1.51	10.7	1.64	22.6	11.6	39.5	32.8	9.00
E950025	E950025	30/10/14	204	-	102	487	155	1.44	0.73	48.3	53.7	12.1	45.6	12.1	0.18	2.70	17.5	3.56	10.0	1.49	11.4	1.51	21.6	11.6	39.9	30.2	8.93
E950025	E950025	30/10/14	192	0.55	109	506	161	1.71	2.04	55.7	58.9	13.1	48.3	13.3	0.27	2.71	17.6	3.87	13.0	1.69	12.9	1.69	21.4	12.3	40.9	33.5	9.39
E950025	E950025	30/10/14	211	0.79	113	548	161	1.54	1.90	59.8	66.3	14.1	45.9	12.7	0.19	2.63	18.5	3.96	12.9	1.74	12.1	1.77	22.2	12.9	40.5	33.4	9.04
E950025	E950025	30/10/14	213	-	107	523	169	1.61	1.96	53.9	70.4	13.6	47.8	14.0	0.13	2.83	18.3	4.10	10.9	1.34	10.8	1.59	18.9	11.8	38.7	32.8	9.77
E950025	E950025	30/10/14	208	0.21	113	530	158	1.41	1.06	58.7	72.3	14.9	46.4	14.3	0.08	2.57	21.0	3.35	11.9	1.51	12.5	1.50	22.3	12.7	37.0	33.4	9.65
E950025	E950025	30/10/14	199	-	109	530	154	1.22	1.42	56.2	61.2	14.1	46.5	12.5	0.06	3.10	18.7	3.77	12.6	1.42	11.2	1.65	21.6	12.1	37.7	33.9	9.25
E950025	E950025	30/10/14	226	0.47	112	541	160	1.60	7.90	56.9	84.8	14.2	46.8	12.2	0.27	2.88	17.0	3.74	11.3	1.90	11.3	1.90	22.9	12.4	41.6	33.5	8.92
E950025	E950025	30/10/14	200	-	120	572	169	1.40	1.22	59.6	61.7	14.1	55.4	13.1	0.36	2.68	18.4	4.11	13.7	1.70	14.0	1.63	24.8	12.3	36.0	36.0	9.55
E950025	E950025	30/10/14	211	-	109	507	159	1.79	3.55	56.0	59.8	13.0	46.2	12.2	0.22	2.73	17.0	3.81	10.6	1.77	11.0	1.69	22.2	11.3	38.4	33.2	9.82

.5.2 Bayesian age models

The following pages show the OxCal (Bronk Ramsey, 2009*b*) code and Bayesian age models for the Awassa, Tilo and Chamo sediments. These P_sequences were generated in OxCal using outlier analysis. These models have been corrected for the presence of < 70 cm thick tephras in the archives, which are assumed to have been deposited instantaneously. The age ranges for these tephras were calculated using the *Date* function.

Awassa

Awassa OxCal Script

P_sequence model with outlier analysis

```
 Options()
{
 BCAD=FALSE;
 PlusMinus=FALSE;
};
Plot()
{
 Outlier_Model("General",T(5),U(0,4),"t");
 P_Sequence("",1,0.1,U(-2,2))
 {
  Boundary()
  {
   z=1068.5;
  };
  R_Date("14c 4",6270,130)
  {
   Outlier(0.05);
   z=1025.5;
  };
  Date("AWT5")
  {
   z=980;
  };
  Date("AWT4")
  {
   z=827;
  };
  Date("AWT3")
  {
   z=790;
  };
  R_Date("14c 3",4500,110)
  {
   Outlier(0.05);
   z=669.5;
  };
  Date("AWT2")
  {
   z=532;
  };
  R_Date("14c 2",3180,90)
  {
   Outlier(0.05);
   z=508;
  };
  R_Date("14c 1",1450,80)
  {
   Outlier(0.05);
   z=245;
  };
  Date("AWT1")
  {
   z=239;
  };
  Boundary()
  {
   z=0;
  };
 };
};
```

OxCal output

	Unmodelled (BP)		Modelled (BP)	
Boundary			795	-1713
AWT1			1542	1119
R_Date 14c 1	1535	1187	1546	1190
R_Date 14c 2	3609	3174	3630	3215
AWT2			4089	3261
R_Date 14c 3	5463	4855	5430	4481
AWT3			6309	5524
AWT4			6563	5443
AWT5			7340	6470
R_Date 14c 4	7433	6859	7496	6885
Boundary			8098	6972
P_Sequence Tilo1	-2	2	-2.02	1.412

OxCal age model

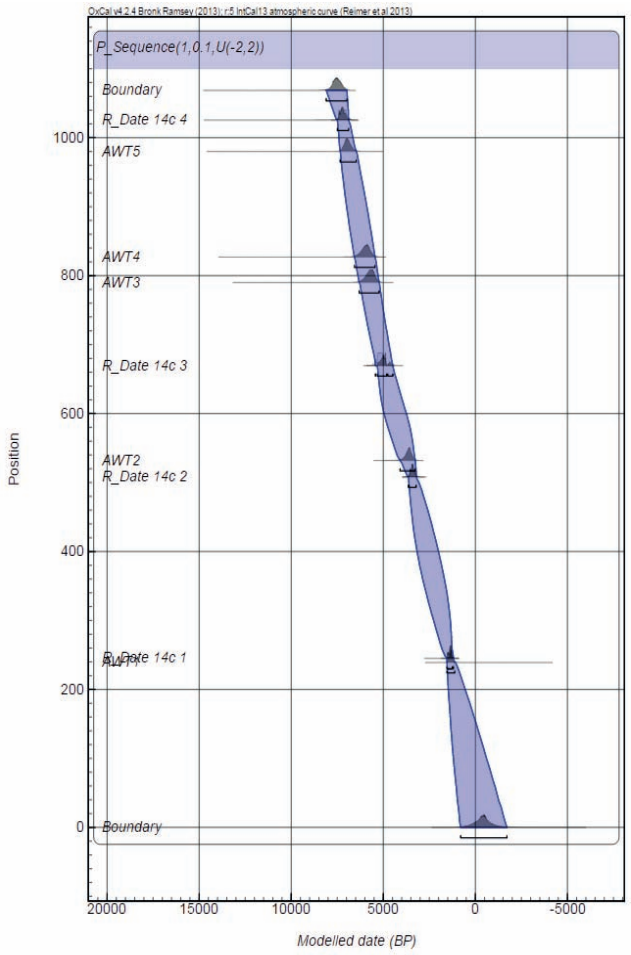

Tilo

Tilo OxCal Script

P_sequence model with outlier analysis

```
Options()
{
 BCAD=FALSE;
 PlusMinus=FALSE;
};
Plot()
{
 Outlier_Model("General",T(5),U(0,4),"t");
 P_Sequence("Tilo1",1,0.05,U(-2,2))
 {
  Boundary()
  {
   z=2117;
  };
  R_Date("14c 7",8840,50)
  {
   Outlier(0.05);
   z=2083.5;
  };
  Date("TT14", )
  {
   z=2039;
  };
  R_Date("14c 6",7930,90)
  {
   Outlier(0.05);
   z=1579;
  };
  Date("TT13", )
  {
   z=1438;
  };
  R_Date("14c 5",6880,50)
  {
   Outlier(0.05);
   z=1109.5;
  };
  Date("TT12", )
  {
   z=735;
  };
  R_Date("14c 4",5520,80)
  {
   Outlier(0.05);
   z=659;
  };
  Date("TT11", )
  {
   z=618.5;
  };
  Date("TT10", )
  {
   z=571;
  };
  R_Date("14c 3",4140,60)
  {
   Outlier(0.05);
   z=485.5;
  };
  Date("TT9", )
  {
   z=479;
  };
  Date("TT8", )
  {
   z=356;
  };
  Date("TT7", )
  {
   z=351;
  };
  R_Date("14c 2",2400,50)
  {
   Outlier(0.05);
   z=314;
  };
  Date("TT6", )
  {
   z=288;
  };
  Date("TT5", )
  {
   z=260;
  };
  Date("TT4", )
  {
   z=245.5;
  };
  Date("TT3", )
  {
   z=213;
  };
  Date("TT2", )
  {
   z=195.5;
  };
  R_Date("14c 1",1390,50)
  {
   Outlier(0.05);
   z=175.5;
  };
  Date("TT1", )
  {
   z=98.5;
  };
  Boundary(Date(N(1995,1)))
  {
   z=0;
  };
 };
};
```

OxCal output

	Unmodelled (BP)		Modelled (BP)	
Boundary	-42	-46	-42	-46
TT1			1308	52
R_Date 14c 1	1390	1186	1394	1185
TT2			2066	1184
TT3			2318	1243
TT4			2480	1295
TT5			2600	1347
TT6			2699	1586
R_Date 14c 2	2702	2342	2703	2340
TT7			3974	2346
TT8			4081	2350
TT9			4853	3928
R_Date 14c 3	4836	4522	4837	4451
TT10			6280	4701
TT11			6432	5060
R_Date 14c 4	6492	6125	6480	6018
TT12			7051	6151
R_Date 14c 5	7828	7617	7827	7613
TT13			7827	7613
R_Date 14c 6	9010	8559	9011	8562
TT14			10175	9394
R_Date 14c 7	10159	9705	10187	9696
Boundary			11086	9681
P_Sequence Tilo1	-2	2	-2.033	-1.6673

OxCal age model

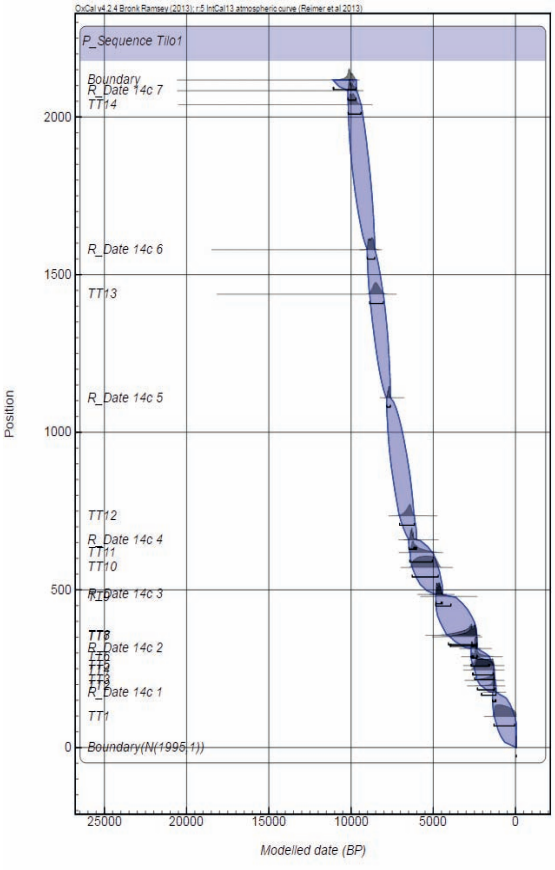

Chamo

Chamo OxCal Script

P_sequence model with outlier analysis

```
Options()
{
 BCAD=FALSE;
 PlusMinus=FALSE;
};
Plot()
{
 Outlier_Model("General",T(5),U(0,4),"t");
 P_Sequence("",1,0.2,U(-2,2))
 {
  Boundary()
  {
   z=1429;
  };
  Date("CHT2")
  {
   z=1360;
  };
  R_Date("14c 7",6578,34)
  {
   Outlier(0.05);
   z=1289;
  };
  R_Date("14c 6",3978,48)
  {
   Outlier(0.05);
   z=987;
  };
  R_Date("14c 5",4081,24)
  {
   Outlier(0.05);
   z=986;
  };
  Date("D2")
  {
   z=920;
  };
  R_Date("14c 3",3304,37)
  {
   Outlier(0.05);
   z=865.5;
  };
  Date("CHT1")
  {
   z=702;
  };
  R_Date("14c 2",1489,81)
  {
   Outlier(0.05);
   z=664;
  };
  R_Date("14c 1",1240,31)
  {
   Outlier(0.05);
   z=639;
  };
  Date("D1")
  {
   z=500;
  };
  Boundary(Date(N(2010,1)))
  {
   z=0;
  };
 };
};
```

OxCal output

	Unmodelled (BP)		Modelled (BP)	
Boundary	-57	-61	-58	-62
AWT1			1542	1119
R_Date 14c 1	1267	1073	1280	1088
R_Date 14c 2	1551	1282	1540	1240
CHT1			2793	1236
R_Date 14c 3	3632	3450	3631	3450
R_Date 14c 5	4801	4447	4872	4438
R_Date 14c 6	4570	4260	4782	4440
R_Date 14c 7	7562	7427	7581	5063
CHT2			9378	5356
Boundary			10264	5644
P_Sequence Chamc	-2	2	-2.02	-1.648

OxCal age model

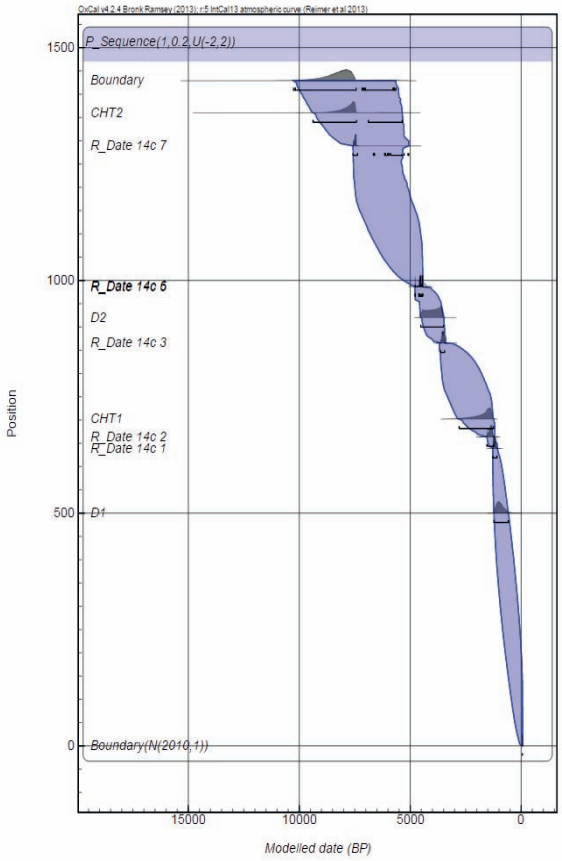

.6 Other outcrop samples

In order to provide greater potential for correlation to source volcanoes, numerous tephra samples from outcrops throughout Ethiopia have been analyses as part of this work. The majority of these outcrop samples have provided an insight into the possible provenance of tephras in archives. However, samples from the Mochena Borago archaeological site (collected by S. Meyer, University of Cologne) were later found to be unsuitable for comparison with Holocene tephras studied here. This is due to uncertainty over the ages of the Mochena Borago tephras, with ages ranging from $\sim$ 3 Ma to Holocene within single tephras. It is possible that these tephras have been reworked, and their stratigraphic integrity compromised. Tephra samples from Ayelu, collected by G. WoldeGabriel (Los Alamos National Laboratory), are late Pleistocene, and significantly older than the Holocene samples identified in this work. Activity from a volcanic centre over this time span would not occur. Nonetheless, these glass analyses are included below, and it is hoped future studies may benefit from these data. Major element glass data are presented to 2 decimal places, trace element data are presented to 3 significant figures. Average silica concentrations in the Ayelu samples, previously determined by G. WoldeGabriel using EPMA, were used as internal standards for LA-ICP-MS analysis.

Limits of detection for all EPMA sessions are given on page 401, the median limits of detection for ATHO-G are given for comparison in the following table headings. Most major elements are present at concentrations above these limits of detection, however, concentrations of MgO and P_2O_5 are below the LLD in many shards.

Trace element analyses were typically undertaken using 20 μm crater diameters, however, †indicates glass shards were analysed using 10 μm crater

diameters. Lower limits of detection (LLD) for LA-ICP-MS analyses are given on page 407. The median LLD concentrations at 20 μm crater diameters of all LA-ICP-MS analytical sessions are given beneath each analyte heading in the following tables. Due to high Sr and Ba concentrations in the gas blanks, coupled with frequent low sample concentrations, some negative concentrations were measured - these are indicated with a dash. Analyses of MPI-DING reference materials were used to check the EPMA and LA-ICP-MS calibrations. These analyses are given on page 398, and are ordered by analysis date.

Unnormalised major element concentrations (wt.%) in tephra samples from Mochena Borago

Label	Tephra	Analysis date	SiO_2 0.08	TiO_2 0.05	Al_2O_3 0.05	MgO 0.04	FeO^T 0.08	MnO 0.07	CaO 0.04	Na_2O 0.08	K_2O 0.03	P_2O_5 0.10	Cl 0.02	Total
MB_3_1	M14 0.75m SE	30/06/15	70.18	0.23	9.98	0.00	3.60	0.12	0.20	2.57	4.89	0.00	0.18	91.95
MB_3_2	M14 0.75m SE	30/06/15	71.94	0.19	9.98	0.00	4.10	0.20	0.18	5.40	4.46	0.01	0.22	96.67
MB_3_4	M14 0.75m SE	30/06/15	70.39	0.20	9.67	0.00	3.54	0.14	0.22	2.58	4.64	0.01	0.16	91.54
MB_3_6	M14 0.75m SE	30/06/15	71.19	0.20	9.33	0.00	4.58	0.17	0.20	4.99	4.21	0.03	0.25	95.15
MB_2_1	M14 0.47m SW	30/06/15	72.52	0.16	9.10	0.00	4.71	0.20	0.15	5.45	4.15	0.04	0.26	96.72
MB_2_2	M14 0.47m SW	30/06/15	71.52	0.21	8.93	0.00	4.69	0.23	0.12	5.06	4.06	0.04	0.25	95.11
MB_2_3	M14 0.47m SW	30/06/15	72.78	0.12	9.36	0.02	4.90	0.20	0.15	5.52	4.28	0.00	0.27	97.60
MB_2_4	M14 0.47m SW	30/06/15	73.01	0.17	9.20	0.00	4.95	0.24	0.19	5.59	4.23	0.00	0.27	97.87
MB_2_5	M14 0.47m SW	30/06/15	72.55	0.17	9.15	0.00	4.63	0.31	0.18	5.36	4.32	0.01	0.30	96.98
MB_2_6	M14 0.47m SW	30/06/15	72.28	0.14	8.90	0.00	5.16	0.29	0.16	5.51	4.24	0.00	0.26	96.93
MB_2_7	M14 0.47m SW	30/06/15	72.35	0.15	9.05	0.00	4.78	0.19	0.13	5.72	4.07	0.01	0.29	96.74
MB_2_8	M14 0.47m SW	30/06/15	73.13	0.14	9.03	0.01	4.71	0.26	0.20	3.57	4.20	0.00	0.29	95.54
MB_2_9	M14 0.47m SW	30/06/15	71.85	0.12	8.97	0.00	5.04	0.26	0.15	5.57	4.07	0.03	0.28	96.32
MB_2_10	M14 0.47m SW	30/06/15	72.17	0.19	9.05	0.00	4.72	0.14	0.20	5.36	4.28	0.00	0.25	96.37
MB_2_11	M14 0.47m SW	30/06/15	72.21	0.14	9.13	0.03	4.57	0.26	0.15	5.33	4.25	0.01	0.26	96.34
MB_2_12	M14 0.47m SW	30/06/15	70.10	0.19	8.93	0.00	4.50	0.33	0.15	5.43	4.08	0.03	0.27	94.02
MB_2_13	M14 0.47m SW	30/06/15	72.82	0.15	9.11	0.00	4.84	0.21	0.16	5.59	4.06	0.00	0.27	97.21
MB_2_14	M14 0.47m SW	30/06/15	72.49	0.18	9.22	0.00	4.92	0.25	0.19	5.61	4.20	0.01	0.27	97.33
MB_2_15	M14 0.47m SW	30/06/15	72.65	0.19	9.42	0.00	4.84	0.22	0.24	5.52	4.32	0.03	0.25	97.70
MB_2_17	M14 0.47m SW	30/06/15	72.46	0.12	9.02	0.05	4.72	0.19	0.19	5.46	4.15	0.00	0.32	96.67
MB_2_18	M14 0.47m SW	30/06/15	70.22	0.16	8.85	0.00	4.83	0.22	0.15	5.01	4.08	0.03	0.22	93.76
MB_2_19	M14 0.47m SW	30/06/15	72.37	0.14	9.21	0.00	4.97	0.21	0.18	5.64	4.12	0.02	0.26	97.12
MB_2_20	M14 0.47m SW	30/06/15	72.38	0.14	9.29	0.00	4.40	0.13	0.13	5.66	4.24	0.02	0.28	96.67
TU2_1	TU2 BWT	03/07/15	68.54	0.25	9.32	0.00	4.46	0.21	0.15	4.91	4.20	0.00	0.20	92.23
TU2_10	TU2 BWT	03/07/15	72.34	0.20	9.44	0.00	4.91	0.24	0.14	5.14	4.13	0.00	0.23	96.77
TU2_11	TU2 BWT	03/07/15	69.97	0.20	8.97	0.00	4.52	0.16	0.17	4.97	4.17	0.03	0.19	93.34
TU2_13	TU2 BWT	03/07/15	71.96	0.22	9.68	0.00	4.63	0.10	0.15	5.10	4.29	0.03	0.19	96.35
TU2_14	TU2 BWT	03/07/15	68.65	0.17	9.03	0.00	4.42	0.22	0.23	5.23	4.24	0.01	0.25	92.45
TU2_15	TU2 BWT	03/07/15	68.75	0.18	9.03	0.01	4.29	0.20	0.19	4.94	4.16	0.00	0.21	91.97
TU2_17†	TU2 BWT	03/07/15	70.23	0.20	9.19	0.03	4.33	0.27	0.15	5.34	4.24	0.09	0.19	94.27
TU2_19	TU2 BWT	03/07/15	70.56	0.27	9.26	0.00	4.51	0.23	0.22	4.94	4.14	0.04	0.23	94.41
TU2_20	TU2 BWT	03/07/15	69.26	0.22	9.17	0.00	4.21	0.21	0.21	5.17	4.15	0.00	0.20	92.80
TU2_21†	TU2 BWT	03/07/15	71.10	0.17	9.51	0.00	4.55	0.24	0.17	5.19	4.26	0.00	0.20	95.40
TU2_22	TU2 BWT	03/07/15	69.75	0.14	9.54	0.00	3.71	0.04	0.09	4.86	3.95	0.00	0.15	92.23
TU2_23	TU2 BWT	03/07/15	69.70	0.29	9.34	0.00	4.63	0.17	0.15	5.38	4.35	0.00	0.24	94.24
TU2_6	TU2 BWT	03/07/15	70.38	0.20	8.96	0.00	4.27	0.27	0.18	5.66	4.38	0.00	0.22	94.51
TU2_7	TU2 BWT	03/07/15	72.06	0.20	9.42	0.00	4.35	0.15	0.17	5.61	4.38	0.02	0.21	96.57
TU2_9	TU2 BWT	03/07/15	69.47	0.19	8.83	0.07	4.34	0.21	0.15	4.88	4.05	0.00	0.29	92.49
M14_0.27_NW_1	M14 0.27m NW	03/07/15	71.33	0.22	9.25	0.04	4.41	0.25	0.16	5.14	4.36	0.01	0.20	95.36
M14_0.27_NW_16	M14 0.27m NW	03/07/15	71.56	0.22	9.16	0.00	4.63	0.17	0.23	5.20	4.54	0.00	0.18	95.88
M14_0.27_NW_18	M14 0.27m NW	03/07/15	72.65	0.28	9.52	0.01	4.83	0.17	0.21	5.25	4.39	0.04	0.19	97.55
M14_0.27_NW_2	M14 0.27m NW	03/07/15	68.08	0.24	9.38	0.00	4.30	0.25	0.33	5.07	4.33	0.00	0.24	92.23
M14_0.27_NW_22	M14 0.27m NW	03/07/15	68.86	0.25	8.84	0.04	4.46	0.19	0.35	5.04	4.30	0.02	0.20	92.55
M14_0.27_NW_24	M14 0.27m NW	03/07/15	71.17	0.23	9.05	0.00	4.68	0.16	0.19	5.23	4.54	0.03	0.22	95.51
M14_0.27_NW_3	M14 0.27m NW	03/07/15	70.82	0.26	9.37	0.00	4.71	0.29	0.18	5.48	4.51	0.02	0.19	95.82
M14_0.27_NW_4	M14 0.27m NW	03/07/15	67.39	0.29	9.11	0.01	4.23	0.20	0.21	4.90	4.21	0.03	0.16	90.74
M14_0.27_NW_5	M14 0.27m NW	03/07/15	71.89	0.23	9.19	0.06	4.33	0.18	0.21	5.25	4.42	0.05	0.23	96.05
BIS_1_1	BIS_1_1	30/06/15	72.83	0.24	9.46	0.00	4.61	0.25	0.18	5.34	4.32	0.00	0.24	97.48
BIS_1_2	BIS_1_2	30/06/15	73.20	0.22	9.38	0.00	4.42	0.28	0.17	4.92	4.38	0.00	0.19	97.18
BIS_1_3	BIS_1_3	30/06/15	72.71	0.21	9.47	0.00	4.38	0.31	0.18	4.93	4.30	0.00	0.23	96.74
BIS_1_4	BIS_1_4	30/06/15	73.39	0.27	9.68	0.00	4.41	0.25	0.16	4.96	4.30	0.00	0.25	97.67
BIS_1_5	BIS_1_5	30/06/15	72.89	0.26	9.35	0.00	4.48	0.26	0.18	5.17	4.31	0.01	0.21	97.13
BIS_1_6	BIS_1_6	30/06/15	73.05	0.26	9.53	0.00	4.63	0.16	0.20	5.08	4.24	0.00	0.20	97.34
BIS_1_7	BIS_1_7	30/06/15	71.47	0.19	9.20	0.01	4.28	0.18	0.17	5.05	4.20	0.00	0.22	94.97
BIS_1_8	BIS_1_8	30/06/15	72.46	0.26	9.36	0.00	4.50	0.19	0.17	4.97	4.29	0.01	0.23	96.44

Continued on next page

Unnormalised major element concentrations (wt.%) in tephra samples from Mochena Borago

Label	Tephra	Analysis date	SiO_2 0.08	TiO_2 0.05	Al_2O_3 0.05	MgO 0.04	FeO^T 0.08	MnO 0.07	CaO 0.04	Na_2O 0.08	K_2O 0.03	P_2O_5 0.10	Cl 0.02	Total
BIS_1_9	BIS_1_9	30/06/15	72.50	0.23	9.36	0.00	4.46	0.22	0.17	5.02	4.39	0.00	0.23	96.59
BIS_1_11	BIS_1_11	30/06/15	73.26	0.24	9.58	0.00	4.56	0.23	0.14	4.89	4.21	0.03	0.20	97.35
BIS_1_12	BIS_1_12	30/06/15	72.78	0.27	9.30	0.00	4.57	0.10	0.18	5.02	4.28	0.04	0.24	96.78
BIS_1_13	BIS_1_13	30/06/15	73.15	0.24	9.51	0.00	4.29	0.26	0.21	5.08	4.25	0.00	0.23	97.22
BIS_1_14	BIS_1_14	30/06/15	73.12	0.22	9.63	0.00	4.50	0.20	0.20	5.38	4.32	0.00	0.23	97.80
BIS_1_15	BIS_1_15	30/06/15	73.14	0.22	9.47	0.00	4.40	0.09	0.18	5.53	4.30	0.00	0.22	97.54
BIS_1_16	BIS_1_16	30/06/15	74.25	0.27	9.53	0.00	4.68	0.32	0.16	2.31	4.30	0.00	0.22	96.03
BIS_1_17	BIS_1_17	30/06/15	73.24	0.24	9.64	0.01	4.39	0.25	0.16	5.28	4.05	0.04	0.22	97.51
BIS_1_19	BIS_1_19	30/06/15	73.17	0.19	9.58	0.05	4.36	0.12	0.22	5.08	4.25	0.02	0.24	97.28
BIS_1_20	BIS_1_20	30/06/15	73.23	0.29	9.27	0.03	4.44	0.24	0.17	4.81	4.56	0.00	0.23	97.27
BIS_2_1	BIS_2_1	30/06/15	72.35	0.29	9.46	0.00	4.32	0.22	0.20	4.90	4.14	0.03	0.20	96.11
BIS_2_2	BIS_2_2	30/06/15	74.39	0.22	9.77	0.00	4.72	0.10	0.17	5.13	4.43	0.05	0.21	99.19
BIS_2_4	BIS_2_4	30/06/15	69.45	0.25	8.60	0.05	5.25	0.23	0.13	5.40	4.00	0.00	0.38	93.73
BIS_2_6	BIS_2_6	30/06/15	70.13	0.26	9.31	0.01	4.53	0.22	0.19	4.77	4.20	0.01	0.22	93.86
BIS_2_7	BIS_2_7	30/06/15	73.38	0.25	9.45	0.00	4.49	0.28	0.15	5.02	4.33	0.00	0.23	97.58
BIS_2_8	BIS_2_8	30/06/15	70.82	0.27	8.87	0.00	4.47	0.22	0.21	5.15	4.02	0.00	0.23	94.25
BIS_2_9	BIS_2_9	30/06/15	69.65	0.25	8.77	0.02	4.27	0.19	0.17	4.79	4.13	0.00	0.25	92.48
BIS_2_10	BIS_2_10	30/06/15	74.22	0.21	9.43	0.00	4.72	0.15	0.17	5.16	4.48	0.00	0.23	98.76
BIS_2_11	BIS_2_11	30/06/15	70.66	0.30	9.03	0.00	4.58	0.28	0.20	4.58	4.10	0.02	0.18	93.93
BIS_2_12	BIS_2_12	30/06/15	73.86	0.23	9.52	0.00	4.57	0.22	0.16	4.93	4.43	0.07	0.23	98.24
BIS_2_13	BIS_2_13	30/06/15	73.29	0.24	9.60	0.00	4.67	0.22	0.17	5.41	4.31	0.03	0.27	98.21
BIS_2_14	BIS_2_14	30/06/15	73.52	0.18	10.16	0.03	3.32	0.12	0.13	4.51	4.24	0.01	0.21	96.43
BIS_2_15	BIS_2_15	30/06/15	69.02	0.35	8.61	0.00	5.06	0.21	0.28	4.54	4.16	0.00	0.30	92.53
BIS_2_16	BIS_2_16	30/06/15	72.40	0.26	9.42	0.00	4.26	0.21	0.19	4.81	4.18	0.01	0.25	95.99
BIS_2_19	BIS_2_19	30/06/15	72.83	0.29	9.68	0.03	4.45	0.12	0.22	5.16	4.33	0.00	0.26	97.38
BIS_2_20	BIS_2_20	30/06/15	70.79	0.27	9.19	0.00	4.53	0.14	0.18	4.83	4.19	0.00	0.19	94.31

Trace element concentrations (ppm) in tephra samples from Mochena Borago

Label	Tephra	Analysis date	Rb 0.62	Sr 1.05	Y 0.17	Zr 0.37	Nb 0.07	Cs 0.19	Ba 1.88	La 0.09	Ce 0.07	Pr 0.06	Nd 0.25	Sm 0.14	Eu 0.13	Tb 0.06	Dy 0.13	Ho 0.04	Er 0.07	Tm 0.05	Yb 0.15	Lu 0.04	Hf 0.08	Ta 0.06	Pb 0.12	Th 0.01	U 0.00
MB_3_1	M14 0.75m SE	28/07/15	106	-	168	1500	187	0.96	64.4	171	339	40.2	156	34.9	3.12	4.89	30.5	6.76	20.2	2.67	18.7	2.42	36.8	12.7	35.1	21.5	5.56
MB_3_2	M14 0.75m SE	28/07/15	116	-	193	1580	206	0.79	78.3	168	347	41.1	173	34.9	4.42	5.45	35.7	6.51	21.1	2.74	20.6	2.63	34.1	14.0	29.9	17.6	5.19
MB_3_4	M14 0.75m SE	28/07/15	125	-	177	1510	188	1.02	50.5	175	338	40.4	149	29.8	2.77	4.61	30.8	6.62	18.3	2.49	17.2	2.76	35.2	13.0	34.1	20.2	5.54
MB_3_6	M14 0.75m SE	28/07/15	147	9.76	274	2220	275	1.61	65.7	247	479	61.1	240	48.9	6.77	7.48	51.0	10.9	29.2	4.42	29.0	4.13	55.1	19.0	47.7	27.2	8.15
MB_2_1	M14 0.47m SW	28/07/15	155	-	359	2910	324	1.27	53.9	308	587	73.6	295	55.7	7.65	10.5	58.9	13.2	39.9	6.04	35.6	5.01	73.2	23.7	51.7	36.2	8.65
MB_2_2	M14 0.47m SW	28/07/15	154	-	314	2650	309	1.17	56.1	296	567	67.5	278	61.3	6.74	9.21	63.6	12.0	33.6	5.15	32.7	4.38	67.7	25.6	51.9	33.1	9.37
MB_2_3	M14 0.47m SW	28/07/15	143	-	296	2380	299	1.37	44.7	266	504	64.6	262	54.2	7.83	9.09	54.5	11.5	34.3	5.14	33.0	4.80	60.8	21.1	47.2	32.0	8.35
MB_2_4	M14 0.47m SW	28/07/15	155	-	339	2790	325	1.22	56.3	316	591	73.6	307	62.5	8.29	10.7	66.4	13.2	39.0	5.16	35.4	4.86	69.6	24.3	52.4	35.1	9.58
MB_2_5	M14 0.47m SW	28/07/15	152	-	301	2490	298	1.43	55.0	283	536	64.2	258	54.6	6.72	9.00	56.5	10.9	35.0	4.60	28.9	4.82	60.1	21.9	47.3	32.7	9.06
MB_2_6	M14 0.47m SW	28/07/15	160	1.06	322	2740	315	1.56	49.3	286	553	68.0	270	55.2	7.03	8.58	55.4	12.4	35.4	4.97	33.5	5.02	67.0	22.2	51.1	33.0	8.62
MB_2_7	M14 0.47m SW	28/07/15	159	-	344	2890	343	1.49	51.3	307	595	72.8	315	62.6	8.82	9.89	63.0	12.9	39.8	5.45	36.7	5.28	72.5	23.7	57.1	37.4	9.17
MB_2_8	M14 0.47m SW	28/07/15	155	-	287	2360	294	1.44	49.2	264	514	62.1	256	50.0	7.01	8.16	54.1	11.4	30.3	4.32	30.3	4.00	58.8	19.9	47.1	30.3	8.45
MB_2_9	M14 0.47m SW	28/07/15	159	1.94	346	2770	337	1.42	62.3	308	604	72.8	299	67.2	9.13	9.93	64.8	13.5	37.3	5.54	32.6	4.70	70.1	24.0	54.9	35.9	9.77
MB_2_10	M14 0.47m SW	28/07/15	157	-	326	2740	322	1.56	53.5	293	593	71.7	292	65.3	7.36	9.93	62.1	12.0	38.9	5.50	36.2	5.55	69.9	24.1	51.6	36.4	9.16
MB_2_11	M14 0.47m SW	28/07/15	155	-	325	2670	320	1.58	48.4	282	574	69.9	281	58.3	7.33	8.90	62.3	11.0	33.3	4.66	32.8	4.94	65.4	22.6	54.2	33.7	8.41
MB_2_12	M14 0.47m SW	28/07/15	150	-	321	2650	317	1.63	52.2	278	573	72.3	279	54.9	7.34	10.2	61.7	12.3	38.1	4.70	33.0	4.78	62.0	22.5	49.5	31.8	8.76
MB_2_13	M14 0.47m SW	28/07/15	165	-	333	2720	328	1.59	57.4	302	575	70.7	278	54.7	7.45	9.86	59.3	12.1	35.6	5.27	35.9	5.10	67.1	23.5	60.2	34.6	9.43
MB_2_14	M14 0.47m SW	28/07/15	153	-	301	2480	291	0.93	58.3	274	539	65.0	274	54.9	6.89	8.79	57.7	12.0	33.6	4.68	30.9	4.49	61.4	21.6	52.9	30.7	8.84
MB_2_15	M14 0.47m SW	28/07/15	138	-	276	2250	277	1.64	55.9	251	521	60.6	248	48.6	5.82	7.90	52.5	9.31	31.5	3.72	27.7	4.74	53.5	19.4	46.6	28.4	7.45
MB_2_17	M14 0.47m SW	28/07/15	160	-	328	2640	336	1.44	49.1	296	583	74.0	268	57.2	7.68	9.66	59.5	10.8	37.2	5.14	34.0	4.72	67.6	24.0	56.0	34.8	9.43
MB_2_18	M14 0.47m SW	28/07/15	142	-	285	2350	274	2.73	70.7	263	515	62.3	248	54.5	6.71	8.03	50.9	10.6	31.5	4.58	30.4	4.17	56.8	19.9	44.1	29.8	8.01
MB_2_19	M14 0.47m SW	28/07/15	155	-	319	2590	318	1.54	50.7	279	545	66.1	277	57.1	7.78	9.14	57.8	11.8	33.8	5.23	29.8	4.49	64.8	21.4	52.3	33.2	8.66
MB_2_20	M14 0.47m SW	28/07/15	157	-	309	2540	317	1.29	47.5	271	538	66.1	272	57.1	6.97	9.95	57.6	10.9	34.1	4.34	30.1	4.58	62.0	20.8	53.6	31.2	9.16
TU2_1	TU2 BWT	29/07/15	164	-	360	2800	334	1.79	112	306	525	73.3	307	63.5	7.97	9.10	59.1	12.7	37.0	6.35	33.6	4.29	66.2	20.4	48.1	36.5	8.32
TU2_10	TU2 BWT	29/07/15	143	4.28	340	2720	321	1.10	56.0	306	564	69.7	295	60.5	7.76	10.0	62.9	12.5	34.7	5.54	31.7	4.95	69.3	23.5	46.6	34.8	8.49
TU2_11	TU2 BWT	29/07/15	135	-	301	2500	286	1.07	59.5	281	532	65.5	291	55.5	6.82	9.44	56.2	11.0	31.2	4.96	33.0	4.34	61.8	21.3	42.2	32.0	7.98
TU2_13	TU2 BWT	29/07/15	131	-	295	2380	282	1.10	58.1	261	499	61.2	263	52.5	6.70	8.86	57.9	11.1	34.5	4.55	29.9	4.50	63.8	20.9	44.3	32.5	7.87
TU2_14	TU2 BWT	29/07/15	138	-	301	2490	284	1.22	61.9	277	506	63.9	266	57.6	6.51	8.73	56.1	11.4	35.5	4.91	31.4	4.69	61.0	21.1	44.5	31.7	7.96
TU2_15	TU2 BWT	29/07/15	132	-	285	2260	287	1.03	55.3	260	481	57.4	250	52.9	6.33	8.31	51.0	9.99	30.8	4.25	27.1	3.97	54.6	18.9	41.9	29.1	7.49
TU2_17	TU2 BWT	29/07/15	127	-	417	3170	333	1.41	137	348	576	83.5	326	69.5	7.35	12.6	73.5	17.6	46.5	6.03	47.6	5.43	84.7	25.3	49.6	44.1	9.84
TU2_19	TU2 BWT	29/07/15	140	-	326	2670	293	0.80	69.2	293	529	68.0	283	54.8	7.97	8.73	62.0	12.3	35.9	5.24	32.8	4.76	64.8	21.2	44.1	32.3	8.22
TU2_20	TU2 BWT	29/07/15	143	-	319	2550	310	1.40	63.1	278	541	68.1	270	64.1	7.53	8.59	52.6	11.0	34.7	4.48	29.7	4.13	63.7	21.0	45.0	32.6	8.32
TU2_21	TU2 BWT	29/07/15	131	-	364	2810	301	1.04	53.7	330	596	76.6	303	64.0	10.7	10.1	73.4	14.7	45.1	6.25	35.7	5.24	78.3	24.0	45.8	41.5	8.14
TU2_22	TU2 BWT	29/07/15	100	-	264	2420	273	0.64	63.0	237	452	56.5	233	52.3	5.52	7.84	49.4	9.86	27.6	4.22	28.5	3.61	59.2	20.4	34.2	28.7	7.90
TU2_23	TU2 BWT	29/07/15	131	-	291	2340	289	1.57	63.7	263	490	61.7	262	59.0	6.26	8.79	58.3	11.9	35.9	4.49	29.3	4.18	58.6	20.0	43.9	30.8	7.45
TU2_6	TU2 BWT	29/07/15	138	-	359	2900	309	1.34	55.8	314	556	73.6	314	65.1	8.02	10.2	62.1	13.1	37.5	5.86	35.5	5.05	70.1	22.7	46.5	36.2	7.60
TU2_7	TU2 BWT	29/07/15	134	-	367	2850	297	1.45	70.8	318	571	73.8	326	62.9	8.39	10.5	63.4	13.0	38.3	5.71	38.0	5.60	70.1	22.1	41.9	36.3	7.60
TU2_9	TU2 BWT	29/07/15	130	-	287	2300	280	0.80	64.6	259	492	61.0	257	53.6	7.14	9.39	54.0	11.7	31.5	4.83	27.8	3.85	59.0	19.5	42.5	30.0	7.64
M14_0.27_NW_1	M14 0.27m NW	29/07/15	131	-	335	2710	301	1.14	74.4	306	557	74.3	319	62.5	7.37	9.87	64.3	12.1	36.3	5.18	32.9	4.95	71.8	22.1	43.3	34.9	7.92
M14_0.27_NW_16	M14 0.27m NW	29/07/15	131	-	277	2400	288	1.10	62.2	265	521	63.6	265	65.7	6.18	8.28	52.2	11.2	33.6	4.33	30.3	4.49	62.6	19.9	43.8	30.9	7.72
M14_0.27_NW_18	M14 0.27m NW	29/07/15	120	-	281	2330	290	1.27	45.7	247	481	59.4	253	55.1	6.39	8.49	59.8	12.0	33.2	4.07	31.1	3.35	48.0	20.3	44.2	30.6	7.15
M14_0.27_NW_2	M14 0.27m NW	29/07/15	130	-	296	2540	280	1.30	74.6	296	529	68.8	312	61.7	6.28	9.95	62.3	11.5	34.7	4.91	31.5	4.98	72.9	20.5	41.7	34.2	6.89

Continued on next page

Trace element concentrations (ppm) in tephra samples from Mochena Borago

Label	Tephra	Analysis date	Rb 0.62	Sr 1.05	Y 0.17	Zr 0.37	Nb 0.07	Cs 0.19	Ba 1.88	La 0.09	Ce 0.07	Pr 0.06	Nd 0.25	Sm 0.14	Eu 0.13	Tb 0.06	Dy 0.13	Ho 0.04	Er 0.07	Tm 0.05	Yb 0.15	Lu 0.04	Hf 0.08	Ta 0.06	Pb 0.12	Th 0.01	U 0.00
M14_0.27_NW_22	M14 0.27m NW	29/07/15	112	-	280	2280	267	0.78	84.5	251	451	60.7	255	51.9	6.50	7.42	53.4	10.9	29.8	4.15	28.4	4.06	57.0	18.9	39.0	27.8	6.13
M14_0.27_NW_24	M14 0.27m NW	29/07/15	128	-	311	2580	288	0.97	58.6	279	491	64.6	268	62.8	7.32	9.02	60.9	11.6	35.8	5.11	32.9	4.71	67.8	19.8	41.2	32.7	6.67
M14_0.27_NW_3	M14 0.27m NW	29/07/15	125	-	301	2460	273	1.12	72.0	287	513	65.5	278	56.6	6.79	9.59	56.1	11.5	36.5	5.14	30.7	4.54	61.0	21.7	45.9	33.1	7.55
M14_0.27_NW_4	M14 0.27m NW	29/07/15	118	-	249	2200	279	0.62	69.9	250	480	57.7	244	50.8	7.42	8.02	50.8	9.96	28.1	4.28	26.8	4.17	55.2	17.6	43.1	29.0	7.20
M14_0.27_NW_5	M14 0.27m NW	29/07/15	119	-	261	2170	267	0.92	53.2	247	473	58.2	238	53.7	5.88	7.84	48.2	10.0	28.9	3.54	25.4	3.42	57.4	17.6	43.3	28.7	6.86
BIS_1_1	BIS_1_1	28/07/15	124	-	271	2240	252	1.07	103	240	463	58.4	251	47.5	5.76	8.29	53.5	9.78	28.9	3.41	28.3	3.84	56.3	16.9	39.5	27.1	5.98
BIS_1_2	BIS_1_2	28/07/15	122	-	284	2280	250	1.05	101	248	466	59.2	264	53.7	7.22	8.77	53.7	10.1	31.7	4.21	29.3	3.59	57.1	19.4	40.2	28.7	6.97
BIS_1_3	BIS_1_3	28/07/15	124	-	268	2260	250	0.99	89.0	234	444	57.2	239	42.6	6.23	7.78	50.4	10.1	29.8	4.18	26.9	3.91	55.7	17.1	38.9	25.9	7.05
BIS_1_4	BIS_1_4	28/07/15	116	-	258	2160	254	0.68	91.3	240	443	55.3	253	48.8	5.53	8.29	46.3	10.2	29.8	4.55	27.1	3.96	52.7	18.3	40.9	27.1	6.20
BIS_1_5	BIS_1_5	28/07/15	118	-	255	2050	238	0.90	87.1	224	446	53.2	235	46.4	6.39	7.85	50.5	9.59	29.1	3.50	27.9	3.32	54.5	16.6	38.8	26.3	6.67
BIS_1_6	BIS_1_6	28/07/15	118	-	250	1970	246	0.99	86.3	221	447	56.7	231	48.9	5.95	6.83	48.9	10.9	30.6	3.67	27.0	3.73	52.0	17.7	37.8	25.0	6.14
BIS_1_7	BIS_1_7	28/07/15	119	-	259	2080	246	1.21	87.8	227	465	56.0	232	47.3	5.47	7.66	45.3	8.61	29.8	4.29	26.2	3.95	53.4	17.3	37.9	27.4	6.53
BIS_1_8	BIS_1_8	28/07/15	128	-	259	2100	251	1.34	100	233	445	57.3	232	48.9	5.25	7.22	42.3	9.70	27.8	4.06	24.9	4.02	51.1	19.5	44.3	27.6	6.16
BIS_1_9	BIS_1_9	28/07/15	115	-	233	1850	233	0.91	83.7	209	422	50.4	206	43.2	6.07	6.83	42.8	8.18	26.2	3.52	21.8	3.20	46.2	15.6	37.4	23.9	6.52
BIS_1_11	BIS_1_11	28/07/15	123	-	220	1920	244	1.11	87.1	212	446	52.1	208	47.9	5.43	7.04	43.7	9.40	27.8	3.80	24.4	3.78	50.2	17.0	42.5	22.4	6.05
BIS_1_12	BIS_1_12	28/07/15	121	-	254	2080	240	1.25	93.1	224	468	58.1	236	48.6	5.91	8.61	49.8	9.76	28.0	4.59	26.9	4.24	53.1	17.3	42.3	26.1	6.92
BIS_1_13	BIS_1_13	28/07/15	115	-	220	1880	243	1.29	98.5	214	437	52.0	203	41.5	5.22	6.89	42.2	8.75	27.1	3.50	23.8	3.55	46.2	16.4	39.6	23.6	6.21
BIS_1_14	BIS_1_14	28/07/15	116	-	250	1990	235	1.09	96.2	222	445	56.3	216	43.0	5.59	7.77	45.0	8.11	26.3	3.73	27.7	3.49	49.0	17.4	39.2	27.2	6.80
BIS_1_15	BIS_1_15	28/07/15	121	-	250	2080	256	0.97	81.6	233	474	53.2	223	44.6	6.52	7.59	46.2	10.5	28.1	3.99	24.5	3.83	48.9	17.9	43.7	25.4	6.80
BIS_1_16	BIS_1_16	28/07/15	128	-	253	2130	254	1.26	102	236	466	56.2	239	46.0	6.56	6.93	51.9	9.89	31.2	4.01	25.7	3.58	55.4	17.9	40.5	27.1	7.24
BIS_1_17	BIS_1_17	28/07/15	115	-	238	2020	245	0.52	82.1	217	446	52.3	215	46.6	6.09	7.83	45.5	9.01	30.0	4.16	23.2	3.78	48.7	16.2	41.6	24.2	7.38
BIS_1_19	BIS_1_19	28/07/15	119	-	252	2120	242	0.85	90.0	234	451	54.6	219	45.0	4.88	7.90	49.6	9.40	28.9	4.02	24.2	3.59	51.2	18.3	41.9	26.5	6.85
BIS_1_20	BIS_1_20	28/07/15	128	-	247	2030	247	0.92	84.9	222	449	52.6	210	45.1	6.37	7.42	48.0	9.47	27.9	4.02	25.3	3.91	53.9	17.8	41.3	26.7	6.68
BIS_2_1	BIS_2_1	28/07/15	123	-	277	2280	259	0.97	74.4	250	467	58.4	256	50.3	6.33	7.60	51.4	10.4	31.6	4.07	30.4	3.93	53.1	18.0	39.4	28.1	6.72
BIS_2_2	BIS_2_2	28/07/15	131	-	265	2230	256	1.14	81.8	251	488	58.5	243	50.5	4.91	7.72	50.2	10.5	28.9	3.80	24.8	3.58	56.3	17.6	41.8	27.3	6.65
BIS_2_4	BIS_2_4	28/07/15	165	-	434	3750	361	0.94	22.3	392	699	87.5	353	72.7	5.67	12.6	76.5	15.8	47.4	7.23	42.7	6.36	93.0	26.4	55.7	45.3	9.33
BIS_2_6	BIS_2_6	28/07/15	143	-	310	2600	303	2.08	102	268	531	63.4	253	51.8	7.53	8.44	55.4	10.6	37.3	6.84	30.0	4.31	62.1	21.7	46.6	33.3	7.91
BIS_2_7	BIS_2_7	28/07/15	124	-	290	2420	252	0.70	84.8	268	485	63.3	250	51.2	6.42	8.55	56.4	10.8	35.3	4.44	29.2	4.25	58.1	17.6	39.4	30.1	7.41
BIS_2_8	BIS_2_8	28/07/15	131	-	316	2590	274	1.26	70.7	277	524	65.2	273	57.4	7.15	9.19	54.9	12.3	33.2	5.02	30.2	4.65	62.2	20.1	41.4	32.9	7.75
BIS_2_9	BIS_2_9	28/07/15	118	-	281	2360	256	1.38	74.0	254	480	62.8	251	50.0	7.54	8.52	56.5	11.9	30.7	4.82	28.7	4.23	57.5	19.7	39.1	30.9	7.14
BIS_2_10	BIS_2_10	28/07/15	120	-	252	2120	248	0.98	75.7	233	464	54.2	226	44.1	5.57	7.68	48.2	10.2	26.5	4.04	26.1	3.97	55.1	18.0	40.8	26.9	6.48
BIS_2_11	BIS_2_11	28/07/15	110	-	161	1410	181	0.57	17.2	168	348	40.2	152	29.3	3.69	4.76	29.6	6.74	16.3	2.34	15.0	2.46	32.9	12.7	24.9	22.7	5.34
BIS_2_12	BIS_2_12	28/07/15	131	-	262	2190	270	1.12	90.0	248	502	59.0	247	52.6	6.81	8.13	48.5	10.2	31.2	4.15	29.6	4.74	55.7	19.1	43.3	29.9	8.26
BIS_2_13	BIS_2_13	28/07/15	122	-	276	2240	257	1.15	94.5	248	492	58.8	247	50.0	6.60	8.23	52.1	9.59	28.8	3.87	27.5	3.96	55.0	18.0	38.4	28.3	7.15
BIS_2_14	BIS_2_14	28/07/15	113	-	182	1680	175	0.81	3.55	148	294	37.8	151	31.1	2.90	6.05	36.4	7.72	21.6	3.01	20.2	2.96	47.8	14.0	35.2	27.2	6.39
BIS_2_15	BIS_2_15	28/07/15	105	-	259	2130	223	0.94	27.0	230	414	51.5	211	42.1	4.97	7.84	49.6	10.6	29.8	4.29	29.0	3.97	58.3	17.6	27.8	29.0	6.33
BIS_2_16	BIS_2_16	28/07/15	130	-	295	2490	263	0.99	76.9	277	506	62.5	251	51.8	6.83	8.56	59.4	11.5	31.6	4.29	28.5	4.64	59.3	20.4	38.9	32.5	7.41
BIS_2_19	BIS_2_19	28/07/15	126	-	298	2520	266	1.28	75.1	279	508	65.7	269	57.7	6.15	9.16	57.5	10.9	32.7	5.16	29.8	4.42	62.0	19.6	38.8	31.8	6.67
BIS_2_20	BIS_2_20	28/07/15	133	-	344	2850	275	1.13	85.8	313	558	76.0	299	62.8	7.98	9.34	62.7	12.2	39.2	5.76	35.1	5.67	75.3	23.2	42.8	35.9	7.96

Trace element concentrations (ppm) in tephra samples from Ayelu

Label	Tephra	Analysis date	Rb 0.62	Sr 1.05	Y 0.17	Zr 0.37	Nb 0.07	Cs 0.19	Ba 1.88	La 0.09	Ce 0.07	Pr 0.06	Nd 0.25	Sm 0.14	Eu 0.13	Tb 0.06	Dy 0.13	Ho 0.04	Er 0.07	Tm 0.05	Yb 0.15	Lu 0.04	Hf 0.08	Ta 0.06	Pb 0.12	Th 0.01	U 0.00
MA002	MA002	31/03/14	109	16.9	72.7	580	112	1.15	875	71.9	134	15.7	53.3	13.0	1.93	1.80	10.8	2.17	5.94	0.86	6.57	1.06	13.5	6.49	15.1	13.8	4.34
MA002	MA002	31/03/14	140	323	76	783	124	2.51	531	73.2	138	16.6	59.5	10.4	1.77	2.27	11.1	2.59	9.27	1.08	7.60	1.17	18.1	6.93	23.6	15.0	3.97
MA002	MA002	31/03/14	139	191	83.3	784	124	1.59	429	87.1	148	17.6	69.1	14.5	1.64	2.30	14.2	3.01	8.70	1.04	7.62	1.52	17.5	8.47	22.2	17.1	4.05
MA002	MA002	31/03/14	132	118	90.4	740	122	1.17	458	86.3	152	19.4	68.7	16.2	1.60	2.32	13.9	2.70	9.39	1.32	10.1	1.05	15.0	8.79	17.9	17.7	4.55
MA002	MA002	31/03/14	139	85.0	95.8	730	128	1.60	405	86.5	156	19.6	75.4	11.9	1.87	2.39	13.8	2.99	9.04	1.44	8.92	1.42	16.6	7.86	18.7	16.8	4.62
MA002	MA002	31/03/14	152	148	81.6	756	127	2.44	694	90.0	156	19.7	69.3	15.2	2.24	2.27	12.9	2.95	7.70	1.20	7.66	1.15	16.7	7.45	22.9	20.2	4.36
MA002	MA002	31/03/14	139	237	86.3	673	127	2.26	481	91.9	156	21.7	75.5	17.6	2.31	2.48	13.3	2.58	10.1	0.86	7.87	1.05	16.3	8.36	19.5	14.9	3.86
MA002	MA002	31/03/14	129	11.1	94.9	734	132	1.28	688	89.5	157	19.3	69.7	14.1	2.05	2.38	15.3	2.97	10.8	1.43	9.42	1.39	18.3	9.43	19.7	18.7	4.86
MA002	MA002	31/03/14	139	19.8	88.6	691	132	1.16	492	84.7	159	18.1	61.8	13.9	2.17	1.87	12.9	3.05	8.38	1.05	8.40	1.06	14.7	8.14	17.0	17.2	5.12
MA002	MA002	31/03/14	121	35.6	83.5	752	130	1.03	735	87.3	163	18.0	65.5	11.4	1.76	2.33	13.5	2.79	8.47	1.34	8.29	1.38	16.3	7.28	16.5	16.6	4.70
MA002	MA002	31/03/14	130	12.0	93.5	749	137	1.29	476	90.4	167	19.9	70.1	14.0	1.90	2.59	16.2	3.28	10.0	1.59	9.44	1.25	14.2	8.24	22.5	17.7	6.94
MA002	MA002	31/03/14	144	55.4	95.4	771	136	1.58	438	92.4	169	19.3	68.4	17.5	1.68	2.45	14.3	3.42	8.3	1.37	9.57	1.30	18.8	8.52	21.0	18.1	5.68
MA002	MA002	31/03/14	136	32.5	94.8	769	135	1.26	517	93.9	169	20.5	72.3	14.1	1.91	2.60	17.0	3.18	10.2	1.40	9.49	1.35	16.7	8.86	17.5	17.6	4.52
MA002	MA002	31/03/14	130	19.7	100	784	134	0.94	541	92.8	169	20.7	77.0	14.2	1.99	2.86	16.7	3.31	10.3	1.47	10.2	1.21	16.7	8.73	16.9	19.3	5.14
MA002	MA002	31/03/14	130	7.28	98.8	786	136	1.12	469	94.1	171	20.0	68.4	14.5	2.10	2.49	16.5	3.34	9.74	1.43	9.46	1.44	19.5	9.07	17.7	19.4	5.65
MA002	MA002	31/03/14	132	44.9	97.5	791	136	1.58	514	92.9	171	19.8	72.1	15.3	2.14	2.94	16.6	3.05	9.69	1.22	8.79	1.25	17.4	8.49	19.1	18.2	6.48
MA002	MA002	31/03/14	138	6.55	102	811	140	1.20	444	95.4	172	21.3	74.5	14.9	1.85	2.93	15.6	3.84	10.1	1.43	10.4	1.42	18.8	8.43	16.7	18.7	5.52
MA002	MA002	31/03/14	128	18.5	101	797	136	1.16	665	98.8	173	21.9	75.9	14.5	2.76	2.30	15.6	3.55	9.38	1.47	9.12	1.44	17.9	9.05	17.6	18.5	5.20
MA002	MA002	31/03/14	128	84.4	101	807	134	1.11	499	94.4	173	21.7	76.9	16.9	2.76	3.09	16.3	3.20	10.4	1.72	9.83	1.15	19.6	8.94	18.4	19.2	5.08
MA002	MA002	31/03/14	129	9.83	90.3	754	134	1.27	490	92.6	174	20.6	70.7	15.5	1.76	2.46	15.6	3.30	11.3	1.43	8.53	1.55	17.2	8.50	18.0	18.1	5.21
MA002	MA002	31/03/14	134	16.8	100	797	138	1.06	457	97.6	176	20.5	70.4	17.0	2.03	2.67	15.0	3.65	9.07	1.27	10.2	1.26	17.7	8.91	17.1	18.6	5.23
MA002	MA002	31/03/14	127	69.6	108	858	134	0.99	516	102	176	21.5	77.1	16.2	1.81	3.01	16.9	3.33	11.2	1.65	12.4	1.69	20.4	8.96	18.7	20.8	5.02
MA002	MA002	31/03/14	134	7.73	98.5	799	143	1.08	491	98.7	178	21.6	70.5	14.0	2.15	2.59	16.8	3.36	10.8	1.57	10.2	1.59	17.5	9.06	18.5	19.0	5.76
MA002	MA002	31/03/14	133	8.07	99.6	818	144	1.17	526	101	181	20.4	75.9	15.9	2.01	2.78	16.8	3.49	9.17	1.41	11.5	1.34	19.1	9.51	18.0	19.2	5.61
MA002	MA002	31/03/14	140	7.96	102	834	142	1.03	520	102	181	22.6	76.6	16.6	2.37	2.84	18.6	3.89	10.5	1.29	9.81	1.60	18.3	8.22	18.2	20.6	5.45
MA002	MA002	31/03/14	139	13.3	103	801	143	1.18	451	100	183	20.3	78.4	16.3	2.05	2.53	17.8	3.75	11.0	1.59	9.56	1.59	18.4	9.09	19.0	20.1	5.94
MA002	MA002	31/03/14	134	22.3	106	817	140	1.10	551	104	183	21.1	73.5	18.5	2.19	2.40	16.8	4.03	10.9	1.47	9.85	1.69	19.9	9.03	19.0	21.2	5.39
MA002	MA002	31/03/14	140	65.0	94.1	745	137	1.20	612	97.6	183	20.1	73.7	15.4	2.12	2.69	13.9	3.13	9.39	1.15	9.51	1.30	15.9	8.53	26.4	18.2	5.54
MA002	MA002	31/03/14	132	30.0	99.2	786	138	1.01	470	94.2	184	19.9	71.5	14.5	2.10	2.50	15.5	3.30	11.2	1.36	10.4	1.26	16.4	8.32	17.8	19.0	5.24
MA002	MA002	31/03/14	136	7.52	102	801	143	1.14	477	101	185	21.6	79.5	16.6	1.88	2.62	18.3	3.29	11.2	1.46	10.0	1.40	18.9	9.58	18.6	20.1	5.72
MA002	MA002	31/03/14	135	9.62	98.5	793	144	1.13	524	99.3	186	21.3	75.5	18.0	2.13	2.79	17.2	4.03	10.9	1.62	10.2	1.70	19.4	8.77	17.6	19.8	5.79
MA002	MA002	31/03/14	139	15.4	103	797	141	1.40	538	102	187	21.8	77.1	19.3	2.09	2.90	15.5	3.76	11.0	1.32	10.1	1.64	17.9	9.64	19.3	20.5	5.47
MA002	MA002	31/03/14	136	7.88	101	820	149	1.19	454	101	188	21.3	84.3	15.7	2.17	2.95	17.9	3.73	12.1	1.56	9.70	1.54	18.5	9.45	18.2	19.3	5.41
MA002	MA002	31/03/14	136	59.1	102	803	135	1.42	498	102	190	21.7	82.8	20.7	2.37	2.64	19.3	3.90	11.7	1.58	10.3	1.61	19.2	9.38	23.8	20.6	5.23
MA002	MA002	31/03/14	139	5.93	107	854	148	1.46	526	106	193	22.9	81.8	16.3	2.03	2.74	20.1	3.65	10.9	1.57	9.09	1.66	18.9	9.97	18.4	20.8	5.78
MA004	MA004	31/03/14	134	57.2	44.8	394	54.5	1.05	707	63.0	102	11.6	38.8	6.51	1.07	1.03	8.61	1.66	4.59	0.93	4.96	0.75	11.4	4.61	17.0	24.1	5.84
MA004	MA004	31/03/14	136	67.7	44	462	56.9	1.09	762	63.9	108	11.6	36.0	8.23	0.75	0.97	7.50	1.76	3.65	0.56	5.23	0.91	10.4	5.27	14.5	23.7	5.14
MA004	MA004	31/03/14	171	71.2	47.2	404	59.8	1.17	754	65.3	110	11.9	41.4	7.32-	0.71	1.10	7.40	1.48	4.84	0.80	5.05	0.96	11.0	4.76	17.4	25.2	5.77
MA004	MA004	31/03/14	130	36.8	62	550	79.8	1.30	765	70.0	129	14.3	52.7	10.0	1.21	1.42	11.3	2.48	8.07	0.87	6.89	1.00	13.6	5.90	16.7	19.0	5.41
MA004	MA004	31/03/14	130	103	59.4	529	83.1	1.12	723	73.3	139	15.7	50.4	10.1	1.51	1.45	11.8	2.46	6.00	1.29	5.75	1.03	13.3	7.22	20.4	17.4	4.79
MA004	MA004	31/03/14	117	290	109	720	89.7	1.40	183	107	160	20.7	72.5	17.0	2.24	2.70	18.1	3.68	10.1	1.53	8.67	1.61	15.2	5.08	20.0	16.3	4.48

Continued on next page

Trace element concentrations (ppm) in tephra samples from Ayelu

Label	Tephra	Analysis date	Rb 0.62	Sr 1.05	Y 0.17	Zr 0.37	Nb 0.07	Cs 0.19	Ba 1.88	La 0.09	Ce 0.07	Pr 0.06	Nd 0.25	Sm 0.14	Eu 0.13	Tb 0.06	Dy 0.13	Ho 0.04	Er 0.07	Tm 0.05	Yb 0.15	Lu 0.04	Hf 0.08	Ta 0.06	Pb 0.12	Th 0.01	U 0.00
MA004	MA004	31/03/14	129	-	141	1150	145	0.95	82.3	88.4	176	21.2	79.1	20.0	1.33	3.99	22.1	4.60	14.9	1.89	13.5	1.60	27.3	9.90	23.5	22.4	5.66
MA004	MA004	31/03/14	139	52.0	107	881	132	1.65	482	108	182	23.3	84.5	19.6	1.62	2.85	18.9	4.28	12.4	1.29	10.3	1.38	21.2	9.13	49.2	25.4	3.83
MA004	MA004	31/03/14	128	4.05	99.1	852	144	1.02	519	96.0	183	20.1	68.6	15.2	1.61	2.64	16.3	3.02	8.78	1.37	10.7	1.66	20.6	9.39	18.1	18.5	5.10
MA004	MA004	31/03/14	127	67.5	96.2	866	140	1.27	445	95.1	184	20.3	70.2	14.0	1.25	2.30	15.8	3.38	9.19	1.52	8.65	1.37	18.2	9.25	16.5	17.8	4.98
MA004	MA004	31/03/14	126	5.60	103	895	150	0.71	534	101	188	22.0	75.4	15.5	1.70	2.69	18.6	3.30	9.40	1.40	10.8	1.43	20.0	9.65	19.0	19.7	5.63
MA004	MA004	31/03/14	124	6.81	113	932	148	0.98	544	110	192	22.4	81.8	16.9	2.19	2.79	17.8	3.88	12.1	1.56	11.7	1.77	25.0	9.92	20.3	22.4	5.52
MA004	MA004	31/03/14	125	7.36	106	909	152	1.09	602	103	192	21.8	76.2	16.9	1.74	2.38	17.8	3.63	10.4	1.82	11.9	1.57	21.1	9.56	19.4	21.0	5.67
MA004	MA004	31/03/14	128	3.67	103	898	152	0.83	478	104	193	21.8	76.1	14.0	1.71	2.71	17.4	3.43	11.5	1.88	11.6	1.69	22.7	9.60	18.4	22.2	5.38
MA004	MA004	31/03/14	128	7.38	110	974	159	0.92	555	110	193	22.3	77.4	18.4	1.94	2.72	18.1	4.05	10.7	1.60	12.4	2.18	22.0	10.7	17.7	22.2	5.61
MA004	MA004	31/03/14	127	7.45	110	947	149	1.27	582	108	194	22.3	76.2	18.9	2.08	2.94	16.8	4.08	11.1	1.89	11.4	1.89	22.1	9.71	19.0	20.3	5.82
MA004	MA004	31/03/14	153	7.52	105	972	156	1.09	349	104	196	23.0	70.2	13.9	1.42	2.24	14.5	3.37	11.2	2.22	11.0	1.29	22.0	11.4	21.5	21.6	5.82
MA004	MA004	31/03/14	125	8.82	111	951	152	1.00	561	112	196	23.4	82.9	17.4	1.82	2.83	18.1	3.86	12.2	1.71	10.6	1.47	20.6	10.1	18.2	21.2	5.85
MA004	MA004	31/03/14	143	22.2	107	960	149	1.25	428	107	196	21.8	79.6	17.3	2.07	2.89	16.8	3.73	10.2	1.71	11.6	1.90	23.6	10.4	21.2	22.1	6.22
MA004	MA004	31/03/14	136	9.69	111	955	156	1.28	552	110	198	23.8	86.1	17.8	1.72	3.33	18.4	4.58	11.9	1.84	12.6	1.75	22.7	11.1	20.8	21.9	5.94
MA004	MA004	31/03/14	135	5.48	107	920	171	1.37	379	106	199	23.1	72.9	13.5	2.10	2.49	18.0	3.86	11.6	1.64	11.7	1.57	21.0	10.8	20.5	23.1	6.91
MA004	MA004	31/03/14	133	4.84	105	911	159	1.20	527	103	199	23.0	84.9	16.6	1.86	3.07	17.5	3.58	9.84	1.37	10.2	1.74	21.6	9.95	21.4	21.5	5.82
MA004	MA004	31/03/14	141	7.25	105	927	155	1.00	562	107	202	23.0	81.8	16.1	2.04	2.85	17.2	3.71	11.4	1.53	11.7	1.67	21.3	10.2	20.1	20.8	5.99
MA004	MA004	31/03/14	138	5.25	111	1030	163	1.28	363	113	203	22.9	82.2	16.8	0.99	2.96	19.5	3.99	10.6	1.78	11.8	1.68	23.9	11.5	20.1	23.3	6.36
MA004	MA004	31/03/14	137	5.73	114	940	168	1.39	393	111	207	22.0	87.6	21.5	1.65	3.10	17.7	4.14	12.0	1.49	11.7	1.62	23.9	11.1	20.5	22.7	5.97
MA004	MA004	02/04/14	143	4.92	115	999	165	1.24	277	115	210	24.1	79.9	16.4	1.63	2.75	20.1	3.92	12.5	1.92	11.3	1.70	24.0	11.4	22.4	22.9	6.19
MA007	MA007	02/04/14	116	8.18	97.1	859	129	0.91	802	99.0	178	21.5	82.1	18.4	2.82	3.02	15.7	3.60	11.8	1.60	9.90	1.45	19.9	8.07	17.1	15.8	4.93
MA007	MA007	02/04/14	115	25.8	102	951	132	1.77	752	100	179	20.9	82.4	18.6	2.28	2.86	17.9	4.05	9.85	1.95	10.2	1.30	20.2	8.07	16.5	16.2	4.43
MA007	MA007	02/04/14	117	9.96	92	880	130	0.79	758	94.6	183	22.1	84.2	14.4	2.31	2.99	14.7	3.67	10.8	1.54	10.3	1.34	20.5	8.40	17.1	16.4	4.87
MA007	MA007	02/04/14	117	12.1	104	921	134	0.94	806	104	190	22.8	82	17.6	2.52	2.95	16.7	3.41	10.7	1.82	9.71	1.41	21.8	8.08	19.1	16.2	5.30
MA007	MA007	02/04/14	112	11.5	106	970	137	1.01	839	107	194	24.1	96.3	17.9	3.23	2.88	20.1	3.66	12.1	1.77	10.9	1.96	21.2	8.65	20.0	17.6	5.42
MA007	MA007	02/04/14	117	50.6	98.7	990	127	1.20	874	105	195	23.8	82.6	18.3	2.27	3.00	17.5	3.49	11.2	1.75	10.0	1.44	21.5	8.06	19.0	18.0	4.86
MA007	MA007	02/04/14	119	12.0	111	1010	136	0.97	872	115	198	25.9	94.9	22.1	3.19	3.52	18.2	4.18	11.9	1.72	11.3	1.66	23.8	9.26	20.5	18.5	5.15
MA007	MA007	02/04/14	115	19.0	107	950	136	1.04	832	111	199	23.9	95.5	20.9	2.64	2.76	19.1	4.28	13.2	1.64	12.0	1.70	21.8	8.87	20.8	18.1	5.16
MA007	MA007	02/04/14	117	67.9	105	1090	130	2.14	940	115	199	23.6	93	18.7	2.74	2.67	17.1	3.68	11.6	1.67	11.7	1.54	24.0	9.45	18.5	19.6	4.86
MA007	MA007	02/04/14	115	9.47	114	1010	143	1.00	891	112	201	24.6	93.9	19.4	3.39	2.88	19.4	4.18	12.3	1.75	11.5	1.66	22.5	8.56	20.9	18.6	5.34
MA007	MA007	02/04/14	116	16.0	108	980	138	1.24	849	106	202	24.1	92.8	18.6	2.67	3.42	19.0	4.01	10.8	1.69	11.0	1.72	21.4	8.30	18.8	18.3	5.32
MA007	MA007	02/04/14	118	12.3	109	1000	135	0.95	858	111	202	24.3	92.6	20.2	3.00	2.98	18.9	4.54	11.2	1.64	11.4	1.71	24.0	8.06	17.5	18.0	4.49
MA007	MA007	02/04/14	113	14.3	112	1020	140	1.06	896	108	204	24.4	98.7	21.1	2.72	3.33	19.3	4.12	11.7	1.62	12.2	1.77	23.6	8.53	18.2	19.1	5.17
MA007	MA007	02/04/14	116	10.8	110	1020	137	0.83	874	114	204	25.2	94.3	17.8	2.92	3.17	17.8	4.26	11.7	1.83	11.8	1.79	24.0	9.07	19.9	19.6	5.41
MA007	MA007	02/04/14	116	12.2	110	1010	145	1.33	839	112	204	25.5	94.9	19.0	2.73	3.45	19.5	3.71	11.7	1.70	11.3	1.71	23.1	9.47	23.1	18.4	4.96
MA007	MA007	02/04/14	120	40.8	129	1140	135	2.06	861	119	205	26.3	99.9	19.8	3.16	3.44	22.7	4.73	13.5	1.67	10.8	2.65	23.5	8.92	19.5	19.6	4.70
MA007	MA007	02/04/14	117	11.0	109	982	141	1.05	906	111	207	25.0	97.3	18.0	2.67	3.06	18.1	3.87	12.1	1.66	12.1	1.80	22.1	8.61	20.3	18.5	5.39
MA007	MA007	02/04/14	114	10.2	113	1040	139	0.91	875	113	209	24.4	96.3	19.4	2.70	3.22	18.5	3.78	12.1	1.53	11.4	1.72	22.5	8.22	18.4	18.8	5.04
MA007	MA007	02/04/14	113	11.4	117	1060	142	1.12	896	115	210	24.3	94.2	21.8	2.73	3.38	19.9	4.16	11.6	1.80	11.6	1.85	23.7	8.67	19.6	19.3	5.29
MA007	MA007	02/04/14	117	12.8	114	1050	149	0.96	936	114	213	25.5	103	19.3	2.96	3.11	18.0	4.11	12.4	1.68	11.9	1.83	24.0	9.18	20.5	19.7	5.53
MA007	MA007	02/04/14	120	16.8	113	1060	140	1.56	868	117	213	25.8	96.9	19.9	2.50	3.23	20.0	4.40	12.6	1.99	13.2	1.56	26.1	8.71	17.1	19.9	4.92
MA007	MA007	02/04/14	111	13.2	114	1030	138	1.13	877	113	213	24.9	95.6	22.0	3.12	3.06	20.3	4.10	11.7	1.41	12.8	1.85	24.7	9.30	20.5	18.8	5.37
MA007	MA007	02/04/14	118	12.6	128	1160	148	1.12	934	131	214	26.7	110	24.8	3.14	3.80	21.8	4.35	13.8	2.14	13.8	1.91	27.0	9.56	19.6	21.4	5.43
MA007	MA007	02/04/14	116	11.8	116	1070	143	1.03	920	118	215	24.9	98.9	20.4	2.63	3.35	20.5	3.92	12.8	1.68	11.5	1.74	25.7	9.96	18.3	21.0	5.29

Continued on next page

Trace element concentrations (ppm) in tephra samples from Ayelu

Label	Tephra	Analysis date	Rb 0.62	Sr 1.05	Y 0.17	Zr 0.37	Nb 0.07	Cs 0.19	Ba 1.88	La 0.09	Ce 0.07	Pr 0.06	Nd 0.25	Sm 0.14	Eu 0.13	Tb 0.06	Dy 0.13	Ho 0.04	Er 0.07	Tm 0.05	Yb 0.15	Lu 0.04	Hf 0.08	Ta 0.06	Pb 0.12	Th 0.01	U 0.00
MA007	MA007	02/04/14	118	10.1	115	1060	142	0.93	876	113	215	25.5	95.6	19.7	2.96	3.25	19.1	4.12	12.4	1.66	11.9	1.84	22.9	9.55	19.2	19.5	4.57
MA007	MA007	02/04/14	115	13.4	115	1040	140	0.99	896	113	215	26.0	100	20.6	3.01	3.46	18.8	4.47	12.2	1.45	12.6	1.84	25.7	8.94	20.6	20.2	5.08
MA007	MA007	02/04/14	124	12.1	122	1100	152	0.74	941	126	218	27.3	111	19.4	3.28	3.27	17.9	4.63	13.0	1.68	12.3	1.86	24.8	8.98	20.5	20.0	5.78
MA007	MA007	02/04/14	111	14.2	121	1070	138	1.18	894	123	227	27.4	101	20.9	3.09	3.48	21.0	4.41	13.0	1.87	12.9	1.82	26.1	9.09	17.8	20.8	5.02
MA007	MA007	02/04/14	116	12.2	118	1080	146	0.88	953	120	227	26.2	109	21.2	3.41	3.48	20.1	4.54	12.7	2.03	13.2	1.78	26.3	9.83	19.3	20.4	5.62
MA007	MA007	02/04/14	120	17.6	133	1210	140	1.37	950	139	227	28.5	117	23.3	2.94	3.71	21.9	5.19	15.2	1.83	12.4	2.09	26.2	10.2	16.1	22.7	5.34
MA007	MA007	02/04/14	117	14.9	143	1290	147	1.17	1070	143	241	30.8	119	24.1	3.87	3.96	24.7	5.45	15.0	2.18	15.3	2.30	31.4	11.0	21.9	25.3	5.44
MA008	MA008	02/04/14	103	18.7	91.1	862	115	0.84	1250	90.5	153	20.6	76.5	14.4	2.90	2.67	16.8	3.04	10.7	1.56	9.56	1.58	19.7	7.95	18.4	16.4	4.32
MA008	MA008	02/04/14	103	12.7	109	988	125	1.09	828	102	155	22.4	85.6	20.3	2.23	3.18	18.4	4.31	11.1	1.82	11.5	1.71	23.6	8.97	17.6	20.0	4.60
MA008	MA008	02/04/14	117	11.1	116	1110	143	0.90	728	118	170	24.1	98.4	19.6	2.18	3.52	19.8	4.12	13.9	1.87	13.3	1.95	28.3	10.2	19.5	21.9	5.69
MA008	MA008	02/04/14	115	8.90	116	1100	136	1.14	583	113	172	26.4	102	18.2	2.50	2.93	20.0	3.86	11.4	1.88	12.0	1.96	25.5	8.71	20.7	20.4	5.54
MA008	MA008	02/04/14	119	7.96	102	958	140	0.91	825	105	174	23.7	86.1	20.5	2.59	2.95	20.1	4.22	11.5	1.66	12.3	1.51	24.3	8.88	20.9	18.7	5.02
MA008	MA008	02/04/14	113	9.74	102	954	133	0.95	737	104	175	23.1	89.0	17.7	2.56	2.83	18.3	3.32	10.0	1.50	10.3	1.63	21.2	8.39	20.2	17.6	5.39
MA008	MA008	02/04/14	120	13.4	105	932	139	1.63	736	104	177	21.9	84.8	20.7	2.35	2.54	16.2	4.26	8.54	1.31	11.3	1.70	20.7	8.42	18.5	16.3	5.04
MA008	MA008	02/04/14	122	28.9	125	1170	145	1.70	880	123	178	26.2	107	21.3	2.93	3.28	20.0	4.66	12.7	2.00	13.0	1.62	25.9	9.77	20.3	19.9	5.26
MA008	MA008	02/04/14	115	13.5	99	930	132	1.06	888	102	180	22.6	89.7	17.5	2.87	3.14	17.4	3.47	11.5	1.57	11.1	1.85	23.4	9.01	22.3	17.5	5.69
MA008	MA008	02/04/14	123	7.08	110	968	141	1.29	567	105	182	23.2	90.5	19.9	1.89	2.95	19.1	4.36	11.0	1.52	12.3	1.55	22.5	8.88	21.1	18.6	6.11
MA008	MA008	02/04/14	121	14.3	102	979	142	1.59	681	102	182	22.9	88.1	22.4	2.14	2.74	15.4	3.65	11.2	1.61	12.2	1.50	24.7	8.87	22.5	17.3	5.35
MA008	MA008	02/04/14	118	18.4	130	1140	141	1.44	878	127	186	27.9	113	22.2	2.99	3.62	22.4	4.92	14.2	1.94	13.7	2.06	29.8	9.38	20.5	22.7	5.79
MA008	MA008	02/04/14	124	8.31	116	1010	147	1.54	613	116	186	24.8	96.6	22.4	2.44	3.32	19.2	4.46	12.2	1.73	12.3	1.73	24.2	9.44	23.1	19.1	5.41
MA008	MA008	02/04/14	119	14.1	123	1160	146	0.98	966	125	190	28.0	101	24.4	3.79	3.65	20.9	4.65	13.4	1.84	13.7	1.86	26.4	9.55	20.4	21.9	5.81
MA008	MA008	02/04/14	117	9.36	109	975	140	0.66	802	109	191	25.5	90.9	20.4	2.47	3.09	18.1	3.46	12.1	1.52	11.8	1.67	21.5	8.86	21.4	18.6	5.28
MA008	MA008	02/04/14	120	8.67	132	1180	152	0.93	807	131	198	29.3	118	23.1	3.18	3.91	24.0	5.34	16.7	2.03	14.8	2.14	27.4	10.3	21.5	22.1	5.46
MA008	MA008	02/04/14	125	10.6	126	1120	152	0.96	810	118	201	27.7	101	22.5	3.19	2.94	21.5	4.42	12.1	2.00	13.1	2.12	26.2	9.73	23.0	20.3	5.75
MA009	MA009	02/04/14	89.8	115	94.8	806	122	0.81	1190	90.2	173	20.1	80.7	14.9	3.44	2.54	15.8	3.52	10.6	1.40	10.3	1.59	20.5	7.90	17.2	15.4	4.11
MA009	MA009	02/04/14	90.9	144	100	829	119	0.96	1200	95.9	179	21.7	86.5	17.6	3.52	3.40	19.8	3.57	11.8	1.79	9.72	1.42	20.9	8.35	16.5	15.7	3.91
MA009	MA009	02/04/14	94.9	140	92.4	773	117	0.75	1110	88.9	181	20.0	80.4	16.6	3.18	2.59	15.6	3.65	11.2	1.24	9.08	1.38	20.1	7.49	25.6	15.0	4.36
MA009	MA009	02/04/14	89.3	149	94	782	109	0.77	1250	92.0	182	21.1	83.4	19.0	3.91	3.06	17.8	3.97	10.4	1.50	11.8	1.82	19.9	8.26	16.9	15.5	5.03
MA009	MA009	02/04/14	105	75.5	108	943	127	0.62	919	104	185	21.9	95.5	18.8	3.30	2.96	17.5	3.49	13.6	1.79	10.7	1.25	22.1	8.95	17.4	16.2	4.44
MA009	MA009	02/04/14	100	86.5	102	856	118	0.87	909	97.7	188	21.5	82.5	20.7	3.32	3.06	19.7	3.75	12.3	1.63	10.7	1.44	18.8	7.56	15.3	15.5	4.12
MA009	MA009	02/04/14	88.1	152	105	864	112	0.68	1270	98.2	188	21.5	90.5	18.3	3.85	3.31	19.0	3.82	10.8	1.88	10.8	1.73	21.3	7.81	18.3	15.6	3.94
MA009	MA009	02/04/14	104	68.9	119	968	131	1.10	906	109	191	23.6	93.4	19.9	3.36	3.19	19.6	4.29	12.9	1.66	11.3	1.78	23.8	8.32	16.8	17.3	4.17
MA009	MA009	02/04/14	98.1	84.8	102	874	127	0.83	1020	101	195	22.7	90.1	18.4	3.06	2.92	16.7	3.97	11.8	1.57	10.2	1.75	19.9	8.35	19.0	17.0	4.46
MA009	MA009	02/04/14	105	70.6	118	978	126	0.76	866	110	196	23.4	99.6	18.1	2.96	3.25	19.2	4.15	11.0	1.74	12.0	1.84	21.7	8.31	17.2	17.3	4.30
MA009	MA009	02/04/14	93.5	154	122	1030	126	1.03	1310	109	197	26.9	103	20.5	4.95	3.59	20.7	4.56	12.3	2.09	11.8	2.05	25.3	8.93	20.5	18.1	4.40
MA009	MA009	02/04/14	94.4	104	124	1030	129	0.71	1130	115	202	25.1	106	23.3	3.56	3.60	21.6	4.91	14.6	1.88	14.3	2.10	27.6	9.77	17.5	19.2	4.60
MA009	MA009	02/04/14	109	43.6	120	994	136	0.92	834	112	205	23.6	97.1	19.5	2.67	3.12	21.3	4.28	13.9	1.55	12.4	1.69	24.8	8.95	19.1	19.4	4.90
MA009	MA009	02/04/14	113	33.8	112	950	141	0.96	702	107	212	23.5	91.9	21.0	3.09	3.36	17.7	4.02	13.0	1.62	12.1	2.03	23.9	9.43	22.5	18.3	5.06
MA009	MA009	02/04/14	110	52.8	134	1070	144	0.83	829	120	215	24.5	97.2	26.4	2.14	4.11	18.9	4.66	15.0	2.30	14.4	2.04	28.0	9.16	20.1	20.4	4.72
MA009	MA009	02/04/14	105	48.0	138	1140	138	0.98	814	129	223	28.5	105	20.9	3.05	4.15	25.2	5.33	15.8	2.47	16.4	2.39	28.2	9.86	33.7	23.0	5.19
MA009	MA009	02/04/14	104	89.4	136	1110	137	0.93	1100	126	226	28.7	109	23.8	3.93	4.11	25.2	4.97	14.0	2.26	15.2	2.10	28.7	10.0	19.0	21.3	4.87
MA0010	MA0010	02/04/14	81.8	122	89.1	764	119	0.69	1210	87.0	163	18.5	79.1	16.6	3.42	2.39	13.4	3.29	9.16	1.40	9.55	1.48	17.9	7.05	17.1	14.0	3.75
MA0010	MA0010	02/04/14	76.3	188	92.6	838	113	0.62	1270	87.6	164	18.8	74.7	16.6	3.62	2.90	14.4	3.10	9.52	1.31	9.66	1.50	18.2	7.73	13.6	14.4	3.55
MA0010	MA0010	02/04/14	92.6	120	88.5	741	118	0.67	1100	88.2	168	19.2	79.2	14.4	3.42	2.53	13.1	2.89	8.26	1.02	9.14	1.28	17.5	6.50	13.3	13.0	3.68

Continued on next page

Trace element concentrations (ppm) in tephra samples from Ayelu

Label	Tephra	Analysis date	Rb 0.62	Sr 1.05	Y 0.17	Zr 0.37	Nb 0.07	Cs 0.19	Ba 1.88	La 0.09	Ce 0.07	Pr 0.06	Nd 0.25	Sm 0.14	Eu 0.13	Tb 0.06	Dy 0.13	Ho 0.04	Er 0.07	Tm 0.05	Yb 0.15	Lu 0.04	Hf 0.08	Ta 0.06	Pb 0.12	Th 0.01	U 0.00
MA0010	MA0010	02/04/14	94.8	113	98.1	883	120	1.01	1150	96.0	171	20.7	89.7	15.0	2.52	2.63	16.7	3.23	10.4	1.74	10.6	1.44	20.5	8.90	17.5	16.7	4.25
MA0010	MA0010	02/04/14	101	76.4	100	796	123	0.90	960	93.7	173	20.2	82.7	17.1	2.60	2.50	16.2	3.50	9.85	1.07	10.1	1.32	18.5	7.94	15.1	15.0	4.12
MA0010	MA0010	02/04/14	104	89.2	106	876	116	0.84	890	98.4	181	20.8	94.1	16.9	2.60	2.74	18.1	3.41	11.7	1.54	9.80	1.28	20.9	7.38	19.4	16.7	3.70
MA0010	MA0010	02/04/14	94.1	67.0	103	903	129	1.06	920	96.8	182	19.9	87.1	14.1	2.30	2.82	17.1	3.66	12.2	1.66	10.8	1.55	21.4	9.14	17.3	16.3	4.03
MA0010	MA0010	02/04/14	92.8	92.2	104	878	126	0.75	1040	98.5	183	21.1	85.8	16.8	3.37	2.75	18.1	3.49	10.3	1.64	9.66	1.45	20.2	8.61	16.2	15.9	4.40
MA0010	MA0010	02/04/14	92.4	79.4	99.1	857	125	0.59	999	95.9	183	21.3	78.1	17.3	2.86	3.00	17.9	3.32	12.0	1.62	8.99	1.72	19.5	8.12	16.0	16.0	4.04
MA0010	MA0010	02/04/14	90.3	93.4	104	874	126	0.72	1020	94.4	184	20.2	86.4	17.2	3.82	2.71	17.5	3.28	10.2	1.66	9.73	1.54	19.4	7.94	16.3	16.0	3.93
MA0010	MA0010	02/04/14	103	65.1	107	923	129	1.04	933	103	187	22.4	89.6	21.0	2.86	2.40	17.3	4.00	12.3	1.66	12.2	1.54	23.0	8.48	14.5	17.3	3.96
MA0010	MA0010	02/04/14	105	52.7	112	921	131	1.07	835	100	188	21.2	91.8	15.4	2.44	3.20	18.2	3.69	11.5	1.62	10.3	1.65	21.7	9.30	17.5	15.9	4.33
MA0010	MA0010	02/04/14	98.3	75.7	104	819	126	0.80	981	102	189	21.7	89.1	15.5	3.08	2.50	17.3	3.43	10.8	1.47	10.2	1.85	19.2	8.29	18.5	17.3	4.36
MA0010	MA0010	02/04/14	98.9	70.2	106	918	129	0.96	910	98.3	190	21.5	92.9	19.7	3.10	3.14	17.5	4.01	12.9	1.73	11.4	1.53	21.6	8.45	15.3	17.1	3.92
MA0010	MA0010	02/04/14	99.4	57.8	107	905	137	0.53	773	102	191	22.4	88.9	17.2	2.26	2.25	17.8	3.62	12.4	1.74	11.3	1.58	21.6	9.96	18.7	16.6	4.96
MA0010	MA0010	02/04/14	100	72.5	109	922	135	0.69	1000	100	195	21.8	86	18.2	2.69	2.75	18.1	4.19	11.7	1.45	10.7	1.45	20.3	8.73	18.6	16.3	4.60
MA0010	MA0010	02/04/14	102	58.4	110	952	131	1.06	806	107	196	21.9	87.8	18.2	2.72	3.11	18.5	4.17	11.8	1.84	12.5	1.57	24.3	8.67	18.6	17.4	4.30
MA0010	MA0010	02/04/14	99.7	92.4	110	964	135	0.46	1030	110	197	24.3	93.2	20.8	3.80	3.49	18.6	4.25	11.9	1.58	11.5	1.62	22.4	8.22	16.1	17.1	4.55
MA0010	MA0010	02/04/14	99.1	54.4	110	937	136	0.78	875	105	197	22.8	91.2	18.2	2.63	3.02	20.0	3.52	12.4	1.64	11.4	1.97	21.9	9.57	21.5	18.9	4.74
MA0010	MA0010	02/04/14	91.3	79.2	111	916	141	0.87	1010	102	203	22.2	90	14.8	3.27	3.13	18.3	4.20	12.3	1.89	10.7	1.76	20.6	8.65	17.7	18.4	4.44
MA0010	MA0010	02/04/14	102	52.8	107	953	141	0.83	894	104	206	21.9	92.5	19.3	3.04	2.91	18.0	4.18	11.2	1.51	11.6	1.76	22.0	8.15	17.6	16.8	4.74
MA0010	MA0010	02/04/14	102	67.0	116	955	133	0.94	940	111	208	24.5	99.4	19.2	3.33	3.65	20.2	3.96	12.3	1.70	11.6	1.65	21.4	8.26	19.1	16.3	4.29
MA0010	MA0010	02/04/14	102	71.5	111	903	119	0.78	909	104	211	21.3	84.2	17.7	2.68	3.13	19.1	4.09	10.0	2.01	11.3	1.60	18.6	7.79	18.0	17.3	3.54
MA0010	MA0010	02/04/14	98.7	40.0	120	1020	136	1.03	772	115	211	23.6	101	18.2	2.17	3.39	26.8	4.86	13.0	1.77	11.2	1.66	24.5	7.85	16.4	17.8	4.38
MA0010	MA0010	02/04/14	99.3	74.3	120	943	132	0.88	939	111	216	24.3	106	21.3	2.75	3.11	20.2	4.07	12.3	1.72	12.7	1.69	20.9	9.53	18.3	16.4	4.63
MA0010	MA0010	02/04/14	103	56.8	119	930	139	0.98	859	104	236	21.3	98.1	18.4	3.02	3.15	19.8	4.28	12.4	1.85	11.6	1.75	22.4	8.51	19.3	17.3	4.54
MA0010	MA0010	02/04/14	119	47.4	140	1190	151	0.80	906	136	241	28.6	122	26.6	3.29	3.46	22.5	5.08	14.6	2.04	15.6	2.31	31.9	10.2	33.2	21.4	4.88
MA0011	MA0011	03/04/14	105	107	82.7	728	115	0.89	1000	85.5	158	18.8	71.8	15.7	2.91	2.18	15.3	3.06	8.53	1.31	7.53	1.20	17.1	6.92	16.8	13.0	5.21
MA0011	MA0011	03/04/14	96.8	131	89.6	752	115	0.97	1120	85.4	168	20.1	75.5	17.1	3.71	2.56	16.6	3.06	10.7	1.79	8.50	1.40	18.2	7.09	18.1	14.2	4.13
MA0011	MA0011	03/04/14	95.5	76.4	93.4	743	118	0.78	942	87.7	173	19.1	80.1	14.9	3.26	2.36	15.6	3.49	10.3	1.70	9.34	1.24	17.7	7.39	18.6	13.4	4.30
MA0011	MA0011	03/04/14	100	71.8	102	849	123	0.83	903	94.5	173	20.3	82	16.2	3.13	2.58	15.3	3.54	10.5	1.41	10.7	1.28	21.0	7.23	17.0	14.8	4.02
MA0011	MA0011	03/04/14	114	61.3	96.6	805	117	0.92	737	94.9	179	20.3	88.7	17.2	2.55	2.54	16.2	3.37	9.78	1.47	8.90	1.30	17.8	7.25	18.1	13.8	3.72
MA0011	MA0011	03/04/14	129	96.5	106	867	122	0.90	956	106	180	22.4	89.9	18.8	3.30	2.85	17.3	3.51	10.2	1.23	10.6	1.34	20.7	7.17	21.1	16.3	4.03
MA0011	MA0011	03/04/14	114	65.7	94.1	811	124	0.82	835	95.6	181	20.8	84.7	16.4	2.85	2.51	17.5	3.37	10.1	1.68	10.0	1.45	19.6	7.71	17.2	15.4	4.38
MA0011	MA0011	03/04/14	99.9	60.7	98.5	836	135	0.65	852	96.5	181	21.5	85.9	18.0	2.38	2.70	18.2	3.83	10.5	1.38	10.4	1.50	20.1	8.32	16.7	15.3	4.04
MA0011	MA0011	03/04/14	97.6	54.3	101	810	124	0.65	816	93.6	184	20.3	82.4	15.6	2.59	2.53	17.0	3.52	9.77	1.71	9.59	1.50	20.1	7.14	17.8	15.4	4.06
MA0011	MA0011	03/04/14	104	94.2	105	844	137	0.92	1010	97.9	184	21.1	87.3	18.2	2.99	2.65	16.9	3.75	11.3	1.68	9.76	1.61	20.5	8.58	18.9	15.6	4.55
MA0011	MA0011	03/04/14	102	66.7	94.1	789	125	0.94	867	90.9	185	20.6	82.1	16.8	2.55	2.59	17.5	3.20	9.61	1.56	10.2	1.48	19.1	8.24	20.9	15.6	4.41
MA0011	MA0011	03/04/14	99.2	99.9	103	892	128	0.72	993	102	188	23.3	92.9	17.1	3.81	2.80	17.6	2.91	10.3	1.45	10.8	1.52	19.1	7.47	16.6	15.1	3.90
MA0011	MA0011	03/04/14	108	51.8	95.3	799	125	0.98	867	95.1	188	21.3	85	16.5	3.36	2.71	18.2	3.60	10.6	1.44	10.9	1.42	22.0	8.07	19.8	15.8	5.04
MA0011	MA0011	03/04/14	100	63.3	101	857	125	0.74	884	98.1	188	22.1	87.3	17.7	2.73	2.98	17.9	3.69	10.1	1.40	10.5	1.78	21.3	7.94	17.3	15.1	4.40
MA0011	MA0011	03/04/14	101	75.0	99.0	848	129	0.81	919	97.4	188	21.7	83.4	20.2	3.09	2.45	18.2	3.59	10.4	1.37	10.2	1.33	20.9	7.88	19.0	15.7	4.42
MA0011	MA0011	03/04/14	101	82.8	100	832	123	0.84	1000	97.1	190	22.1	90.6	15.9	2.67	2.92	16.2	3.40	11.3	1.76	10.4	1.65	21.6	8.52	18.3	15.5	5.10
MA0011	MA0011	03/04/14	112	54.2	101	870	135	0.86	788	102	191	22.3	93.5	18.4	2.68	2.77	15.8	3.92	11.7	1.60	15.6	1.51	21.1	8.15	20.1	16.6	4.34
MA0011	MA0011	03/04/14	105	54.1	103	847	130	0.91	856	99.5	192	21.4	92.1	16.6	3.60	2.85	18.0	3.46	10.2	1.61	9.66	1.51	20.6	8.29	19.0	15.4	4.52
MA0011	MA0011	03/04/14	106	55.7	108	867	129	0.95	843	101	193	21.9	87.3	16.8	2.87	3.01	19.1	3.82	10.8	1.64	10.4	1.55	21.7	8.10	19.0	16.7	4.65
MA0011	MA0011	03/04/14	119	91.2	111	892	124	0.75	968	109	195	22.2	96.9	16.7	3.34	2.83	19.4	3.36	11.2	1.62	11.2	1.71	21.9	8.27	17.8	17.4	4.11

Continued on next page

Trace element concentrations (ppm) in tephra samples from Ayelu

Label	Tephra	Analysis date	Rb 0.62	Sr 1.05	Y 0.17	Zr 0.37	Nb 0.07	Cs 0.19	Ba 1.88	La 0.09	Ce 0.07	Pr 0.06	Nd 0.25	Sm 0.14	Eu 0.13	Tb 0.06	Dy 0.13	Ho 0.04	Er 0.07	Tm 0.05	Yb 0.15	Lu 0.04	Hf 0.08	Ta 0.06	Pb 0.12	Th 0.01	U 0.00
MA0011	MA0011	03/04/14	103	61.2	103	872	144	0.74	913	97.7	195	22.2	86.8	16.9	3.29	2.93	18.0	3.38	12.1	1.52	10.7	1.62	19.2	7.98	18.0	16.3	4.58
MA0011	MA0011	03/04/14	108	79.4	109	855	129	0.89	933	104	197	23.4	94.3	18.4	2.87	3.01	19.5	3.89	11.7	1.66	11.4	1.77	20.8	8.37	18.8	16.2	4.15
MA0011	MA0011	03/04/14	105	65.5	108	933	131	0.53	917	110	199	23.5	100	18.7	3.11	3.37	19.7	3.98	13.6	1.66	13.0	1.74	24.2	9.28	18.4	18.7	4.63
MA0011	MA0011	03/04/14	102	56.1	107	896	129	0.68	894	107	202	23.9	95.8	19.0	3.06	2.95	18.5	3.94	13.0	1.62	10.6	1.67	22.1	9.26	18.7	16.1	4.88
MA0011	MA0011	03/04/14	109	49.3	114	946	136	0.74	713	111	203	23.9	91.8	17.9	2.20	3.20	20.2	4.35	13.0	1.69	11.0	1.99	23.5	8.30	23.4	18.8	4.51
MA0011	MA0011	03/04/14	106	37.4	116	951	141	0.88	761	112	210	23.9	98	19.5	2.73	2.96	19.2	4.28	12.6	1.79	10.8	1.96	23.0	8.78	18.8	17.3	4.79
MA0012	MA0012	03/04/14	107	9.85	117	1000	138	0.63	828	114	211	23.4	96.2	20.2	2.67	3.23	22.2	4.43	12.4	1.91	10.6	1.83	24.4	9.68	18.4	19.2	5.00
MA0012	MA0012	03/04/14	121	11.6	117	1020	142	1.26	832	110	212	24	93.3	19.4	2.71	3.17	19.4	3.54	14.6	1.60	11.6	1.95	23.2	9.61	18.2	19.6	5.00
MA0012	MA0012	03/04/14	119	11.4	118	1030	146	0.99	877	115	217	25.2	101	19.8	2.88	3.31	20.3	4.11	12.6	1.83	12.3	1.65	26.2	9.96	19.6	19.9	5.48
MA0012	MA0012	03/04/14	116	8.17	117	1010	139	0.93	847	116	218	24.9	93.3	21.8	2.85	3.30	21.1	4.37	12.7	2.02	11.7	1.39	23.3	9.29	18.3	19.5	5.31
MA0012	MA0012	03/04/14	113	13.7	122	1050	137	0.90	870	116	220	25	97.8	20.1	3.00	3.33	18.9	4.43	12.9	1.80	12.7	1.78	24.4	9.55	17.8	19.1	5.12
MA0012	MA0012	03/04/14	115	10.2	125	1050	147	1.13	873	119	225	25.1	96.8	23.8	2.89	3.05	20.9	4.38	13.0	1.85	12.6	1.68	27.1	9.26	19.3	20.3	5.23
MA0012	MA0012	03/04/14	117	13.0	122	1040	145	0.97	891	118	226	25.3	97.2	20.0	2.44	3.18	21.3	4.47	12.4	1.74	11.9	1.99	26.1	9.74	20.7	19.8	5.08
MA0012	MA0012	03/04/14	114	13.2	125	1090	149	1.02	953	120	228	26.7	103	17.9	2.75	3.27	22.5	4.47	13.4	1.95	13.6	2.05	26.0	9.76	18.8	20.3	5.11
MA0012	MA0012	03/04/14	113	10.5	133	1160	149	0.97	961	125	230	27.1	108	21.8	2.77	3.66	23.5	4.75	14.9	1.95	14.1	2.12	25.9	9.69	18.6	21.4	4.70
MA0012	MA0012	03/04/14	119	20.7	135	1190	145	0.81	922	131	230	27.5	112	22.5	3.18	3.36	22.7	4.68	14.3	2.56	13.6	2.10	28.9	10.5	17.3	22.9	4.93
MA0012	MA0012	03/04/14	112	11.4	128	1050	142	1.02	877	115	230	26.1	108	20.0	3.64	3.08	21.2	4.59	12.9	1.82	12.9	1.93	25.3	10.1	19.7	20.7	4.92
MA0012	MA0012	03/04/14	115	11.1	132	1080	149	1.06	925	121	231	25.4	104	22.4	3.42	3.23	21.5	4.84	13.8	1.75	12.7	1.86	28.3	10.1	18.6	22.5	5.53
MA0012	MA0012	03/04/14	116	12.8	128	1120	152	0.86	927	126	231	26.9	99.9	20.4	3.41	3.50	22.5	5.16	14.0	1.89	13.7	2.01	27.5	10.5	19.9	20.3	5.49
MA0012	MA0012	03/04/14	114	13.2	138	1140	150	0.80	910	131	232	27.9	113	24.9	3.40	3.61	20.8	5.00	13.6	2.09	13.4	2.21	29.6	9.36	19.0	22.2	5.17
MA0012	MA0012	03/04/14	113	10.4	122	1090	144	1.07	898	120	232	26.3	104	22.2	2.32	3.44	19.1	4.51	11.6	2.11	13.2	2.08	28.7	9.96	19.3	20.2	5.21
MA0012	MA0012	03/04/14	115	11.6	132	1130	151	1.14	953	124	232	28.2	108	22.1	3.12	3.45	22.4	4.72	15.4	1.87	14.1	2.06	28.7	10.7	17.5	21.6	5.46
MA0012	MA0012	03/04/14	119	12.6	121	1050	147	0.99	907	122	233	26.9	106	18.7	2.95	3.24	19.9	4.67	12.7	1.92	12.2	1.82	25.7	9.51	19.4	20.1	5.13
MA0012	MA0012	03/04/14	117	13.2	128	1110	148	0.93	930	126	236	26.9	103	20.8	3.08	3.71	20.6	4.70	13.8	2.11	13.7	2.15	26.5	10.2	20.4	21.6	5.22
MA0012	MA0012	03/04/14	113	12.8	137	1160	157	0.84	971	133	238	26.9	113	22.0	3.21	3.19	23.7	4.84	14.7	2.21	14.5	2.02	28.6	10.9	18.9	22.3	5.13
MA0012	MA0012	03/04/14	115	11.8	130	1120	149	0.85	981	129	240	26.6	107	25.2	3.24	3.63	24.9	4.36	15.0	2.13	14.4	1.97	29.4	10.6	19.5	23.3	5.43
MA0012	MA0012	03/04/14	114	10.9	138	1190	147	0.91	969	128	241	27.0	114	22.9	3.13	3.70	22.5	4.55	15.2	2.18	14.9	1.87	30.8	11.1	18.5	23.1	5.57
MA0012	MA0012	03/04/14	117	11.9	133	1160	153	0.91	959	129	243	27.8	110	22.7	3.25	3.74	22.7	5.33	14.6	1.99	14.2	2.10	27.6	10.7	21.4	23.0	5.38
MA0012	MA0012	03/04/14	113	10.3	134	1140	155	0.92	963	128	244	28.0	118	22.7	3.34	3.61	22.5	4.84	14.6	1.99	14.2	2.15	28.9	10.1	19.3	22.5	5.73
MA0012	MA0012	03/04/14	116	13.7	128	1140	156	1.12	985	133	246	27.4	109	20.4	3.43	3.43	23.0	4.83	14.1	2.13	15.3	2.15	29.1	10.7	19.1	22.6	5.88
MA0012	MA0012	03/04/14	113	11.9	141	1230	161	0.97	995	135	268	30.0	112	22.2	3.53	3.82	24.2	4.70	14.2	2.20	16.4	2.09	31.8	11.5	19.5	25.5	6.41
MA0013	MA0013	04/04/14	112	13.3	109	983	133	0.93	806	104	183	22.2	91.6	18.3	2.99	3.08	17.1	3.73	12.1	1.63	11.1	1.74	23.7	8.67	19.7	17.2	4.81
MA0013	MA0013	04/04/14	110	30.3	113	1030	141	0.97	820	109	185	24.2	93.5	19.7	3.20	3.20	19.5	4.66	12.8	1.67	11.5	1.76	28.1	9.42	24.0	18.9	4.69
MA0013	MA0013	04/04/14	114	15.5	118	1050	142	0.93	887	113	186	24.4	98.3	19.0	2.67	3.24	21.3	4.73	13.8	1.73	13.8	1.76	27.3	9.82	21.4	20.1	5.54
MA0013	MA0013	04/04/14	109	23.5	110	972	138	0.81	836	111	188	23.2	94.9	18.5	2.52	3.07	19.4	4.01	11.8	1.66	12.3	1.59	23.2	9.16	19.1	19.7	4.97
MA0013	MA0013	04/04/14	122	31.7	127	1110	144	0.83	889	120	189	25.7	98.4	19.6	3.46	3.53	21.3	4.50	13.7	2.19	13.4	2.03	26.2	10.1	25.4	21.6	5.69
MA0013	MA0013	04/04/14	117	22.2	115	1020	141	1.00	890	110	189	23.9	89.9	19.7	2.98	2.88	19.6	3.89	12.5	1.95	11.0	1.80	25.0	9.08	20.2	17.7	4.61
MA0013	MA0013	04/04/14	115	9.01	107	955	139	0.84	823	107	190	23.6	96.3	17.3	3.00	3.23	18.2	4.00	11.2	1.86	11.6	1.79	24.3	8.55	18.7	17.1	4.82
MA0013	MA0013	04/04/14	112	11.9	118	1070	140	0.88	853	112	192	24.5	91.2	19.3	2.62	3.07	19.6	3.78	13.1	2.07	12.7	1.86	25.0	9.73	20.1	20.2	5.11
MA0013	MA0013	04/04/14	113	14.1	113	1020	140	0.96	863	111	194	24.8	90.5	19.9	3.16	3.66	17.9	4.05	13.4	1.69	11.6	1.74	25.8	9.15	21.5	19.7	5.82
MA0013	MA0013	04/04/14	121	25.3	126	1110	144	0.99	918	118	194	26.5	105	20.1	3.10	3.82	21.9	4.51	14.0	1.75	14.2	1.79	27.1	10.8	21.9	21.7	5.14
MA0013	MA0013	04/04/14	124	27.5	129	1140	146	0.94	937	122	195	26.7	101	22.4	3.00	3.43	20.9	4.59	13.7	2.04	14.2	1.97	28.2	10.1	20.7	21.5	5.39
MA0013	MA0013	04/04/14	140	15.7	130	1130	145	1.01	884	122	197	26.3	98.4	19.7	3.27	3.57	20.5	4.11	13.1	2.23	12.9	1.98	24.8	9.58	18.7	19.9	5.45
MA0013	MA0013	04/04/14	112	11.8	128	1100	146	0.88	892	122	197	26.1	105	24.0	2.86	3.74	21.6	4.59	13.7	1.92	13.6	1.87	25.1	10.4	19.5	21.0	5.50

Continued on next page

Trace element concentrations (ppm) in tephra samples from Ayelu

Label	Tephra	Analysis date	Rb 0.62	Sr 1.05	Y 0.17	Zr 0.37	Nb 0.07	Cs 0.19	Ba 1.88	La 0.09	Ce 0.07	Pr 0.06	Nd 0.25	Sm 0.14	Eu 0.13	Tb 0.06	Dy 0.13	Ho 0.04	Er 0.07	Tm 0.05	Yb 0.15	Lu 0.04	Hf 0.08	Ta 0.06	Pb 0.12	Th 0.01	U 0.00
MA0013	MA0013	04/04/14	120	19.2	131	1150	150	1.09	945	124	198	25.7	101	21.3	3.06	3.68	22.7	4.33	13.6	1.84	13.9	1.97	28.8	10.6	21.4	21.8	5.52
MA0013	MA0013	04/04/14	111	16.1	118	1050	145	0.89	881	115	198	26.2	97.5	18.7	2.82	2.96	20.7	3.92	13.0	1.75	11.5	1.93	23.7	9.12	20.8	19.2	5.53
MA0013	MA0013	04/04/14	120	15.8	128	1130	155	1.11	935	124	203	27.1	98.2	22.9	2.82	3.65	22.4	4.83	15.4	1.85	15.1	1.83	29.0	9.94	20.0	21.1	5.58
MA0013	MA0013	04/04/14	116	18.6	135	1200	142	1.32	899	131	203	26.1	105	21.2	3.21	4.05	21.7	4.45	15.5	2.18	13.8	2.14	29.0	10.3	17.3	22.8	5.25
MA0013	MA0013	04/04/14	112	16.8	138	1210	149	0.95	957	134	204	28.5	110	22.0	3.38	3.48	23.9	4.75	14.4	2.19	14.9	2.20	28.1	9.95	18.5	21.6	5.25
MA0013	MA0013	04/04/14	121	18.4	133	1170	146	1.21	971	122	204	26.3	110	20.8	2.96	3.63	21.1	4.95	14.9	2.06	13.4	1.99	27.0	10.7	20.1	20.2	5.15
MA0013	MA0013	04/04/14	111	16.1	120	1060	138	1.04	907	120	207	24.6	103	19.3	2.98	3.46	18.8	4.20	10.8	1.79	12.2	1.79	24.2	9.61	19.8	20.2	5.37
MA0013	MA0013	04/04/14	118	76.2	128	1150	136	1.19	945	127	208	28.0	109	27.0	3.32	3.57	21.0	5.11	14.6	2.46	13.4	1.96	26.2	9.27	31.8	19.8	4.33
MA0013	MA0013	04/04/14	117	13.2	119	1050	146	1.07	930	122	211	26.4	105	22.0	3.64	3.82	21.5	4.85	14.6	1.97	14.3	1.74	29.3	10.6	22.7	20.6	5.63
MA0013	MA0013	04/04/14	119	49.1	145	1310	152	0.95	1020	141	223	30.6	109	24.2	4.02	4.03	24.1	6.12	16.4	1.95	16.7	2.36	29.7	11.9	22.6	25.7	5.82
MA0013	MA0013	04/04/14	122	19.5	141	1200	153	0.94	1040	132	224	27.3	116	22.0	3.63	4.11	24.5	4.59	13.5	1.93	13.8	2.13	26.6	10.3	19.1	21.2	5.83
MA0013	MA0013	04/04/14	117	74.3	133	1210	151	1.00	1000	149	230	30.0	116	23.5	3.19	3.99	22.6	4.69	14.7	2.35	15.4	2.20	28.6	10.7	31.5	22.8	5.89
MA0014	MA0014	04/04/14	103	19.4	92.5	768	99.1	0.75	745	82.3	156	18.7	69.4	15.4	1.94	2.28	16.3	3.25	11.0	1.58	8.72	1.37	19.6	6.43	14.8	15.0	4.22
MA0014	MA0014	04/04/14	116	19.6	96.3	810	113	0.89	802	81.1	165	18.7	76.0	14.7	2.39	2.79	14.7	3.65	10.3	1.41	10.7	1.49	21.3	7.33	17.2	16.0	4.93
MA0014	MA0014	04/04/14	118	18.3	96.8	825	113	0.92	822	85.0	170	18.9	75.8	15.1	2.16	2.51	15.5	3.51	11.3	1.45	11.0	1.48	20.6	6.92	16.5	16.3	4.62
MA0014	MA0014	04/04/14	128	29.0	105	914	116	1.19	903	93.1	175	20.9	84.4	16.7	1.57	3.29	17.8	3.28	12.0	1.79	11.1	1.34	25.8	7.02	29.5	18.3	4.62
MA0014	MA0014	04/04/14	119	18.4	108	905	115	0.85	904	92.8	177	21.6	81.1	17.1	1.92	2.80	18.0	4.39	12.7	1.94	12.6	1.75	25.1	7.70	20.7	18.5	4.49
MA0014	MA0014	04/04/14	121	19.4	101	878	118	0.98	857	90.8	178	20.6	82.8	16.8	2.57	2.55	16.3	4.00	11.2	1.79	11.5	1.87	23.9	7.60	19.9	18.6	4.88
MA0014	MA0014	04/04/14	122	30.8	108	935	118	0.77	900	99.8	180	21.9	89.9	18.2	2.69	3.40	18.8	3.95	11.2	2.01	12.1	1.60	23.3	8.13	23.8	18.3	5.61
MA0014	MA0014	04/04/14	136	28.1	113	968	111	1.05	905	99.5	181	23.3	84.2	18.5	2.36	2.76	18.2	4.26	12.8	1.84	13.6	1.79	26.4	7.62	21.2	20.2	4.50
MA0014	MA0014	04/04/14	123	19.4	102	855	118	0.88	863	96.0	181	21.0	82.8	17.3	1.87	2.71	15.8	3.61	12.0	1.40	11.8	1.58	22.4	7.10	15.7	17.3	5.86
MA0014	MA0014	04/04/14	112	22.0	110	927	119	0.80	902	94.6	184	20.8	90.4	16.0	2.34	3.37	22.2	4.13	11.8	1.97	13.3	1.75	24.2	8.87	19.2	20.1	4.98
MA0014	MA0014	04/04/14	131	28.7	109	921	114	1.17	869	95.3	184	21.1	86.4	15.7	2.22	3.06	17.5	4.03	11.0	1.90	11.8	1.45	23.6	7.02	21.4	17.4	4.33
MA0014	MA0014	04/04/14	129	19.7	102	869	113	0.96	842	90.8	185	20.5	80.8	16.1	2.67	3.08	17.3	3.68	11.8	1.96	11.4	1.71	23.1	7.53	17.3	17.0	5.13
MA0014	MA0014	04/04/14	118	22.4	118	989	119	0.88	907	102	187	23.0	85.9	17.5	2.30	3.19	19.7	4.62	13.5	2.02	12.4	1.83	25.9	8.59	21.7	21.1	5.34
MA0014	MA0014	04/04/14	127	22.2	109	926	121	1.21	920	98.5	187	22.1	84.6	17.8	2.34	2.94	19.9	4.38	12.6	2.00	13.4	1.62	24.1	7.83	19.9	19.6	5.55
MA0014	MA0014	04/04/14	126	21.5	113	965	118	1.01	907	101	188	23.4	82.7	16.8	2.45	3.26	23.0	4.46	12.6	1.82	11.5	1.95	26.4	7.95	18.8	18.5	4.86
MA0014	MA0014	04/04/14	112	20.8	108	894	118	1.00	862	96.1	190	22.2	86.7	20.1	2.21	3.06	18.7	4.23	14.2	1.82	12.2	1.85	25.4	7.81	20.8	19.2	5.17
MA0014	MA0014	04/04/14	121	21.5	116	1010	123	1.15	985	104	192	22.6	89.4	17.2	2.70	3.35	21.1	4.47	14.1	2.06	12.6	1.80	25.6	8.77	23.8	20.1	4.94
MA0014	MA0014	04/04/14	119	26.2	130	1130	126	0.89	984	112	193	25.9	105	19.5	2.90	3.66	21.8	4.90	15.4	2.38	14.9	2.06	27.3	9.58	22.9	21.8	5.36
MA0014	MA0014	04/04/14	113	25.1	128	1090	121	0.73	979	108	198	24.3	97.0	18.8	2.42	3.64	23.6	4.95	14.4	2.14	15.0	2.11	27.8	8.98	18.5	22.5	10.5
MA0014	MA0014	04/04/14	125	22.4	133	1130	128	0.86	1030	116	198	26.5	111	19.8	2.84	3.41	21.9	5.26	14.6	2.23	15.3	2.30	28.4	9.31	26.5	23.7	5.56
MA0014	MA0014	04/04/14	129	27.9	137	1170	127	0.87	1010	118	214	25.5	101	23.5	3.57	3.85	23.5	5.12	15.1	1.96	14.8	2.22	28.0	9.24	19.6	23.2	4.85
MA0014	MA0014	04/04/14	125	28.5	127	1070	134	0.84	1010	115	219	25.3	95.6	20.2	2.51	2.99	21.1	4.78	14.7	2.50	14.2	1.88	28.8	9.24	21.6	23.4	5.36

.7 Reference materials

This Appendix provides analyses of MPI-DING glass reference materials, which were used to check the calibration of the EPMA and LA-ICP-MS.

.7.1 EPMA reference materials

The MPI-DING reference materials, ATHO-G (rhyolite), St-Hs6/80-G (andesite), GOR128-G (komatiite) and ML3B-G (basalt) were analysed throughout each analytical session. These analyses are given below, and the date of analysis indicated. The average and 2σ of these analyses are given alongside published major element concentrations from the GeoReM online database (Jochum *et al.*, 2005).

Normalised major element concentrations (wt.%) in MPI-DING reference materials

Label	MPI-DING glass	Analysis date	SiO_2	TiO_2	Al_2O_3	MgO	FeO^T	MnO	CaO	Na_2O	K_2O	P_2O_5	Cl
ATH-G/1	ATHO-G	20/02/14	75.29	0.22	12.45	0.12	3.35	0.14	1.75	4.04	2.76	0.02	0.05
ATH-G/2	ATHO-G	20/02/14	75.82	0.28	12.42	0.09	3.39	0.10	1.82	2.23	2.76	0.02	0.06
ATH-G/3	ATHO-G	20/02/14	74.53	0.27	12.43	0.11	3.10	0.12	1.69	4.05	2.74	0.00	0.06
ATH-G/4	ATHO-G	20/02/14	74.83	0.28	12.45	0.09	3.15	0.12	1.66	4.17	2.72	0.00	0.06
ATH-G/5	ATHO-G	20/02/14	74.32	0.22	12.19	0.07	3.14	0.11	1.79	4.10	2.66	0.03	0.03
ATH-G/6	ATHO-G	20/02/14	75.10	0.25	12.38	0.09	3.32	0.14	1.67	4.05	2.76	0.01	0.05
ATH-G/7	ATHO-G	20/02/14	75.28	0.28	12.38	0.10	3.19	0.10	1.73	1.98	2.75	0.00	0.06
ATHO-G/3	ATHO-G	20/02/14	75.44	0.19	12.38	0.10	3.24	0.18	1.74	3.41	2.71	0.00	0.04
ATHO/1	ATHO-G	21/02/14	75.05	0.28	12.33	0.09	3.00	0.01	1.80	4.22	2.69	0.00	0.05
ATHO/10	ATHO-G	21/02/14	75.53	0.22	12.52	0.12	3.20	0.12	1.75	4.09	2.66	0.04	0.06
ATHO/11	ATHO-G	21/02/14	75.26	0.28	12.55	0.10	3.09	0.10	1.73	4.20	2.68	0.04	0.04
ATHO/12	ATHO-G	21/02/14	75.63	0.24	12.39	0.10	3.26	0.09	1.71	4.13	2.73	0.02	0.06
ATHO/13	ATHO-G	21/02/14	75.03	0.23	12.38	0.08	3.26	0.04	1.76	4.10	2.74	0.04	0.06
ATHO/14	ATHO-G	21/02/14	76.24	0.24	12.50	0.11	3.40	0.07	1.70	4.25	2.72	0.05	0.05
ATHO/15	ATHO-G	21/02/14	74.88	0.28	12.29	0.07	3.28	0.08	1.75	4.15	2.85	0.01	0.11
ATHO/16	ATHO-G	21/02/14	75.07	0.25	12.16	0.13	3.28	0.07	1.76	4.07	2.79	0.02	0.06
ATHO/17	ATHO-G	21/02/14	75.18	0.26	12.31	0.10	3.26	0.17	1.74	4.44	2.75	0.04	0.06
ATHO/18	ATHO-G	21/02/14	74.86	0.28	12.18	0.08	3.25	0.06	1.68	4.14	2.68	0.01	0.06
ATHO/19	ATHO-G	21/02/14	74.85	0.24	12.28	0.09	3.30	0.11	1.72	4.22	2.69	0.02	0.06
ATHO/2	ATHO-G	21/02/14	72.78	0.20	11.97	0.10	3.15	0.08	1.63	4.06	2.60	0.00	0.07
ATHO/20	ATHO-G	21/02/14	75.43	0.29	12.29	0.13	3.32	0.05	1.73	3.75	2.70	0.00	0.03
ATHO/3	ATHO-G	21/02/14	73.39	0.29	12.05	0.13	3.11	0.13	1.73	4.28	2.67	0.01	0.05
ATHO/4	ATHO-G	21/02/14	75.29	0.27	12.39	0.11	3.17	0.12	1.73	4.27	2.74	0.00	0.05
ATHO/5	ATHO-G	21/02/14	75.46	0.24	12.49	0.10	3.39	0.14	1.71	3.31	2.67	0.00	0.03
ATHO/6	ATHO-G	21/02/14	75.08	0.21	12.49	0.12	3.26	0.12	1.73	4.27	2.63	0.02	0.05
ATHO/7	ATHO-G	21/02/14	75.25	0.20	12.13	0.11	3.10	0.17	1.78	2.58	2.70	0.04	0.03
ATHO/8	ATHO-G	21/02/14	74.84	0.22	12.36	0.09	3.22	0.11	1.73	3.80	2.69	0.02	0.06
ATHO/9	ATHO-G	21/02/14	74.74	0.29	12.32	0.07	3.23	0.13	1.74	3.98	2.73	0.00	0.04
ATHO-G/2	ATHO-G	21/02/14	75.04	0.28	12.41	0.12	3.44	0.05	1.75	4.15	2.74	0.01	0.03
ATHO-G/2	ATHO-G	21/02/14	75.56	0.24	12.34	0.12	3.07	0.07	1.69	4.10	2.70	0.00	0.06
ATHO-G_1	ATHO-G	26/08/14	75.67	0.26	12.33	0.08	3.17	0.10	1.70	4.17	2.73	0.04	
ATHO-G_2	ATHO-G	26/08/14	75.40	0.17	12.37	0.07	3.30	0.07	1.60	4.22	2.75	0.04	
ATHO-G_3	ATHO-G	26/08/14	75.31	0.25	12.34	0.12	3.21	0.11	1.67	4.30	2.72	0.05	
ATHO-G_4	ATHO-G	26/08/14	75.47	0.26	12.37	0.10	3.43	0.13	1.65	4.14	2.84	0.02	
ATHO-G_1	ATHO-G	26/08/14	75.19	0.25	12.19	0.07	3.37	0.06	1.72	4.38	2.75	0.05	
ATHO-G_2	ATHO-G	26/08/14	75.25	0.28	12.24	0.12	3.25	0.07	1.64	4.29	2.73	0.00	
ATHO-G_3	ATHO-G	26/08/14	74.76	0.23	12.33	0.15	3.27	0.07	1.60	4.29	2.79	0.00	
ATHO-G_4	ATHO-G	26/08/14	74.86	0.25	12.36	0.09	3.17	0.06	1.67	4.22	2.81	0.00	
ATHO-G_5	ATHO-G	26/08/14	75.40	0.25	12.14	0.08	3.19	0.14	1.66	4.19	2.74	0.04	
ATHO-G_6	ATHO-G	26/08/14	75.73	0.28	12.34	0.11	3.36	0.12	1.70	4.30	2.75	0.00	
ATHO-G_1	ATHO-G	27/08/14	75.44	0.21	12.37	0.12	3.50	0.12	1.66	4.16	2.75	0.00	
ATHO-G_2	ATHO-G	27/08/14	75.60	0.22	12.36	0.11	3.41	0.11	1.70	4.16	2.66	0.01	

Continued on next page

Normalised major element concentrations (wt.%) in MPI-DING reference materials

Label	MPI-DING glass	Analysis date	SiO_2	TiO_2	Al_2O_3	MgO	FeO^T	MnO	CaO	Na_2O	K_2O	P_2O_5	Cl
ATHO-G_5	ATHO-G	27/08/14	75.27	0.26	12.07	0.09	3.26	0.16	1.67	4.20	2.76	0.03	
ATHO-G_6	ATHO-G	27/08/14	75.29	0.27	12.17	0.11	3.24	0.13	1.64	3.93	2.66	0.02	
ATHO-G_3	ATHO-G	27/08/14	75.34	0.29	12.16	0.10	3.38	0.09	1.66	4.47	2.71	0.06	
ATHO-G_4	ATHO-G	27/08/14	75.51	0.17	12.29	0.09	3.38	0.12	1.63	4.30	2.86	0.00	
ATHO-G_1	ATHO-G	28/08/14	75.19	0.25	12.19	0.07	3.37	0.06	1.72	4.38	2.75	0.05	
ATHO-G_2	ATHO-G	28/08/14	75.25	0.28	12.24	0.12	3.25	0.07	1.64	4.29	2.73	0.00	
ATHO-G_3	ATHO-G	28/08/14	74.76	0.23	12.33	0.15	3.27	0.07	1.60	4.29	2.79	0.00	
ATHO-G_4	ATHO-G	28/08/14	74.86	0.25	12.36	0.09	3.17	0.06	1.67	4.22	2.81	0.00	
ATHO-G_5	ATHO-G	28/08/14	75.40	0.25	12.14	0.08	3.19	0.14	1.66	4.19	2.74	0.04	
ATHO-G_6	ATHO-G	28/08/14	75.73	0.28	12.34	0.11	3.36	0.12	1.70	4.30	2.75	0.00	
ATHO1G_6	ATHO-G	29/06/15	74.54	0.28	12.32	0.09	3.06	0.09	1.70	4.23	2.69	0.02	0.05
ATHO1G_1	ATHO-G	29/06/15	75.01	0.16	12.31	0.12	3.25	0.11	1.60	4.45	2.70	0.00	0.04
ATHO1G_2	ATHO-G	29/06/15	74.83	0.26	12.33	0.06	3.22	0.09	1.70	3.99	2.75	0.00	0.05
ATHO1G_3	ATHO-G	29/06/15	74.85	0.28	11.98	0.10	3.10	0.10	1.62	4.19	2.67	0.08	0.04
ATHO1G_4	ATHO-G	29/06/15	75.21	0.26	12.24	0.16	3.33	0.16	1.62	4.04	2.76	0.00	0.04
ATHO1G_5	ATHO-G	29/06/15	75.02	0.25	12.24	0.06	3.22	0.10	1.73	4.11	2.71	0.02	0.03
ATHO1G_10	ATHO-G	29/06/15	74.99	0.23	12.18	0.07	3.19	0.17	1.70	4.05	2.72	0.05	0.06
ATHO-G_6	ATHO-G	30/06/15	74.78	0.23	12.24	0.10	3.22	0.09	1.59	4.29	2.72	0.06	0.06
ATHO-G_9	ATHO-G	30/06/15	75.00	0.23	12.25	0.08	3.19	0.11	1.66	4.14	2.72	0.02	0.01
ATHO-G_10	ATHO-G	30/06/15	74.92	0.28	12.35	0.09	3.11	0.16	1.70	4.04	2.64	0.01	0.05
ATHO-G_1	ATHO-G	30/06/15	75.21	0.21	12.08	0.11	3.21	0.12	1.66	3.98	2.68	0.00	0.02
ATHO-G_3	ATHO-G	30/06/15	75.24	0.31	12.15	0.14	3.30	0.13	1.69	4.05	2.79	0.03	0.03
ATHO-G_2	ATHO-G	30/06/15	75.44	0.28	12.23	0.09	3.21	0.10	1.64	4.23	2.73	0.00	0.04
ATHO-G_4	ATHO-G	30/06/15	74.74	0.27	12.22	0.06	3.10	0.21	1.70	4.21	2.79	0.02	0.03
ATHO-G_5	ATHO-G	30/06/15	74.90	0.23	12.02	0.07	3.19	0.09	1.60	4.21	2.66	0.00	0.03
ATHO-G_1	ATHO-G	03/07/15	74.04	0.26	12.42	0.11	3.36	0.10	1.67	4.44	2.74	0.05	0.02
ATHO-G_2	ATHO-G	03/07/15	74.34	0.28	12.33	0.15	3.38	0.08	1.64	4.12	2.72	0.05	0.04
ATHO-G_3	ATHO-G	03/07/15	74.87	0.26	12.31	0.11	3.16	0.14	1.61	4.11	2.80	0.01	0.06
ATHO-G_4	ATHO-G	03/07/15	75.28	0.19	12.17	0.09	3.35	0.20	1.65	4.04	2.74	0.00	0.03
ATHO-G_5	ATHO-G	03/07/15	75.20	0.28	12.26	0.08	3.41	0.10	1.55	4.36	2.67	0.04	0.03
		Average	**75.09**	**0.25**	**12.29**	**0.10**	**3.25**	**0.11**	**1.69**	**4.07**	**2.73**	**0.02**	**0.05**
		2 σ	1.01	0.06	0.25	0.04	0.21	0.08	0.11	0.86	0.10	0.04	0.03
		GeoReM	75.60	0.26	12.20	0.10	3.27	0.11	1.70	3.75	2.64	0.04	0.03
StHs/6/80-G/3	StHs6/80-G	20/02/14	63.24	0.69	17.94	2.01	4.19	0.03	5.12	4.60	1.30	0.11	0.00
StHS6/80-G/1	StHs6/80-G	20/02/14	63.41	0.68	17.92	1.96	4.30	0.05	5.25	4.55	1.32	0.12	0.00
StHS6/80-G/2	StHs6/80-G	20/02/14	63.62	0.62	18.11	1.92	4.44	0.08	5.28	4.89	1.30	0.14	0.02
StHS6/80-G/3	StHs6/80-G	20/02/14	63.22	0.66	17.79	1.97	4.45	0.07	5.16	4.35	1.21	0.11	0.01
StHS6/80-G/4	StHs6/80-G	20/02/14	62.84	0.69	17.76	1.95	4.33	0.07	5.24	4.68	1.36	0.15	0.01
StHS6/80-G/5	StHs6/80-G	20/02/14	63.52	0.71	17.97	1.98	4.33	0.10	5.24	3.93	1.33	0.15	0.01
StHS6/80-G/6	StHs6/80-G	20/02/14	63.00	0.78	17.63	1.98	4.30	0.05	5.26	4.33	1.34	0.14	0.00
StHS6/80-G/7	StHs6/80-G	20/02/14	63.22	0.69	17.69	1.96	4.53	0.04	5.25	4.40	1.30	0.12	0.01
StHs6/80-G/2	StHs6/80-G	21/02/14	63.32	0.74	17.67	1.94	4.28	0.08	5.29	4.48	1.27	0.14	0.00
StHs/1	StHs6/80-G	21/02/14	63.06	0.70	17.58	1.91	4.54	0.07	5.19	4.43	1.27	0.15	0.00
StHs/9	StHs6/80-G	21/02/14	63.77	0.71	17.61	1.91	4.10	0.15	5.21	3.91	1.34	0.15	0.01
StHs/11	StHs6/80-G	21/02/14	64.46	0.69	18.27	1.91	4.50	0.02	5.35	4.08	1.29	0.11	0.00
StHs/12	StHs6/80-G	21/02/14	64.08	0.69	17.90	1.97	4.66	0.04	5.28	3.70	1.32	0.16	0.03
StHs/13	StHs6/80-G	21/02/14	63.66	0.70	17.80	1.96	4.38	0.06	5.23	4.69	1.31	0.14	0.02
StHs/14	StHs6/80-G	21/02/14	63.75	0.67	17.79	2.01	4.50	0.02	5.29	4.56	1.33	0.10	0.03
StHs/15	StHs6/80-G	21/02/14	63.44	0.76	17.78	1.91	4.36	0.07	5.35	4.66	1.34	0.11	0.01
StHs/16	StHs6/80-G	21/02/14	63.70	0.66	17.93	1.98	4.38	0.07	5.20	4.67	1.34	0.09	0.00
StHs/17	StHs6/80-G	21/02/14	63.68	0.70	17.86	1.89	4.31	0.11	5.13	4.67	1.33	0.14	0.00
StHs/18	StHs6/80-G	21/02/14	63.40	0.66	17.78	1.96	4.41	0.15	5.24	4.70	1.27	0.14	0.01
StHs/19	StHs6/80-G	21/02/14	63.71	0.70	17.84	1.89	4.49	0.14	5.35	4.50	1.31	0.16	0.01
StHs/20	StHs6/80-G	21/02/14	64.07	0.77	17.75	1.97	4.44	0.09	5.31	4.47	1.35	0.14	0.00
StHs6/80-G_2	StHs6/80-G	26/08/14	63.60	0.67	17.52	1.94	4.27	0.04	5.32	4.59	1.33	0.14	
StHs6/80-G_1	StHs6/80-G	26/08/14	63.67	0.77	17.64	1.91	4.16	0.11	5.26	4.73	1.31	0.11	
StHs6/80-G_3	StHs6/80-G	26/08/14	63.53	0.73	17.67	1.96	4.45	0.10	5.33	4.52	1.36	0.14	
StHs6/80-G_4	StHs6/80-G	26/08/14	63.88	0.76	17.50	1.95	4.35	0.12	5.17	4.83	1.34	0.19	
StHs6/80-G_1	StHs6/80-G	26/08/14	63.74	0.65	17.84	1.91	4.41	0.05	5.17	4.77	1.35	0.09	
StHs6/80-G_2	StHs6/80-G	26/08/14	63.94	0.73	17.63	1.94	4.29	0.05	5.22	4.51	1.35	0.11	
StHs6/80-G_3	StHs6/80-G	26/08/14	63.89	0.71	17.47	1.94	4.25	0.05	5.30	4.63	1.35	0.12	
StHs6/80-G_4	StHs6/80-G	26/08/14	63.96	0.72	17.34	1.93	4.37	0.08	5.26	4.54	1.32	0.11	
StHs6/80-G_5	StHs6/80-G	26/08/14	63.36	0.66	17.76	1.83	4.44	0.07	5.14	4.67	1.30	0.14	
StHs6/80-G_1	StHs6/80-G	27/08/14	63.87	0.70	17.70	1.83	4.31	0.05	5.22	4.61	1.29	0.14	
StHs6/80-G_2	StHs6/80-G	27/08/14	63.34	0.74	17.91	1.93	4.43	0.03	5.38	4.33	1.36	0.14	
StHs6/80-G_4	StHs6/80-G	27/08/14	63.64	0.66	17.64	1.82	4.32	0.06	5.21	4.57	1.33	0.10	
StHs6/80-G_3	StHs6/80-G	27/08/14	63.79	0.75	17.74	1.91	4.33	0.08	5.30	4.64	1.28	0.17	
StHs6/80-G_5	StHs6/80-G	27/08/14	63.59	0.70	17.52	1.92	4.55	0.04	5.26	4.72	1.33	0.13	
StHs6/80-G_6	StHs6/80-G	27/08/14	63.78	0.75	17.55	1.95	4.36	0.07	5.28	4.73	1.34	0.13	
StHs6/80-G_1	StHs6/80-G	28/08/14	63.74	0.65	17.84	1.91	4.41	0.05	5.17	4.77	1.35	0.09	
StHs6/80-G_2	StHs6/80-G	28/08/14	63.94	0.73	17.63	1.94	4.29	0.05	5.22	4.51	1.35	0.11	
StHs6/80-G_3	StHs6/80-G	28/08/14	63.89	0.71	17.47	1.94	4.25	0.05	5.30	4.63	1.35	0.12	
StHs6/80-G_4	StHs6/80-G	28/08/14	63.96	0.72	17.34	1.93	4.37	0.08	5.26	4.54	1.32	0.11	
StHs6/80-G_5	StHs6/80-G	28/08/14	63.36	0.66	17.76	1.83	4.44	0.07	5.14	4.67	1.30	0.14	
StHs_5	StHs6/80-G	29/06/15	63.53	0.69	17.43	1.88	4.36	0.09	5.33	4.64	1.29	0.26	0.03
StHs_1	StHs6/80-G	29/06/15	63.73	0.73	17.70	2.03	4.50	0.15	5.33	4.25	1.25	0.19	0.02
StHs_2	StHs6/80-G	29/06/15	63.50	0.69	17.56	1.83	4.46	0.01	5.22	4.72	1.32	0.20	0.00
StHs_4	StHs6/80-G	29/06/15	63.48	0.74	17.63	2.00	4.39	0.04	5.23	4.66	1.34	0.18	0.00
StHs_7	StHs6/80-G	29/06/15	63.08	0.75	17.74	2.01	4.55	0.04	5.29	4.71	1.35	0.20	0.01
StHs_10	StHs6/80-G	29/06/15	63.84	0.73	17.55	1.92	4.29	0.03	5.22	4.78	1.36	0.13	0.02
StHS6/80-G_8	StHs6/80-G	30/06/15	63.42	0.76	17.44	1.92	4.34	0.02	5.38	4.62	1.32	0.15	0.01
StHS6/80-G_9	StHs6/80-G	30/06/15	63.62	0.72	17.48	2.06	4.51	0.05	5.20	4.67	1.24	0.20	0.01
StHS6/80-G_10	StHs6/80-G	30/06/15	63.49	0.72	17.73	1.97	4.46	0.04	5.26	4.07	1.36	0.10	0.00

Continued on next page

Normalised major element concentrations (wt.%) in MPI-DING reference materials

Label	MPI-DING glass	Analysis date	SiO_2	TiO_2	Al_2O_3	MgO	FeO^T	MnO	CaO	Na_2O	K_2O	P_2O_5	Cl
StHS6/80-G_5	StHs6/80-G	30/06/15	63.64	0.64	17.47	1.96	4.38	0.10	5.15	4.37	1.25	0.12	0.03
StHS6/80-G_2	StHs6/80-G	30/06/15	63.45	0.70	17.54	1.97	4.36	0.17	5.24	4.51	1.31	0.21	0.02
StHS6/80-G_4	StHs6/80-G	30/06/15	63.52	0.70	17.70	1.92	4.38	0.09	5.12	4.41	1.31	0.17	0.01
StHS6/80-G_3	StHs6/80-G	30/06/15	63.43	0.78	17.56	1.93	4.56	0.05	5.28	4.84	1.30	0.12	0.01
StHS6/80-G_6	StHs6/80-G	30/06/15	62.94	0.72	17.52	2.02	4.62	0.17	5.17	4.54	1.29	0.22	0.02
StHS6/80-G_7	StHs6/80-G	30/06/15	62.93	0.69	17.39	1.99	4.40	0.10	5.22	4.54	1.21	0.21	0.03
StHs6/80-G_1	StHs6/80-G	03/07/15	63.55	0.66	17.90	1.90	4.51	0.04	5.16	4.78	1.31	0.06	0.02
StHs6/80-G_2	StHs6/80-G	03/07/15	63.26	0.68	17.44	1.90	4.34	0.08	5.24	4.31	1.28	0.08	0.01
StHs6/80-G_3	StHs6/80-G	03/07/15	63.75	0.66	17.50	1.90	4.60	0.02	5.30	4.52	1.30	0.02	0.01
StHs6/80-G_4	StHs6/80-G	03/07/15	63.42	0.70	17.52	1.96	4.30	0.04	5.35	4.55	1.30	0.10	0.02
StHs6/80-G_5	StHs6/80-G	03/07/15	63.57	0.74	17.27	1.95	4.41	0.06	5.20	4.35	1.28	0.09	0.00
StHs6/80-G_6	StHs6/80-G	03/07/15	63.37	0.66	17.63	1.88	4.37	0.04	5.28	4.61	1.31	0.04	0.01
		Average	**63.57**	**0.70**	**17.67**	**1.94**	**4.39**	**0.07**	**5.25**	**4.54**	**1.31**	**0.14**	**0.01**
		2 σ	0.61	0.07	0.39	0.10	0.22	0.08	0.13	0.46	0.07	0.08	0.02
		GeoReM	63.70	0.70	17.80	1.97	4.37	0.08	5.28	4.44	1.29	0.16	0.01
GO128-G/1	GOR128-G	20/02/14	45.64	0.23	10.01	25.75	9.85	0.22	6.16	0.63	0.03	0.03	0.01
GO128-G/2	GOR128-G	20/02/14	45.90	0.32	9.92	25.89	10.20	0.17	6.16	0.52	0.02	0.01	0.02
GO128-G/3	GOR128-G	20/02/14	45.40	0.29	9.72	25.54	9.87	0.07	6.15	0.50	0.04	0.01	0.00
GO128-G/4	GOR128-G	20/02/14	45.52	0.31	10.09	25.95	10.16	0.26	6.23	0.54	0.04	0.04	0.01
GO128-G/5	GOR128-G	20/02/14	45.83	0.30	10.22	25.32	9.33	0.20	6.25	0.67	0.02	0.04	0.00
GO128-G/6	GOR128-G	20/02/14	45.60	0.30	10.13	25.65	9.56	0.20	6.44	0.52	0.04	0.01	0.00
GO128-G/7	GOR128-G	20/02/14	45.48	0.31	10.17	26.02	9.59	0.24	6.03	0.59	0.03	0.04	0.01
GOR128-G/3	GOR128-G	20/02/14	46.20	0.31	10.13	25.60	9.84	0.25	6.21	0.56	0.03	0.03	0.00
GOR128/1	GOR128-G	21/02/14	46.28	0.31	9.98	25.39	9.58	0.17	6.18	0.50	0.03	0.00	0.00
GOR128/10	GOR128-G	21/02/14	46.43	0.34	10.10	25.52	9.72	0.23	6.33	0.56	0.01	0.02	0.01
GOR128/11	GOR128-G	21/02/14	46.49	0.29	10.05	25.64	9.74	0.14	6.10	0.61	0.06	0.00	0.00
GOR128/2	GOR128-G	21/02/14	46.46	0.31	9.95	25.53	9.56	0.15	6.15	0.51	0.06	0.01	0.02
GOR128/3	GOR128-G	21/02/14	46.32	0.30	10.10	25.54	9.34	0.18	6.20	0.53	0.02	0.05	0.01
GOR128/4	GOR128-G	21/02/14	46.39	0.29	9.88	25.39	9.69	0.22	6.33	0.53	0.06	0.04	0.00
GOR128/5	GOR128-G	21/02/14	46.48	0.32	10.05	25.58	10.14	0.20	6.25	0.46	0.04	0.04	0.00
GOR128/6	GOR128-G	21/02/14	46.76	0.25	10.15	25.81	9.53	0.18	6.29	0.48	0.03	0.00	0.00
GOR128/7	GOR128-G	21/02/14	46.38	0.28	10.12	25.45	9.93	0.26	6.30	0.57	0.06	0.02	0.01
GOR128/8	GOR128-G	21/02/14	46.53	0.32	10.02	25.61	9.77	0.24	6.07	0.61	0.01	0.03	0.00
GOR128/9	GOR128-G	21/02/14	46.07	0.26	10.10	25.55	9.77	0.27	6.35	0.50	0.02	0.02	0.00
GOR128-G/1	GOR128-G	21/02/14	46.00	0.24	10.11	25.57	9.64	0.21	6.27	0.65	0.03	0.02	0.00
GOR128-G/2	GOR128-G	21/02/14	46.23	0.29	10.08	25.41	9.79	0.18	6.18	0.58	0.02	0.03	0.00
GOR128/1	GOR128-G	21/02/14	46.40	0.26	9.92	25.78	9.77	0.12	6.23	0.58	0.02	0.00	0.00
GOR128/10	GOR128-G	21/02/14	46.55	0.29	10.20	25.62	9.73	0.08	6.35	0.49	0.06	0.01	0.01
GOR128/11	GOR128-G	21/02/14	46.24	0.21	10.02	25.70	9.81	0.15	6.19	0.54	0.07	0.02	0.01
GOR128/2	GOR128-G	21/02/14	45.14	0.26	9.98	24.69	9.33	0.16	6.05	0.77	0.05	0.04	0.10
GOR128/3	GOR128-G	21/02/14	46.38	0.30	9.99	25.75	10.07	0.16	6.20	0.57	0.04	0.01	0.01
GOR128/4	GOR128-G	21/02/14	45.91	0.21	10.06	25.84	10.01	0.15	6.14	0.53	0.04	0.02	0.00
GOR128/5	GOR128-G	21/02/14	46.06	0.24	9.86	25.63	9.81	0.18	6.24	0.63	0.07	0.04	0.00
GOR128/6	GOR128-G	21/02/14	46.53	0.27	10.10	25.73	9.78	0.20	6.17	0.55	0.02	0.01	0.02
GOR132_6	GOR128-G	29/06/15	45.27	0.38	10.87	21.93	10.51	0.12	8.36	0.85	0.03	0.05	0.00
GOR132_1	GOR128-G	29/06/15	45.28	0.29	10.81	22.33	10.11	0.19	8.33	0.83	0.04	0.00	0.01
GOR132_2	GOR128-G	29/06/15	45.30	0.32	10.80	22.05	10.17	0.20	8.49	0.85	0.01	0.07	0.00
GOR132_3	GOR128-G	29/06/15	45.38	0.27	10.91	22.39	10.05	0.11	8.39	0.75	0.05	0.02	0.02
GOR132_4	GOR128-G	29/06/15	45.58	0.32	10.86	22.21	10.40	0.11	8.46	0.86	0.00	0.06	0.02
GOR132_5	GOR128-G	29/06/15	45.21	0.34	10.77	22.18	10.29	0.18	8.43	0.72	0.04	0.05	0.01
GOR132_10	GOR128-G	29/06/15	45.28	0.30	10.99	22.32	10.33	0.20	8.53	0.88	0.02	0.05	0.02
GOR132-G_7	GOR128-G	30/06/15	45.58	0.35	10.83	22.23	10.10	0.19	8.31	0.74	0.03	0.04	0.04
GOR132-G_8	GOR128-G	30/06/15	45.18	0.29	10.72	22.21	10.56	0.13	8.48	0.86	0.02	0.00	0.00
GOR132-G_9	GOR128-G	30/06/15	45.49	0.27	10.85	22.38	10.41	0.10	8.44	0.72	0.05	0.01	0.02
GOR132-G_10	GOR128-G	30/06/15	45.74	0.24	10.78	22.31	10.20	0.20	8.50	0.74	0.04	0.07	0.00
GOR132-G_6	GOR128-G	30/06/15	45.28	0.25	10.87	22.11	10.47	0.13	8.35	0.79	0.03	0.04	0.00
GOR132-G_3	GOR128-G	30/06/15	45.38	0.30	10.79	22.41	10.38	0.21	8.32	0.75	0.02	0.02	0.00
GOR132-G_2	GOR128-G	30/06/15	45.40	0.34	10.77	22.27	10.62	0.16	8.40	0.72	0.03	0.02	0.00
GOR132-G_4	GOR128-G	30/06/15	45.58	0.33	10.83	22.26	10.67	0.13	8.48	0.77	0.04	0.08	0.01
GOR132-G_5	GOR128-G	30/06/15	45.54	0.30	10.84	22.18	10.29	0.16	8.70	0.79	0.04	0.03	0.00
GOR132-G_1	GOR128-G	03/07/15	44.98	0.31	10.92	22.46	10.35	0.23	8.51	0.84	0.04	0.07	0.00
GOR132-G_2	GOR128-G	03/07/15	45.07	0.33	10.84	22.31	9.99	0.11	8.61	0.83	0.04	0.05	0.02
GOR132-G_3	GOR128-G	03/07/15	45.26	0.37	10.99	22.23	10.37	0.05	8.62	0.80	0.04	0.04	0.01
GOR132-G_4	GOR128-G	03/07/15	45.15	0.24	11.04	22.35	9.93	0.09	8.43	0.76	0.01	0.04	0.01
GOR132-G_5	GOR128-G	03/07/15	45.81	0.27	11.11	22.47	10.32	0.16	8.36	0.76	0.04	0.05	0.00
GOR132-G_6	GOR128-G	03/07/15	45.72	0.28	10.89	22.32	10.00	0.10	8.49	0.76	0.04	0.00	0.00
		Average	**45.81**	**0.29**	**10.40**	**24.16**	**9.99**	**0.17**	**7.18**	**0.66**	**0.03**	**0.03**	**0.01**
		2 σ	1.00	0.07	0.85	3.36	0.70	0.10	2.25	0.26	0.03	0.04	0.03
		GeoReM	45.39	0.30	10.87	22.27	10.30	0.15	8.45	0.79	0.03	0.04	0.01
ML3B-G_1	ML3B-G	26/08/14	51.54	2.12	13.86	6.57	11.10	0.19	10.33	2.26	0.39	0.22	
ML3B-G_2	ML3B-G	26/08/14	51.69	2.10	13.81	6.55	10.76	0.23	10.56	2.09	0.36	0.27	
ML3B-G_3	ML3B-G	26/08/14	51.84	2.04	13.89	6.60	11.22	0.20	10.26	2.35	0.38	0.25	
ML3B-G_4	ML3B-G	26/08/14	51.90	2.02	13.84	6.49	10.84	0.18	10.32	2.37	0.38	0.20	
ML3B-G_1	ML3B-G	27/08/14	51.76	2.14	13.87	6.51	11.39	0.25	10.44	2.41	0.39	0.22	
ML3B-G_2	ML3B-G	27/08/14	52.12	2.08	13.75	6.37	10.86	0.20	10.52	2.42	0.39	0.24	
ML3B-G_4	ML3B-G	27/08/14	51.93	2.13	13.93	6.51	11.34	0.20	10.60	2.42	0.33	0.21	
ML3B-G_3	ML3B-G	27/08/14	51.94	2.13	13.55	6.55	11.02	0.22	10.50	2.23	0.41	0.25	
ML3B-G_6	ML3B-G	27/08/14	52.01	2.17	13.74	6.44	10.97	0.17	10.44	2.37	0.39	0.23	
ML3B-G_5	ML3B-G	27/08/14	51.57	2.18	13.79	6.36	10.77	0.19	10.47	2.34	0.39	0.23	
ML3B-G_1	ML3B-G	28/08/14	52.06	2.11	13.46	6.70	11.33	0.21	10.46	2.15	0.39	0.24	
ML3B-G_2	ML3B-G	28/08/14	52.18	2.10	13.71	6.55	11.00	0.21	10.36	2.41	0.38	0.26	

Continued on next page

Normalised major element concentrations (wt.%) in MPI-DING reference materials

Label	MPI-DING glass	Analysis date	SiO_2	TiO_2	Al_2O_3	MgO	FeO^T	MnO	CaO	Na_2O	K_2O	P_2O_5	Cl
ML3B-G_3	ML3B-G	28/08/14	51.46	2.18	13.64	6.62	11.41	0.19	10.63	2.45	0.45	0.25	
ML3B-G_4	ML3B-G	28/08/14	52.06	2.06	13.62	6.57	10.81	0.16	10.51	2.17	0.40	0.24	
ML3B-G_5	ML3B-G	28/08/14	52.04	2.14	13.62	6.56	10.93	0.16	10.60	2.52	0.39	0.26	
ML3B-G_6	ML3B-G	28/08/14	51.77	2.08	13.67	6.53	11.53	0.23	10.64	2.31	0.39	0.24	
		Average	**51.87**	**2.11**	**13.74**	**6.53**	**11.08**	**0.20**	**10.48**	**2.33**	**0.39**	**0.24**	
		2 σ	0.44	0.09	0.27	0.17	0.51	0.05	0.23	0.24	0.05	0.04	
		GeoReM	51.87	2.11	13.74	6.53	11.08	0.20	10.48	2.33	0.39	0.24	

.7.2 EPMA lower limits of detection

Lower limits of detection (LLD) for EPMA analyses are given in the Table below. The LLD is defined as the concentration at which an element is detected above the instrument back ground noise (Perkins and Pearce, 1995), and is calculated using Equation 1. These limits of detection are calculated from repeat analyses of three different MPI-DING glass standards, analysed during each analytical session. The median limit of detection for ATHO-G over all analytical sessions is given, this has the most similar composition to samples analysed in this study.

$$LLD = 3 \times \sigma \text{ of gas blanks} \times (\text{ concentrations} / \text{ avg. sample cps}) \quad (1)$$

where cps is counts per second

EPMA lower limits of detection, concentrations are in wt. %

Analysis date	MPI-DING glass	SiO_2	TiO_2	Al_2O_3	MgO	FeO^T	MnO	CaO	Na_2O	K_2O	P_2O_5	Cl
20/02/14	ATHO-G	0.06	0.02	0.04	0.02	0.07	0.02	0.03	0.05	0.04	0.10	0.02
20/02/14	GOR 128-G	0.06	0.03	0.04	0.05	0.12	0.08	0.04	0.09	0.02	0.04	0.15
20/02/14	StHs6/80-G	0.03	0.04	0.04	0.04	0.10	0.07	0.02	0.06	0.04	0.04	0.02
21/02/14	ATHO-G	0.07	0.05	0.03	0.03	0.08	0.10	0.04	0.07	0.03	0.04	0.02
21/02/14	GOR 128-G	0.06	0.05	0.04	0.04	0.11	0.08	0.04	0.06	0.01	0.05	1.80
21/02/14	StHs6/80-G	0.05	0.05	0.03	0.03	0.10	0.06	0.04	0.07	0.04	0.05	0.04
28/08/14	ATHO-G	0.05	0.05	0.03	0.04	0.09	0.08	0.03	0.07	0.03	0.12	
28/08/14	ML3B-G	0.03	0.08	0.05	0.04	0.07	0.09	0.05	0.05	0.03	0.05	
28/08/14	StHs6/80-G	0.04	0.04	0.04	0.04	0.08	0.05	0.01	0.07	0.02	0.05	
27/08/14	ATHO-G	0.04	0.03	0.03	0.02	0.06	0.05	0.05	0.06	0.03	0.08	
27/08/14	ML3B-G	0.05	0.02	0.02	0.02	0.14	0.09	0.04	0.07	0.05	0.05	
27/08/14	StHs6/80-G	0.03	0.06	0.03	0.06	0.08	0.10	0.02	0.03	0.03	0.05	
26/08/14	ATHO-G	0.03	0.04	0.04	0.03	0.04	0.04	0.03	0.01	0.03	0.01	
26/08/14	ML3B-G	0.04	0.06	0.03	0.04	0.15	0.08	0.04	0.07	0.03	0.06	
26/08/14	StHs6/80-G	0.06	0.03	0.04	0.01	0.13	0.05	0.03	0.04	0.02	0.05	
29/06/15	ATHO-G	0.10	0.06	0.09	0.03	0.08	0.06	0.03	0.11	0.02	0.24	0.02
29/06/15	GOR 128-G	0.09	0.05	0.06	0.10	0.03	0.08	0.04	0.07	0.04	0.05	0.02
29/06/15	StHs6/80-G	0.12	0.05	0.06	0.11	0.09	0.12	0.02	0.14	0.03	0.04	0.02
30/06/15	ATHO-G	0.15	0.05	0.10	0.06	0.07	0.07	0.05	0.20	0.03	0.18	0.03

Continued on next page

EPMA lower limits of detection, concentrations are in wt. %

Analysis date	MPI-DING glass	SiO_2	TiO_2	Al_2O_3	MgO	FeO^T	MnO	CaO	Na_2O	K_2O	P_2O_5	Cl
30/06/15	GOR 128-G	0.15	0.05	0.07	0.09	0.10	0.05	0.03	0.11	0.01	0.09	0.02
30/06/15	StHs6/80-G	0.09	0.03	0.09	0.02	0.09	0.05	0.03	0.14	0.03	0.10	0.02
03/07/15	ATHO-G	0.13	0.08	0.05	0.06	0.15	0.13	0.04	0.05	0.03	0.03	0.03
03/07/15	GOR 128-G	0.15	0.06	0.07	0.09	0.05	0.11	0.02	0.09	0.02	0.07	0.05
03/07/15	StHs6/80-G	0.17	0.01	0.09	0.07	0.12	0.11	0.03	0.14	0.03	0.20	0.03
	Median ATHO-G	0.08	0.05	0.05	0.04	0.08	0.07	0.04	0.08	0.03	0.10	0.02

.7.3 LA-ICP-MS reference materials

During each LA-ICP-MS analytical run, the MPI-DING reference material, ATHO-G, was analysed five times using a 20 μm crater diameter to check the calibration. These analyses are given below and are ordered according to analysis date. The average and 2σ of these analyses are given alongside published trace element concentrations from the GeoReM online database (Jochum *et al.*, 2005).

Trace element concentrations (ppm) in MPI-DING reference materials

MPI-DING glass	Analysis date	Rb	Sr	Y	Zr	Nb	Cs	Ba	La	Ce	Pr	Nd	Sm	Eu	Tb	Dy	Ho	Er	Tm	Yb	Lu	Hf	Ta	Pb	Th	U
ATHO-G	31/03/14	65.5	95.2	104	552	62.5	0.93	551	56.1	113	14.8	60.3	14.4	2.83	3.01	18.6	3.81	12.5	1.80	11.4	1.49	14.9	4.24	6.62	7.84	2.06
ATHO-G	31/03/14	65.0	97.6	102	533	61.0	0.99	570	56.0	115	15.0	60.8	14.8	2.93	2.51	17.0	3.83	10.6	1.81	10.4	1.53	15.2	3.90	6.58	7.27	2.45
ATHO-G	31/03/14	66.1	90.3	93.2	510	60.8	0.92	548	52.9	110	14.2	56.3	13.2	2.39	2.48	16.8	3.54	10.9	1.43	9.46	1.29	12.9	3.70	5.09	6.76	2.43
ATHO-G	31/03/14	70.0	101	102	528	61.2	1.06	612	56.9	122	15.6	57.6	14.4	3.22	2.91	15.8	3.72	11.6	1.45	10.0	1.76	12.9	3.86	6.22	7.45	2.41
ATHO-G	31/03/14	65.2	92.6	89.1	484	56.1	1.04	530	50.3	108	13.3	52.2	14.3	2.65	2.43	15.5	3.25	10.8	1.49	9.20	1.50	13.8	3.73	5.54	6.59	2.46
ATHO-G	02/04/14	66.4	105	105	537	62.4	1.17	580	53.1	112	13.9	65.7	14.6	2.84	2.92	18.1	3.98	12.3	1.92	12.1	1.77	16.5	5.33	18.90	8.08	2.49
ATHO-G	02/04/14	66.9	97.5	100	521	63.5	1.06	579	55.4	116	14.3	65.7	14.7	3.10	2.63	19.3	3.70	12.6	1.64	11.6	1.77	14.7	4.17	6.10	8.28	2.58
ATHO-G	02/04/14	68.5	94.4	98.2	491	63.4	1.21	584	53.2	112	13.7	64.8	14.8	3.08	2.54	16.8	3.74	11.3	1.69	10.9	1.69	13.3	3.90	5.99	7.65	2.70
ATHO-G	02/04/14	67.6	97.9	94.6	501	63.8	1.22	557	53.8	111	13.9	63.8	14.7	2.88	2.56	17.1	3.70	11.1	1.57	11.4	1.57	14.0	4.14	6.13	7.64	2.50
ATHO-G	02/04/14	69.3	94.6	94.6	487	59.4	1.13	567	53.2	112	13.6	66.0	14.3	2.85	2.78	17.2	3.75	11.7	1.74	11.1	1.63	14.6	4.10	6.26	7.55	2.59
ATHO-G	03/04/14	70.0	98.9	107	531	59.7	1.26	566	55.1	116	15.5	60.4	14.7	2.61	3.09	18.2	3.85	13.5	1.88	12.2	1.69	15.8	4.61	6.15	8.31	2.43
ATHO-G	03/04/14	71.1	98.7	100	508	60.0	1.06	559	54.0	118	14.5	62.9	14.3	3.04	2.85	18.3	3.52	12.0	1.83	11.9	1.84	15.6	4.43	5.98	8.21	2.82
ATHO-G	03/04/14	70.0	92.2	97.7	495	59.5	1.16	565	56.3	114	14.3	58.6	14.0	2.77	2.74	16.6	3.60	10.7	1.46	11.3	1.93	15.3	3.83	6.58	7.61	2.78
ATHO-G	03/04/14	76.2	92.4	94.7	478	62.0	1.11	565	54.6	117	14.0	60.7	16.1	3.32	2.83	16.9	3.73	10.5	1.37	11.3	1.47	13.9	3.89	6.44	7.53	2.93
ATHO-G	03/04/14	68.2	91.0	92.8	465	61.0	1.01	532	49.0	114	13.9	60.5	13.6	2.86	2.66	16.3	3.65	10.1	1.53	11.5	1.44	13.0	3.97	6.25	7.63	2.42
ATHO-G	04/04/14	71.6	97.3	95.2	503	60.2	0.99	572	55.0	111	13.9	60.8	14.8	3.20	2.57	17.2	4.03	11.7	1.64	11.0	1.71	15.5	3.87	7.74	7.67	2.63
ATHO-G	04/04/14	71.5	101	97.0	496	59.3	1.11	578	54.3	110	14.0	63.6	14.8	2.89	2.78	17.1	3.67	11.2	1.53	10.8	1.76	14.7	3.90	6.47	8.22	2.57
ATHO-G	04/04/14	78.5	98.0	94.7	489	60.6	1.16	580	52.5	111	14.5	61.7	14.0	2.92	2.64	16.8	3.55	10.9	1.58	11.4	1.50	14.1	3.65	6.23	7.48	3.10
ATHO-G	04/04/14	74.1	96.1	89.2	466	58.5	1.24	569	51.0	108	14.6	64.2	13.4	3.04	2.60	16.6	3.78	11.3	1.61	10.7	1.50	13.9	3.78	6.92	7.76	2.79
ATHO-G	04/04/14	70.3	97.2	90.4	477	58.2	1.03	568	52.1	113	13.9	59.5	12.1	2.94	2.77	15.7	3.50	11.9	1.48	10.9	1.63	12.1	3.77	7.13	7.27	2.89
ATHO-G	09/07/14	57.2	83.7	95.2	439	57.8	0.86	453	52.5	102	12.9	53.3	13.5	2.61	2.51	16.2	3.67	10.5	1.63	9.56	1.55	12.0	3.36	5.09	6.26	2.40
ATHO-G	09/07/14	62.1	94.9	104	474	66.4	1.25	506	54.6	110	14.3	53.0	14.9	2.39	2.37	18.6	3.54	10.5	1.37	10.3	1.71	13.7	3.75	4.91	7.90	2.32
ATHO-G	09/07/14	60.3	88.6	95.3	449	59.5	0.92	475	54.2	107	13.3	56.7	15.5	2.34	2.50	15.4	3.91	10.7	1.65	10.3	1.54	13.3	3.68	4.25	7.23	2.41
ATHO-G	09/07/14	69.5	95.3	103	473	66.3	1.07	505	59.6	114	15.1	64.7	15.1	2.80	2.63	18.1	3.27	11.1	1.47	11.3	1.78	13.6	4.07	4.73	7.40	2.37
ATHO-G	09/07/14	61.1	91.6	94.7	453	61.7	0.83	483	54.9	111	14.4	58.0	14.3	2.92	2.42	14.7	3.54	10.3	1.38	10.1	1.65	14.3	3.73	4.75	7.64	2.29
ATHO-G	10/07/14	63.2	99.5	99.6	525	64.9	1.03	518	54.0	110	14.0	67.8	16.0	3.26	2.97	18.1	3.98	11.9	1.51	11.3	1.58	14.5	4.08	5.43	7.98	2.51
ATHO-G	10/07/14	66.6	96.4	102	515	62.7	1.23	502	54.9	110	13.8	61.4	13.6	2.88	2.95	16.4	3.49	12.3	1.64	10.7	1.60	14.7	4.25	4.75	7.51	2.53
ATHO-G	10/07/14	65.1	91.8	98.0	490	61.3	1.01	527	54.5	111	15.0	60.3	14.6	3.09	2.67	15.7	3.75	11.5	1.66	11.5	1.65	15.7	4.03	5.37	7.12	2.33
ATHO-G	10/07/14	66.8	99.0	104	532	63.7	1.25	520	57.3	123	15.0	69.6	14.2	2.70	2.90	18.5	3.81	10.8	1.41	10.4	1.63	14.9	4.25	5.87	8.31	2.58
ATHO-G	10/07/14	73.6	97.2	100	513	63.3	1.15	513	53.8	114	13.8	62.9	13.5	2.98	2.64	16.5	3.90	11.4	1.52	11.5	1.50	15.3	4.25	5.60	7.96	2.40
ATHO-G	11/07/14	62.5	99.0	111	535	63.6	1.15	519	55.2	113	14.6	63.1	15.0	2.84	2.45	19.6	3.80	11.3	1.78	11.3	1.60	16.2	4.27	9.28	7.61	2.37
ATHO-G	11/07/14	65.1	104	114	573	65.4	1.07	572	62.0	125	15.7	66.0	17.5	3.23	3.22	19.6	4.13	11.8	1.96	11.6	1.97	17.6	4.76	5.44	8.30	2.58
ATHO-G	11/07/14	64.8	100	104	529	62.8	1.23	547	57.7	123	14.7	65.7	15.9	3.28	2.83	18.1	3.33	11.8	1.47	11.0	1.37	13.5	4.11	5.00	7.92	2.26
ATHO-G	11/07/14	62.1	91.9	103	519	60.7	1.22	528	55.5	117	14.3	65.3	14.1	3.04	2.64	15.7	3.08	11.9	1.50	10.6	1.61	13.9	4.40	8.58	8.42	2.64
ATHO-G	11/07/14	63.0	93.9	100	518	66.8	0.96	537	57.2	124	14.3	60.3	13.6	3.00	2.58	17.2	3.22	11.1	1.37	10.6	1.52	14.0	3.55	5.40	8.07	2.55
ATHO-G	16/07/14	70.0	102	108	559	68.7	1.31	551	58.4	121	14.6	60.2	17.8	3.27	2.90	17.4	3.85	11.7	1.88	11.9	1.99	15.0	4.30	5.92	8.30	2.69
ATHO-G	16/07/14	68.7	99.9	103	530	64.1	1.11	569	59.7	124	14.7	60.0	14.3	2.85	3.28	20.0	4.12	10.9	2.00	12.0	1.80	16.3	4.14	5.82	8.12	2.57
ATHO-G	16/07/14	64.1	93.2	97.3	508	62.3	1.13	522	54.7	121	14.2	63.8	13.1	2.92	2.64	16.8	3.28	11.6	1.59	11.6	1.69	15.8	4.53	5.93	8.78	2.38
ATHO-G	16/07/14	69.9	97.7	102	528	63.9	1.06	530	55.2	125	15.0	63.6	15.6	2.92	2.37	17.1	3.57	12.2	1.46	11.3	1.85	16.6	4.07	6.21	7.55	2.39
ATHO-G	16/07/14	73.5	102	103	521	65.2	1.06	541	57.4	130	13.6	55.7	14.4	3.12	2.69	16.7	3.94	12.0	1.63	12.9	1.82	14.5	4.34	6.27	7.99	2.79
ATHO-G	18/07/14	64.2	89.3	92.9	484	60.6	1.14	522	52.7	112	12.7	55.9	13.0	2.65	2.48	18.1	3.49	8.66	1.79	9.94	1.34	13.8	4.04	5.18	6.97	2.19
ATHO-G	18/07/14	66.1	88.9	90.1	510	61.5	0.95	528	54.3	115	13.4	61.3	13.5	2.47	2.36	14.6	3.44	10.3	1.54	9.38	1.59	12.0	3.79	5.22	7.33	2.22

Continued on next page

Trace element concentrations (ppm) in MPI-DING reference materials

MPI-DING glass	Analysis date	Rb	Sr	Y	Zr	Nb	Cs	Ba	La	Ce	Pr	Nd	Sm	Eu	Tb	Dy	Ho	Er	Tm	Yb	Lu	Hf	Ta	Pb	Th	U
ATHO-G	18/07/14	70.0	89.5	94.2	494	62.3	0.92	527	50.7	116	14.2	58.8	11.5	2.33	2.40	17.6	3.39	10.4	1.53	10.5	1.67	13.5	3.30	5.50	7.26	2.26
ATHO-G	18/07/14	68.3	85.5	91.6	472	62.4	1.11	533	50.5	115	12.5	60.1	15.0	2.38	2.26	15.8	3.60	10.4	1.53	9.80	1.39	13.3	3.99	5.21	6.64	2.30
ATHO-G	18/07/14	66.2	87.3	95.7	493	62.5	1.10	516	54.3	115	13.4	61.9	13.2	2.76	2.38	17.5	3.12	10.9	1.61	10.2	1.54	14.6	3.89	5.54	7.18	2.39
ATHO-G	22/07/14	62.2	95.9	101	533	64.3	1.13	494	54.1	108	14.2	60.8	14.3	3.27	2.72	18.8	3.28	13.6	1.50	10.4	1.74	14.4	4.39	4.51	7.79	2.14
ATHO-G	22/07/14	61.4	92.8	98.7	517	63.3	0.98	489	53.4	112	14.0	56.1	12.6	2.48	2.60	15.9	3.71	12.8	1.45	10.5	1.36	14.5	3.83	4.51	7.40	2.27
ATHO-G	22/07/14	61.9	94.8	93.7	514	60.0	1.08	481	53.2	111	14.3	54.5	15.6	2.75	2.21	14.9	3.87	11.4	1.54	10.7	1.67	13.1	4.07	4.88	6.84	2.45
ATHO-G	22/07/14	62.7	92.2	92.2	488	61.2	1.02	475	49.2	112	13.3	54.4	12.7	2.91	2.51	16.2	3.14	10.9	1.44	9.59	1.48	13.7	3.69	4.98	7.37	2.36
ATHO-G	22/07/14	63.7	98.7	99.8	509	65.5	0.98	501	54.7	120	14.8	62.6	14.5	2.56	2.82	17.5	4.10	12.5	1.40	9.90	1.61	13.5	3.97	5.93	8.06	2.44
ATHO-G	28/10/14	68.0	107	103	531	63.3	1.15	628	60.4	114	16.5	64.2	16.4	2.98	3.02	19.0	3.87	13.2	2.04	11.9	1.92	13.7	4.50	7.47	8.56	2.48
ATHO-G	28/10/14	68.5	107	104	520	62.5	1.08	671	59.2	111	16.4	63.9	15.2	3.31	2.69	18.4	3.73	11.7	1.80	11.3	1.76	16.2	4.35	7.20	8.21	2.62
ATHO-G	28/10/14	68.6	102	95.9	491	61.7	1.05	647	57.1	110	15.6	63.1	15.2	3.17	2.55	17.8	3.97	12.6	1.68	10.6	1.50	15.4	4.22	7.28	7.21	2.75
ATHO-G	28/10/14	65.3	101	99.4	519	61.1	0.91	592	52.7	110	14.4	63.2	13.7	3.09	2.61	16.5	3.63	10.2	1.38	10.9	1.63	13.4	3.91	5.70	7.39	2.28
ATHO-G	28/10/14	70.7	106	99.5	495	61.9	1.01	662	58.0	111	16.1	65.4	15.7	3.39	2.90	19.0	4.12	11.8	1.56	11.3	1.80	15.1	4.05	6.81	7.83	2.81
ATHO-G	30/10/14	72.5	108	99.7	511	58.7	1.28	615	56.6	123	15.3	69.4	15.8	3.03	2.41	18.7	3.94	12.6	1.74	11.7	1.90	14.6	3.75	5.94	7.61	2.36
ATHO-G	30/10/14	73.0	109	99.9	510	60.7	1.21	622	55.2	114	15.8	64.4	14.1	2.69	2.65	17.9	3.79	11.0	1.76	11.9	1.63	15.2	3.95	6.75	8.11	2.67
ATHO-G	30/10/14	76.5	104	94.7	485	62.8	1.14	633	56.2	113	15.8	65.6	15.4	2.64	2.43	17.3	3.51	10.8	1.69	12.0	1.73	13.4	4.03	7.32	7.75	3.02
ATHO-G	30/10/14	68.3	98.6	90.3	463	58.1	1.22	563	53.7	125	14.3	57.9	15.4	2.59	2.45	15.5	3.42	10.4	1.56	10.4	1.47	13.6	3.71	7.07	7.30	2.73
ATHO-G	30/10/14	72.3	108	94.5	495	62.1	1.14	601	53.0	123	14.4	59.7	15.5	3.15	2.45	16.2	3.45	9.60	1.59	11.6	1.48	13.5	3.70	5.97	7.17	2.72
ATHO-G	12/01/15	61.8	90.2	102	502	60.2	0.84	495	54.7	111	13.7	59.6	16.0	3.11	2.33	16.1	3.58	9.33	1.85	8.38	1.47	13.3	3.60	5.96	7.42	2.51
ATHO-G	12/01/15	65.3	94.8	104	519	62.8	0.91	521	56.1	120	14.8	60.4	14.3	2.48	2.95	18.3	3.68	11.3	1.44	10.3	1.33	14.0	4.15	5.70	7.87	2.05
ATHO-G	12/01/15	67.3	93.5	100	500	61.7	1.10	522	56.0	127	14.4	62.7	12.8	2.71	2.73	16.7	4.12	10.4	1.78	10.7	1.41	15.0	4.23	4.78	6.95	2.22
ATHO-G	12/01/15	65.9	96.6	94.9	497	61.8	1.26	513	54.3	116	14.2	61.6	16.0	3.17	2.93	15.2	3.37	10.1	1.72	10.7	1.46	13.8	4.09	5.07	7.05	2.30
ATHO-G	12/01/15	65.7	94.5	95.4	484	63.3	1.21	532	54.4	120	14.2	62.5	14.4	2.45	2.46	17.1	3.82	10.3	1.47	11.2	1.33	13.4	4.04	5.66	7.53	2.19
ATHO-G	13/01/15	74.0	105	85.4	339	54.7	1.17	510	48.5	117	10.0	53.8	12.9	2.35	1.79	13.8	2.59	9.04	1.20	9.44	1.57	13.7	4.31	7.39	6.20	3.52
ATHO-G	13/01/15	71.1	103	89.7	343	55.6	1.06	533	46.7	124	10.1	56.8	14.3	2.20	2.55	12.4	2.96	9.37	1.38	9.20	1.52	12.7	4.21	6.92	5.58	4.11
ATHO-G	13/01/15	73.3	101	85.2	334	59.6	1.29	525	46.4	112	10.4	57.1	14.7	2.28	2.24	11.7	2.35	9.84	1.27	9.06	1.49	11.9	4.13	6.42	6.15	4.13
ATHO-G	13/01/15	71.2	98.9	86.2	322	54.7	1.09	523	44.7	117	9.8	55.2	15.0	2.19	2.26	12.5	2.53	9.18	1.28	8.55	1.39	12.6	4.37	7.47	6.14	3.76
ATHO-G	13/01/15	72.1	105	85.4	326	59.0	1.21	528	47.6	113	10.7	57.2	16.7	2.22	1.90	12.1	2.71	8.30	1.01	8.91	1.29	11.4	4.20	7.01	5.70	4.11
ATHO-G	14/01/15	62.8	97.7	104	519	61.9	0.90	493	56.7	114	14.4	56.7	15.3	2.70	2.71	15.3	3.24	12.2	1.73	9.70	2.04	14.2	3.91	6.42	7.07	2.16
ATHO-G	14/01/15	64.9	94.0	101	535	65.4	0.88	517	57.5	118	14.7	59.4	15.7	2.73	2.84	17.4	3.34	10.8	1.86	11.2	1.72	13.7	4.06	5.87	7.01	2.56
ATHO-G	14/01/15	63.2	92.9	92.2	484	65.3	1.17	509	54.6	111	13.7	57.3	13.4	2.64	2.55	16.0	3.17	9.89	1.49	9.11	1.75	12.9	3.89	3.91	7.16	2.25
ATHO-G	14/01/15	62.3	90.6	102	499	63.0	1.12	520	57.9	118	14.3	56.6	14.2	2.66	2.51	15.8	3.42	11.0	1.62	10.7	1.48	13.3	3.98	5.62	7.53	2.35
ATHO-G	14/01/15	67.8	91.1	97.7	484	64.9	1.24	495	52.0	116	15.0	56.5	14.7	2.71	2.61	16.3	3.46	10.0	1.80	10.3	1.45	14.3	3.88	4.99	6.34	2.42
ATHO-G	15/01/15	63.9	90.2	96.0	511	63.2	1.08	492	55.5	112	12.5	58.2	14.9	2.96	2.47	15.9	3.28	9.29	1.54	8.16	1.57	13.9	3.36	5.31	6.29	2.21
ATHO-G	15/01/15	64.5	92.9	96.9	511	64.6	0.79	504	52.3	116	13.6	56.0	12.3	3.11	2.37	15.2	3.63	9.13	1.45	9.70	1.48	14.8	3.25	6.15	7.88	1.87
ATHO-G	15/01/15	67.0	88.6	90.7	496	63.0	1.07	469	50.0	112	13.2	55.0	13.1	2.27	2.02	14.6	3.19	9.79	1.61	9.27	1.12	13.8	4.20	4.64	6.84	2.11
ATHO-G	15/01/15	69.5	90.2	94.6	499	65.1	1.01	489	52.7	117	14.2	57.7	14.3	2.46	2.45	16.0	3.41	11.2	1.38	9.32	1.36	14.2	4.36	4.70	6.67	2.58
ATHO-G	15/01/15	66.6	91.9	95.3	475	64.1	1.10	526	50.7	113	13.0	52.8	12.9	2.33	2.29	15.7	3.58	9.23	1.40	9.35	1.38	13.8	4.03	4.69	6.97	2.27
ATHO-G	16/01/15	59.4	90.8	98.8	508	63.0	0.56	402	55.4	113	14.2	52.0	14.1	2.62	2.65	15.1	4.02	13.0	1.46	11.7	1.99	15.1	4.53	6.72	7.71	2.70
ATHO-G	16/01/15	65.7	91.8	98.2	507	64.8	0.97	424	54.0	117	13.7	61.5	13.5	2.47	2.37	18.1	3.57	11.4	1.78	10.6	1.80	16.5	3.95	5.43	8.23	2.29
ATHO-G	16/01/15	74.5	94.8	100	526	63.6	1.39	422	56.9	119	14.9	62.3	13.1	2.31	2.15	15.2	3.71	11.5	1.77	11.6	1.44	13.2	4.53	5.27	7.65	2.59
ATHO-G	16/01/15	63.6	91.0	90.6	500	64.1	1.00	403	50.9	112	12.8	58.2	13.5	2.43	2.63	13.0	3.86	9.79	1.49	9.82	1.70	15.0	3.92	4.01	6.44	2.21
ATHO-G	16/01/15	63.5	86.7	93.4	485	61.9	0.95	418	51.4	119	13.5	58.1	13.5	3.21	2.22	15.9	3.53	9.88	1.50	9.23	1.32	12.6	4.31	4.99	8.10	2.58
ATHO-G	19/01/15	61.6	91.2	107	556	63.7	1.13	484	56.4	112	14.8	56.6	15.6	2.77	2.76	17.6	3.61	11.9	1.74	10.9	1.31	17.6	3.90	5.34	7.92	2.09

Continued on next page

Trace element concentrations (ppm) in MPI-DING reference materials

MPI-DING glass	Analysis date	Rb	Sr	Y	Zr	Nb	Cs	Ba	La	Ce	Pr	Nd	Sm	Eu	Tb	Dy	Ho	Er	Tm	Yb	Lu	Hf	Ta	Pb	Th	U
ATHO-G	19/01/15	61.6	92.5	110	571	63.6	1.34	532	59.0	118	14.6	60.3	14.5	2.59	3.03	17.1	3.58	10.4	1.91	11.2	1.98	13.4	3.99	4.50	7.83	2.17
ATHO-G	19/01/15	61.4	90.4	101	519	61.0	1.02	508	54.8	114	14.3	62.2	14.2	2.45	2.86	16.1	3.66	10.3	1.43	11.5	1.46	14.3	3.81	5.07	7.56	2.19
ATHO-G	19/01/15	64.2	97.8	103	546	62.8	1.07	524	57.4	116	14.5	61.1	14.3	2.83	2.77	17.6	4.10	9.31	1.62	10.2	1.45	13.0	4.20	4.46	7.60	2.39
ATHO-G	19/01/15	67.3	91.6	100	521	67.0	1.08	563	56.5	117	14.2	65.9	13.9	2.63	2.79	16.5	3.36	11.2	1.45	10.6	1.82	14.1	4.11	5.54	7.37	2.53
ATHO-G	20/01/15	61.4	92.2	106	549	64.7	0.99	499	56.5	110	13.6	58.7	16.4	2.87	2.95	16.2	3.74	11.1	1.71	12.0	1.63	15.1	3.38	9.40	7.74	1.97
ATHO-G	20/01/15	59.4	97.6	105	563	63.5	1.22	527	56.1	111	13.9	53.9	14.3	2.68	2.74	17.4	4.48	11.6	1.68	10.6	1.79	16.7	4.04	4.58	7.34	1.84
ATHO-G	20/01/15	67.3	97.9	101	538	64.3	1.06	503	57.5	110	14.9	61.0	15.4	2.19	2.68	15.9	3.28	11.5	1.63	9.86	1.67	14.7	4.12	4.76	7.65	2.12
ATHO-G	20/01/15	64.3	93.0	96.3	516	59.1	1.06	520	54.5	106	14.1	58.1	14.1	2.67	2.69	16.3	3.34	9.36	1.46	11.7	1.49	14.1	3.76	4.87	6.71	2.22
ATHO-G	20/01/15	63.1	92.8	94.5	489	58.5	1.09	507	55.3	103	13.9	58.1	13.8	2.45	2.50	16.3	3.37	10.3	1.64	10.3	1.66	13.3	4.07	5.39	6.98	2.37
ATHO-G	21/01/15	65.7	94.4	104	539	64.3	0.83	498	52.9	112	13.8	65.6	13.8	2.36	2.92	16.2	3.60	10.5	1.27	12.7	1.99	14.7	3.64	5.63	7.17	2.02
ATHO-G	21/01/15	60.2	90.7	102	536	63.2	1.13	529	56.3	109	14.1	62.0	13.6	2.99	2.86	18.5	3.72	10.4	1.55	11.6	1.98	14.8	4.17	9.33	7.48	1.94
ATHO-G	21/01/15	61.5	90.0	105	553	64.6	1.35	507	55.0	116	14.8	61.2	12.5	3.35	2.61	17.7	3.41	10.6	1.81	10.5	1.70	15.0	4.20	4.57	7.56	2.42
ATHO-G	21/01/15	67.5	95.9	105	542	66.0	1.30	529	55.1	115	14.6	64.7	14.1	3.07	2.66	16.6	3.64	11.5	1.41	10.5	1.61	16.5	4.19	4.70	7.59	2.51
ATHO-G	21/01/15	65.5	93.9	97.2	530	64.9	1.16	495	56.5	110	13.2	57.6	13.9	2.83	2.41	15.5	3.50	9.60	1.45	9.50	1.77	13.4	3.82	8.42	7.17	2.22
ATHO-G	05/05/15	63.4	95.9	108	570	64.7	1.31	548	59.0	121	14.8	61.7	14.7	3.02	2.93	20.0	4.23	12.2	1.67	10.6	1.62	16.1	4.02	13.40	7.59	2.16
ATHO-G	05/05/15	67.6	103	111	591	70.1	1.29	584	63.6	130	15.8	63.5	14.8	3.49	3.09	18.5	4.03	12.3	1.58	13.2	1.74	16.1	4.79	4.93	8.16	2.10
ATHO-G	05/05/15	63.6	95.1	107	535	63.3	1.08	577	59.7	126	15.4	65.1	15.7	2.77	2.66	17.8	3.87	10.9	1.92	10.3	1.69	15.3	3.85	5.08	7.59	2.19
ATHO-G	05/05/15	68.3	98.9	107	547	69.7	0.81	587	58.6	122	16.0	72.4	12.8	2.87	2.66	16.9	3.89	11.5	1.55	10.3	1.40	16.3	4.48	4.67	7.26	2.54
ATHO-G	05/05/15	62.7	104	104	532	63.9	1.00	556	57.6	120	14.4	58.0	14.0	2.39	2.47	15.9	3.53	12.4	1.74	10.3	1.53	16.7	3.81	4.16	8.12	2.22
ATHO-G	06/05/15	66.1	92.0	110	578	69.0	1.34	516	56.9	120	14.3	70.6	14.3	3.15	2.48	16.6	3.99	11.6	1.70	12.2	2.01	15.4	4.28	16.20	8.30	2.35
ATHO-G	06/05/15	64.1	98.6	113	562	68.6	1.09	544	55.6	117	15.1	65.2	15.1	2.62	2.68	17.1	3.82	11.3	1.54	10.7	1.61	13.5	4.66	5.50	7.62	2.25
ATHO-G	06/05/15	63.6	96.2	104	539	67.0	1.02	504	55.9	120	13.9	63.2	12.9	3.07	2.55	16.7	3.86	10.6	1.58	10.4	1.73	16.3	4.32	5.18	7.86	2.44
ATHO-G	06/05/15	70.7	96.1	103	531	69.4	1.19	511	55.5	117	14.5	59.1	13.6	2.98	2.34	18.0	3.44	10.9	1.54	10.7	1.56	15.5	4.46	4.79	7.57	2.41
ATHO-G	06/05/15	63.0	91.7	97.8	509	62.3	1.09	517	52.2	114	13.6	60.6	12.6	2.47	2.26	15.1	3.43	11.1	1.51	11.1	1.21	13.4	3.93	5.23	6.95	2.24
ATHO-G	07/05/15	64.4	95.0	110	563	67.6	1.22	549	54.9	117	15.0	68.6	16.4	2.71	2.33	17.5	4.23	12.9	1.61	11.4	1.68	15.4	3.97	5.41	8.00	2.44
ATHO-G	07/05/15	67.5	103	104	542	65.7	1.47	572	56.7	118	15.4	62.8	14.9	3.02	2.67	17.9	3.47	12.0	1.54	11.8	1.66	15.7	3.77	4.99	7.79	2.55
ATHO-G	07/05/15	70.7	98.3	99.8	533	65.2	0.98	566	55.4	118	14.2	64.8	14.6	2.87	2.65	14.8	3.87	11.2	1.60	10.8	1.59	14.1	3.69	5.19	7.59	2.55
ATHO-G	07/05/15	70.7	101	103	524	64.9	1.02	561	55.9	119	14.9	62.0	14.6	3.13	2.21	16.7	3.10	11.3	1.38	11.4	1.46	14.9	3.72	5.25	7.71	2.63
ATHO-G	07/05/15	64.4	90.3	104	549	64.4	1.10	567	55.6	122	14.9	63.3	15.4	3.30	2.43	16.6	3.89	10.6	1.51	10.7	1.41	15.6	3.83	5.00	7.33	2.64
ATHO-G	20/07/15	68.2	119	112	619	63.9	1.20	583	63.8	131	15.5	67.4	15.2	3.23	3.16	17.6	4.35	11.7	1.77	12.2	1.87	17.9	4.16	8.41	8.56	2.27
ATHO-G	20/07/15	63.7	103	109	544	60.9	0.99	520	57.4	124	14.0	65.0	13.2	2.82	2.67	19.1	3.42	11.4	1.30	10.2	1.70	14.9	3.72	6.01	8.10	2.01
ATHO-G	20/07/15	64.4	103	109	582	64.0	0.82	578	65.0	133	15.6	65.5	15.1	3.05	2.84	18.4	3.62	12.7	1.59	12.7	1.81	16.1	4.43	6.64	8.07	2.28
ATHO-G	20/07/15	67.0	104	105	550	64.9	0.92	557	62.1	131	14.8	64.5	15.9	2.94	2.79	17.0	3.62	11.5	1.74	10.1	1.96	14.5	3.55	4.73	8.20	2.23
ATHO-G	20/07/15	68.9	99.8	107	565	64.2	1.23	567	59.8	131	15.8	68.4	15.9	3.04	2.93	17.2	3.19	12.6	1.77	9.76	1.66	14.5	4.56	6.19	7.01	2.55
ATHO-G	21/07/15	65.4	81.2	102	525	61.72	0.99	592	57.30	123	15.5	60.6	13.1	1.95	2.75	17.4	3.53	11.1	1.64	11.4	1.83	13.1	4.17	4.70	7.72	1.91
ATHO-G	21/07/15	69.0	95.5	98.2	499	61.39	0.93	583	55.04	120	14.3	56.7	13.3	2.48	2.42	17.6	4.11	10.8	1.51	11.0	1.55	15.2	4.24	5.92	8.01	5.46
ATHO-G	21/07/15	65.3	93.1	101	505	60.81	1.06	584	57.49	126	14.9	63.8	16.7	2.91	2.77	15.6	3.81	11.9	1.37	12.0	1.67	15.8	3.92	5.12	8.29	5.51
ATHO-G	21/07/15	69.5	94.0	103	504	66.33	1.27	635	60.13	133	14.9	64.9	13.9	3.50	2.94	19.9	3.84	11.7	1.28	10.3	1.55	14.5	4.25	6.19	7.67	0.29
ATHO-G	21/07/15	65.3	94.1	97.2	486	55.98	0.83	534	55.31	133	13.6	57.0	14.1	2.44	2.43	16.3	3.40	10.1	1.46	10.3	1.55	13.2	3.77	4.79	7.81	0.13
ATHO-G	23/07/15	64.2	110	108	566	69.14	1.15	596	61.76	130	16.1	67.2	18.2	3.08	2.98	21.1	4.09	12.6	2.24	12.1	1.94	15.7	5.03	10.4	9.44	2.46
ATHO-G	23/07/15	75.8	114	112	558	71.50	1.08	643	61.07	145	17.4	73.3	17.1	4.07	2.84	20.0	4.09	13.3	2.16	13.1	1.54	17.2	4.33	11.8	8.57	2.84
ATHO-G	23/07/15	64.0	109	102	528	67.49	1.03	609	63.80	141	16.0	69.0	17.2	3.17	2.63	18.6	4.23	11.2	1.74	11.8	1.49	14.9	4.47	8.99	8.85	2.65
ATHO-G	23/07/15	65.3	110	110	543	68.23	0.98	602	62.71	140	15.6	68.9	16.9	2.98	2.72	19.9	4.33	12.0	1.86	13.9	1.69	17.7	4.34	10.5	8.41	2.66
ATHO-G	23/07/15	69.9	108	114	581	68.83	0.77	661	63.39	140	17.3	71.8	19.8	3.36	2.70	16.8	4.15	12.0	2.47	12.6	1.90	14.4	4.51	6.72	8.68	2.81

Continued on next page

Trace element concentrations (ppm) in MPI-DING reference materials

MPI-DING glass	Analysis date	Rb	Sr	Y	Zr	Nb	Cs	Ba	La	Ce	Pr	Nd	Sm	Eu	Tb	Dy	Ho	Er	Tm	Yb	Lu	Hf	Ta	Pb	Th	U
ATHO-G	24/07/15	67.5	108	107	546	68.15	0.85	669	61.78	133	15.3	73.2	15.6	2.91	2.69	18.4	4.18	13.2	1.89	11.9	2.37	14.7	4.56	5.69	8.71	2.47
ATHO-G	24/07/15	70.4	91.3	108	542	81.97	1.25	707	66.13	138	16.2	64.1	16.7	3.27	3.48	18.2	4.09	12.5	1.64	11.7	1.75	15.4	4.15	4.83	9.25	2.57
ATHO-G	24/07/15	68.5	98.7	110	518	64.42	0.86	593	60.58	132	16.5	69.7	15.2	3.60	2.83	19.0	3.65	12.5	1.75	12.8	1.94	15.2	4.76	4.51	9.14	3.01
ATHO-G	24/07/15	73.1	90.9	105	486	63.74	1.17	639	63.07	138	16.5	64.8	16.4	2.52	2.76	17.3	3.65	10.6	1.63	12.2	1.56	14.1	4.07	5.15	8.60	2.90
ATHO-G	24/07/15	71.4	92.3	101	546	66.65	1.27	698	64.61	136	18.5	65.2	16.2	3.24	2.60	19.3	3.84	11.6	1.94	11.9	1.41	16.3	4.49	6.28	8.89	2.50
ATHO-G	28/07/15	66.1	109	110	558	64.29	1.17	602	56.57	124	15.1	68.3	14.1	2.47	3.28	16.1	3.85	12.3	1.87	11.7	1.62	16.7	4.17	4.64	7.46	2.27
ATHO-G	28/07/15	59.8	105	107	536	62.87	1.02	589	56.63	125	15.7	63.1	15.3	2.68	2.86	17.7	3.76	12.7	1.87	9.34	1.53	13.3	4.17	4.95	8.76	2.86
ATHO-G	28/07/15	60.2	90.3	93.9	487	58.56	1.08	535	51.53	117	14.0	55.0	14.2	2.28	2.38	16.2	3.59	12.2	1.36	9.05	1.58	13.2	3.96	4.99	6.74	2.41
ATHO-G	28/07/15	62.9	92.8	97.9	493	59.31	0.86	566	50.65	122	14.9	60.4	13.6	2.65	2.52	17.3	3.55	10.2	1.57	9.56	1.52	13.5	3.99	6.38	7.77	2.54
ATHO-G	29/07/15	56.7	76.9	103	563	62.5	0.94	560	58.8	118	15.5	56.3	16.0	2.71	3.20	17.0	4.34	11.2	1.40	12.4	1.55	15.0	4.23	6.95	8.29	2.31
ATHO-G	29/07/15	59.1	90.2	101	551	65.2	1.04	602	59.7	123	15.1	62.7	14.8	3.34	2.40	16.2	4.02	11.8	1.81	10.4	1.69	12.6	4.03	5.37	7.38	2.17
ATHO-G	29/07/15	67.2	91.0	95.7	519	64.7	0.93	586	58.6	132	16.1	55.0	13.9	3.09	2.30	15.9	3.57	10.1	1.70	10.8	1.58	13.0	4.16	4.57	7.78	2.38
ATHO-G	29/07/15	60.2	85.6	95.3	489	60.4	0.72	551	55.5	118	15.2	60.4	13.9	2.57	2.86	16.2	3.56	11.7	1.33	9.28	1.39	15.3	3.49	4.65	7.17	2.16
ATHO-G	29/07/15	61.4	91.3	91.7	494	63.0	0.99	569	53.8	121	14.5	63.3	14.2	2.72	2.15	15.2	3.48	9.50	1.16	11.3	1.33	13.3	3.62	5.27	6.95	2.17
Average		**66.5**	**96.4**	**100**	**512**	**63.2**	**1.08**	**546**	**55.7**	**118**	**14.4**	**61.5**	**14.6**	**2.83**	**2.64**	**16.9**	**3.65**	**11.2**	**1.61**	**10.8**	**1.62**	**14.5**	**4.07**	**6.09**	**7.62**	**2.49**
2 σ		4.18	6.58	6.34	45.89	3.47	0.15	53.98	3.77	8.17	1.26	4.54	1.28	0.35	0.27	1.59	0.35	1.07	0.21	1.05	0.20	1.29	0.33	2.00	0.67	0.58
GeoReM		65.3	94.1	94.5	512	62.4	1.08	547	55.6	121	14.6	60.9	14.2	2.76	2.51	16.2	3.43	10.3	1.52	10.5	1.54	13.7	3.90	5.67	7.40	2.37

.7.4 LA-ICP-MS lower limits of detection

Lower limits of detection (LLD) for all LA-ICP-MS analytical sessions are given in the following table.

Limits of detection are low for most analytes, particularly using 20 μm crater diameters. Using 10 μm crater diameters, the ^{29}Si signal to background ratio decreases, causing LLD concentrations to increase. Glass shards analysed in this study are highly evolved, containing incompatible elements typically exceeding these limits of detections when using 20 μm diameter craters. Limits of detection are sensitive to instrumental variations, associated with tuning and gas blanks (Pearce *et al.*, 2011). Background counts for Sr, Rb, Cs and Ba increase over time, due to their 'sticky' nature causing them to adhere to the glassware and interface cones of the ICP-MS (Pearce *et al.*, 2011). This behaviour, coupled with low Sr concentrations in these fractionated glass compositions, causes their higher LLD concentrations. Barium was found to be useful for discrimminating the Tilo tephras, however, concentrations in the glass shards fall well above the LLD for this analyte.

LA-ICP-MS lower limits of detection, concentrations are in ppm

Date	Session	Crater diameter, μm	Rb	Sr	Y	Zr	Nb	Cs	Ba	La	Ce	Pr	Nd	Sm	Eu	Tb	Dy	Ho	Er	Tm	Yb	Lu	Hf	Ta	Pb	Th	U
31/03/14	AM	20	0.69	0.33	0.12	0.12	0.07	0.31	5.67	0.05	0.06	0.01	0.42	0.11	0.12	0.05	0.07	0.04	0.12	0.05	0.25	0.04	0.09	0.04	0.27	0.01	0.00
31/03/14	AM	10	7.32	9.47	0.70	0.92	0.33	0.74	17.3	0.52	0.53	0.12	1.67	0.67	0.37	0.13	0.56	0.08	0.51	0.30	0.67	0.09	0.48	0.41	0.94	0.10	0.00
02/04/14	AM	20	0.36	2.50	0.04	0.22	0.02	0.14	5.25	0.18	0.06	0.02	0.33	0.12	0.04	0.02	0.07	0.02	0.11	0.09	0.19	0.05	0.10	0.04	0.21	0.00	0.00
02/04/14	AM	10	4.70	7.08	1.79	2.67	0.69	1.18	10.4	0.25	0.67	0.62	1.86	2.50	1.89	0.33	0.25	0.26	0.24	0.59	0.34	0.32	0.24	0.55	0.42	0.15	0.04
02/04/14	PM	20	1.14	4.89	0.08	0.38	0.09	0.24	3.12	0.06	0.20	0.02	0.24	0.12	0.11	0.03	0.07	0.04	0.18	0.11	0.17	0.11	0.16	0.09	0.14	0.02	0.00
02/04/14	PM	10	3.51	13.6	2.35	1.12	0.18	0.48	14.0	0.47	0.78	0.82	0.84	0.31	0.78	0.25	0.82	0.39	0.79	0.22	0.95	0.16	0.20	0.57	0.32	0.08	0.00
03/04/14	AM	20	0.10	1.52	0.13	0.40	0.10	0.41	1.19	0.03	0.11	0.01	0.67	0.12	0.11	0.06	0.11	0.04	0.09	0.01	0.09	0.05	0.08	0.11	0.18	0.01	0.00
03/04/14	AM	10	2.27	15.7	0.42	2.37	0.51	0.50	12.5	0.79	0.45	0.16	0.44	0.97	1.16	0.16	0.44	0.20	1.10	0.15	1.25	0.51	0.47	0.70	1.06	0.13	0.00
04/04/14	AM	20	0.92	0.52	0.22	0.33	0.06	0.17	2.98	0.05	0.03	0.04	0.06	0.31	0.22	0.03	0.20	0.05	0.04	0.04	0.07	0.04	0.04	0.07	0.09	0.00	0.02
04/04/14	AM	10	4.99	14.2	0.16	1.22	0.20	1.55	23.8	0.35	0.35	0.45	1.87	0.76	0.75	0.24	0.13	0.16	0.57	0.06	0.69	0.75	0.28	0.47	0.82	0.11	0.19
09/07/14	AM	20	0.26	0.75	0.23	0.63	0.09	0.16	2.67	0.19	0.13	0.06	0.32	0.37	0.18	0.09	0.37	0.08	0.12	0.10	0.27	0.01	0.08	0.18	0.13	0.02	0.00
09/07/14	AM	10	1.72	2.22	1.09	3.27	0.25	0.74	11.7	1.00	0.81	0.23	2.42	1.05	1.62	0.63	0.73	0.08	0.39	0.15	2.20	0.32	0.00	0.13	0.95	0.24	0.00
09/07/14	PM	20	1.14	1.47	0.29	0.39	0.06	0.08	1.01	0.04	0.17	0.05	0.04	0.13	0.16	0.11	0.34	0.02	0.06	0.05	0.03	0.05	0.04	0.04	0.11	0.00	0.00
09/07/14	PM	10	1.09	2.13	1.06	1.44	0.30	0.58	15.9	0.20	0.36	0.32	2.01	1.77	0.95	0.21	0.58	0.48	0.22	0.48	0.46	0.39	0.27	0.21	0.60	0.10	0.00
10/07/14	AM	20	0.15	1.14	0.02	0.27	0.07	0.05	2.81	0.09	0.07	0.14	0.25	0.21	0.13	0.05	0.12	0.03	0.03	0.05	0.06	0.02	0.12	0.08	0.09	0.04	0.00
10/07/14	AM	10	3.88	4.24	1.11	0.36	0.20	0.41	12.7	0.85	0.56	0.12	3.24	0.74	0.95	0.24	1.19	0.37	0.51	0.50	0.42	0.22	0.27	0.15	0.56	0.05	0.03
10/07/14	PM	20	0.64	1.68	0.17	0.42	0.07	0.10	3.63	0.03	0.07	0.11	0.15	0.14	0.09	0.09	0.18	0.17	0.03	0.07	0.23	0.07	0.02	0.06	0.04	0.01	0.00
10/07/14	PM	10	1.06	4.57	1.21	1.40	0.26	1.10	16.9	0.43	2.23	0.58	2.50	1.96	0.98	0.18	0.44	0.29	1.75	0.18	1.55	0.23	1.19	0.17	0.29	0.07	0.00
11/07/14	AM	20	0.38	0.79	0.18	0.25	0.13	0.08	3.70	0.04	0.07	0.06	0.16	0.00	0.09	0.06	0.18	0.05	0.23	0.01	0.07	0.04	0.04	0.05	0.05	0.01	0.01
11/07/14	AM	10	2.93	2.14	0.61	1.05	0.37	0.25	0.73	0.12	0.28	0.44	0.49	1.19	0.55	0.15	0.21	0.38	0.16	0.44	0.44	0.42	0.25	0.29	0.34	0.00	0.00
11/07/14	PM	20	0.34	1.00	0.09	0.46	0.02	0.13	2.24	0.04	0.15	0.09	0.03	0.24	0.36	0.05	0.05	0.07	0.13	0.04	0.17	0.06	0.21	0.07	0.06	0.01	0.00
11/07/14	PM	10	3.53	1.16	0.62	1.96	0.35	0.90	9.58	0.80	0.29	0.56	1.77	0.98	0.97	0.41	1.47	0.30	0.87	0.31	0.88	0.44	0.37	0.38	1.14	0.00	0.00
16/07/14	AM	20	0.39	1.77	0.18	0.29	0.09	0.13	2.16	0.07	0.07	0.05	0.11	0.26	0.03	0.06	0.08	0.03	0.06	0.06	0.05	0.02	0.00	0.09	0.22	0.03	0.00
16/07/14	AM	10	3.73	2.21	0.69	0.57	0.75	0.95	5.63	0.83	0.35	0.06	0.64	0.00	0.47	0.28	0.89	0.08	0.16	0.59	0.36	0.15	0.62	0.23	0.03	0.00	0.00
16/07/14	PM	20	0.32	0.66	0.18	0.83	0.05	0.18	0.51	0.04	0.18	0.12	0.36	0.23	0.17	0.01	0.11	0.03	0.03	0.04	0.15	0.02	0.11	0.03	0.09	0.00	0.00
16/07/14	PM	10	2.28	15.2	1.17	1.87	0.68	0.25	16.8	0.33	0.43	0.74	1.51	0.53	0.11	0.40	0.76	0.38	2.90	0.28	1.65	0.43	0.00	0.85	0.58	0.13	0.00
18/07/14	AM	20	0.57	0.97	0.04	0.27	0.07	0.21	1.33	0.18	0.11	0.09	0.58	0.19	0.11	0.10	0.14	0.04	0.13	0.05	0.13	0.02	0.04	0.06	0.22	0.00	0.00
18/07/14	AM	10	2.90	0.77	2.03	2.95	0.63	0.54	12.2	0.92	1.03	0.63	0.85	2.08	1.01	0.37	2.24	0.94	0.32	1.13	1.41	0.37	1.99	0.41	1.03	0.19	0.00
22/07/14	AM	20	0.41	0.67	0.19	0.40	0.08	0.26	0.55	0.12	0.08	0.07	0.16	0.00	0.21	0.11	0.13	0.12	0.00	0.11	0.22	0.07	0.06	0.10	0.04	0.00	0.02
22/07/14	AM	10	3.43	15.4	0.65	4.61	0.83	0.70	8.57	0.51	0.91	0.13	2.18	1.89	0.94	0.68	2.10	0.29	1.07	0.26	0.45	0.58	0.00	0.78	2.28	0.35	0.22
22/07/14	PM	20	0.92	0.67	0.31	0.42	0.05	0.07	2.05	0.07	0.08	0.02	0.14	0.07	0.13	0.09	0.11	0.07	0.11	0.15	0.07	0.09	0.18	0.02	0.08	0.04	0.00
22/07/14	PM	10	2.36	4.65	1.54	3.82	0.24	0.87	26.0	0.57	0.27	0.40	1.63	1.29	1.50	0.16	2.15	0.34	3.39	0.22	3.43	0.58	0.48	0.53	0.60	0.09	0.05
28/10/14	AM	20	0.39	0.93	0.32	0.38	0.07	0.18	1.86	0.12	0.03	0.13	0.45	0.00	0.35	0.05	0.07	0.04	0.08	0.02	0.29	0.06	0.11	0.05	0.14	0.00	0.00
28/10/14	AM	10	5.19	7.47	1.53	5.03	0.43	0.40	4.64	0.35	0.11	0.43	3.99	4.09	1.33	0.64	0.81	0.31	1.21	0.63	0.74	0.62	0.38	0.66	1.59	0.07	0.00
28/10/14	PM	20	0.66	0.53	0.20	0.11	0.03	0.21	0.46	0.12	0.08	0.10	0.32	0.13	0.26	0.07	0.06	0.06	0.11	0.05	0.07	0.07	0.04	0.06	0.12	0.07	0.00
28/10/14	PM	10	4.50	5.72	0.54	3.65	0.72	1.66	31.4	0.59	0.08	0.71	4.66	0.26	1.41	1.23	2.19	0.99	0.36	0.26	0.63	0.35	1.05	0.26	0.64	0.00	0.00
29/10/14	AM	20	0.83	1.20	0.17	0.53	0.07	0.26	1.58	0.07	0.03	0.06	0.03	0.26	0.06	0.11	0.13	0.04	0.03	0.03	0.10	0.06	0.00	0.08	0.08	0.01	0.04
29/10/14	AM	10	3.93	4.53	0.94	0.63	0.03	0.34	29.6	0.97	0.05	0.55	0.55	1.79	0.79	0.46	0.54	0.25	0.37	0.24	0.19	0.32	0.24	0.08	0.70	0.09	0.00
29/10/14	PM	20	0.68	1.44	0.24	0.45	0.07	0.19	2.57	0.10	0.06	0.03	0.52	0.15	0.06	0.05	0.08	0.03	0.04	0.03	0.11	0.03	0.09	0.03	0.21	0.02	0.00
29/10/14	PM	10	3.20	0.09	0.04	1.23	0.04	0.76	22.3	0.69	0.20	0.27	0.84	0.30	0.74	0.21	1.63	0.37	0.04	0.06	0.14	0.43	0.68	0.28	0.20	0.00	0.00
30/10/14	AM	20	0.21	1.10	0.09	0.21	0.06	0.28	1.96	0.06	0.06	0.07	0.10	0.05	0.23	0.07	0.00	0.04	0.02	0.02	0.34	0.04	0.08	0.02	0.05	0.01	0.00
30/10/14	AM	10	4.84	4.45	0.43	1.82	0.12	0.85	9.29	0.05	0.28	0.58	0.92	1.26	0.10	0.11	1.65	0.26	0.24	0.19	0.21	0.28	0.18	0.32	0.18	0.00	0.00
30/10/14	PM	20	0.96	1.11	0.19	0.55	0.05	0.15	1.90	0.23	0.05	0.03	0.30	0.16	0.22	0.06	0.35	0.06	0.08	0.03	0.06	0.09	0.07	0.08	0.10	0.00	0.00

Continued on next page

LA-ICP-MS lower limits of detection, concentrations are in ppm

Date	Session	Crater diameter, μm	Rb	Sr	Y	Zr	Nb	Cs	Ba	La	Ce	Pr	Nd	Sm	Eu	Tb	Dy	Ho	Er	Tm	Yb	Lu	Hf	Ta	Pb	Th	U
30/10/14	PM	10	3.45	8.50	0.87	1.18	0.54	0.85	2.76	0.97	0.27	0.33	1.82	0.48	0.99	0.07	0.34	0.09	0.40	0.35	1.02	0.18	0.25	0.15	0.47	0.06	0.00
12/01/15	AM	20	0.93	1.01	0.03	0.36	0.06	0.09	1.42	0.03	0.09	0.03	0.30	0.00	0.11	0.02	0.07	0.07	0.04	0.02	0.06	0.04	0.03	0.07	0.05	0.03	0.00
12/01/15	AM	10	4.16	4.29	0.47	1.00	0.43	0.46	8.45	0.43	0.20	0.14	1.67	0.77	0.46	0.17	0.36	0.00	0.27	0.08	0.37	0.14	0.17	0.23	0.60	0.05	0.00
12/01/15	PM	20	0.82	0.55	0.09	0.12	0.08	0.09	0.27	0.08	0.05	0.01	0.45	0.25	0.03	0.03	0.08	0.00	0.03	0.04	0.10	0.01	0.00	0.06	0.10	0.01	0.00
12/01/15	PM	10	0.98	1.79	0.10	1.64	0.36	0.59	3.22	0.23	0.24	0.32	0.44	0.42	1.00	0.08	0.45	0.07	0.20	0.49	0.37	0.11	0.13	0.30	0.12	0.06	0.00
13/01/15	AM	20	0.87	0.17	0.16	0.30	0.11	0.20	1.22	0.09	0.06	0.07	0.34	0.07	0.06	0.02	0.05	0.02	0.00	0.06	0.04	0.05	0.07	0.03	0.15	0.02	0.00
13/01/15	AM	10	4.47	3.32	0.26	1.15	0.57	0.59	1.54	0.20	0.09	0.14	0.79	0.80	0.24	0.13	0.74	0.06	0.17	0.07	0.13	0.07	0.13	0.11	0.64	0.00	0.08
13/01/15	PM	20	0.52	0.84	0.05	0.28	0.04	0.06	0.94	0.03	0.07	0.08	0.24	0.20	0.13	0.05	0.04	0.02	0.05	0.02	0.15	0.02	0.05	0.04	0.07	0.01	0.00
13/01/15	PM	10	0.25	0.71	0.52	1.63	0.47	0.33	4.44	0.13	0.61	0.15	0.62	0.46	0.98	0.15	0.56	0.16	0.37	0.20	0.23	0.09	0.44	0.26	0.44	0.12	0.00
14/01/15	AM	20	0.72	0.20	0.41	0.56	0.09	0.19	1.25	0.07	0.13	0.06	0.09	0.00	0.10	0.08	0.13	0.05	0.11	0.02	0.18	0.02	0.10	0.02	0.03	0.01	0.00
14/01/15	AM	10	2.06	5.03	0.92	1.70	0.44	1.07	6.78	0.48	0.60	0.18	0.14	0.00	1.09	0.37	0.00	0.16	0.16	0.12	0.33	0.02	0.55	0.16	0.05	0.06	0.00
15/01/15	AM	20	0.23	0.69	0.11	0.09	0.20	0.15	1.42	0.12	0.06	0.03	0.08	0.21	0.12	0.03	0.16	0.02	0.06	0.04	0.15	0.03	0.00	0.03	0.06	0.01	0.00
15/01/15	AM	10	5.17	3.21	1.13	1.93	0.48	1.47	2.68	0.76	0.08	0.32	1.50	0.57	0.44	0.19	1.10	0.00	0.24	0.29	0.65	0.11	0.00	0.10	0.69	0.06	0.00
15/01/15	PM	20	0.28	0.34	0.17	0.28	0.04	0.20	1.64	0.12	0.04	0.03	0.18	0.07	0.08	0.03	0.09	0.08	0.08	0.03	0.14	0.02	0.11	0.05	0.02	0.02	0.00
15/01/15	PM	10	7.24	8.07	0.48	1.22	0.23	0.72	2.40	0.36	0.56	0.45	1.14	0.35	0.81	0.21	0.55	0.25	0.47	0.33	0.51	0.22	0.18	0.35	0.62	0.07	0.04
16/01/15	AM	20	0.48	0.65	0.15	0.31	0.06	0.34	1.77	0.14	0.05	0.05	0.23	0.08	0.13	0.03	0.05	0.04	0.04	0.02	0.13	0.02	0.22	0.07	0.02	0.01	0.00
16/01/15	AM	10	1.53	2.46	0.89	2.23	0.27	0.30	7.02	0.67	0.48	0.26	0.25	0.87	1.74	0.36	0.67	0.00	0.20	0.02	0.99	0.19	0.63	0.43	0.25	0.13	0.00
19/01/15	AM	20	0.31	0.44	0.36	0.38	0.15	0.09	0.99	0.11	0.04	0.08	0.26	0.00	0.10	0.02	0.05	0.05	0.04	0.07	0.10	0.01	0.18	0.12	0.12	0.04	0.00
19/01/15	AM	10	2.53	3.71	0.55	2.19	0.53	0.81	2.97	0.07	0.50	0.09	0.68	0.49	0.39	0.22	0.81	0.04	0.53	0.23	0.57	0.24	0.40	0.30	0.32	0.05	0.03
19/01/15	PM	20	0.48	0.12	0.07	0.66	0.09	0.22	0.99	0.01	0.06	0.04	0.08	0.15	0.08	0.02	0.00	0.03	0.07	0.05	0.08	0.03	0.04	0.07	0.21	0.01	0.00
19/01/15	PM	10	3.72	2.22	0.71	0.56	0.74	0.94	5.64	0.80	0.36	0.07	0.65	0.00	0.49	0.25	0.99	0.09	0.15	0.49	0.37	0.15	0.67	0.27	0.09	0.00	0.00
20/01/15	AM	20	1.06	0.65	0.11	0.17	0.22	0.28	0.57	0.11	0.03	0.01	0.15	0.11	0.11	0.06	0.07	0.05	0.07	0.01	0.11	0.09	0.10	0.13	0.13	0.02	0.00
20/01/15	AM	10	0.96	0.45	0.83	1.07	0.83	0.77	10.9	0.31	0.59	0.33	0.16	1.25	0.50	0.19	0.27	0.18	0.62	0.02	0.05	0.18	0.27	0.01	0.25	0.10	0.00
20/01/15	PM	20	0.74	0.76	0.05	0.34	0.13	0.14	1.71	0.11	0.15	0.01	0.24	0.12	0.17	0.11	0.10	0.02	0.00	0.04	0.20	0.03	0.06	0.09	0.04	0.04	0.01
20/01/15	PM	10	4.60	4.13	1.40	5.67	0.95	0.54	2.46	0.21	0.27	0.34	0.83	0.89	0.22	0.36	0.26	0.00	0.33	0.38	0.44	0.20	1.14	0.34	0.65	0.16	0.00
21/01/15	AM	20	1.18	0.34	0.14	0.60	0.03	0.19	1.96	0.13	0.04	0.10	0.41	0.10	0.17	0.05	0.11	0.00	0.04	0.03	0.23	0.08	0.15	0.05	0.08	0.04	0.00
21/01/15	AM	10	2.64	1.18	0.37	2.24	0.36	0.98	2.46	0.09	0.83	0.33	3.09	0.45	0.47	0.10	0.50	0.23	0.58	0.04	1.19	0.02	0.47	0.50	0.52	0.00	0.00
21/01/15	PM	20	0.04	0.86	0.18	0.45	0.15	0.14	1.31	0.03	0.10	0.01	0.07	0.00	0.11	0.08	0.25	0.05	0.00	0.06	0.18	0.09	0.08	0.02	0.16	0.00	0.00
21/01/15	PM	10	4.57	4.63	1.58	1.92	0.61	1.80	11.0	0.38	0.83	0.41	1.47	0.70	1.67	0.17	1.13	0.18	0.38	0.12	0.56	0.50	0.80	0.37	0.41	0.14	0.00
05/05/15	AM	20	1.06	4.04	0.20	0.08	0.18	0.24	2.45	0.07	0.16	0.07	0.27	0.33	0.21	0.04	0.31	0.03	0.05	0.01	0.06	0.09	0.25	0.12	0.27	0.04	0.00
05/05/15	AM	10	4.45	17.9	1.10	1.80	0.59	0.73	16.7	1.16	1.03	0.52	2.48	0.34	2.64	0.34	2.18	0.30	0.46	0.11	0.07	0.98	0.34	0.69	0.86	0.00	0.05
06/05/15	AM	20	0.80	1.40	0.19	0.53	0.18	0.10	0.90	0.19	0.11	0.04	0.25	0.00	0.35	0.08	0.17	0.05	0.05	0.06	0.24	0.04	0.16	0.15	0.26	0.01	0.01
06/05/15	AM	10	5.01	2.21	1.05	2.27	0.38	0.51	17.3	0.88	0.35	0.40	4.35	1.56	1.37	0.32	0.39	0.15	0.70	0.31	1.19	0.39	0.37	0.45	0.53	0.10	0.00
06/05/15	PM	20	0.59	1.26	0.25	0.36	0.07	0.30	0.74	0.07	0.14	0.06	0.11	0.29	0.08	0.06	0.20	0.06	0.03	0.02	0.24	0.09	0.08	0.03	0.06	0.03	0.00
06/05/15	PM	10	6.05	16.6	0.63	1.46	0.79	0.93	23.6	0.98	0.78	0.68	1.46	0.56	0.84	0.50	0.69	0.43	1.42	0.37	1.90	1.10	1.45	0.08	0.93	0.08	0.10
07/05/15	AM	20	0.94	2.65	0.10	0.13	0.09	0.34	1.30	0.07	0.16	0.05	0.17	0.19	0.17	0.04	0.23	0.03	0.08	0.06	0.26	0.03	0.03	0.01	0.25	0.02	0.00
07/05/15	AM	10	5.18	6.63	1.52	5.90	0.52	2.98	3.57	0.34	0.55	0.43	3.04	3.30	1.77	0.16	1.74	0.30	0.61	0.31	0.83	1.16	0.76	0.73	0.55	0.19	0.05
20/07/15	AM	20	0.60	27.8	0.18	0.47	0.15	0.92	5.43	0.15	0.15	0.15	0.10	0.18	0.03	0.05	0.32	0.07	0.09	0.04	0.23	0.04	0.00	0.05	0.30	0.02	0.02
20/07/15	AM	10	4.45	150	1.97	3.11	0.26	1.24	29.8	0.16	0.48	0.62	3.86	1.78	2.33	1.03	1.42	0.77	0.39	0.26	1.56	0.39	0.19	0.85	1.19	0.08	0.00
21/07/15	AM	20	1.01	10.2	0.37	0.20	0.19	0.11	4.51	0.16	0.06	0.04	0.55	0.04	0.10	0.11	0.14	0.14	0.17	0.08	0.13	0.03	0.09	0.11	0.14	0.01	0.00
21/07/15	AM	10	3.79	69.7	1.42	1.12	0.28	1.29	11.6	1.06	0.38	0.52	5.02	1.16	0.93	0.37	1.25	0.58	0.64	0.63	0.85	0.95	0.43	0.67	1.62	0.27	0.05
21/07/15	PM	20	0.38	9.62	0.08	0.40	0.06	0.08	2.19	0.03	0.16	0.03	0.56	0.33	0.22	0.04	0.18	0.12	0.06	0.06	0.06	0.07	0.22	0.01	0.09	0.00	0.00
21/07/15	PM	10	3.69	84.1	0.95	2.42	0.23	1.12	6.89	0.90	0.69	0.11	1.72	1.47	1.75	0.90	0.57	0.23	1.78	0.68	1.14	1.06	0.31	0.84	1.07	0.06	0.00
23/07/15	AM	20	1.57	21.7	0.15	0.11	0.07	0.37	3.33	0.28	0.17	0.12	0.02	0.47	0.28	0.10	0.28	0.14	0.13	0.05	0.25	0.08	0.18	0.08	0.22	0.02	0.00
23/07/15	AM	10	0.29	0.36	0.15	3.20	0.03	0.18	1.63	0.10	0.05	0.01	0.17	0.06	0.07	0.02	0.10	0.09	0.07	0.02	0.15	0.01	0.12	0.06	0.03	0.03	0.00

Continued on next page

LA-ICP-MS lower limits of detection, concentrations are in ppm

Date	Session	Crater diameter, μm	Rb	Sr	Y	Zr	Nb	Cs	Ba	La	Ce	Pr	Nd	Sm	Eu	Tb	Dy	Ho	Er	Tm	Yb	Lu	Hf	Ta	Pb	Th	U
23/07/15	PM	20	0.60	18.4	0.24	0.82	0.07	0.08	4.98	0.15	0.01	0.22	0.44	0.17	0.50	0.10	0.29	0.07	0.12	0.08	0.25	0.10	0.04	0.14	0.24	0.02	0.01
23/07/15	PM	10	6.34	48.6	1.69	1.90	0.23	0.51	26.4	0.68	0.67	0.34	2.28	2.40	1.62	0.33	1.58	1.06	0.37	0.66	0.97	1.15	1.15	0.75	1.00	0.06	0.05
24/07/15	AM	20	0.65	14.6	0.28	0.42	0.01	0.26	4.42	0.10	0.09	0.11	0.14	0.29	0.31	0.13	0.25	0.04	0.13	0.08	0.24	0.03	0.05	0.08	0.02	0.00	0.00
24/07/15	AM	10	2.79	176	3.43	2.84	0.33	2.27	11.5	0.75	0.39	0.34	2.17	2.00	0.98	0.42	1.78	0.37	0.07	0.58	0.26	0.28	0.87	0.57	2.03	0.16	0.00
24/07/15	PM	20	0.53	9.15	0.28	0.65	0.10	0.46	0.53	0.20	0.04	0.11	0.28	0.19	0.23	0.14	0.18	0.07	0.16	0.07	0.19	0.02	0.08	0.07	0.14	0.01	0.02
24/07/15	PM	10	1.39	110	2.17	1.02	0.50	1.09	17.5	1.72	0.80	0.23	4.66	1.94	1.42	0.63	2.82	0.17	1.09	0.28	1.30	0.13	2.40	1.03	0.89	0.18	0.00
28/07/15	AM	20	0.19	4.31	0.09	0.46	0.13	0.25	3.89	0.20	0.21	0.04	0.25	0.25	0.17	0.05	0.14	0.08	0.12	0.05	0.33	0.12	0.04	0.04	0.18	0.00	0.00
28/07/15	AM	10	5.12	29.2	3.02	0.47	0.22	0.11	16.0	1.05	1.06	0.30	6.09	0.43	1.20	0.93	0.81	0.88	0.28	0.82	1.50	0.49	0.32	0.46	0.61	0.00	0.06
28/07/15	PM	20	1.02	12.4	0.10	0.26	0.09	0.48	2.30	0.16	0.09	0.07	0.30	0.14	0.21	0.18	0.43	0.03	0.31	0.03	0.17	0.12	0.09	0.01	0.15	0.00	0.00
28/07/15	PM	10	4.12	123	2.75	1.86	0.03	1.92	35.7	0.63	0.53	0.76	2.75	0.72	2.83	0.44	0.75	0.29	0.76	0.37	0.86	1.38	1.60	0.74	0.68	0.25	0.00
29/07/15	AM	20	0.63	8.19	0.12	0.12	0.08	0.31	2.89	0.18	0.03	0.14	0.71	0.41	0.33	0.03	0.16	0.02	0.12	0.08	0.11	0.11	0.18	0.10	0.31	0.01	0.01
29/07/15	AM	10	6.13	98.5	0.84	4.75	0.29	2.31	18.8	0.81	1.44	0.38	3.36	0.91	0.22	0.66	1.60	0.63	2.05	0.67	1.72	1.02	0.35	0.37	1.47	0.14	0.00
Median		20	0.62	1.05	0.17	0.37	0.07	0.19	1.88	0.09	0.07	0.06	0.25	0.14	0.13	0.06	0.13	0.04	0.07	0.05	0.15	0.04	0.08	0.06	0.12	0.01	0.00
Median		10	3.73	4.64	0.93	1.84	0.37	0.76	11.3	0.55	0.48	0.34	1.67	0.84	0.96	0.26	0.75	0.25	0.40	0.29	0.66	0.32	0.37	0.37	0.61	0.08	0.00

.8 Calculations

.8.1 Calculation of Q Ab Or normative positions in the Haplogranite System

Equations 2 to 4, from Blundy and Cashman (2001), were used to calculate the quartz, albite and orthoclase normative positions of rhyolitic tephras. These calculations compensate for the effect of anorthite, which displaces the quartz-feldspar cotectic to higher quartz contents. None of the samples contained normative kalisiite, or normative leucite, but if they had these would have to be included in the calculation for Ks'. The new normative positions could then be plotted on the haplogranite (Q-Ab-Or) system.

$$Qz' = Qz_n \times (1 - 0.03An + 6 \times 10^{-5}[Or_n \times An] + 10^{-5}[Ab_n \times Or_n \times An] \quad (2)$$

$$Or' = Or_n \times (1 - 0.07An + 10^{-3}[Qz_n \times A_n]) \quad (3)$$

$$Ab' = 100 - Qz' - Or' \quad (4)$$

where Qz' is the position of quartz on the haplogranite system, and Qz_n is normative quartz normalised to an anorthite free basis.

.8.2 Calculation of Q Ne Ks normative positions in Petrogeny's Residua Sytem

The CIPW norms of quartz, nepheline and kalsilite in trachytic-phonolitic tephras were recast to an an alkali feldspar free basis (i.e. converting alkali feldspar end-members to their equivalent contents of Ne, Ks and Q) using Equations 5 to 7. These normative positions could then be plotted on Petrogeny's Residua System.

$$Qz' = Q + Or \times ([4 \times Q_{mw}]/[2 \times Or_{mw}]) + Ab \times ([4 \times Q_{mw}]/[2 \times Ab_{mw}]) \quad (5)$$

$$Ne' = Ab \times ([2 \times Ne_{mw}]/[2 \times Ab_{mw}]) + Ne \quad (6)$$

$$Ks' = Or \times ([2 \times Ks_{mw}]/[2 \times Or_{mw}]) \quad (7)$$

where Q_{mw} is the molecular weight of quartz.

—